



20 SEP 1954

MINISTRY OF SUPPLY

AERONAUTICAL RESEARCH COUNCIL
REPORTS AND MEMORANDA

The High-Speed Laboratory
of the
Aerodynamics Division, N.P.L.

By D. W. HOLDER

LONDON: HER MAJESTY'S STATIONERY OFFICE

1954

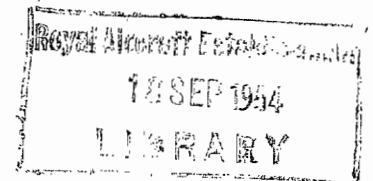
PRICE £3 10s 0d NET

R. & M. No. 2560
A.R.C. Monograph

MINISTRY OF SUPPLY
AERONAUTICAL RESEARCH COUNCIL
REPORTS AND MEMORANDA

The High-Speed Laboratory of the
Aerodynamics Division, N.P.L.

By
D. W. HOLDER



PART I
Description of the Installation

PART II
Experimental Techniques

PART III
Experimental Results

LONDON : HER MAJESTY'S STATIONERY OFFICE

1954

Crown Copyright Reserved

PRINTED AND PUBLISHED BY HER MAJESTY'S STATIONERY OFFICE

To be purchased from

York House, Kingsway, LONDON, W.C.2 423 Oxford Street, LONDON, W.1

P.O. Box 569, LONDON, S.E.1

13a Castle Street, EDINBURGH, 2 1 St. Andrew's Crescent, CARDIFF

39 King Street, MANCHESTER, 2 Tower Lane, BRISTOL, 1

2 Edmund Street, BIRMINGHAM, 3 80 Chichester Street, BELFAST

or from any Bookseller

1954

Price £3 10s 0d net

PRINTED IN GREAT BRITAIN

S.O. Code No. 23-2560

The High-Speed Laboratory of the Aerodynamics Division, N.P.L.

Parts I, II and III

By

D. W. HOLDER

Reports and Memoranda No. 2560

December, 1946

General Summary.—The first part of this report describes the high-speed tunnel installation in the Aerodynamics Division of the National Physical Laboratory. The installation consists of the 12-in. diameter High-Speed Tunnel, the 20 × 8-in. High-Speed Tunnel and a number of smaller tunnels all of which are operated on the induction principle from a common compressed-air storage capacity. An account is included of a series of experiments which were made to investigate the influence of the design on the efficiency of an induced-flow tunnel, and finally the new 18 × 14-in. High-Speed tunnel is described.

The second part describes some of the experimental techniques which have been used. Many of these are similar in principle to those of low-speed tunnel practice, but some of them (*e.g.*, the schlieren and shadowgraph techniques) are peculiar to compressible-flow experiments.

The third part of the report reviews the experimental results obtained in the high-speed tunnels during and immediately before the war. The phenomena which occur on a particular aerofoil as the Mach number is increased from a low value are described in detail and the effects of the aerofoil shape are then discussed. This approach is used also for supersonic flow where the flow round a particular aerofoil is again described in detail and the effects of aerofoil shape and Mach number are discussed. The flow round an aerofoil with a control flap is discussed for both subsonic and supersonic flow and an account is included of a number of other fundamental and *ad hoc* investigations.

The report was written in 1946 as a contribution to the series of monographs intended for the Scientific War Records.

CONTENTS

<i>Section</i>	<i>Title</i>	<i>Page No.</i>
	General Summary	1
PART I		
1.1	Introduction	5
1.2	The Production of a High-Velocity Airstream	6
1.3	Power Supply and General Description	7
1.4	History of the High-Speed Tunnels in the Aerodynamics Division of the N.P.L.	8
1.5	Description of the Installation in the Aerodynamics Division of the N.P.L.	9
1.5.1	The 1-ft dia. Tunnel	10
1.5.2	The 20 × 8-in. Tunnel	10
1.5.3	The 5 × 2-in. Tunnel	11
1.6	The Advantages of the Induction Principle	11
1.7	Variation of Stagnation Temperature in a Closed-Circuit Tunnel	13

CONTENTS—*continued*

<i>Section</i>	<i>Title</i>	<i>Page No.</i>
1.8	The Efficiency of Induction-Type Tunnels	13
1.8.1	Energy Ratio	14
1.8.2	Energy Ratio for Continuous Operation	15
1.8.3	Energy Ratio for Operation from Storage	15
1.8.4	Energy Required to Charge Storage Reservoirs	16
1.8.5	Variation of Energy Ratio with Tunnel Stagnation Pressure	17
1.9	The Influence of the Tunnel Design on Efficiency	17
1.9.1	Effects of Asymmetry of Injection	18
1.9.2	The Influence of the Diffuser Design	18
1.9.3	The Influence of the Injector Slot Width and Angle of Injection	19
1.9.4	The Use of an Injector of Convergent-Divergent Section	19
1.9.5	Comparison between the Efficiencies of the Model and Larger Tunnels	20
1.9.6	The Influence of a Model in the Working Section	20
1.9.7	Influence of the Return Duct on Efficiency	20
1.10	The Influence of the Injection on the Distribution of Velocity along the Tunnel Axis	20
1.11	The use of the Model Results in the Design of Induction-type Tunnels	21
1.12	The Proposed new 18 × 14-in. Tunnel	22
PART II		
2.1	Introduction	55
2.2	Regulation of Tunnel Speed	55
2.2.1	Regulation at Constant Injector-Slot Area	56
2.2.2	Regulation by Variation of the Injector-Slot Area	56
2.2.3	Regulation by a Throat Downstream of the Working Section	56
2.2.4	Regulation at Supersonic Speeds	57
2.3	Measurement of Tunnel Speed	57
2.4	Direct Force Measurement	58
2.4.1	The Three-Component Electrical Balance	59
2.4.2	Strain-Gauge Balance	59
2.4.3	Drag Balance	60
2.5	Indirect Force Measurement	61
2.5.1	Pressure-Plotting Technique	61
2.5.1.1	Pressure-plotting models	62
2.5.1.2	Pressure-plotting manometer	63
2.5.2	Determination of Profile Drag at High Speeds by a Wake-Traverse Method	63
2.5.2.1	Correction for finite diameter of pitot tube	67
2.5.2.2	Pitot and static tubes	67
2.6	Factors which may cause the behaviour of the Working Fluid in a Wind Tunnel to Depart from that of a Perfect Gas	67
2.6.1	Relaxation-Time Effects	68
2.6.2	Possibility of Liquefaction at High Mach Number	68
2.6.3	Influence of Humidity	69
2.6.4	Driers	71
2.6.4.1	Control of stagnation temperature	71
2.6.4.2	Control of stagnation pressure	72
2.6.4.3	Drying in a compression-expansion cycle	72
2.6.4.4	Drying in a refrigeration-reheating cycle	73
2.6.4.5	Chemical driers	73
2.6.4.6	The application of drying methods to wind tunnels	73
2.6.5	The Influence of Moisture on the Reading of a Pitot Tube	73
2.6.6	The Influence of Condensation on the Profile Drag Measured by the Wake-Traverse Method	75

CONTENTS—*continued*

<i>Section</i>	<i>Title</i>	<i>Page No.</i>
2.7	Effects of Reynolds Number and Turbulence	75
2.7.1	Effects of Turbulence	75
2.8	Interference due to the Constraint of the walls of a Closed Rectangular Tunnel on an Aerofoil Spanning the Working Section	76
2.8.1	Blockage	76
2.8.2	Lift Effect	76
2.8.3	Corrections at Low Speed	77
2.8.4	Corrections at Compressibility Speeds	78
2.8.5	Tunnel Choking	80
2.8.6	Interference due to the boundary layer of the side walls	81
2.9	The Adjustable Walls of the N.P.L. 20 × 8-in. Tunnel	81
2.9.1	Streamlines and Pressures round a Doublet, Vortex and Source	82
2.9.2	Experimental Observations Using the Adjustable Walls	83
2.9.3	Lift by the Integration of Wall Pressures	84
2.10	Intercomparison of Observations with Straight and Streamlined Walls	84
2.11	Wall Interference at Supersonic Speeds	84
2.12	Yawmeters	86
2.12.1	Aerofoil Yawmeter	86
2.12.2	The Circular-Cylinder Yawmeter	86
2.12.3	Bent-Tube Yawmeter	87
2.13	Optical Systems for Flow Exploration	87
2.13.1	The Schlieren Method	89
2.13.2	The Direct-Shadow Method	90
2.13.3	Notes on Optical Components	91
2.13.4	Notes on the Arrangement of the Optical System	92
2.13.5	Glass for Wind-Tunnel Walls	93
2.13.6	General Remarks on the Use of Optical Methods at the N.P.L.	93
2.13.7	The Interferometer Method	94
2.14	Measurement of Wave Angles	94
2.15	Attempts to Visualize Streamlines	94
2.16	Methods of Indicating Transition Position	94
2.17	Methods of Fixing Transition	95
2.18	The Measurement of Stagnation Temperature	97
2.18.1	Measurements of the Stagnation Temperature in the Wake of an Aerofoil	97
2.19	The Measurement of Surface Temperature	98
2.20	Measurement of Inducing-Air Supply to Tunnels	98
2.21	Supersonic Nozzle Design	99

PART III

3.1	Introduction	145
3.2	Experiments at Subsonic and Transonic Speeds	145
3.2.1	The Flow round an Aerofoil at High Subsonic Mach Number	145
3.2.1.1	Changes of flow pattern with free-stream Mach number	146
3.2.1.2	Flow pattern changes at low incidence	147
3.2.1.3	Flow pattern changes at high incidence	147
3.2.1.4	Variation of normal force and moment coefficients with free-stream Mach number	148
3.2.1.5	Variation of profile-drag coefficient with free-stream Mach number	149
3.2.1.6	General discussion of the overall force and moment-coefficient changes	150
3.2.1.7	Note on the diffuse nature of some of the shock-waves of Figs. 4 to 18	150

CONTENTS—*continued*

<i>Section</i>	<i>Title</i>	<i>Page No.</i>
3.2.2	The Influence of the Aerofoil Shape	151
3.2.2.1	Lift	151
	Influence of aerofoil thickness	151
	Influence of camber	152
	Influence of trailing-edge angle	152
	Critical Mach number for lift fall	152
3.2.2.2	Pitching moment	152
	Influence of aerofoil thickness	152
	Influence of camber	152
	Influence of trailing-edge angle	152
	Critical Mach number for pitching moment	152
3.2.2.3	Profile drag	153
	Influence of aerofoil thickness	153
	Influence of position of maximum thickness	153
	Influence of leading-edge radius	153
	Influence of camber	153
	Critical Mach number for drag rise	153
3.2.3	Aerofoil Tests at Subsonic Speeds in the 1-ft Diameter Tunnel	153
3.2.4	Aerofoil Tests at Subsonic Speeds in the 20 × 8-in. Tunnel	154
3.2.5	Schlieren Photography in the 20 × 8-in. Tunnel	154
3.2.6	Intercomparison of N.P.L. and R.A.E. High-Speed Tunnel Observations	154
3.2.7	Intercomparison of High-Speed Wind Tunnel and Flight Observations	154
3.2.8	The Influence of Reynolds Number	155
3.2.9	Transition Indication	156
3.2.10	The Interaction of Shock-waves and Boundary Layers	156
3.2.11	Boundary-Layer Suction	158
3.2.12	Controls on Subsonic Aerofoils	159
3.2.13	Tests with Brake Flaps	161
3.2.14	Fin-Tailplane Interference	162
3.2.15	Sharp-Nosed Aerofoils at Subsonic Speeds	162
3.2.16	Sweep Back	163
3.2.17	Experiments with a Circular Cylinder at High Mach Number	164
3.2.18	Velocity-Measuring Instruments	165
3.2.19	The Measurement of Surface Temperature	166
	Flat Plates	166
	Streamline Bars	166
	Circular Cylinder	166
	NACA 0020	167
3.3	Experiments at Supersonic Speeds	167
3.3.1	Supersonic Tests on Sharp-Nosed Aerofoils	167
3.3.1.1	Tests with 3-component balance	167
3.3.1.2	Pressure-plotting and flow-visualization experiments	168
3.3.2	Round-Nosed Aerofoils at Supersonic Speeds	170
3.3.3	Controls on Supersonic Aerofoils	170
3.4	Miscellaneous Experiments	171
3.4.1	Body-Wing Combinations	172
3.4.2	Aspect-ratio Tests	172
3.4.3	Complete Aircraft Models	172
3.4.4	Other Tests	172
Appendix I.	Table of Aerofoils tested in the High-Speed Laboratory of the Aerodynamics Division, N.P.L.	173
Appendix II.	Reference List of Compressibility Reports by the Staff of the High-Speed Laboratory and others at the Aerodynamics Division, N.P.L., June, 1947	176
References	183

PART I

1.1. *Introduction.*—The principal purpose of wind-tunnel tests is to enable the aerodynamic forces on a full-scale body moving through the air to be predicted from observations made in controlled tests on a scale model, and also to enable a study of the flow pattern around the body to be made in greater detail than would be possible in free flight.

It is well known^{1,2,3,4} that if forces due to viscosity and inertia alone are of importance, the flows around two geometrically similar bodies completely immersed in a fluid will be similar if the Reynolds number^{1,2,3,5,6,7} is the same in each case. If the forces due to viscosity are negligible, compared with those arising from the compressibility or elasticity of the fluid, then the criterion for similarity is the Mach number^{2,8,9} defined as the ratio of the local velocity to the speed of sound at the local temperature. This latter speed is that at which disturbances of small amplitude are propagated in the fluid. Both Reynolds and Mach numbers have certain critical ranges in which the flow pattern experiences considerable changes.

Since air is both viscous and compressible, the motions round the prototype body, and the scale model in the tunnel, will only be truly similar if the Reynolds and Mach numbers are separately identical. At high Mach number, however, it is difficult, if the prototype body is large, to achieve full-scale Reynolds number without a very large expenditure of power. Indeed, there is no British tunnel which enables this identity of Reynolds and Mach numbers to be achieved if the latter is high.

In order, therefore, that the results of high-speed tunnel tests may be applied to the motion of the prototype body, it is necessary to assume that at high Mach number the influence of the viscous forces is small compared with those due to compressibility and, therefore, if identity of Mach number is achieved a large Reynolds number difference may be tolerated provided that the Reynolds number is not in a critical region. The extent to which this assumption is justifiable is uncertain, particularly as it is generally accepted¹⁰ that the mechanism of the shock-stall is closely associated with the inter-action of shock-waves and boundary layers^{11,12,13,14}. There is, indeed, very little information concerning the influence of Reynolds number on the flow round a body at high Mach number. The most obvious comparison is between the results of high-speed tunnel tests and flight tests at the same Mach number but increased Reynolds number. Such comparisons have been made, however, only in a small number of cases owing to the limited number of flight tests that have been carried out, and the difficulties of instrumentation in these tests.

Even if identity of Mach number is achieved, and it is assumed that the Reynolds number discrepancy is tolerable, there may still be differences between the tunnel and free-air flows which have an important effect on the forces experienced by a body. In this connection differences of the turbulence and humidity of the airstream must be considered together with the interference due to the constraint of the boundaries of the working section. In certain cases it may also be necessary to consider the relaxation time^{15,16} of the working fluid and its behaviour on approaching its liquefaction point.^{17,18}

To provide information on these points (and also to give information in the transonic velocity region) comparative tests have been made in this country,¹⁹ in Germany,^{20,21} and in the United States,²² between models in a tunnel and models either dropped from an altitude or projected into free air.

There is little systematic evidence on the effects of turbulence mainly because of the extreme difficulty of obtaining a quantitative measure of turbulence at high Mach number. Airstream turbulence does, however, appear to have a considerable effect on the flow around a model particularly in the transonic speed range, and the wind-tunnel turbulence estimated by this criterion appears to be influenced considerably by the arrangement and uniformity of the gauze screens at the tunnel intake.

The interference of the tunnel walls may be eliminated at all Mach numbers by shaping them²³ to coincide with streamlines of the flow round the body in an unlimited stream. This method has proved valuable in subsonic tests on two-dimensional bodies at the National Physical Laboratory, but at Mach numbers close to unity it becomes very difficult to determine the correct wall shape accurately. At supersonic speeds it is, in general, not necessary to shape the walls in the manner described²⁴.

The humidity of the airstream may be of considerable importance since the condensation of moisture accompanied by the release of latent heat may have an appreciable effect on the flow.

It is customary to refer to velocities below the local speed of sound as subsonic, and to velocities in excess of this speed as supersonic. A region of velocity centred approximately about the local speed of sound and characterized by the existence in the flow pattern of regions of both subsonic and supersonic velocity is referred to as the transonic or mixed velocity range.

The apparatus which is used in the Aerodynamics Division of the N.P.L. to investigate the flow round bodies at high Mach number will be briefly described in this section of the monograph. A second section²⁵ will describe the experimental techniques which are used, and a third²⁶ section some of the more important experimental results obtained during and immediately before the war.

1.2. *The Production of an Airstream of High Mach Number.*—The high-velocity airstream at the working sections of the wind tunnel is produced by an acceleration from rest and approximately atmospheric conditions. This acceleration takes place in a continuous channel of varying cross-sectional area termed the effuser and may be regarded as isentropic. Using the equations of state and of constancy of total energy together with the equations for isentropic pressure changes it is possible²⁷ to obtain relations between the Mach number at the working section and the pressure, density, temperature and velocity at this region in terms of the stagnation values. Moreover, by the use of Sutherland's equation²⁸ or a simple power relationship²⁹, it is possible to calculate the viscosity of the air at the working section from the temperature computed above. Thus, the Reynolds number of an experiment on a model placed in the working section may be expressed in terms of the Mach number and the stagnation conditions of the airstream. Some of the more important variables are plotted as functions of working-section Mach number in Figs. 1 and 2 for standard atmospheric stagnation conditions.

On the assumption of an isentropic expansion, the mass velocity (ρV) rises to a maximum at a Mach number of unity and then falls again with further increase of Mach number. In a continuous channel the cross-sectional area must (on the assumption of approximately constant conditions across a cross-section) be inversely proportional to the mass velocity in order to satisfy the condition of continuity of mass flow, and it is, therefore, clear that whilst the cross-sectional area must be decreased in order to accelerate a subsonic flow the converse is true if the flow is initially supersonic. Thus, in order to produce a supersonic flow it is necessary first to contract the channel to a throat^{30, 31, 32} at which the velocity will be approximately equal to the critical sonic value, and then expand the channel in order to produce further acceleration to a supersonic velocity. Such a convergent-divergent channel placed at the upstream end of a high-speed tunnel is usually referred to as a supersonic effuser or nozzle.

No such nozzle is required for a subsonic tunnel in which a range of Mach numbers may be obtained by adjusting the working-section pressure in accordance with the curve given in Fig. 1. A limit to the working-section Mach number is, however, reached when the velocity across any section becomes equal to the sonic value at the local temperature. Conditions then become critical in the sense that the mass flow through the tunnel reaches a maximum value, and the tunnel is referred to as choked. Further decrease of pressure downstream of the section at which choking has taken place then produces no further increase of velocity upstream.

If a supersonic effuser is fitted, the ratio of the throat area to that of the working section A^*/A will determine approximately the mean working-section Mach number which is achieved according to a relationship similar to that plotted in Fig. 2. This curve indicates only the area ratio,

however, and gives no indication of the geometry between the throat and working section. This geometry is of some importance if a uniform flow is to be achieved at the working section and will be further discussed in Part II. Only one supersonic Mach number may be achieved for a particular nozzle geometry, and if a range of Mach number is required it is necessary to have either a number of separate nozzles or adjustable tunnel walls.

Considering once again the curve of mass velocity plotted in Fig. 2 it would appear to be impossible to pass continuously from a subsonic to a supersonic, or from a supersonic to a subsonic, velocity in a channel of constant cross-sectional area. A deceleration from a supersonic to a subsonic velocity may, however, also take place discontinuously through a normal shock-wave^{8, 9, 33, 34}. Deceleration through a convergent-divergent channel may, in theory, be isentropic, but deceleration through a shock-wave is accompanied by an increase of entropy, and if the flow is to be maintained power must be supplied continuously from an external agency. Such a shock-wave at the downstream end of the working section of a supersonic tunnel is referred to as the tunnel or breakdown shock-wave. A discontinuous acceleration from a subsonic to a supersonic Mach number cannot take place since this would involve a decrease of entropy and a violation of the second law of thermodynamics. The changes which take place through a normal compressive shock-wave are shown in Fig. 3(a).

The variation of static pressure with working-section Mach number is shown in Fig. 1 for an isentropic acceleration. The relation between these two quantities is commonly used to deduce the latter from a measurement of the former. Fig. 1 also shows the fall of temperature which accompanies the acceleration. It should be noted that this temperature is not reached by a body placed in the flow, nor by the tunnel walls, since it may be shown^{35, 36, 37} that re-heating to a temperature very close to the stagnation value occurs in the boundary layers of these surfaces.

From Fig. 1 it may be seen that if a fundamental linear dimension of the model (this may be the aerofoil chord) and the stagnation pressure are constant, the Reynolds number of the experiment rises to a maximum at a Mach number of about 1.2. The dynamic head ($\frac{1}{2}\rho V^2$) rises to a maximum at a Mach number of $\sqrt{2}$ and the kinetic energy per unit area ($1/2\rho V^3$) at $\sqrt{3}$. This is shown in Fig. 2.

In the Aerodynamics Division of the N.P.L. no attempt has been made to use a second convergent-divergent duct or other form of supersonic diffuser when the working-section velocity is supersonic. Thus the supersonic recompression is always through an approximately normal shock-wave. At the Mach number commonly used in these tunnels, however, ($M < 1.5$) there is evidence³⁸ that in practice, it is difficult to achieve diffuser efficiencies in excess of that given by a normal shock-wave. At higher Mach numbers, however, increased efficiencies may be obtained³⁸ by suitable design. The ratio of the total head at the tunnel intake to that at the diffuser exit (termed the overall tunnel pressure ratio) is plotted in Fig. 3(b) as a function of working-section Mach number. Three curves are given; one applies to the case in which the supersonic recompression takes place through a normal shock-wave followed by completely efficient subsonic diffusion. A second curve applies to a normal shock-wave without subsequent subsonic diffusion, and a third shows values obtained in practice. In the first two curves the losses occurring in the supersonic diffusion have been calculated from the simple shock-wave equations.

1.3. General Description and Power Supply.—Considering the channel sketched in Fig. 4(a), the air accelerates isentropically from rest at atmospheric conditions at the tunnel intake up to the working-section Mach number. Recompression then takes place in the diffuser. If the whole process is isentropic, and recompression is complete (that is, there is no residual kinetic energy at the diffuser exit) then no power is required to maintain the flow. In practice, however, there is a gain of entropy due to losses of total head arising from skin friction, eddying motion and in shock-waves. Moreover, because of the adverse pressure gradient, conversion of kinetic to pressure energy in the diffuser is seldom efficient, and in an open circuit tunnel there is always some rejection of kinetic energy at the diffuser exit. Thus, to maintain the flow, it is necessary to supply an amount of energy to the airstream which is equal to that dissipated in these losses. In the National Physical Laboratory (N.P.L.) high-speed tunnels this energy is supplied by an

annular jet of air issuing with high velocity from a slot into the tunnel downstream of the working section. This jet mixes with the air in the tunnel and induces a flow through the working section. The high-velocity jet is, therefore, referred to as the inducing airstream, and the air flowing through the working section as the induced airstream. A sketch of the general arrangement of this 'induction-type' wind tunnel is given in Fig. 4(b). The inducing airstream is supplied from a pressure chamber which encircles the tunnel in the region of the injector slot. The pressure chamber is supplied by a pipe system from compressed-air storage reservoirs which are charged by reciprocating compressors. For subsonic operation the velocity of the induced airflow depends on the pressure in the pressure chamber which is regulated by a throttle valve of the gate type situated in the pipeline between the compressed-air reservoir and the tunnel pressure chamber. For supersonic operation it is found that the velocity is independent of the blowing pressure provided that the value of this pressure lies between certain well defined limits (*see* section 1.10). Since the pressure in the pressure chamber may be high and considerable pressure differences may exist between the interior of the working section and the surrounding atmosphere, the tunnels are of robust construction, the main structure being of steel.

1.4. *History of the High-Speed Tunnels in the Aerodynamics Division of the National Physical Laboratory.*—The first British high-speed tunnels were constructed by Stanton^{39, 40} in the Engineering Division of the N.P.L. from 1921 onwards. In these early tunnels, which were of very small working-section size (0.8 in. diameter and 3 in. diameter), a number of projectile and aerofoil models^{41, 42} were tested at both subsonic and supersonic velocities. These tunnels were operated by the direct discharge of compressed air from either a compressor or reservoir.

The first high-speed tunnel in the Aerodynamics Division, N.P.L., was installed in 1935 in the Compressed Air Tunnel⁴³ (C.A.T.) building and was of circular cross-section with a working-section diameter of 12 in. It was operated on the induction principle by the discharge of air from the C.A.T. at the completion of a run at high Reynolds number. Thus, the frequency and duration of runs by this high-speed tunnel were controlled by the C.A.T. test programme. This high-speed tunnel installation was in all respects very similar to the National Advisory Committee for Aeronautics (U.S.A.) installation⁴⁴ constructed in 1928 to operate from the American Variable Density Tunnel⁴⁵. From November 1935 until May 1939 a considerable number of tests at subsonic working-section velocities were carried out in this tunnel under the direction of Mr. C. N. H. Lock. During this period an experimental investigation into the possibility of building a high-speed induction type tunnel of rectangular cross-section with adjustable walls at the working section was carried out⁴⁶ in the Engineering Division, N.P.L., under the direction of Dr. Gough.

In 1939 the circular high-speed tunnel was moved to its present position in the new High-Speed Tunnel laboratory with a separate compressed-air storage capacity charged by the existing C.A.T. compressors. Before installation in the new building, modifications, which had been found desirable during previous runs, were made to the tunnel design. The modified tunnel was first run in its new position in November, 1939.

A tunnel of rectangular cross-section with a working section 20×8 in. fitted with adjustable walls on its two shorter sides to reduce the wall interference was completed in May, 1941. This tunnel, which was intended for tests at subsonic speeds on aerofoil models completely spanning the working section, was operated on the induction principle and was housed in the new building. The compressed-air supply was drawn from the existing storage capacity.

In November, 1943, the original circular tunnel was fitted with a convergent-divergent effuser upstream of the working section and was successfully operated at a supersonic working section Mach number of 1.4. Since this date a number of tests at supersonic velocities have been made in this tunnel at Mach numbers of about 1.2, 1.4 and 1.55. The 20×8 in. tunnel has also been run empty at a low supersonic Mach number (1.15) by using the adjustable walls to form a convergent-divergent nozzle.

Since 1942 when a tunnel of working-section dimensions 5×2 in. was transferred to the new building from the Engineering Division, a number of small tunnels each devoted to specialised research work have been constructed to operate from the new compressed-air storage reservoirs.

Experimental work carried out on the 12-in diameter tunnel has led to the publication of some 45 Aeronautical Research Council (A.R.C.) reports of which 10 were issued whilst the tunnel was in the C.A.T. building. Experiments made in the 20×8 -in. tunnel have been described in 24 reports and work carried out in the other smaller tunnels in about 14 reports. Altogether some 125 A.R.C. reports were prepared by the High-Speed Tunnel staff before September, 1945, those not mentioned above being of a theoretical or general nature. A list of the reports is given in an Appendix to Part III²⁶.

Up to June, 1945, all the high-speed tunnels had been of the open-circuit type, but in this month return ducts were fitted to the two larger tunnels and one of the smaller tunnels so that the airstream could be dried. Most of the work to be described was, however, carried out before the return ducts were installed.

1.5. *Description of the Installation at the Aerodynamics Division N.P.L.*—A plan of the high-speed wind-tunnel installation of the N.P.L. Aerodynamics Division is given in Fig. 5(a), and a photograph of the interior of the tunnel room in Fig. 5(b). This plan shows the installation as it was in May, 1945, and the corresponding elevation is shown in Fig. 5(c). A sketch of the recently fitted return ducts is given in Fig. 5(d). The two largest tunnels alone, and only the main supply pipework are shown for clarity. A network of piping with a maximum operational pressure of 100 lb/sq in. supplied from the receivers through a reducing valve is not shown in full.

A battery of three intercooled three-stage reciprocating compressors situated in the Compressed Air Tunnel building may be used singly or in parallel to charge three compressed-air storage receivers at the rear of the High-Speed Tunnel Laboratory through a 4-in. diameter main. The compressors were manufactured by Messrs. Fullerton, Hodgart and Barclay and operate at a constant speed of 300 r.p.m. Each was designed to give a constant delivery of 1100 cu ft of free air per minute at all delivery pressures up to the maximum of 350 lb/sq in. gauge, with an isothermal efficiency of 80 per cent. Each compressor is driven by a Crompton-Parkinson auto-synchronous motor absorbing 400 horsepower at maximum compressor delivery pressure. The three storage receivers together have a total volume of 5,000 cu ft, and a maximum storage pressure of 350 lb/sq in. gauge. The Compressed Air Tunnel has a volume of 10,000 cu ft at the same maximum storage pressure.

The compressors take in air at the ambient atmospheric conditions, and, the atmospheric humidity at Teddington being seldom below 50 per cent, and the compression sensibly isothermal, a considerable amount of condensation occurs in the compressed-air storage receivers. Pools of water collect in the bases of the receivers, and are periodically removed through drain cocks provided for this purpose.

The inducing-air supply for the tunnels is drawn from the receivers through 6-in. diameter mains discharging into a pipe whose diameter expands from 6 in. at the first receiver to 9 in. downstream of the third receiver. The flow of inducing air from this pipe to the two largest tunnels is regulated by throttle valves of the gate type and smaller by-pass valves. The larger throttle valves are of 6-in diameter, the pipes leading from the 12-in. diameter main to the two tunnels being of this size. Valves arranged in the pipework between compressors and receivers, and receivers and the supply main to the tunnels enable any of the receivers to be isolated. Provision is also made to supply the high-speed tunnels from the C.A.T. when this is available as a storage reservoir.

Apart from the two larger tunnels shown, there are (at May, 1945) three smaller tunnels situated in the tunnel room devoted to specialised research work. These are supplied with inducing air from the storage receivers, two of them through a reducing valve designed to limit the maximum inducing-air pressure to 100 lb/sq in. gauge.

A $5\frac{1}{2}$ -horse power 'Broomwade' rotary vacuum pump situated in the tunnel room may be used to evacuate a suction receiver of 200 cu ft volume or one of the three larger storage receivers. Suction mains are situated near to both of the largest tunnels.

1.5.1. *The 1-ft Diameter Tunnel.*—The 1-ft diameter tunnel in its present form is sketched in Fig. 6(a), and photographs of the tunnel in its original and present forms are shown in Fig. 6(b). It is mounted with its axis vertical and draws air from the intake chamber beneath the tunnel room floor and discharges it through the roof. The portion of the tunnel upstream of the injector slot is made up in cylindrical sections which mate into each other and into the tunnel intake and pressure chamber. These sections may be removed by lowering the tunnel intake on four supporting screws, and replaced by other sections to give differing tunnel characteristics. In this manner one of a number of effusers may be inserted upstream of the working section to enable a supersonic velocity to be obtained there, and the balance shown in position in Fig. 6(a) may be replaced by a cylindrical section of 'Perspex' to permit flow visualization.

The injector slot (Fig. 7) is annular, and of constant width (0.105 in.) round the tunnel periphery. The mixing chamber and diffuser is a cone of $6\frac{1}{4}$ deg full angle and exit area-expansion ratio (based on working-section area) $7\frac{1}{2}$, the divergence being continuous from injector slot to diffuser exit. The injector design is such that the inducing air is injected in a direction parallel to the axis of the tunnel. The inducing-air supply is led into the pressure chamber through a single radial pipe, and radial perforated baffles are arranged in the pressure chamber in an attempt to ensure a uniform flow from the injector slot.

The original intake was surrounded by a hexagon of 100-mesh gauze, and had six straightening vanes parallel to the tunnel axis arranged radially in the intake at 60 deg intervals to remove any large-scale swirl. Recently a new intake has been fitted, and this is shown in Fig. 6(c). The bottom of the intake is solid so that the whole of the induced air enters the intake space in a radial direction before turning through a right-angle and passing into the tunnel contraction. The contraction was not designed by a theoretical method but on the basis of experimental experience, the contraction ratio of the metal flare being 16:1.

The aerofoil models tested in the tunnel are normally of 2-in. chord and completely span the tunnel. Apart from the balance shown in the sketch (*see Part II*²⁵) provision is made for the measurement of profile drag by total-head traverse of the aerofoil wake. Tests have also been made on three-dimensional bodies supported on the axis of the tunnel. In these tests successful force measurements have been made by the use of electrical strain gauges of the resistance type.²⁵ With aerofoils of moderate thickness at zero incidence subsonic tests at Mach numbers up to about 0.85 may be made, and effusers for supersonic operation at Mach numbers of 1.2, 1.4 and 1.6 are available.

The possible duration of the tunnel run before the storage receivers are exhausted depends on the nature of the model and the Mach number of the test, but it is of the order of from 2 to 3 minutes at the highest test Mach numbers. This period is found to be adequate for the necessary experimental observations.

1.5.2. *The 20 × 8-in. Rectangular Tunnel.*—The 20 × 8-in. tunnel is sketched in Fig. 8(a) and also shown in Figs. 8(b) and 8(c); the general arrangement is similar to that of the 1-ft diameter tunnel. Upstream of the injector slot the walls on the two shorter sides of the tunnel are of 0.020 in. spring steel and may be adjusted by a number of micrometers²³. The tunnel is intended primarily for the testing of aerofoil models at subsonic speeds. The models completely span the tunnel between the two larger sides and are normally of 5-in. chord. They are mounted at the centres of turntables which may be rotated to vary the incidence and have glass walls which enable the flow to be observed optically.

At the downstream end of the adjustable tunnel walls there is an adjustable throat which may be closed until the velocity in this region becomes equal to the critical sonic velocity²⁵. This method may be used to regulate the tunnel speed and achieve steadier conditions at the working

section. Static-pressure holes in the flexible walls at each micrometer, and in the region of the flexible throat, enable the walls to be set to the pressure distributions corresponding to minimum model interference²⁵. There are 17 micrometers on each side of the tunnel, the spacing being $1\frac{1}{2}$ in. in the region of the model and 3 in. elsewhere. The adjustable throat has two adjusting screws on each side of the tunnel.

There is no balance, and the forces experienced by the model are deduced either from explorations in the model wake, or by pressure-plotting observations at the model surface.

The pressure chamber completely encircles the tunnel, and the injector slot, Fig. 7, is continuous round the four walls and is 0.067 in. wide. The injection of inducing air is parallel to the tunnel axis and there are two inducing-air entries to the pressure chamber arranged at the centres of the two longer sides. The mixing region and diffuser is of rectangular cross-section and diverges continually from the injector slot to diffuser exit. The area-expansion ratio of the diffuser at exit (based on working-section area) is 7, and the equivalent conical angle of expansion (based on rate of area increase) is 8 deg.

By use of the adjustable walls, models may normally be tested up to Mach numbers of from 0.85 to 0.90 and the running time at top speed is adequate for all but the longest experimental observations (about 4 minutes at the highest speed).

1.5.3. *The 5 × 2-in. Tunnel.*—This tunnel was originally situated in the Engineering Division N.P.L.⁴⁶ but was moved to the Aerodynamics Division in 1942. The tunnel in its present form is shown in Fig. 9 and it was used to make the original experimental investigations leading to the design of the 20 × 8-in. tunnel. It may be fitted either with adjustable walls on the two shorter sides for subsonic operation, or rigid effuser liners for supersonic operation. Glass plates may be placed on the two longer sides for flow visualization.

The tunnel has been used in the Aerodynamics Division for experiments in connection with the use of boundary-layer suction on an aerofoil at high subsonic speeds⁴⁷, and for pressure plotting and flow photography⁴⁸ on wedge sections at a supersonic Mach number (1.4).

1.6. *The Advantages of the Induction Principle.*—The original adoption of the induction principle for the high-speed wind tunnels in the Aerodynamics Division of the N.P.L. must to some extent be attributed to the existence of the compressed-air supply which was available from the compressor installation and storage capacity of the Compressed Air Tunnel. There are, however, certain advantages inherent in this type of tunnel which make it very suitable for use at the N.P.L. It should, perhaps, be stated at this stage that many of these advantages are of an economic rather than a technical nature.

The power required to operate a high-speed tunnel of moderate size is large, and it is possible that the available power supply may be inadequate. Moreover, the power requirements are of an intermittent nature and may be unsuitable for the supply system (which may be the electricity grid). By the use of the induction principle with receivers to store energy in the form of compressed air (or any system involving the direct discharge of compressed air, or discharge into an evacuated reservoir), the power requirements may be reduced to a low continuous load. The induction principle is more favourable at Mach number below about 1.5 than a system involving the direct discharge of compressed air from storage since, by suitable design, it is possible to obtain mass ratios considerably greater than unity in the former case. In tunnels of the latter type, moreover, it may prove difficult to maintain a constant total head and stagnation temperature in the working section of the tunnel as the storage receiver pressure and temperature fall during the tunnel run. The storage of energy by evacuation is not economical in the initial cost of the installation since, if the tunnel is of appreciable size and the required duration of run long, the necessary volume of the evacuated receiver may become very large.

It may, however, prove necessary to adopt one of these two direct-action systems if high supersonic Mach numbers (> 2.0) are required in the working section of the tunnel, since there is some evidence at least in the case of a single-stage injector of the type now used that the

induction principle is unable to maintain the pressure ratios required for operation at these Mach numbers. If this becomes necessary, an adequate supply of compressed air is already available for a direct blow-off tunnel in the storage receivers used at present for induction drive.

By a sufficiently rapid expansion of the stored air, extremely high powers may be obtained, and the installation is, therefore, very flexible. For example, the 1-ft diameter tunnel, which was originally intended for use for subsonic tests, has recently been operated extensively at supersonic Mach numbers without the provision of any additional equipment other than a supersonic effuser section, although the power requirements are considerably increased.

In an induction-type installation, the tunnels may be of a comparatively simple nature, and the major fraction of the total initial cost of the installation lies in the compressor and storage receivers. When a central set of compressors and storage receivers has been installed, an indefinite number of tunnels may be constructed at relatively low cost without separate power plants, and by a suitable arrangement, the whole of the available storage capacity may be made available to any tunnel. This has, in fact, been done at the N.P.L. where first the 20×8 -in. tunnel and then three smaller tunnels were constructed to operate from the original storage receiver of the 1-ft tunnel, and where it is proposed to construct the 18×14 -in. tunnel⁴⁹.

The induction system has a considerable advantage over a system involving the use of compressors in the tunnel circuit in that tunnels operating on the former system require no elaborate cooling apparatus since the compressed air may either be cooled as it leaves the compressor (the rate of flow being small), or allowed to cool in the storage reservoirs. In a continuously operated direct-action tunnel the cooling apparatus may be of a complicated nature (*e.g.*, the Royal Aircraft Establishment High-Speed Wind Tunnel⁵⁰), although a relatively simple system of air exchange has been used with some success in certain high-speed tunnels (*e.g.*, 2.7 m at D.V.L.)⁵¹. It should be pointed out, however, that the fall of stagnation temperature observed in the N.P.L. return-flow induction type tunnels (and which is inevitable with tunnels of this type) will aggravate difficulties associated with the condensation of water vapour in the working section, and it has been suggested that electrical heaters be installed in these tunnels.

The compression of the inducing air for storage has proved an extremely convenient method of drying the air used in the tunnel circuits at the N.P.L.

It is doubtful if the efficiency of a tunnel of the induced-flow type on a continuous basis (without storage) can be as great as that of a tunnel driven by a fan or internal compressor. It would, therefore, seem that if continuous or semi-continuous operation is required a fan-driven tunnel will be used in preference to an induced-flow tunnel. In Fig. 10, the energy ratios (*see* section 1.8.1) of the existing N.P.L. tunnels expressed on the assumption of continuous operation (without storage) are compared with those of the R.A.E. and D.V.L. fan-driven tunnels. The curve for the $2\frac{1}{4}$ -in. tunnel may be compared with those of the fan-driven tunnels since the former tunnel was designed to operate efficiently continuously (*i.e.*, without storage) although the assumption of isothermal compression may be questionable in this case. Since, however, the 1-ft diameter and 20×8 -in. tunnels were designed to operate intermittently, a comparison between the energy ratios of these tunnels expressed on the basis of continuous operation (without storage) with those of the fan-driven tunnels may be misleading. This matter is further discussed in section 1.8.3. It appears that the highest efficiencies which have so far been obtained with an induction-type tunnel (*see* curve for the $2\frac{1}{4}$ -in. tunnel) are at subsonic speeds comparable with those of the R.A.E. tunnel. A comparison of the efficiency of the latter with that of the D.V.L. tunnel indicates, however, that the R.A.E. tunnel may be rather an inefficient example of a fan-driven, high-speed tunnel.

The flexibility and simplicity of the induction system which makes it very suitable for research work of a fundamental nature, and the limited nature of the available power supply have led to the choice of the induction system in the proposals for new high-speed wind tunnels in the Aerodynamics Division of the N.P.L. It is proposed, however, to consider the design of some form of direct-action supersonic tunnel for the Aerodynamics Division even though a model induction-type tunnel has succeeded in reaching a Mach number of 2.0 (very inefficiently).

1.7. *Variation of Stagnation Temperature in a Closed-Circuit Tunnel.*—If the stagnation temperatures of the induced and inducing airstreams differ, and are represented by T_H and T_A respectively, it is clear that in the simplest case of an open-circuit tunnel, the stagnation temperature T_B of the airstream after mixing will be given by:

$$C_p T_A + m C_p T_H = (m + 1) C_p T_B \quad \dots \quad (1)$$

$$\text{or } T_B = \frac{T_A + m T_H}{m + 1} \quad \dots \quad (2)$$

where m is the mass ratio.

In the case of a closed (return)-circuit tunnel, it may be assumed that the stagnation temperature of the induced air at the working section is equal to that of the induced and inducing airstreams after mixing, and it is necessary to express equation (2) in differential form obtaining an equation for the rate of fall of stagnation temperature at the tunnel intake in terms of the stagnation temperature of the inducing airstream, the rate of supply of inducing air, and the volume of the tunnel circuit.

If it is assumed that there is no change of the stagnation temperature of the inducing air at the throttle valve, and therefore, that the stagnation temperature of the inducing air is equal to the temperature of the air in the storage receivers, it is possible, by assuming some arbitrary equation for the mode of expansion from the storage receivers, to obtain an expression for the rate of change of receiver temperature (and therefore inducing-air stagnation temperature) in terms of the initial storage conditions and the rate of discharge to the tunnel. It is thus possible to express the rate of change of stagnation temperature at the tunnel intake in terms of the dimensions of the installation, the initial storage conditions, and the rate of discharge of inducing air to the tunnel, it being assumed that there is no heat transfer through the tunnel walls.

Since no attempt is made to conserve any internal (*i.e.*, heat) energy acquired by the inducing air in compression before storage, the most efficient compression cycle is the isothermal. This is approximately achieved at the N.P.L. by the use of three-stage intercooled compressors. Thus the temperature of the stored air before a tunnel run will be approximately equal to that of the atmosphere. During the tunnel run the receiver temperature will, in general, fall because of the rapid expansion of the stored air. Thus, in general, the stagnation temperature at the intake of a closed-circuit tunnel of the induction type will also fall during a tunnel run from a value equal to that of the atmosphere at the beginning of the run. It is clear that this fall of temperature is basically due to the extraction of heat from the air during compression by the compressor inter and after coolers. In fact, an installation of the type used at the N.P.L. incorporates inherently the simplest possible type of air refrigerator in the isothermal—quasi adiabatic compression—expansion cycle of the inducing air.

The fall of stagnation temperature predicted by the above argument is observed in the 1-ft diameter and 20 × 8-in. tunnels now that they have been fitted with return ducts. The observed temperature fall is less than that calculated on the above assumptions, since the tunnel structure has a considerable thermal capacity, and heat transfer occurs through the thin metal walls of the return circuit and elsewhere in the tunnel circuit. A typical example of the observed fall of stagnation temperature is shown in Fig. 11.

1.8. *The Efficiency of Induction-Type Tunnels.*—

Notation:

Suffix	0	atmospheric conditions.
	w	working-section conditions.
	s	conditions at injector slot.
	i	receiver conditions at the beginning of a tunnel run.
	t	receiver conditions after running time t .

Symbols	A	cross-sectional area.
	P	blowing pressure (defined below).
	p	pressure.
	ρ	density.
	a	velocity of sound.
	M	Mach number.
	m	mass ratio (defined below).

It is convenient to express measurements of the efficiency of induction-type tunnels in terms of the following variables:

- (a) The blowing pressure, defined as the total head of the inducing air in the tunnel pressure chamber.
- (b) The mass ratio, defined as the ratio of the rate of mass flow of induced air to that of inducing air.

It has been shown that the discharge coefficient of injector slots of the type used at the N.P.L. is closely equal to unity. Thus, if the ratio of the blowing pressure to the static pressure in the tunnel downstream of the injector slot exceeds a value of about 2, the discharge from the slot may be calculated to a fair degree of accuracy on the assumption that the velocity of the inducing air at the section of minimum cross-sectional area of the slot (normally the slot exit) is equal to the critical sonic velocity, and that the acceleration from rest in the pressure chamber up to this velocity is isentropic.

If this assumption is made and it is further assumed that the stagnation temperatures of the induced and inducing airstreams are equal and that the total head of the induced air is atmospheric, the mass ratio may be written ($\gamma = 1.40$):

$$m = 1.728M \left(\frac{5}{5 + M^2} \right)^3 \frac{p_0 A_w}{P A_s} \quad \dots \quad (3)$$

Most of the following equations may, therefore, be expressed in terms of the blowing pressure and tunnel geometry. The mass ratio has, however, been retained, since it gives simple expressions, and the rate of supply of inducing air was normally measured in the experimental work in addition to the blowing pressure.

1.8.1. *Energy Ratio*.—The definition of the energy ratio depends on the cycle followed by the inducing air before entering the pressure chamber of the tunnel.

It is useful to consider two different types of operation—

- (a) The compressor is connected directly to the pressure chamber of the tunnel so that the compressor delivery pressure is equal to the blowing pressure, and the rate of mass delivery equal to the rate of mass flow of the inducing air.
- (b) The compressor is used to charge storage reservoirs before the tunnel is run, and the energy so stored is then used to drive the tunnel. The power supplied to the tunnel may, in this case, be less or greater than the compressor power depending on the rate at which the stored energy is used.

In case (1) the energy ratio may, on the assumption of isothermal compression*, be defined as the ratio of the rate of flow of kinetic energy at the working section of the tunnel to the power required to compress the inducing air isothermally from atmospheric conditions to the blowing pressure.

* In many cases it may be more realistic to assume adiabatic compression followed by cooling to the initial temperature. At the N.P.L., however, isothermal compression is achieved approximately for storage purposes (the rate of delivery being low) by using multi-stage intercooled compressors and it has, therefore, been customary to base the energy ratio on a compression cycle of this type.

In case (b) the energy ratio must be defined, in common with that of all intermittent tunnels, as the ratio of the rate of flow of kinetic energy at the working section multiplied by the maximum time for which it is possible to run the tunnel (with the required working-section conditions) to the energy required by the compressor to charge the storage receiver⁵². Thus, in case (b) the energy ratio will, for constant initial receiver and working-section conditions, be proportional to the maximum possible duration of a tunnel run on one receiver charge.

The value of this latter quantity will depend on the method which is used to regulate the supply of inducing air to the tunnel. Such regulation will be necessary if constant working-section conditions are to be maintained, since the receiver pressure will fall continuously during a tunnel run. Under case (b), therefore, it is necessary to consider two alternative methods of regulation⁵²:

- (a.I) The pressure chamber is connected to the storage receiver through a throttle valve which is progressively opened, as the tunnel run proceeds and the storage pressure falls, to maintain a constant blowing pressure. In this case the injector slot area will be constant, and the tunnel run will end when the storage pressure becomes equal to the required blowing pressure.
- (a.II) The pressure chamber is connected directly to the storage receiver so that the storage and blowing pressures are equal. The area of the injector slot is then progressively increased as the tunnel run proceeds and the blowing pressure falls. By this method it should be possible to maintain constant working section conditions throughout the tunnel run.

The latter method of regulation is possible since it has been found that a tunnel of this type may be operated over a wide range of blowing pressure by an adjustment of the area of the injector slot^{52, 53}. A typical family of curves showing the variation of blowing pressure with injector slot area for a range of working-section Mach numbers is plotted in Fig. 36.

The two alternative methods of operation (a) and (b) will be referred to as continuous operation and operation from storage respectively. The two alternative methods of regulation (a.I) and (a.II) will be referred to as valve and variable-slot regulation.

1.8.2. *Energy Ratio for Continuous Operation.*—This quantity, defined in the previous paragraph, may be written:

$$\begin{aligned}
 (\text{E.R.})_1 &= \frac{\frac{1}{2}\rho_w V_w^3 A_w}{\frac{\rho_w V_w A_w \dot{p}_0}{m} \log_e \frac{P}{\dot{p}_0}} \quad \dots \quad \dots \quad \dots \quad \dots \quad \dots \quad \dots \quad (4) \\
 &= \frac{\frac{1}{2}m V_w^2}{\dot{p}_0 \log_e \frac{P}{\dot{p}_0}}.
 \end{aligned}$$

If the temperature at the tunnel intake is atmospheric this expression may be written:

$$(\text{E.R.})_1 = \frac{3.5mM^2}{(5 + M^2) \left(\log_e \frac{P}{\dot{p}_0} \right)} \quad \dots \quad \dots \quad \dots \quad \dots \quad \dots \quad (5)$$

1.8.3. *Energy Ratio for Operation from Storage.*—Since for given working section and initial receiver conditions this quantity is proportional to the time for which it is possible to operate the tunnel on the receiver charge of compressed air, it is convenient to calculate the magnitude of this

time first. Thus if, in tunnel running time, dt , the receiver pressure falls from p to $(p - dp)$, and the temperature from T to $(T - dT)$ and it is assumed that the rate of mass flow of inducing air to the tunnel is constant over the time element considered,

$$Q dt = V \frac{\rho_0 T_0}{p_0} \left(\frac{p}{T} - \frac{p - dp}{T - dT} \right). \quad \dots \quad \dots \quad \dots \quad \dots \quad \dots \quad \dots \quad \dots \quad (6)$$

Neglecting second-order terms, this may be written

$$QT^2 dt = V \frac{\rho_0 T_0}{p_0} (T dp - p dT). \quad \dots \quad \dots \quad \dots \quad \dots \quad \dots \quad \dots \quad \dots \quad (7)$$

If the expansion from the receiver is assumed to follow the arbitrary polytropic equation $p/\rho^n = \text{constant}$ and to start from conditions suffix 1, then:

$$T = T_1 \left(\frac{p}{p_1} \right)^{(n-1)/n} \quad \dots \quad \dots \quad \dots \quad \dots \quad \dots \quad \dots \quad \dots \quad (8)$$

$$dT = \frac{n-1}{n} \frac{T_1}{p_1} \left(\frac{p_1}{p} \right)^{1/n} dp \quad \dots \quad \dots \quad \dots \quad \dots \quad \dots \quad \dots \quad \dots \quad (9)$$

inserting (8) and (9) in (7) and assuming that the initial temperature of the stored air T_L is equal to the atmospheric temperature T_0

$$Q dt = V \frac{\rho_0}{p_0} \frac{1}{n} \left(\frac{p_1}{p} \right)^{(n-1)/n} dp \quad \dots \quad \dots \quad \dots \quad \dots \quad \dots \quad \dots \quad \dots \quad (10)$$

or, in terms of the mass ratio and working-section conditions

$$dt = \frac{Vm(5 + M^2)^3}{125p_0 a_0 M A_w n} \left(\frac{p_1}{p} \right)^{(n-1)/n} dp. \quad \dots \quad \dots \quad \dots \quad \dots \quad \dots \quad \dots \quad \dots \quad (11)$$

If valve regulation is used, the mass ratio and blowing pressure will be constant and equation (11) may be integrated between conditions suffix 1 and t to give

$$t = \frac{Vm(5 + M^2)^3}{125p_0 a_0 M A_w} \left\{ p_1 - p_t \left(\frac{p_1}{p_t} \right)^{(n-1)/n} \right\}. \quad \dots \quad \dots \quad \dots \quad \dots \quad \dots \quad \dots \quad \dots \quad (12)$$

If this type of regulation is used, the maximum duration of a tunnel run may be found by inserting the value of the blowing pressure for p_t in equation (12) and using the corresponding value of the mass ratio m . If variable-slot regulation is used, equation (11) may be integrated numerically to estimate the possible duration of a tunnel run.

1.8.4. *Energy required to charge Storage Receivers.*—Since no attempt is made to conserve any internal energy acquired by the inducing air in compression, the most efficient compression cycle is the isothermal.

The work done by the compressor in charging the receiver may be divided into two parts: one representing the work done on the air passing through the machine, and the other the work done on the air already in the receiver by compressing it as the new air is added. If p_A is the pressure at the intake of the compressor and p_0 and p are the initial and final pressures in the receiver the first quantity of work W_1 is given by

$$W_1 = V \left[p \log_e \frac{p}{p_A} - p_0 \log_e \frac{p_0}{p_A} - (p - p_0) \right], \quad \dots \quad \dots \quad \dots \quad \dots \quad \dots \quad \dots \quad \dots \quad (13)$$

and the second quantity W_2 by

$$W_2 = V(p - p_0). \quad \dots \quad \dots \quad \dots \quad \dots \quad \dots \quad \dots \quad \dots \quad (14)$$

The total quantity W is therefore given by the equation

$$W = V \left(p \log_e \frac{p}{p_A} - p_0 \log_e \frac{p_0}{p_A} \right), \quad \dots \quad (15)$$

which reduces to

$$W = V p \log_e \frac{p}{p_A} \quad \dots \quad (16)$$

if the initial pressure in the receiver is equal to the (constant) pressure at the intake to the compressor.

The equations of this and the previous section enable the value of the energy ratio for operation from storage (E.R.)₂ to be calculated.

1.8.5. *Variation of Energy Ratio with Tunnel Stagnation Pressure.*—If the tunnel stagnation pressure is varied, the blowing pressure will be proportional to the tunnel stagnation pressure, and the mass ratio will not vary.

Thus, for continuous operation

$$(E.R.)_1 \propto \frac{1}{\log_e \frac{P}{p_0}} \quad \dots \quad (17)$$

It is here assumed that the compressor-intake pressure remains constant with variation of the stagnation pressure. If the compressor intake is coupled to the tunnel bleed-off there will be no change of energy ratio with change of stagnation pressure. With constant compressor-intake conditions, however, there will, in general, be a change of energy ratio, as the stagnation pressure is varied. If the stagnation pressure is increased from atmospheric pressure to a pressure λ times the atmospheric pressure the energy ratios will be related by the expression

$$\frac{(E.R.)_{1\lambda}}{(E.R.)_1} = \frac{\log_e \frac{P}{p_0}}{\log_e \frac{\lambda P}{p_0}} \quad \dots \quad (18)$$

If the stagnation pressure is to be below one atmosphere, power will be required to maintain this low pressure, and the energy ratio will be equal to that at one atmosphere.

1.9. *The Influence of the Tunnel Design on the Efficiency.*—If the blowing pressure is known as a function of working-section Mach number and tunnel geometry, it is possible to predict, by methods similar to those outlined in the previous paragraphs, the complete performance characteristics of the tunnel. If certain assumptions concerning the mixing and diffuser efficiencies are made, it is possible to calculate the blowing pressure by methods similar to those used by Crocco⁵⁴. The validity of some of these assumptions is, however, rather uncertain, and it is perhaps better to measure the blowing pressure experimentally. This has been done on the two larger N.P.L. tunnels⁵⁷, but since it is not possible to vary the geometry of these tunnels, the influence of such variations on the efficiency cannot be investigated. A model tunnel^{55, 56, 57} with a working section of 2½-in. diameter was, therefore, constructed in 1944 to enable the influence of the tunnel geometry on the efficiency characteristics to be determined experimentally.

The following parameters could be varied:—

- (a) Injector slot area.
- (b) Angle of injection (defined below).
- (c) Diffuser Angle.
- (d) Diffuser exit area.
- (e) Width of injector slot around the periphery of the tunnel.

Provision was also made for operation over a range of subsonic and supersonic Mach numbers, variation of the working-section length, the insertion of a model into the working section and the use of injector slots of convergent-divergent shape.

The tunnel is sketched in Fig. 12(a) and shown in Fig. 12(b). For the greater part of the work described here it was of the open-circuit type illustrated, but towards the end of this work a return circuit was constructed. The return-circuit tunnel is shown in Figs. 13(a) and 13(b).

The rate of mass flow of inducing air to the tunnel was measured by an orifice plate inserted in the inducing-air supply pipe, and that of induced air deduced from measurements of the static pressure at the wall of the working section and of the total head at the tunnel intake. The blowing pressure was measured as the stagnation pressure of the air in the pressure chamber of the tunnel.

Because of the difficulty of separating the influence of variations of the tunnel design on the efficiency of the various processes involved (mixing, diffusion, etc.) the results of the experimental work have been expressed in terms of variations of the overall efficiency of the tunnel. Some attempts have been made to analyse the experimental observations further, but these are at present incomplete and are not described here.

1.9.1. *Effect of Asymmetry of Injection.*—The inlets of the inducing-air supply to the pressure chambers of the 1-ft and 2¼-in. diameter tunnels are asymmetrical, consisting of single radial pipes. A number of radial baffles are placed inside the pressure chamber of the former tunnel in an attempt to compensate for this, but these have not been found wholly satisfactory. Fig. 14 shows the distribution of velocity across the exit of the diffuser of the 1-ft tunnel when the working-section Mach number is 1.4. The greater part of the flow takes place in the region of the cross-section diametrically opposite the inlet to the pressure chamber, and, the velocity distribution across the working section being sensibly constant, this must be due to asymmetry of injection. On the 2¼-in. tunnel compensation for the asymmetry of inlet to the pressure chamber may be effected by a lateral displacement of the nozzle. This has the effect of narrowing the slot in the region diametrically opposite to, and widening the slot adjacent to, the inlet. The effect of such compensation on the velocity distribution at the diffuser exit is shown in Fig. 15 and produces a velocity distribution which is symmetrical about the tunnel centre-line. The peaks in the velocity distributions shown are due to incomplete mixing of the induced and inducing air and are discussed in a subsequent section. The effect of asymmetry of injection on the energy ratio of the tunnel is shown in Fig. 16, from which it is clear that the efficiency is a maximum when the injection becomes symmetrical. In the whole of the experimental work carried out on the model tunnel described here compensation for asymmetry of entry into the pressure chamber has been made unless a statement to the contrary is given.

A second model tunnel, shown in Fig. 17, was constructed in 1946 with a symmetrical system of four inducing-air supply pipes. It was found that the values of the efficiency characteristics measured with this tunnel were in agreement with those measured on the original tunnel compensated for asymmetry of entry.

1.9.2. *The Influence of the Diffuser Design.*—In general, it appears that the major problem of the design of high-speed wind tunnels from the aspect of power economy lies in the design of an efficient diffuser. For subsonic tunnels of the direct-action type it appears that a simple divergent diffuser^{58, 59} of equivalent conical angle below about 5 deg may give a high efficiency provided that the expansion ratio at exit (or at the first cascade in a closed-circuit tunnel) is adequate. In the case of a supersonic tunnel, diffusion to a subsonic velocity³⁸ must be effected upstream of the subsonic diffuser which may then be of similar design to that used in a subsonic tunnel. At low supersonic Mach numbers it seems that it is impossible to obtain a supersonic diffuser with a greater efficiency than that of a normal shock-wave, but at high Mach numbers losses due both to the gain of entropy through the shock and phenomena occurring in the region of the interaction of the shock-wave and the boundary layer of the tunnel walls are considerable. Much work has, therefore, been done upon the design of efficient supersonic diffusers both in connection with wind-tunnel design, and the construction of entries to supersonic propulsive units (*e.g.*, the ram jet or athodyd). In this connection the design of oblique shock-wave (Oswatitach) diffusers³⁸ is noteworthy.

It has already been stated that in the N.P.L. induction-type tunnels no attempt is made to use any form of supersonic diffuser other than a normal shock-wave. Thus, it is only the influence of the subsonic diffuser downstream of the injector slot which has been investigated. In the present tunnels the channel downstream of the injector slot also serves as a mixing zone in which mixing of the induced and inducing airstreams takes place. It is very difficult in experimental work, therefore, to separate the influence of changes of the geometry downstream of the injector slot into its influence on the efficiencies of mixing and diffusion. This is particularly so, since in many cases mixing is not complete at the downstream end of the diffuser even if the area ratio (based on working-section area) at this region is as much as 18 to 1. The model tunnel was, for a large part of the experimental work, fitted with a mixing zone of constant area⁶⁰ for about one diameter downstream of the injector slot before the expanding region of the diffuser commenced. The presence of this constant area region was found to lead to an improvement of efficiency over a tunnel fitted with a diffuser expanding directly from the injector slot. This is illustrated in Fig. 18. An attempt to produce further improvement of efficiency by a variation of the length of the constant area region (between the limits $\frac{1}{2}$ to $1\frac{1}{2}$ working-section diameters) was unsuccessful. The design of the tunnel did not permit the use of a greater range of lengths.

In the description which follows, the first diameter of the channel downstream of the injector slot was of constant cross-sectional area blending into a conical divergent region of 4 deg whole angle. Downstream of this region the diffuser angle could be varied by the addition of separate wooden diffusers of either 4 deg, 8 deg or 12 deg whole angle. A faired transition piece $1\frac{1}{2}$ diameters long was inserted upstream of the wooden cone when its angle differed from 4 deg. The lengths of the wooden diffusers could be varied to give a range of area ratios at diffuser exit. With diffusers of this type it was found that, with a high subsonic Mach number (0.9) at the working section, variation of the angle of the wooden diffuser between 4 deg and 12 deg had little influence, at constant exit area ratio, on the efficiency characteristics of the tunnel. This is illustrated by Figs. 19, 20, 21, where the blowing pressure, mass ratio and energy ratio (for continuous operation) are plotted as functions of injector-slot width for a number of different diffusers. It may be seen that the points for the three separate diffusers of the same exit area ratio lie closely on a single curve. The same three efficiency variables are plotted as functions of the exit area ratio of the diffuser at a number of injector-slot widths in Fig. 22.

Similar curves for a supersonic working-section Mach number (1.4) are given in Figs. 23, 24, 25, 26. It may be seen that the diffuser angle now has a considerable influence on the efficiency characteristics, and that the 4 deg diffuser is most efficient. The 12 deg diffuser will not permit the required working-section Mach number to be reached at all over the larger part of the range of injector-slot widths.

It should be noted that the relative merits of the different diffusers are substantially independent of the injector-slot width so that it is not necessary to vary the diffuser design if the slot width is changed.

1.9.3. The Influence of the Injector-Slot Width and Angle of Injection.—Considering any curve for a constant diffuser geometry in Figs. 19, 20, 21, 23, 24, 25, it may be seen that as the injector slot is widened the blowing pressure and mass ratio fall and the energy ratio for continuous operation rises. This is more clearly illustrated by Figs. 27, 28, in which the distinct curves apply to different angles of injection⁵³, θ , defined as the angle which the inducing airstream immersing from the injector slot subtends with the tunnel axis (Fig. 4(b)). It may be seen that the greatest efficiency is attained by the use of zero angle of injection. It was not possible over the greater part of the range of slot width to achieve a supersonic Mach number of 1.37 at an angle of injection of 25 deg.

1.9.4. The Use of an Injector of Convergent-Divergent Section.—An attempt has been made⁵³ to obtain improvements of efficiency by the use of an injector slot of convergent-divergent section to reduce the pressure of the inducing airstream to that of the induced airstream before the two streams meet. This has, however, not proved successful, but there is evidence that this failure may be due to a breakaway at the section of minimum area of the slot.

1.9.5. *Comparison Between Efficiencies of Model and Larger Tunnels.*—The 2¼-in. diameter tunnel was modified to a scale model of the 1-ft diameter tunnel (scale 1/5.3). Values of the three efficiency variables for the two tunnels are plotted as functions of the working-section Mach number in Fig. 29. From this figure it may be seen that the agreement is satisfactory, the larger tunnel being slightly superior. The efficiencies of the 2¼-in. diameter and 20 × 8-in. tunnels are compared in Fig. 29 at equal values of the ratio of the injector-slot area to the working-section area and equivalent diffuser angles and exit area ratios. The agreement between the efficiencies of the two tunnels is surprisingly good.

From these comparisons it may be concluded that apart from indicating the most efficient form of the tunnel design, the model results may be expected to give a fairly reliable quantitative prediction of the efficiency of a proposed larger tunnel.

1.9.6. *The Influence of a Model in the Working Section.*—The results given in the previous sections apply to an empty working section. If the extra power required to operate the tunnel when a model is placed in the working section is that required to overcome the drag of the model in an unlimited flow then:

$$\text{Additional Power} = \frac{1}{2}\rho V^3 S C_D, \quad \dots \dots \dots (19)$$

where C_D is the drag coefficient of the model and S the area on which it is based. It has been found^{56, 53, 61} that, in wind tunnels of the induction type, the additional power is between ten and twenty times as great as that predicted by equation (19) at both supersonic and high subsonic Mach numbers. This large additional power requirement is due mainly to an increase of the losses downstream of the injector slot connected with the increase of blowing pressure required to supply the additional power required when the model is present. The increase of power required to maintain the flow when the model is present is compared with that calculated by equation (19) in Fig. 30. This figure is based upon measurements made in the 2¼-in. tunnel; the drag coefficient of the subsonic aerofoil model being that measured in the 1-ft diameter tunnel, and that of the supersonic aerofoil being calculated by Ackeret's theory. Similar results are obtained in both the 1-ft diameter and 20 × 8-in. tunnels.

The results of a limited number of explorations on the tunnel axis downstream of the injector slot at a range of blowing pressures are shown in Fig. 33 and discussed in section 1.10. These results give some explanation of the increased losses in this region which arise from an increase of the blowing pressure above the value required to maintain the flow in the empty tunnel.

1.9.7. *Influence of the Return Duct on Efficiency.*—It is found that the return ducts which have been fitted to the two larger tunnels have very little influence on the efficiency, and that the return circuit which has been fitted to the 2¼-in. tunnel produces a slight improvement of efficiency over that of an open-circuit tunnel with an exit area ratio equal to that at the first corner of the return-flow tunnel.

1.10. *The Influence of the Injection on the Distribution of Velocity Along the Tunnel Axis.*—In a subsonic wind tunnel disturbances arising from the injection of inducing air may be propagated upstream, and influence the flow round a model placed in the working section. This effect may be eliminated* by the use of a choked throat at the downstream end of the working section. Such a throat is provided on the 20 × 8-in. tunnel, and observations at the working section have been made both with and without the throat present. It has been found that no changes of the pressure distribution or profile drag of the model are produced by the insertion of the throat.

Several accounts have been published of the influence of back pressure upon the flow in a Laval nozzle (corresponding to the effuser of a supersonic wind tunnel)^{63, 64}. It is found⁶² in a supersonic tunnel of the induction type that variations of the nature of the injection of inducing air influences the back pressure on the effuser with resultant changes of velocity distribution which are very similar to those described in these accounts. As the blowing pressure is increased, the velocity

* It is still possible for disturbances to be propagated upstream through the boundary layers of the tunnel walls.

at the working section increases until the velocity at the effuser throat become sensibly equal to the critical sonic speed. Further increase of blowing pressure then produces a region of supersonic velocity downstream of this point terminating in a shock-wave. As the blowing pressure is increased this tunnel shock-wave moves downstream until a position is reached beyond which further pressure increase causes the wave to recede upstream. Observations of the variation of tunnel shock-wave position and energy ratio (for direct operation) with changes of the blowing pressure made in the $2\frac{1}{4}$ -in. tunnel are shown in Fig. 31 at a number of injector-slot widths and angles of injection. It has been found in the model tunnel that, for working-section lengths of $1\frac{1}{2}$, $2\frac{1}{2}$ and 4 diameters, the tunnel shock-wave may be moved downstream to the injector slot if the angle of injection is zero. Increase of angle of injection results in an upstream movement of this most downstream position as shown in Fig. 32. These observations led to the assumption that the injection of inducing air tends to form a constriction to the flow of induced air downstream of the injector slot, the constriction being most severe (at constant slot width) when the angle of injection and blowing pressure are high.

This assumption is partly justified by the results of explorations along the axis of the tunnel in the neighbourhood of the injector slot. The results of such explorations in the $2\frac{1}{4}$ -in. and 12-in. diameter tunnels are shown in Fig. 33. These figures apply to constant injector-slot width and angle of injection, the blowing pressure alone being varied. The sharp drop of Mach number towards the left of the figures indicates the position of the tunnel shock-wave. It may be seen that as the blowing pressure is increased there is a tendency for the inducing air to be re-accelerated in passing through the constriction caused by the injection, and in some cases the flow on the tunnel axis may become supersonic again, the second régime of supersonic flow terminating in a second shock-wave. It has been indicated in section 1.9.6 that these figures give some explanation of the high apparent power absorption of a model placed at the working section; they also explain to some extent the high power absorption of a supersonic induction-type tunnel.

The influence of the injector slot width on the flow in the neighbourhood of the injector slot is also shown in Fig. 34. These observations were made in the $2\frac{1}{4}$ -in. tunnel with three working-section lengths. It appears that with the tunnel shock-wave in its most downstream position the constricting effect of the inducing airstream is most severe at intermediate slot widths. Since at very narrow slot widths the mass ratio is high, and little inducing air is injected, and at very wide slot widths the blowing pressure and inducing air density is low and, therefore, mixing occurs early, this result is, perhaps, not unexpected.

The curves of Fig. 34 also show that the working-section length (over the range tested) appears to have no effect on the most downstream position of the tunnel shock-wave which seems, rather, to occur at a fixed distance upstream of the injector slot.

1.11. *Use of the Model Results in the Design of Induction-Type Tunnels.*—The results of the experiments with the model tunnel indicate that it is possible to design a diffuser which is efficient over a range of injector-slot areas and working-section Mach numbers. Such a diffuser appears to consist of a cone of about 4 deg whole angle preceded by a short 'mixing zone' of constant cross-sectional area and about one working-section diameter long. In general, there is no great improvement of efficiency to be achieved by increasing the exit area ratio of the diffuser to a value in excess of about 8. At all injector-slot areas it seems that the angle of injection should be zero.

Considering a tunnel of this shape, therefore, it is possible to maintain the required working-section conditions with a range of injector slot areas, and, therefore, at a range of blowing pressures and mass ratios. The value of the injector-slot area selected will depend on the characteristics of the method which is adopted to supply and regulate the inducing air.

The variation of the energy ratio for continuous operation, with blowing pressure and working-section Mach number is shown in Fig. 35. The most efficient operation is achieved by the use of a wide injector slot and a low blowing pressure. The variation of mass ratio and blowing pressure with injector slot area is shown in Fig. 36. The use of a low blowing pressure involves, however, a large mass flow of inducing air, and this may present serious ducting problems.

Fig. 37 shows some examples of the calculated variation of the possible duration of a tunnel run from a storage receiver. The initial storage pressure has been taken as 350 lb/sq in. above atmospheric pressure, and the index of expansion from the receiver has been assumed to be 1.2 (*i.e.*, the expansion is assumed to follow the equation $p/\rho^n = \text{constant}$ where, $n = 1.2$). The figure shows the variation of running time for valve regulation with variations of the area of the injector slot (constant throughout a tunnel run), and it may be seen that the running time has a maximum value at a particular optimum injector-slot area. The occurrence of such an optimum value may be crudely explained by noting that as the injector-slot area is increased the blowing pressure (and therefore the value to which the receiver pressure may be lowered) falls, but at the same time the rate of consumption of inducing air rises (*i.e.*, the mass ratio falls). The variation of this optimum value of the injector-slot area with the working-section Mach number, the tunnel stagnation and the initial storage pressures, is shown in Figs. 38, 39, 40.

If regulation is by variation of the injector-slot area the variation of the running time with the value of the area to which the slot has been widened will be similar to that shown in Fig. 41. In general, it appears that a running time some 20–30 per cent in excess of that obtained with valve regulation at the optimum slot area may be obtained by this method of regulation. It may, therefore, be concluded that, if the tunnel is to be operated from storage over a range of working section and initial storage conditions, there is a strong case for the provision of an injector slot whose area may be varied. If possible, a continuous variation whilst the tunnel is in operation should be arranged, and such variation used to regulate the supply of inducing air.

There is some evidence that the efficiency measurements made on the model tunnel are not subject to serious scale effect (*see* section 1.9.5). Moreover, it appears that provided that the ratio of the injector-slot area to the working section area, and the equivalent angle and exit area ratio of the diffuser are similar, these measurements are not critical to changes of the cross-sectional shape of the tunnel (*see* section 1.9.5). Thus, as well as indicating the most efficient design of this type of tunnel, the measurements described may, in the absence of more reliable data, be used to predict quantitatively the performance of tunnels by the use of the simple equations derived in section 1.8.

Until the 18 × 14-in. tunnel (*see* below) has been constructed, there is no evidence that this procedure is reliable, but it is clear that methods similar to those described may be used to determine the most efficient method of operation of a particular tunnel from values of the blowing pressure and mass ratio measured on the new tunnel itself. Thus, if efficient operation is to be achieved, some time must be spent early in the life of the new tunnel in determining the variation of the efficiency characteristics with changes of the variable tunnel components (*e.g.*, injector-slot area, stagnation pressure).

1.12. *The Proposed New 18 × 14-in. Tunnel.*—It is proposed⁴⁹ to construct a new high-speed wind tunnel of the induction type in the Aerodynamics Division of the N.P.L. Owing to the present shortage of building materials and labour, this tunnel will be housed in the existing High-Speed Tunnel Laboratory (Fig. 5(a)), on the south side. The tunnel axis will be horizontal, and the flow in the working section in a direction away from the storage receivers. A sketch is given in Fig. 42; the tunnel is of the return-flow type, the return duct being above the roof of the building.

Compressed-Air Storage Capacity.—It is proposed to double* the existing storage capacity (now 5,000 cu ft) by the installation of three new receivers which will be placed above the three existing receivers at the rear of the tunnel room.

Tunnel Intake Contraction.—This has been designed by Cheers⁶⁵ on the basis of a method due to Goldstein. It will give the necessary contraction (16.1) in the shortest possible axial length compatible with a favourable pressure gradient at the walls. Measurements of wall pressures in a model contraction have indicated that the design is satisfactory over the range of speeds which are contemplated.

*The capacity has been trebled by the addition of two 5,000 cu ft receivers in addition to the three new receivers mentioned above. (August, 1949.)

Adjustable Walls.—The two shorter sides of the tunnel are to be adjustable with a range of movement adequate both for the reduction of tunnel interference at subsonic test speeds, and the formation of an effuser for supersonic operation. Since it is not known whether it will be possible to form a satisfactory supersonic effuser in this manner, provision is to be made for the easy removal of the adjustable walls which will then be replaced by rigid liners. The micrometer spacing will be 2 in. over the greater part of the length of the adjustable wall. It is hoped that these walls will enable an investigation to be made into the influence of a supersonic diffuser (*e.g.*, in the form of a second throat) at the downstream end of the working section on the performance of the tunnel.

Injector Slot.—The widths of the injector slots on the four sides of the tunnel are to be separately variable whilst the tunnel is not running and simultaneously variable whilst the tunnel is in operation. Thus, provision is made to compensate for any asymmetry of entry to the pressure chamber, and for regulation of the supply of inducing air by continuous variation of the injector-slot width. The limits of the injector-slot width will be zero and 1/2 in. At all slot widths the inducing air will enter the tunnel in a direction parallel to the tunnel axis. There are four entries to the pressure chamber arranged symmetrically at the extremities of the diagonals of the cross section.

Mixing Region and Diffuser.—The duct immediately downstream of the injector slot will be of constant cross-sectional area for a short length, and will then diverge at an equivalent conical angle (based on rate of area increase) of 4 deg. The area ratio at the first corner will be 4.0. Downstream of the first corner, the cross-section changes from rectangular to circular in a transition length in which the equivalent 4 deg expansion is maintained. The expansion is complete at the third corner at which the area ratio is 16.0. The airstream is then ducted back to the tunnel intake by a duct of constant cross-sectional area through a second transition length from circular to rectangular cross-section.

Cascades.—The cascade vanes will be of sheet metal⁶⁶ and will turn the air through a right-angle in a single stage. Each vane will be a quadrant in section with short tangential extensions at the leading and trailing edges. The vane chord will be 8 in. and the gap chord ratio 0.25. The leading edges will be at an incidence of 5 deg.

Settling Length.—There will be a settling length upstream of the intake contraction with provision for the insertion of gauze damping screens.

Bleed-off Valve.—The bleed-off valve will be placed immediately downstream of the second corner and the bleed-off area will be controlled by the rotation of an annular sleeve valve encircling the bleed-off chamber.

Stagnation Pressure.—By a suitable reduction of the bleed-off area it is hoped to run the tunnel at stagnation pressures up to three atmospheres absolute. The whole of the tunnel shell is stressed to withstand this internal pressure. At this maximum stagnation pressure, the Reynolds number of a test for a 6-in. chord model at $M = 0.9$ will be of the order of seven million.

Running Time.—It is expected that with the inducing-air storage capacity which will be available, the running time will be adequate for test work at all tunnel speeds.⁵²

Flow Visualization.—The working section is to be provided with an adequate area of glass wall to enable the flow round the model to be observed optically.

Working-Section Mach Number.—The tunnel will be operated at both subsonic and supersonic working-section Mach numbers up to a maximum value of about 1.6.

General.—The control of the inducing-air supply, and the bleed-off area is to be manual in the first instance, but provision is to be made for the subsequent installation of automatic control.

The tunnel has been designed on the 'unit' principle so that all the major components may be removed and replaced readily.

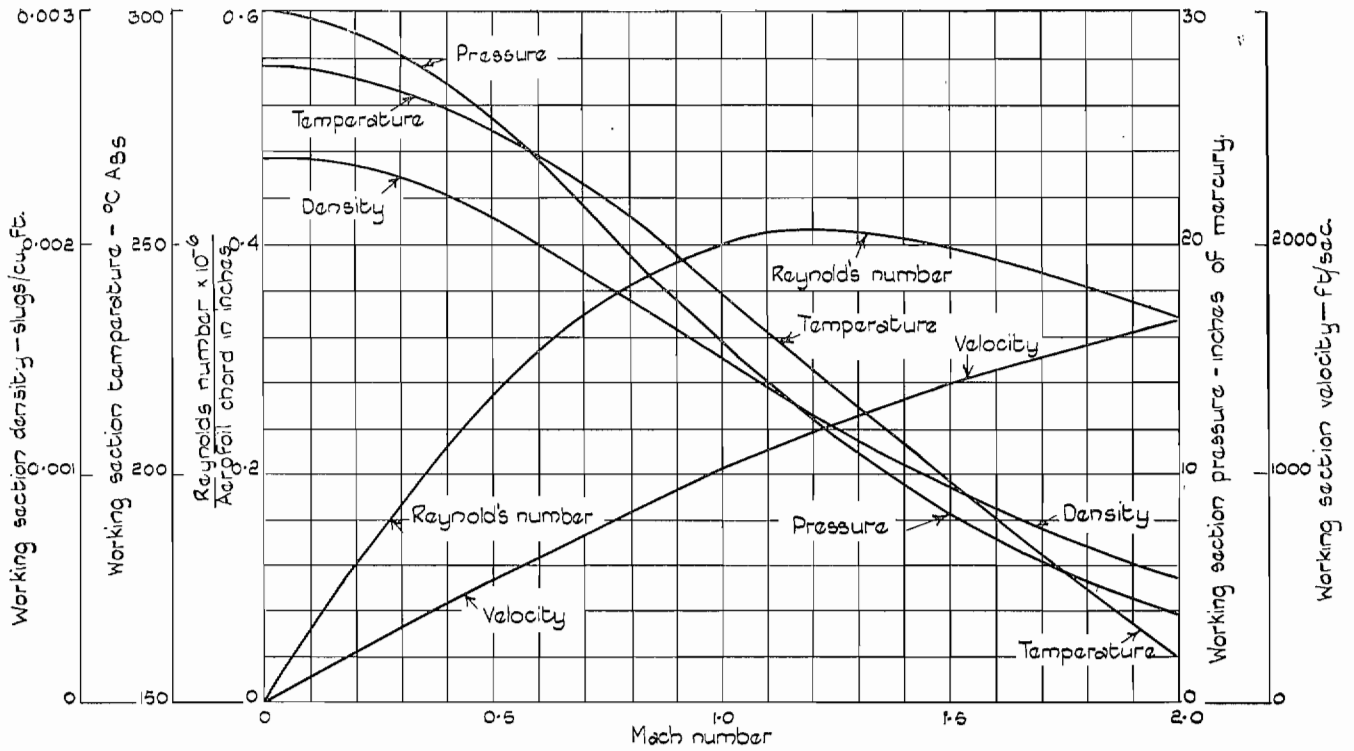


FIG. 1. Conditions of air at working section as a function of working-section Mach number assuming isentropic acceleration from intake conditions $p = 30$ in. Hg. $\rho = 0.002378$ slugs/cu ft. $T = 288^\circ\text{C}$ abs. $V = 0$.

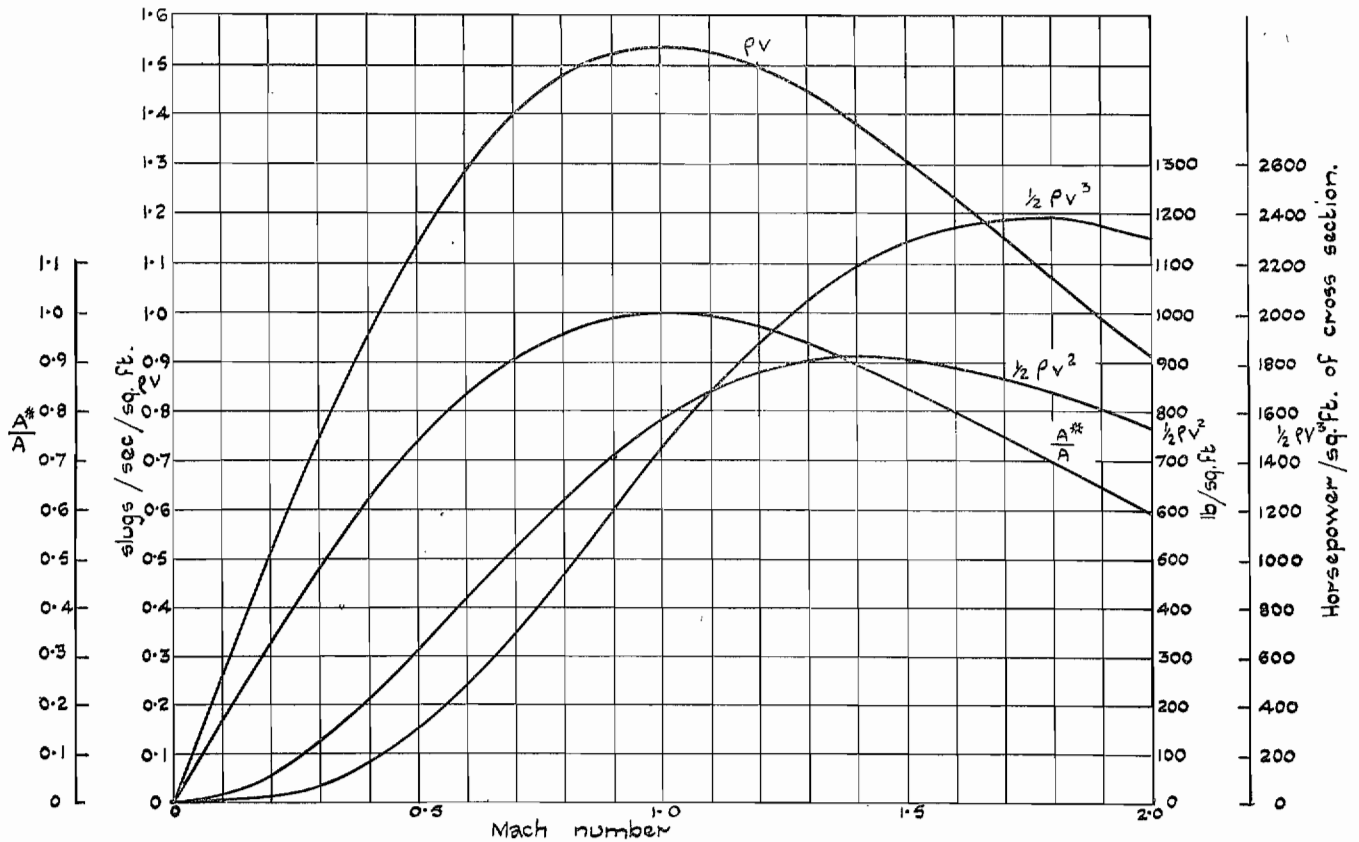


FIG. 2. Conditions of air at working section as a function of working-section Mach number assuming isentropic acceleration from intake conditions $p = 30$ in. Hg. $\rho = 0.002378$ slugs/cu ft. $T = 288^\circ\text{C}$ abs. $V = 0$.

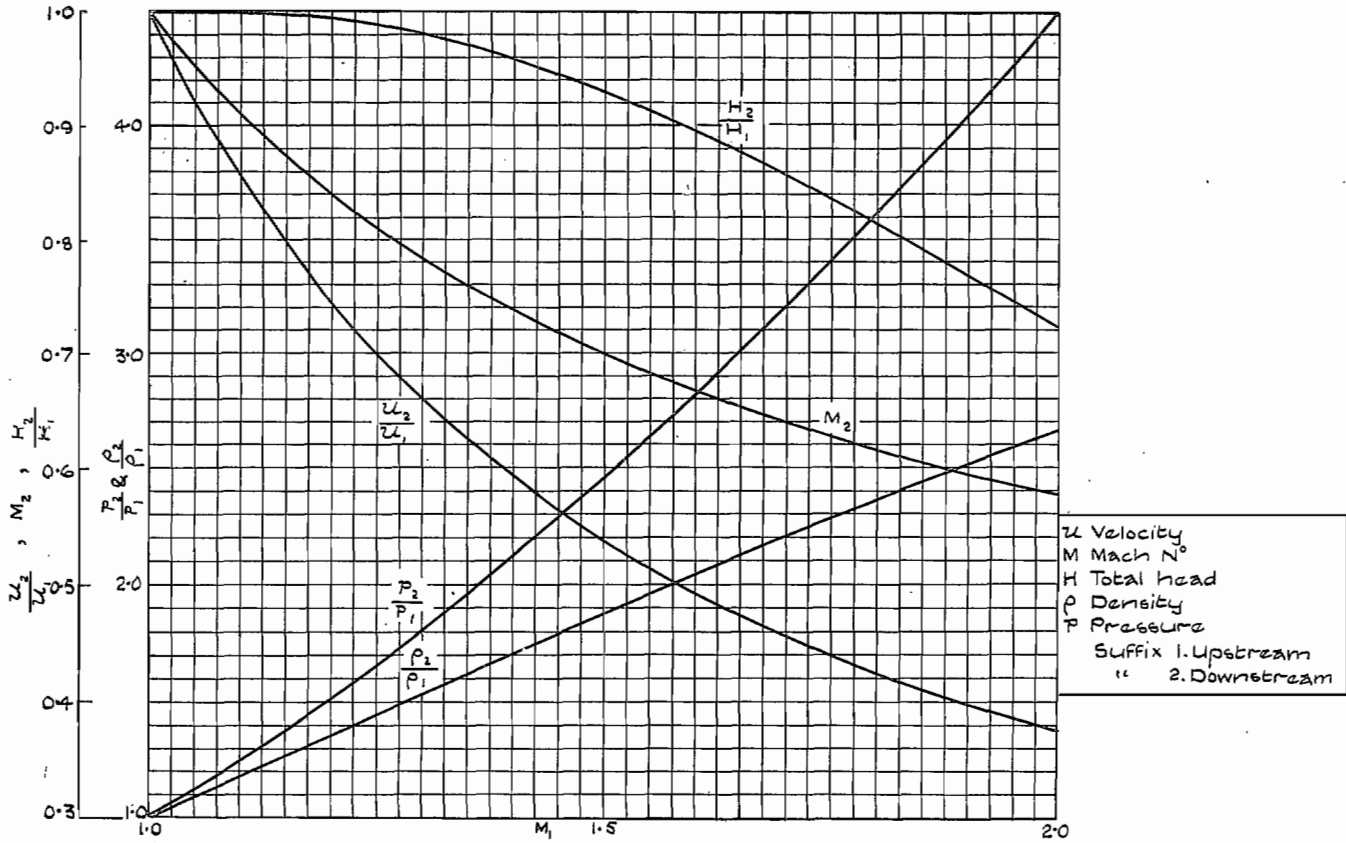


FIG. 3(a). Changes through a normal shock-wave.

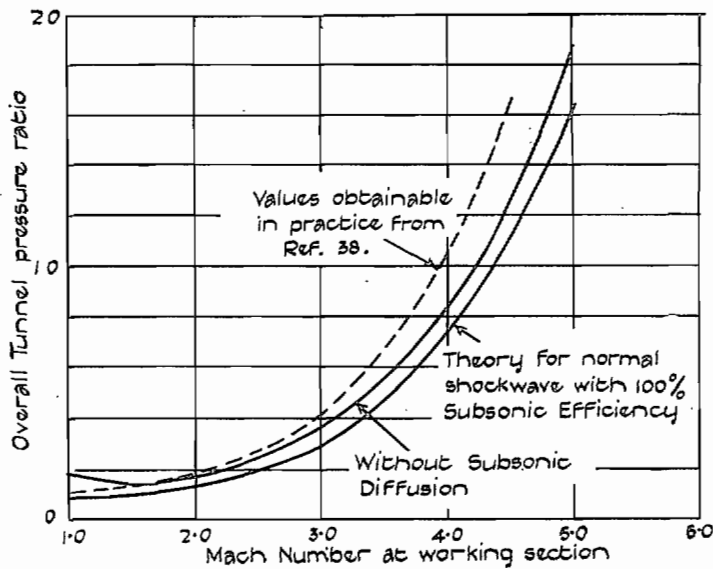


FIG. 3(b). Variation of overall pressure ratio required to operate tunnel with working-section Mach number.

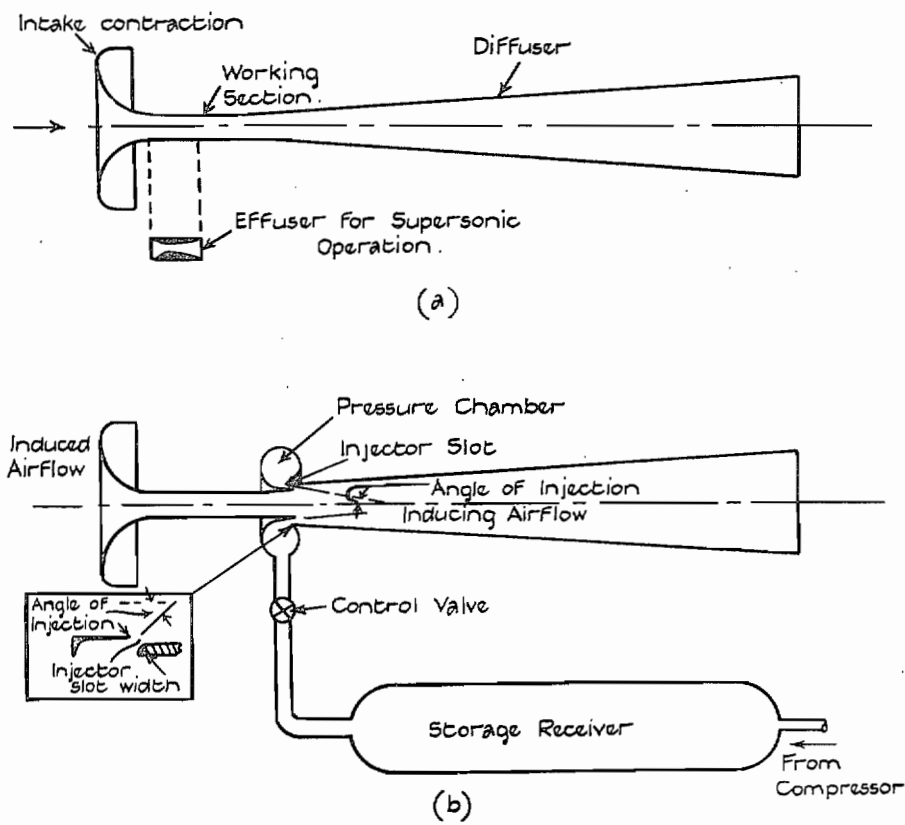
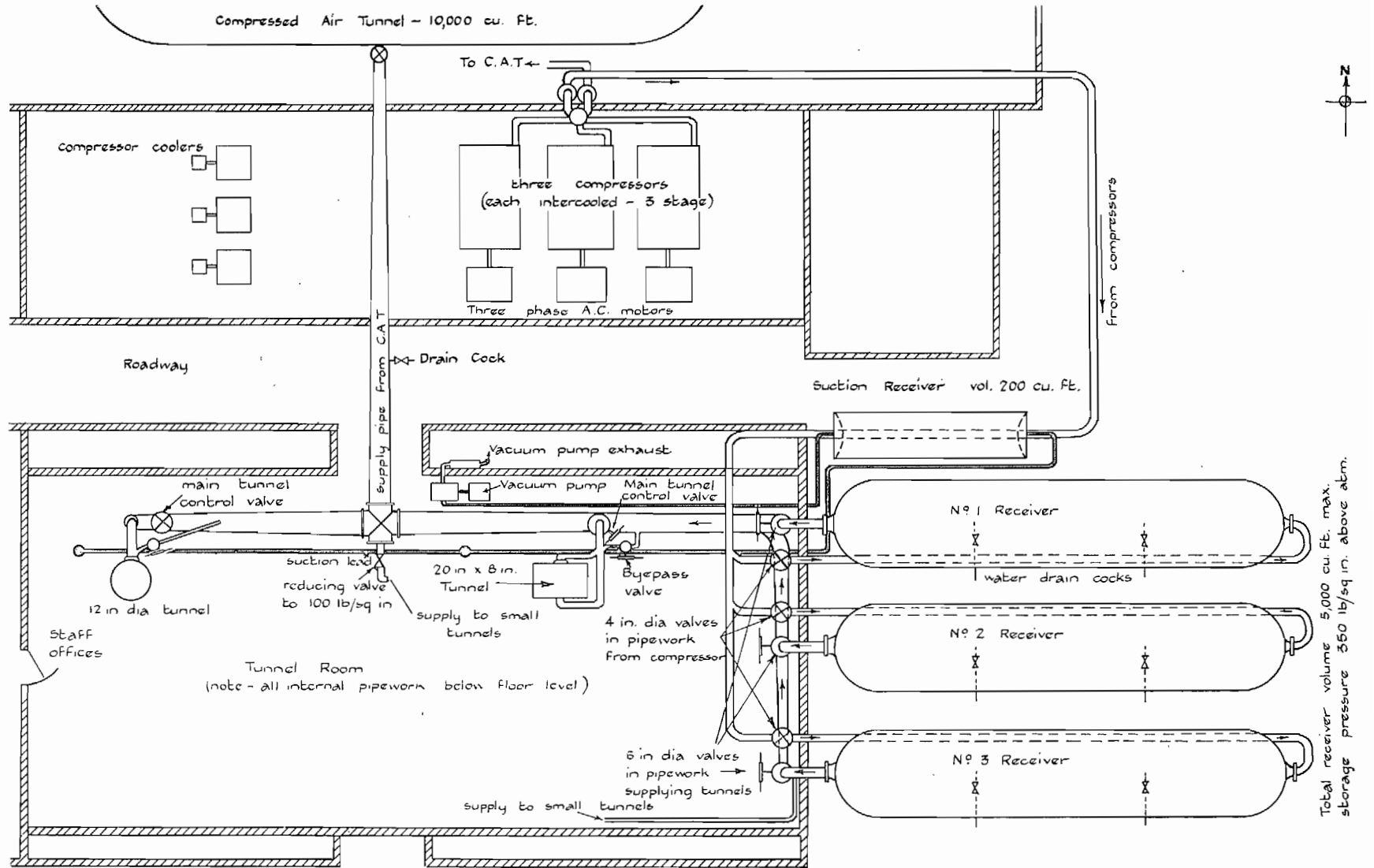


FIG. 4. Sketch of induction-type tunnel installation.



Total receiver volume 5,000 cu. Ft. max.
 storage pressure 350 lb/sq in. above atm.

FIG. 5(a). Layout of N.P.L. high-speed wind tunnels.



FIG. 5(b). General view of interior of tunnel room.

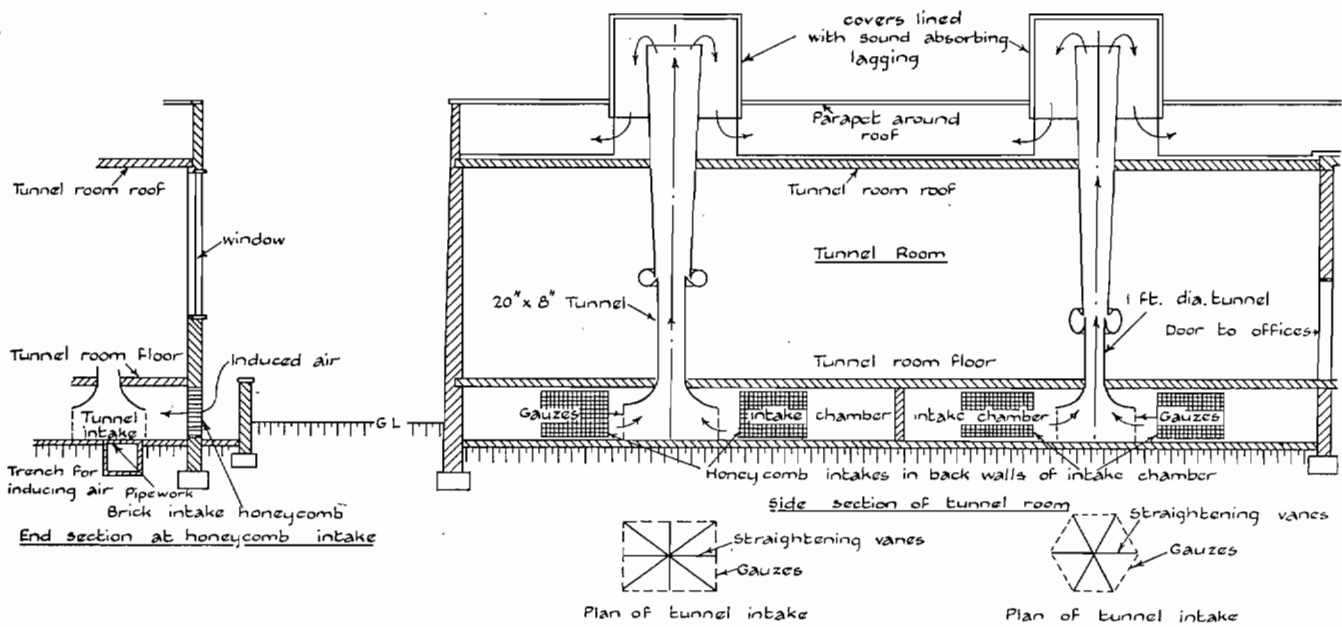


FIG. 5(c). Sketch of induced-air system of high-speed tunnels.

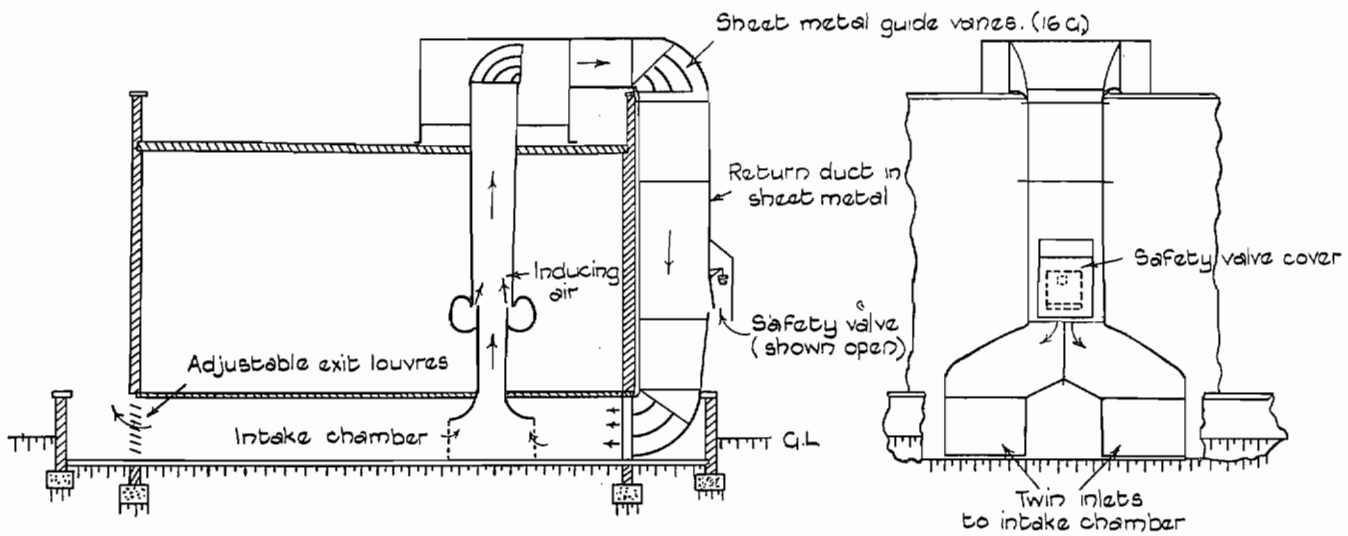


FIG. 5(d). Sketch of return duct.

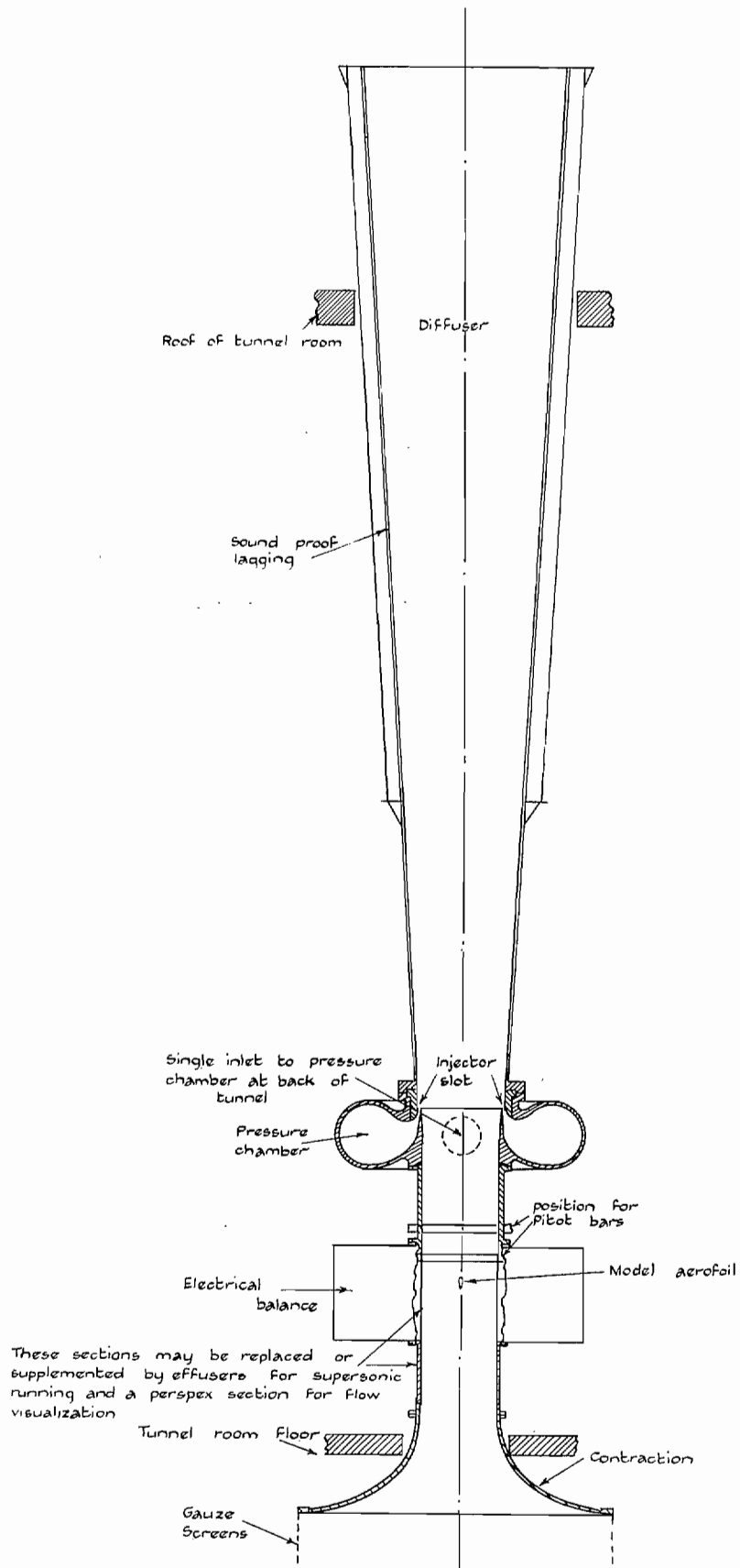
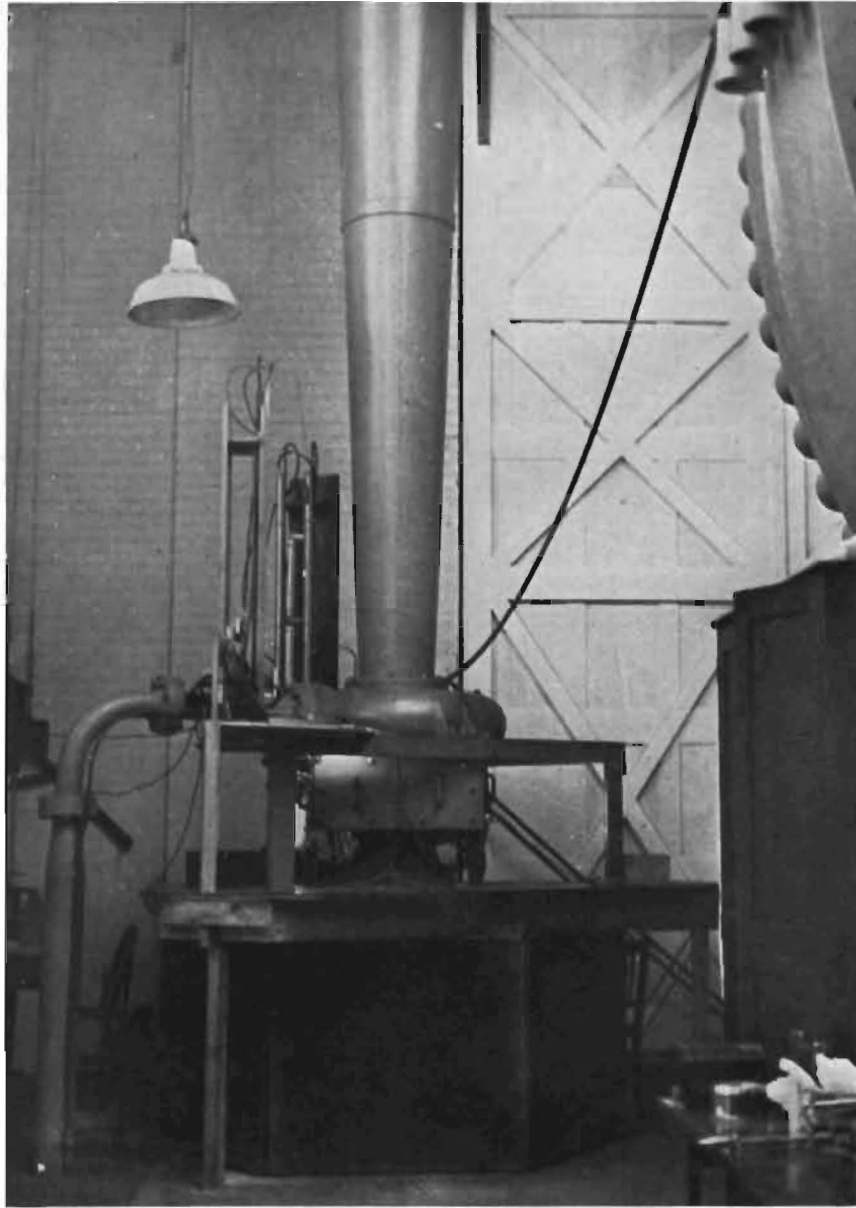
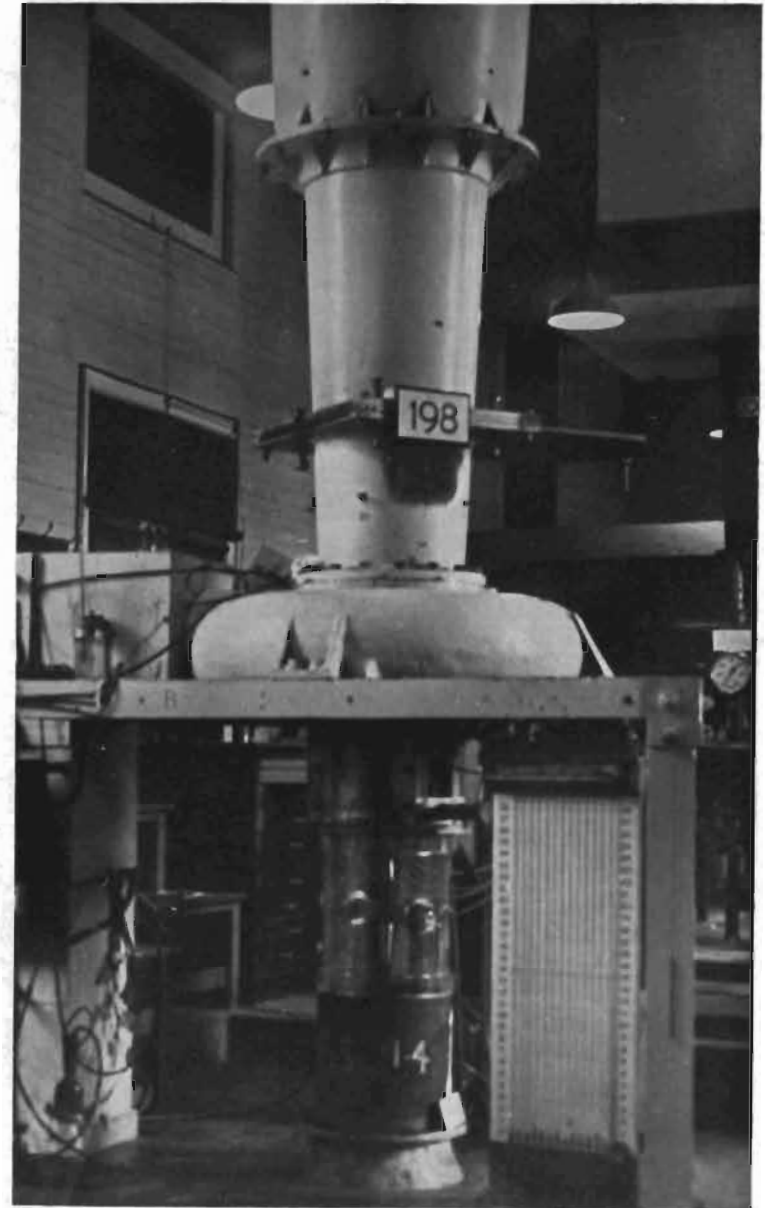


FIG. 6(a). 12-in. diameter high-speed tunnel.



1-ft diameter tunnel in original position in compressed-air tunnel building and fitted with electric balance.



1-ft diameter tunnel in present position and fitted with a nozzle for supersonic operation and a 'Perspex' working section.

FIG. 6(b).

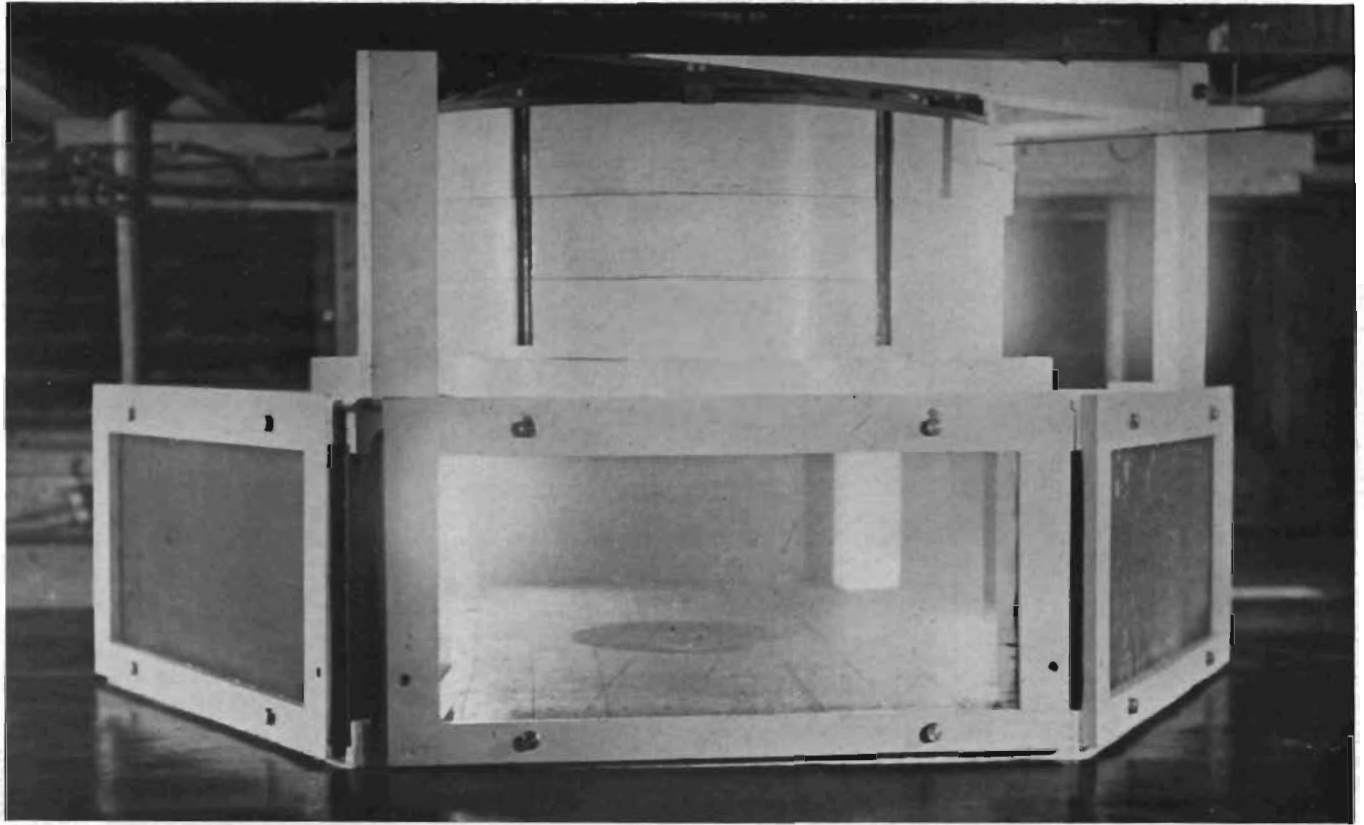


FIG. 6(c). New intake to 1-ft diameter high-speed tunnel.

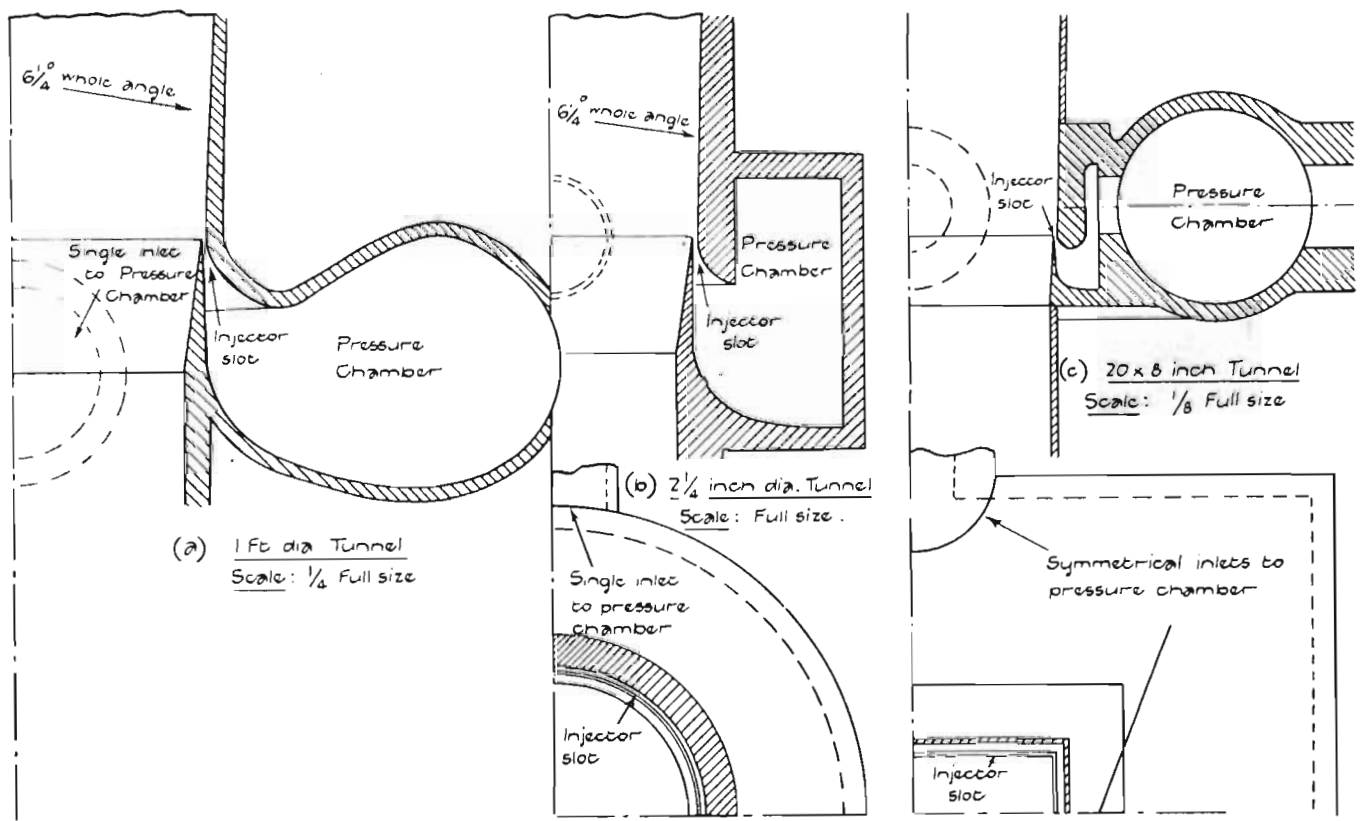


FIG. 7. Comparison of injectors of the 1-ft diameter, $2\frac{1}{4}$ -in. diameter and 20×8 -in. tunnels.

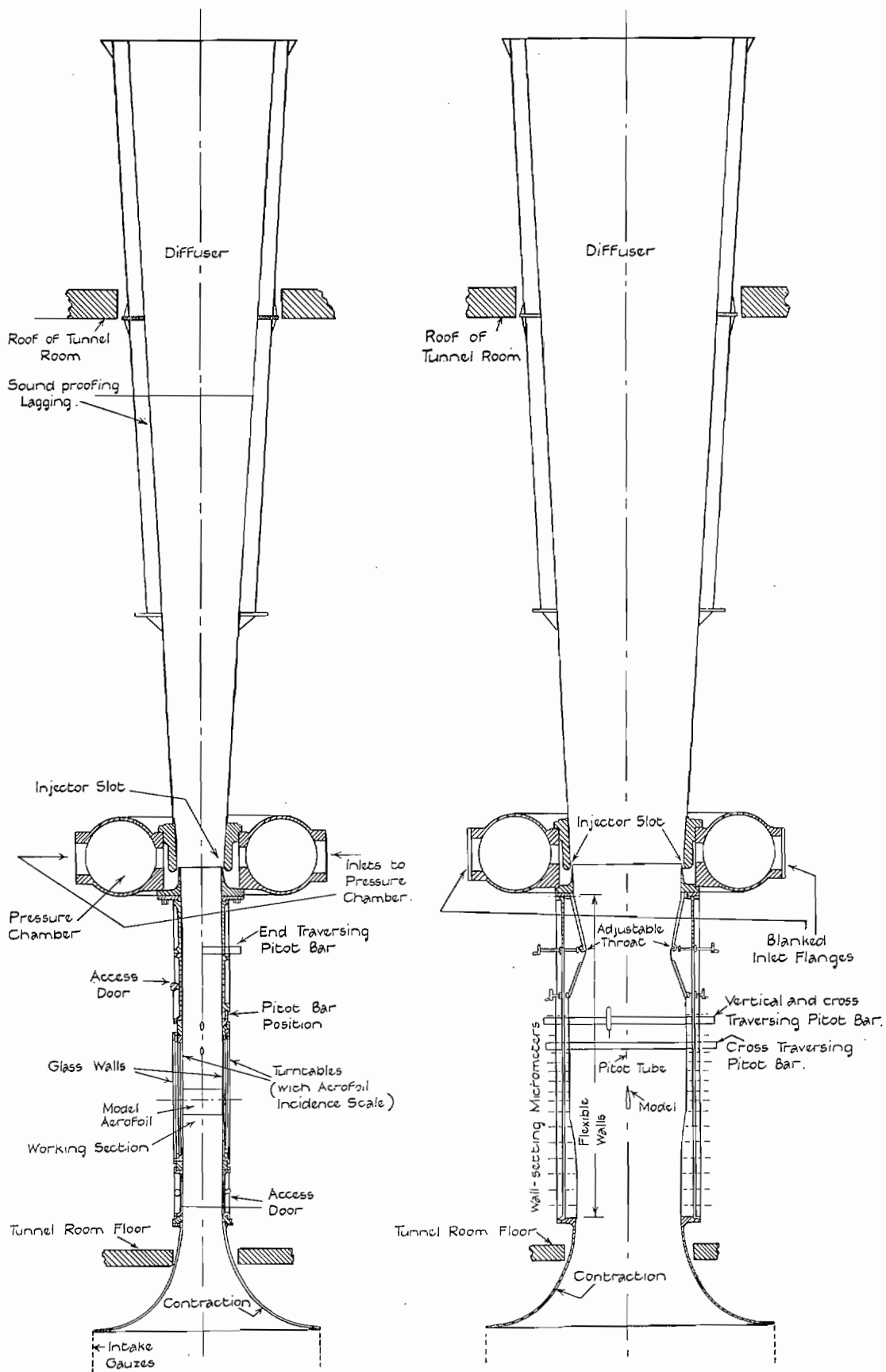


FIG. 8(a). 20 x 8-in. high-speed tunnel.



FIG. 8(b). 20 × 8-in. high-speed tunnel.

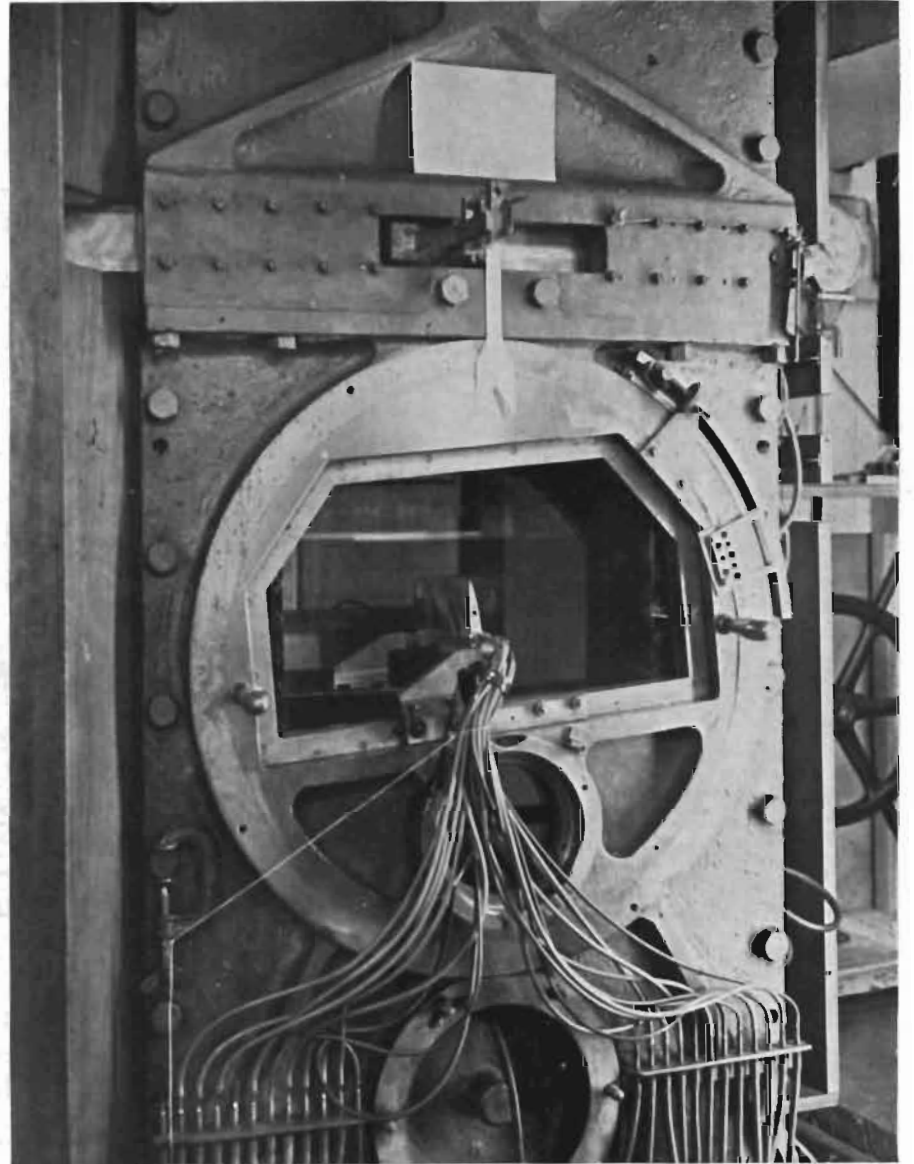


FIG. 8(c). 20 × 8-in. high-speed tunnel. Working section.

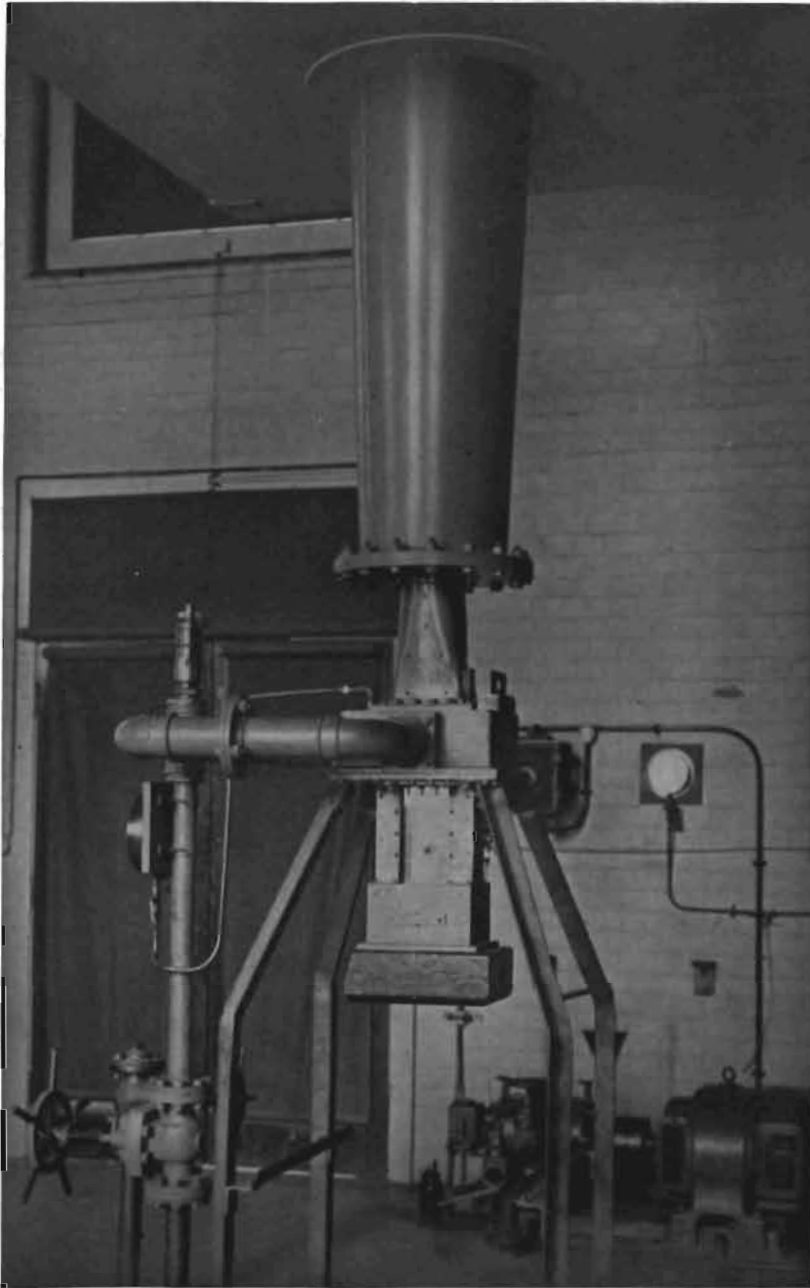
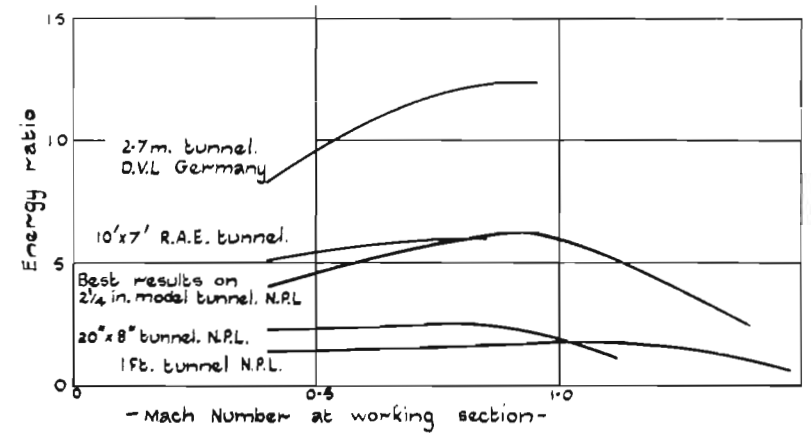


FIG. 9. 5 × 2-in. high-speed tunnel.



Note:- For fan driven tunnel (D.V.L. & R.A.E.)
 Energy ratio = $\frac{\text{Rate of flow of kinetic energy at working section}}{\text{Fan power.}}$
 For induction type tunnel (N.P.L.)
 Energy ratio = $\frac{\text{Rate of flow of kinetic energy at working section}}{\text{Power to compress inducing air isothermally from atm. pressure to blowing pressure.}}$

FIG. 10. Variation of energy ratio of high-speed wind tunnels with working-section Mach number. Empty tunnel.

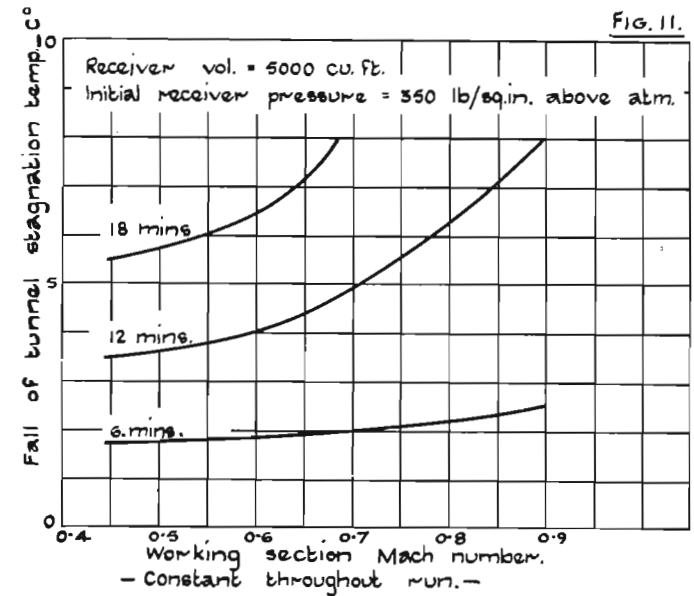


FIG. 11. Observed fall of stagnation temperature in 20 × 8-in. return duct tunnel. (Times are durations of tunnel runs.)

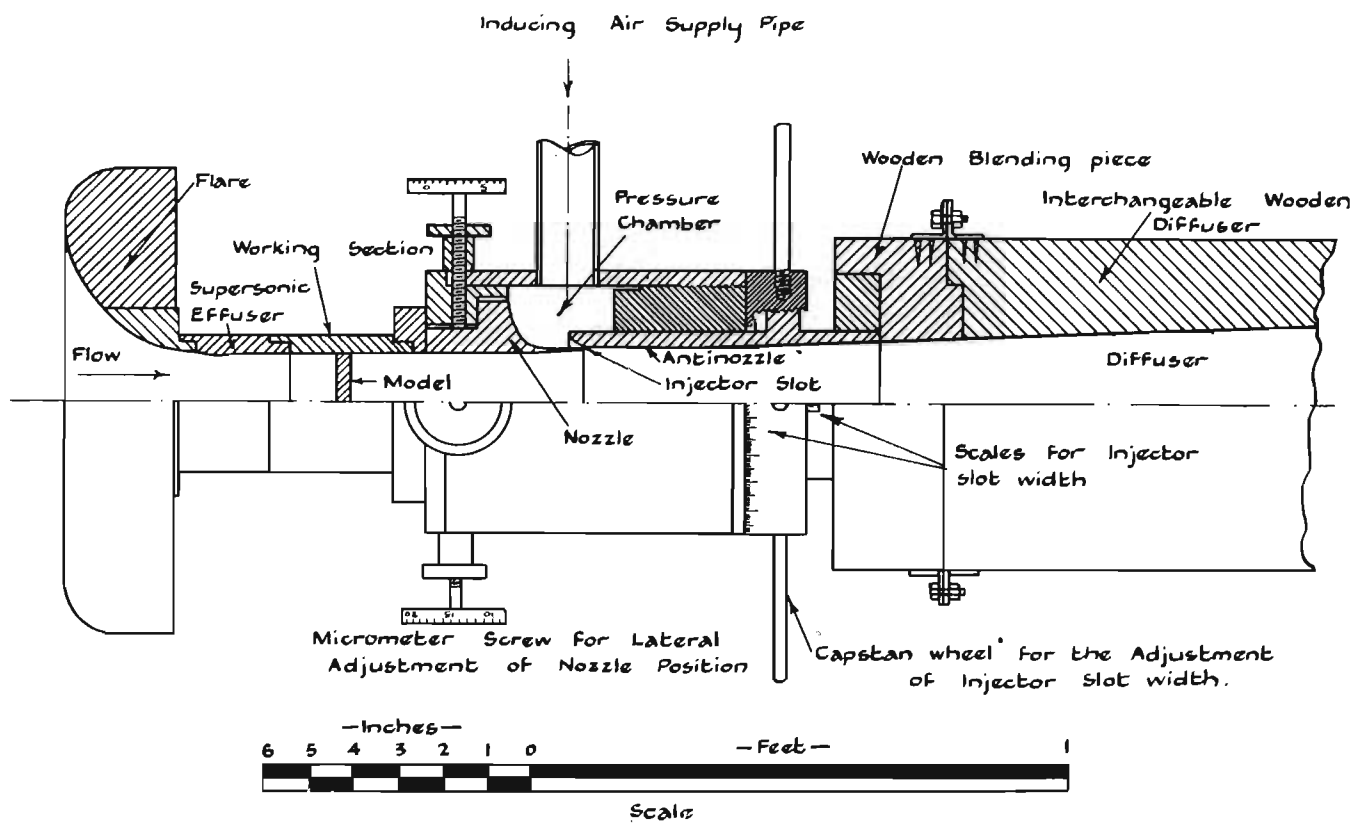


FIG. 12(a). Plan of 2 $\frac{1}{4}$ -in. diameter open-circuit induced-flow tunnel.

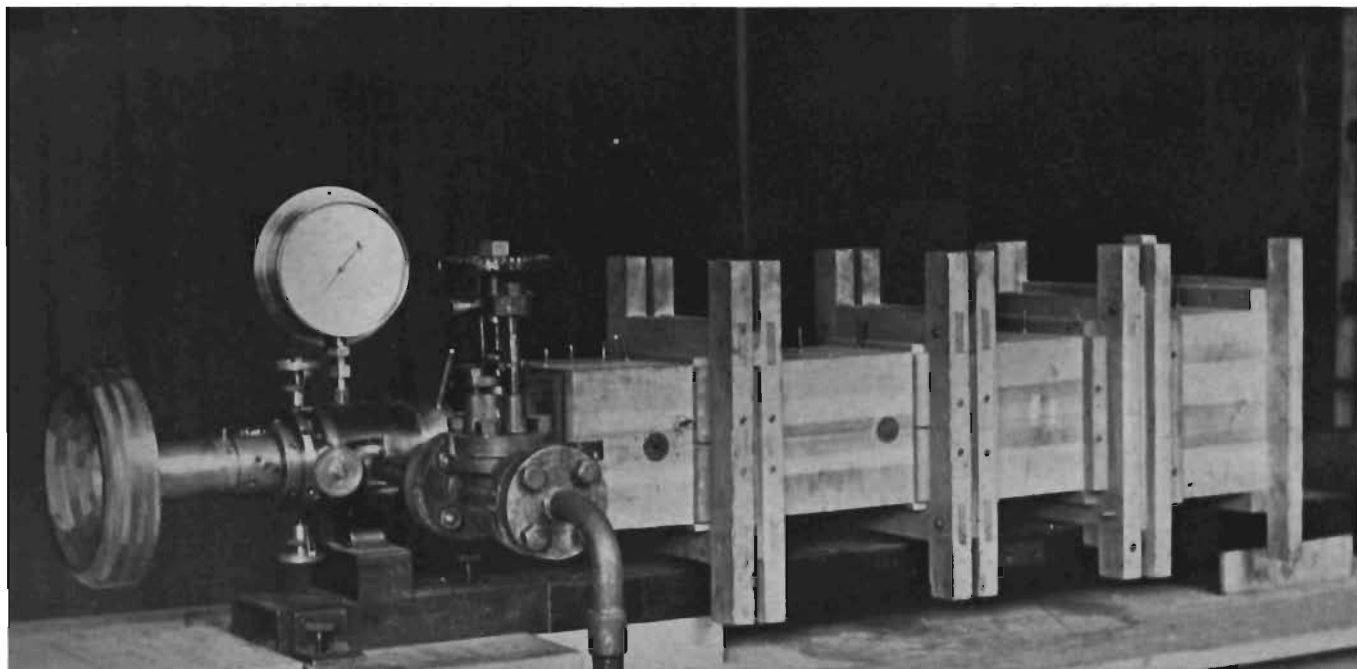


FIG. 12(b). 2 $\frac{1}{4}$ -in. diameter high-speed tunnel.

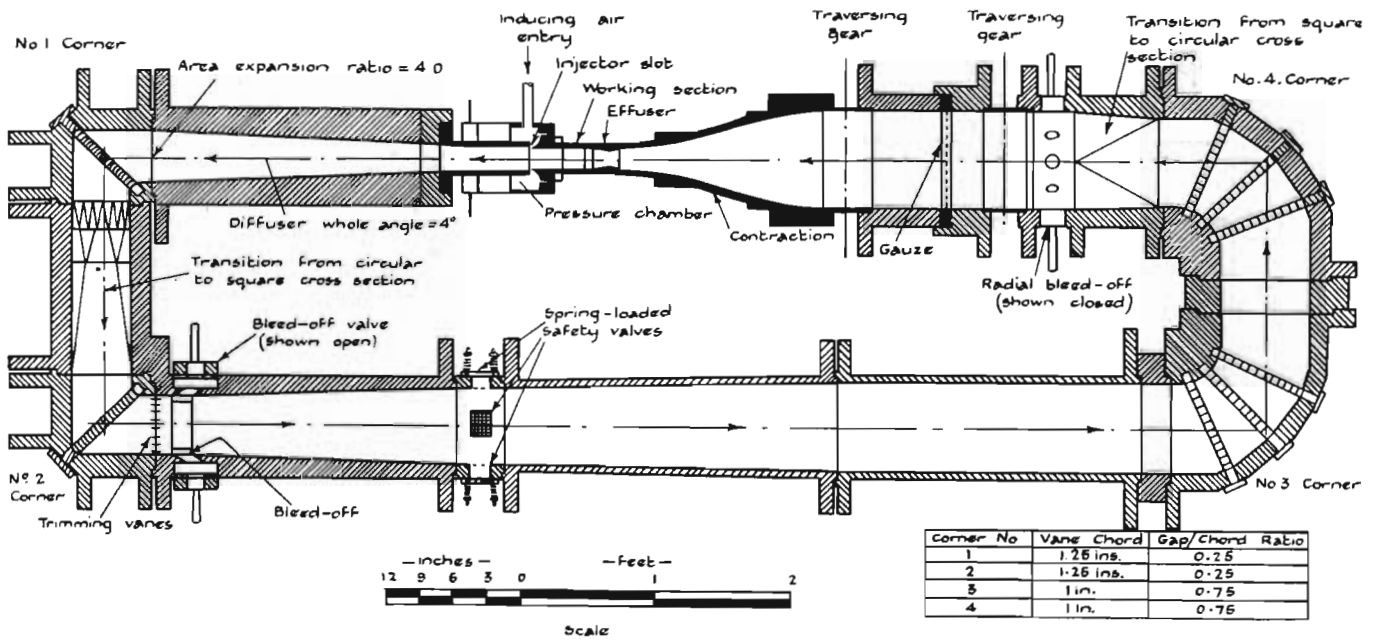


FIG. 13(a). 2½-in. diameter return-flow induction-type tunnel.

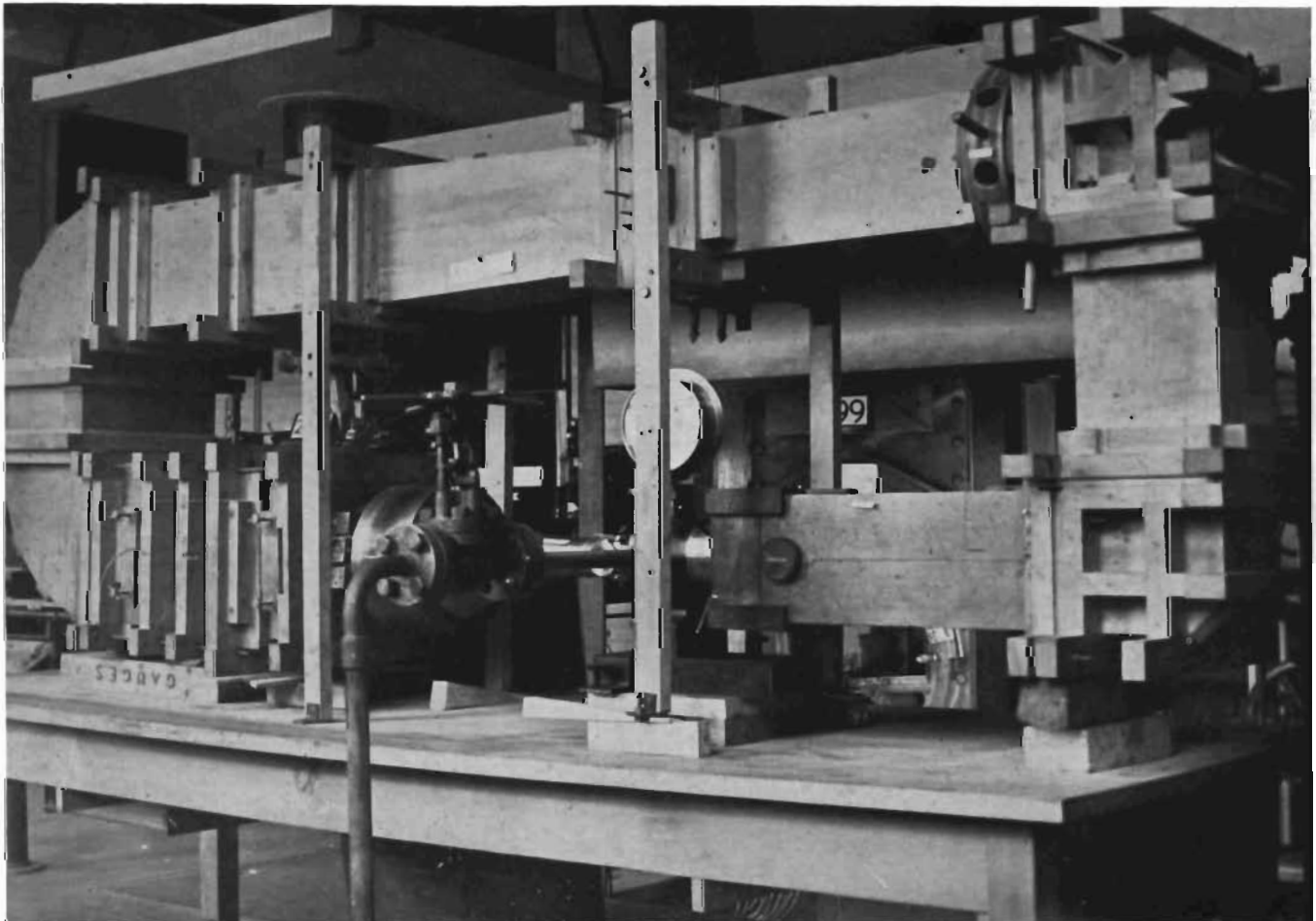


FIG. 13(b). 2½-in. diameter tunnel fitted with return duct.

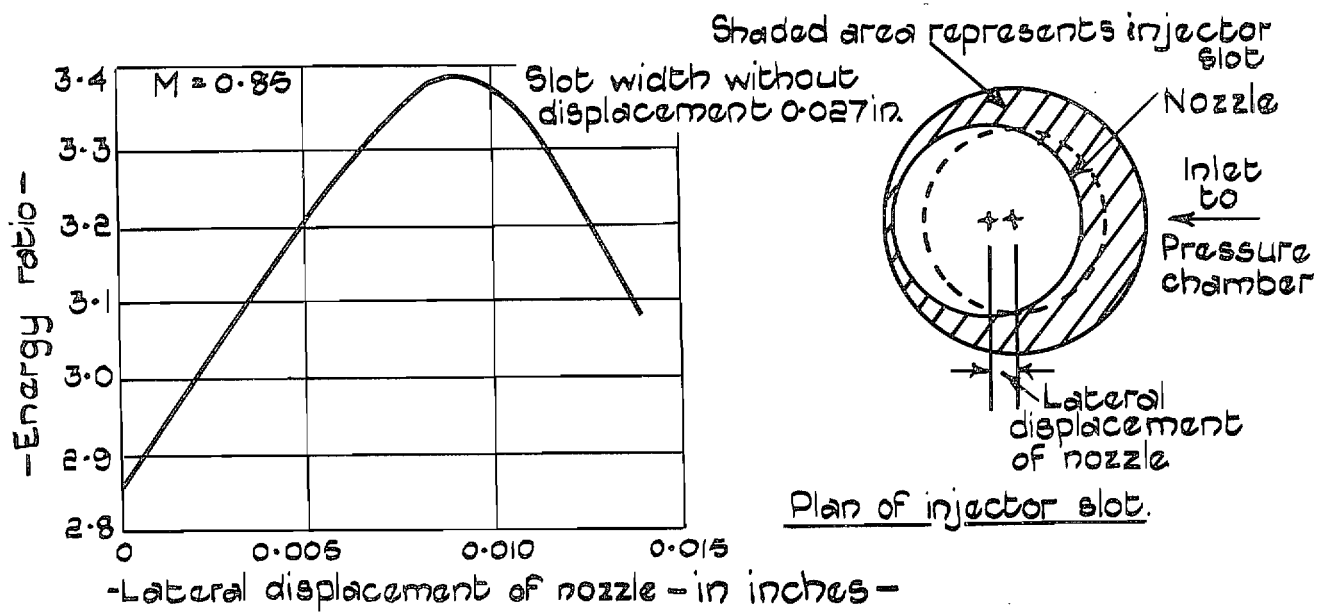


FIG. 14. Effects of asymmetry of entry to the pressure chamber and compensation for this by an adjustment of the peripheral distribution of injector slot area on energy ratio.

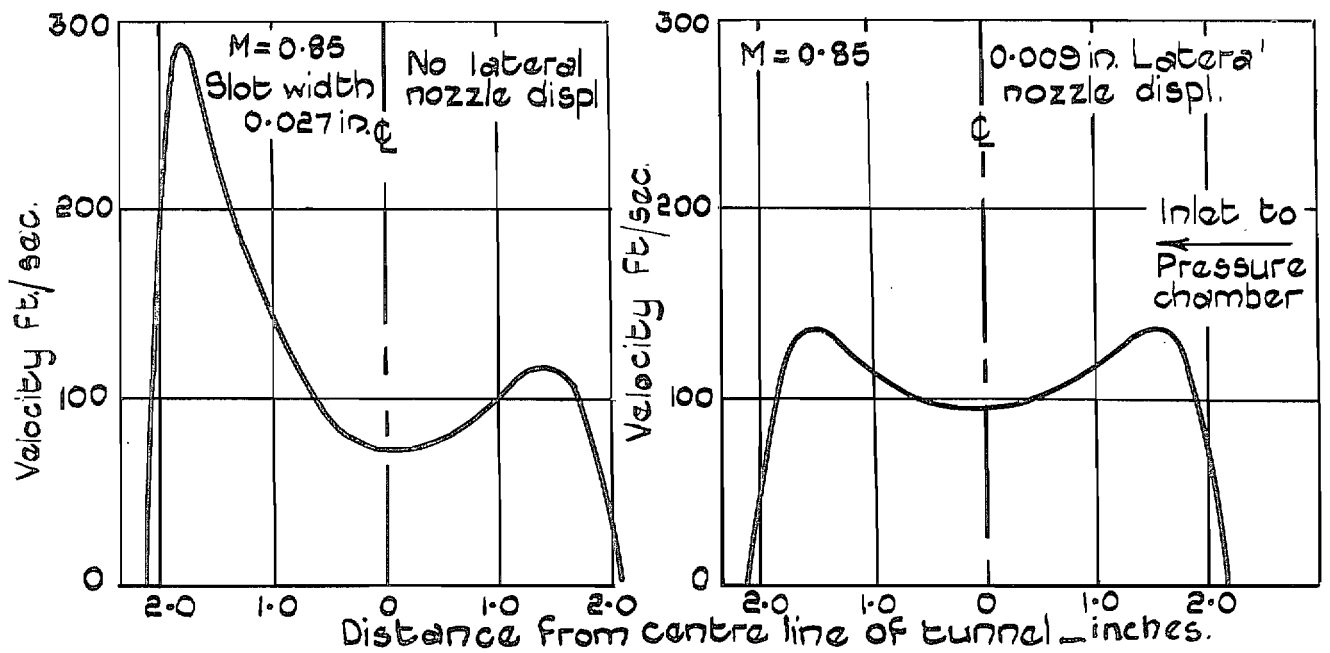


FIG. 15. Distribution of velocity across the diffuser downstream of the injector slot with and without nozzle displacement.

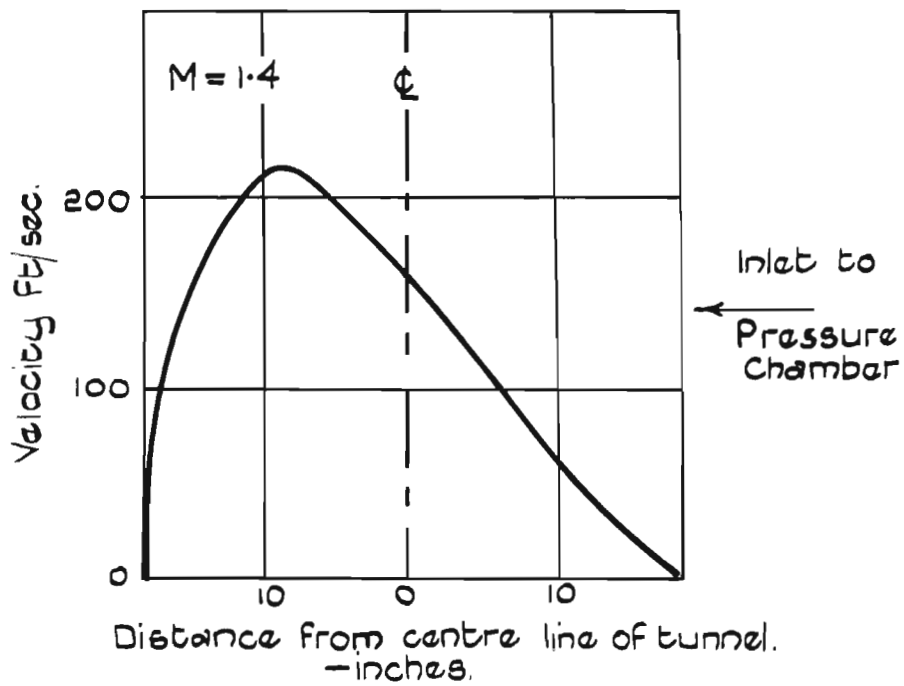


FIG. 16. Distribution of velocity at exit of diffuser of 1-ft diameter tunnel showing asymmetry due to single inlet to pressure chamber.

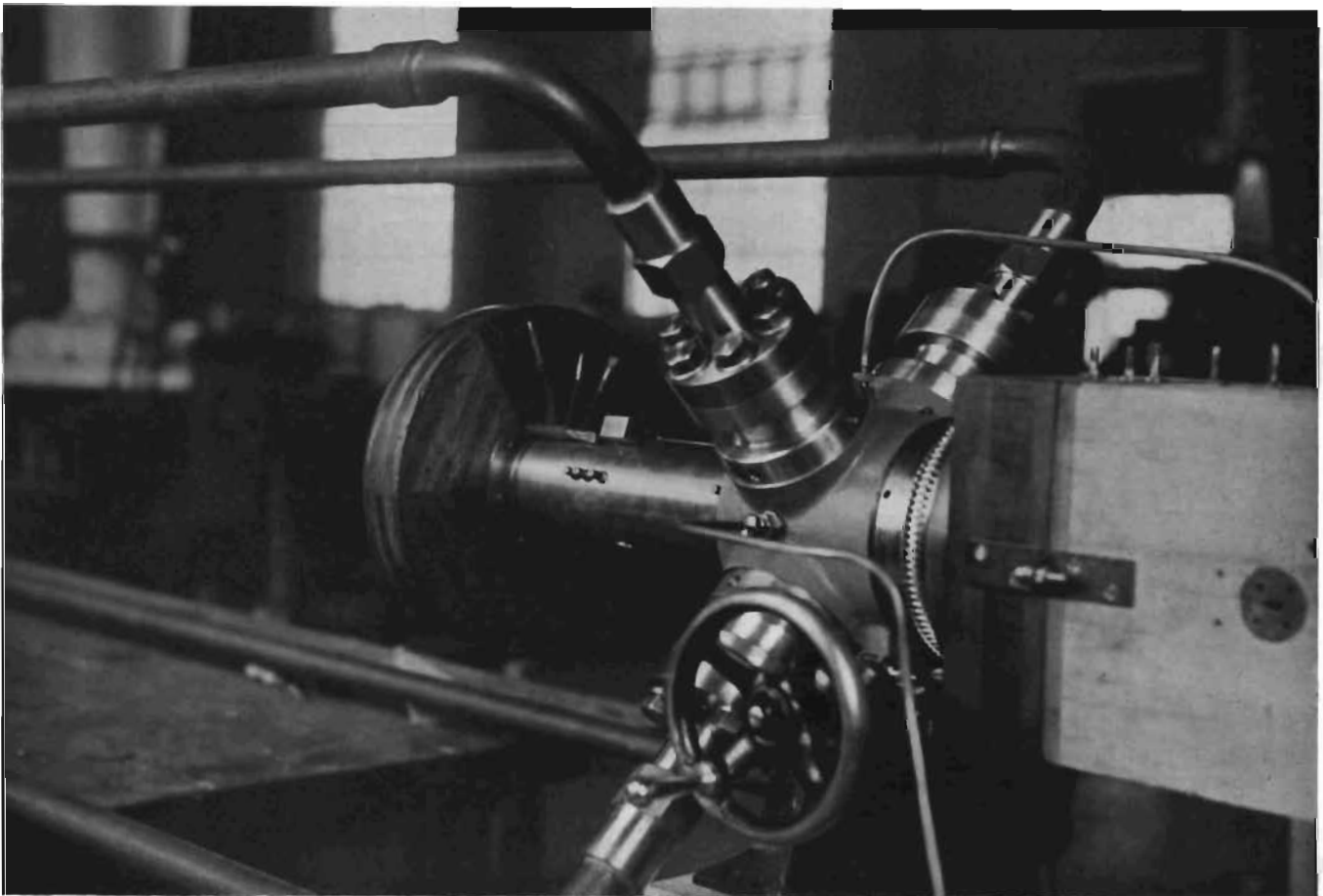


FIG. 17. 2 1/2-in. diameter model tunnel with 4 inducing-air entries.

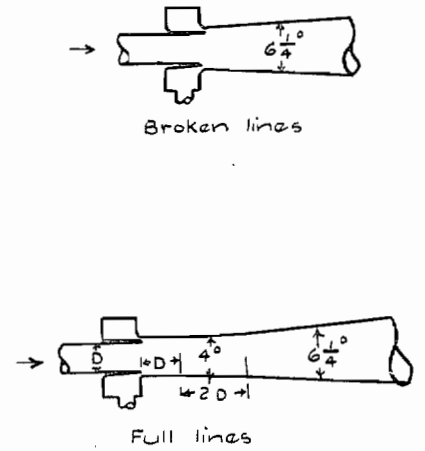
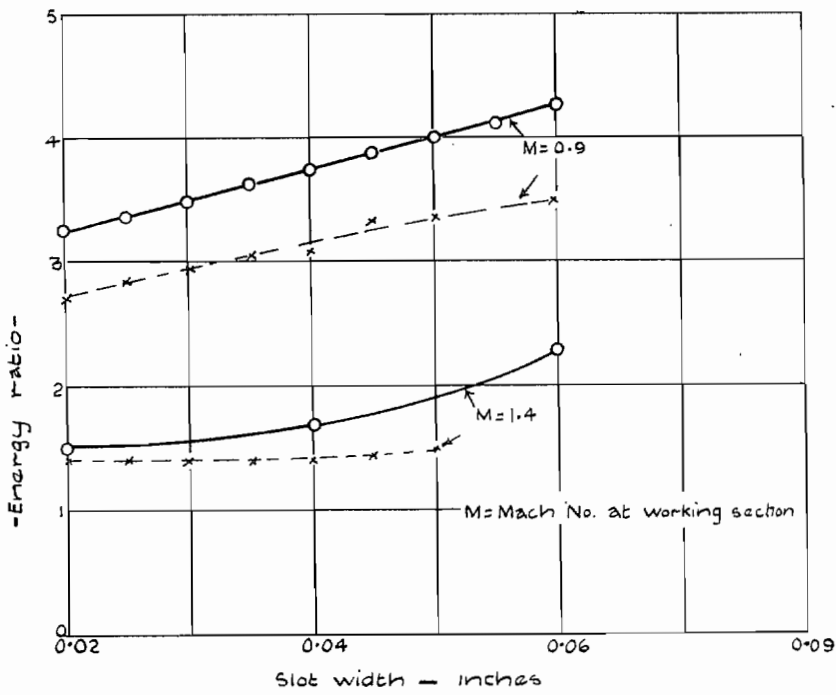


FIG. 18. Influence of constant area region downstream of injector slot upon efficiency.

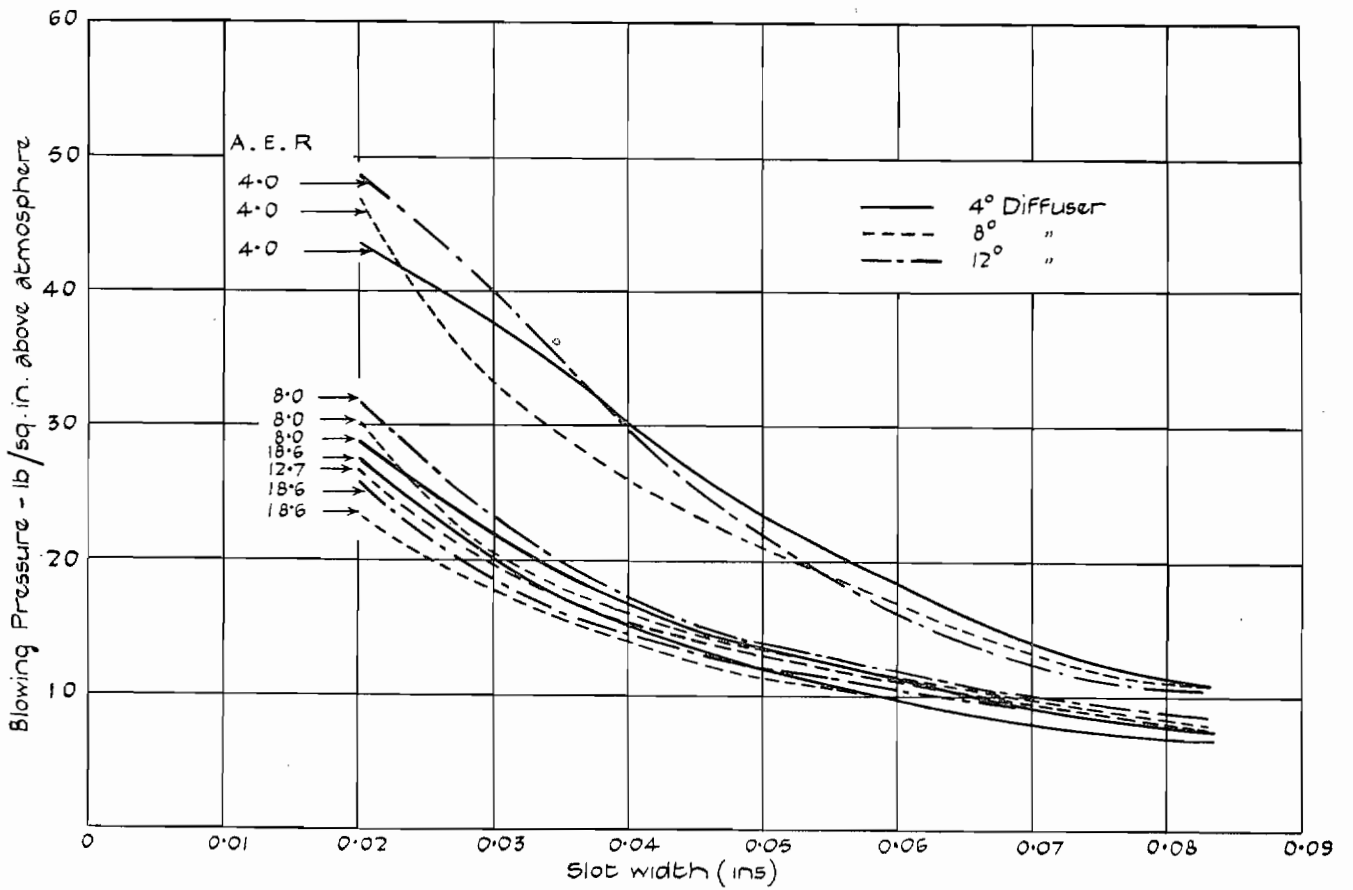


FIG. 19. Variation of blowing pressure with slot width for diffusers of varying whole angle and area expansion ratio. $M = 0.9$.

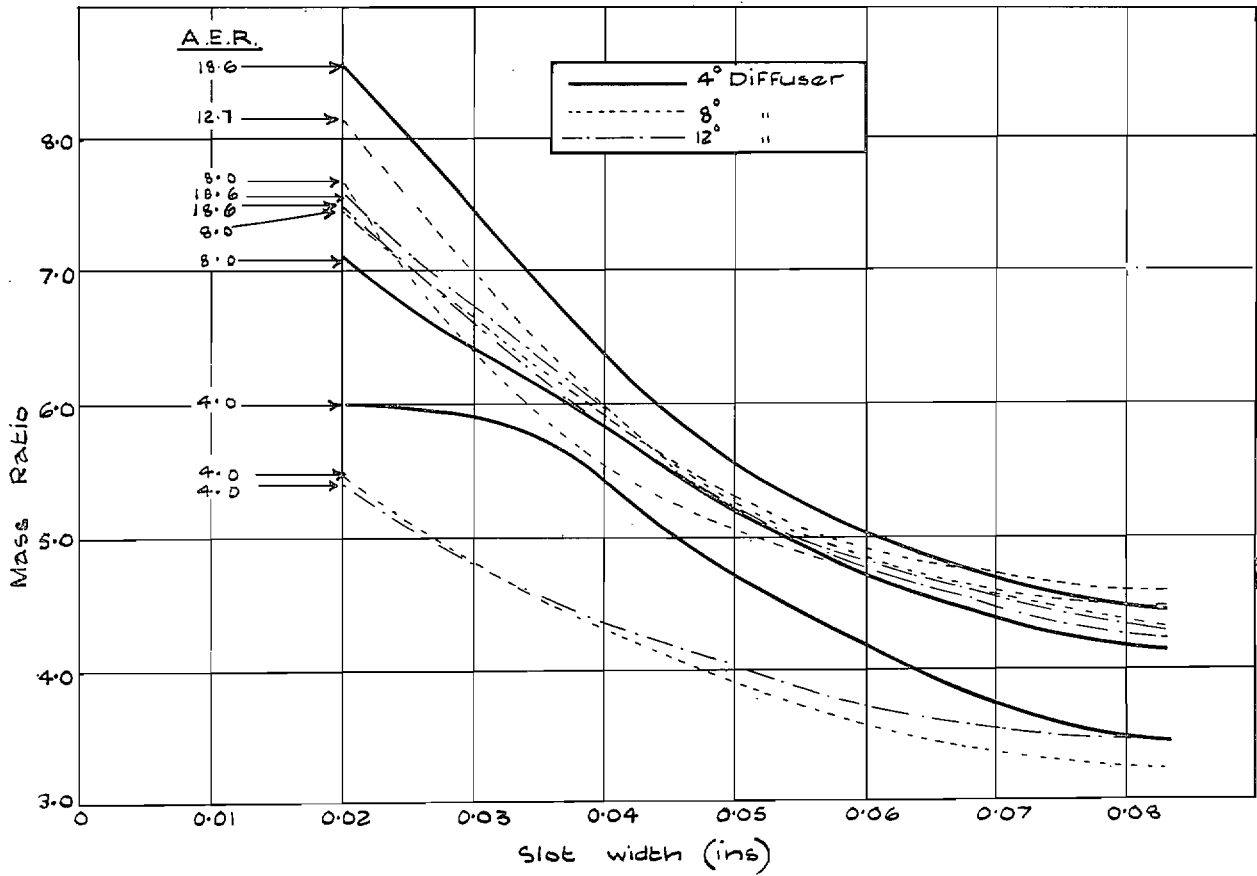


FIG. 20. Variation of mass ratio with slot width for diffusers of varying whole angle and area expansion ratio.

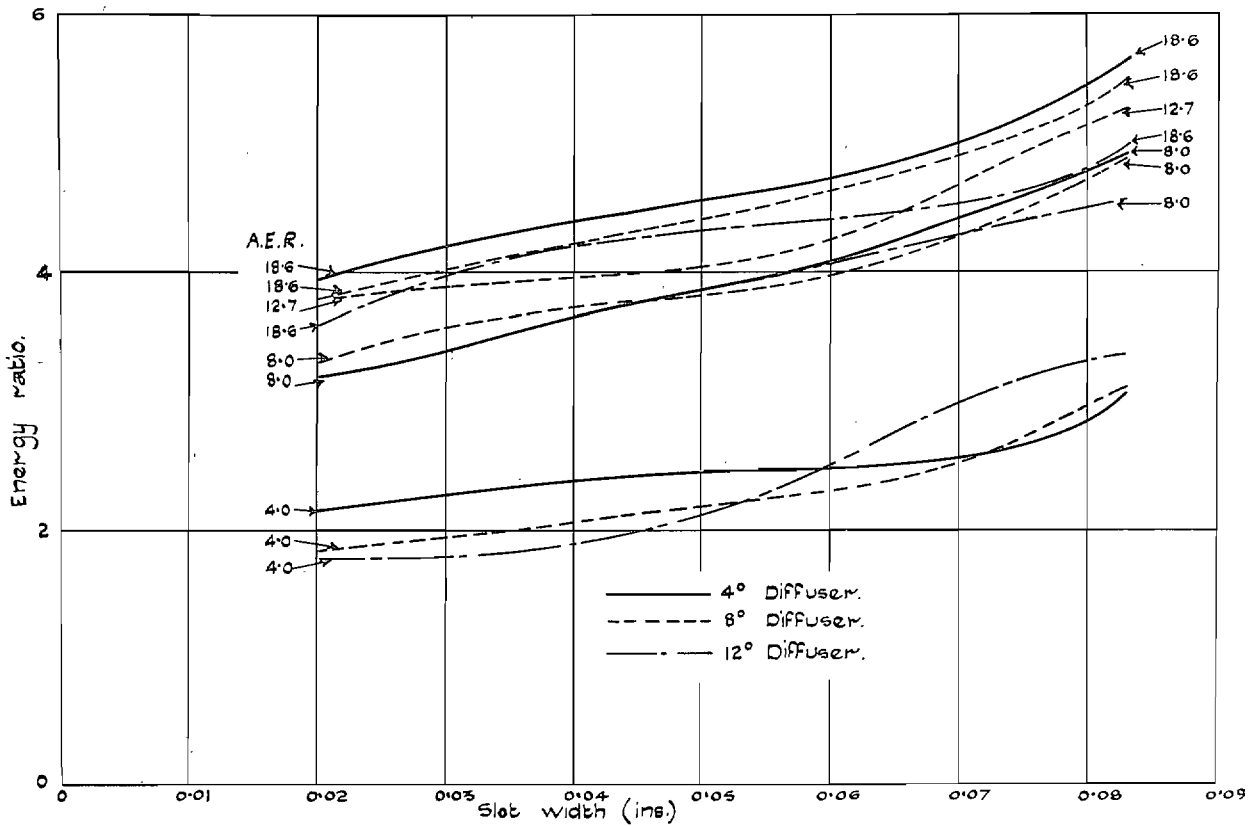


FIG. 21. Variation of energy ratio with slot width for diffusers of varying whole angle and area expansion ratio.
 $M = 0.9$.

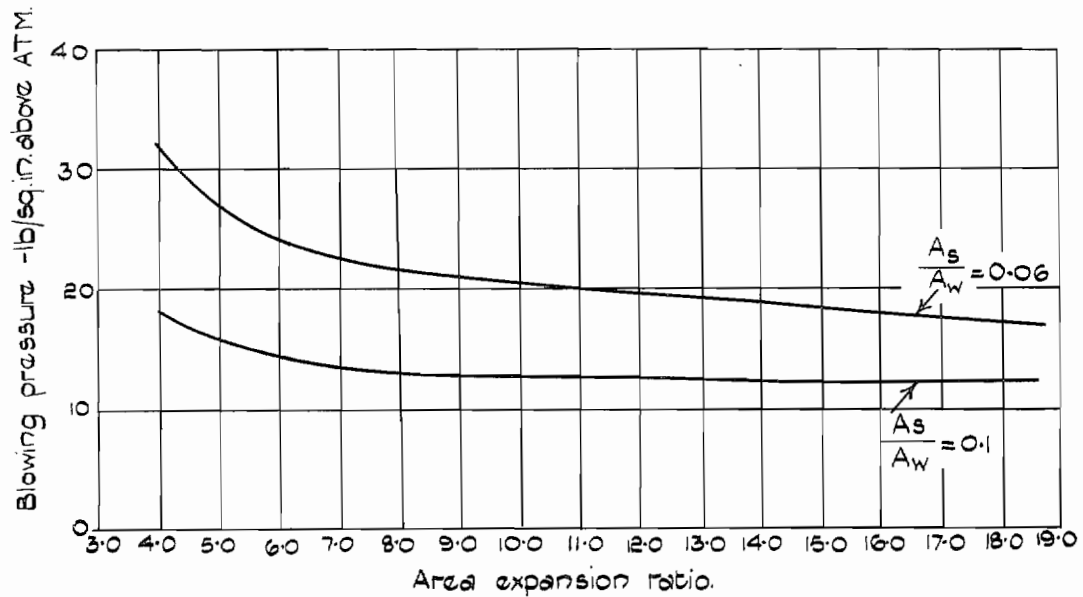
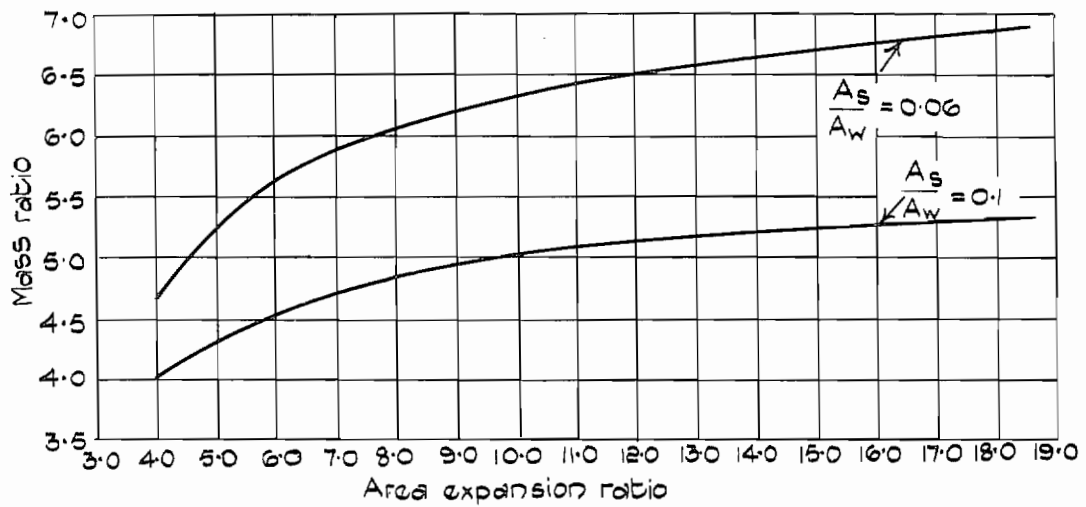
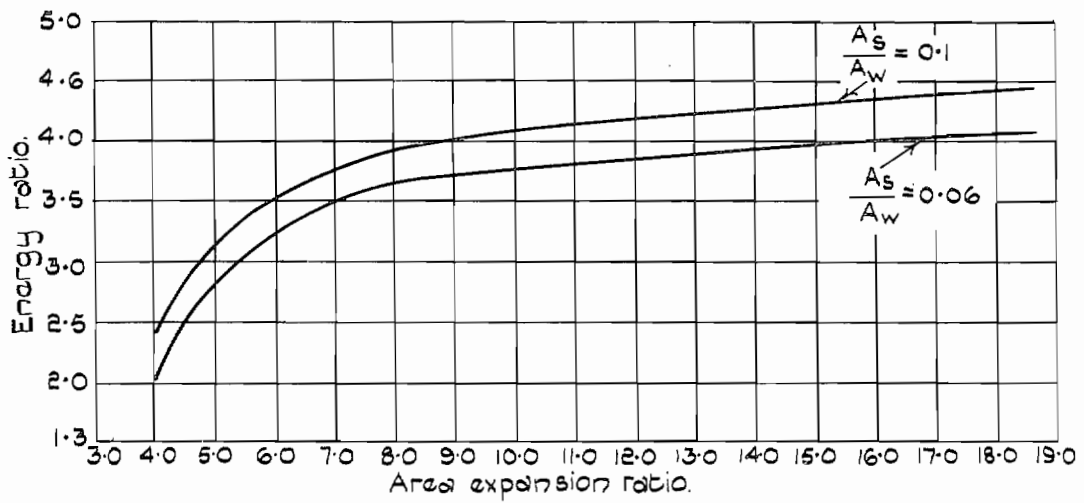


FIG. 22. Variation of efficiency with area expansion ratio of diffuser of 4, 8 or 12 deg whole angle. At working-section $M = 0.9$.

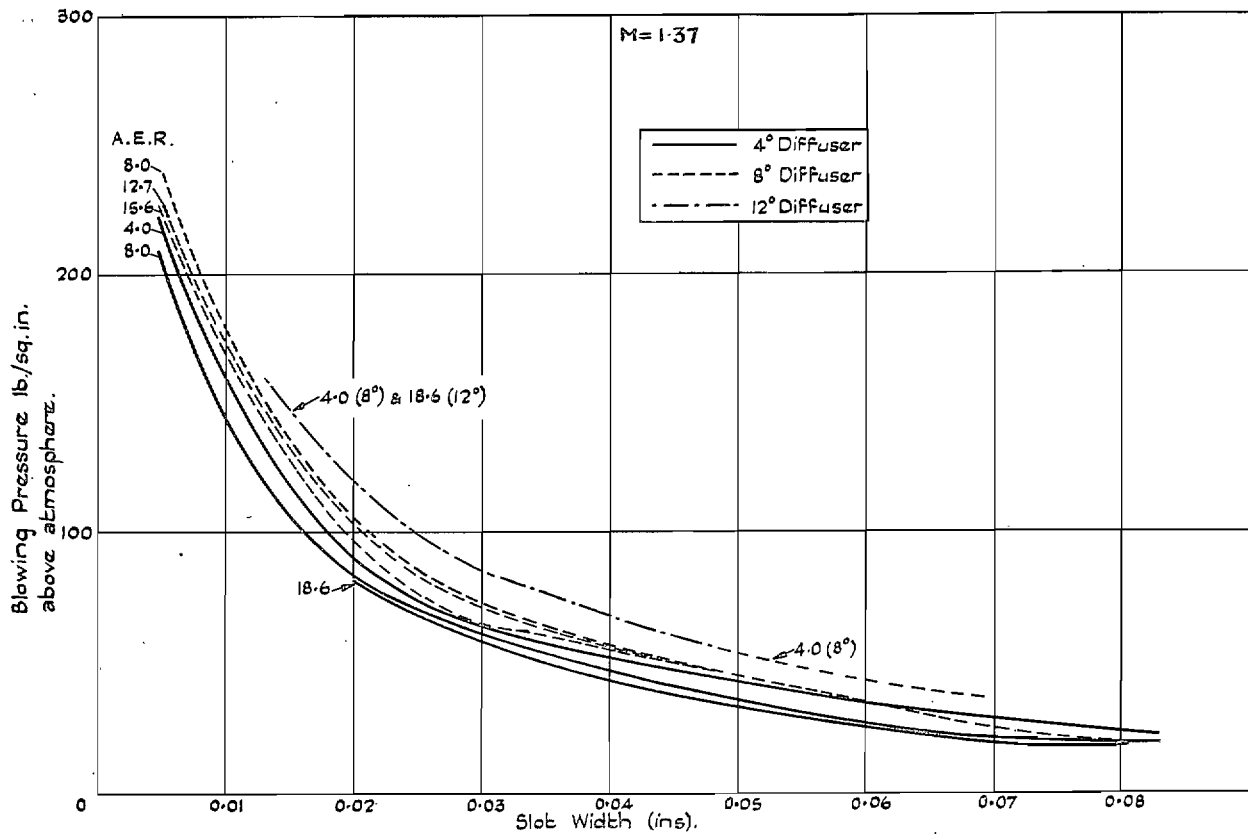


FIG. 23. Variation of blowing pressure with slot width for diffusers of varying whole angle and area expansion ratio.

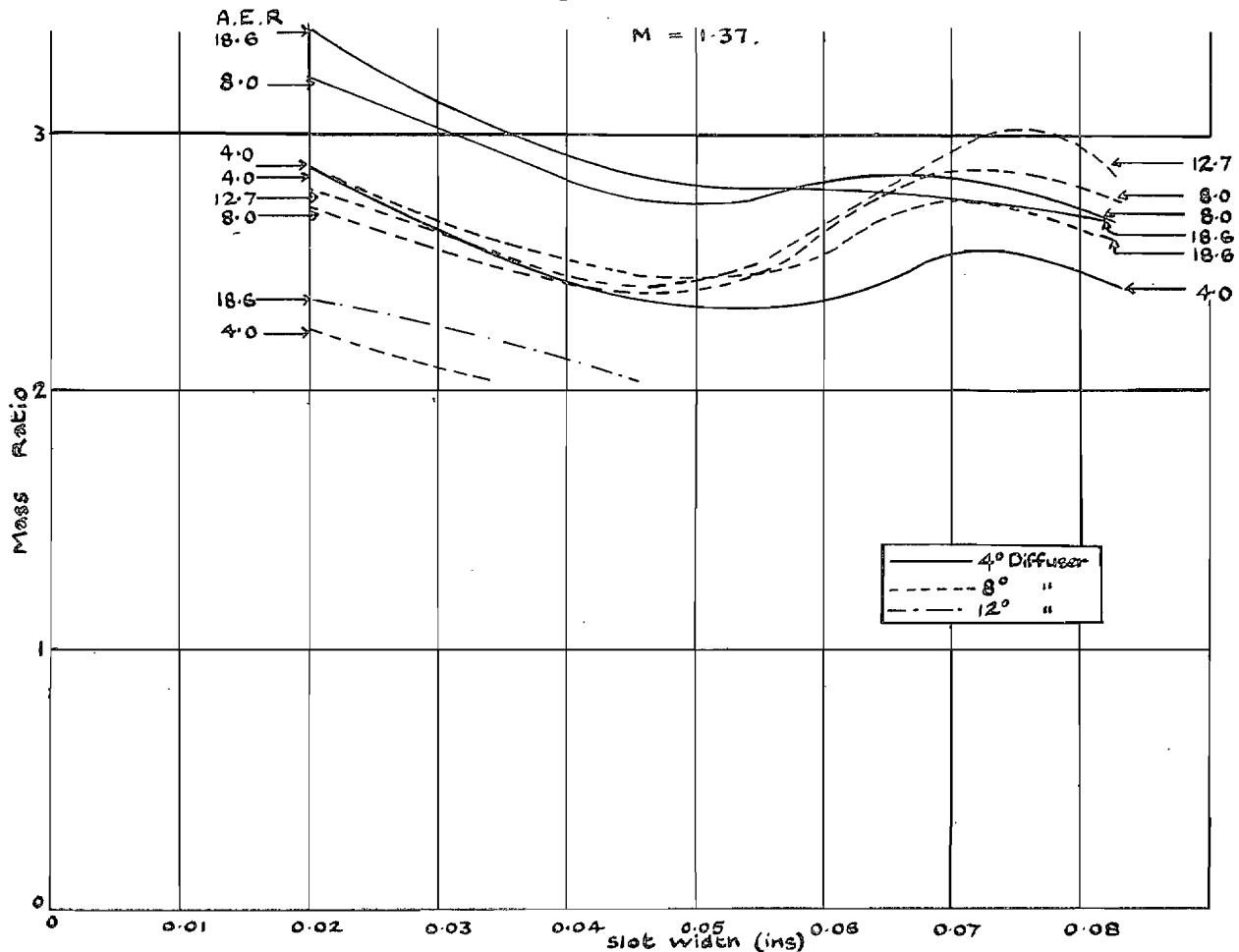


FIG. 24. Variation of mass ratio with slot width for diffusers of varying whole angle and area expansion ratio.

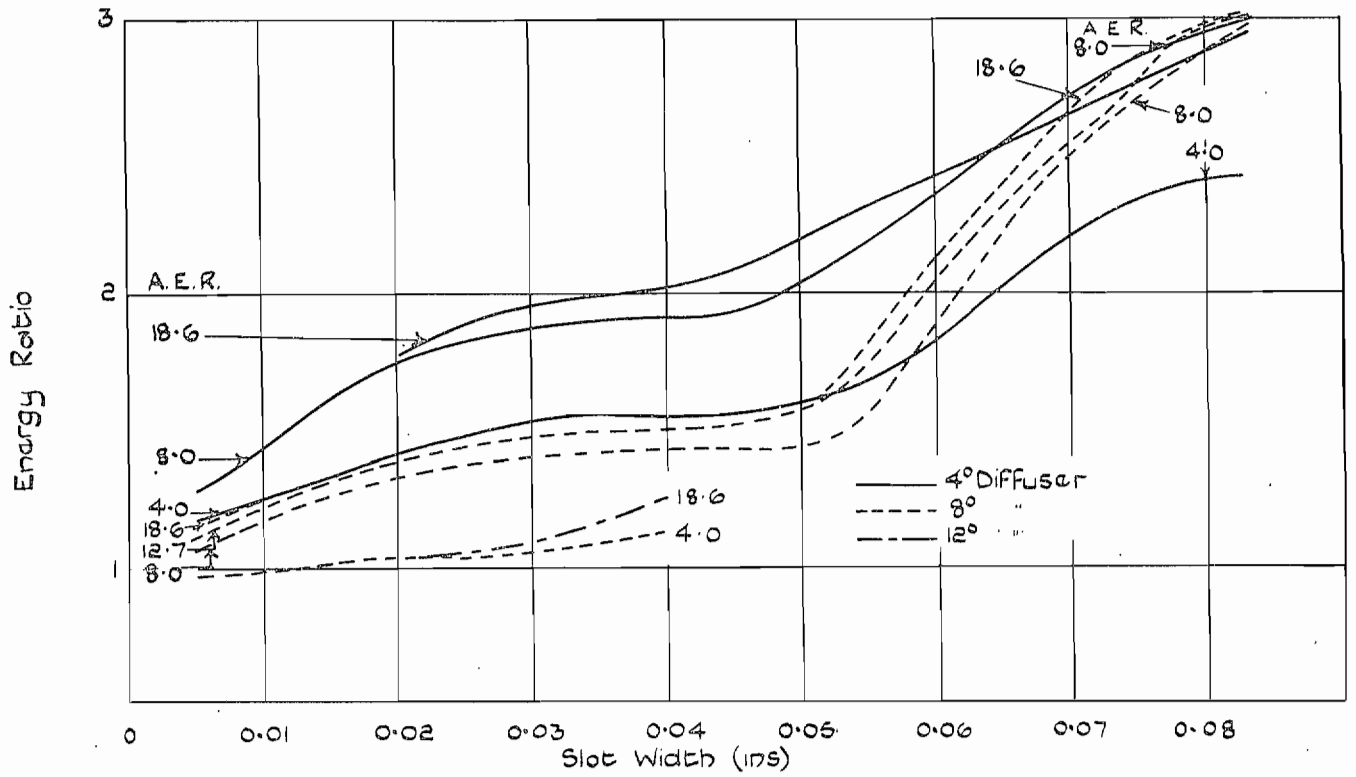


FIG. 25. Variation of energy ratio with slot width for diffusers of varying whole angle and area expansion ratio.
 $M = 1.37$.

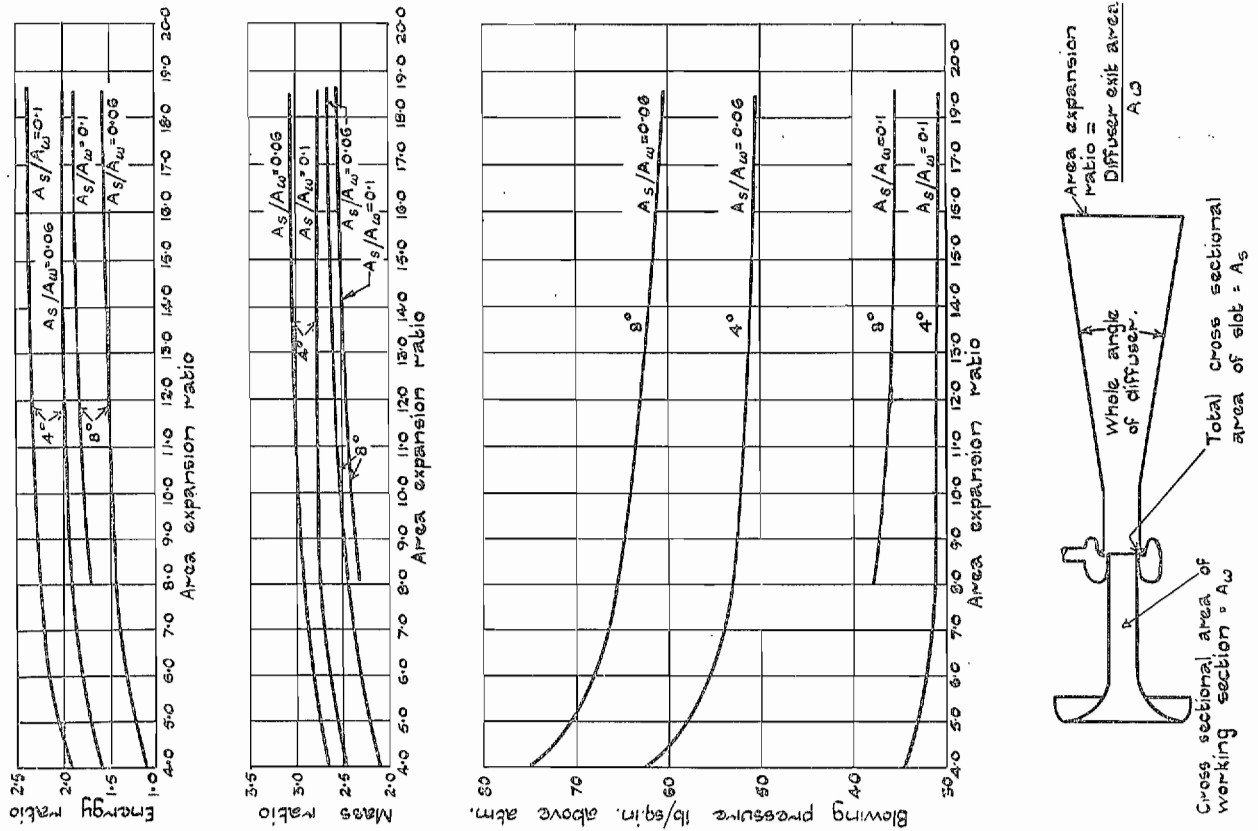


FIG. 26. Variation of efficiency with area expansion ratio and whole angle of diffuser. At working-section $M = 1.4$.

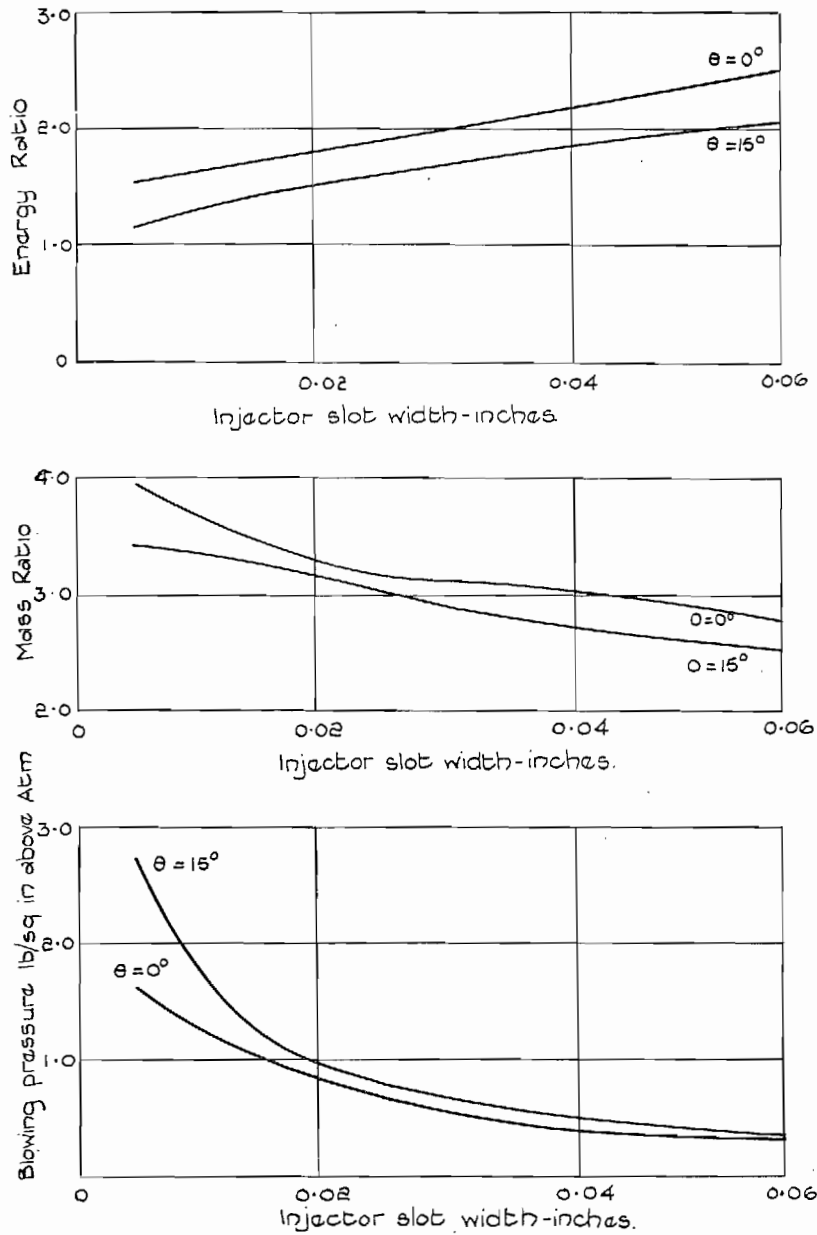


FIG. 27. Variation of energy and mass ratio and blowing pressure with injector-slot width and angle of injection. Working-section Mach number 1.37. ($2\frac{1}{4}$ -in. diameter tunnel; diffuser of 4 deg whole angle and exit area ratio 8.0.)

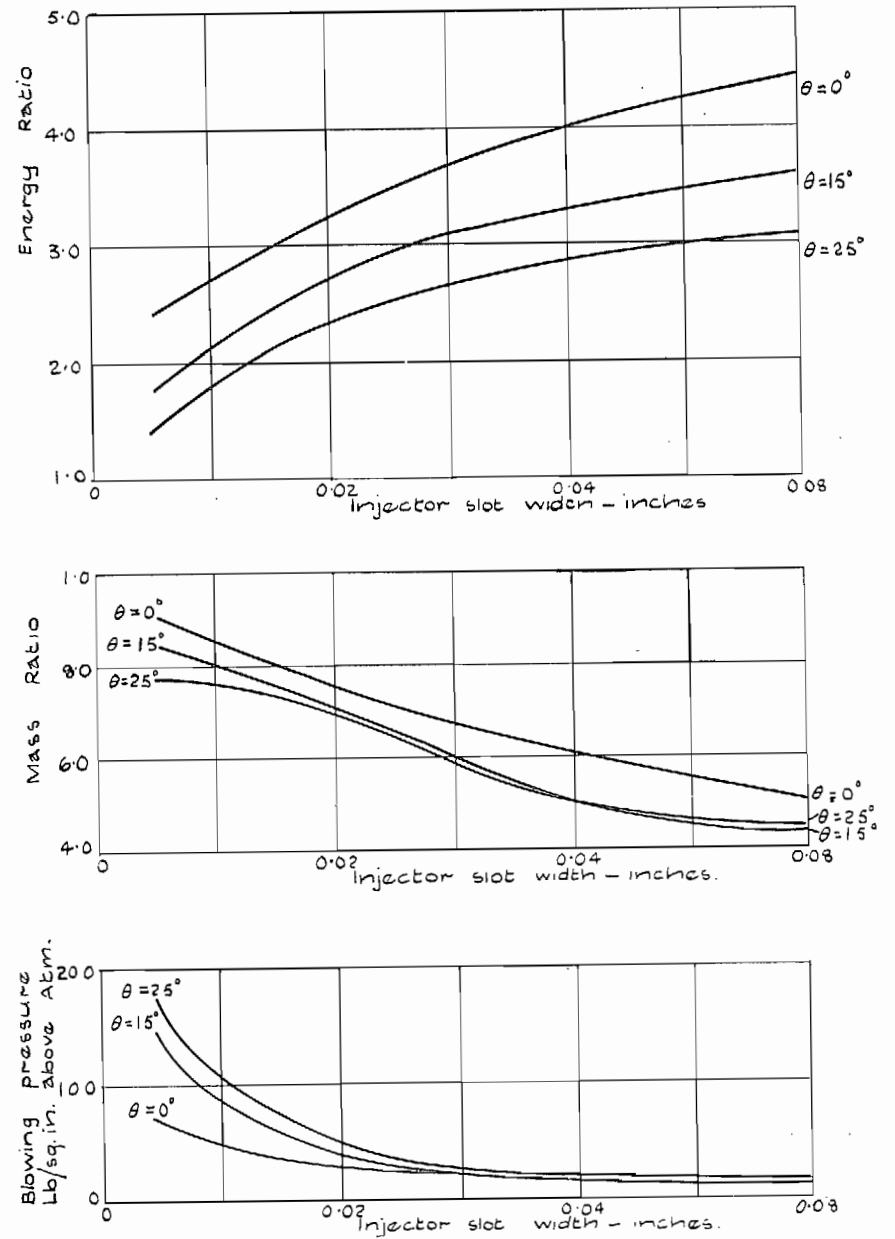


FIG. 28. Variation of energy and mass ratio and blowing pressure with injector-slot width and angle of injection. Working-section Mach number = 0.9. ($2\frac{1}{4}$ -in. diameter tunnel; diffuser of 4 deg whole angle and exit area ratio 8.0.)

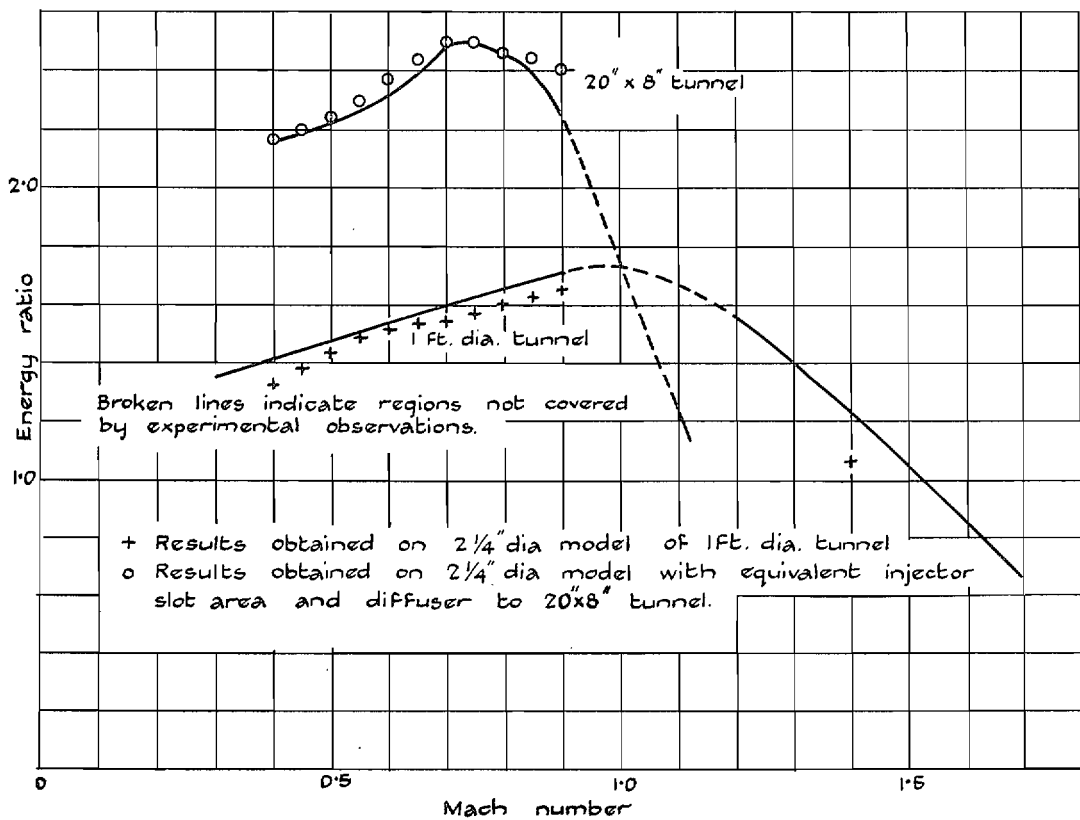
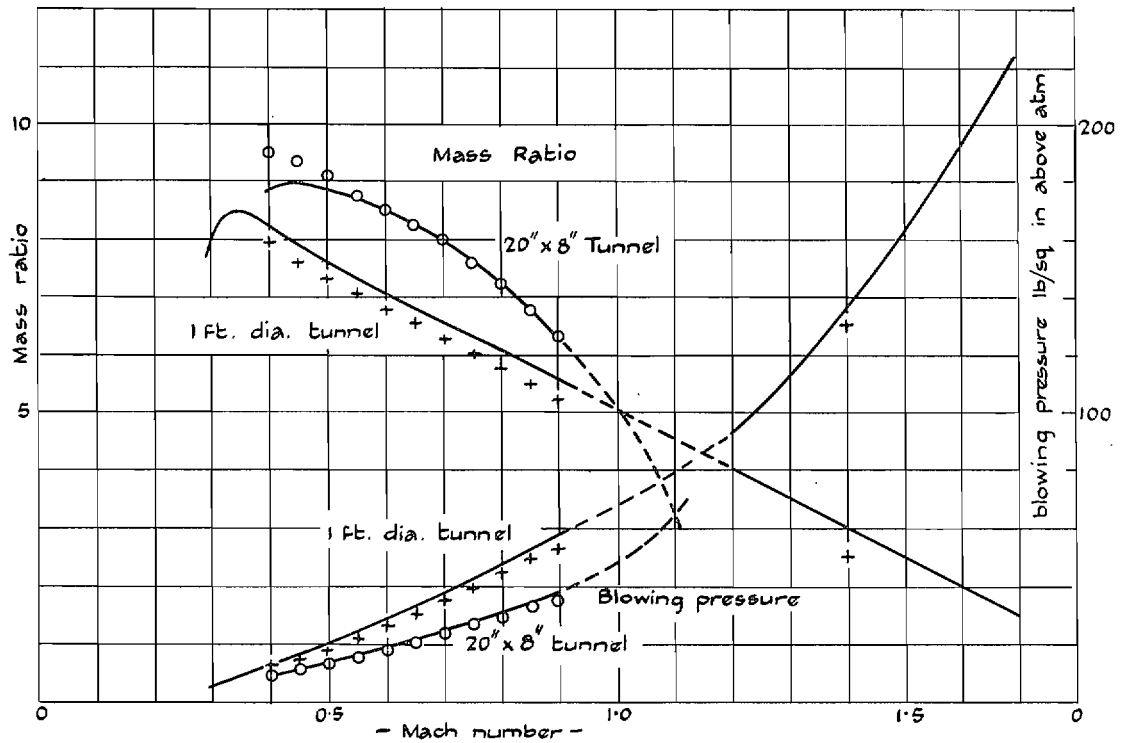


FIG. 29. Variation of blowing pressure and mass and energy ratios with working-section Mach number.

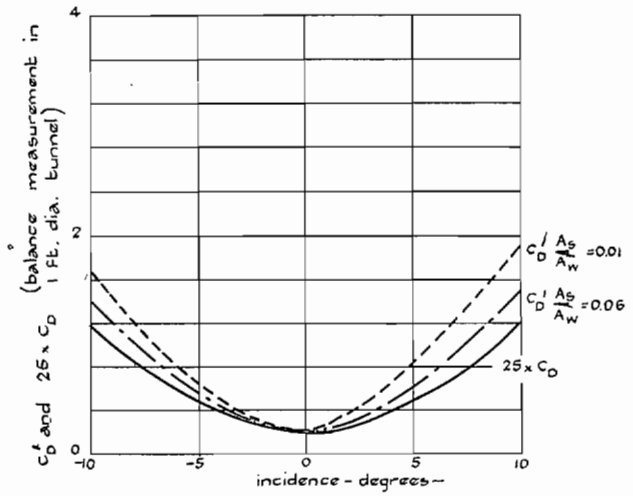
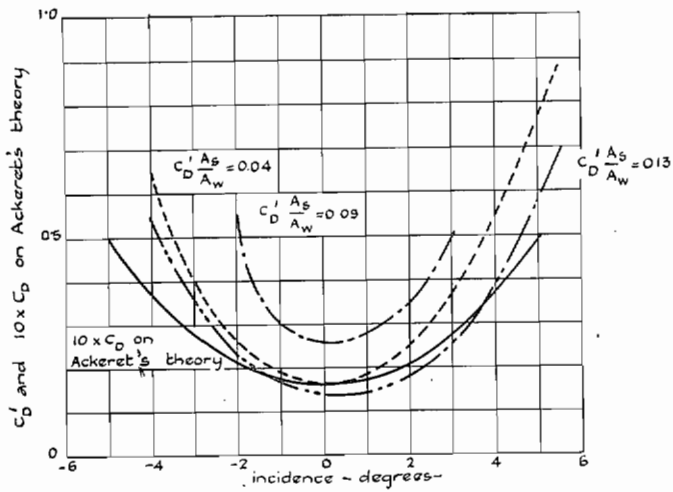


FIG. 30. Power absorption of aerofoil models of $\frac{\text{span}}{\text{chord}}$ ratio 6.5 completely spanning working section.

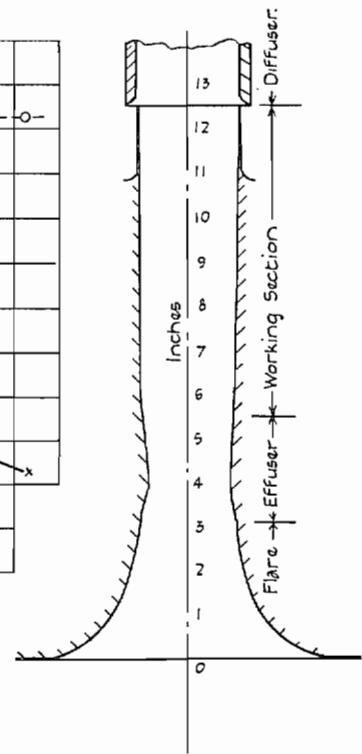
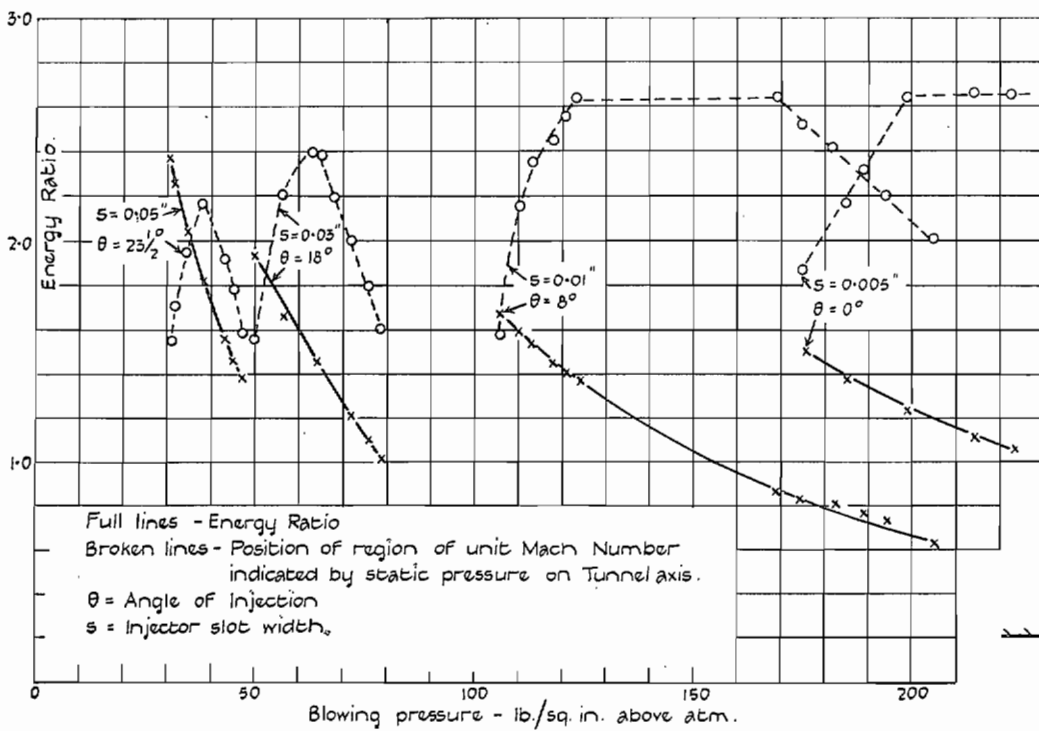


FIG. 31. Variation of shock-wave position and energy ratio with blowing pressure. $2\frac{1}{4}$ -in. tunnel. 4 deg diffuser of exit area ratio 8.0.

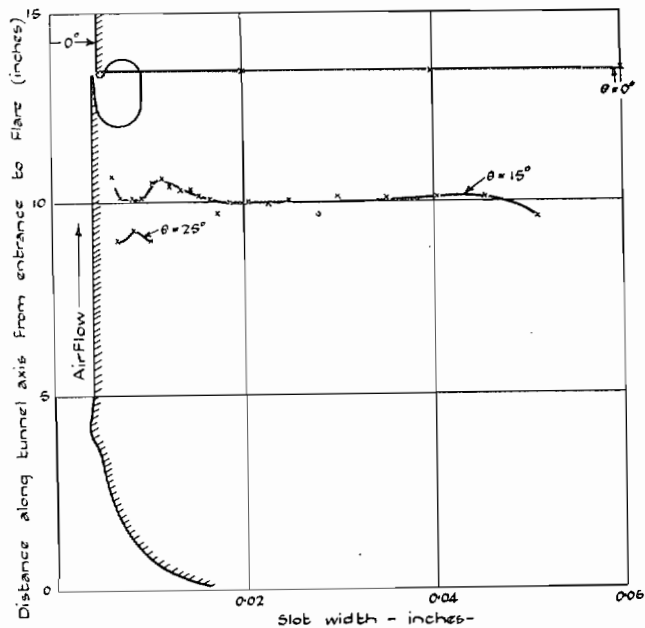


FIG. 32. Variation of most downstream position of tunnel shock-wave with injector slot width and angle of injection (4 deg diffuser preceded by short parallel portion.) $M = 1.4$.

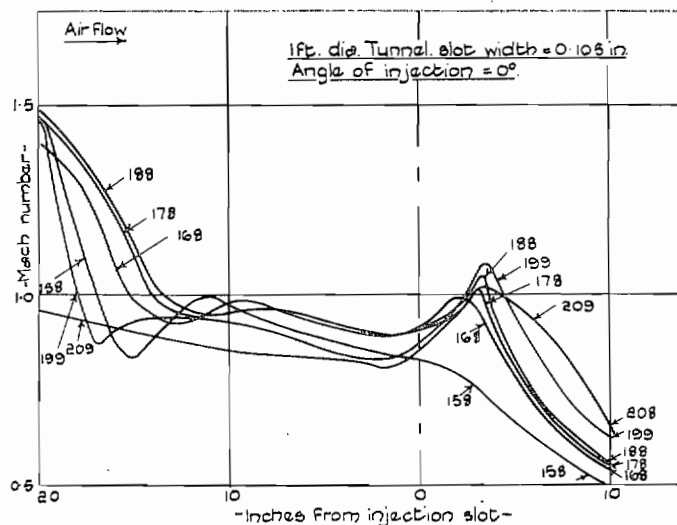
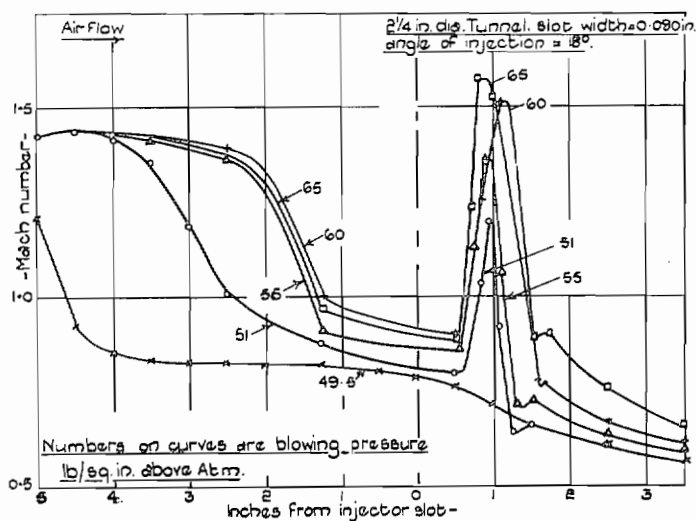


FIG. 33. Variation of Mach number in the region of the injector slot with changes of blowing pressure.

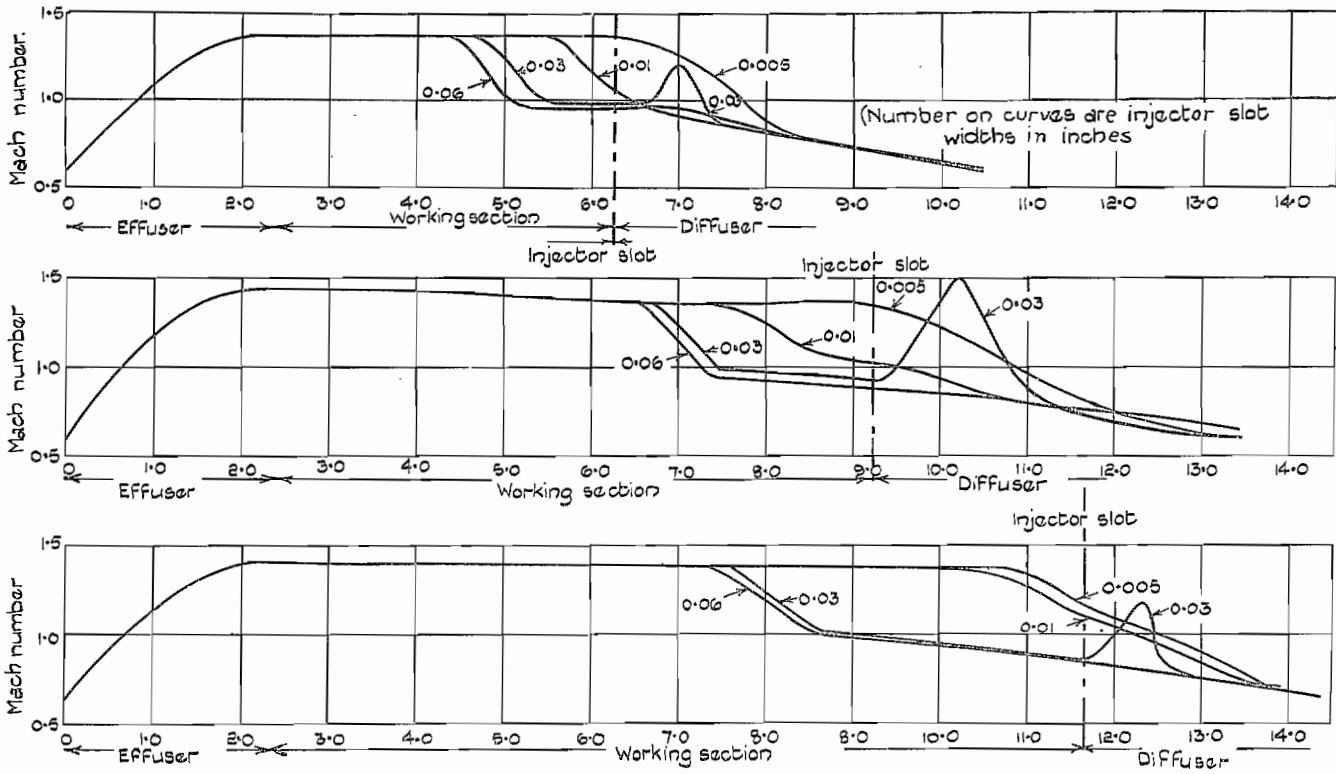


FIG. 34. Distance from upstream end of effuser—inches.

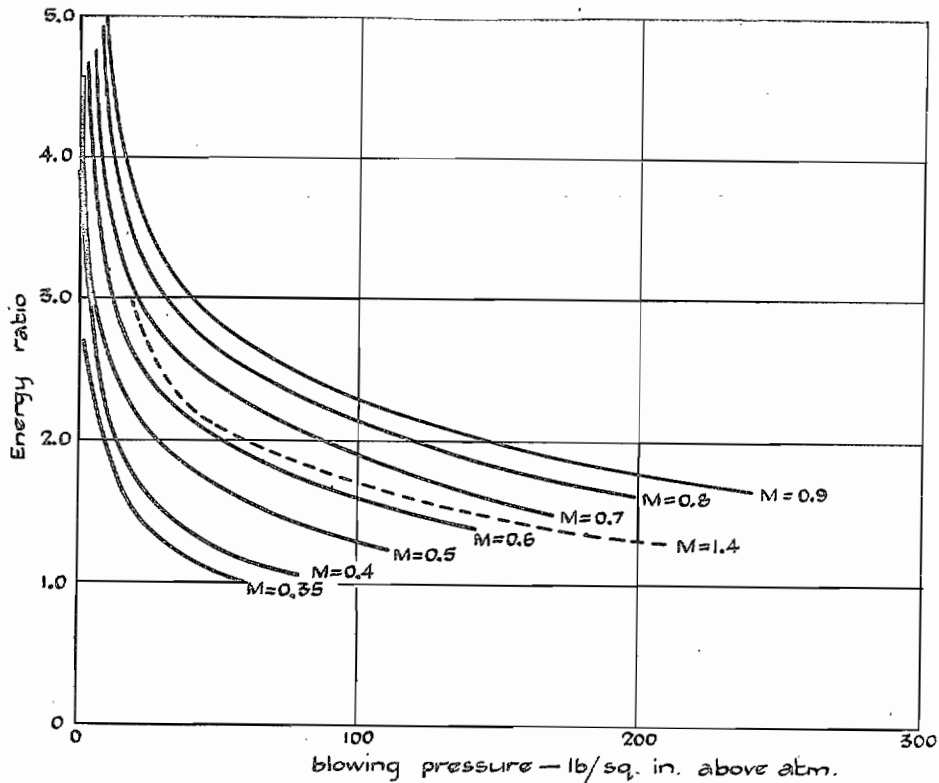


FIG. 35. Variation of energy ratio for direct operation with blowing pressure and working-section Mach number. (Stagnation pressure = 1 atm. Blowing pressure = compressor delivery pressure.)

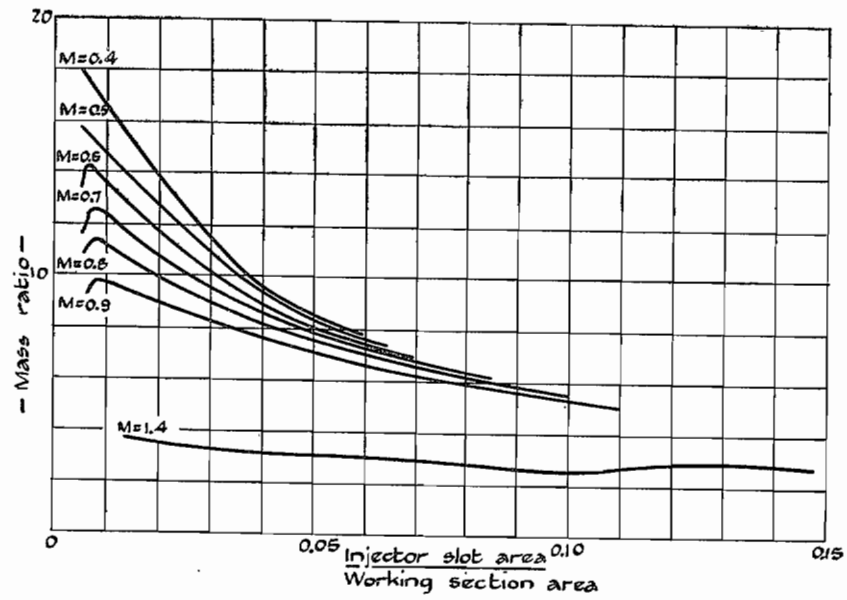
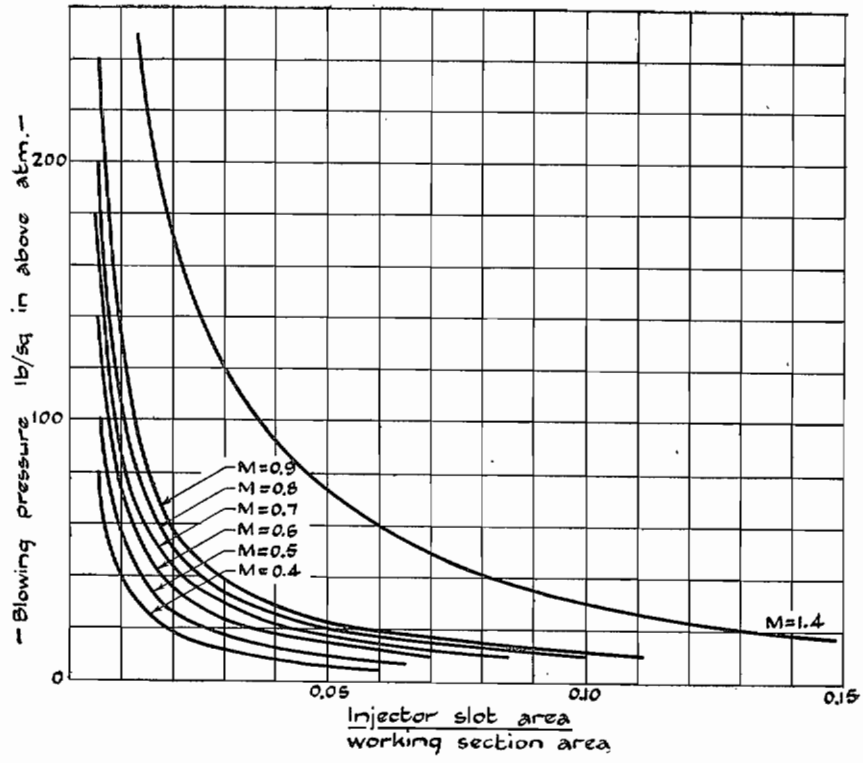


FIG. 36. Variation of mass ratio and blowing pressure with injector-slot area and working-section Mach number. Stagnation pressure = 1 atm.

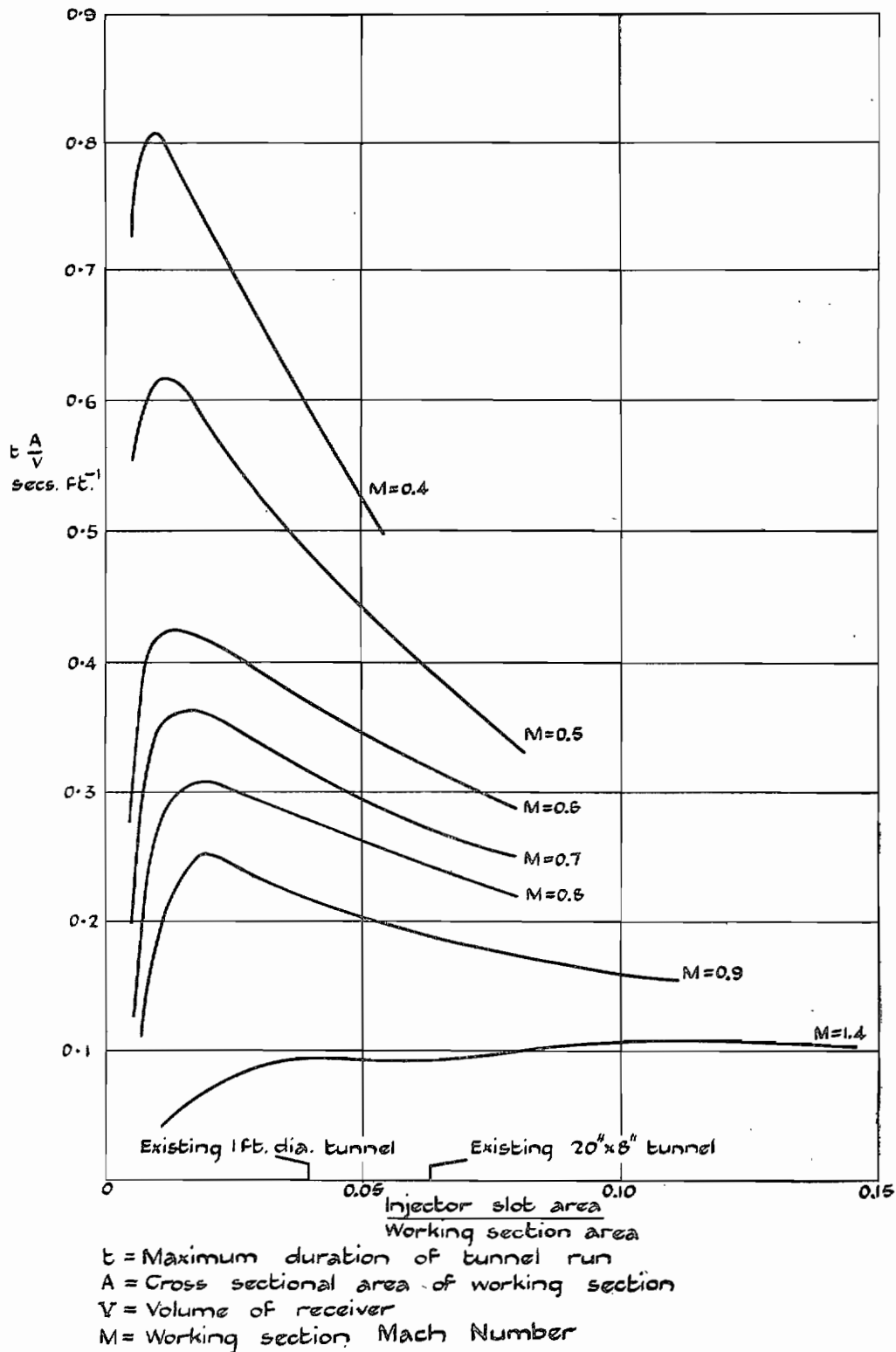


FIG. 37. Running time for 1 atm stagnation pressure. Valve regulation. (Receiver pressure at beginning of run = 350 lb/sq in. above atmosphere. Index of expansion $n = 1.2$.)

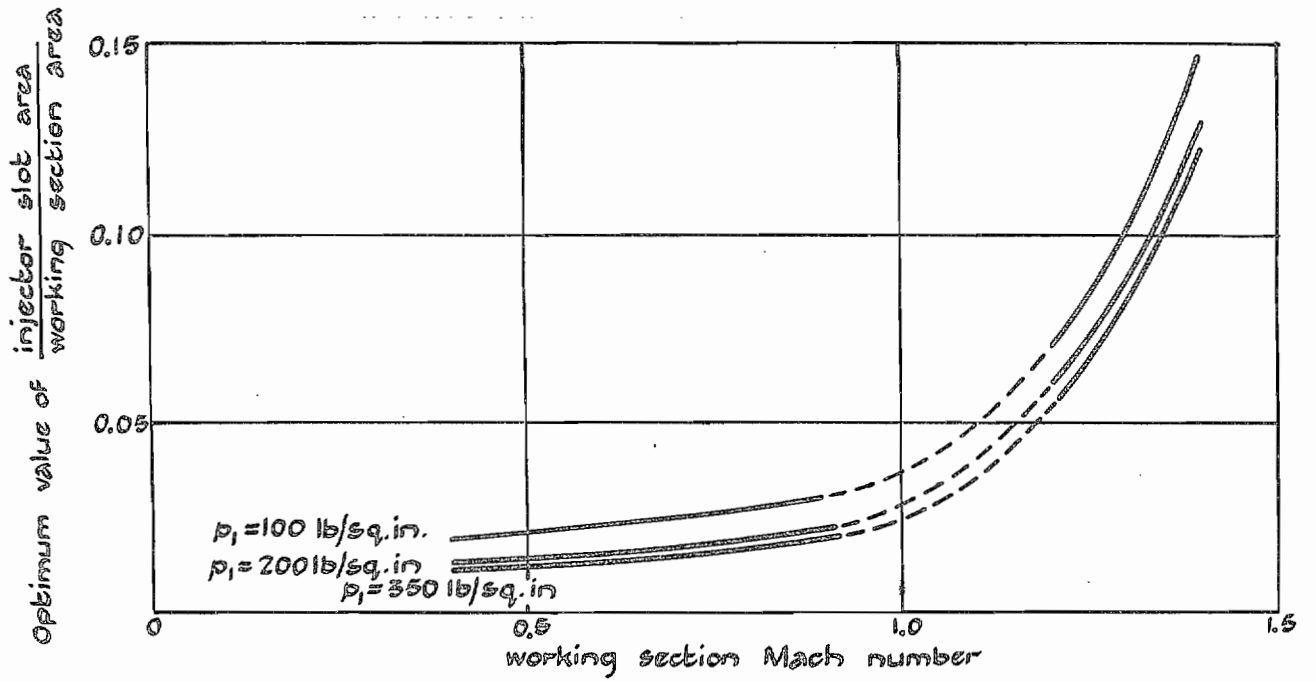


FIG. 38. Variation of optimum injector-slot area with working-section Mach number. 1 atm stagnation pressure. Valve regulation.

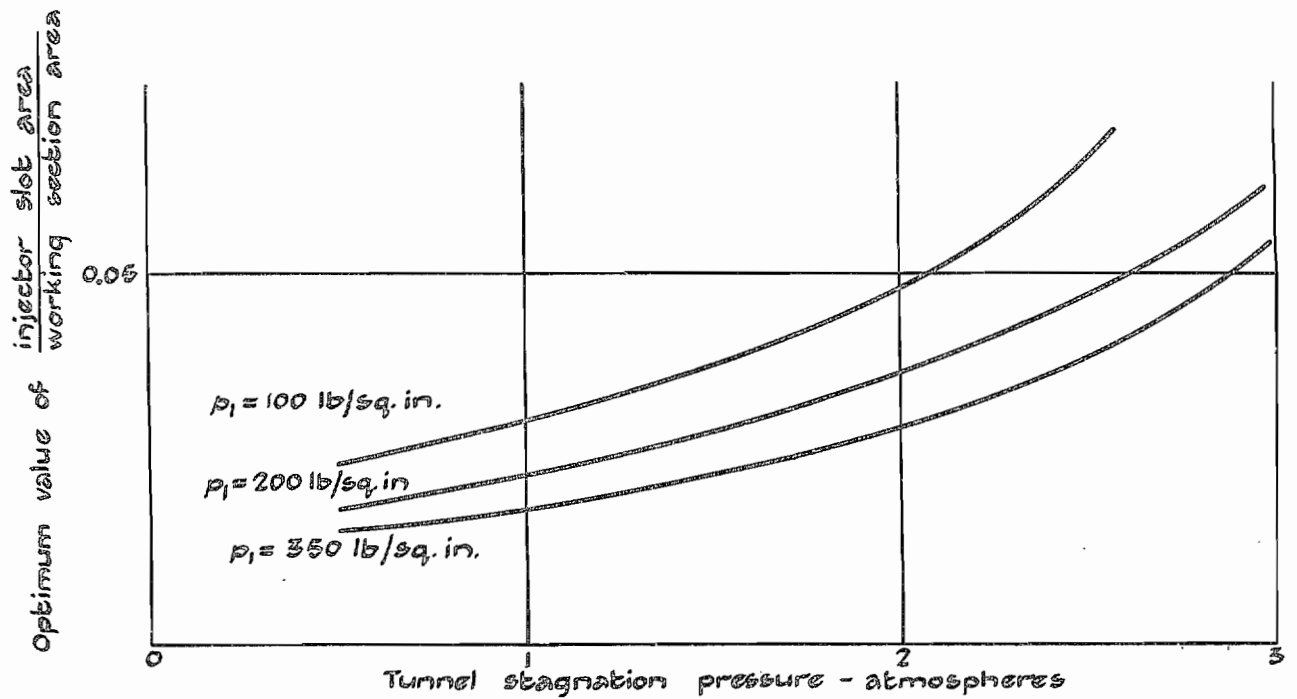


FIG. 39. Variation of optimum injector-slot area with tunnel stagnation pressure. Mach number 0.9. Valve regulation.

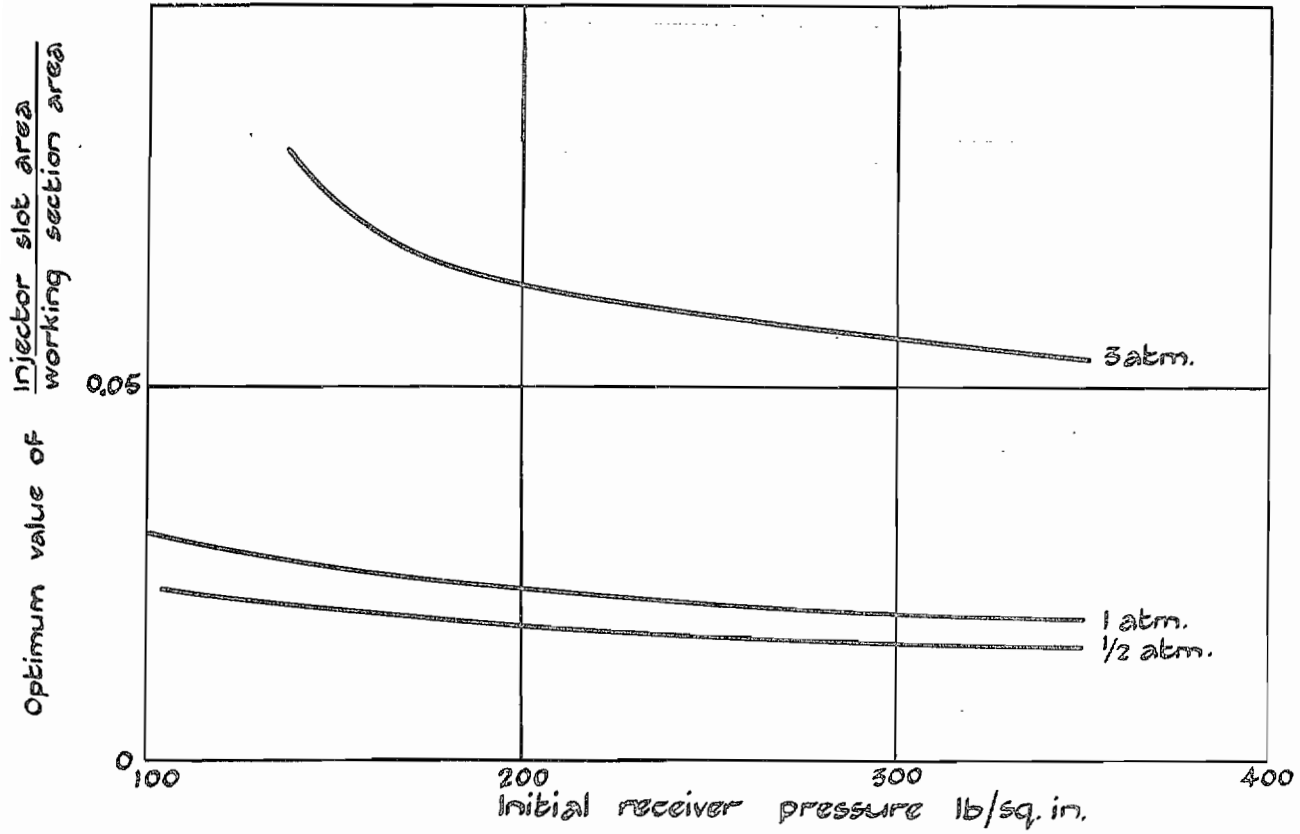


FIG. 40. Variation of optimum injector-slot area with receiver pressure at beginning of tunnel run. Mach number 0.9. Valve regulation.

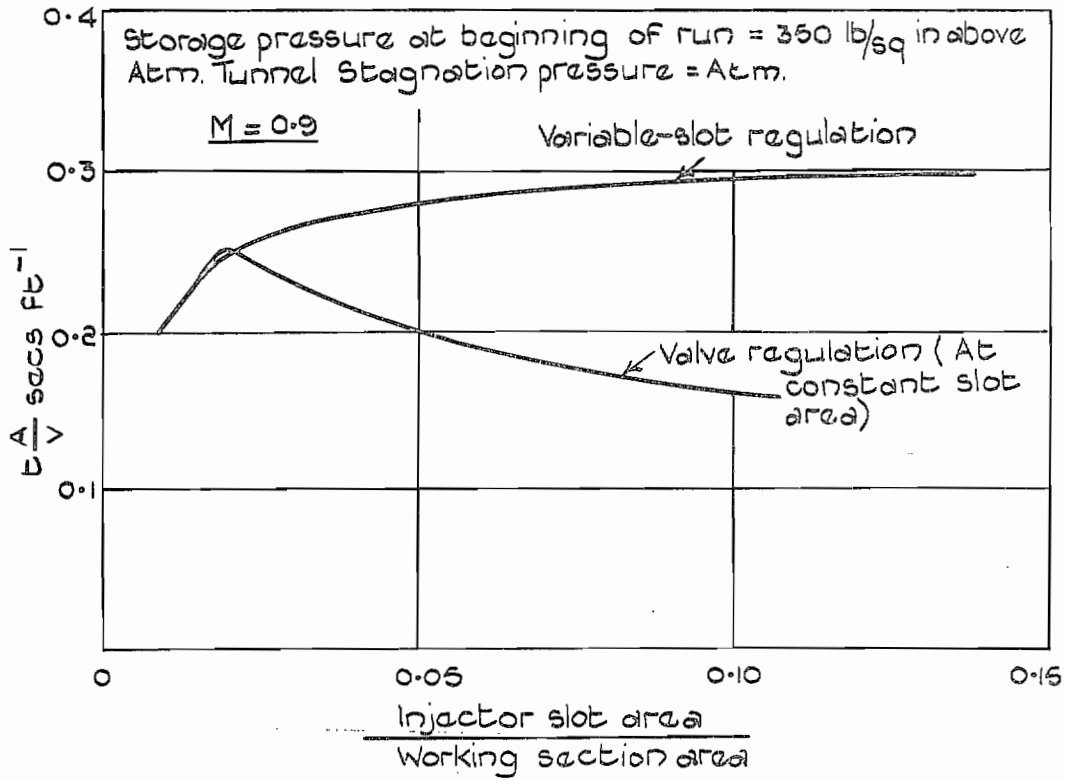


FIG. 41. Intercomparison of running times with valve and variable-slot regulation.

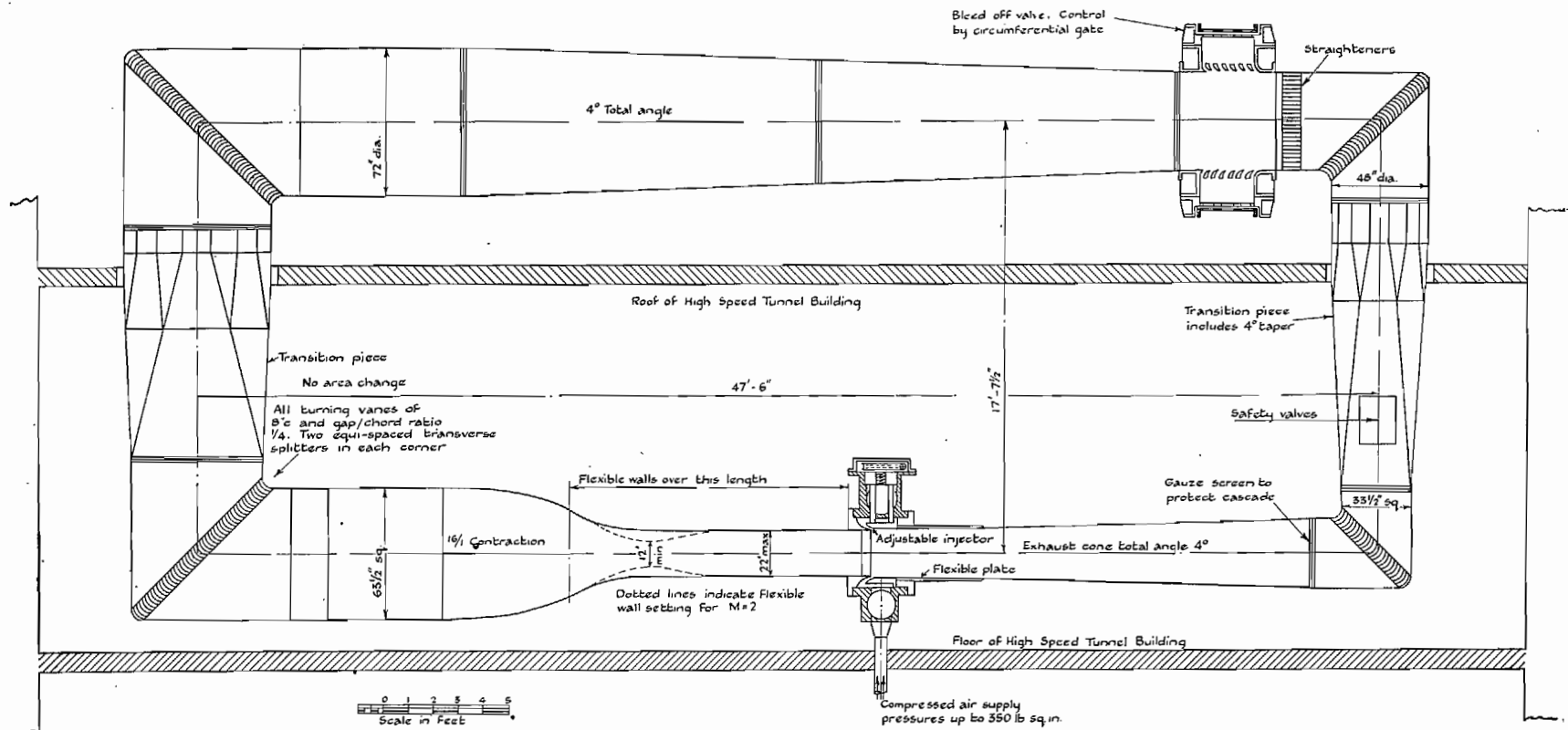


FIG. 42. General arrangement of 18 x 14-in. high-speed tunnel.

PART II

2.1. Introduction.—The experimental techniques which are used in high-speed tunnel work include adaptations of many of the standard methods of low-speed tunnel technique. Thus, the method of pressure plotting aerofoil models⁶⁷ by the use of small pressure holes distributed over the surface has been used extensively in the N.P.L. high-speed tunnels. The method of profile drag measurement by wake traverse⁶⁸ has also been used up to high subsonic Mach numbers, and it has been shown^{69, 70, 71} that for most models it is sufficient, even at these speeds, to measure the total head and static pressure distributions alone. A three-component electrical balance⁷² has been used to measure the lift, drag and pitching moment on two-dimensional aerofoil models and certain other bodies at both subsonic and supersonic speeds.

Many of the more common methods of flow visualization which are used in low-speed tunnels are not applicable to high-speed tunnel practice, but extensive use has been made at the N.P.L. and elsewhere of schlieren and direct-shadow techniques.

In high-speed tunnel tests the interference of supporting wires and struts^{73, 74} may be large and care is needed in the design of these components. Much of the work at the N.P.L. has been done with two-dimensional aerofoil models completely spanning the tunnel between the walls. In this case the support interference arises from the decay of the circulation in the boundary layers of the tunnels walls⁷⁵ and from the spread of turbulence from the wall boundary layers by transverse contamination^{78, 90}. These effects are, however, in most cases small. Some tests have, however, been made on three-dimensional bodies supported on the tunnel axis, and in this case the method of support has usually been by a sting protruding from the base of the model. For this type of support, special methods have been developed for the measurement of the aerodynamic forces and moments. Normal force and moments have been measured by the use of electrical strain gauges^{76, 77} of the resistance type, and drag by a mechanical balance.

Pitot and static tubes have been used extensively for flow exploration, and some use has also been made of yawmeters of several different types. At supersonic speeds explorations have also been made by the observation of the inclination of the bow-waves of cones and wedges of known apex angle.

Several methods have been developed⁷⁸ for the indication of the transition position on the surfaces of aerofoil models at high subsonic speeds. The conventional methods of fixing transition appear to involve difficulties at high speeds, but a satisfactory method has been developed⁷⁹ and involves the introduction of minute quantities of air into the boundary layer from a spanwise row of small surface holes.

Measurements of the temperature distribution over the surfaces of a model aerofoil⁸⁶ and other bodies⁸⁵ have been made by the use of thermo-junctions buried in the model surfaces. An instrument for the measurement of stagnation temperature has been developed, and has been used to explore the wakes of aerofoil models.

Turbulence measurements with spheres⁸⁰ have been made in the high-speed tunnels at low speeds, but the measurements cannot be extended to higher speeds because of the early shock-stall of the sphere. It has so far proved impossible to develop any method for the quantitative measurement of turbulence at high speeds.

2.2. Regulation of Tunnel Speed.—If useful results are to be obtained with a wind tunnel it must be possible to maintain constant conditions at the working section for a period which is sufficiently long to enable the flow pattern and the readings of the measuring instruments to become steady, and to enable a record of the required observations to be made. If tests are to be made at a number of different speeds, moreover, the method of speed regulation must be capable of covering this range.

The problem is complicated in the N.P.L. installation by the continuous fall of the pressure in the storage reservoirs which takes place as either of the two larger tunnels is operated. Thus, in general, it is necessary to adjust the speed regulating device continuously whilst the tunnel is running to compensate for the fall of storage pressure.

2.2.1. Regulation at Constant Injector-Slot Area.—In Part I⁸¹ it has been indicated that with a constant injector-slot area the working-section Mach number may be varied up to a certain maximum (less than unity) by an adjustment of the blowing pressure. If constant conditions are to be maintained in the working section, therefore, it is necessary to maintain the blowing pressure* at a constant value.

This method of regulation is normally used at the N.P.L. where a throttle valve is placed between the storage reservoir and the tunnel pressure chamber. The valve is initially opened until the required working-section conditions are attained, and then further continuously opened to maintain a constant blowing pressure as the storage pressure falls. The tunnel run ends when the storage pressure has fallen to the blowing pressure.

2.2.2. Regulation by a Variation of the Injector-Slot Area.—This method is not used at present, but since it is more efficient than the method described above it is proposed to adopt it for the new 18 × 14-in. tunnel⁴⁹. The storage reservoirs and tunnel pressure chamber are connected without an intermediate throttle so that the blowing pressure is always approximately equal to the storage pressure, and the area of the injector slot is then increased continuously during the tunnel run to compensate for the falling storage pressure.

2.2.3. Regulation by a Throat Downstream of the Working Section.—If sonic speed is reached across a section of the tunnel at the downstream end of the working section, the conditions at the working section will not be influenced by changes of the flow pattern downstream of the region of sonic speed. In particular, the conditions at the working section will not be influenced by variations of the injection provided that the region of sonic speed is maintained. By a variation of the cross-sectional area of the tunnel at the sonic region, the mass flow and Mach number at the working section may be varied over a wide range up to a maximum value which occurs when the tunnel chokes elsewhere. Moreover, the mass flow calculated from a knowledge of the cross-sectional area of the tunnel at the sonic region provides a convenient check on the working-section Mach number as deduced from a pressure measurement at some point upstream of the model.

Thus, provided that the power input to the tunnel is sufficient to produce the region of sonic speed, fluctuations of the power can have no influence on the flow at the working section. Moreover, transient disturbances^{82, 83, 84} originating in the region of the injector and in the diffuser cannot be propagated upstream into the working section† unless they pass through the subsonic boundary layers of the tunnel walls or through the wake of the model placed in the working section.

The 20 × 8-in. tunnel at the N.P.L. is fitted with an adjustable throat of the type described above and this has been used to regulate the working-section Mach number. In practice a region of supersonic velocity terminating in a shock-wave is formed in the diverging channel downstream of the throat and it is found that regulation by this method leads to an appreciable wastage of power. Although there is now evidence^{82, 83, 84} that the influence of disturbances from downstream of the working section may be considerable, experiments have shown that in the 20 × 8-in. tunnel the pressure distributions on model aerofoils measured with and without the throat in operation are in excellent agreement‡. Thus, in general, the throat of the 20 × 8-in. tunnel is not used in routine experiments, and the method of regulation is that described in section 2.2.1.

* In practice small adjustments of the blowing pressure are necessary during a tunnel run to compensate for the fall of stagnation temperature which accompanies the expansion from the receivers.

† Since such disturbances may be of finite amplitude it is strictly necessary that a region of supersonic velocity shall exist, at the downstream end of the working section. As described above, however, in practice such a region is always present when a throat is used.

‡ There is evidence that in many cases the injection of inducing air forms an effective throat before mixing takes place. Since the velocity of the inducing air immediately downstream of the injector slot is supersonic in most cases, and the induced air is accelerated to a supersonic velocity by the effective throat formed by the inducing air, it is possible that the propagation of disturbances from downstream of the injector into the working section is prevented.

2.2.4. *Regulation at Supersonic Speeds.*—If a convergent-divergent effuser is fitted at the upstream end of the working section and a supersonic velocity is produced, variations of the power input to the tunnel only produce variations in the position and amplitude of the breakdown or tunnel shock-wave which defines the downstream limit of the supersonic region. Either of the methods in Section 2.2.1 and 2.2.2 may be used to regulate the tunnel speed and, provided that the blowing pressure is large enough to maintain the position of the tunnel shock-wave well downstream of the model under test, small fluctuations of this pressure are found to be unimportant.

2.3. *Measurement of the Tunnel Speed.*—If the acceleration of the air from rest at the tunnel intake up to the working section is isentropic, the ratio of the total head at the intake to the static pressure at the working section is an explicit function of the working-section Mach number. Assuming that the air behaves as a perfect gas with constant specific heats, the ratio of the local static pressure p to the total head H will be related to the local Mach number by the equation²⁷

$$\frac{p}{H} = \left(\frac{2}{2 + (\gamma - 1)M^2} \right)^{\gamma/(\gamma-1)}, \quad \dots \quad \dots \quad \dots \quad \dots \quad (1)$$

where M is the Mach number and γ the ratio of the specific heats at constant pressure and volume. For $\gamma = 1.40$ equation becomes

$$\frac{p}{H} = \left(\frac{5}{5 + M^2} \right)^{7/2} \quad \dots \quad \dots \quad \dots \quad \dots \quad (2)$$

There appears to be some uncertainty as to the value of γ for dry air at the temperatures occurring in high-speed tunnels. A value of 1.40 seems, however, to be a reasonable average of the values that have been suggested and leads to a considerable simplification of the equations. This value has, therefore, been used at the N.P.L. and R.A.E., but different values are used elsewhere in this country and abroad.

It is difficult to measure the pressure ratio of equation (2) directly and it is, therefore, more usual to measure the pressure difference $(H - p)$ and the value of H as a small difference from the barometric pressure. In the past the method of measuring $(H - p)$ was by a mercury manometer (Fig. 1) the pressure of the air at rest at the intake (H) being connected to one side, and the working-section static pressure (p) to the other. Thus, a visual observation of the quantity $(H - p)$ was obtained and read on a scale graduated in inches and tenths behind the mercury column. It was extremely difficult with this method to maintain an exact subsonic Mach number at the working section since the corresponding height of the mercury column often involved odd hundredths of an inch and varied with barometric pressure. Thus, the need for some mechanical device enabling a given Mach number to be maintained easily was apparent, and the N.P.L. Mach number gauge⁸⁵ was constructed.

The Mach number is a function of the ratio $(H - p)/H$ and thus, for constant Mach number

$$(H - p) \propto H \quad \dots \quad \dots \quad \dots \quad \dots \quad (3)$$

Since the pressure at the intake to the tunnel depends entirely* on the barometric pressure H_0 , equation may be written

$$(H - p) \propto H_0 \quad \dots \quad \dots \quad \dots \quad \dots \quad (4)$$

The Mach number gauge (Fig. 2) develops the mechanics of this statement. It consists of a manometric balance with a beam freely supported on two points, one located in a cup and the other transversely only in a groove. Two copper bellows with sealed ends, thus forming pressure capsules, are fixed on either side of the beam to a baseplate which forms the earth for the suspension unit. The free end of each capsule is connected to the balance beam by a shackle through a point and cup suspension giving a frictionless force transfer from the capsule to the beam. The earthed end of each capsule is drilled and fitted with a nipple. One nipple is connected to the tunnel intake pressure (H) and the other to the working-section static pressure (p).

* Strictly the scale pan should be adjusted to a position which is dependent on the total head at the intake and not the barometric pressure. The difference between these two quantities is usually small and is due to the loss of total head incurred on passage through the intake gauze screens. It is usual at the N.P.L. to measure this pressure drop on a water manometer during a preliminary tunnel run before the Machmeter is finally adjusted.

The centres at which the forces are transferred from the pressure capsules to the balance beam are adjusted until there is no change of moment about the point of suspension with change of an equal pressure applied to each capsule. Thus there is no change of zero with pressure change. The initial tension of the capsules is adjusted to a minimum so that the extra stability thus introduced is as small as possible.

If L is the distance of each capsule from the point of the beam suspension, a moment is exerted on the beam proportional to $(H - \phi)L$. This amount is balanced by a weight W , different for each Mach number, placed on a scale pan at distance R from the point of suspension thus, omitting the constant introduced for the area of the capsules,

$$(H - \phi)L = WR \dots \dots \dots (5)$$

If the Mach number is constant equation (5) then shows that, for a constant value of L ,

$$WR \propto H_0 \dots \dots \dots (6)$$

If, therefore, W is to be constant for each Mach number, R must vary as the barometric pressure H_0 . The scale-pan leverage is adjustable; the pan being suspended from a point fixed to a block which may be traversed along the beam by a screwed shaft rotated by a micrometer calibrated in terms of the barometric pressure. A balance-block of weight equal to that of the scale pan is traversed by the same shaft in the opposite direction to compensate for the change of moment of the scale-pan weight.

A small secondary beam attached to the main beam carries a rider which enables Mach numbers between the values corresponding to the set of weights to be obtained. The rider beam is of hexagonal section and may be rotated so that any face is uppermost. Each face carries a scale which applies to a different barometric pressure, and the rider beam must be rotated until the scale most appropriate to the ambient barometric pressure is visible before the rider is set. This method of using the rider is possible over the Mach number range 0.4 to 0.9 since in this range the relationship between $(H - \phi)$ and M is approximately linear. At lower Mach numbers a calibration curve is used.

An electrical indicator ⁸⁶ of the type used on many N.P.L. balances is mounted on the balance beam to indicate when balance is achieved. The indicator is connected to a dynamometer ammeter which gives a null reading when the beam is balanced as shown in Fig. 3. Damping is effected by an oil dashpot at one end of the beam, and a clamp is provided at the other end for locking the beam in a neutral position when not in use.

Thus, with the scale-pan position set to the correct position for the barometric pressure* and the appropriate Mach-number weight on the scale pan, the tunnel speed is manually regulated to maintain a null reading on the indicator scale. This procedure is only possible at subsonic Mach numbers below the choking value. When an effuser is fitted for supersonic operation the effuser geometry determines the working-section Mach number which is then measured by a mercury manometer, or by observations of the inclination of the bow-wave of a wedge or cone.

2.4. Direct Force Measurement.—For two-dimensional tests, particularly on aerofoil models, the method of direct force measurement by a balance is less valuable than indirect methods involving pressure plotting and wake traverses, since these latter methods give a clearer insight into the mechanism which results in a change of overall force. Apart from some early work, therefore, indirect force measurement has been used recently more extensively at the N.P.L. for two-dimensional subsonic aerofoil tests than have direct (balance) methods.

At supersonic speeds, however, owing to the necessarily small model chord, little pressure plotting has been done, and the wake-traverse method has not been used at all. In such tests balances have been used almost exclusively for force measurement. The original 1-ft diameter tunnel was fitted with a three-component electric balance of design similar to that used in the

* See footnote on previous page.

C.A.T.⁸⁸ This balance is designed to measure lift drag and pitching moment on 2-in. chord models of 12-in. span, and has, during the last ten years, been used extensively for this purpose. For three-dimensional models, particularly models including bodies in the form of solids of revolution, indirect methods of force measurement are laborious and, in general, balance tests are essential. For this purpose both the original three-component balance and specially designed strain-gauge⁷⁶ and drag balances have been used in the 1-ft diameter tunnel.

2.4.1. *The Three-Component Electrical Balance* (Fig. 4).—This balance⁷² is used with two-dimensional aerofoil models in the 1-ft diameter tunnel. In order that leakage should not take place from the atmosphere to the low pressure region in the working section along the ends of the aerofoil it was essential to design a balance which could be enclosed and operated in a chamber which could be completely isolated from the atmosphere. An electrically operated balance similar in principle to that used in the Compressed Air Tunnel⁸⁸ was, therefore, designed and constructed.

In principle the balance is a device for measuring the moment of the aerodynamic forces experienced by the aerofoil about each of three axes parallel to the span. From these three measurements it is possible to deduce the lift, drag and pitching moment of the aerofoil. The aerofoil C passes through the walls of the working section and is clamped outside the tunnel to two end blocks. The end blocks are arranged so that there is no discontinuity of the tunnel walls at the ends of the aerofoil, and can rotate with the aerofoil model with a radial clearance of 0.030 in. from the rigid tunnel walls. When measurements are being made the aerofoil and end blocks are rigidly attached to the main swinging member of the balance which lies in a plane roughly normal to the aerofoil chord. The swinging member is suspended on six strips of spring steel (D), under high tension, three on each side of the tunnel, arranged at intervals of 120 deg to the axis of suspension. A coil (E) is attached to the end of the swinging member with its axis vertical and is arranged to float between two similar coils (F) and (G) which are rigidly attached to the main tunnel structure. Balance weights for the coil are attached to the swinging member on the opposite side of the axis of suspension to the coil. An oil dash-pot (H) for damping, an electrical stability device, and an indicator⁸⁶ for the position of the swinging member are attached to the opposite end of the swinging member to that of the coil.

The position of the axis of suspension may be given three alternative positions, two in the plane of the aerofoil (lift and moment axes), and a third (drag axis) at some distance from this plane. The axis position is adjusted by removing the four suspension bolts (A), adjusting the position of the member (B), and reinserting bolts of different length. The third axis is obtained by replacing the suspension bolts at alternative positions in the swinging frame.

The incidence may be adjusted when the tunnel is not running by rotating the incidence horseshoe (J) on engaging a dog clutch. The aerofoil is rigidly attached to the incidence horseshoe which, except during incidence changing, is rigidly attached to the main swinging member. To maintain a constant centre of gravity position of the swinging member with variations of the incidence horseshoe position, a cam (K), attached to the horseshoe, moves a jockey weight (I) along one arm of the swinging member.

The electrical contacts from the floating coil are carried from the swinging member through mercury cup contacts arranged close to the suspension axis. A direct current is passed through the two fixed coils and the floating coil (in the opposite direction). By a variation of the magnitude of this current the aerodynamic forces experienced by the aerofoil may be compensated, and the swinging member balanced (balance being indicated by the electrical indicator). A measurement of the magnitude of the current is then used to deduce the moment of the aerodynamic force about the suspension axis. Three such measurements about the three axes enable lift, drag and pitching moment to be deduced. The direction of the electromagnetic balancing force may be reversed by reversing the direction of the current in the two fixed coils.

2.4.2. *Strain-Gauge Balance*.—A limited number of tests have been made in the 1-ft diameter tunnel on bodies in the form of solids of revolution located on the tunnel axis. In some of these tests the body has been supported at the centre of an aerofoil, and the aerodynamic forces

measured with the three-component electric balance. In view of the interference between the body and the aerofoil support, however, a more usual method of support, particularly for supersonic tests, has been by a sting, projecting from the rear of the body and held downstream. With this method of support attempts have been made to measure the drag with the drag balance described in section 2.3.3. Measurements of normal force and moment have been made by the use of electrical strain gauges of the resistance type⁷⁷ attached to the supporting sting. The development of this latter technique has been described by Wingham in R. & M. 2316⁷⁶.

The test model is hollow and is attached to the sting at the nose. The sting passes up through the model and projects from the rear downstream of which it is supported through a variable-incidence knuckle to an axial member rigidly attached to the tunnel. Strain-gauges are attached to the sting within the model and are used to measure the distortion of the sting produced by the aerodynamic forces experienced by the model. From a knowledge of the geometry of the assembly, the elastic properties and cross-section of the sting, and measurements of the distortion of the sting, the position and magnitude of the normal aerodynamic force on the model may be calculated.

The wire strain-gauges used are of the N.P.L. type in which the resistance element is wound in the form of a flattened coil and then bonded with phenol formaldehyde resin impregnated paper. The gauges are cemented to the sting with 'Durafix' and, after baking, a coat of resin is applied as a protection against moisture. The unstrained gauge resistance is 500 ohms.

The electrical circuit finally developed involved mounting eight strain-gauges on the sting (Fig. 5). The gauges formed two complete Wheatstone bridges G_1 and G_2 . A potential difference was maintained across each bridge, and the mid-points of the included branches were connected to a vernier potentiometer reading to one microvolt. The potentiometer was used to measure the open-circuit potential difference across the mid-points, and the change e in this quantity produced by a resistance change δS of each gauge due to straining.

Thus

$$e = \frac{\delta S}{S} E, \quad \dots \quad \dots \quad \dots \quad \dots \quad \dots \quad (7)$$

where S is the unstrained gauge resistance. For the sting size used it was possible with this electrical circuit to measure bending moments to 1/250 lb/in. under steady conditions. Temperature compensation was the best possible with the arrangement used since each bridge was at one temperature. It was not possible to neglect the thermo-electric e.m.f. since the bridge was never balanced, and a reversing switch was included in the battery circuit to give two readings for each bending moment measured from which it was possible to eliminate the thermo-electric effect.

A sketch of the sting and electrical circuit is given in Fig. 5. The model is attached by means of the machined lug at the base of the sting, the lug mating with keyways cut in the nose of the model and giving a positive but easily removeable form of attachment.

It is easy to show that the change of gauge resistance due to straining is proportional to the bending moment about the mid-point of the gauge. Thus, by mounting gauges at two points along the sting, it is possible to deduce the normal force and moment applied to the sting at its point of attachment to the model nose. From the values of these quantities the normal aerodynamic force and moment experienced by the model may be deduced. The chief disadvantage of the method was found to be the impossibility of providing a damping device for motion of the sting. It was also necessary to measure the model incidence whilst the tunnel was running because of the incidence change produced by the bending of the sting under load.

2.4.3. Drag Balance.—It is possible to measure the normal force and moment on a three-dimensional model supported on the axis of the circular tunnel by the use of the strain-gauge technique described in the previous section. It is not, however, possible to measure drag by this balance. For the measurement of the drag of three-dimensional bodies, therefore, the balance

shown in Fig. 6 was constructed. The balance was of a very simple type and had several disadvantages, chief amongst which was the inability to measure drag when the model was experiencing lift. It was used for subsonic and supersonic tests in the 1-ft diameter tunnel. At the time when these tests were made the tunnel was not fitted with return ducts and used moist atmospheric air. The variations of static pressure along the working section (particularly on the axis) necessitated very large buoyancy corrections, particularly at supersonic speeds, and the experimental observations were not, therefore, very reliable.

2.5. Indirect Force Measurement.—In section 2.3 it has been stated that indirect methods are of great value in two-dimensional subsonic work. The two most important are the measurement of the normal pressure distribution over the model surface and the measurement of pitot and static-pressure distributions in the wake. Besides enabling the lift, pitching moment, profile and form drags to be deduced, these methods also enable a good insight into the mechanisms resulting in the changes of force and moment to be obtained. They also give information which is valuable as a basis for comparison with theory.

Both methods are in common use for low-speed tests, and the technique of pressure plotting differs very little at high and low speeds. A theory of the wake-traverse method at high speeds has been developed⁶⁹ which involves observations of the same quantities as those required at low speeds. This theory is based on certain assumptions which have been experimentally verified to a certain approximation, and appear to be valid for most aerofoil sections.

2.5.1. Pressure-Plotting Technique.—The measurement of the pressure distribution over the surfaces of an aerofoil model enables the lift, pitching moment, form drag, and centre of pressure position to be deduced; and a measurement over a range of incidence and speed, the derivatives of the above quantities to be calculated. Moreover, the measured pressure distribution enables the Mach number distribution to be determined* and the extent of supersonic regions at the aerofoil surfaces to be observed. The method, therefore, not only gives the magnitudes and positions of the overall forces, but a great deal of more fundamental information which is of value as a basis for and comparison with theory.

In the N.P.L. high-speed tunnel tests the observed pressure distributions are expressed either in the form of the pressure coefficient C_p given by

$$C_p = \frac{p - p_0}{\frac{1}{2}\rho_0 V_0^2}, \quad \dots \dots \dots \quad (8)$$

(where p is local static pressure, p_0 free-stream static pressure, ρ_0 free-stream density and V_0 free-stream velocity) or in the form of the pressure coefficient p/H_0 , where H_0 is the free-stream total head. The former coefficient has the advantage that it enables the influence of pressure distribution changes on the overall force coefficients experienced by the aerofoil to be easily seen, and further gives a pressure distribution which is sensibly independent of Mach number at low speeds. The second coefficient has the advantage that a scale of local Mach number (which is exact ahead of the shock-wave) may be appended to the pressure-coefficient scale. This enables changes in the local Mach number, and the appearance of supersonic regions, to be seen at once.

It is usual to express the pressure distribution in terms of both the above coefficients as functions of either the ratio x/c (where x is the distance from the leading edge and c the aerofoil chord), or the parameter θ . This quantity is connected to x/c by the relation:

$$\cos \theta = \left(1 - \frac{2x}{c}\right), \quad \dots \dots \dots \quad (9)$$

and has the advantage that it spreads out the pressure distribution over the nose and tail of the aerofoil, and is, therefore, of particular value when the pressure changes rapidly in these regions. For the purpose of calculating the forces experienced by the aerofoil it is usual to plot the observed

* Errors in the determination of the Mach number may arise in practice from the loss of total head in shock-waves or flow separations.

pressure differences ($H_0 - p$) first on a θ basis, and then replot the observations on abscissæ more suitable for force integration. Thus, for lift, the observations are replotted on an x/c basis, for moment on a basis of $z = (x - \frac{1}{4}c)^2/2c^2$, and for form drag on a y/c basis.

The areas under the three curves are then measured, and converted to the usual coefficients by the relations

$$C_L = \frac{\int (H_0 - p) \frac{dx}{c}}{\frac{1}{2}\rho_0 V_0^2} = \frac{\text{area}}{\frac{1}{2}\rho_0 V_0^2} \quad \dots \quad (10)$$

$$C_M = \frac{\int (H_0 - p)(x - \frac{1}{4}c) \frac{dx}{c^2}}{\frac{1}{2}\rho_0 V_0^2} = \frac{\int (H_0 - p) dz}{\frac{1}{2}\rho_0 V_0^2} = \frac{\text{area}}{\frac{1}{2}\rho_0 V_0^2} \quad \dots \quad (11)$$

$$C_{D \text{ FORM}} = \frac{\int (H_0 - p) \frac{dy}{c}}{\frac{1}{2}\rho_0 V_0^2} = \frac{\text{area}}{\frac{1}{2}\rho_0 V_0^2} \quad \dots \quad (12)$$

The quantity $\frac{1}{2}\rho_0 V_0^2$ is tabulated as a function of ($H_0 - p$) and is then independent of barometric pressure. More recently for lift and moment it has become usual to use a single plotting and a moment integrator in addition to a planimeter to derive the required quantities.

In reporting the results of experiments, it is usual to show both pressure coefficients (Cp and p/H_0) as functions of x/c alone, since at high Mach number the pressure changes at the nose and tail of the aerofoil are of relatively little significance in comparison with the pressure changes over the central chord region.

2.5.1.1. *Pressure-plotting models.*—The original method of constructing pressure-plotting models for the 20×8 in. tunnel consisted of cutting grooves in the aerofoil surfaces which communicated with the pressure holes and were covered by brass inserts. By this method it was not found possible to secure a sufficiently good surface finish, particularly in the case of pressure holes near the leading edge. For this reason, and from considerations of model strength and ease of manufacture, the method was abandoned in favour of the present method of construction which is illustrated in Fig. 7. Models of this type with 34 pressure holes (total in both surfaces) have been successfully constructed and tested with thickness/chord ratios down to 10 per cent, the model chord being 5 in. Models of thicknesses 5 per cent and $6\frac{1}{2}$ per cent are under construction with 30 pressure holes. All pressure-plotting models used at the N.P.L. have been of brass.

The models are usually supported by steel pins which are drilled to permit the hypodermic tubing from the pressure holes to be brought out of the tunnel. A single pin is attached to one end of the aerofoil, and passes out through a clearance hole in the glass wall to a supporting bracket outside the tunnel. The clearance between the glass wall and pin is sealed by a rubber sleeve. Three pins are attached to the other end of the model and these are similarly carried out through clearance holes in the glass wall to a steel bracket. The glass wall and supporting bracket on the three-pin side may be rotated about the axis of the single pin to vary the model incidence. The brackets are arranged to have a minimum obstruction to the optical system which is used to visualize the field of flow round the model. The brass models of 5 per cent and $6\frac{1}{2}$ per cent thickness are not to be supported by pins, but by rectangular brass tongues at each end of the model. With this method of support it will no longer be possible to visualize the flow round the model close to the surface, but steel models of the same section without pressure holes are being constructed for this purpose. These latter models will be supported by pins in the manner of the thicker models described above.

The pressure holes, which are usually of 0.01 in. diameter, are not arranged in a single chordwise plane, but are staggered across the centre of the span. This is done to minimise the effects of small-surface irregularities and leaks at any particular pressure hole upon the readings of downstream

holes. It is well known^{90, 78} that the effects of such disturbances may, by transverse contamination of the boundary layer, spread across the span downstream. Variations of the uniformity of the stream across the centre part of the span of the aerofoil are found to have a negligible effect on the readings of the pressure holes. The positions of the pressure holes are selected by experience, or by a previous knowledge of the pressure distribution of the aerofoil in question or of a similar aerofoil. The general form of the pressure distribution may be known either from previous experimental work or from calculation.

2.5.1.2. Pressure-plotting manometer.—The pressure holes in the surfaces of the aerofoil are connected to a multi-tube manometer which is also used for the measurement of the pressure distributions along the adjustable tunnel walls. This instrument, in common with the majority of the manometers used in the high-speed tunnel building, is fitted with a device for ‘freezing’ the manometer readings when they have become steady. This consists of a series of eccentrics which may be rotated to press clamps against rubber tubes placed at the tops of the manometer tubes. The sequence of events is, therefore, for the tunnel to be run up to the required working-section Mach number as indicated by the Mach meter, and the pressure readings at the model surface to be frozen when steady. The tunnel is then shut down after which the manometer readings are read and tabulated in an observations book.

Some method of either freezing or rapidly recording the manometer readings is essential since the wastage of power in maintaining a tunnel run of sufficient length to enable the readings to be recorded individually would be large. The photographic recording of manometric readings is extensively used elsewhere, but the following advantages* are claimed for the method used at the N.P.L.

- (a) Whilst the time taken to record the manometer readings after freezing is considerable, it is less than that required to process and read from the equivalent photograph.
- (b) Inconsistencies are at once discovered, and repeat tunnel runs are easily made since they do not involve the re-rigging which would probably be required if the manometer records were examined some time after the experiment was made.

The tubes of the N.P.L. pressure-plotting manometer are equi-spaced, and their spacing has, therefore, little relation to the spacing of pressure holes along the model chord. At the D.V.L.⁵¹ a manometer has been constructed with the tube spacing proportional to the pressure-hole spacing of the model. Photographic records of this instrument are directly planimetered to give the normal force and moment. This method must result in a considerable saving of time and labour. The construction of an integrating manometer has also been considered at the N.P.L.

The present manometer has 47 tubes containing mercury and having a range of 0 to 30 in., and 47 water tubes arranged between the mercury tubes and having a range 0 to 60 in. It is thus possible to measure a pressure by either a mercury or a water column. The sensitivity range thus obtained is found to be adequate for most purposes but in certain cases the use of a gauging liquid of intermediate density would be useful. Several such liquids exist^{91, 51} and are widely used elsewhere but, since most are corrosive, special precautions must be taken in the design of the manometer in which they are used. No great use of such liquids has yet been made in the N.P.L. high-speed tunnel laboratory.

2.5.2. Determination of Profile Drag at High Speeds by a Wake-Traverse Method.—At speeds at which the compressibility of the air may be neglected it is known that the profile drag of an aerofoil section can be determined with sufficient accuracy from measurements of total head† and static pressure across a section of the wake. When compressibility is important the measurement of a third quantity (*e.g.*, air density or temperature) becomes theoretically necessary. In R. & M. 1971⁹²,

* These advantages are probably peculiar to the induction-type tunnel and to other intermittent tunnels, since it is inconvenient to shut down a fan-driven tunnel after each set of observations.

† The total head is defined as the pressure of the air after isentropic deceleration to rest. At subsonic speeds this is equal to the pitot pressure.

however, it is shown that if the assumption is made that the total energy per unit mass of air is constant across a section of the wake, the profile drag may be derived to a high degree of accuracy from measurements of total head and static pressure alone.

The assumptions on which the method is based are that:

- (a) The air behaves as a perfect gas with constant specific heats.
- (b) The pressure at the mouth of a pitot tube is equal to the total head if the velocity is subsonic, and that this condition is satisfied in the wake of the aerofoil.
- (c) The entropy is constant everywhere outside the boundary layer and wake.
- (d) There is no flux of energy across the streamlines bounding the boundary layer and wake.
- (e) Any inclination of the stream at the measuring section to the normal to the section is negligible.
- (f) The total energy per unit mass of air is constant everywhere (including the wake).
- (g) Mean streamlines may be drawn in the wake such that the total head is constant along each stream tube at least between the measuring section and a section sufficiently far downstream for the static pressure there to be equal to the free-stream value.
- (h) The tunnel walls and aerofoil are perfectly non-conducting.

Assumption (g) above is similar to that made in the derivation of Jones' original method⁶⁸ and assumption (f) has been checked experimentally (*see* R. & M. 1971⁶⁹). The fact that the assumptions are justifiable is to some extent checked by the agreement between drags deduced by the pitot-traverse method and measured by balance Fig. 11 (*see* R. & M. 1971⁶⁹) and the agreement of drags deduced from wake traverse at different distances behind the trailing edge Fig. 10.

The method described below is the standard means of measuring profile drag in the 20 × 8-in. tunnel at the N.P.L. A similar method is used in flight tests and elsewhere. It should be noted that the presence of condensed moisture in the working section^{92,93,94} will vitiate the arguments on which the method is based. The method should be applicable when limited shock-waves are present on the aerofoil; in common with other methods of measurement, however, it will be subject to the influence of tunnel constraint and this effect may be large at high Mach number. At high Mach number it may also be difficult to cover the whole wake of the shock-wave. The pitot-traverse method has so far not been used to measure drag at supersonic speeds, but an attempt is now being made at the N.P.L. to use the method for this purpose.

Considering the flow past the aerofoil sketched in Fig. 8 let AA be a section sufficiently far upstream for the velocity, pressure and density to be constant across it, these constant values being denoted by V , p_0 and ρ_0 respectively. Let BB be a section sufficiently far downstream for the static pressure to have become constant at its upstream value p_0 . Let TT' be the boundaries of the wake (including that of any shock-waves present) at BB, and let PQST, P'Q'S'T' be streamlines of the steady flow past the aerofoil. Let the velocity and density at BB inside the wake be u and ρ respectively. Let CC be the section across which the wake is to be explored cutting the streamlines shown in S and S'. Denote the velocity, pressure and density at CC between S and S' by u , p , and ρ_1 respectively. Denote the total heads at AA, BB and CC by H_0 , H and H_1 respectively.

From considerations of momentum the drag D per unit length of span is given by

$$D = \int \rho u (V - u) dy, \quad \dots \dots \dots (13)$$

where the integral is taken across the wake at section BB. (For compressible flow this is proved in the Appendix of R. & M. 1971⁶⁹.) Let dy in this equation be the breadth of a stream tube, and

let its breadth at section CC be dy_1 . The continuity equation is then

$$\rho u dy = \rho_1 u_1 dy_1. \quad \dots \quad (14)$$

so that

$$D = \int \rho_1 u_1 (V - u) dy_1, \quad \dots \quad (15)$$

and if c is the chord of the aerofoil it is convenient to write the drag coefficient, C_D , as

$$C_D = \frac{D}{\frac{1}{2} \rho_0 V^2 c} = \int C_D' \frac{dy}{c}, \quad \dots \quad (16)$$

where

$$C_D' = 2 \frac{\rho_1 u_1}{\rho_0 V} \left(1 - \frac{u}{V}\right). \quad \dots \quad (17)$$

The integrals in equations (15), (16) are taken across the wake at section CC and u is the velocity at section BB on the streamline through the point at which the velocity is u_1 , on section CC.

In order that the method should be readily applicable to the results of experimental observations it is necessary to express C_D' in terms of the measurable quantities p_1 and H . Making assumptions (f) and (g) above and using the equations for the flow of a perfect compressible fluid it is possible to obtain from equation (17).

$$C_D' = 2 \left(\frac{H_1}{H_0}\right)^{(\gamma-1)/\gamma} \left(\frac{p_1}{p_0}\right)^{1/\gamma} \left\{ \frac{1 - \left(\frac{p_1}{H_1}\right)^{(\gamma-1)/\gamma}}{1 - \left(\frac{p_0}{H_0}\right)^{(\gamma-1)/\gamma}} \right\}^{1/2} \\ \times \left\{ 1 - \left[\frac{1 - \left(\frac{p_0}{H_1}\right)^{(\gamma-1)/\gamma}}{1 - \left(\frac{p_0}{H_0}\right)^{(\gamma-1)/\gamma}} \right]^{1/2} \right\} dy. \quad \dots \quad (18)$$

This equation may be transformed into a more useful form by the introduction of a fictitious Mach number M_2 defined by

$$M_2 = \frac{2}{\gamma - 1} \left\{ \left(\frac{H_0}{H_1}\right)^{(\gamma-1)/\gamma} - 1 \right\}. \quad \dots \quad (19)$$

Then by defining $\lambda = \frac{1}{2} \gamma M^2$, equation (18) may be written

$$C_D' = 2 \left(\frac{H_1}{H_0}\right)^{(\gamma-1)/2\gamma} \left(\frac{p_1}{p_0}\right)^{(\gamma+1)/2\gamma} \left(\frac{\lambda_1}{\lambda_0}\right)^{1/2} \left\{ 1 - \left(1 - \frac{\lambda_2}{\lambda_0}\right)^{1/2} \right\} \dots \quad (20)$$

or with $\gamma = 1.4$

$$C_D' = 2 \left(\frac{H_1}{H_0}\right)^{1/7} \left(\frac{p_1}{p_0}\right)^{6/7} \left(\frac{\lambda_1}{\lambda_0}\right)^{1/2} \left\{ 1 - \left(1 - \frac{\lambda_2}{\lambda_0}\right)^{1/2} \right\}. \quad \dots \quad (21)$$

Tables for $(H_1/H_0)^{1/7}$, $(p_1/p_0)^{6/7}$ are given in R. & M. 1971⁶⁹, which should also be consulted for a detailed derivation of the above equations. Values of the expression in $\{ \}$ are also tabulated in this reference.

The above formula is more convenient than some other exact formulae since it involves the use of single-entry tables or single curves whereas other methods involve the use of double-entry tables or families of curves. Moreover, the above method is more accurate since other methods tend to lose accuracy when H_1 is nearly equal to H_0 (as it is near the edge of the wake) or when M_0 is small. The method is, however, rather laborious and simpler approximate methods are commonly used in practice.

In R. & M. 1971⁶⁸, equation (21) is further transformed to a function of the Mach number ahead of the model and the two variables g and p (defined as in R. & M. 1688) alone where

$$g = \frac{H_1 - p_0}{H_0 - p_0} \text{ and } p = \frac{p_1 - p_0}{H_0 - p_0} \quad \dots \quad (22)$$

Thus

$$C_D' = 2(g - p)^{1/2} (1 - g^{1/2}) \{ [1 + \frac{1}{8}(M_0^2)3 - 2\gamma + 3p - 2g - (2\gamma - 1)g^{1/2}] \} \quad \dots \quad (23)$$

and this form may in some cases be preferable to the form of equation (21).

One approximate method which has been used at the N.P.L. is described by Beavan and Manwell in R. & M. 2233⁹⁵. It was observed that the value of C_D' (equation (17)) was roughly proportional to $(H_0 - H_1)$ at any given speed and it was thought that a simple expansion, to only a few terms, might be used. This did not prove to be the case, but it was found that it was possible to prepare tables of new functions⁹⁵ which reduced the labour of the reduction of experimental results especially when it was sufficient to evaluate the integral

$$C_D = \int C_D' d \frac{y_1}{c} \quad \dots \quad (24)$$

by the simple trapezium rule. The tables have the advantage that no interpolation is required at any stage.

The value of C_D' was expressed in the form

$$\frac{1}{2}C_D' = \frac{1}{7}Qh + \varepsilon_1 + \varepsilon_2s + \varepsilon_3s^2, \quad \dots \quad (25)$$

where

$$h = \frac{H_0 - H_1}{H_0}, \quad s = \frac{p_1 - p_0}{p_0}, \quad \dots \quad (26)$$

$$\frac{1}{Q} = \left(\frac{H_0}{p_0} \right)^{2/7} - 1 = (1 + z)^{2/7} - 1 \text{ and } z = \frac{H_0 - p_0}{p_0} \quad \dots \quad (26)$$

The quantities ε_1 , ε_2 and ε_3 are functions of h (ε_1 of order h^2 , ε_2 and ε_3 of order h) and z . These functions were tabulated together with the value of $1/7.Q$ (a function of z alone). The method of arranging the calculations is discussed in R. & M. 2233⁹⁵.

Even this approximate method is found to be rather laborious, and rapid methods of calculating the drag have been given by Thompson⁸⁷ and by Beavan. These methods are only moderately accurate, but on account of the limited accuracy of experimental observation they are normally used in the reduction of observations. In exceptional cases, however, either the exact method or the first approximate method described above are used.

The rapid method of drag calculation given by Beavan is based on the observed fact that in the more usual practical cases the static pressure is constant across the wake at the measuring section which is usually 1-chord behind the trailing edge. The formula is drastically simplified and is quoted below for a 5-in. chord aerofoil in the rectangular tunnel at the N.P.L.

$$C_D = \frac{K \times \text{Area under } (H_0 - H_1) \text{ curve} + \frac{1}{10} \times (H_0 - H_1)_{\text{max}}}{(H_0 - p_0)} \times 10^{-3} \quad \dots \quad (28)$$

where the total-head difference-curve $(H_0 - H_1)$ is plotted in inches of water against distance across the tunnel in inches, the area being taken in units of inches of water pressure difference and 0.1-in. intervals of traverse. The value of $(H_0 - p_0)$ is expressed in inches of mercury and represents the tunnel speed. The quantity K has been tabulated as a function of the variables $(H_0 - p_0)$ and $(H_0 - H_1)$ for standard conditions which assume a value of the total head upstream of the model of 30 in. of mercury, a pitot-tube diameter of 0.025 in., and a ratio of the quantities $(p_1 - p_0)/(H_0 - p_0)$ of 0.04. Correction tables have been constructed for different values of these standard conditions. Similar formulae are used for models of differing chord and the accuracy obtained by their use is found to be adequate in most cases.

2.5.2.1. *Correction for finite diameter of pitot-tube.*—When there is a transverse gradient of total head across the mouth of a pitot-tube the effective centre of the tube is displaced from the geometrical centre towards the region of higher velocity⁶⁶. Thus, the area under the total-pressure curve is less than it should be. For the usual type of pitot-tube used in the high-speed tunnels it is sufficiently accurate to take this displacement as 0.18 times the external diameter of the tube. This correction is applied both at low and high speeds, and although there is no direct experimental evidence of its validity at high speeds, the relative importance of the correction diminishes rapidly with increase of speed above the shock-stall because of the increase of the drag coefficient. The corrections can be applied in practice⁶⁹ by the addition, to the value of C_D of 0.36 times the maximum ordinate of the C_D -curve times the diameter of the tube divided by the chord.

2.5.2.2. *Pitot and static-tubes.*—Apart from some early observations⁶⁹ when a comb of ten tubes was used, traverses are now almost invariably made with a single pitot-tube. A number of tubes of circular cross-section and varying diameter are available the standard external diameters being 0.055 in., 0.03 in. and 0.025 in. for most experimental work. A typical tube is drawn in Fig. 9; other tubes differ only in the diameter of the extreme tube. The tubes may be fitted either directly into the pitot-traverse gear shown in Fig. 9 or to extension tubes of external diameter 0.25 in. Typical static tubes are also shown in Fig. 9. Traverses are normally made in a plane at 1-chord behind the trailing edge.

For explorations in supersonic flow, pitot-tubes of the type described above are used, and the Rayleigh correction³³ for the loss of total head through the bow-wave (assumed normal over the mouth of the tube) is applied to the reading in order to obtain the total head. In order to ensure that the bow-wave is normal at the mouth of the tube it was the practice in Germany to use tubes with a large ratio of external diameter to bore. The static-tubes used at the N.P.L. for supersonic operation are fitted with ogival heads and the static holes are arranged in a single plane some 8 to 10-tube diameters downstream of the nose.

2.6. *Factors which may Cause the Behaviour of the Working Fluid in a Wind Tunnel to Depart from that of a Perfect Gas.*—In the reduction of experimental observations as well as in theoretical work it is usual to assume that the working fluid behaves as a perfect gas with constant specific heats and obeying an equation of state.

$$\frac{p}{\rho} = RT, \quad \dots \dots \dots (29)$$

where R is a constant for a particular gas. It is also usually assumed that the energy content is capable of instantaneous change following the external conditions so that the internal energy is always a uniquely defined function of the temperature. With certain exceptions the behaviour of the atmosphere under the conditions of pressure and temperature usually encountered in free flight is very close to that of a perfect gas. The temperature and pressure in a wind tunnel will, however, usually differ from the values in flight, and, particularly if working substances other than air are used, it is necessary to ensure that the behaviour of the fluid in the tunnel does not depart appreciably from that of a perfect gas.

Real gases are superheated vapours or mixtures of such vapours, and, whilst the behaviour may approximate to that of a perfect gas when the degree of superheat is high, this will no longer be the case when any of the constituents approaches its liquefaction point. At normal temperature and pressure dry air is highly superheated, and it has been shown that for practical purposes it may be regarded as a perfect gas over the range of these quantities usually encountered in wind-tunnel practice. If the air contains water vapour, however, saturation and condensation of this constituent may take place under the conditions of temperature and pressure which exist at the working section of a wind tunnel and, it is usually necessary to control the humidity conditions with care.

2.6.1. *Relaxation-Time Effects.*—The internal energy E of unit mass of the working substance may be written

$$E = E_t + E_r + E_i, \quad \dots \quad \dots \quad \dots \quad (30)$$

where E_t , E_r and E_i denote the energies due to translation, rotation and vibration of the molecules respectively. At any temperature each of these quantities has an equilibrium value which may be calculated from statistical mechanics. If the temperature changes, the translational and rotational energies become adapted to their new equilibrium values very rapidly, but the vibrational energy is relatively much less rapidly adjusted. The relaxation time is a measure of the time constant representing the time taken for the vibrational energy to achieve equilibrium conditions. For air, the departure of the behaviour from that of a perfect gas produced by the relaxation-time phenomena is negligible over the temperature range encountered in flight or in wind tunnel or turbine practice. For certain other working fluids, however, some of which have been suggested for power economy in wind tunnels⁹⁷, relaxation time may produce serious departures from a perfect-gas behaviour. The use of such fluids in wind tunnels is, therefore, usually not possible for this and other reasons. A detailed discussion of the effects of relaxation time in gas dynamics is given in papers by Gunn¹⁵ and by Kantrowitz¹⁶ and in the references cited in these papers.

2.6.2. *The possibility of Liquefaction at High Mach Number.*—Goldstein¹⁷ has examined the behaviour of dry air in a high-speed wind tunnel, and concludes that if the liquefaction point (or dew point) is not approached the departure of the behaviour from that of a perfect gas with $\gamma = C_p/C_v = 1.40$ has a negligible influence on the results of calculations relating to the flow at the working section.

The logarithms of the vapour pressures of oxygen and nitrogen are plotted against the reciprocal of the absolute temperature in Fig. 12. This method of plotting has been suggested by Dodge and Davis⁹⁸ who find that the vapour pressure may be calculated from the following empirical expressions over a wide range of pressure and temperature.

$$\log_{10} P = 4.06295 - \frac{366.523}{T} \text{ for oxygen} \quad \dots \quad \dots \quad \dots \quad (31)$$

$$\log_{10} P = 3.93352 - \frac{304.494}{T} \text{ for nitrogen} \quad \dots \quad \dots \quad \dots \quad (32)$$

where P is the vapour pressure in atmospheres, and T the absolute temperature in deg K . The vapour pressure curves of Fig. 12 have been drawn with the aid of these equations together with experimental data reported by Dodge and Davis and by other workers.

The liquefaction point of curve for dry air is also included in Fig. 12. This has been drawn by the use of data reported by Dodge and Dunbar⁹⁹ and by Inglis¹⁰⁰ together with the data from the International Critical Tables. The expression¹⁸

$$\phi = \frac{\Pi_o \Pi_N}{\Pi_o - (\Pi_o - \Pi_N)z_o}, \quad \dots \quad \dots \quad \dots \quad (33)$$

which applies to a perfect solution whose vapour behaves as a perfect gas, may also be used to calculate the liquefaction point with sufficient accuracy. Here ϕ is the total pressure, Π_o and Π_N the vapour pressures of oxygen and nitrogen and z_o the mol fraction of oxygen in the vapour mixture. In the derivation of the liquefaction point plotted in Fig. 12 air was taken as a binary mixture of oxygen and nitrogen with a mol fraction of oxygen 0.21. Goldstein¹⁷ has pointed out that the vapour pressure of argon lies between those of oxygen and nitrogen fairly close to that of oxygen, and that the presence of argon in the air will, therefore, have little influence on the liquefaction-point curve.

Curves representing the conditions at the working section of a wind tunnel for a number of stagnation pressures and temperatures are also given in Fig. 12. For the range of stagnation conditions and Mach numbers at present in use or contemplated for high-speed tunnel practice,

the conditions are far removed from the liquefaction point. Thus, for stagnation pressures of one atmosphere or less, and stagnation temperatures above 0 deg C it appears that the liquefaction point is still not approached at a Mach number of four.

2.6.3. *The Influence of Humidity.*—If w is the weight of water vapour per unit weight of air in a mixture of air and water vapour, it follows from Avogadro's hypothesis that

$$p_w = w p_A \frac{W_A}{W_w} \quad \dots \quad (34)$$

where p_w and p_A are the partial vapour pressures of water vapour and air respectively, w_A is the molecular weight of air, and W_w that of water vapour. Inserting numerical values for the molecular weights this becomes

$$w = \frac{18 p_w}{29 p_A} \quad \dots \quad (35)$$

The specific humidity τ is usually defined as the weight of water vapour per unit weight of the mixture of air and water vapour. Thus

$$\tau = \frac{w}{1+w} = \frac{18 p_w}{18 p_w + 29 p_A} \quad \dots \quad (36)$$

and since the total static pressure p is equal to the sum of the partial pressures of the air and water vapour

$$\tau = \frac{18 p_w}{29 p - 11 p_w}, \quad \dots \quad (37)$$

at the intake of a wind tunnel, p_w will usually be small compared with p , and it is, therefore, usually sufficiently accurate to write

$$\tau = \frac{18 p_w}{29 p} \quad \dots \quad (38)$$

The relative humidity, β , is defined by the relation

$$\beta = \frac{p_w}{p_s}, \quad \dots \quad (39)$$

where p_s is the saturation vapour pressure. Thus equation (38) becomes

$$\tau = \frac{18}{29} \beta \frac{p_s}{p} \quad \dots \quad (40)$$

If the flow in a wind tunnel between the intake, denoted by suffix 1, and the working section denoted by suffix 2, is considered, and it is assumed that no moisture is removed from the air-stream between the two sections, equation (35) shows that

$$\frac{p_{A1}}{p_{w1}} = \frac{p_{A2}}{p_{w2}} \quad \dots \quad (41)$$

Further, if it is assumed that the flow is isentropic and that the velocity at section 1 is zero,

$$\frac{T_2}{T_1} = \frac{2}{2 + (\gamma - 1) M_2^2}, \quad \dots \quad (42)$$

$$\frac{p_2}{p_1} = \left(\frac{T_2}{T_1} \right)^{\gamma/(\gamma-1)}, \quad \dots \quad (43)$$

where T_2 and T_1 , are the absolute stream temperatures, M_2 , the working-section Mach number, and γ the ratio of the specific heats which is assumed to be constant between the two sections.

Thus

$$\frac{p_{A2} + p_{w2}}{p_{A1} + p_{w1}} = \left(\frac{2}{2 + (\gamma - 1)M_2^2} \right)^{\gamma/(\gamma-1)}, \quad \dots \quad (44)$$

and with equation (41) this becomes

$$\frac{p_{w2}}{p_{w1}} = \left(\frac{2}{2 + (\gamma - 1)M_2^2} \right)^{\gamma/(\gamma-1)} \quad \dots \quad (45)$$

Thus the relative humidities at the two sections are related by

$$\beta_2 = \beta_1 \frac{p_{s1}}{p_{s2}} \left(\frac{2}{2 + (\gamma - 1)M_2^2} \right)^{\gamma/(\gamma-1)} \quad \dots \quad (46)$$

The saturation vapour pressure is a function of temperature alone, and thus the ratio of the saturation vapour pressures may be determined from a knowledge of the intake temperature by the use of equation (42). The relationship between saturation vapour pressure and temperature is given in Fig. 13 which is based on values tabulated in the International Critical Tables. If condensation does not take place the influence of moisture on the flow in a wind tunnel is unimportant. If condensation occurs, however, important changes of the flow may follow. There will be a release of latent heat, a removal of the partial vapour pressure of the water vapour and, possible, a change in the values of the specific heats and of their ratio γ . The presence of water particles in the airstream after condensation may also make it difficult to interpret the readings of measuring instruments, in particular, the pitot-tube.

Of these effects, the release of latent heat is usually the most important and depends in magnitude on the amount of water vapour condensed and whether water or ice particles are formed on condensation. The influence of heat addition on the flow in a channel is discussed in Refs. 101, 102. The effect on Mach number and static pressure may be seen from the equations

$$\frac{dM^2}{M^2} = \frac{1 + \gamma M^2}{1 - M^2} \left(\frac{dQ}{H} - \frac{dA}{A} \right), \quad \dots \quad (47)$$

and

$$\frac{dp}{p} = \frac{-\gamma M^2}{1 - M^2} \left(\frac{dQ}{H} - \frac{dA}{A} \right), \quad \dots \quad (48)$$

where dQ is the quantity of heat added, H the enthalpy before heat addition, A the cross-sectional area and dA the change of this quantity. These equations indicate that condensation in a channel of constant cross-sectional area will produce an expansion and increase of Mach number if the initial Mach number is subsonic, and a compression and decrease of Mach number if the latter is initially supersonic.

The influence on the flow in a wind tunnel depends on the region in which condensation takes place. In subsonic tunnels condensation may, for example, occur downstream of the position at which the working-section Mach number is measured, and this will produce an apparent decrease of the choking Mach number of the tunnel. In supersonic tunnels condensation often occurs between the nozzle throat and the working section, and produces a decrease of the working-section Mach number below that obtained with dry air or calculated from the nozzle geometry on the assumption of an isentropic expansion. Moreover, in a supersonic tunnel the compressive disturbances produced by condensation may be reflected at the walls and produce more concentrated disturbances further downstream. This is illustrated by Fig. 14 which shows measurements made in a 2-in. square tunnel at the N.P.L. The phenomena have been known for a considerable time in connection with condensation in steam nozzles, and are, for example, discussed by Stodala⁶⁴ and by Binnie and Woods¹⁰³. The latter work, in particular, was carried out in considerable detail and should be referred to for further information. Fig. 15, which is due to Binnie and Woods shows the influence of condensation on the static pressure in a steam nozzle at varying intake temperature.

In practice it is found that condensation does not begin immediately saturation is reached and that a considerable degree of supersaturation may be tolerable. The factors governing the quantitative value of the degree of supersaturation at which condensation commences are complex and are, for example, discussed by Wilson¹⁰⁴ and by Binnie and Woods¹⁰³ and in references given in their paper. Condensation of a supersaturated airstream will usually be accelerated by the presence of small solid particles,* and may also be initiated at some region of disturbance (*e.g.*, at the model or a shock-wave present in the flow). At the N.P.L. it has been found that the degree of supersaturation may be more than fourfold before condensation begins.

Condensation cannot take place if saturation does not occur, thus equation (46) may be used to define a value of the intake relative humidity below which condensation at the working section will be impossible for given stagnation temperature and Mach number. Similar intake humidity conditions may also be defined for any value of the degree of supersaturation at the working section. Values of the intake relative humidity which will produce saturation and four, six and eightfold saturation at the working section are given in Figs. 16 to 18 for a range of working-section Mach numbers and intake temperatures.

It has, however, been found by Hermann¹⁰⁵ that the effects of condensation are negligible up to Mach numbers of 2.29 provided that the specific humidity (which is a measure of the maximum amount of heat release which may take place on condensation) is less than 0.5 gm per kilogramme. Subsequent work¹⁰⁶ in Germany has indicated that this limit is satisfactory up to Mach numbers of 4.4. It is clear, therefore, that both the relative and specific humidities are of importance in considerations of the influence of moisture on the flow in a wind tunnel. For given temperature and Mach number the former will define the degree of supersaturation at the working section, and will, largely, decide whether condensation takes place or not and the latter will define the influence which condensation will have on the flow. In order to completely define the humidity conditions at the intake of a wind tunnel it is, therefore, necessary to specify either:

- (a) The relative humidity, temperature and pressure.
- (b) The specific humidity, temperature and pressure.
- (c) The partial vapour pressure of the water vapour, the pressure and the temperature.

Other possible combinations may be used, (*e.g.*, a definition involving the dew point) and are readily deduced from equations (46), (40), (39), (38).

2.6.4. Driers.—In order that the effects of condensation may be avoided or controlled it is necessary to control the humidity conditions at the tunnel intake. The object of such control may be either to avoid condensation completely (this will usually involve a reduction of relative humidity), or to reduce the effects of condensation (which will involve a decrease of specific humidity).

2.6.4.1. Control of stagnation temperature.—It is clear from Fig. 13 that the saturation vapour pressure may be raised by an increase of temperature. Thus, if the stagnation temperature of the air in the tunnel is raised, the relative humidity will fall and it may be possible to avoid condensation. Equation (34), however, indicates that the specific humidity will not be changed if the pressure is constant. The effects of heat release at condensation may, however, be less severe at high temperature since the enthalpy in equations (47), (48) will itself be increased.

The method is particularly convenient for application to closed-circuit tunnels driven directly by a fan or compressor, since the stagnation temperature may then be raised by a reduction of the degree of cooling. The details of the arrangement of the system will depend on the method which is used to cool the tunnel. Thus, for tunnels cooled by liquid coolant the temperature rise is effected by a decrease of the rate of flow of coolant. For tunnels cooled by air exchange the rate of entry of cold air is restricted.

* Since the completion of the present paper it has been suggested by Lukasiewicz that this is probably not true for the rapid processes involved in condensation in a supersonic stream. Refs. 89 and 137 should therefore be read in conjunction with the above.

Whilst an increase of stagnation temperature may also be necessary at very high Mach number to prevent the liquefaction of other constituents of the air, a large increase of temperature has certain practical disadvantages. Thus, for example, the whole tunnel structure including the working section and model will attain a temperature only a little below the stagnation temperature. The power requirements for given Mach and Reynolds numbers will also be increased by stagnation temperature. Nevertheless, stagnation temperature up to about 40 deg C have been used successfully in practice^{51, 21}.

2.6.4.2. *Control of Stagnation Pressure.*—Equation (40) indicates that for constant specific humidity and stagnation temperature the relative humidity at the tunnel intake is proportional to the stagnation pressure. Thus, if no attempt is made to remove water vapour from the airstream the tendency for condensation will increase as the stagnation pressure is increased. Conversely, the possibility of condensation will be reduced at constant specific humidity by a reduction of stagnation pressure. With constant relative humidity and temperature the specific humidity is inversely proportional to the stagnation pressure so that under these conditions the effects of condensation will decrease with increase of stagnation pressure. The stagnation pressure will, however, usually be determined by other considerations and it is only necessary to note that the need for a drier is usually greatest in a pressurized tunnel (*e.g.*, in the proposed 18 × 14 in. N.P.L. tunnel⁴⁹).

2.6.4.3. *Drying in a compression-expansion cycle.*—If air, initially at conditions denoted by suffix 1, is compressed to conditions denoted by suffix 2, at constant temperature (this may be achieved in practice either by isothermal compression or by cooling after compression) the relative humidities before and after compression, are related by

$$\beta_2 = \frac{p_2}{p_1} \beta_1, \quad \dots \quad \dots \quad \dots \quad \dots \quad \dots \quad \dots \quad \dots \quad \dots \quad \dots \quad (49)$$

where it is assumed that no moisture is removed during the compression and that the specific humidity is, therefore, constant. If the pressure ratio is adequate, saturation and condensation will take place, and if all condensed and supersaturated moisture is removed the air may be regarded as saturated at conditions 2. The value of β_2 will then be unity, and the specific humidity τ_2' will become

$$\tau_2' = \frac{18 p_s}{29 p_2} \quad \dots \quad \dots \quad \dots \quad \dots \quad \dots \quad \dots \quad \dots \quad \dots \quad \dots \quad (50)$$

If the air is then expanded back to pressure p_1 at the same temperature, the final relative humidity β_3 is given by

$$\beta_3 = \frac{p_1}{p_2} \quad \dots \quad \dots \quad \dots \quad \dots \quad \dots \quad \dots \quad \dots \quad \dots \quad \dots \quad (51)$$

so that both relative and specific humidities may be substantially reduced by a cycle of this type.

Such a cycle is used in the N.P.L. induction-type tunnel installation which is sketched in Fig. 19. Here the air is compressed for storage up to a maximum pressure of 25 atmospheres. The three compressor stages are intercooled, and an aftercooler is fitted. Final cooling also takes place in the unlagged storage reservoirs. Condensed moisture is removed by water traps, and by blow-off valves in the bases of the reservoirs. Expansion from the reservoirs then takes place into the tunnel circuits through the injector slots, and the tunnels being fitted with return ducts, the whole of the air in the circuit is, after a short preliminary run, derived from the reservoirs. Unfortunately, the stagnation temperature in the tunnel falls slightly during a tunnel run because of the fall in the stagnation temperature of the inducing air which accompanies the expansion from the reservoirs. Nevertheless the departure from atmospheric stagnation temperature is not sufficiently great to aggravate the humidity conditions seriously, and a considerable degree of drying is obtained.

Equation (24) indicates that with compression to 25 atmospheres final relative humidities of the order of 4 per cent should be obtained. In practice, however, in the N.P.L. tunnels the value does not fall below about 12 per cent and the discrepancy is attributed partly to the carrying over of moisture in a supersaturated state and as mist, and partly to the porosity of the brickwork which constitutes part of the tunnel circuit. Thermograph and hygrograph records taken in the intake of the 20 × 8-in. tunnel before and after the return ducts were fitted are shown in Figs. 20, 21.

2.6.4.4. *Drying in a refrigeration-reheating cycle.*—If air is cooled the saturation vapour pressure will fall, and if the pressure does not fall saturation and condensation will take place. If supersaturated and condensed moisture is removed, and the saturation vapour pressure then increased again by reheating, it is possible to achieve a low final relative humidity. The removal of moisture will also produce a decrease of specific humidity. This cycle may be used in conjunction with the compression-expansion cycle described above.

2.6.4.5. *Chemical driers.*—Drying may also be accomplished by the adsorption of water vapour from the air by one of a number of chemical drying agents such as silica gel and activated alumina. Silica gel appears at present to be the most promising material for use in connection with high-speed wind-tunnel installations although the evidence is scanty.

The drying agent is usually placed in beds across the airstream to be dried. The beds must be reactivated periodically and this may be accomplished by blowing heated air through them. If the efficiency of the bed is to be maintained at a high level during use, it is also necessary to cool it continuously or at frequent intervals. This is usually done by checking the flow of moist air and applying a blast of cold dry air. Fig. 22 illustrates typical¹⁰⁶ properties of silica gel as a drying agent. For further information reference should be made to the literature (*e.g.*, Ref. 107) or to catalogues issued by the manufacturers.

2.6.4.6. *The application of drying methods to wind tunnels.*—In general it is desirable that a high-speed tunnel shall be fitted with a return circuit. In this case it is necessary only to dry the air in the circuit before a series of tunnel runs after which further drying is unnecessary. A return circuit also permits the possibility of operation at an increased stagnation temperature by a control of the degree of cooling. In addition to temperature control, other physical or chemical drying methods may be used.

In an open-circuit tunnel (*e.g.*, those operated by the discharge of atmospheric air into an evacuated reservoir) the power required to dry the large mass flow by physical methods may be excessive, and chemical driers will usually be employed. The drying beds will be placed at a section of large cross-sectional area and low velocity upstream of the contraction. By this method the efficiency of the drier will be increased and the power losses in resistance minimised. An example of this type of drier installation is shown in Fig. 23, and values for the pressure drop due to the resistance of the drying beds are given in Fig. 24.

The provision of a chemical drier in a by-pass circuit may prove a convenient method for drying the air in a closed-circuit tunnel before a run is commenced, and by this method, the power loss associated with the resistance of the drying bed may be avoided during the tunnel run.

2.6.5. *The Influence of Moisture on the Reading of a Pitot-Tube.*—The significance of the reading of a pitot-tube placed in a moist airstream has been discussed by Taylor⁹³ who used a (p, v) diagram to illustrate the problem. Such a diagram is also of value in connection with other problems of the condensation of moisture.

Fig. 25 shows such a diagram; the ordinate represents the pressure, and the abscissa $1/\rho$, where ρ is the mean density of the moist air (with or without water drops). The point A represents the conditions of the unsaturated air at rest at the tunnel intake, and the curve ABC an adiabatic expansion without condensation. This curve is very close to an adiabatic for dry air. As the

representative point moves down ABC (the point now representing the conditions at some point in the effuser or working section of the tunnel) the temperature will fall, and saturation may occur at some point B. If condensation then takes place immediately and continues at a sufficient rate to keep the air in a saturated condition, the representative point will follow the saturation adiabatic BD. If condensation does not begin at B, the representative point will continue to move down ABC to a point C at which the air is supersaturated before condensation begins. The conditions after C will follow some curve CD, the exact shape depending on the relative rates of condensation and expansion. If saturation occurs at D (condensation beginning at C) the representative point will then move along the saturation adiabatic BDE to the point E which corresponds to the minimum expansion pressure.

If a pitot-tube is placed in the water-laden airstream, the drops of water may evaporate so rapidly that saturation conditions are maintained, and the representative point will move back along EDB to B, and then up the dry adiabatic towards A. If the drops do not evaporate at all, the representative point will travel up a curve EF which will be practically identical to the dry adiabatic through E. Partial evaporation will be represented by an intermediate curve.

Bernoulli's equation may be written

$$\frac{1}{2}u^2 = \int_p^{p_0} \frac{dp}{\rho}, \quad \dots \dots \dots \dots \dots \dots \quad (52)$$

where p_0 is the pressure of the air at rest at the tunnel intake, and u the stream velocity at pressure p . A pitot-tube brings the air to rest, so that if p_1 is the pitot pressure,

$$\int_{p_1}^{p_0} \frac{dp}{\rho} = 0, \quad \dots \dots \dots \dots \dots \dots \quad (53)$$

the integral being taken round the path followed by the representative point on the (p, v) diagram. The pitot pressure may, therefore, be found by following the representative point until the total area swept out by the abscissa is zero. If no condensation occurs, this condition is satisfied by $p_1 = p_0$. If, for example, the representative point travels down the dry adiabatic until a degree of supersaturation represented by C is reached, and then follows the path CDEGH until all drops are evaporated before reaching the pitot-tube at H (on the dry adiabatic), it will move up the line BHA to a point K, where the area HBCDEGH is equal to the area LAKN. The ordinate KS of K will then represent the pitot pressure p_1 .

If the drops do not evaporate before reaching the pitot-tube, the abscissa of the representative point will have swept out zero area before reaching the dry adiabatic. This case is represented by the path ABCDEO. If OR is the abscissa of O, and OR cuts the dry adiabatic at Q, O is determined by the condition that the area OQCDEO is equal to the area ABQRLA. In this case the pitot pressure is represented by the ordinate OT of O.

In R. & M. 2248⁹⁴ Taylor proceeds to use the (p, v) diagram to discuss the readings of a pitot-tube when evaporation of the water drops does not occur. Two cases are considered:—

- (a) The drops are deflected with the air at the mouth of the pitot-tube.
- (b) The drops pass through the mouth and strike the back of the tube without contributing to the recorded pressure.

Equations are derived enabling the density, velocity and the mass of water drops per unit mass of air to be determined if the static pressure and either of the above pitot pressures are known. In practice, however, it is not certain which of the pitot pressures will be measured, and the possible error which may arise is discussed by Taylor. Thus, for example, a possible error of 12 per cent in the determination of the mass of water drops may occur. On physical grounds it would seem that a pitot-tube of small diameter should read the first pitot pressure, and a tube of large diameter the second. At present, however, there is no systematic experimental evidence to confirm this.

2.6.6. *The Influence of Condensation on the Profile Drag Measured by the Wake-Transpose Method.*—Fig. 26 is included to illustrate the influence of moisture condensation on experimental observations. The figure gives values of the profile-drag coefficient for an aerofoil at subsonic Mach numbers in the 20×8 -in. N.P.L. tunnel deduced from a pitot-traverse in the wake. The Mach number plotted as abscissa was calculated from the observed static pressure of the undisturbed stream upstream of the model on the assumption of an isentropic expansion from the measured stagnation pressure at the tunnel intake, and the pitot observations reduced in the usual manner on the assumption of isentropic flow everywhere outside of the wake of the model. The influence on the measured drag is considerable, but the relative values of the contributions of the various departures from the assumed conditions is not certain.

2.7. *Effects of Reynolds Number and Turbulence.*—There is little evidence concerning the effects of Reynolds number and airstream turbulence on the flow pattern round a body at supersonic speeds. The effects of Reynolds number on model projectiles has been investigated by the Engineering Division, N.P.L. by an analysis^{108, 109} of results obtained in the Ordnance Board tunnel and on the shell range, and there appears to be in some cases a considerable effect on the pressures on the base of the projectile.

No evidence of the effects of either Reynolds number or turbulence at supersonic speeds have been obtained in the Aerodynamics Division tunnels. The effects may be particularly large close to a region where a shock-wave meets the boundary layer on the surface of the body under test. An investigation of the interaction of a shock-wave and the boundary layer on a flat surface with varying shock strength has been made by Fage and Sargent¹¹, and similar, but rather more detailed, investigations with variations of both shock strength and Reynolds number by Ackeret¹², and by Liepmann¹³. From the results of Ackeret's and Liepmann's tests it seems that the state of the boundary layer and hence the Reynolds number has a considerable influence on the nature of the interaction.

In common with all low-speed tunnel tests at low Reynolds numbers, tests in the N.P.L. high-speed tunnels will be subject to the possibility of laminar separation. At low speeds the effects of laminar separation will be very similar to those observed in many other tunnels, but at higher Mach numbers the effects are less well known. It is important to consider the possibility of laminar separation when comparing the results of measurements in the N.P.L. high-speed tunnels with results at higher Reynolds number, or applying them to full-scale aircraft.

2.7.1. *Effects of Turbulence.*—There is little information on the effects of airstream turbulence on the flow pattern round an aerofoil at high speeds. In the past, turbulence effects in the N.P.L. high-speed tunnels have been confused by the effects of condensation of moisture in the working section. Now that return ducts have been fitted, and moderately dry air can be used, it should be possible to investigate the influence of turbulence more thoroughly but so far this work has not been done.

The problem is complicated by the absence of a reliable method of obtaining a quantitative measure of the turbulence at high speeds. Sphere tests⁸⁰ were made in both the 1-ft diameter and 20×8 -in. tunnels in 1942, but it was impossible to extend the tests to high Mach numbers because of the early shock-stall of the sphere. These tests, which are reported in R. & M. 1959⁸⁰, indicated that the turbulence at the working section was greatly influenced by the nature and arrangement of gauzes at the tunnel intake. With the best entry conditions tested it was found that the critical Reynolds number of a sphere was of the same order as that measured in the N.P.L. low-speed tunnels. It is doubtful, however, if these measurements have much relation to the degree of turbulence at the working sections of the tunnels in their present form, since the tunnel entries have both been considerably modified since the original observations were made.

There is evidence that the turbulence of the airstream has a considerable effect on the drag of an aerofoil model particularly above the shock-stall. Drag changes below the shock-stall with variations of the tunnel turbulence are, presumably, due to changes of the transition positions

on the aerofoil surfaces. Above the shock-stall drag variation is possibly due to the dependence of the nature of the interaction of shock-waves and boundary layers on the condition of the latter upstream of the shock-wave. The effect of airstream turbulence, as modified by alterations of the tunnel entry, on the drag of an aerofoil below the shock-stall is illustrated by Figs. 27, 28, 29. The effect on the drag rise above the shock-stall, and on the free-stream Mach number at which the drag rise commences, is illustrated by Figs. 28, 29. The phenomena illustrated by these figures are purely qualitative and, apart from indicating that the airstream turbulence is of considerable importance, inconclusive.

The intake arrangements of the 1-ft diameter and 20×8 -in. tunnels have now been modified to the forms shown in Figs. 5(c) and 6(c) of Ref. 81, and it is found that, provided the gauze screens are kept clean, drag observations may be repeated satisfactorily, and it is concluded that the degree of turbulence may be maintained sensibly constant. There is no evidence that the insertion of a honeycomb in the entry of the 1-ft tunnel has improved the turbulence, and it appears to have had an adverse effect on the uniformity of the flow across the working section. In view of the above, the proposed insertion of a honeycomb at the entry of the 20×8 in. tunnel has been postponed. It was found that the provision of straightener vanes (Fig. 5(c) and 6, Ref. 81) in the tunnel intake improved the turbulence as estimated by the drag of an aerofoil provided that the vanes were of good form, and that the junction at the centre of the vanes was carefully formed. It has been suggested that a gauze be placed at a small distance above the floor of the entry chambers to the 1-ft and 20×8 -in. tunnels to minimise the effects of separation of the boundary layer on the floor.

2.8. Interference Due to the Constraint of the Walls of a Closed Rectangular Tunnel on an Aerofoil Spanning the Working Section.—The corrections which must be applied for the influence of boundary constraint at low speeds have been summarised by Glauert¹¹⁰. In general, the method of calculating the magnitudes of the corrections involves the replacement of the tunnel boundaries by the appropriate image system (to satisfy the original boundary conditions) and the use of combinations of doublets, vortices and sources to represent the aerofoil. It is usual to divide the total interference into two components which may be termed the blockage and lift effects. These are assumed to be independent and are finally superposed to obtain the magnitude of the required correction.

2.8.1. Blockage.—Since the lateral expansion of the flow in passing the model will be constrained by the presence of the solid walls (assumed straight) the velocity at the model will be increased above the value in free air for a given relative velocity of the airstream far ahead. Thus, it is necessary to add a correction to the 'tunnel speed' in order to obtain the actual speed at the model. In addition to this 'solid blockage' effect, a similar effect will occur due to the 'wake blockage'. Thus, since the wake is a region of reduced velocity, the requirement of continuity of mass flow in the tunnel will involve an increase of the speed of the stream surrounding the wake above the relative speed far ahead of the model. It is necessary, therefore, to add an additional correction to the tunnel speed for the wake blockage. In addition, the presence of the wake will produce a pressure gradient along the tunnel axis* which will give a spurious drag increase for which it is necessary to apply a correction. It should be noted that blockage influences only the axial velocity distribution and has no influence on the transverse velocity.

2.8.2. Lift Effect.—This effect arises from the constraint of the boundaries on the velocity field of the circulation associated with the lift. The lift effect on the axial velocity component is zero, and it is only the transverse velocities which are influenced. The constraint is equivalent to a curvature of the flow in an unlimited stream and involves an effective change of camber and (since the centroid of the bound vortex system is situated at approximately the quarter-chord point and not at half chord) incidence. In practice it is inconvenient to apply a correction to

* It is assumed that there is no pressure gradient along the axis of the empty tunnel. If the cross-sectional area is constant along the working section, a pressure gradient will occur due to the growth of the boundary layer of the walls. This may be avoided, however, by the provision of a suitable gradual expansion of cross-section.

camber (since data are required for an aerofoil of given camber) and it is, therefore, usual to assume a plausible relation between camber, lift and pitching moment, and to apply corrections to the latter quantities alone. Similarly it is often inconvenient to correct incidence, and the lift curve slope (which is usually known with sufficient accuracy) is used to convert this correction to a correction to lift at constant incidence.

2.8.3. *Corrections at Low Speed.*—In addition to the corrections summarised by Glauert¹¹⁰, equations have been given by Goldstein¹¹⁶, by Young and Squire¹¹² and by others. The equations given by Glauert neglect, in general, terms of higher degree than

$$\left(\frac{c}{2h}\right)^2, \left(\frac{t}{2h}\right)^2, C_D \left(\frac{c}{2h}\right), \eta \left(\frac{t}{2h}\right),$$

where c is the aerofoil chord and t its maximum thickness, $2h$ is the tunnel height normal to the chord-span plane. C_D is the drag coefficient and η is an empirical factor used by Glauert to represent the width of the wake. Goldstein¹¹⁶ has given the corrections to the order $(c/h)^4$.

The equations given by Glauert may be written:

	Lift Effect	Solid-blockage Effect	Wake-blockage Effect
$V_f - V$		$+\frac{\pi^2}{12} \lambda \left(\frac{t}{2h}\right)^2 V \quad \{= \varepsilon_s V\}$	$+\left(\frac{t}{2h}\right) \eta V \quad \{= \varepsilon_w V\}$
$C_{L,f} - C_L$	$+\frac{\pi^2}{24} \left(\frac{c}{2h}\right)^2 (C_L + 2C_M)$	$-\frac{\pi^2}{6} \lambda \left(\frac{t}{2h}\right)^2 C_L$	$-2 \left(\frac{t}{2h}\right) \eta C_L$
$C_{M,f} - C_M$	$+\frac{\pi^2}{192} \left(\frac{c}{2h}\right)^2 C_L$	$-\frac{\pi^2}{6} \lambda \left(\frac{t}{2h}\right)^2 C_M$	$-2 \left(\frac{t}{2h}\right) \eta C_M$
$C_{D,f} - C_D$		$-\frac{\pi^2}{6} \lambda \left(\frac{t}{2h}\right)^2 C_D$	$-2 \left(\frac{t}{2h}\right) \eta C_D$

Note.— C_M is the pitching-moment coefficient about the quarter-chord point.

where the terms without suffix apply to the measured values, and the terms with suffix f to the values corrected to free-air conditions. The corrected coefficients apply to an incidence equal to the value in the tunnel and have been obtained in the above form on the assumption of a lift-curve slope of 2π . The blockage corrections to the lift and moment coefficients enter purely as corrections to dynamic head. λ is a factor dependent on the shape of the 'basic profile' of the aerofoil (defined as the shape obtained when the camber is removed and the resultant symmetrical aerofoil placed at zero incidence) and is plotted in R. & M. 1566¹¹⁰ for a variety of shapes. The corrections given above do not include a correction for the pressure gradient arising from wake blockage as this is usually negligibly small, and also assume the drag coefficient constant over the small effective incidence change involved in the corrections.

It will be noted that the wake-blockage factor ε_w defined above is independent of the drag coefficient. This will clearly not be true in practice since the factor must increase as the the drag coefficient rises and the wake widens. Such a factor may be obtained by the device of representing the wake by a source suggested by Prandtl¹¹⁵. By this method the factor

$$\varepsilon_w = 1/4 \left(\frac{c}{2h}\right) C_D \quad \dots \quad \dots \quad \dots \quad \dots \quad \dots \quad \dots \quad \dots \quad (54)$$

is obtained. This must then be added to the solid-blockage factor ε_s tabulated above to give the final correction which, for velocity is, for example, of the form

$$V_f = (1 + \varepsilon_s + \varepsilon_w) V \quad \dots \quad \dots \quad \dots \quad \dots \quad \dots \quad \dots \quad \dots \quad (55)$$

More recently Thom¹¹¹ and Young and Squire¹¹² have shown that the blockage may be expressed in terms of the volume of the body. This method is, in general, more convenient than that given above for three-dimensional bodies and wing-body combinations. Thus, for example, for a two-dimensional wing of average thickness Young and Squire give the solid-blockage factor ϵ_s as

$$\epsilon_s = 0.62 \frac{B}{4h^2s} \quad \dots \quad \dots \quad \dots \quad \dots \quad \dots \quad \dots \quad (56)$$

where B is the wing volume and s the span.

Thom gives

$$\begin{aligned} \epsilon_s &= \frac{0.77 ct}{8\pi h^2} \cdot \frac{\pi^2}{3} \\ &= \frac{\pi^2 \left(\frac{t}{2h}\right)^2}{12} \cdot 0.49 \frac{c}{t} \quad \dots \quad \dots \quad \dots \quad \dots \quad \dots \quad \dots \quad (57) \end{aligned}$$

Comparison with the values tabulated above indicate that this is equivalent to replacing λ by $0.49 c/t$. An inspection of the values of λ plotted in R. & M. 1566¹¹⁰ shows that the value $\lambda = 0.49c/t$ is in good agreement with the original values for aerofoils of usual thickness/chord ratio.

2.8.4. Corrections at Compressibility Speeds.—The linear-perturbation theory has been used by Goldstein and Young¹¹⁷, by Thom¹¹¹, by Allen and Vincenti¹¹³ and by others¹¹⁸ to obtain equations for the corrections for boundary constraint at high Mach number. In general it is possible to retain the form of the low-speed corrections given above, and introduce the effects of compressibility by multiplication by some appropriate power of β , where $\beta = (1 - M^2)^{1/2}$. Strictly the method of superposition on which all low-speed corrections are based is not applicable at high Mach number where the differential equations are no longer linear in the physical plane. On the assumption that the disturbing velocity is small compared with the free-stream velocity, however, it is possible to obtain approximate linear equations. The resultant expressions are, however, only strictly applicable to thin aerofoils of small camber at low incidence and become inaccurate as the Mach number is increased. They are all based on low-speed corrections of the order of accuracy (*i.e.*, $(c/h)^2$) given by Glauert¹¹⁰. The corrections given by Goldstein and Young¹¹⁷ are based on the equations summarised by Glauert¹¹⁰ but include no correction to the lift and moment coefficients for the change of dynamic head associated with the correction to velocity (and, therefore, density) due to blockage. The corrections retain the empirical factor η in the wake-blockage terms and neglect the correction to drag due to the pressure gradient associated with wake blockage. Thom¹¹¹ concludes that this latter correction is negligible and gives corrections for blockage for all force and moment coefficients basing the wake-blockage correction on the drag coefficient by the use of a source to represent the wake. Allen and Vincenti¹¹³ give corrections for both the lift and blockage effects basing the wake blockage on the drag coefficient, and including a term to allow for the influence of the associated pressure gradient on the drag. The corrections in the form used at the N.P.L. are given in Table 1. Since it is usually inconvenient to correct the incidence, this correction has been written in the form of a correction to lift coefficient at constant incidence. At present there is no evidence that these corrections are the best. Allen and Vincenti¹¹³ give a method for the correction of the aerofoil pressure distribution for the influence of wall interference. Such a method has not, however, been used to date at the N.P.L.

There is experimental evidence that the corrections given above and based on the linear-perturbation theory underestimate the blockage at high Mach number (greater than 0.8 of the choking Mach number say) if the β terms are based on the uncorrected Mach number*. By considering the mass flow through the tunnel Thom¹¹⁴, ¹¹⁹ suggests that it is necessary to apply an additional blockage correction which increases rapidly as the Mach number approaches the

* There is some doubt concerning the appropriate value of M to be used in the determination of the powers of $\beta = (1 - M^2)^{1/2}$ which appear in the equations. The uncorrected values have often been used, but it has been argued that it is more appropriate to use the corrected values. The latter method is rather difficult to apply as a process of successive approximation is necessary.

choking value. Two alternative methods for the determination of this correction have been suggested—the first involves the multiplication of the solid-blockage factor determined by the linear perturbation theory by a factor μ , and the second is based on measurements of the pressures at the tunnel walls. Values of the factor μ are given in R. & M. 2385¹¹⁴ for a range of values of the ratio of the tunnel Mach number to the choking tunnel Mach number and of the ratio of the two-dimensional aerofoil chord to the tunnel height. If the blockage factor ε is determined by this method the corrections to the Mach number and force coefficients follow from the expressions:—

$$M_f - M = \varepsilon(1 + 0.2M^2)M \quad \dots \dots \dots (58)$$

$$C_f - C = -\varepsilon(2 - M^2)C \quad \dots \dots \dots (59)$$

where C stands for C_L , C_M or C_D .

TABLE 1

Corrections for Wall Interference for an Aerofoil Completely Spanning a Closed Rectangular Tunnel of Height $2h$

	Lift Effect	Solid-blockage Effect	Wake-blockage Effect	
			(i)	(ii)
$V_f - V$		$+\frac{1}{\beta^3} \frac{\pi^2}{12} \lambda \left(\frac{t}{2h}\right)^2 V \{=\varepsilon_s V\}$	$+\frac{1+0.4M^2}{\beta^2} \frac{1}{4} \left(\frac{c}{2h}\right) C_D V \{=\varepsilon_w V\}$	
$M_f - M$		$+\frac{1+0.2M^2}{\beta^3} \frac{\pi^2}{12} \lambda \left(\frac{t}{2h}\right)^2 V$	$+\frac{(1+0.4M^2)(1+0.2M^2)}{\beta^2} \times \frac{1}{4} \left(\frac{c}{2h}\right) C_D M$	
$C_{L,f} - C_L$	$-\frac{1}{\beta^2} \frac{\pi^2}{24} \left(\frac{c}{2h}\right)^2 (C_L + 2C_M)^*$	$-\frac{2-M^2}{\beta^3} \frac{\pi^2}{12} \lambda \left(\frac{t}{2h}\right)^2 C_L$	$-\frac{(2-M^2)(1+0.4M^2)}{\beta^2} \times \frac{1}{4} \left(\frac{c}{2h}\right) C_D C_L$	
$C_{M,f} - C_M$	$+\frac{1}{\beta^2} \frac{\pi^2}{192} \left(\frac{c}{2h}\right)^2 C_L$	$-\frac{2-M^2}{\beta^3} \frac{\pi^2}{12} \lambda \left(\frac{t}{2h}\right)^2 C_M$	$-\frac{(2-M^2)(1+0.4M^2)}{\beta^2} \times \frac{1}{4} \left(\frac{c}{2h}\right) C_D C_M$	
$C_{D,f} - C_D$		$-\frac{2-M^2}{\beta^3} \frac{\pi^2}{12} \lambda \left(\frac{t}{2h}\right)^2 C_D$	$-\frac{(2-M^2)(1+0.4M^2)}{\beta^2} \times \frac{1}{4} \left(\frac{c}{2h}\right) C_D^2$	$-\frac{1+0.4M^2}{\beta^3} \times \frac{\pi^2}{12} \lambda \left(\frac{t}{2h}\right)^2 C_D$

Notes.— $\beta = (1 - M^2)^{1/2}$. $\gamma = 1.40$. Terms without suffix refer to values measured in the tunnel.

Terms with suffix f refer to corrected values. The corrected lift and moment coefficients apply at the tunnel incidence α . C_M is the pitching-moment coefficient about quarter-chord.

* It is generally more accurate to use the experimental lift-curve slope a_0 rather than the theoretical low-speed value 2π . This may be included by multiplying the expression by $a_0 \beta / 2\pi$.

The solid blockage and wake blockage (i) corrections to the force and moment coefficients are corrections due to the change of dynamic head.

The wake blockage (ii) correction to drag is for the effect of the pressure gradient.

In the 12-in. diameter tunnel it has been the practice to apply a correction for blockage alone. The correction employed is based on some early experiments on two aerofoils of N.2030 section and of 2 and 1.2-in. chord. The speed at the model is taken to be the speed well upstream plus 0.4 of the difference between this latter speed and that at the wall opposite the model. More recently, the interference at high speed in a closed circular tunnel has been discussed on a theoretical basis by Vincenti and Graham¹²⁴.

The requirement of the above correction makes it difficult (in common with all high-speed tunnels with unstreamlined walls) to use the Machmeter to obtain even values of the Mach number at the model. This difficulty has been overcome in the 12-in. diameter tunnel by the use of a system of capillary tubing in a leak connection between pressure holes opposite and upstream of the model thus enabling a pressure equivalent to the static pressure corresponding to the corrected tunnel speed to be connected to one side of the Machmeter.

It is realized that this correction in the 12-in. diameter tunnel may be inaccurate, particularly as the choking speed is approached. In view of other sources of error of comparable magnitude, however, a more complex correction seems unjustifiable, particularly in the case of balance measurements.

2.8.5. Tunnel Choking.—A high-speed subsonic tunnel is said to be 'choked' when further increase of power input to the prime mover produces no increase of Mach number in the working section ahead of the model. This is equivalent to defining the choked condition as the condition when the rate of mass flow through the tunnel reaches a maximum. When the tunnel is empty (*i.e.*, there is no model in the working section) choking normally occurs when the velocity across some cross-section of the tunnel becomes equal to the critical sonic value. As shown in Fig. 2 of Ref. 81 the mass flow through the choked section is a maximum when this condition is reached. In a direct-action tunnel choking may be produced at the downstream end of the working section by the growth of the boundary layers of the tunnel walls. In an induction-type tunnel, however, there is evidence that empty tunnel choking may in some instances be due to the formation of a choked throat in the region of the injector slot.

When a model is placed in the working section it is, in general, found that the choking speed* of the tunnel is lowered. Choking under these conditions normally occurs in the region of the model. This phenomenon may be explained by the assumption that choking occurs when sonic velocity spreads uniformly between the model and the tunnel walls. On this assumption the choking speed can be calculated with moderate accuracy, and the rise of drag without further increase of Mach number ahead of the model explained. Thom^{111, 114} has recently given an alternative analysis which suggests that choking occurs when the regions of supersonic velocity near the model extend so far that further rise of the velocity ahead of the model produces such a reduction of mass flow through the supersonic regions that it neutralizes the increased mass flow in the region of subsonic velocity nearer the tunnel walls. This explanation is also compatible with the observed increase of the drag of the model with increase of the power input to the tunnel after choking has occurred. This drag rise is due to the increase of the size of the supersonic regions and of the amplitude and extent of the associated shock-waves and flow separations.

There is at present no reliable method of reducing measurements made in a tunnel after choking has occurred to an equivalent flow in free air. Indeed it is doubtful if the flow pattern round the model in the choked condition corresponds to any flow which may occur in an unlimited stream. None of the methods of calculating the corrections for wall interference based on the representation of the model by source, sink and vortex combinations can account for the phenomenon of choking, but Thom¹¹⁴ has suggested an alternative method based on considerations of the mass flow through the tunnel, of calculating the blockage corrections below the choking speed which does predict choking. The accuracy of all corrections for wall interference becomes uncertain, however, as the choking speed is approached.

* The choking speed is defined as the tunnel speed (*i.e.*, the speed in the working section sufficiently far upstream to be uninfluenced by the presence of the model) at which choking takes place. The choking Mach number is the Mach number corresponding to this value of the tunnel speed.

Since heat release in a channel is accompanied by a Mach number change towards unity it should be noted that, if the airstream contains moisture, condensation may lead to a decrease of the choking speed of a subsonic tunnel. This is discussed in section 2.6.3.

By the use of adjustable walls it is, in theory, possible to streamline them and to eliminate tunnel interference and choking at all Mach numbers. Since at unit Mach number the Mach number is infinitely sensitive to changes of the cross-sectional area, however (*see* Fig. 2 of Ref. 81), it is not possible to streamline the walls in practice at Mach numbers close to unity. Moreover, the theoretical considerations on which the standard N.P.L. method of determining the streamline shape is based certainly became invalid when the shock-wave from the aerofoil extends to the wall and are probably inaccurate at a lower Mach number. Since a streamline is deflected suddenly at an oblique shock-wave the adjustable walls must be capable of such sudden changes of slope if they are used to imitate streamlines in a supersonic flow. It is indicated below, however, that it is not necessary, in general, to streamline the walls of a supersonic tunnel.

The observed limiting working-section Mach numbers for the N.P.L. 20×8 -in. tunnel are plotted in Fig. 30 for straight walls and for walls streamlined by the standard method. It should be noted that the measurements on which this figure is based were subject to the influence of the condensation of atmospheric humidity. More recent observations with dry air have indicated that the limiting tunnel speeds are now increased above the values plotted. The experimental values are compared with the theoretical choking Mach numbers calculated on the basis of the original one-dimensional theory described above. It would be expected that this simple theory would over rather than under-estimate the choking speed, but Fig. 30 indicates that the converse is apparently true for the 20×8 -in. tunnel. This discrepancy which does not appear to be confirmed by experiments at the R.A.E.¹⁷⁴ and in America¹²³ must be attributed partly to a departure of the flow from uniformity across the tunnel and chiefly to the condensation of moisture. It may also be connected with the small longitudinal gaps at the sides of the adjustable walls.

2.8.6. *Interference due to the Boundary Layer of the Side Walls.*—The presence of the boundary layer of the side walls has three effects:—

- (a) The spread of turbulence from the wall boundary layer by transverse contamination along the aerofoil span may have an appreciable effect on the force coefficients and pressure distribution, particularly if a large part of the aerofoil boundary layer is naturally laminar. In the N.P.L. 20×8 -in. tunnel, however, explorations and observations with chemical transition indicators⁷⁸ have shown that the flow over the centre part of the aerofoil (on which all measurements are made) is not influenced by this phenomenon.
- (b) Interference will arise from the induced velocity of the images of the trailing vortices formed as the lift of the aerofoil decays in the boundary layers of the side walls. With a 5-in. chord model the correction required for this effect is, according to Preston⁷⁵, of the order* of 2 to 3 per cent on incidence, and is often neglected.
- (c) The presence of the boundary layers on the side walls may also result in a slight departure from two-dimensional flow over a large part of the span. Thus, for example, spanwise flow has been observed close to the surface of an aerofoil at the leading and trailing edges by the use of an oil-film technique. It seems, however, that this effect is unimportant in most tests in the 20×8 -in. tunnel.

2.9. *The Adjustable Walls of the N.P.L. 20×8 -in. Tunnel.*—The adjustable walls of the 20×8 -in. tunnel are shown in Fig. 31 diagrammatically, and a drawing of one of the micrometers together with its attachment to the wall is shown in Fig. 32. The walls are fitted with surface

* There is evidence that Preston's theory overestimates the magnitude of this effect. This may be because he assumes the flow to be two-dimensional at each element of the span.

pressure holes at each micrometer and the method of setting the walls is based on pressure measurements at these. The tunnel speed is measured on hole 13B upstream of the model as shown in Fig. 31.

Up to the end of 1944 the standard method of setting the walls for no lift was based on some early theoretical work by Taylor and by Goldstein (*see* Appendix II of R. & M. 2005²³). This shows that for compressible flow past a corrugated wall analysable into a Fourier series, the pressure variations along a straight wall parallel to it are twice those at the same points in the absence of the wall. Thus the tunnel wall settings corresponding to free-air conditions should be such that the pressure variations along the walls produced by the presence of the model are half those which would be observed on a straight wall. Assuming linearity between pressures and tunnel width, it was concluded that it would be sufficient to set the walls half-way between the straight position and the position for uniform pressures when the model was in the tunnel. The wall settings for uniform pressure were determined experimentally, and the 'straight' position was taken as that giving zero pressure gradient with the tunnel empty. Thus the straight wall setting included an allowance for the growth of the wall boundary layer.

When the aerofoil is experiencing a lift, equal uniform pressures on the two walls can only be obtained by bending the axis of the tunnel through a finite angle θ , which is related to the lift coefficient by the expression

$$\theta = \frac{cC_L}{4\pi}, \text{ to the first order in } C_L, \quad \dots \quad (60)$$

where c is the aerofoil chord, C_L the lift coefficient and $2h$ the tunnel height. Such a shape could not be imitated in the existing tunnel and the following alternative scheme was adopted. The walls were adjusted to give a constant pressure along each but differing on the two sides of the tunnel, the value of the difference depending on the lift. The walls were then set to a position half-way between the straight setting and the position for level pressures with the model present as in the case of zero lift. Lock and Beavan have examined the problem in detail in R. & M. 2005²³, and have concluded that a better approximation to the streamline wall settings can be obtained at zero lift by setting the walls 0.6 of the distance between the straight settings and the settings for level pressures with the model present (closer to the latter). For a finite lift the following method is now generally used at the N.P.L.

With the aerofoil at its test incidence the walls are first experimentally set for constant pressures (unequal on the two sides). Then 0.6 of the mean change of the two sides from the straight condition of uniform pressure in the empty tunnel is added to the latter together with an amount, positive on one side and negative on the other, calculated from equation (61) below for a single vortex in free air based on the estimated lift coefficient at the particular Mach number considered. The lift coefficient is usually known to a sufficient degree of accuracy from preliminary tests, either by the measurement of the normal pressure distribution over the model or by the integration of the tunnel wall pressures.

Since the wall settings will, in general, differ for each Mach number and lift coefficient the above method involves a considerable amount of labour in practice, and the use of adjustable walls in future high speed tunnels has been criticised on this and other grounds in Ref. 74.

2.9.1. *Streamlines and Pressures round a Doublet, Vortex and Source.*—In R. & M. 2005²³, Lock and Beavan use image systems and the linear-perturbation theory as given by Goldstein and Young¹¹⁷ to calculate the streamline deflections and pressure changes produced by the introduction of a doublet, vortex and source at the origin. The equation for the deflection δ of the streamline (o, h) produced by a vortex of strength k without tunnel walls is alone reproduced here since it is used directly in the calculation of the wall setting (*see* section 2.11).

$$\frac{2\pi U}{\beta k} \delta = -\frac{1}{2} \log \left(1 + \left\{ \frac{x}{\beta h} \right\}^2 \right). \quad \dots \quad (61)$$

Here U is the streamwise velocity, x the distance from the origin parallel to the tunnel axis and, as before, $\beta = (1 - M^2)^{1/2}$. Equations for the streamline deflection and pressure change due to a doublet and source as well as a vortex are given in R. & M. 2005²³ with no walls, straight walls and constant pressure walls. The results are summarised in Fig. 33 where expressions proportional to the streamline deflection and pressure change are plotted as ordinate against the quantity $x/\beta h$ as abscissa for straight and constant pressure walls and the free-air case for a doublet, source and vortex at the origin. It appears from this figure that for either a doublet or source (no lift) at the origin the free-air wall shape lies approximately 0.6 of the way between straight and constant pressure settings. For finite lift the free-stream wall shape for a vortex can be imitated without difficulty by the adjustable walls of the 20 × 8-in. tunnel over their available length in spite of the logarithmic infinity of equation (61).

If the aerofoil could be replaced by a known system of doublets, vortices and sources, it would be possible to calculate the ideal streamline wall setting at each Mach number and lift coefficient. In practice, however, this system is quite unknown. The wall settings for a simple doublet and source together with the additional displacement required to allow for the lift on the basis of a single vortex have, however, been used in the derivation of the method of wall setting described in section 2.11 below. Since this method of wall setting is based on the use of doublets, vortices and sources to represent the aerofoil, on the method of superposition, and on the linear-perturbation theory, its theoretical basis is no more sound than that of the corrections discussed above for the wall interference in a straight-walled tunnel. Nevertheless, the use of adjustable walls increases the choking speed of the tunnel, and an examination of experimental results has indicated that the results appear to be reliable up to nearly the top speed of the tunnel.

2.9.2. *Experimental Observations using the Adjustable Walls.*—Typical examples of the pressure distributions along the straight walls with a 5-in. chord aerofoil of EC 1250 section at 2 deg incidence in the working section are shown in Fig. 34. The difference between the pressure at a reference point in one of the longer (side) walls ahead of the model and at the adjustable walls in inches of water is plotted against distance along the tunnel axis for a number of Mach numbers measured at hole 13B ahead of the model. An approximate scale of Mach number is appended to the ordinate. The local increment of Mach number due to the presence of the aerofoil is separated into the effects of blockage and lift in the lower parts of Fig. 34, where the sums and differences of the pressure differences on the two sides of the tunnel are plotted for a range of Mach numbers. The blockage figure illustrates typically the effects of this phenomenon on the axial velocity distribution. It would be anticipated from theory that the peaks of the blockage curves would occur opposite the mid-chord of the aerofoil (position of maximum thickness) and that those of the lift effect would occur opposite the quarter-chord point (centroid of the bound vortex system). This is well fulfilled at the lower Mach numbers, but both peaks move downstream at higher Mach number.

An examination of the blockage curve illustrates the effects of solid and wake blockage, but the latter is best seen from Fig. 35 where the changes of pressure and Mach number 1.7 chords behind the trailing edge are plotted against the Mach number well ahead of the aerofoil for a range of incidence. Theoretical curves calculated by a method due to Thom¹¹¹ are included and the agreement is reasonably good up to the highest Mach number. The effects of blockage are summarised in Fig. 36 where the peak pressure difference opposite the model is plotted against the Mach number ahead of the model. Curves calculated by potential theory for an ellipse of the same thickness and at the same incidence as the aerofoil are added, and it can be seen that the curves begin to diverge appreciably at Mach numbers greater than about 0.7. Beyond this point up to the top speed of the tunnel (even, it is found, after the shock-wave from the aerofoil has reached the wall on one side) the curve of rise is smooth. A large part of this excess rise is due to the increasing importance of the wake-blockage component at the higher tunnel speeds. This is best seen in Fig. 37 where sample blockage curves at high Mach number have been analysed into the solid and wake-blockage components, the latter being assumed to be of the form produced by a source. The full lines for the solid-blockage component are obtained as

the difference between the total and wake blockage, and the broken lines are calculated for doublets of strength sufficient to give the same peak solid blockage. It may be seen that, if the wake blockage is large (as it is when the drag rises at the shock-stall), it will add to the solid blockage opposite the centre of the aerofoil (which is all that can be predicted by potential theory) and will account for the rearward shift of the peak blockage pressure at the higher Mach numbers.

On the basis of the above and other evidence it seems that simple doublet and source system may be used to replace the aerofoil as regards blockage up to a very high Mach number. The alternative analyses of Fig. 37 show, however, that the positioning of the equivalent source may be of importance as regards the choice of the magnitude of the equivalent doublet.

The lift effect is shown in Fig. 38 where the difference between the pressures at the two walls (the mean values at equal positive and negative incidences) are plotted as a function of Mach number. Theoretical curves for a vortex of strength based on the lift coefficient of the aerofoil are added, and it may be seen that these curves are in good agreement with the experimental observations over the greater part of the range of Mach number. Thus it appears that the simple vortex may be used with satisfactory accuracy to represent the lift of the aerofoil. The assumption that the lift and blockage effects are independent is also justified.

2.9.3. Lift by the Integration of Wall Pressures.—It has been indicated that when the aerofoil is experiencing lift it is impossible to shape the walls of the tunnel to give pressures which are constant on each and equal on the two sides of the tunnel. In practice it is found that for any given value of the lift there is a particular value of this pressure difference which is most easy to obtain. If it is assumed that any force on the aerofoil normal to the stream is transmitted by pressure to the walls it should be possible to deduce the lift by an integration of the differential wall pressures.

With the straight walls the available length is sufficient to enable the lift to be deduced, but with the streamline settings the wall pressure variations fall off more gradually and a greater length than that provided in the 20×8 -in. tunnel is required. In Fig. 39 the lift coefficients deduced from surface-pressure plotting at the aerofoil are compared with values deduced from the integration of the pressures on the available length of the straight walls. The form of the two curves is similar, but there is a discrepancy of the order of from 5 to 10 per cent, although theoretically this should be only 1 per cent (based on the curve of Fig. 33 for the pressures around a vortex). This discrepancy is attributed in R. & M. 2005²³ to the fact that the wall pressures are measured at the middle of the wall and that the pressure is not uniform across the wall. It would seem to be reasonable to use a factor to correct for this. With the available length of streamlined walls the discrepancy would theoretically be of the order of 20 per cent and this has been confirmed experimentally. Again a correction factor appears to be permissible.

Apart from certain special applications, the lift is usually obtained by the integration of normal pressures over the model rather than the wall at the N.P.L. since the former gives a considerable amount of useful information in addition to the lift coefficient.

2.10. Intercomparison of Observations with Straight and Streamlined Walls.—The lift, moment and drag coefficients of a 10 per cent thick NACA (N 1050/1650) aerofoil with straight and streamlined walls are shown in Figs. 40 to 42. The points shown correspond to the corrected values of the measurements with straight walls. The corrections have been applied by the equations given in Table 1 above, and based on the uncorrected Mach number, together with the additional factor μ suggested by Thom. In general it appears that, with the exception of lift at high incidence, the corrected observations with the straight walls are in satisfactory agreement with the observations made with the walls streamlined. The lift curves were corrected by the use of the experimental value of the lift-curve slope and not the theoretical value.

2.11. Wall Interference at Supersonic Speeds.—The interference due to the presence of the tunnel walls on a two-dimensional aerofoil in a supersonic stream has been considered by Hilton²⁴ and others. In the usual manner, the boundary condition of zero normal velocity may be satisfied

by replacing the wall by an infinite series of images. A single image is shown in Fig. 43 and it is clear that if the flow is everywhere supersonic no interference will be experienced by the aerofoil provided that it is upstream of the bow-wave of the image A, the portion CB of this wave coinciding with the reflection of the aerofoil bow-wave from the tunnel wall. On the assumption of wholly supersonic flow, therefore, the criterion for zero wall interference is that the reflection of the bow-wave shall not strike the aerofoil. A similar criterion applies to models other than the two-dimensional aerofoil.

In a real flow, regions of subsonic velocity always exist in the boundary-layers of the tunnel walls and in the aerofoil wake. Thus it is possible for the model to be influenced by the propagation of disturbances upstream in these regions. All possibility of upstream propagation in the wake could be eliminated by ensuring that reflected bow-wave only meets the wake sufficiently far downstream of the trailing edge for flow in the wake to be supersonic. The possibility of upstream propagation in the tunnel-wall boundary layers is, however, always present. There is, however, experimental evidence to indicate that the model will be free from wall interference provided that the reflected bow-wave does not strike the wake too close to the trailing edge (less than 1 chord behind the trailing edge for an aerofoil or 3 calibres behind the base of a projectile).

If the nose of the aerofoil is blunt, the incidence high or the free-stream Mach number low, deceleration to a subsonic velocity may take place behind the bow-wave. If the region of subsonic velocity extends to the wall the aerofoil will become subject to wall interference or, more strictly, all parts of the aerofoil over which the velocity is subsonic will experience interference from all parts of the wall over which the velocity is subsonic provided that a region of supersonic velocity does not intervene. In addition to observing the reflected bow-wave it is also necessary, therefore, to ensure that the pressure at the tunnel wall in the vicinity of the model never falls to a value corresponding to a subsonic velocity.

It is, therefore, possible (and necessary) to ensure that a model in a supersonic tunnel is free from wall interference provided that the Mach number is sufficiently high. As the Mach number falls towards unity, however, it is necessary to decrease the model size (to zero at $M = 1$) if interference is to be avoided.

If the cross-section of the tunnel is circular, and the model completely spans the tunnel, the regions of the span close to the walls will always be subject to interference from the reflected bow-wave. Moreover, there is some evidence, both experimental⁹² and theoretical¹⁵², that disturbances on the axis of a circular tunnel are more violent than elsewhere in the flow. For example, it seems that a disturbance originating around the periphery of the tunnel must build up into a disturbance of high amplitude towards the apex of the disturbance cone near the tunnel axis. Thus a circular cross-section besides being unsuitable for two-dimensional work is also unsuitable for three-dimensional tests since in the latter the model will be supported close to the axis and moreover may be long in the direction of the stream so that axial variations have an important effect.

Moreover, the use of a circular cross-section does not permit the use of sensitive optical systems of either the direct shadow, schlieren or interferometer type. The construction of nozzle liners is simpler with a tunnel of rectangular section than with a circular tunnel. Also, it is probable that it is easier to make an experimental correction for errors in the initial design of the nozzle in a two-dimensional than in a three-dimensional nozzle.

There is, therefore, an overwhelming argument against the use of a circular cross-section for supersonic wind tunnels. As regards the choice of suitable relative dimensions for the rectangular section, considerations of the possibility of testing both two and three-dimensional models and of obtaining a reasonable depth of optical field appear to favour a section approximating to square. If, however, the tunnel is also to be used for two-dimensional tests at high subsonic and low supersonic Mach numbers it may be desirable for the tunnel dimension normal to the chord-span plane to be increased so that the wall interference is reduced. These considerations led to the choice of the cross-sectional shape of the proposed 18 × 14-in. N.P.L. subsonic and supersonic tunnel.

Apart from a number of small tunnels and a few supersonic runs of the 20×8 -in. tunnel, the only large tunnel available for supersonic operation in the N.P.L. Aerodynamics Division has been the 1-ft diameter tunnel. This tunnel was not originally intended for supersonic running but has recently been extensively used for this purpose. Many interesting results have been obtained, but, for the reasons outlined above, tests have not been as complete as might be desired, and many of the results may be subject to errors of uncertain magnitude. Nevertheless, two-dimensional supersonic tests in this tunnel have been in good agreement with theory and the results of tests made elsewhere. A cylindrical working section of 'Perspex' has enabled some limited flow visualization to be done. It is hoped* in the near future to install a working section $9\frac{1}{2}$ -in. square to fit on to the injector and diffuser of the existing tunnel with an intermediate transition piece.

2.12. Yawmeters.—Some work was done early in the life of the N.P.L. high-speed tunnels to investigate the effects of increasing Mach number on the sensitivity of various types of yawmeter, and to develop an instrument suitable for use at high speeds. The use of such an instrument is of importance in the calibration of the flow in the working section, and in exploring the flow round, and downstream of, an aerofoil model. Several types of yawmeter including the aerofoil, circular cylinder and several instruments of the bent pitot-tube type were tested.

2.12.1. Aerofoil Yawmeter.—This instrument consists of a 2-in. chord, 2-in. span aerofoil of EC 1250 section with a single pressure hole in each surface 0.15 of the chord from the leading edge. This pressure-hole position was chosen to give maximum sensitivity to yaw over the required range of Mach number by a consideration of the pressure distributions measured on a 5-in. chord model in the 20×8 -in. tunnel. The aerofoil is usually mounted at the centre of a streamline strut ($1\frac{1}{2}$ -in. chord) which completely spans the tunnel, but it may also be mounted on an end bar. The instrument has been used extensively to determine the yaw and swirl at the working sections of the 12-in. diameter and 20×8 -in. tunnels, the swirl being deduced from a measurement of yaw at several points across the section.

The method of yaw measurement consists of varying the incidence of the yawmeter until equal pressures are recorded at the two measuring holes. The incidence of the yawmeter is varied in the 12-in. diameter tunnel by using the incidence changing gear of the three-component electric balance in which the instrument is mounted. In the 20×8 -in. tunnel the yawmeter is usually mounted at the position of the two small portholes (Fig. 8(a) of Ref. 81) upstream of the normal model position, and a specially constructed gear is used for varying the incidence.

A sketch of the aerofoil yawmeter is given in Fig. 44(a) and typical calibration curves in Fig. 44(b); the influence of tunnel speed on the sensitivity is indicated in Fig. 44(c). The instrument has been found satisfactory for tunnel calibration, and has also been used to measure the downwash downstream of a 5-in. chord aerofoil in the 20×8 -in. tunnel. It is, however, rather unsatisfactory (and quite useless with its present size) for detailed explorations of the flow round an aerofoil because of the disturbance which it produces. Moreover, at very high speeds, the static pressure on the surface is limited by the attainment of sonic speed further downstream and it might be expected that at such speeds the sensitivity of the instrument would fall. This is shown in Fig. 44(c).

2.12.2. The Circular-Cylinder Yawmeter.—This instrument has the advantage that it may be rotated without giving rise to additional disturbances of the flow. The method of operation of the instrument again involves a rotation until equal pressures are recorded at two holes in the surface. Preliminary tests only have been made with this yawmeter in the N.P.L. high-speed tunnels, and these indicate that the instrument is satisfactory. The positions of the pressure holes for maximum sensitivity were calculated from Stanton's original measurements of the pressure distribution round a cylinder at high speeds⁴¹. In Stanton's paper the value of $\kappa = p/\rho V^2$

* This was done in January, 1948.

(where p is the pressure on the cylinder at a point subtending an angle θ with the leading edge, ρ is the free-stream density and V the free-stream velocity) is plotted against θ . From these observations the value of $d\alpha/d\theta$ has been plotted in Fig. 45 as a function of θ and free-stream Mach number.

It has been suggested that by the use of a third hole at the trailing edge of the cylinder, it should be possible to obtain measurements of velocity simultaneously with those of yaw. A sketch of the head of the instrument used at the N.P.L. is given in Fig. 46.

2.12.3. *Bent-Tube Yawmeters.*—This type of instrument consists of two or more pitot-tubes inclined to the airstream. The tubes are arranged symmetrically, and the whole yaw head inclined until equal pressures are recorded at each tube. The original instrument tested consisted of two pitot-tubes inclined towards each other at angles of 45 deg to the axis of the instrument (Fig. 47), the design being similar to that of the usual low-speed type¹²⁰. The tube mouths are arranged close together so that errors associated with small space variations of yaw and speed are minimised. The instrument was found to be satisfactory at low speeds, but to give very unsteady and unreliable readings at higher speeds due, presumably, to the increased mutual interference of the two tubes. In an attempt to obtain a more satisfactory instrument a yawmeter consisting of two pitot-tubes inclined apart in the form of a Y was tested. Whilst steadier observations were obtained with this than with the original instrument, it was still unsatisfactory and has the additional disadvantage of magnifying the effects of space fluctuations. It appears that an instrument of this type, whilst lending itself to construction on a small scale, is not very suitable for use at high speeds.

2.13. *Optical Systems of Flow Exploration.*—Methods of flow exploration depending on measurements of the distribution of stagnation and static pressure have several disadvantages.

- (a) With the exception of the measurement of normal surface pressure, all such methods involve the introduction of a disturbance into the flow field.
- (b) The inertia of the measuring apparatus is usually high (with the exception of certain types of pressure capsule), and such methods are, therefore, suitable for measurements in steady flow alone.
- (c) The labour involved in the exploration of large fields is considerable, particularly at high Mach number where the disturbance and interference of a comb of exploring tubes is usually prohibitive.
- (d) Unless yawmeters are used the observations are often subject to the effects of yaw.
- (e) In the case of the measurement of static pressure the boundary layer of the exploring tube may prevent the accurate recording of a sharp pressure change.
- (f) It may be difficult to avoid vibration of the exploring tube thus, introducing an unknown effect on the recorded pressure. This implies the necessity of a rigid support and should also be classified under (a).
- (g) Static pressure tubes in a supersonic stream are subject to a small extent to the influence of the bow-wave of the tube, and at high subsonic Mach numbers to the possible formation of local shock waves.

These considerations suggest that an alternative method of flow exploration may be of value in high-speed tunnel work. If the density is known at all points in the flow field it is possible on certain assumptions and with a knowledge of the total head to deduce the pressure and velocity. Moreover, it is well known that the density ρ is related to the refractive index n by the equation of Lorenz which may be written approximately

$$\frac{n - 1}{\rho} = \text{constant} . \quad \dots \dots \dots (62)$$

Thus, the problem of flow exploration may often be reduced to that of determining the refractive index at all points in the field. This suggests the use of one of a number of optical methods which are not subject to any of the limitations of the pressure exploration methods discussed above. Before proceeding to a more detailed description, it may first be of value to outline some simple aspects of the theoretical basis on which the optical methods depend.

Referring to Fig. 48, let Oz represent the undisturbed path of a ray of light, and let A and B represent points on an element of the wave front at O. Suppose now that a disturbance is introduced into the light path with a refractive index gradient normal to Oz which is represented by $\partial n/\partial x$. Then if n is the refractive index at O, the refractive indices n_A and n_B at A and B respectively will be given by

$$n_A = n + \frac{\partial n}{\partial x} \delta x,$$

and

$$n_B = n - \frac{\partial n}{\partial x} \delta x.$$

If v is the velocity of propagation of the wave-front at O, the velocities v_A and v_B at A and B will be

$$v_A = v \frac{n}{n + \frac{\partial n}{\partial x} \delta x},$$

$$v_B = v \frac{n}{n - \frac{\partial n}{\partial x} \delta x}.$$

After a time interval δt , let the wave-front be at A'O'B'. Then the angle BCB' is given by

$$\delta\theta = \frac{AA'}{AC} = \frac{BB'}{BC}$$

and hence if CO, the radius of curvature of the ray, is denoted by R

$$\frac{v \frac{n}{n + \frac{\partial n}{\partial x} \delta x} \delta t}{R - \delta x} = \frac{v \frac{n}{n - \frac{\partial n}{\partial x} \delta x} \delta t}{R + \delta x} \quad \dots \quad \dots \quad \dots \quad \dots \quad \dots \quad \dots \quad \dots \quad (63)$$

or

$$\frac{1}{R} = \frac{1}{n} \frac{\partial n}{\partial x}.$$

Denoting the distance along the ray between O and O' by δs , the deflection $\delta\theta$ of the ray from its undisturbed path is given by

$$\delta\theta = \frac{1}{n} \frac{\partial n}{\partial x} \delta s, \quad \dots \quad \dots \quad \dots \quad \dots \quad \dots \quad \dots \quad \dots \quad (64)$$

and the total deflection θ_x in the x, z plane by

$$\theta_x = \int \frac{1}{n} \frac{\partial n}{\partial x} ds. \quad \dots \quad \dots \quad \dots \quad \dots \quad \dots \quad \dots \quad \dots \quad (65)$$

Similarly the deflection due to the density gradient $\delta n/\delta y$ in the y, z plane is given by

$$\theta_y = \int \frac{1}{n} \frac{\partial n}{\partial y} ds. \quad \dots \quad \dots \quad \dots \quad \dots \quad \dots \quad \dots \quad \dots \quad (66)$$

For the purpose of deducing the refractive index from experimental observations it is then usual¹²¹ to assume that the deviation of the ray from its undisturbed path within the disturbance is infinitesimal so that ds may be replaced by dz in the above equations.

2.13.1. *The Schlieren Method.*—The form of the schlieren^{121, 122, 123} or striation method which is most commonly employed is that usually attributed to Töpler, and in this method an attempt is made to record some quantity from which it is possible to deduce the deflection θ of equation (65). An extended line source of light is usually employed, and the light is generally converted into a parallel beam before passing through the tunnel. Referring to Fig. 49, the light from the source S is converted into a parallel beam by the lens (or mirror) L_1 before entering the working section. Beyond the working section, a second lens L_2 is used to produce an image of the source in the plane K beyond which a camera produces an image of the flow in the working section on a screen or photographic plate. By a suitable choice of camera lens the size of the resultant image may be adjusted over a wide range, and it is usually possible, therefore, to obtain an adequate intensity of illumination.

If the source is of uniform intensity, and the angle ω (Fig. 49) is sufficiently small ($\omega \leq 4$ deg), the image obtained at the screen will be of uniform brilliance. If now an opaque cut-off is introduced in the plane K so that a fraction of the image of the source is obscured, the illumination at the screen will remain uniform (since K is at the focus of L_2) but will be reduced. Referring to Fig. 49, the illumination at the screen will be proportional to the distance a . When a disturbance is introduced into the working section a deflection of the light will take place, and the corresponding part of the image of the source will move a distance Δa relative to the cut-off. Since both this movement and the change of illumination are proportional to the angular deflection θ of equation (65), observations of the change of illumination will be a measure of the density gradient in the tunnel. Thus assuming that θ is small:

$$\Delta a = f_2 \theta, \quad \dots \quad \dots \quad \dots \quad \dots \quad \dots \quad \dots \quad \dots \quad \dots \quad \dots \quad (67)$$

where f_2 is the focal length of the lens L_2 , and

$$\frac{\Delta I}{I} = \frac{\Delta a}{a}, \quad \dots \quad \dots \quad \dots \quad \dots \quad \dots \quad \dots \quad \dots \quad \dots \quad \dots \quad (68)$$

where ΔI is the change of illumination at the screen and I the original value. Hence,

$$\frac{\Delta I}{I} = \frac{f_2}{a} \theta = \frac{f_2}{a} \int \frac{1}{n} \frac{\partial n}{\partial x} dz, \quad \dots \quad \dots \quad \dots \quad \dots \quad \dots \quad \dots \quad \dots \quad \dots \quad \dots \quad (69)$$

from equation (65).

Fig. 50 shows the cut-off as seen from the direction of the axis of the optical system. Considering some particular point of the image of the source originally focused at P_1 , the introduction of the disturbance will displace P_1 to either P_2 or P_0 . The optical system will only indicate the component Δa of this displacement normal to the edge of the cut-off, and since this displacement is a function of the component of the density gradient in this direction, it follows that the line source and cut-out must be placed in a direction perpendicular to that of the density gradient which is to be observed. It is clear that the illumination will be proportional to the image displacement only so long as the image of the source is not deflected right off (or on to) the cut-off.

The sensitivity of the system is directly proportional to the focal length of the second lens or mirror and to the extent of the initial cut-off of the image. If, however, the initial cut-off is too great the system will be insensitive to deflections of the image towards the opaque portion of the cut-off and diffraction effects may become serious. Thus, in practice it is necessary to adjust the cut-off initially so that an image of uniform finite intensity of illumination is obtained. It may be shown that the sensitivity is inversely proportional to the range of deflections over which the image of the source remains partially cut off. Thus, in practice, the sensitivity must not be too high or this range will be exceeded.

The method of operation of a schlieren arrangement of the type described above may be understood by considering Fig. 51 which shows a photograph of the flow around a double-wedge aerofoil at $M = 1.4$ in the 5×2 -in. tunnel at the N.P.L. The cut-off was parallel to the chord with the opaque side in the position shown. The directions of the positive components of the density gradient perpendicular to the edge of the cut-off are shown in Fig. 52, and it is clear from equation (65) that deflections of the light will take place in these directions. Thus, on one side of the chord, expansions cause a deflection off the cut-off and increased illumination, and on the other side, a deflection onto the cut-off and decreased illumination. The converse is true for compressions, and the photographic record is, therefore, symmetrical about a line through the aerofoil chord except that the images of the flow phenomena are of opposite sign on each side. It should be noted that the arrangement indicates only density gradients, and that except in the wake, shock-waves and regions of expansion where the density gradient is finite, the illumination is constant.

Whilst it is theoretically possible to deduce the density quantitatively from records obtained with the arrangement described above, it is found in practice that considerable difficulties arise in the accurate photometric analysis of the record. Thus, few attempts have been made to use this arrangement for determining the density. A more promising method for quantitative use is of the type usually attributed to Ronchi¹²⁵ in which the deflection of the beam of light is effectively measured directly by observing the image of a grid placed a little to one side of the focus of the second lens (Fig. 53).

2.13.2. *The Direct-Shadow Method.*—The direct-shadow or shadowgraph method^{121, 122} which is usually attributed to Dvorak requires simpler optical apparatus than either of the other two optical methods discussed here. It is admirably suited to the demonstration of compressibility phenomena (particularly to the visualization of shock-waves and wakes) and also for routine use in high-speed tunnel work in conjunction with other observations. Of the three methods discussed, it is, however, the least amenable to the numerical determination of the variation of density in the flow field.

In its simplest form the method consists of a light source S on one side of the tunnel, and a screen Q on the other (see Fig. 54). This type of set-up, which is characterised by the use of divergent light, has been extensively used on ballistic ranges for the photography of the flow pattern round projectiles and for this purpose a spark discharge is employed as the light source. For the visualization of the flow round a two-dimensional body placed between the glass walls of the tunnel, however, a more satisfactory arrangement is obtained by collimating the light from the source into a parallel beam before passage through the working section. For this purpose a suitable lens or mirror may be used, and the best results are obtained with a point-light source.

The physical process by which a deflection of the light is caused by the presence of the disturbance is outlined in section 2.13, but in order to understand the mechanism of the action of the direct-shadow method it is necessary to consider the conditions within the disturbance in rather more detail. Referring to Fig. 55 let AB and CD be the undisturbed paths of two adjacent rays. Upon the introduction of the disturbance, the rays will be deflected, and if the refractive index gradient $\partial n/\partial x$ is constant (i.e., $\partial^2 n/\partial x^2 = 0$) the deflected rays will remain parallel as shown in Fig. 55(a). If however, $\partial^2 n/\partial x^2$ is positive, the rays will be deflected as shown in Fig. 55(b), and will diverge, and if $\partial^2 n/\partial x^2$ is negative the deflected rays will converge as shown in Fig. 55(c).

Thus, for example, Fig. 56 shows the variation of the density and its first and second derivatives through a shock-wave. At the front of the shock-wave $\partial^2 n/\partial x^2$ is positive and the rays will diverge giving a region of decreased intensity at the screen, and at the rear of the shock-wave the rays will converge and increase the intensity of illumination. Thus direct-shadow records of shock-waves are characterised by two bands, one dark and the other light, of which the dark band always indicates the front (low pressure) side. This phenomenon is illustrated by Fig. 57. The direct-shadow method will only indicate regions of the flow in which the second derivative of

the density is finite. Thus, whilst the method is particularly suitable for shock-wave observations in which the change of this derivative is large, it is unsuitable for the visualization of regions of expansion in which the density changes are usually gradual.

From general considerations or from equation (70) below, the sensitivity of the system will increase as the distance of the screen or photographic plate from the tunnel is increased. Since, however, even in two-dimensional flow the density will not be free from small fluctuations across the tunnel and since the source is never a true point it is found that the definition of the image decreases as the distance from the tunnel is increased (*see* Fig. 58) and that, in practice, the distance of the screen from the tunnel should not exceed one tunnel width. In particular, if an attempt is made to use a camera to focus on the median plane of the disturbance (*i.e.*, the distance of the screen from the disturbance is zero), it will be very difficult to obtain any image at all. Thus it follows that the image size will be approximately that of the flow field to be observed, and in certain cases this may introduce difficulties in obtaining adequate illumination.

It may be shown¹²¹ that the change of illumination produced by the introduction of the disturbance is given approximately by

$$\frac{\Delta I}{I} = l \int \left(\frac{\partial^2}{\partial x^2} + \frac{\partial^2}{\partial y^2} \right) \log n \, dz, \quad \dots \quad (70)$$

from which it seems, subject to the loss of definition discussed above, the sensitivity increases as the distance l of the screen from the disturbance is increased.

2.13.3. Notes on the Optical Components.—For a schlieren set-up, the parallel light beam and the image of the source may be produced either by a lens or mirror system. The required quality of these optical components is high and, in general, for a given diameter and focal length a mirror will be less expensive than a lens. Indeed, for large diameters it is very difficult to obtain satisfactory lenses, and mirrors are almost invariably used. With a mirror, only a single glass surface must be figured, and the internal quality of the glass is unimportant; chromatic aberration is eliminated, and the amount of light absorbed is reduced.

Suitable mirrors are formed by coating the surface of a figured glass plate with a thin deposit of some metal (*e.g.*, aluminium, which is applied by a sputtering process). The required surface geometry of the mirror depends on the optical arrangement which is used. In most cases a parabolic mirror is strictly necessary in order to avoid spherical aberration, but if the focal length is large, the differences between a parabolic and spherical shape become small and the latter may be tolerable.

Referring to Fig. 59(a) it is, in general, necessary to place the source and cut-off outside the axis of the two mirrors in order to remove them from the field of the parallel light beam. Strictly, this implies that the mirrors should be figured off the axis, but, provided that the angles α and β are small, axially figured mirrors may usually be employed successfully if the precautions discussed below are taken to minimise the aberrations introduced.

With a line cut-off the greatest sensitivity is obtained with a line source of uniform brightness placed parallel to the cut-off and normal to the direction of the density gradient which is to be observed. A uniform sensitivity to density gradients in all directions normal to the optical axis may, however, be obtained by the use of a point source and circular cut-off, and in certain cases this arrangement may be preferable.

Certain types of lamp give an effectively linear source directly, but such a source may be formed with almost any lamp by using a condenser to illuminate a slit or the edge of a small mirror. For continuous observation certain workers have recommended a high-pressure mercury-vapour lamp of 1,000 watts as the light source. This lamp (Mazda type B-H6) gives an effectively linear source (1×25 mm), and may be operated either continuously or flashed to give exposures of the order of 4 microseconds for photography. At the N.P.L. a mercury-vapour lamp of 250 watts (Mazda Box Type ME) has been used to illuminate a slit for continuous observations, and replaced by

a spark gap for photography. The arrangement of the spark gap is shown in Fig. 60 and with this it is possible to obtain exposures of less than 1 microsecond. Care must be taken to ensure that only a single spark is discharged at each make and break of the induction coil primary circuit. Multiple sparks may be detected either by their noise, or by the observation of some rapidly moving object placed in the light field. They may be eliminated by adjusting the length of the spark gap, the input voltage to the primary and by providing a small flow of dry air through the discharge tube to remove moisture and ionised gases from previous discharges.

It is essential that the whole of the optical system should be carried on rigid supports insulated from vibrations introduced by the tunnel and its compressors. Adequate provision should be made for the necessary optical adjustments, wherever possible by the use of micrometer screws.

At the N.P.L. the arrangement shown in Fig. 59(b) is used on the 20 × 8-in. tunnel. Here the source is supported on the optical axis in the shadow of the aerofoil model and its supporting bracket. The first mirror has a diameter of some 28 cm and a focal length of about 100 cm, and the second mirror a diameter of 35 cm and a focal length of 350 cm. Whilst the short focal length of the first mirror is necessitated by the limited space around the tunnel, the high magnification of the source image produced and the increased powers of light collection are valuable features of the arrangement. Typical photographs obtained with this arrangement are given in Figs. 50 to 53 of Part III¹⁵³.

For direct-shadow work a point source is desirable. This may, for continuous observation, be formed by illuminating an iris by a condenser and mercury-vapour lamp. For photography the spark gap shown in Fig. 60 may be used. The parallel light beam may be produced either by a lens or mirror but the required quality is lower than for schlieren work.

2.13.4. Notes on the Arrangement of the Optical System.—In setting up the schlieren apparatus, the following points should be remembered. The angles α and β of Fig. 59(a) should be as small as possible and also of opposite sign so that the source and cut-off are on opposite sides of the axis of the two mirrors. The former precaution minimises the effects of astigmatism and the latter those of coma. It is also desirable to arrange the apparatus so that astigmatism distorts the image only in a direction parallel to the source and cut-off edge. This may be achieved by placing the optical axis SOO'I in a horizontal plane when the source and cut-off are horizontal, and in a vertical plane when they are vertical. In particular, systems in which SO is in a vertical plane and O'I in a horizontal plane (or *vice versa*) are to be avoided. The distance OO' between the two mirrors should in general be a minimum as all disturbances between them, whether in the wind tunnel or not, may appear on the screen.

The source must be located accurately at the focus of the mirror O, and this may be achieved either by reflecting an image of the source back on to a screen held close to the source (by placing a plane mirror between the two concave mirrors), or by measurements of the diameter of the beam OO' at different positions along its length. Similarly, the cut-off must be located at the focus of the mirror O' by adjusting the position of the cut-off along O'I until the image on the screen darkens uniformly as the cut-off is moved across the image of the source.

It is also necessary to ensure that the axis of the mirrors is parallel to the aerofoil span, and this may be done by sighting along the trailing edge by eye or with a cathetometer on to the image of the source in the mirror O, or on to some other suitably illuminated object placed at the position of the source.

The above procedure may be readily adapted to the setting up of a schlieren system employing lenses instead of mirrors, and to direct-shadow systems. With lens-schlieren systems, the flare spots, observed on looking through the system from a direction a little above or to one side of the optical axis, may be used as a very convenient aid to the alignment.

A good bibliography of papers relevant to the optical design and adjustment of schlieren and shadowgraph systems is given in Ref. 126.

2.13.5. *Glass for Wind-Tunnel Walls.*—If any form of optical method is to be attempted it is necessary that the walls of the wind tunnel should be transparent. Glass walls are usually used for this purpose since most alternatives (*e.g.*, 'Perspex') distort too much under load or are too soft to avoid being scratched during use. Figs. 61 and 62 show direct-shadow and schlieren photographs of a sheet of 'Perspex'. Apart from the surface irregularities visible in the schlieren photograph the optical qualities of the sheet appear to be comparatively good.

The most common faults which have been found in glass walls are:

- (a) Internal striations (ream).
- (b) Small surface blemishes.
- (c) Large-scale surface irregularities, waviness, etc.

Of these it seems that (a) is due to lack of homogeneity of the molten glass before rolling and arises from the lack of adequate stirring of the melt. Faults (b) and (c) may be eliminated by adequate surface grinding and polishing.

Figs. 63 and 64 show direct-shadow and schlieren photographs of a typical sample of 1/8-in. window glass. The ream or internal striations are clearly visible. In Fig. 64(b) the schlieren arrangement has been adjusted to indicate the surface waves whose crests appear to run obliquely across the photograph. Figs. 65 and 66 show schlieren photographs of a piece of 1 1/4-in. plate glass supplied for use as a wind-tunnel wall. Fig. 67 shows a direct-shadow photograph of the same glass sheet. Fig. 68 shows a direct-shadow photograph of a 1-in. sheet of selected plate glass which is almost free from internal striations. Small surface faults are visible in this photograph. Fig. 69 shows two schlieren photographs of the same glass sheet taken with the same schlieren set-up. In the second photograph the glass has been rotated through 180 deg from its original position. The difference in the illumination of the two photographs indicates that the glass is wedge-shaped (*i.e.*, that the two glass-air surfaces are not parallel). This effect would not be serious in practice, since the schlieren arrangement could be adjusted as a compensation.

Figs. 70 and 71 show direct-shadow and schlieren photographs of 3/4-in. plate glass made as a special melt in which the molten glass was carefully stirred. Glass prepared by this method appears to be suitable for direct-shadow and schlieren photography and is used at present for the walls of the 20 × 8-in. tunnel at the N.P.L. It is not known whether the internal uniformity of this glass is adequate for use with the interferometer. With this instrument a considerably greater degree of accuracy of the surface finish will be required if elaborate corrections to the photographic records are to be avoided. Thus, it appears that the surfaces must be plane and parallel to within about 1/3 of the wavelength of the light to be used.

2.13.6. *General Remarks on the Use of Optical Methods at the N.P.L.*—The direct-shadow and schlieren arrangements alone have been used, the design of each optical arrangement being determined largely by the characteristics of the available optical components, and the available space in the tunnel room. The principal items of optical equipment which have been available for use at the N.P.L. consist of:

- One Zeiss Jena Triplet* lens 1:5, $f = 70$ cm, about 4 1/2-in. diameter.
- One Goerz Dogma* lens 1:7, $f = 125$ cm, about 6-in. diameter.
- Two spherical mirrors .. $f = 3$ ft, 12-in. diameter.

Recently these have been supplemented by two Zeiss spherical mirrors with $f = 350$ cm and of 14-in. diameter. The two lenses have been used in a lens form of the direct-shadow and schlieren

* These lenses which are designed for photographic purposes are probably not the most suitable for schlieren or direct-shadow work in which the objects to be observed are not far off the axis. It is probable that a simple doublet may be preferable.

arrangement on both the 5×2 -in. and 20×8 -in. tunnels. The mirrors have been used to form a schlieren set-up on the 20×8 -in. tunnel. Optical benches have been constructed for the 5×2 -in. tunnel and 20×8 -in. tunnel.

It is usual to observe the shock-waves on the aerofoil surfaces as a routine part of a test in the 20×8 -in. tunnel, and a direct-shadow system is commonly employed for this purpose. The 1-ft diameter tunnel is not suitable for optical work because of the shape of its cross-section. A cylindrical Perspex working section has, however, been used to replace the balance section for flow visualization using the direct-shadow method with divergent light. Whilst the section acts as a cylindrical lens, and the Perspex has poor optical qualities, this method has proved of value in certain experiments. The schlieren arrangement has been used on a number of small tunnels (about 2-in. square) to observe, in particular the interaction of shock-waves and boundary layers, and the effects of the condensation of humidity.

2.13.7. *The Interferometer Method.*—This method has not been used in the Aerodynamics Division and will not, therefore, be described. Of the available optical systems, however, it appears to be the most promising for the quantitative analysis of the density field and in Germany^{82, 127, 128, 129} an instrument of the Mach-Zehnder type has been used with some success for this purpose.

2.14. *Measurement of Wave Angles.*—By the use of either the schlieren or the direct-shadow method it is possible to obtain photographs of the flow round an obstacle in a supersonic flow from which the geometry of the shock-wave pattern may be measured. An application of this method is the introduction of a wedge or a cone of known shape into the flow for the purpose of observing and measuring the angle of the bow-wave and hence deducing the Mach number. The apex angle of the wedge or cone is chosen to give an attached bow-wave¹³⁰ of sufficient intensity to be readily visible on the optical system. A few measurements of this type have been made in the 5×2 -in. tunnel at a Mach number of 1.4. The scale of the experiment did not, however, permit a detailed exploration of the flow to be made, and the observations were made at one point in the flow only and were used to find the free-stream Mach number.

An analogous method has been used in Germany for the correction of the shape of a supersonic nozzle. Here small transverse grooves were cut in the walls so that weak disturbances were put into the flow. The nozzle shape was then adjusted until these wavelets were parallel at the end of the nozzle.

2.15. *Attempts to Visualize Streamlines.*—Work has been done in the 5×2 -in. tunnel in an attempt to visualize the filament lines of the supersonic flow round a 1-in. chord double-wedge aerofoil (6 per cent thick). The injection of streams of carbon dioxide and smoke into the air-stream from small orifices upstream of the model was tried, but, on the scale of the experiment, it was not found possible to obtain a sufficiently thin filament. The most successful method involved the use of a row of 0.008-in. diameter unheated wires at about 0.3-in. intervals across the tunnel upstream of the model. The wakes from these widened very little downstream and the refractive index gradient was sufficient to give an indication on a schlieren apparatus. It was not possible because of the small scale of the experiment to use wires of sufficiently small relative diameter, and the wakes in this experiment were rather broad. It appeared, however, that the method might be used successfully on a larger scale. Experiments using heated wires have been made under Ackeret in the Zurich high-speed tunnel. This method seems to give excellent results as judged by photographs taken by the schlieren method.

A photograph of the supersonic flow past a double-wedge aerofoil taken in the 5×2 -in. tunnel at the N.P.L. using the unheated wire grid is shown in Fig. 72.

2.16. *Methods of Indicating Transition Position.*—Measurements, particularly those of profile drag, in the N.P.L. high-speed tunnels have at times been inconsistent. The influence of the condensation of atmospheric humidity has now been largely eliminated by the use of return ducts,

and inconsistencies are attributed to variations of the airstream turbulence. Below the free-stream Mach number at which the drag rises sharply, such inconsistencies will be due largely to variations of the transition positions on the aerofoil surfaces. In order to correlate drag measurements in particular, therefore, and to give general information on movements of the transition position with variations of the free-stream Mach number, it is necessary to have some method of indicating the transition position. This is more desirable than the use of a fixed transition position, since it has been found difficult to devise a method of fixing the transition without giving rise to shock-waves when the Mach number approaches its critical value.

Deposits of atmospheric dust and oil from the compressors have from time to time been observed on aerofoil models behind a spanwise line which has been assumed to indicate the position of transition. This assumption is justified by the formation of similar deposits indicating the spread of turbulence behind irregularities near the leading edge of the aerofoil, such deposits taking the form of the familiar cusp-shaped surfaces. The occurrence of such deposits is, however, somewhat random, and more reliable methods have been developed⁴⁶. These methods are, however, rather difficult to apply to routine tunnel tests largely because of the difficulty of access to the model. The most successful method which has been used is an adaptation of the 'china clay' method originally described in R. & M. 2126¹⁵⁴. This has been used with the 5-in. chord models of the 20 × 8-in. tunnel and depends on the differential rates of evaporation from the surface of the model in the laminar and turbulent regions of the boundary layer. The surface is coated with a layer of a colourless solid of fine crystalline structure (china clay) appearing white when dry, which is then covered with a volatile oil of approximately the same refractive index (iso-safrole) so that the solid layer becomes virtually transparent. As the oil is evaporated during the tunnel run the white appearance of the dry solid is once more seen, and evaporation being more rapid in the turbulent than in the laminar region of the boundary layer, a white layer appears on the aerofoil surface aft of the transition point. Results obtained with this method of transition indication are discussed in R. & M. 2079⁷⁸, and in Part III of this report²⁶.

2.17. Methods for Fixing Transition.—The usual method for fixing the position of transition from laminar to turbulent flow in the boundary layer of an aerofoil at low speeds is either by a fine spanwise wire or by a narrow band of roughness in the form of fine particles attached to the surface. In the N.P.L. high-speed tunnels attempts have been made by Pearcey to fix transition by means of spanwise wires and grooves^{133, 134}, and the use of a band of roughness has been tried by Fowler (unreported). The problem of transition fixing at high speeds is discussed by Fage and Sargent in R. & M. 2106⁷⁹, in which a new method, particularly suited to high-speed work, is described. The criterion for transition to occur close behind a wire is $u_h h/\nu \simeq 400$, where h is the diameter of the wire, u_h the velocity in the boundary layer, without the wire, at distance h from the surface, and ν is the kinematic viscosity. The Pohlhausen solution of the laminar boundary layer equations is $u_h = h u_\tau^2/\nu$, where u_τ is the frictional velocity $(\tau_0/\rho)^{1/2}$, and τ_0 is the surface shearing stress. Thus the transition criterion may be written $u_\tau h/\nu = 20$.

A similar criterion for transition behind a narrow rough strip may be written $u_\tau h/\nu = k$, where h is now the average height of the excrescences forming the roughness, and k is a constant for an assigned form of roughness. The value of k must be determined experimentally but for roughness caused by sand or carborundum particles it will be greater than 5.5, the value for which the roughness just begins to increase the resistance to flow.

For a laminar boundary layer, the Pohlhausen theory gives $u_\tau x/\nu \propto (u_1 x/\nu)^{3/4}$, where x is the distance from the leading edge of the aerofoil and u_1 is the velocity just outside the boundary layer. The transition criterion $u_\tau h/\nu = k$ can, therefore, be written $h/x \propto (u_1 x/\nu)^{-3/4}$.

If the wire or roughness size selected is just adequate to cause transition at the lowest test speed, the value of h and, therefore, the disturbances created at a higher speed, will be greater than the optimum. The diameter of the wire or the height of the excrescences should, therefore, be progressively decreased with an increase of speed.

A more serious disadvantage of the use of either a wire or band of roughness at high speeds is that the increase of velocity close to the excrescence may cause a shock-wave. This was borne out in the experiments reported in R. & M. 2252^{133, 134}, and in Fowler's unreported experiments with a band of roughness. If this occurs it is usually found that the rise of drag coefficient associated with the formation of shock-waves on the aerofoil surface occurs earlier when the excrescence is present than when it is not present.

This shortcoming was overcome in the method developed by Fage and Sargent and described in R. & M. 2106⁷⁹. The method consisted of injecting minute air jets into the boundary layer from a spanwise row of small surface holes. A great advantage of the method is that the rate of air injection can be adjusted at each test speed to give the minimum disturbance necessary to fix transition. It is found that this minimum rate of air injection is so small that a local shock-wave is not formed at even the highest test speeds. It is suggested in R. & M. 2106⁷⁹ that, owing to the local acceleration of the flow, the formation of wavelets just outside a transition region is inevitable at a sufficiently high speed, even when transition occurs naturally.

In R. & M. 2252¹³³, Pearcey describes tests with wires of 0.006-in. diameter on a 5-in. chord model of NACA 2218 section in the 20 × 8-in. tunnel at Reynolds numbers varying from 1.0×10^6 to 1.8×10^6 and Mach numbers from 0.35 to 0.8. It is concluded, for the reasons given above, that the use of wires is not suitable for transition fixing at high Mach numbers. Further tests by Pearcey with wires of the same diameter attached to an aerofoil of EC 1250 section and 12-in. chord are described in R. & M. 2252¹³⁴. The Reynolds number range in these experiments was 1×10^6 to 4×10^6 and the Mach number range 0.15 to 0.68. At these Reynolds numbers it appeared that the performance of a wire was more satisfactory.

The attempted use of grooves of the forms sketched in Fig. 73(b) on a 2-in. chord model of NACA 2417 section in the 1-ft diameter tunnel to fix transition is described in R. & M. 2252¹³³. It appeared that such grooves were quite ineffective.

After some preliminary experiments in a low-speed tunnel of 8 × 3-in. section in which air was injected from small surface holes into the boundary layer of one tunnel wall, and in which two different hole diameters were tested, Fage and Sargent applied their method of transition fixing to a 12-in. chord model of EC 1250 section placed in the 20 × 8-in. tunnel. The air was injected from two rows of 53 holes spaced at 0.075 in. across the middle 4 in. of the upper and lower surfaces of the 8-in. span. The hole diameter was 0.0135 in. and the holes were arranged in spanwise lines 0.15 chord from the leading edge. Pitot-traverse measurements of profile drag were made at 0 deg incidence with and without air injection over a range of Mach numbers from 0.575 to 0.784.

It was found that the value of the profile-drag coefficient rose rapidly at all Mach numbers tested with increase of the ratio from zero, but that the drag coefficient reached a constant value for $m/m_b = 0.015$, above which further increase of this quantity did not influence the drag. In this expression m is the mass of air injected into the boundary layer per unit span per second, and m_b is the mass of air flowing in the laminar boundary layer per unit span per second.

Observations of the flow pattern by a direct-shadow method indicated that for Mach numbers up to the highest used there was no disturbance of the flow just outside the boundary layer near the holes provided that m was less than $0.04m_b$. At this value a weak shock-wave extending about 0.2 in. from the surface appeared. It was concluded that the method of transition fixing could be used satisfactorily at high Mach numbers.

The influence of air injection (at the optimum rate) on the drag coefficient of the aerofoil is illustrated in Fig. 73(c). This figure indicates the importance of avoiding leakage of air into the boundary layer of an aerofoil in practice, and since leakage of air from the boundary layer into the aerofoil has a favourable tendency, it was stressed in R. & M. 2106⁷⁹ that if leakage was unavoidable provision should be made for the maintenance of a pressure within an aircraft wing below the external pressure.

2.18. *The Measurement of Stagnation Temperature.*—The measurement of the stagnation temperature of a high-speed airstream is important in problems involving heat release either by combustion or the condensation of moisture, for assessing the surface temperature of a model placed in the airstream, and for checking one of the fundamental theoretical assumptions on which the wake-traverse method of profile-drag measurement is based. The accurate measurement of this quantity is complicated by heat losses to the surrounding air by conduction, convection and radiation, and by conduction losses through the measuring instrument itself.

Bulb-type thermometers and thermo-junctions have been used for this purpose, but the latter have many advantages, the most obvious being facility of remote reading. The essential feature of a 'pitot thermocouple' is a thermo-junction mounted in the head of a pitot-tube. An instrument of this type can, however, give erratic and incorrect readings if badly designed.

On the basis of experience at the N.P.L. and elsewhere the principal design requirements for a successful instrument appear to be:

- (a) To ensure a sufficient heat transfer from the air that is being dammed at the mouth of the pitot-tube to the measuring body (thermo-junction or thermometer bulb).
 - (i) The measuring body is placed in a region of low velocity rather than a stagnation region by 'ventilating', or allowing a small flow to take place through the pitot-tube.
 - (ii) The measuring body is constructed of small dimensions and low heat capacity.
- (b) To guard against conduction, convection and radiation losses from the air in the stagnation, or low velocity, region, to regions of lower temperature.
 - (i) The pitot-tube and support, and the wires of the thermo-junction are made of materials of low thermal conductivity.
 - (ii) The thermo-junction is made with small surface area.
 - (iii) Adequate screening is provided to minimize radiation and convection losses.

It appears that a 'pitot thermocouple' of the Franz type^{135, 136} is the most reliable instrument so far developed. The instrument is sketched in Fig. 74(b), and consists of a thermo-junction mounted at the downstream end of a diffuser the entry to which is the mouth of the pitot-tube. A small airflow is allowed to take place through the instrument by small vents downstream of the thermo-junction. The calibration curve reproduced in Fig. 74(c) from Ref. 136 indicates that the instrument measures the stagnation temperature to a high degree of accuracy. The instrument which has been used at the N.P.L. is of the same type but omits the diffuser. This instrument is sketched in Fig. 74(a) and calibration curves obtained in the 1-ft diameter tunnel at the N.P.L. are given in Fig. 74(d). The effect of a variation of the size of the ventilating hole downstream of the thermo-junction is indicated in Fig. 74(e). With a hole diameter of 0.03 in. the reading of the instrument is sensibly independent of airspeed although the flow velocity past the thermo-junction is higher than in the Franz-type instrument. An inspection of Fig. 74(e) indicates that the N.P.L. type instrument is less satisfactory than an instrument of the Franz type, and it is recommended that the latter type be used in preference to the former. The potential difference across the N.P.L. thermocouple was measured with a vernier potentiometer, reading to one microvolt (*i.e.*, to 1/53 deg C for the thermo-junction used).

2.18.1. *Measurements of Stagnation Temperature in the Wake of an Aerofoil.*—The variation of the stagnation temperature across the wake of a 2-in. chord brass model of NACA 0020 section at zero incidence has been measured in the 1-ft diameter tunnel over a range of Mach number. Typical results are plotted in Fig. 75 from which it can be seen that the stagnation temperature at the centre of the wake is less than that outside the wake, and that the stagnation temperature at the edges of the wake is greater than this reference value. The variations of stagnation temperature are, however, so small that they will not cause appreciable errors in the calculation of the profile drag coefficient by the method described in R. & M. 1971⁶⁹ and based on the assumption of constant total energy (*i.e.*, constant stagnation temperature).

Fig. 76 compares the stagnation temperature and C_D' variations across the wake. At low Mach numbers it is found that the widths of the regions over which the stagnation temperature and C_D' (and, therefore, loss of total head) vary, agree well. At higher Mach numbers, however, the width of the C_D' wake begins to exceed the stagnation temperature wake. The sideways extension of the C_D' curve is largely due to the loss of total head through the shock-wave, and, since theoretically the stagnation temperature does not vary through a shock-wave, the observed phenomenon is not unexpected.

2.19. *The Measurement of Surface Temperature.*—The temperature distribution over the surface of a 2-in. chord model of NACA 0020 section was measured in the 1-ft diameter tunnel in an attempt to provide an experimental comparison with Squire's theory, and evidence of the influence of shock-waves on the temperature. A description of the results obtained in this experiment is given in R. & M. 2230³⁶.

The aerofoil was constructed of Tufnol as it was essential that the model should be a poor conductor. Fourteen iron-constantan thermo-junctions were spot welded, flush with the aerofoil surface, and the leads were carried out through channels in the interior of the model. In an original model the junctions were staggered across the aerofoil span, but it was found that a slight swirl of the flow which was, at the time, present in the tunnel made this arrangement unsuitable, and it was abandoned in favour of an arrangement of the thermo-junctions in one chordwise line. A sketch of the model in its final form is given in Fig. 77. The junctions were all situated in one surface, and the aerofoil being symmetrical, the temperatures on the upper and lower surfaces were found by reversing the incidence. The exact local wind direction in the tunnel was found by a yawmeter traverse. A reference thermo-junction was placed in the intake of the tunnel, and the potential differences between this junction and each of the aerofoil junctions were measured on a Tinsley vernier potentiometer reading to one microvolt. A dust-proof selector switch with silver contacts designed by Mr. Hickman of the Physics Division, N.P.L., enabled any one of the fourteen thermo-junctions to be selected at will. The calibration factor for the iron-constantan thermo-junctions was 53 microvolts per deg C temperature difference.

The measurements were expressed in terms of a coefficient C_θ defined by:

$$C_\theta = \frac{\Delta T}{T_H - T}, \quad \dots \dots \dots \dots \dots \dots \dots \dots \dots \quad (71)$$

where ΔT is the increase of surface temperature over free-stream static temperature, and T is the free-stream static temperature. T_H is the stagnation temperature which is equal to the temperature of the air at rest in the tunnel intake. The value of T can be calculated if the Mach number and intake temperature are known, so that ΔT and the value of C_θ can be deduced from a knowledge of these quantities and the measured temperature difference between the model surface and tunnel intake.

The experimental results were confused by the condensation of atmospheric moisture at the higher Mach numbers. This was found to be of considerable importance, and could not be avoided since the tunnel was not fitted with return ducts at the time of the experiment. The experiment also indicated that a larger test model would be desirable, and that 'Ebonite' would be a more suitable material than 'Tufnol' because of the lower thermal conductivity.

The electrical circuit (Fig. 78) has the advantage that a direct reading of the temperature difference between the aerofoil surface and tunnel intake is obtained and a suggested modification using a water bath is indicated in Fig. 79. It is also felt that a copper or nickel-constantan junction would be preferable to an iron-constantan junction because of the tendency of the latter to rust. The nickel junction has the advantage of a lower thermal conductivity than either the iron or copper junctions.

2.20. *Measurement of Inducing-Air Supply to Tunnels.*—The inducing-air supply to the N.P.L. induction-type high-speed tunnels has been measured on numerous occasions in connection with measurements of efficiency. These measurements were normally made by a standard Hodgson

orifice plate placed in the supply pipe. For measurements of the inducing-air supply to the larger tunnels, orifices of either 1, 2 or 3-in. diameters were placed in one of the 4 1/8-in. diameter mains connecting to the storage reservoirs. For measurements with model tunnels orifices of diameter varying from 1/8 to 5/8 in. were placed in a 7/8-in. diameter supply main. The differential heads over these orifices were measured by the high-pressure mercury manometer shown in Fig. 80 which also permitted the pressure upstream of the orifice to be measured. A similar method of flow measurement has also been used to measure the delivery of the compressors in routine trials.

2.21. *Supersonic Nozzle Design.*—The one-dimensional theory (sometimes called the hydraulic theory) of compressible flow indicates that in order to achieve a supersonic velocity in a continuous channel it is necessary to contract the cross-sectional area to a throat at which the velocity is equal to the critical sonic value, and then expand to produce further acceleration to a supersonic velocity. Applying this theory to the design of a wind-tunnel nozzle, and assuming that the acceleration is isentropic and the velocity components normal to the axis are negligible, a relation is obtained between the working-section Mach number M and the ratio of working-section area A to the throat area A^*

$$\frac{A^*}{A} = M \left(\frac{\gamma + 1}{2 + (\gamma - 1)M^2} \right)^{(\gamma+1)/2(\gamma-1)} \quad \dots \quad (72)$$

or with $\gamma = 1.40$

$$\frac{A^*}{A} = 216 \frac{M}{(5 + M^2)^3} \quad \dots \quad (73)$$

In practice, however, the assumption of one-dimensional flow is not valid, and whilst equations (72), (73), will still give the required overall nozzle-area ratio with moderate accuracy, methods must be obtained for the design of the nozzle on the basis of two-dimensional flow.

Methods for the conversion of a given shock-free supersonic flow to a second shock-free flow at a different supersonic Mach number have been given by Busemann¹³⁸ and others^{139, 140}. Most of these methods are based on the method of graphical characteristics, but Atkin¹⁴¹ has given an analytical method based on the original method of Busemann. In particular, it is possible by the use of these methods to design a channel which will give a final uniform shock-free supersonic flow from a given initial supersonic distribution. The problem of supersonic nozzle design is, therefore, to some extent reduced to that of determining the velocity distribution at, or a little downstream of, the throat. The conditions at the throat of a nozzle have been examined by Taylor³⁰, Hooker³¹, Görtler¹⁴⁴, Sauer³², Atkin¹⁴¹ and others. Measurements by Stanton¹⁴⁵ have shown excellent agreement with the calculations of Hooker³¹ for a three-dimensional nozzle (based on Taylor's original calculations for the two-dimensional case³⁰). At present, however, there is insufficient experimental evidence to determine which of these methods is the most reliable.

Certain methods^{*143, 132} have also been given for a nozzle design based on the assumption of a plane sonic line at the throat. Such methods are rather simpler to use than any of the methods discussed above since they involve centered expansions (Prandtl-Meyer) alone. In general, the shortest possible nozzle for a given final Mach number is obtained by using this assumption and a sudden expansion at the throat. Other nozzle shapes are, however, readily obtained by using the geometry of any streamline of the flow. An approximate method of nozzle design has been suggested by Bailey and Wood. Lighthill¹⁴⁶ has recently given a method for the analytical design of nozzles including that of the subsonic region and throat. This method is based upon the hodograph transformation.

All the methods of nozzle design discussed above ignore the boundary layers of the nozzle walls. In practice, it is necessary to displace the nozzle walls by a distance equal to the displacement thickness of the boundary layer. This displacement is usually applied as a small correction to

* A method of this type was suggested by Sargent at the N.P.L. in 1945 and has been used in the design of a number of nozzles.

the nozzle ordinates obtained by the potential-flow design. In the past, the rate of growth of displacement thickness has been determined on the basis of experiment and has usually been assumed to be constant over the length of the nozzle. In practice, with a rectangular or square tunnel it is very inconvenient and in some cases impracticable to apply a taper to the two side walls for boundary-layer growth. Thus, for example, it is desirable that the two glass side walls of the working section should be parallel if flow visualization is to be attempted. In general, therefore, it is usual to allow for the boundary-layer growth, on all four tunnel walls, by a displacement of two of the walls alone sufficient to maintain the cross-sectional area constant at the value assumed in the calculation of the nozzle shape. At the W.V.A.¹³² at Kochel, Germany, an allowance of from 0.004 to 0.012 in. per in. was given on each of the two nozzle walls for boundary-layer growth (the boundary-layer thickness being taken as zero at the throat). Puckett¹⁴² gives corresponding values of from 0.007 to 0.010 in. per in. for Mach numbers of from 1.5 to 2.5 and Reynolds numbers (based on working section height) of from 5×10^5 to 5×10^6 . These values all apply to tunnels with square working sections and correspond to a rate of growth of displacement thickness of from 0.002 to 0.006 in. per in. Values of this order have also been deduced from measurements at the N.P.L. It is sometimes the practice to calculate the rate of growth of displacement thickness from the methods which are now available^{149, 150, 151} rather than to rely upon experimental values.

A method has been developed in Germany¹³² for the experimental correction of a nozzle design for errors arising, for example, from the use of an erroneous boundary-layer allowance. This method involves the observation by a schlieren method of wavelets introduced into the flow by small transverse grooves in the nozzle profile. The nozzle geometry is, by this method, adjusted (by scraping) until the wavelets in the final supersonic flow are parallel. The material used for the nozzle construction was a plaster (monolith) which was found to obviate the warping associated with wooden nozzles and the difficulty of machining metal nozzles. The use of this material also permitted adjustments to the shape to be made conveniently.

At the N.P.L. the only tunnel which was available for supersonic operation was the original 1-ft diameter tunnel. This was originally intended for subsonic operation alone, and the maximum length of the nozzle which was determined by the distance between the existing intake and working section, was therefore limited. A number of cylindrical nozzles were designed by Bailey and Woods¹⁴⁷ approximate method to give Mach numbers of about 1.2, 1.4 and 1.6. In the tunnel's original form, the actual Mach number which was achieved varied with the humidity of the atmosphere due to the condensation of moisture in the tunnel, but now that a return duct has been fitted, consistent Mach numbers are obtained. More recently, a number of smaller supersonic tunnels with square or rectangular working sections have been constructed. In most of these tunnels the nozzle design has been based upon the assumption of a plane sonic line.

Mention should be made here of the use of multi-nozzle effusers in Germany during the war. Such effusers have the advantage of shortness and seemed to be particularly promising for application to large wind tunnels. Whilst, however, large-scale irregularities are absent in the supersonic stream, a large number of small-scale disturbances are present. It is found¹⁵⁵ that a considerable distance is required downstream of the nozzle before the wakes of the cells decay. Moreover, the power required to operate a tunnel with a nozzle of this type is considerably greater than that required for a tunnel with a conventional nozzle.

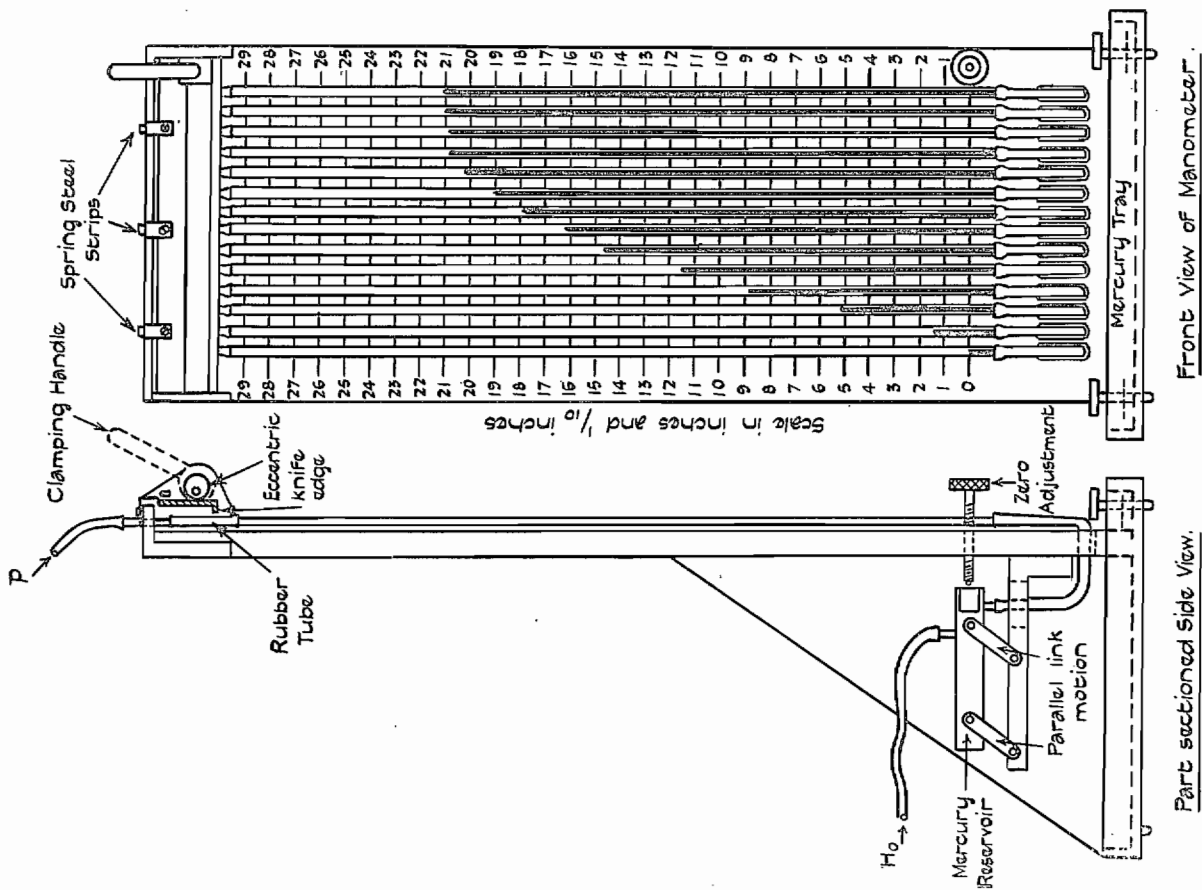


FIG. 1. 14-tube mercury manometer.

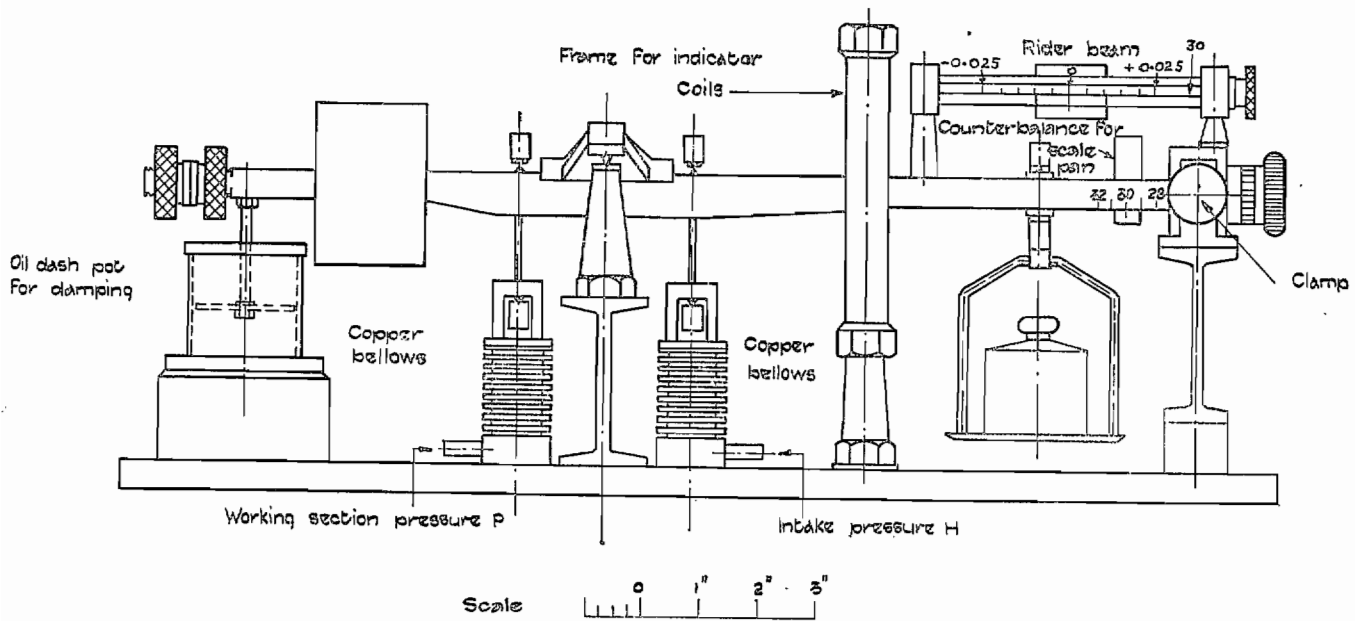


FIG. 2. General arrangement of Mach number gauge.

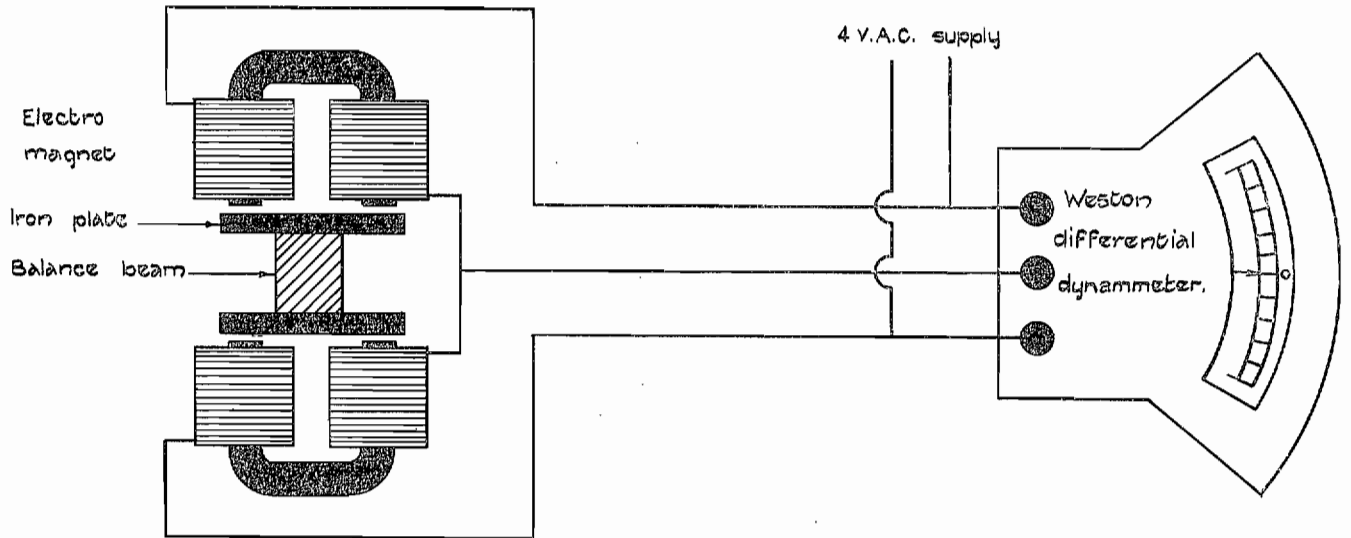


FIG. 3. Balance indicator.

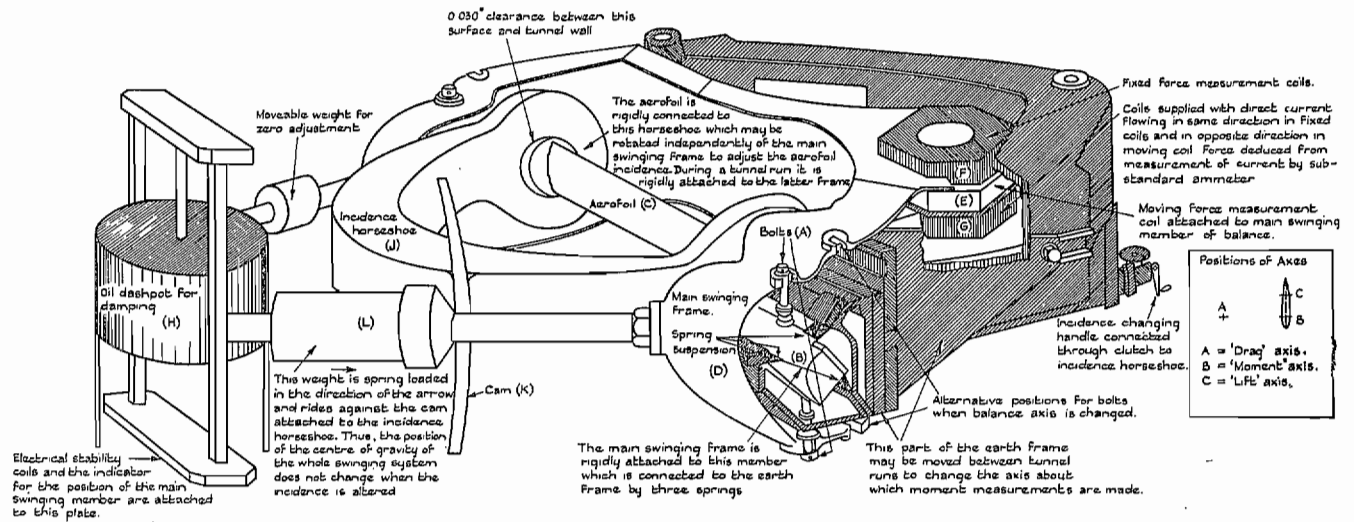


FIG. 4. Sketch of three-component balance—shaded area earthed

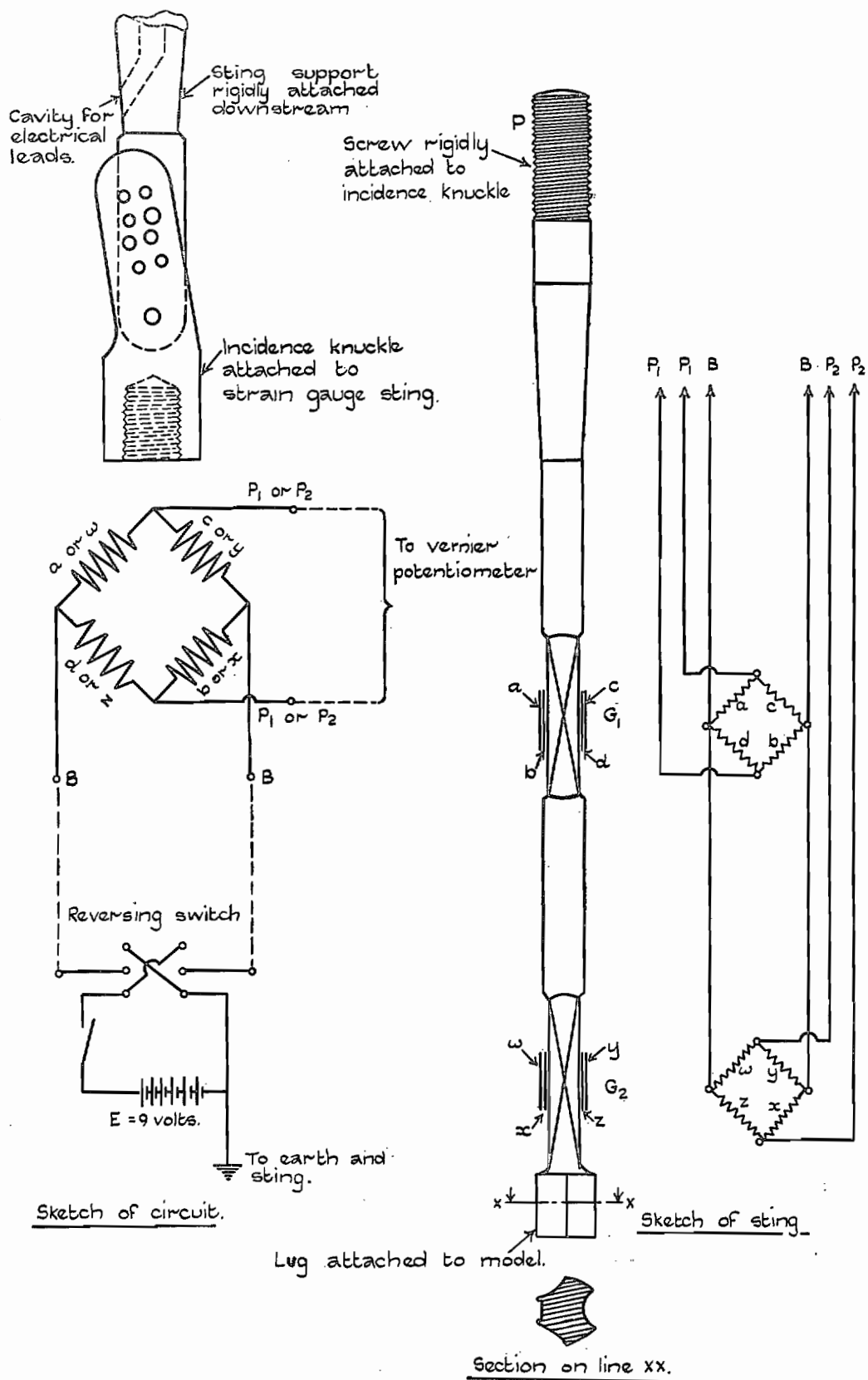


FIG. 5. Strain-gauge sting and gauge circuit for measurement of force normal to sting in plane of paper.

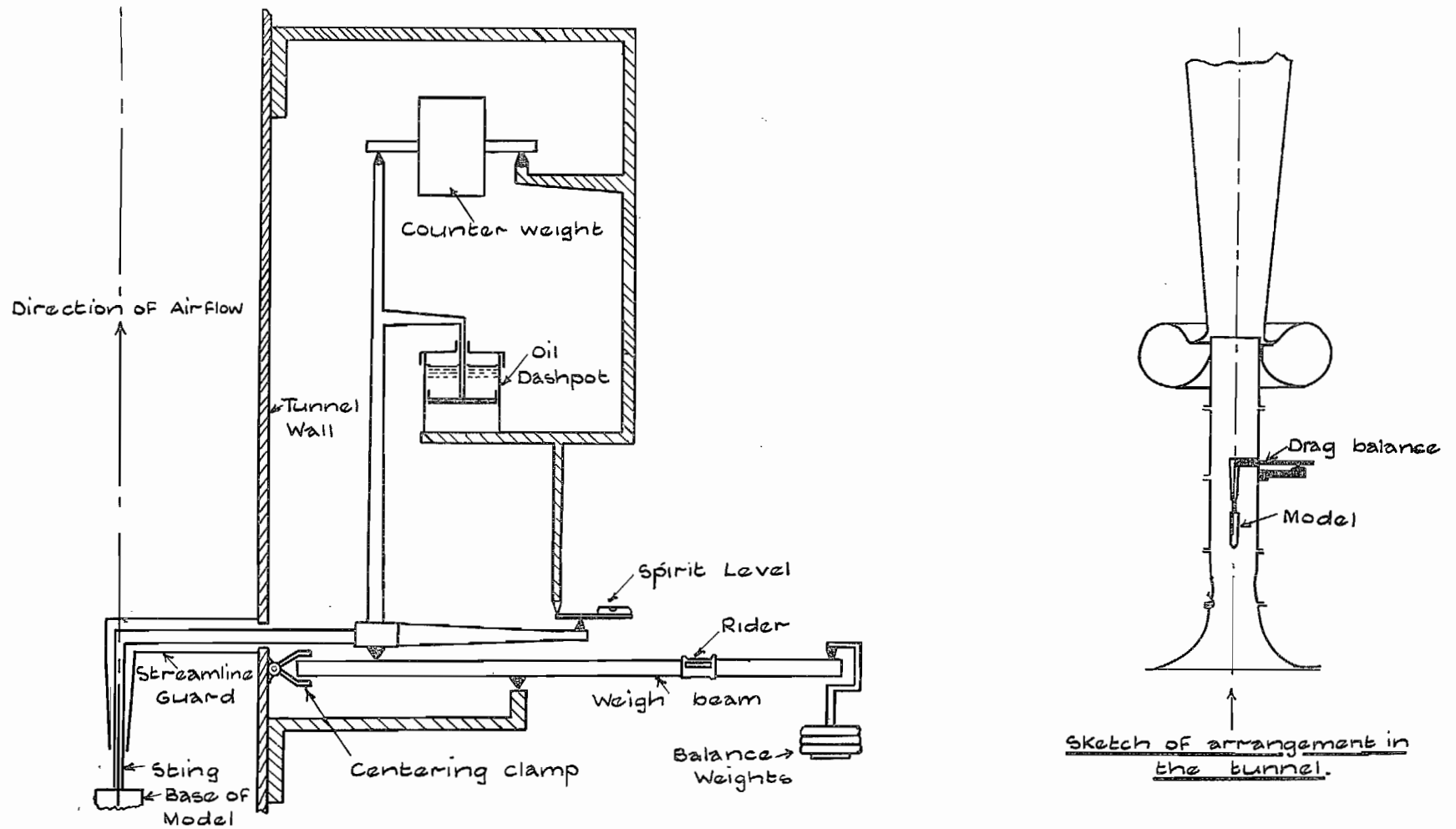


FIG. 6. Diagram of drag balance for three-dimensional bodies in 1-ft diameter tunnel.

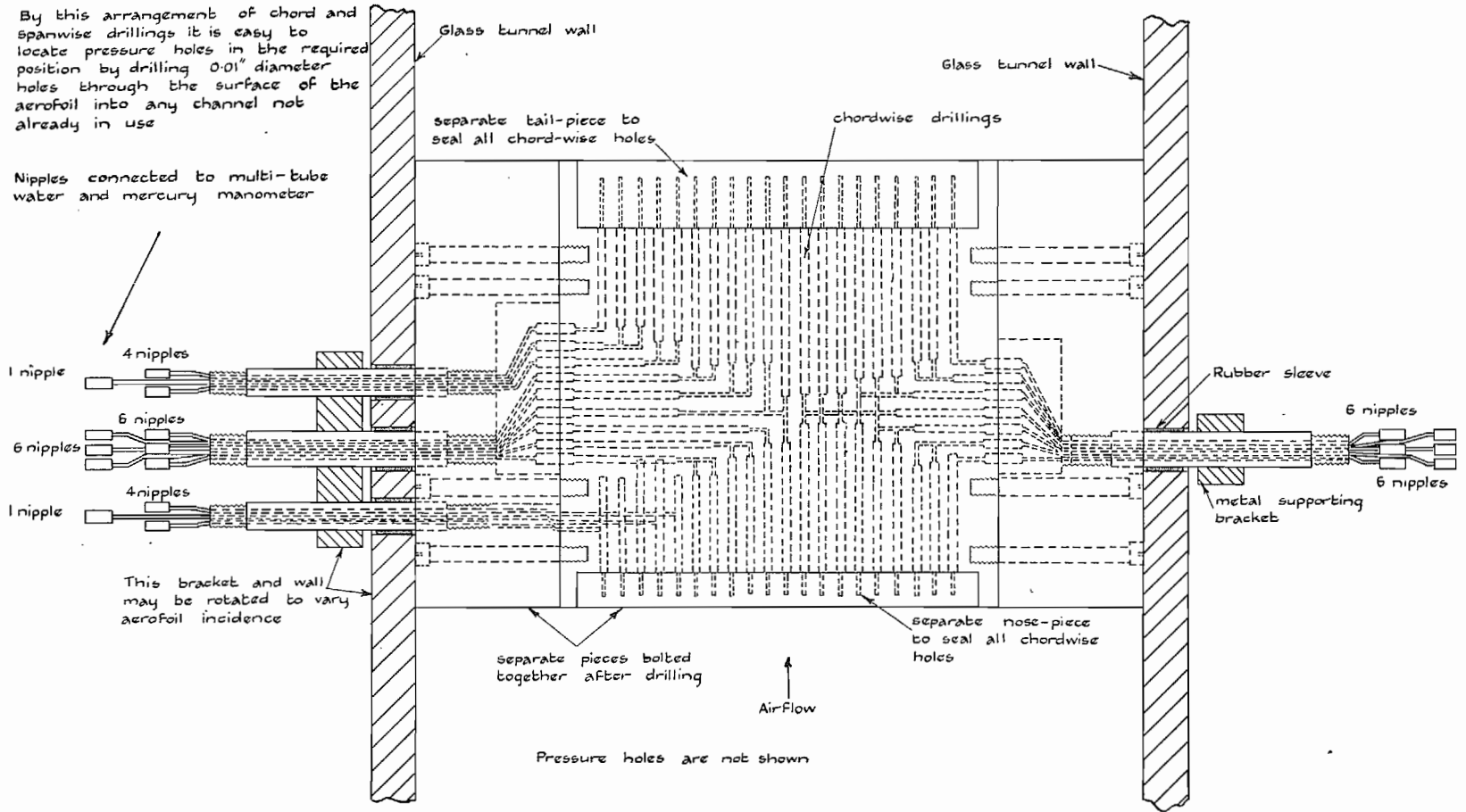


FIG. 7. . Arrangement of typical pressure-plotting aerofoil in 20 × 8-in. high-speed tunnel.—34 pressure holes—brass model.

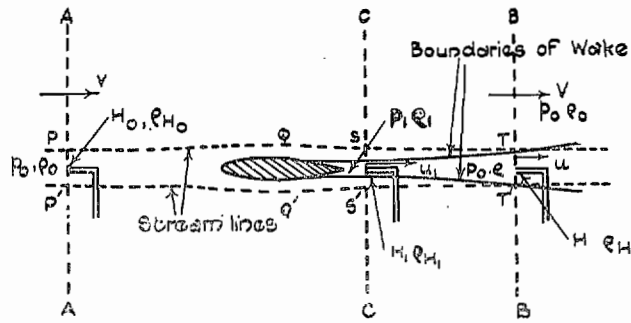


FIG. 8. Steady flow of a compressible fluid past an aerofoil.

Note: TT¹ represents the boundaries of the wake including that of any shock-waves present.

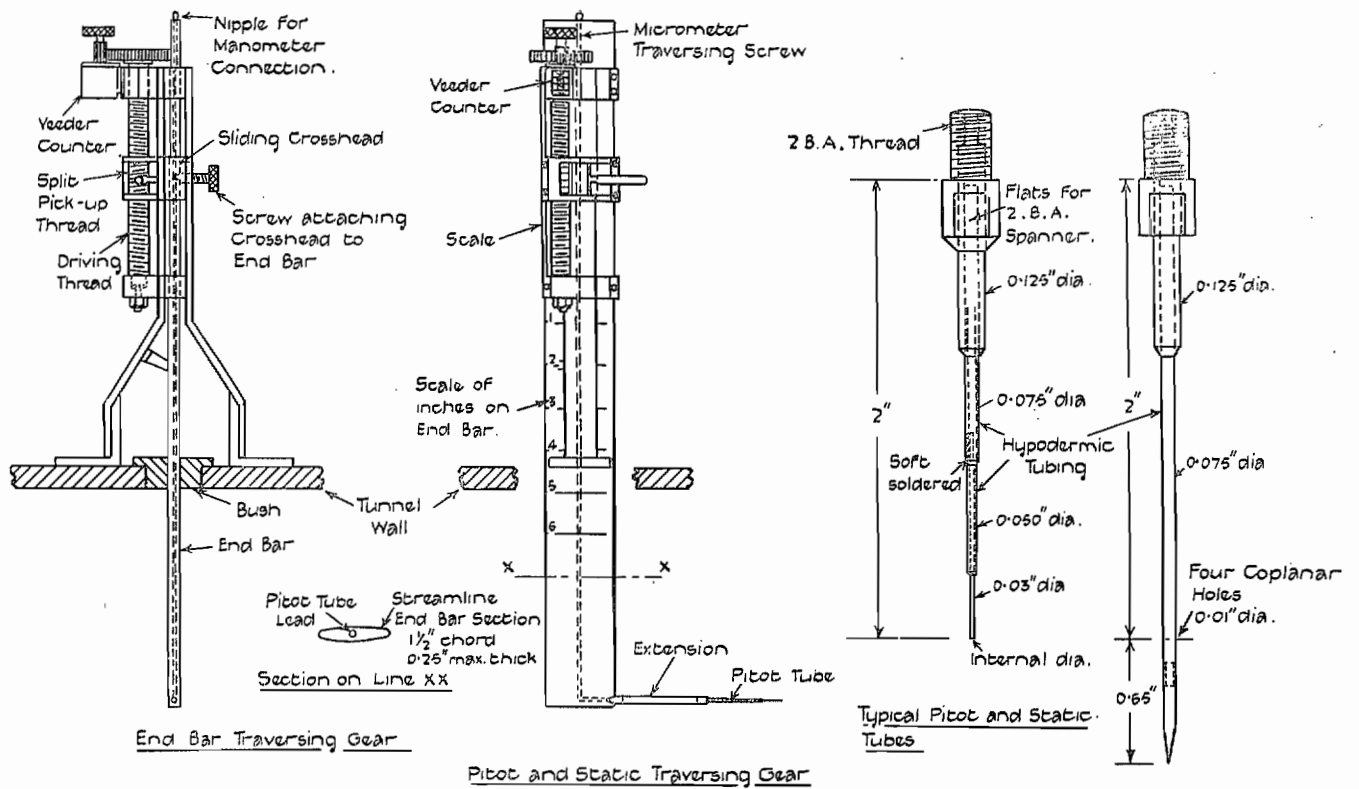


FIG. 9. Pitot and static traversing gear.

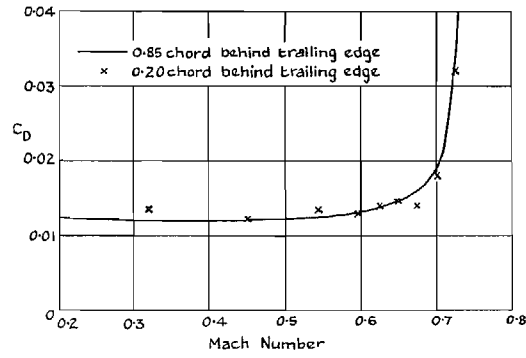
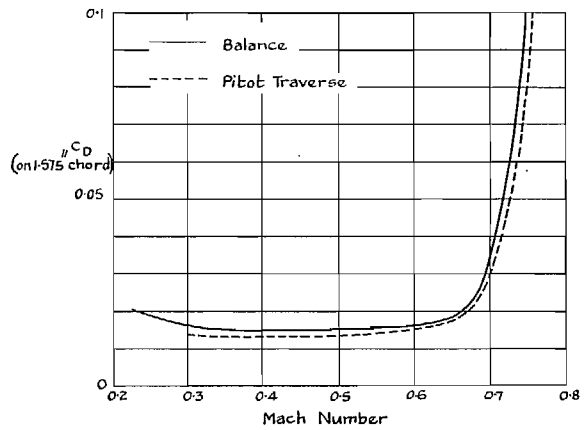


FIG. 10. Profile drag coefficient of NACA 0020 aerofoil (2-in chord) at zero incidence by Pitot traverse at two distances down stream of trailing edge.



Profile Drag Coefficient of Tapered Aerofoil by Balance and Pitot Traverse. -Zero Incidence-

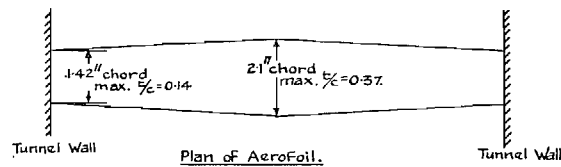


FIG. 11. Profile drag coefficient of tapered aerofoil by balance and pitot traverse—zero incidence.

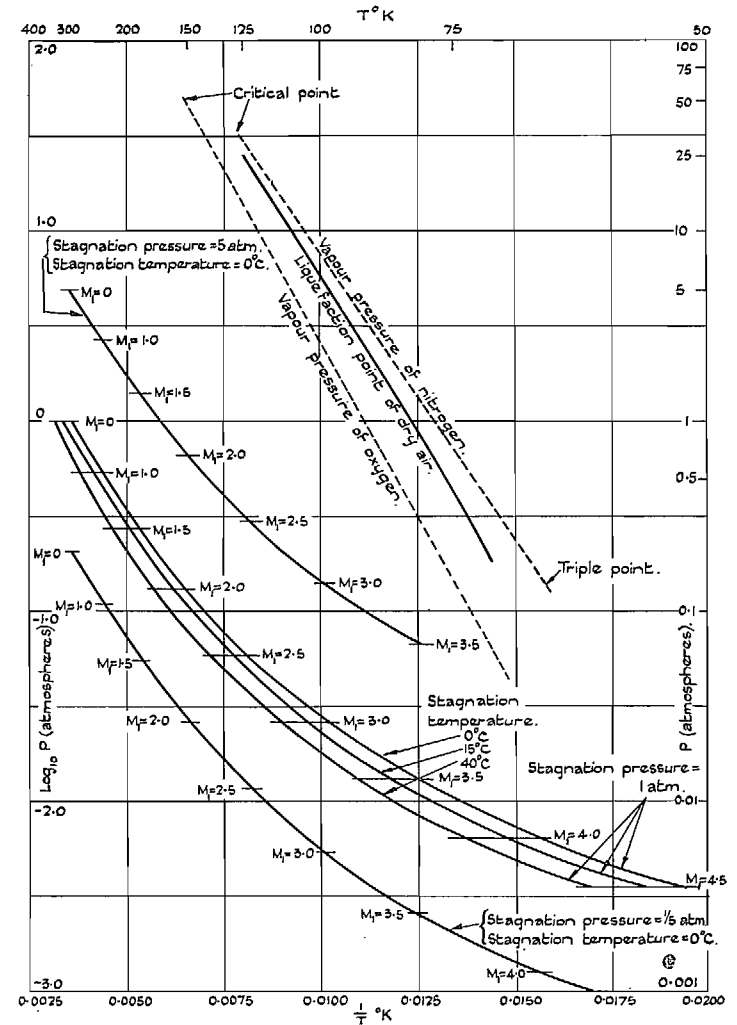


FIG. 12. Vapour pressure of oxygen and nitrogen and liquefaction point of dry air.

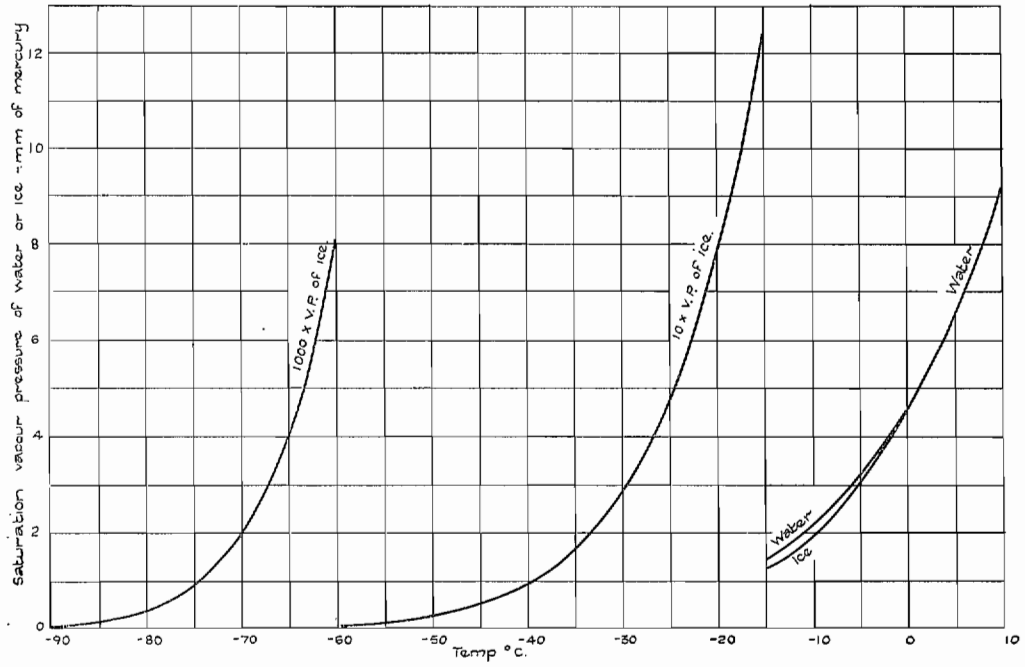


FIG. 13. Variation of saturation vapour pressure of water vapour with temperature.

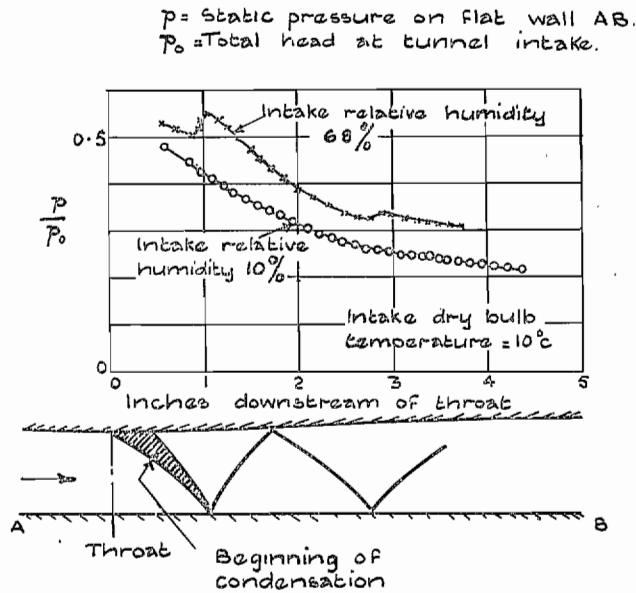


FIG. 14. Measured pressure distributions along 2 × 2-in. supersonic tunnel with high and moderately low intake humidity, and sketch of observed wave pattern at relative humidity = 68 per cent.

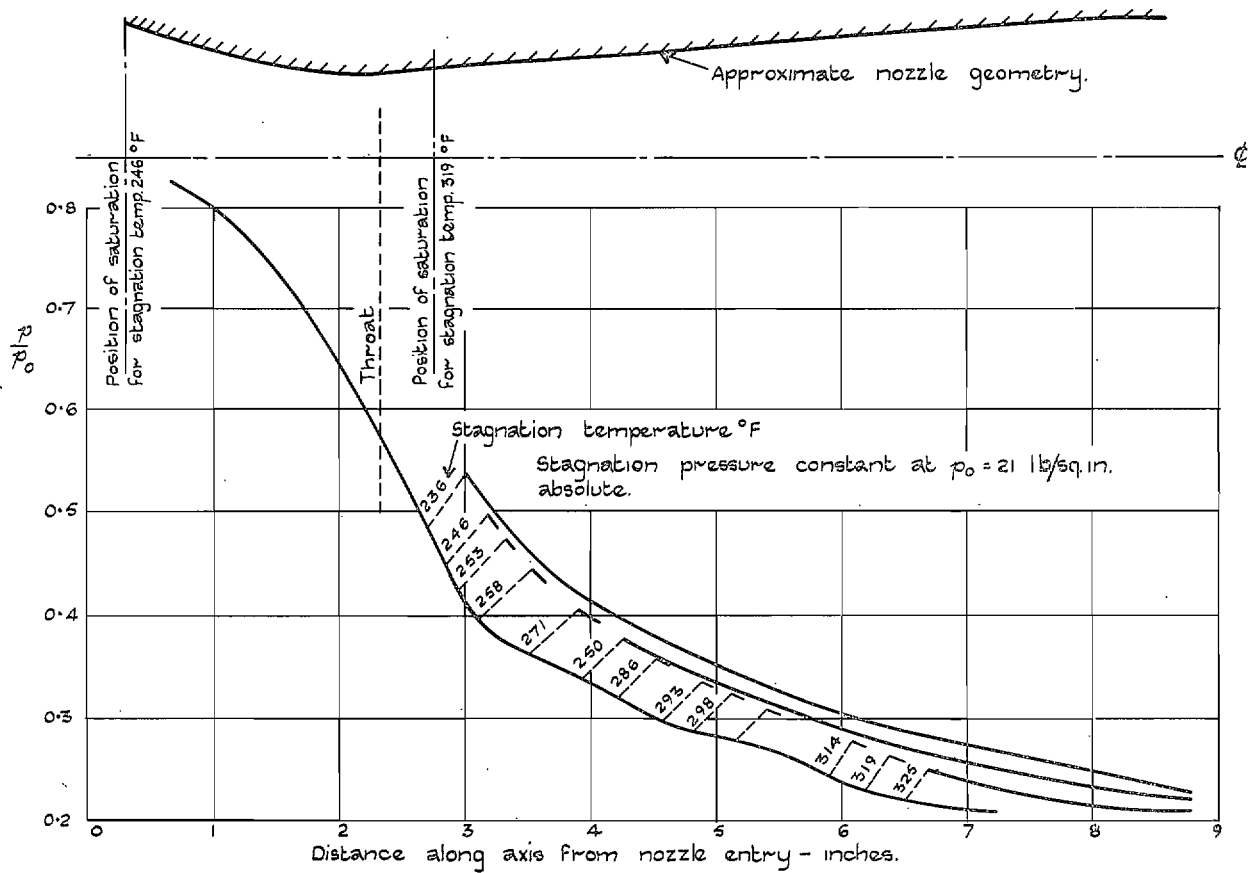


FIG. 15. The influence of condensation upon the flow in a steam nozzle.

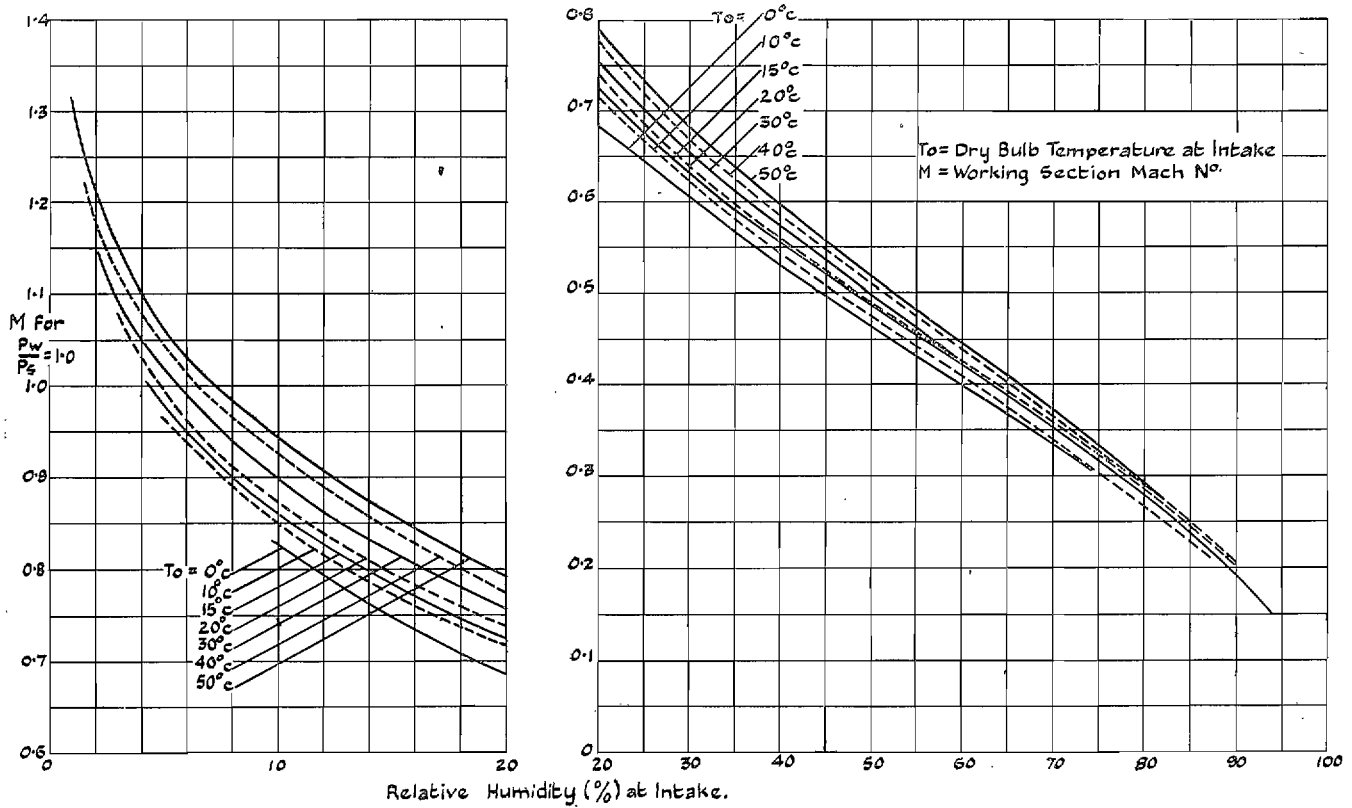


FIG. 16. Conditions for saturation at working section (water vapour over water).

p_w Partial vapour pressure of water vapour.
 p_s Saturation vapour pressure of water vapour.
 T_0 Dry bulb temperature at intake.
 M Working section Mach number.

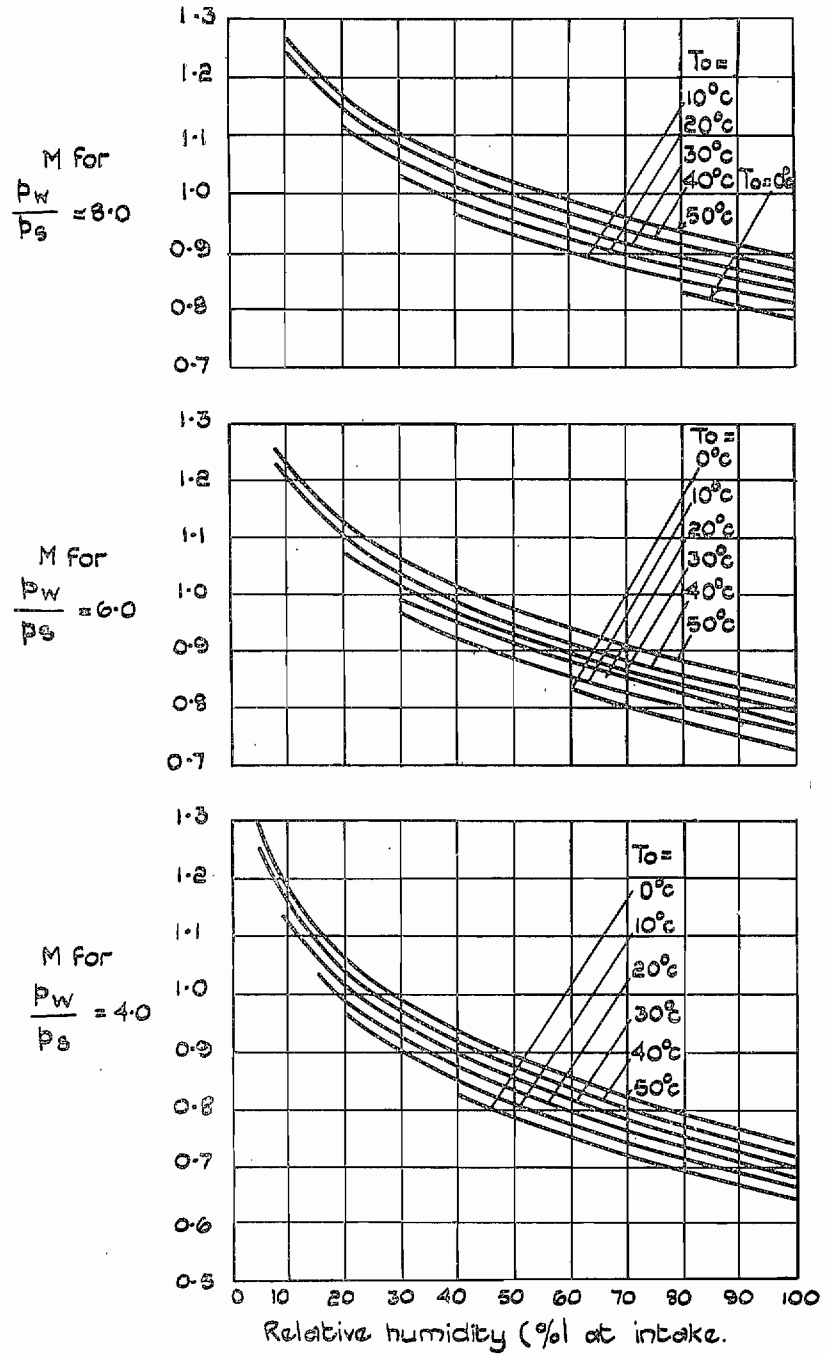


FIG. 17(a). Conditions for 4, 6 and 8-fold saturation at working section (water vapour over water).

p_w = Partial vapour pressure of water vapour.
 p_s = Saturation vapour pressure of water vapour.
 T_o = Dry bulb temperature at intake.
 M = Working section Mach number.

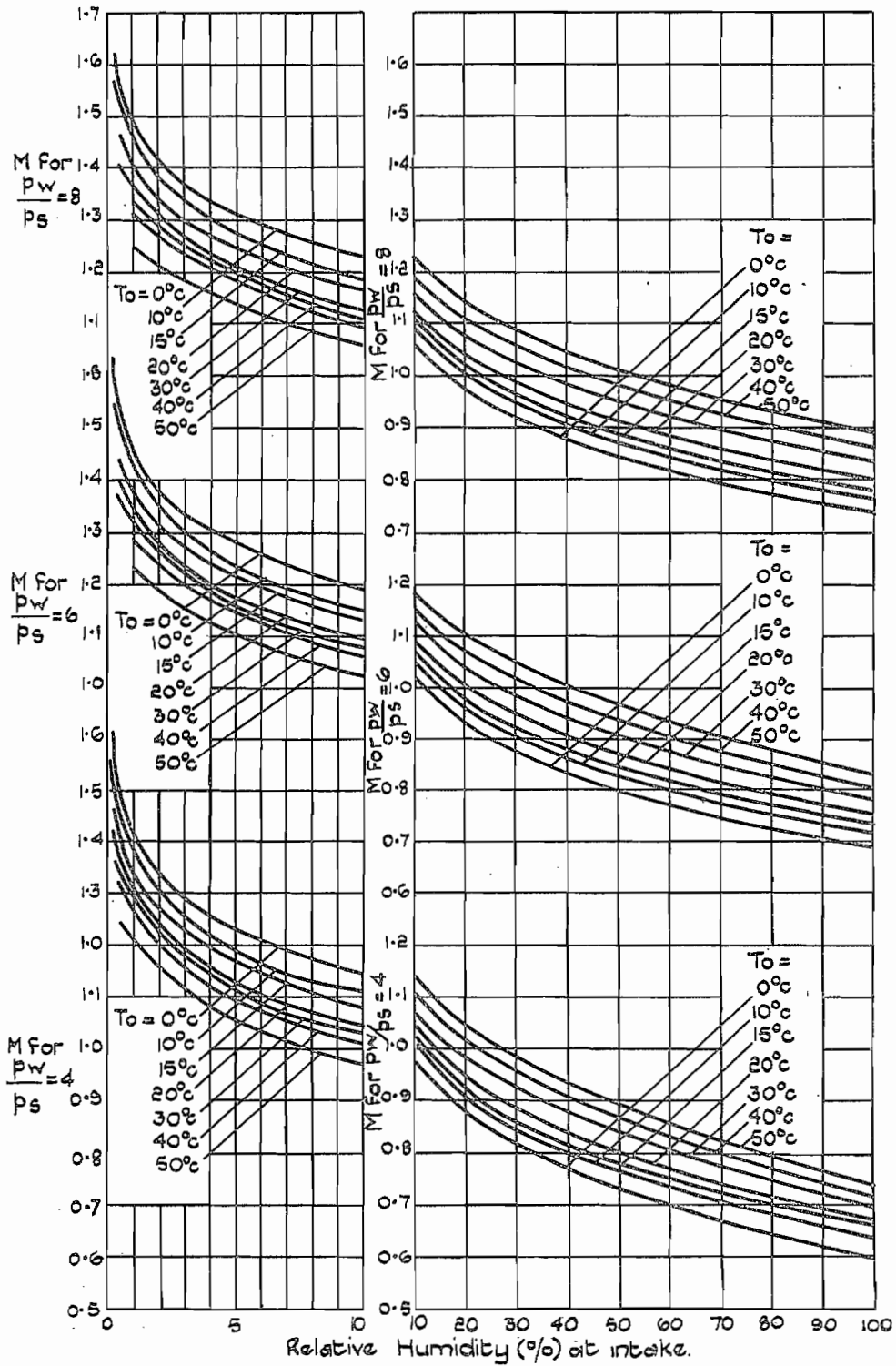


FIG. 17(b). Conditions for 4, 6 and 8-fold saturation at working section (water vapour over ice).

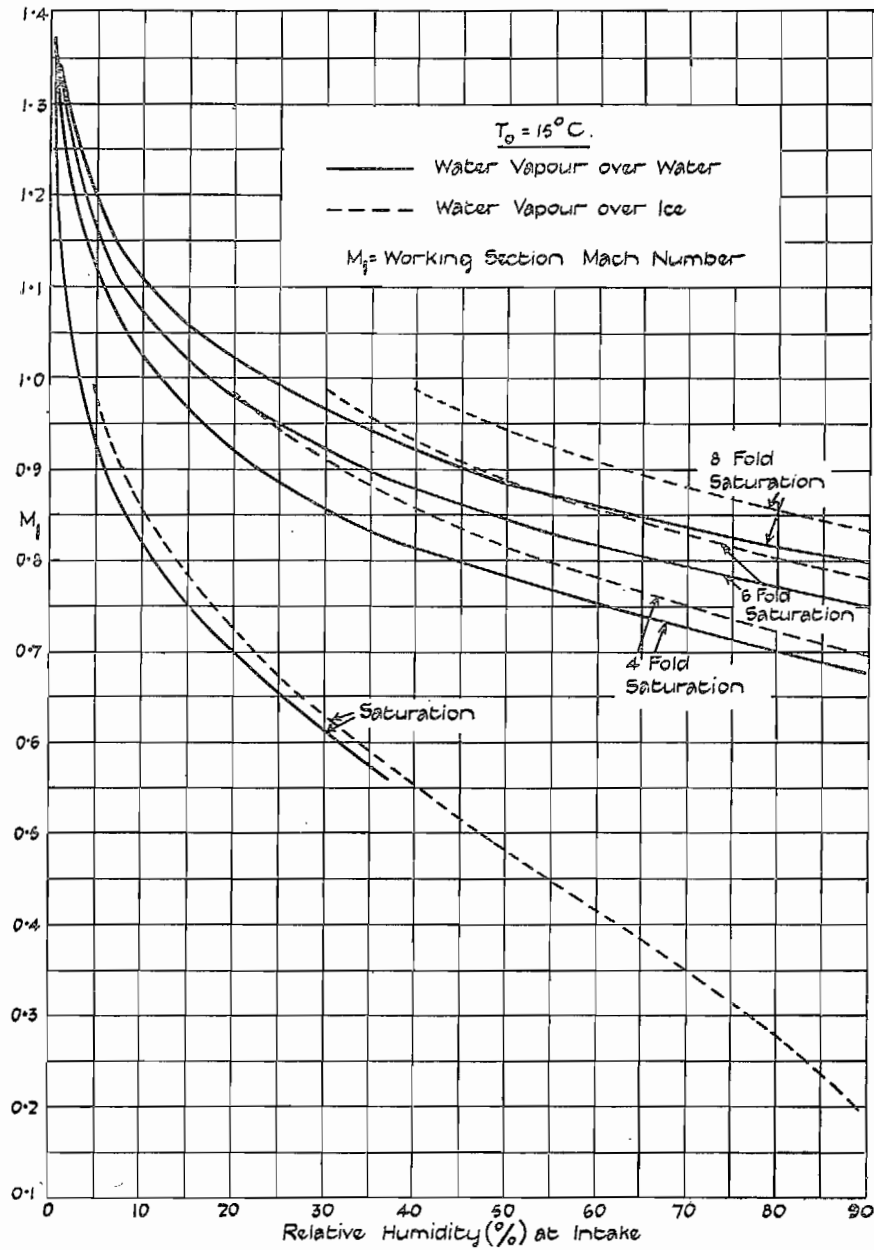


FIG. 18. Conditions for saturation and 4, 6 and 8-fold saturation at working section.

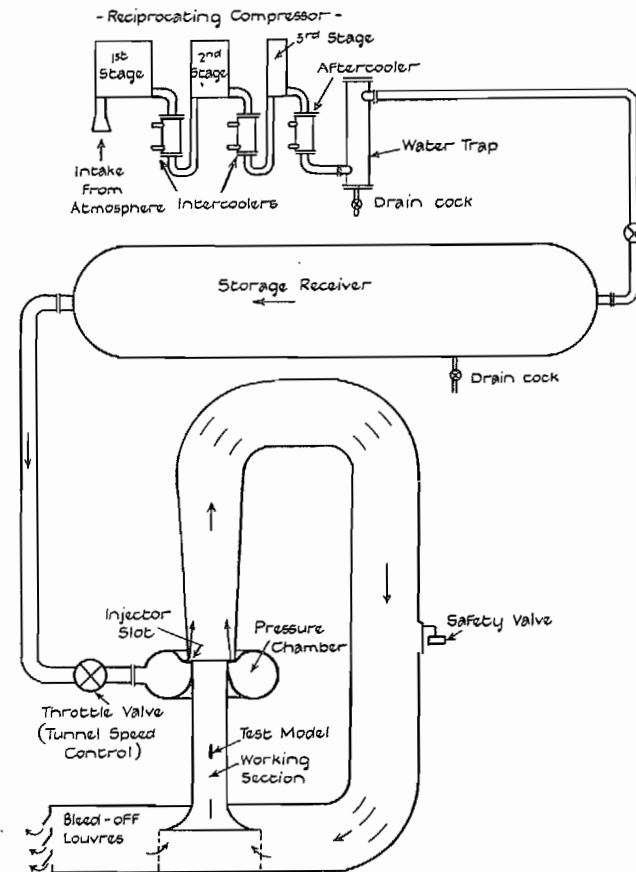


FIG. 19. Sketch of N.P.L. induction-type wind tunnel installation.

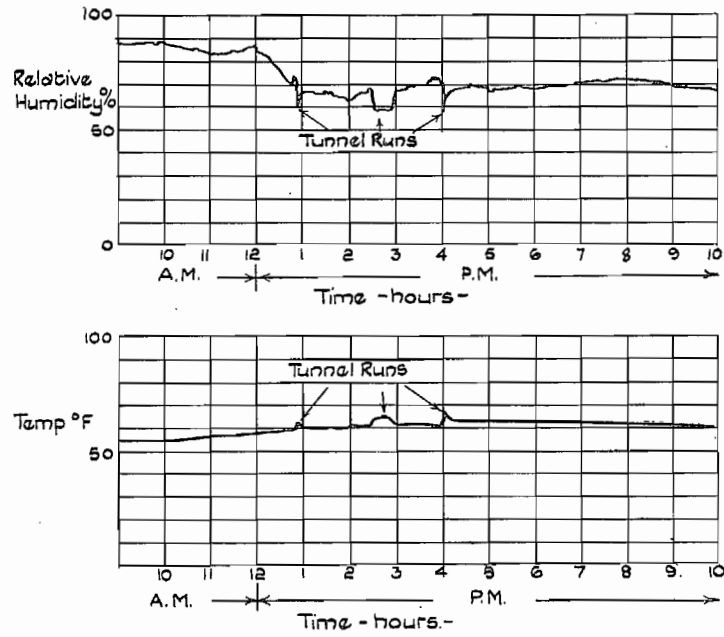


FIG. 20. Hygrograph and thermograph records at tunnel intake without return ducts.

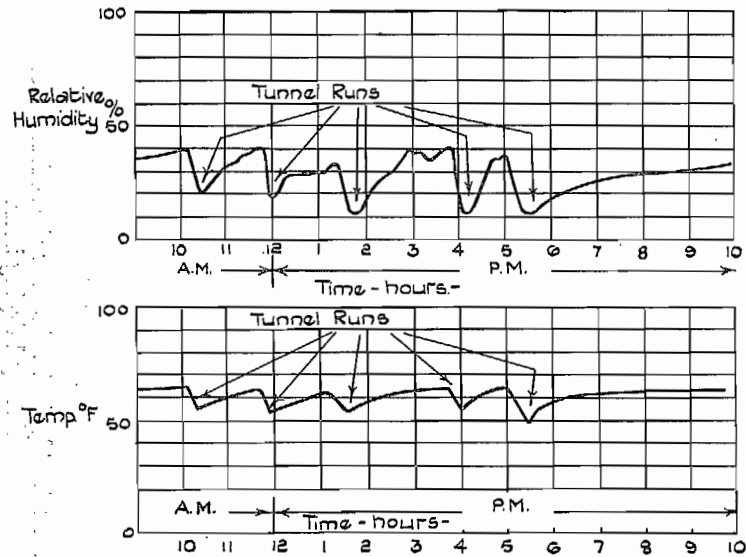


FIG. 21. Hygrograph and thermograph records at tunnel intake with return ducts.

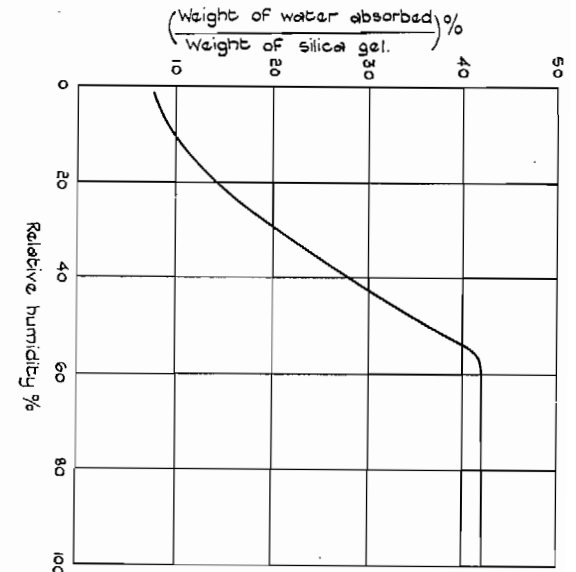


FIG. 22. Typical absorbent properties of silica gel.

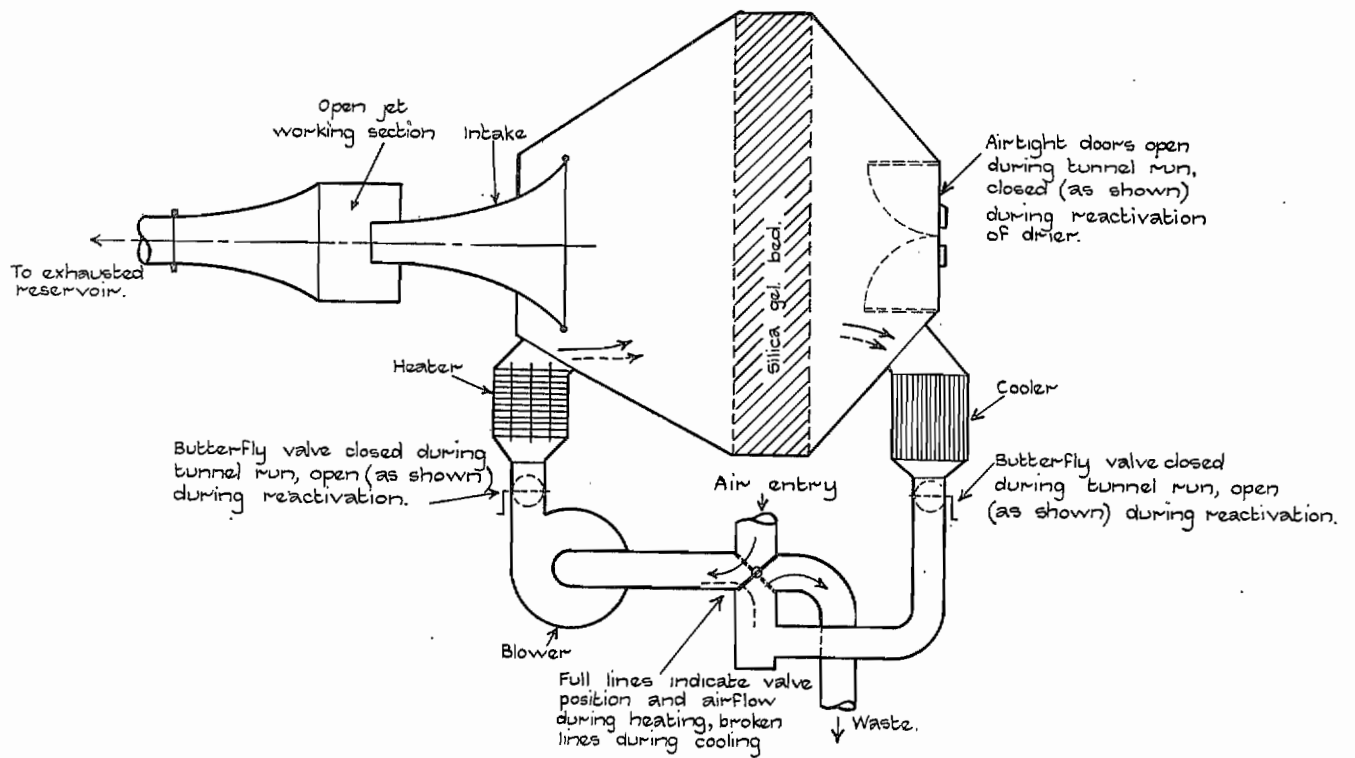


FIG. 23. Sketch of the drier installation on the 215-mm diameter subsonic tunnel at Göttingen.

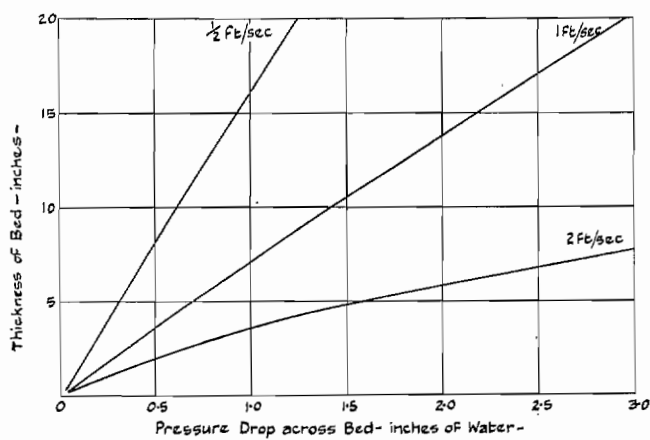


FIG. 24. Typical values for the resistance of silica gel drying beds.

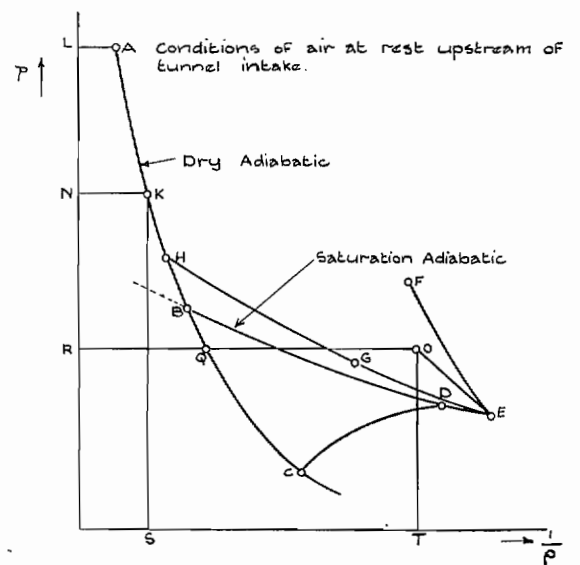


FIG. 25. (p, v) diagram for a pitot-tube in moist airstream.

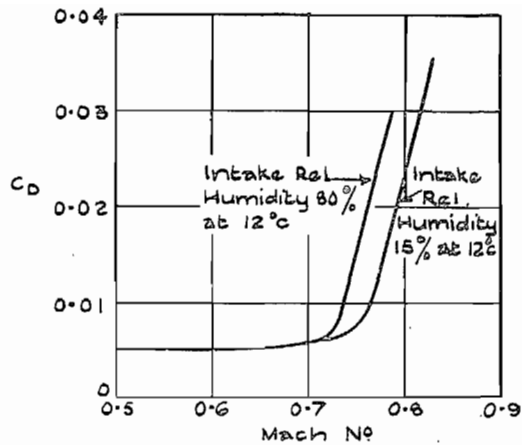


FIG. 26. Influence of humidity on profile-drag coefficient measured by wake-traverse method.

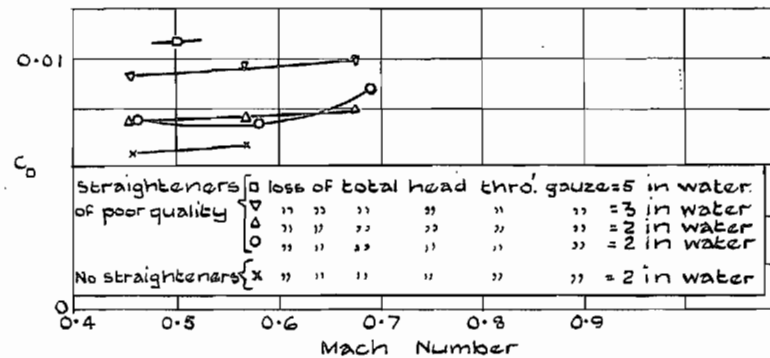


FIG. 27. Goldstein 1442/1547 aerofoil at 0.5 deg incidence below shock-stall.

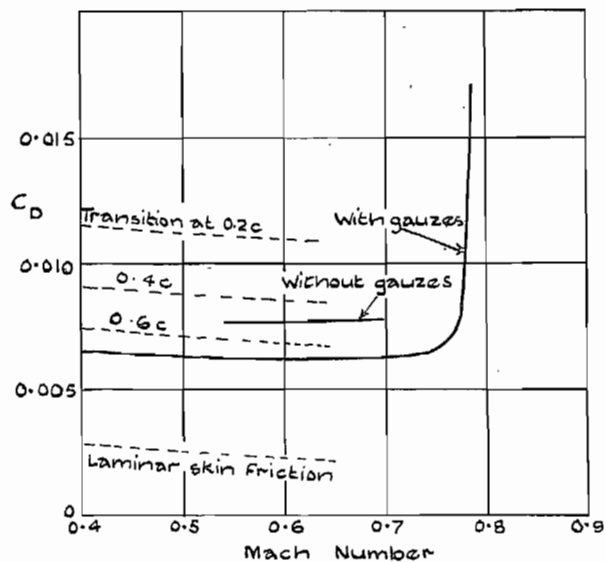
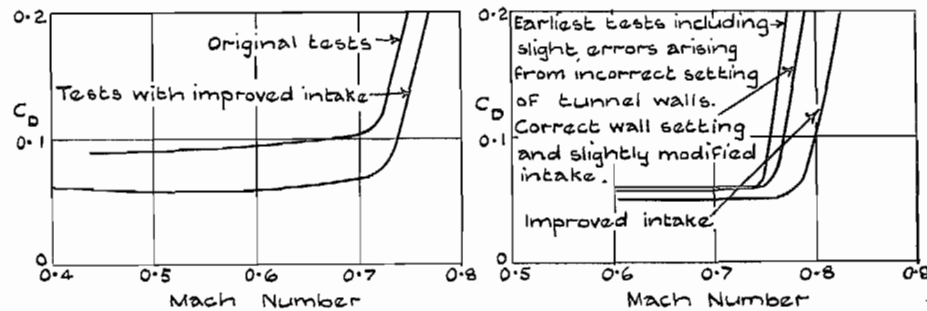


FIG. 28. Aerofoil EC 1250 at 0 deg incidence in 20 x 8-in. high-speed tunnel.



Goldstein 1442/1547 at 0.5 deg incidence. EC 1250 at 0 deg incidence.
 FIG. 29. Effect of tunnel intake upon drag coefficient. 20 x 8-in. tunnel.

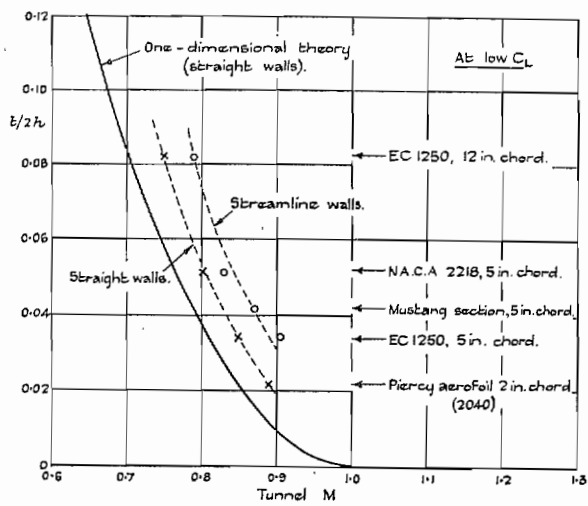
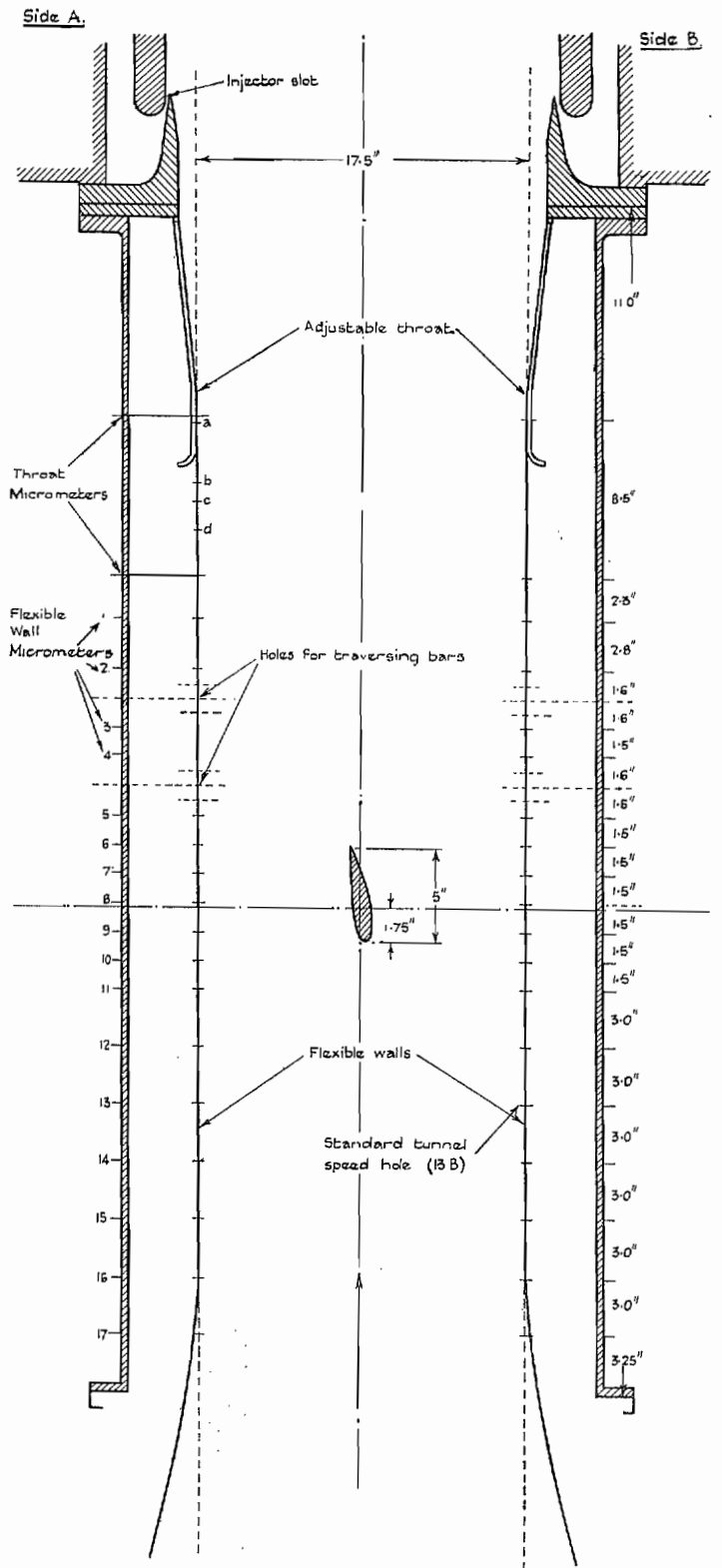


FIG. 30. Comparison of observed choking speeds of 20×8 -in. tunnel with those calculated on one-dimensional theory.



There are pressure holes in the flexible walls opposite each of the micrometers 1-7 and at a, b, c, d

FIG. 31. Diagrammatic view of the flexible walls, set straight and parallel.

117

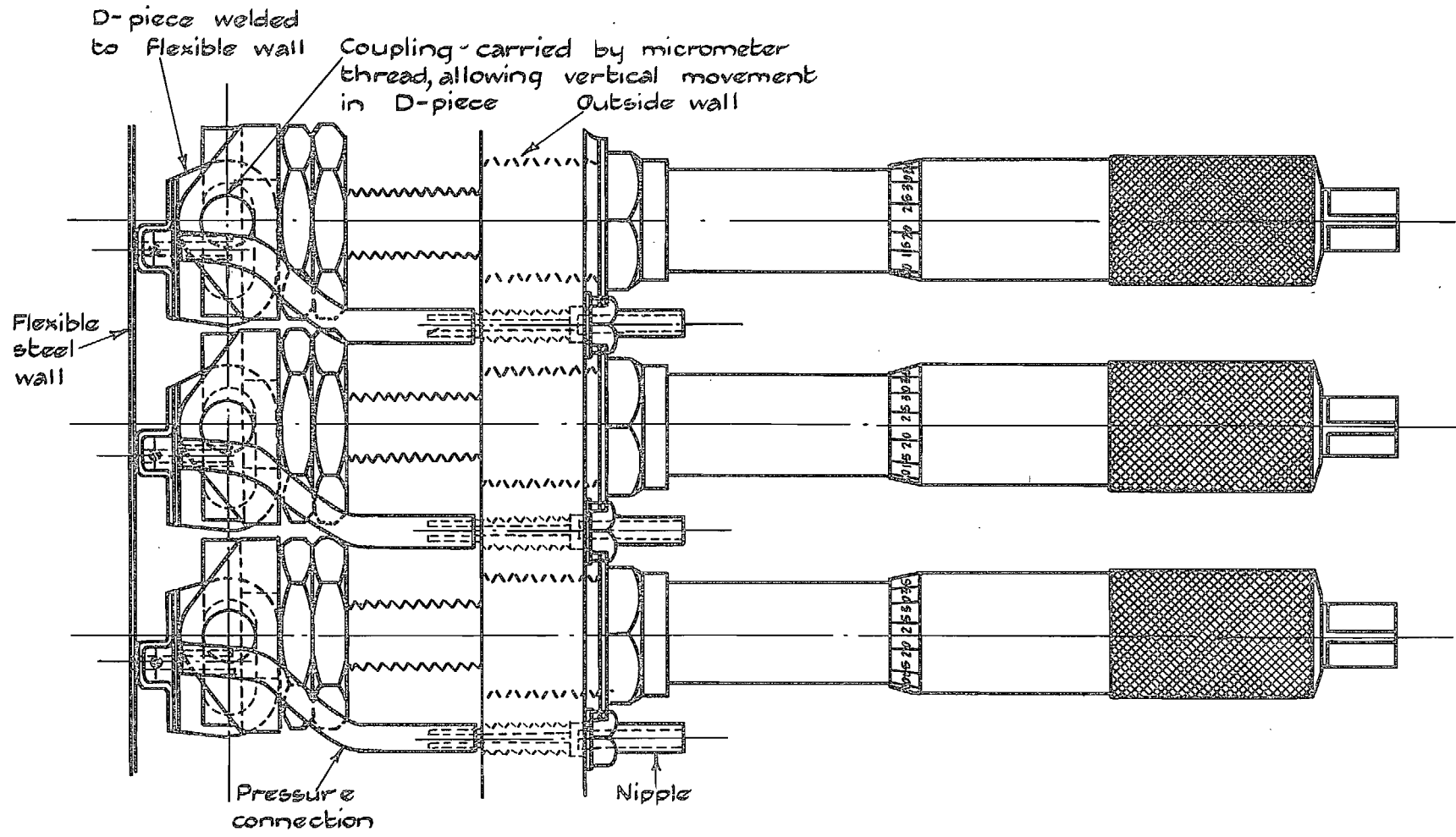


FIG. 32. Details of flexible wall control.

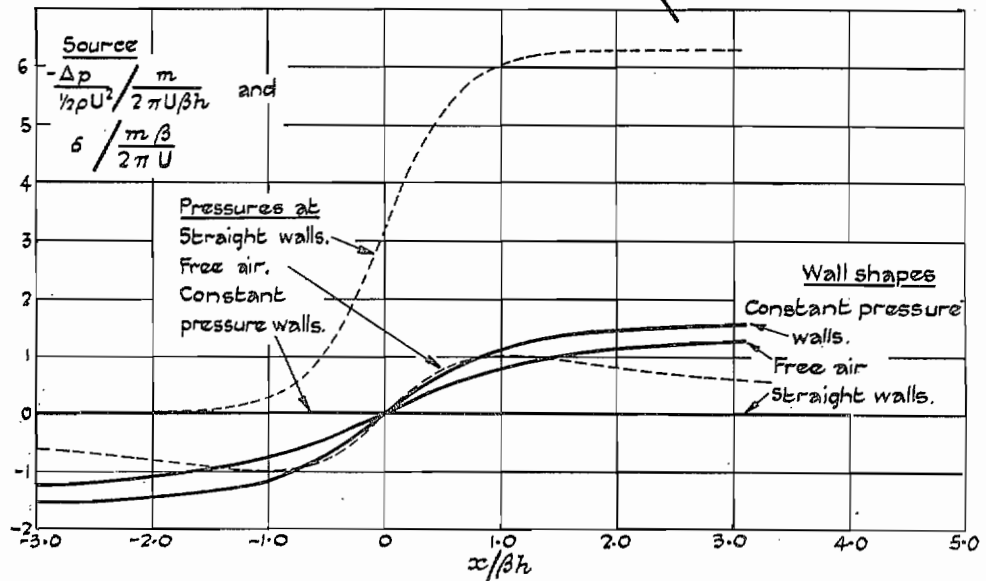
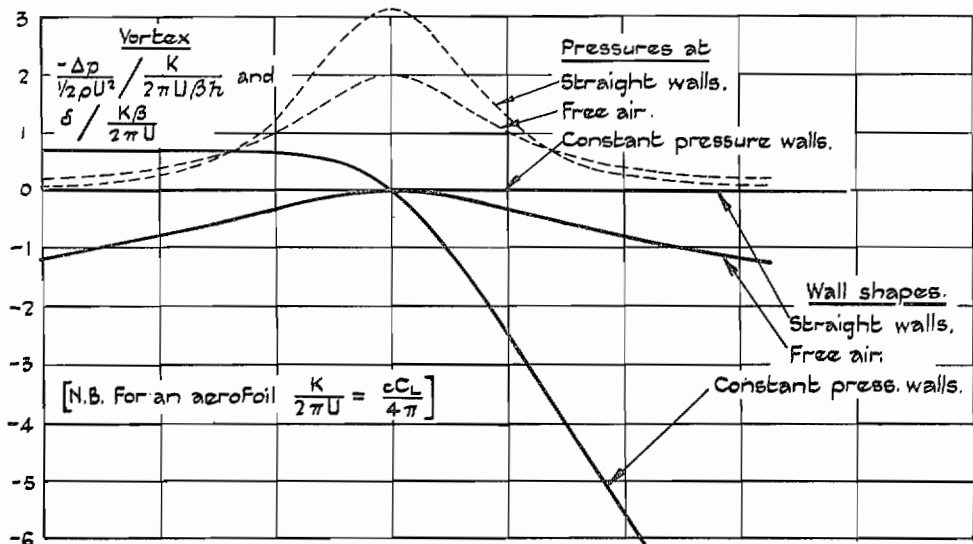
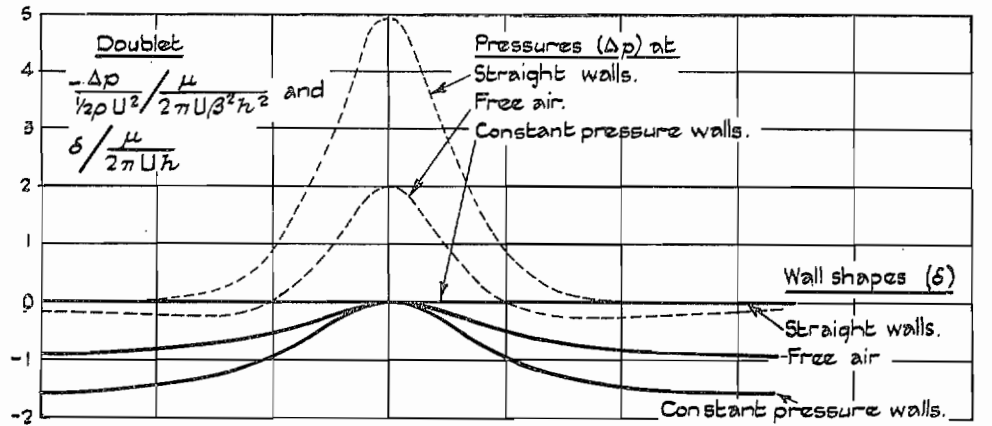


FIG. 33. Streamlines and pressures about doublets, vortices and sources.

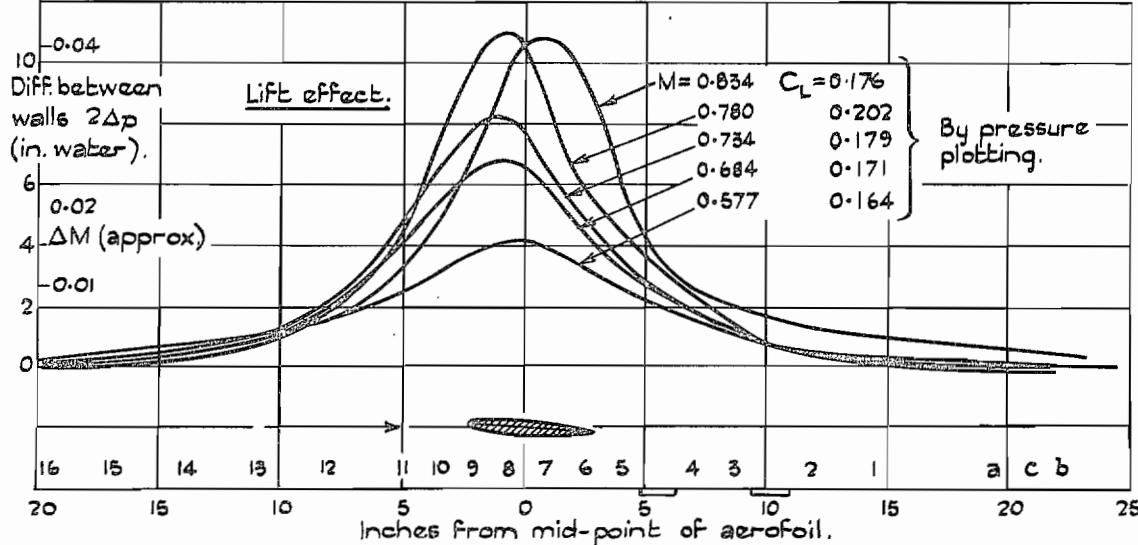
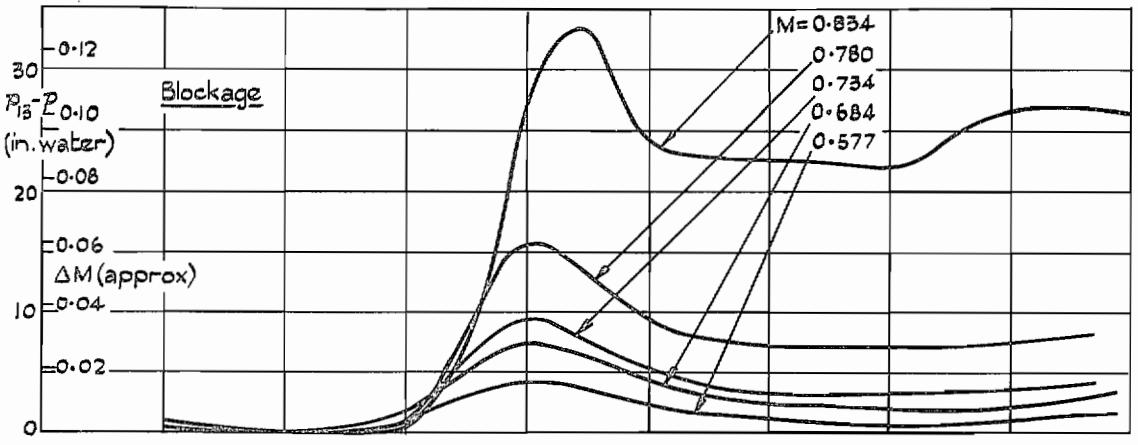
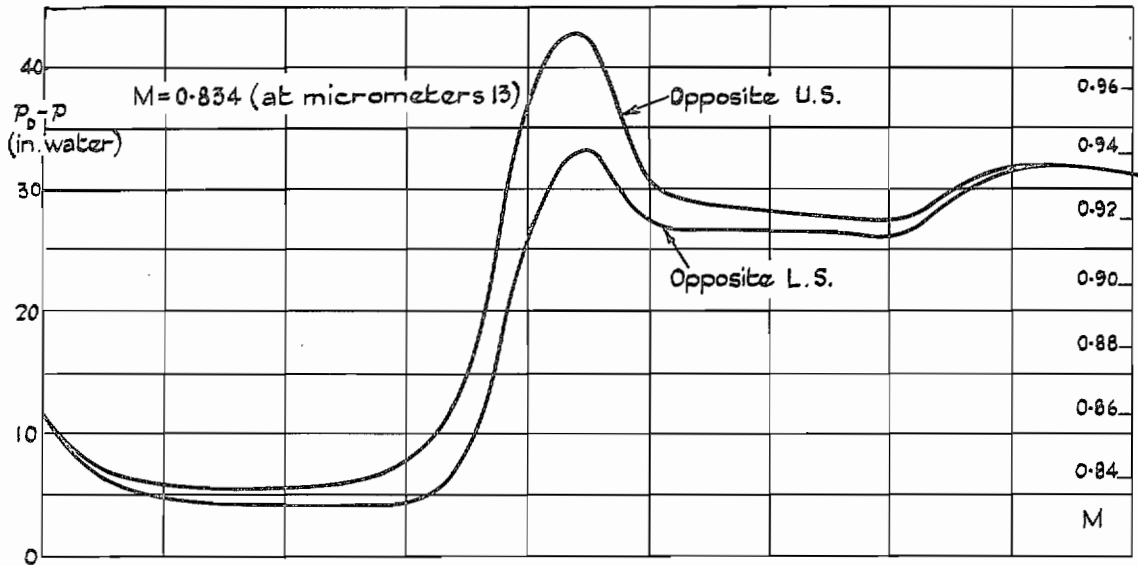


FIG. 34. Wall pressures and velocities with straight walls—aerofoil EC 1250. 5-in. chord at 2 deg.

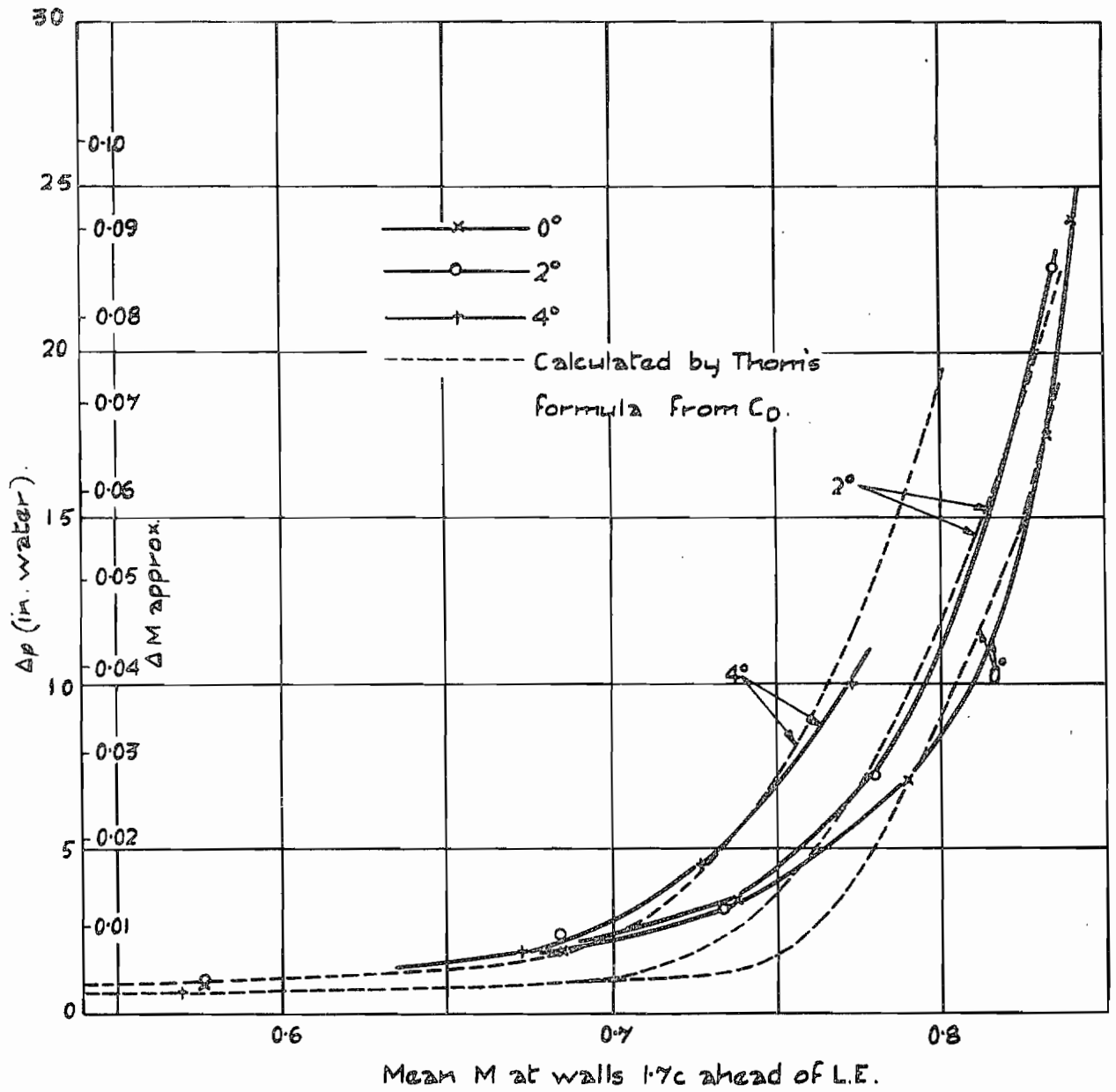


FIG. 35. Change of pressure and velocity behind EC 1250, 5-in. chord, on straight walls (wake blockage effect; increase of velocity at walls 1.7c behind trailing edge).

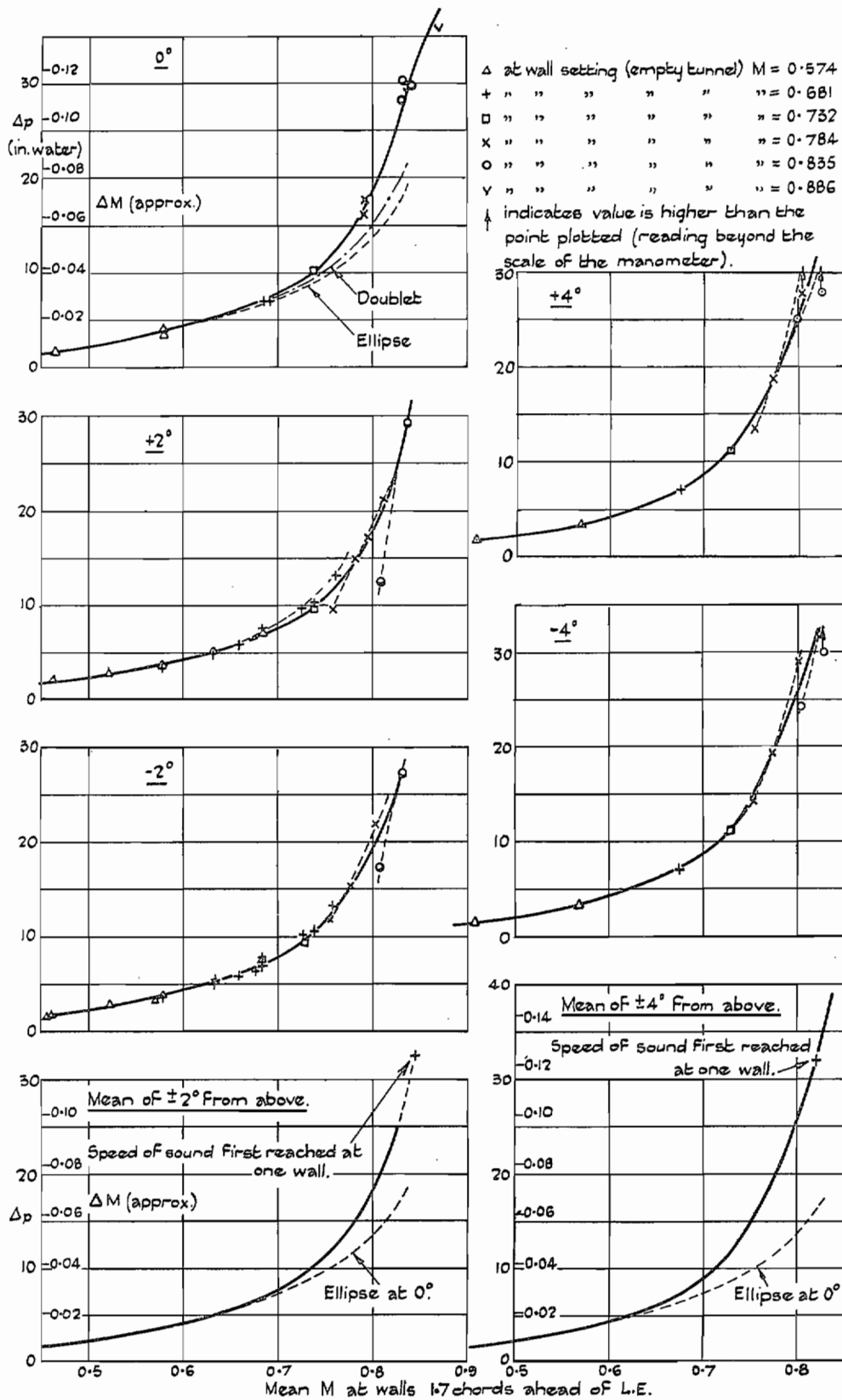


Fig. 36. Change of pressure and velocity opposite EC 1250, 5-in. chord, on straight walls (blockage effect).

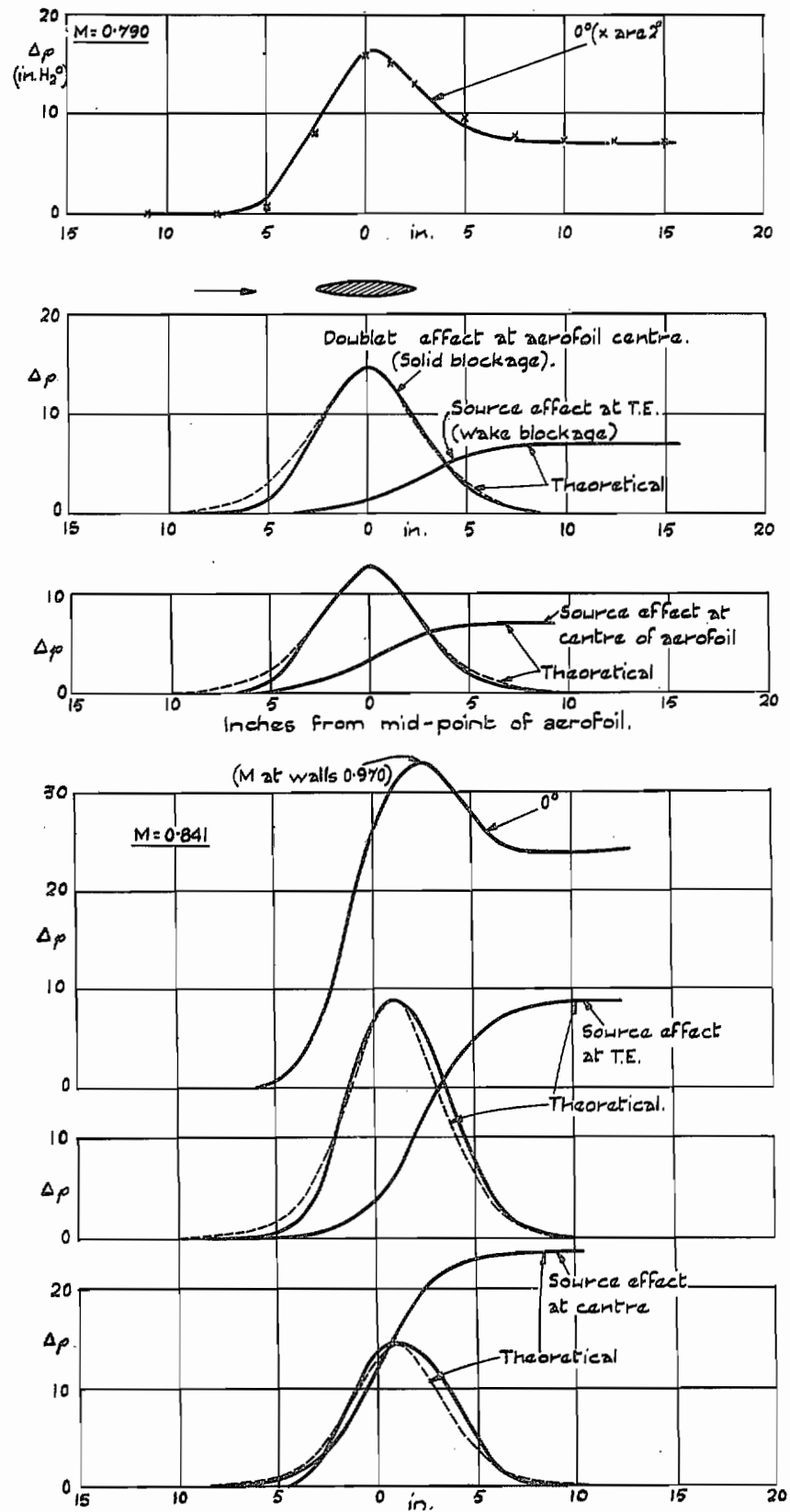


FIG. 37. Analysis of blockage into doublet and source effects.

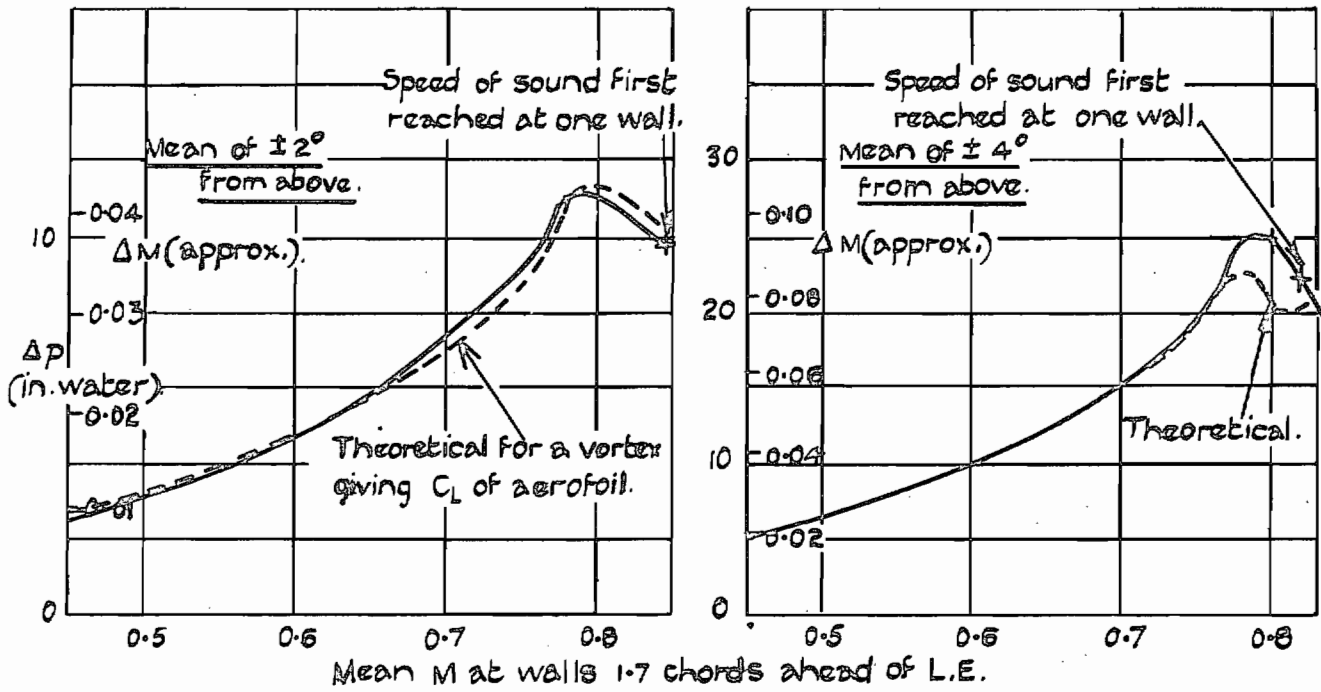


FIG. 38. Difference of pressure and velocity opposite EC 1250, 5-in. chord, on straight walls (lift effect).

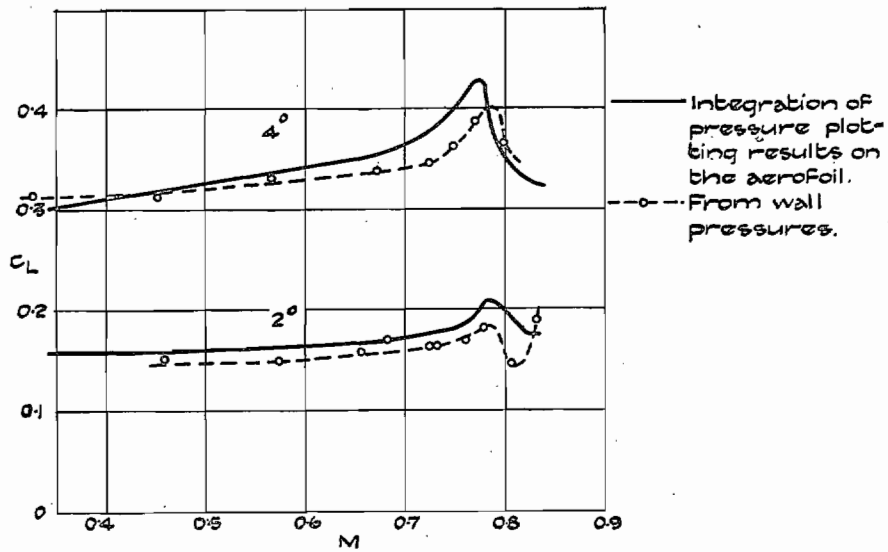


FIG. 39. Lift from wall pressures (straight walls).

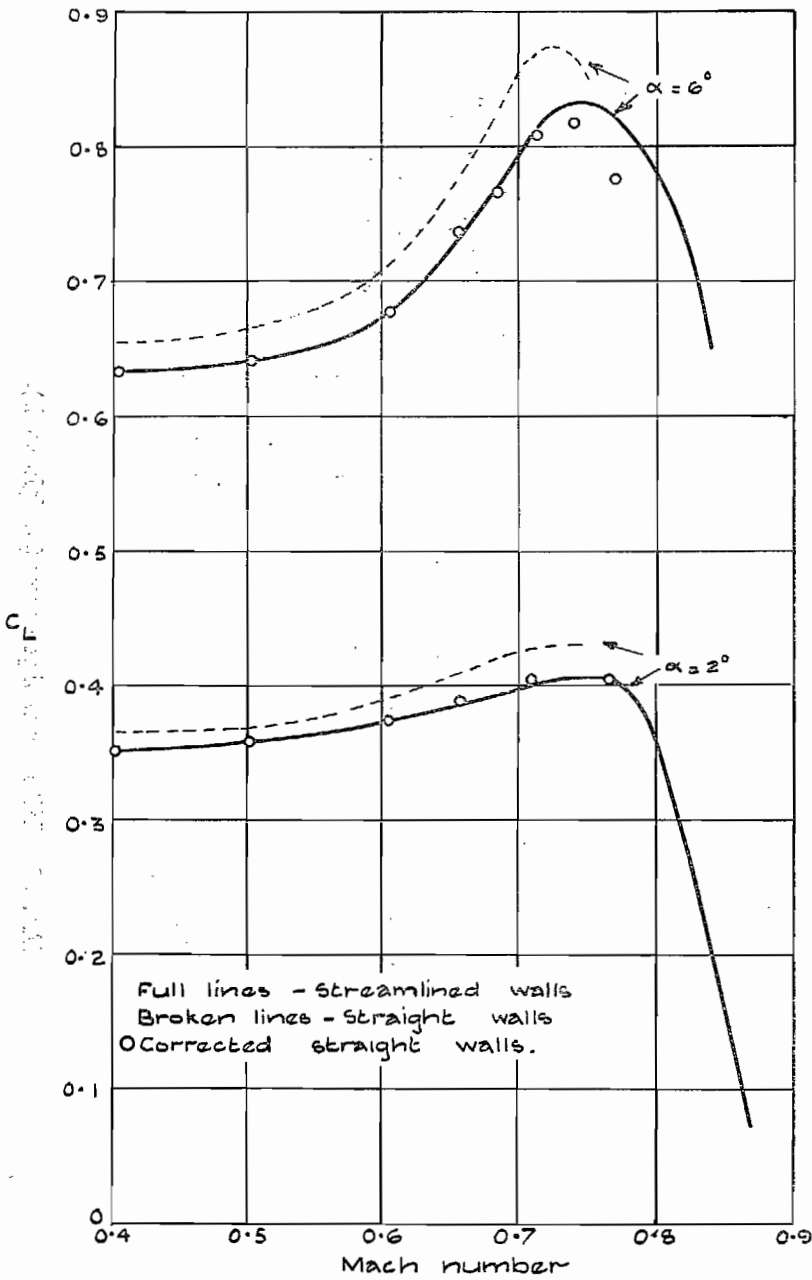
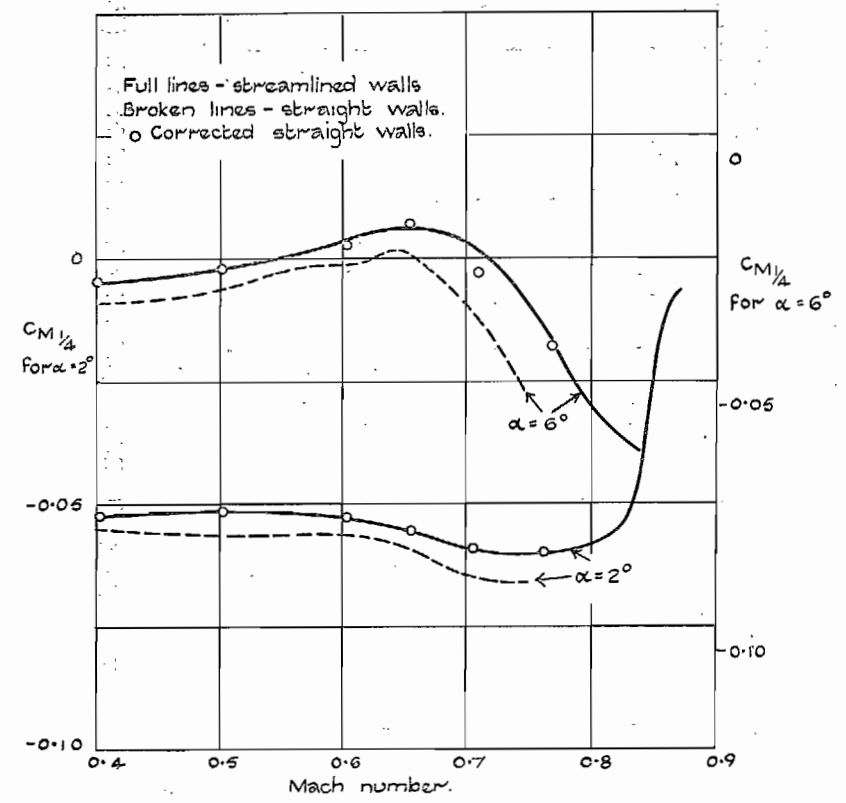


FIG. 40. Lift coefficients with straight and streamlined walls. 10 per cent NACA propeller aerofoil.



10% NACA propeller aerofoil.

FIG. 41. Quarter-chord pitching-moment coefficients with straight and streamlined walls.

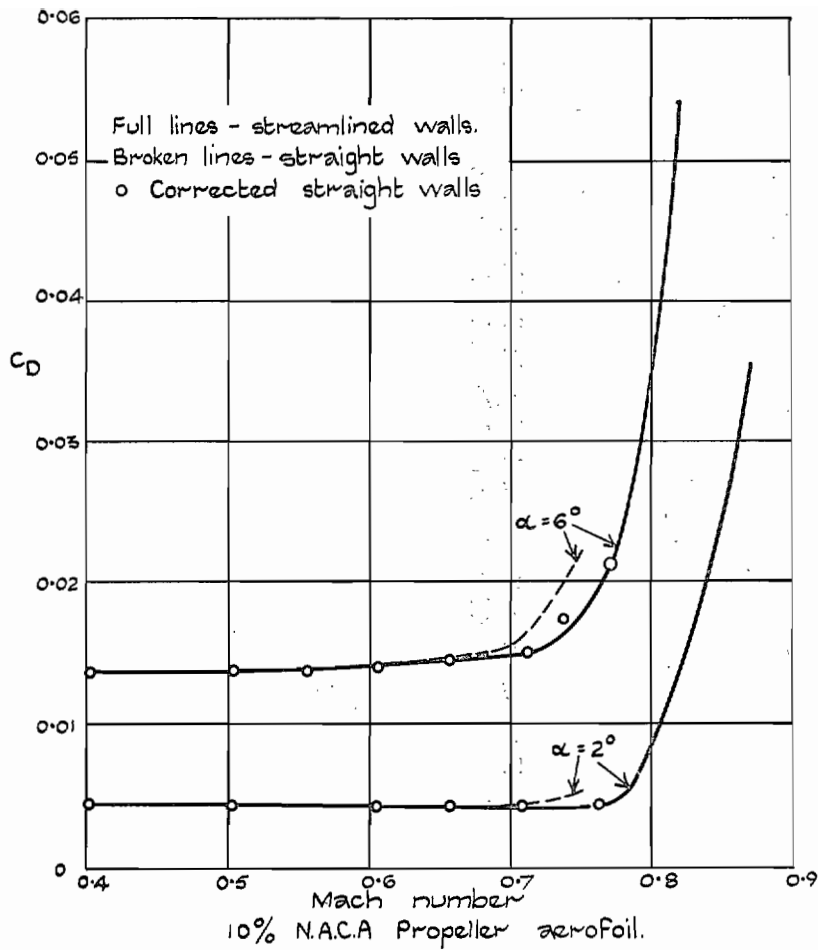


FIG. 42. Profile drag coefficients with straight and streamlined walls.

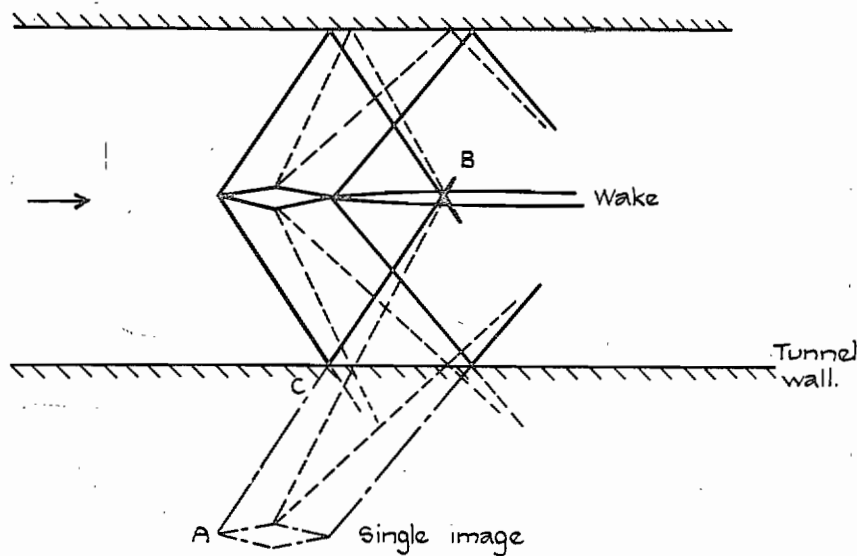


FIG. 43. Sketch of wave pattern from an aerofoil in a supersonic tunnel when the flow is everywhere supersonic.

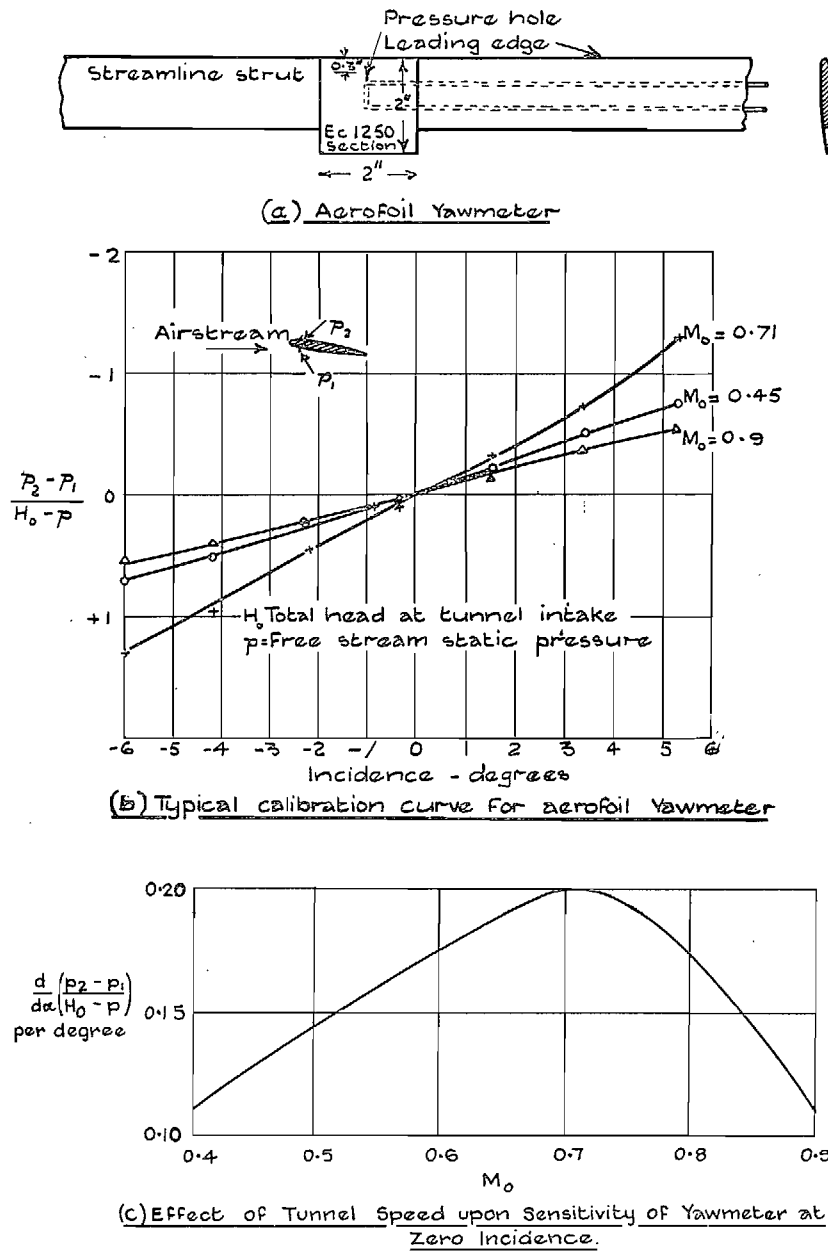


FIG. 44.

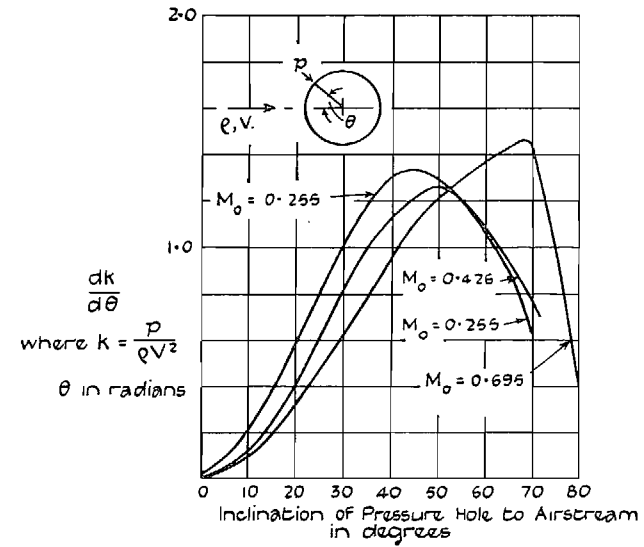


FIG. 45. Variation of sensitivity of cylindrical yawmeter with position of pressure hole and Mach number.

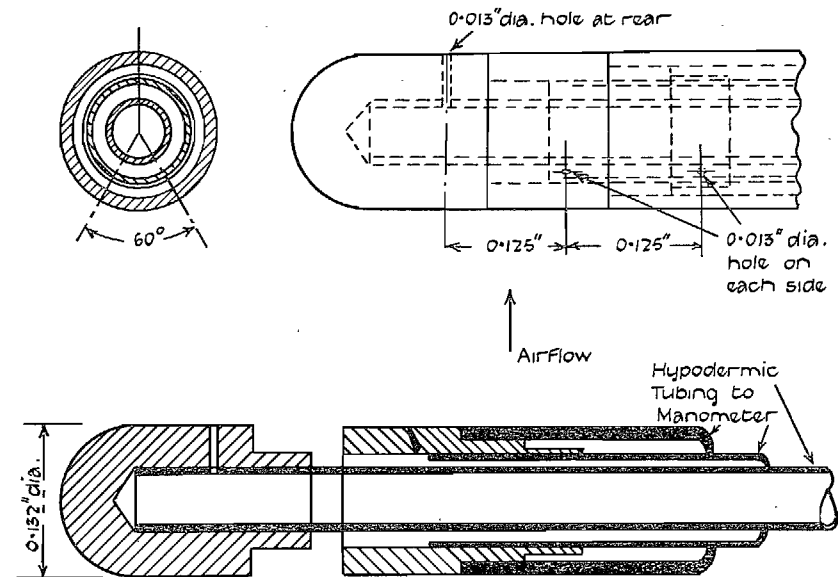
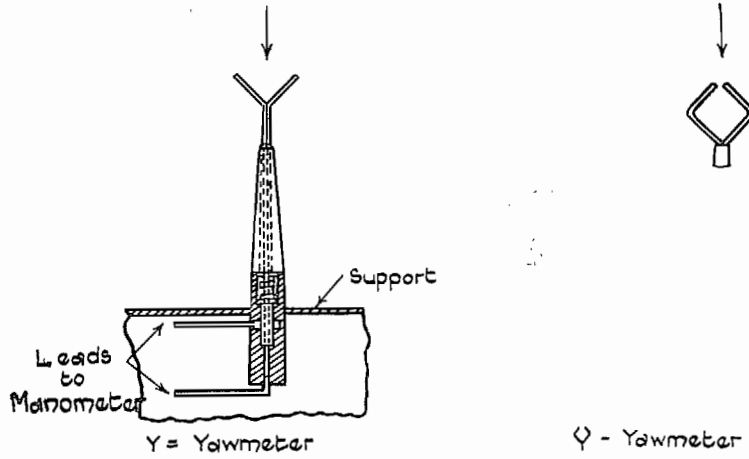


FIG. 46. N.P.L. circular-cylinder yawmeter—sketch of head.



127

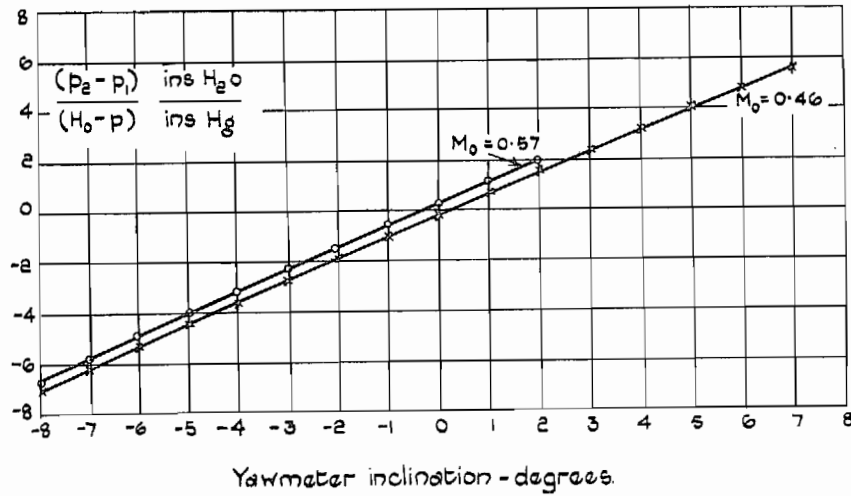


FIG. 47. Low-speed calibration curves for Y-yawmeter. Readings become violently unsteady for $M_0 = 0.8$.

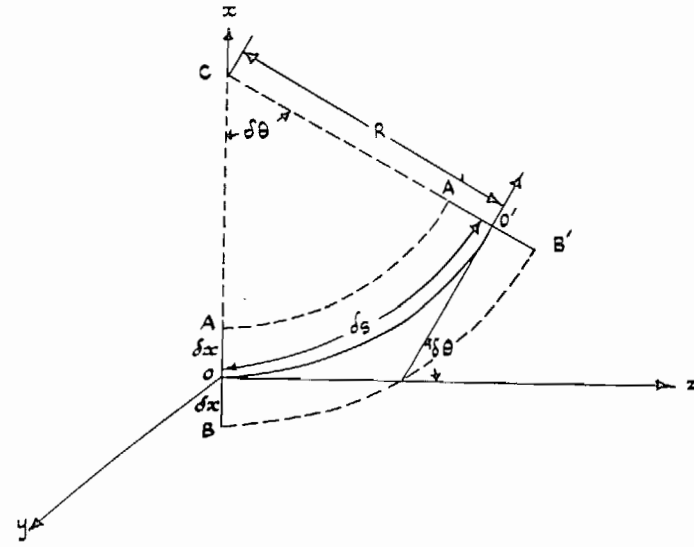


FIG. 48. Deflection of light in a density gradient.

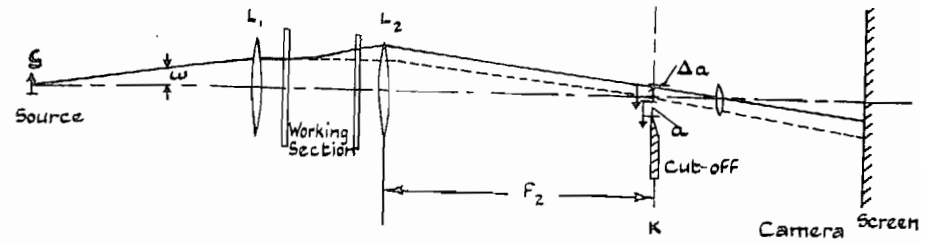


FIG. 49. Sketch of schlieren arrangement.

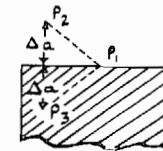
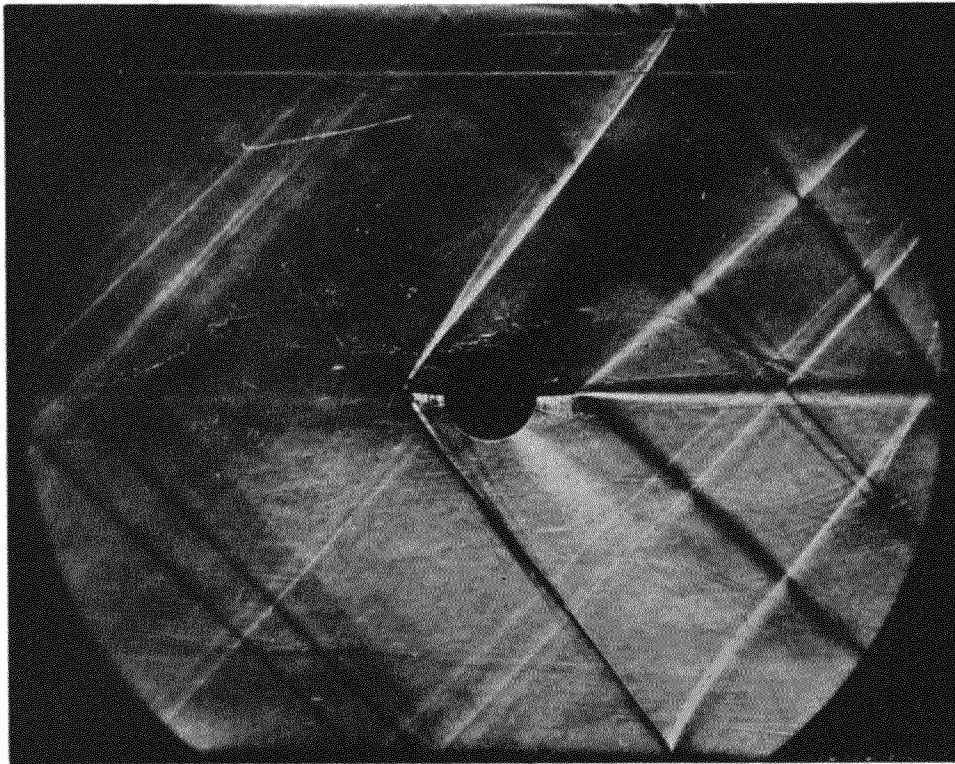


FIG. 50. Sketch of cut-off as seen from direction of optical axis.



Cut off

FIG. 51. Schlieren photograph of 6 per cent double-wedge aerofoil at $M = 1.4$. Cut-off parallel to chord.
 (Note.—The circular object at $\frac{1}{2}$ chord is a support and is outside the tunnel.)

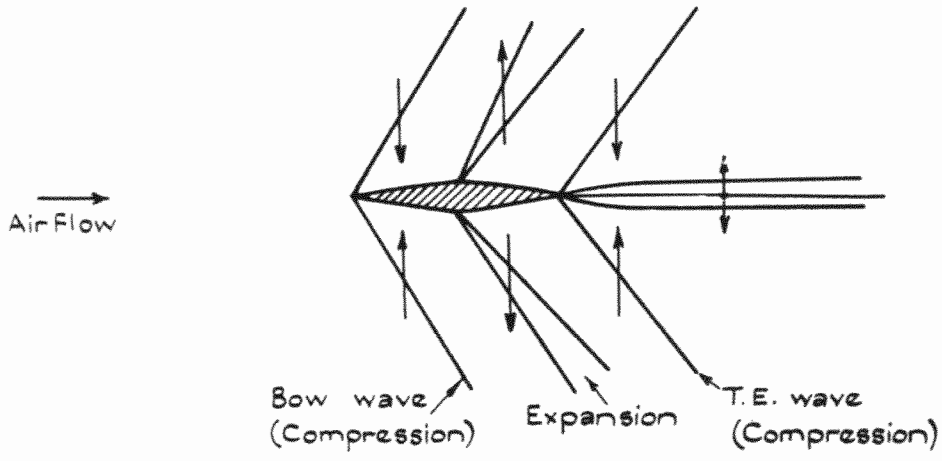


FIG. 52. Sketch of directions of positive density gradient components normal to chord of double-wedge aerofoil at supersonic Mach number.

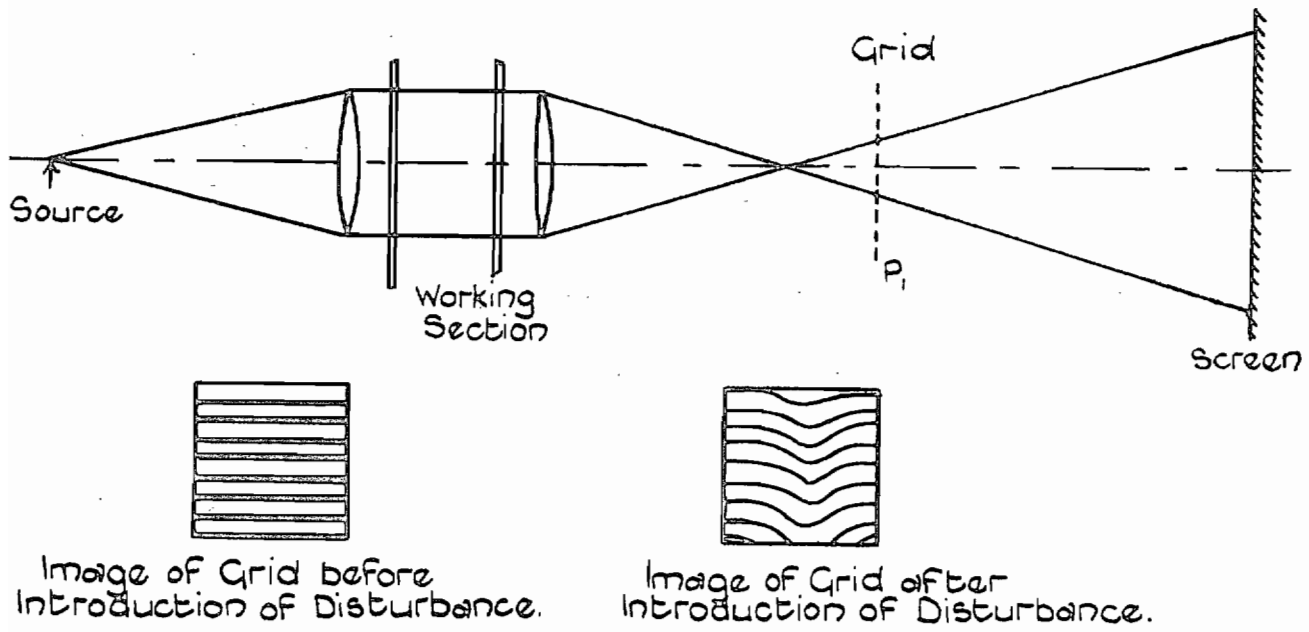


FIG. 53. Simplified-sketch of one form of the Ronchi schlieren arrangement.

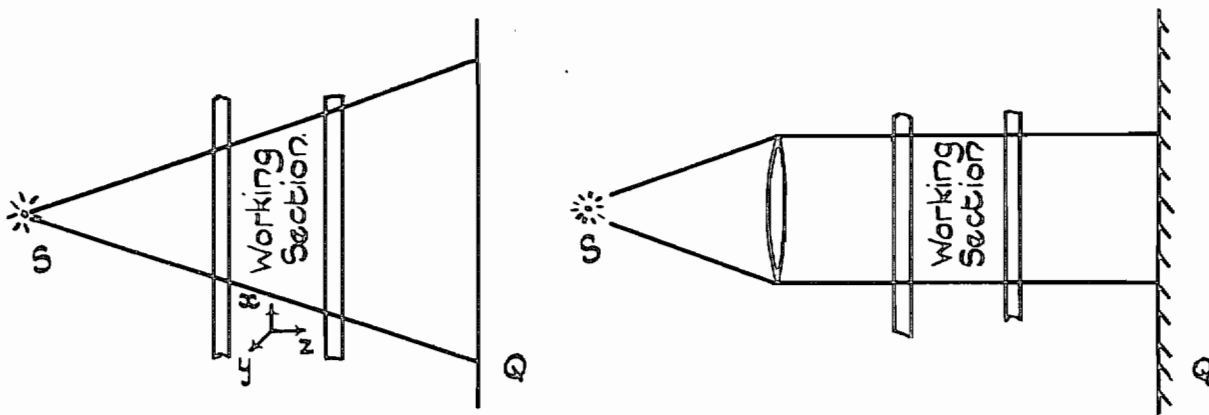


FIG. 54. Direct shadow systems with divergent and parallel light.

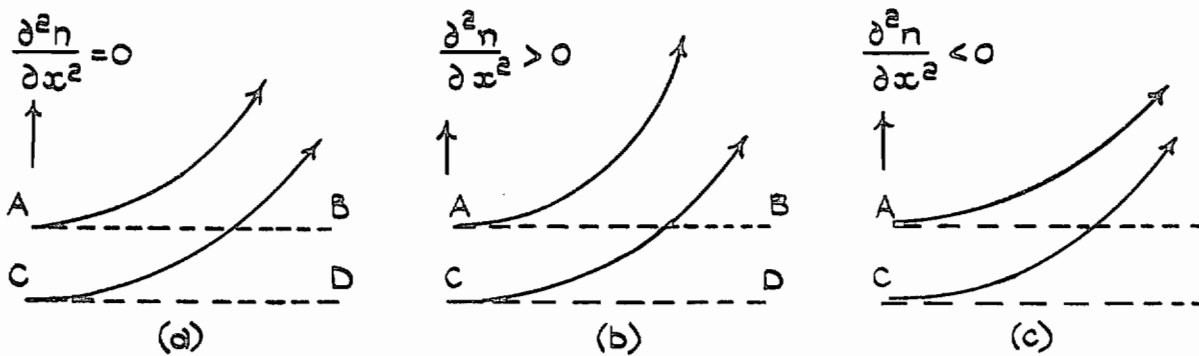


FIG. 55. Deflection of light in a non-uniform density gradient.

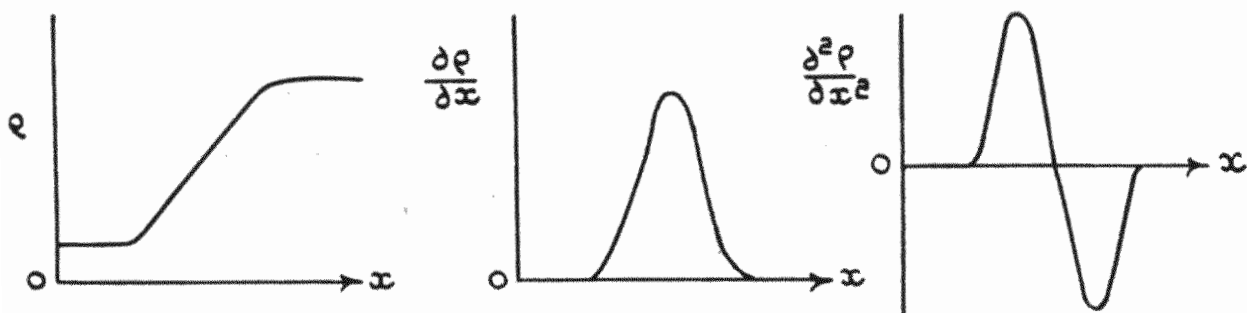
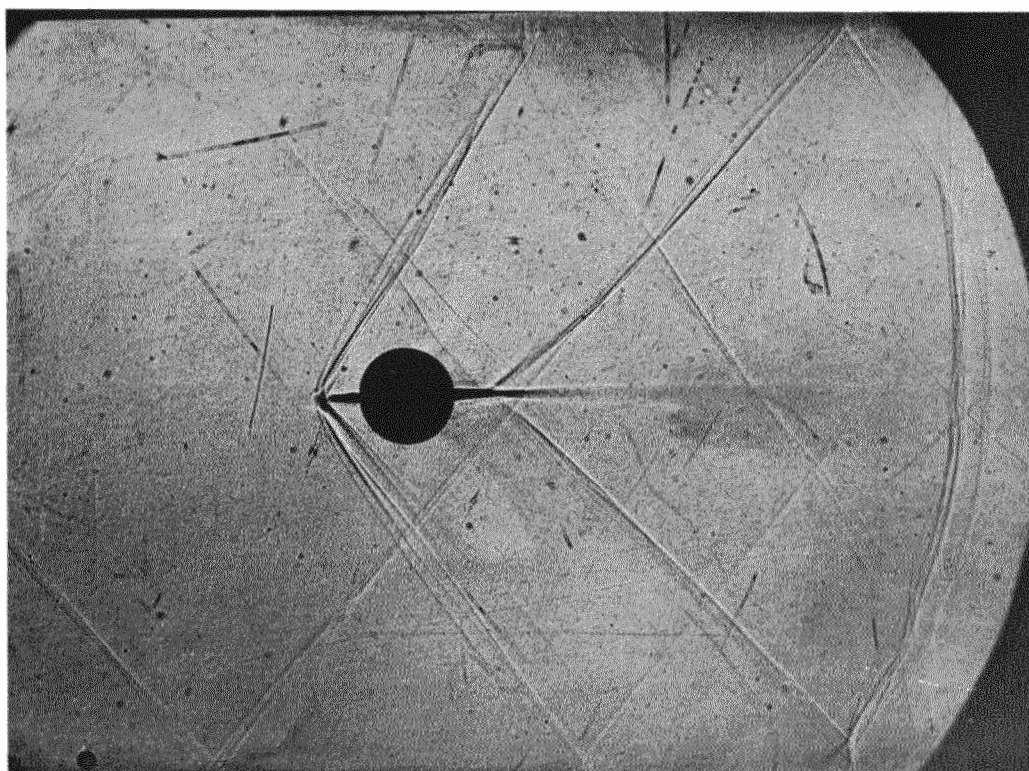


FIG. 56. Density derivatives in a shock-wave.



Airflow \longrightarrow

FIG. 57. Direct shadow photograph of the flow around a double wedge aerofoil at $M = 1.4$.

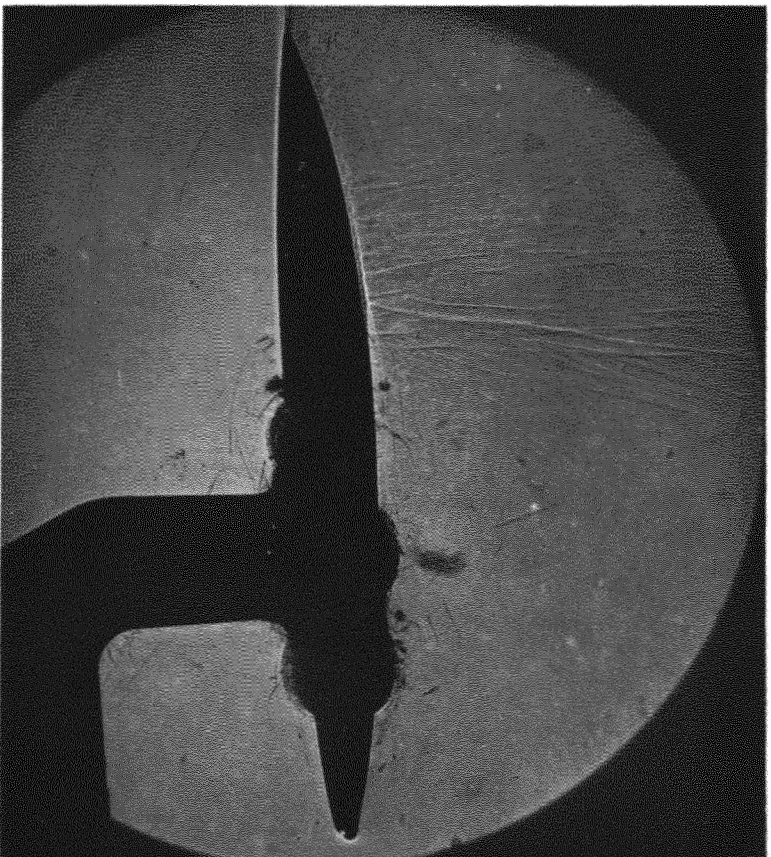


Fig. 58(a). Direct shadow photograph of flow around 10 per cent NACA propeller aerofoil at $\alpha = +4$ deg. $M = 0.78$ ($M_{crit} = 0.65$). Plate 4½ in. from tunnel wall.

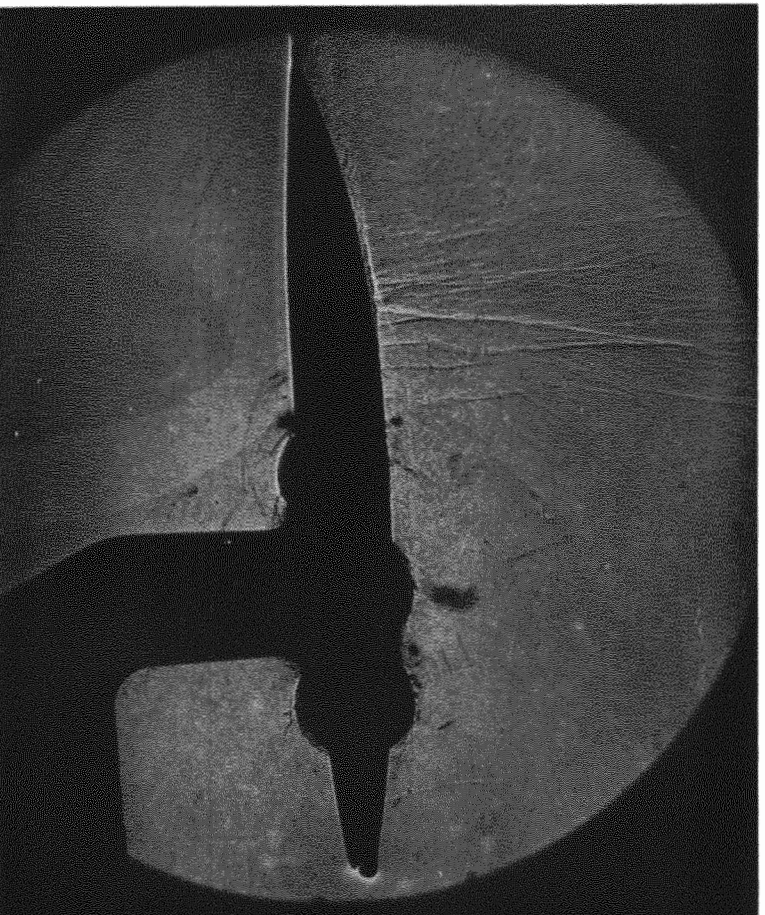


Fig. 58(b). Direct shadow photograph of flow around 10 per cent NACA propeller aerofoil at $\alpha = 4$ deg. $M = 0.78$ ($M_{crit} = 0.65$). Plate 12 in. from tunnel wall.

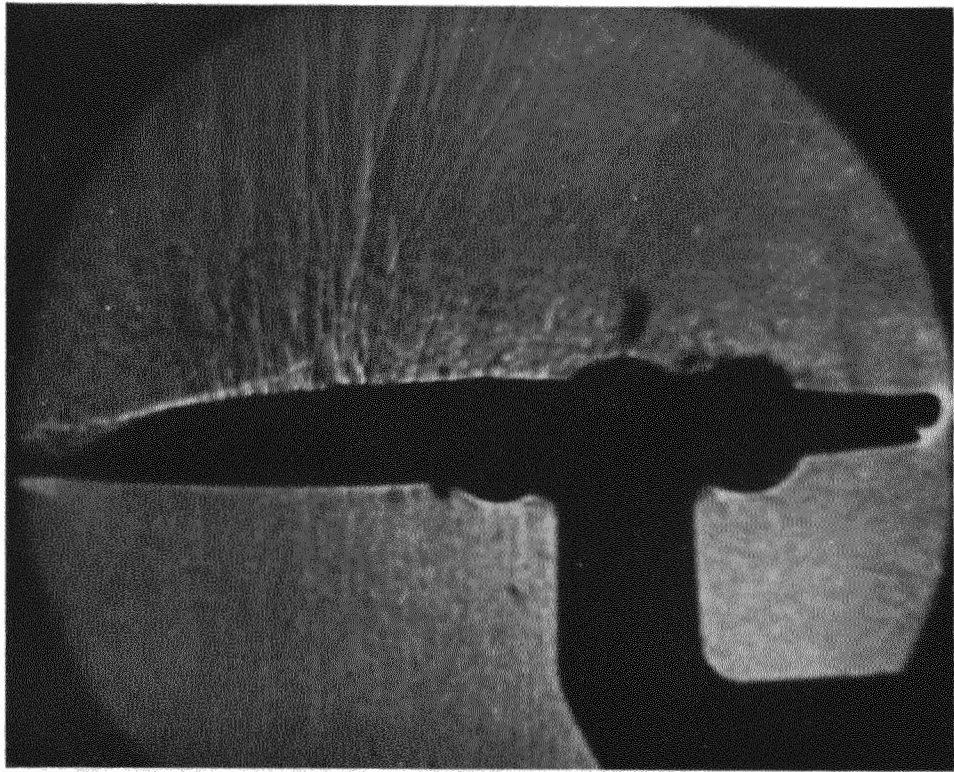


FIG. 58(c). Direct shadow photograph of flow around 10 per cent NACA propeller aerofoil at $\alpha = 4$ deg.
 $M = 0.78$ ($M_{crit} = 0.65$). Plate 60 in. from tunnel wall.

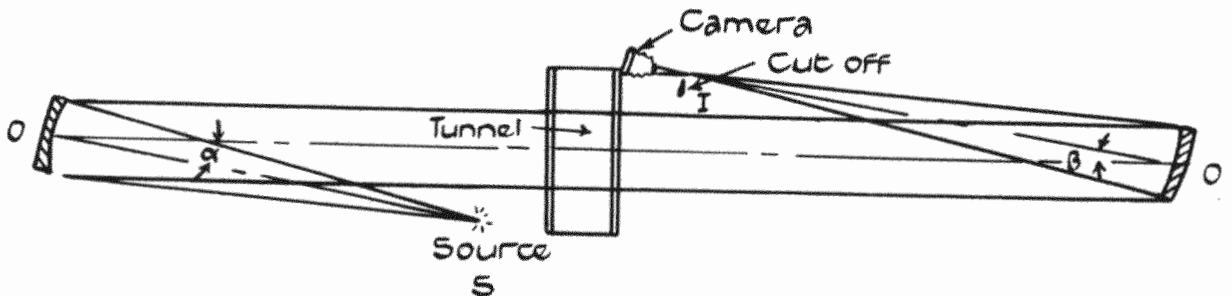


FIG. 59(a). Schlieren set-up with mirrors.

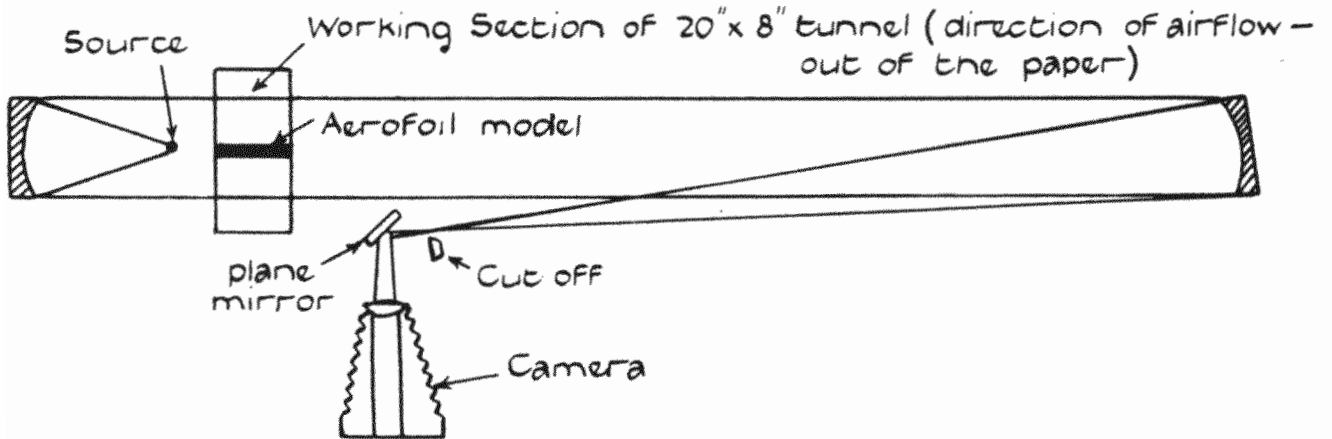
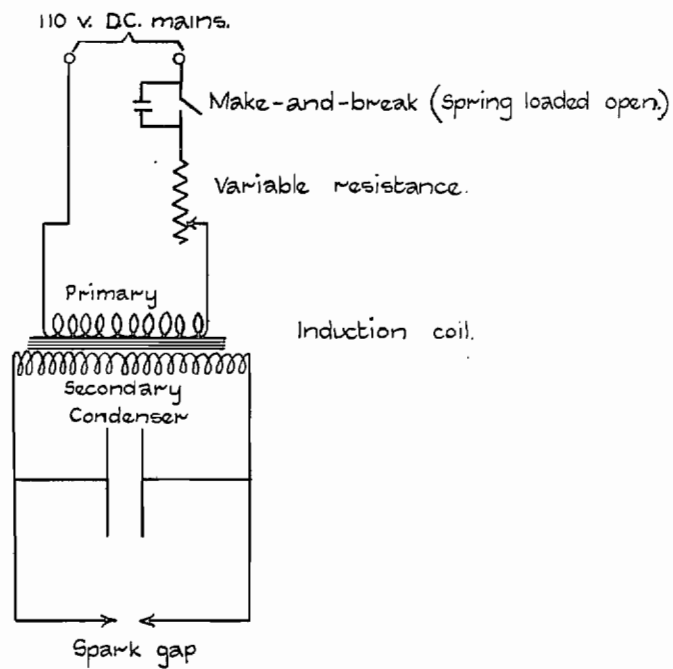
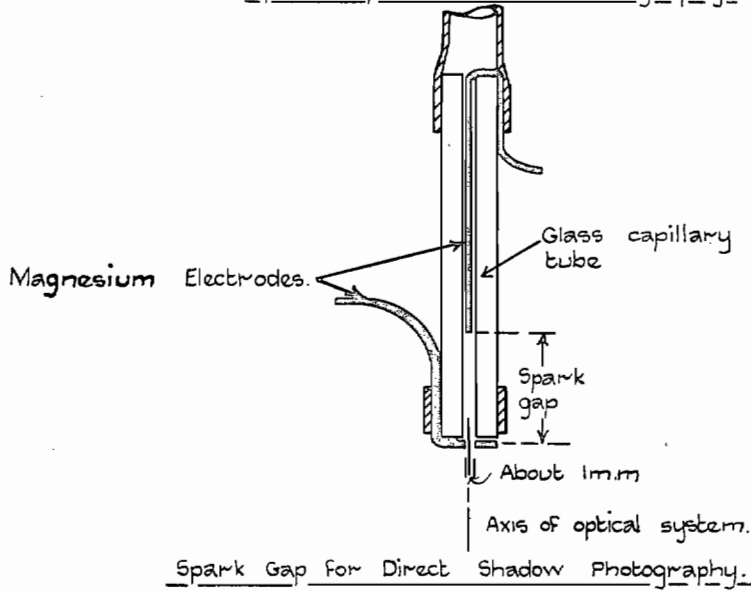
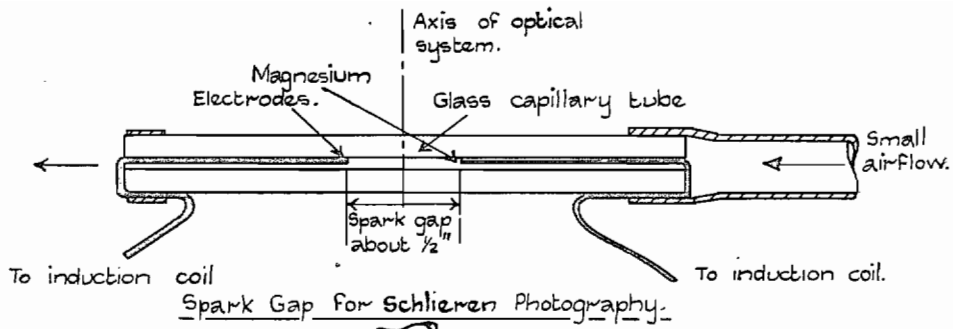


FIG. 59(b). Sketch of schlieren set-up on 20×8 -in. tunnel.



Sketch of Induction Coil Circuit.

FIG. 60.

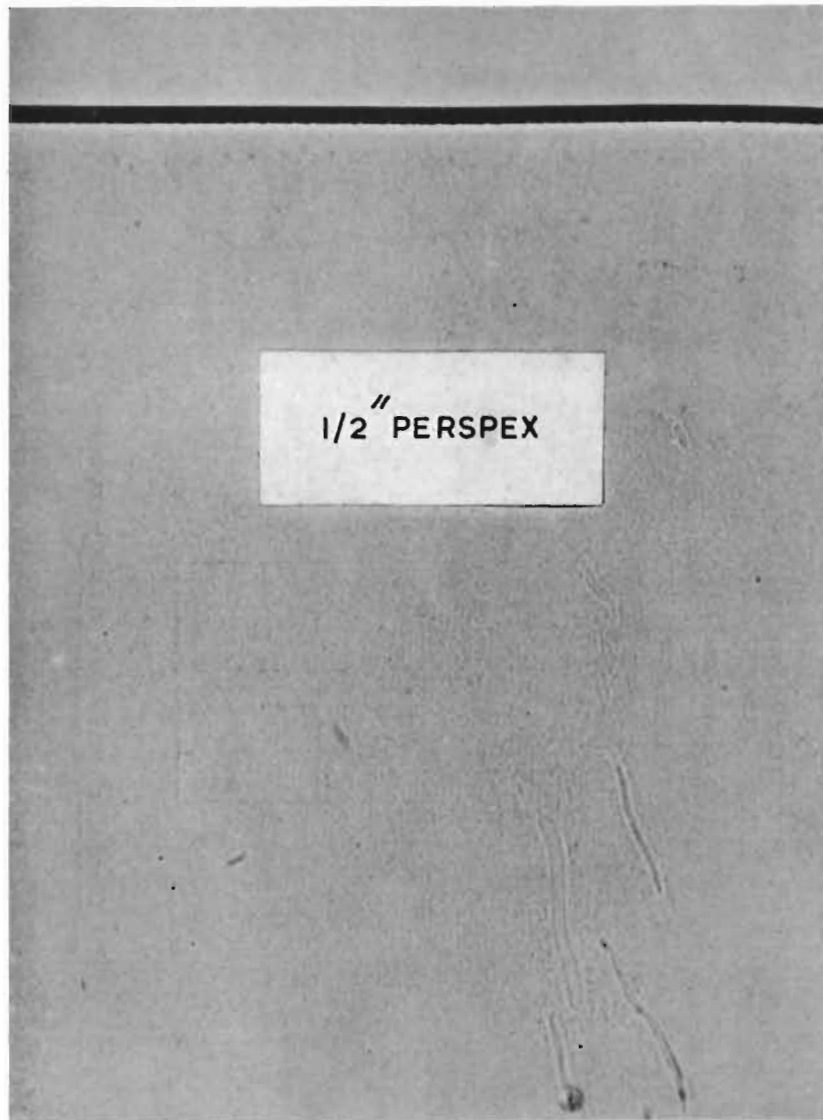


FIG. 61. Direct-shadow photograph of $\frac{1}{2}$ -in. sheet of Perspex.

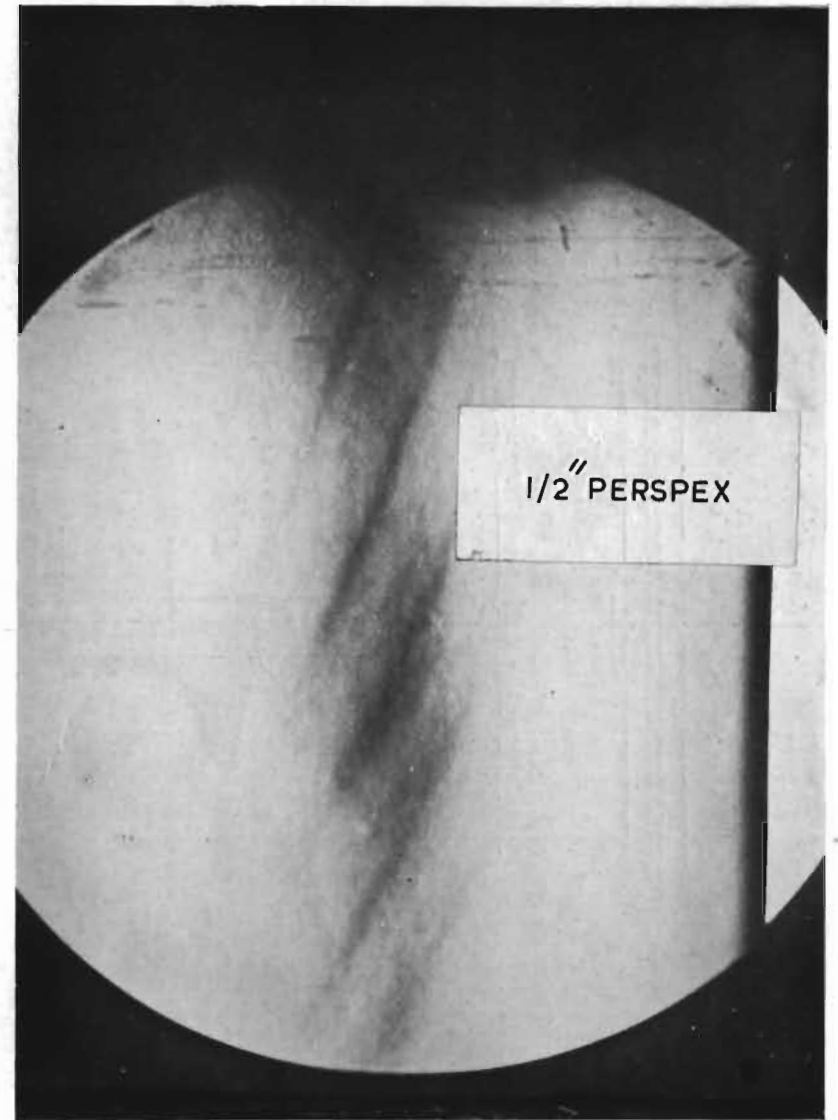
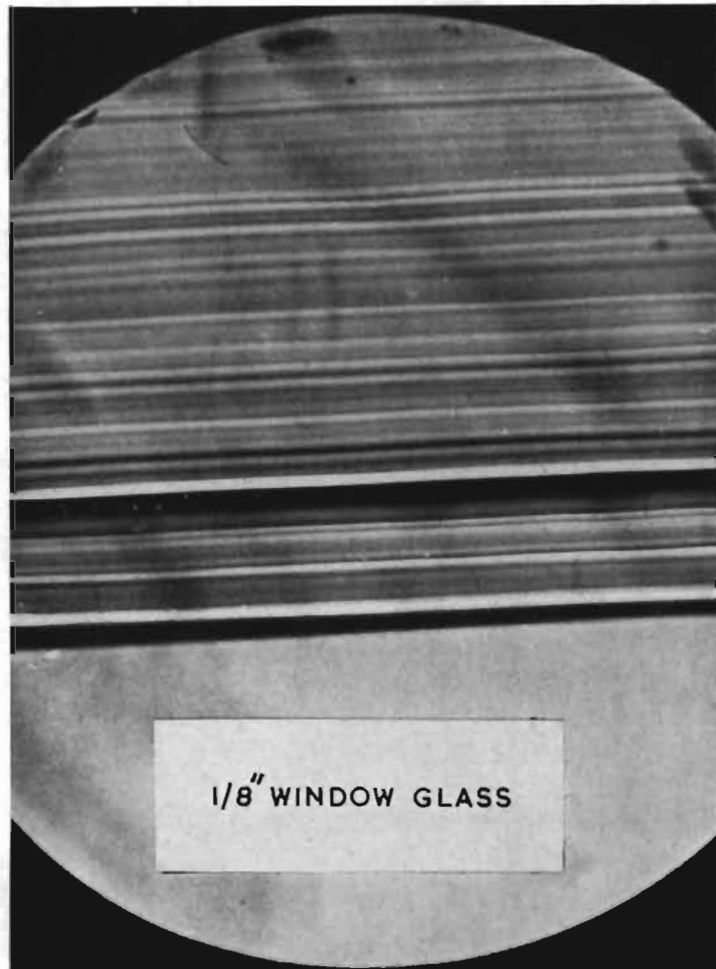


FIG. 62. Schlieren photograph of $\frac{1}{2}$ -in. sheet of 'Perspex', showing surface waves.

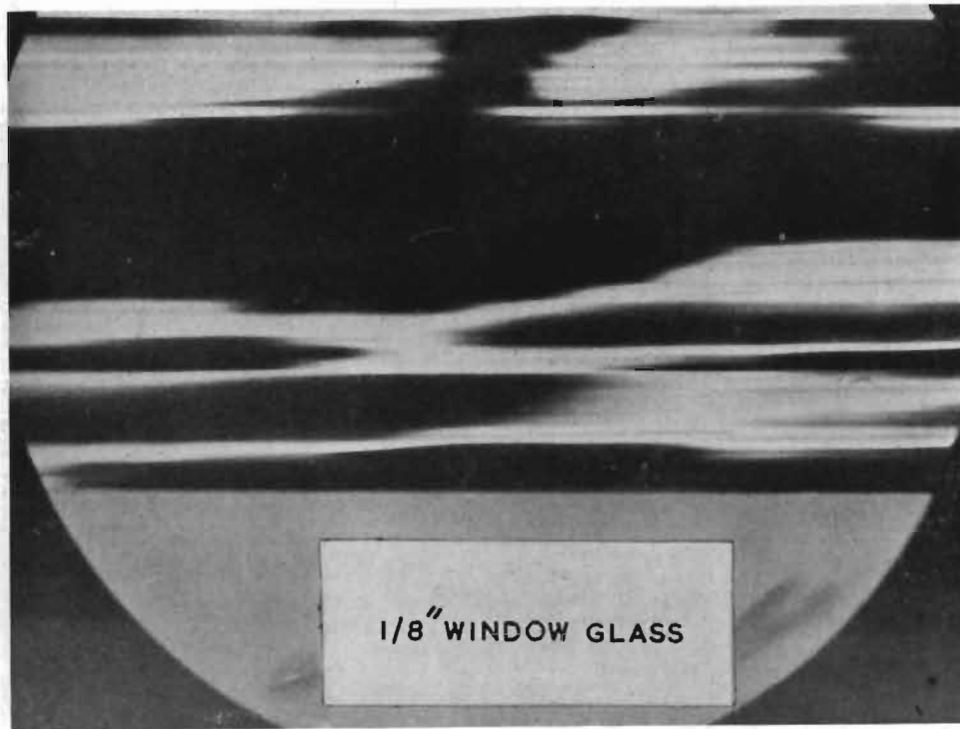


Schlieren photograph of $\frac{1}{8}$ -in. sheet of window glass.
Knife edge normal to edge.



Direct-shadow photograph of $\frac{1}{8}$ -in. sheet of window glass.

FIG. 63.



(a) Schlieren photograph of $\frac{1}{8}$ -in. sheet of window glass.
Knife edge parallel to striations.



(b) Schlieren photograph of $\frac{1}{8}$ -in. sheet of window glass,
showing surface waves.

FIG. 64.

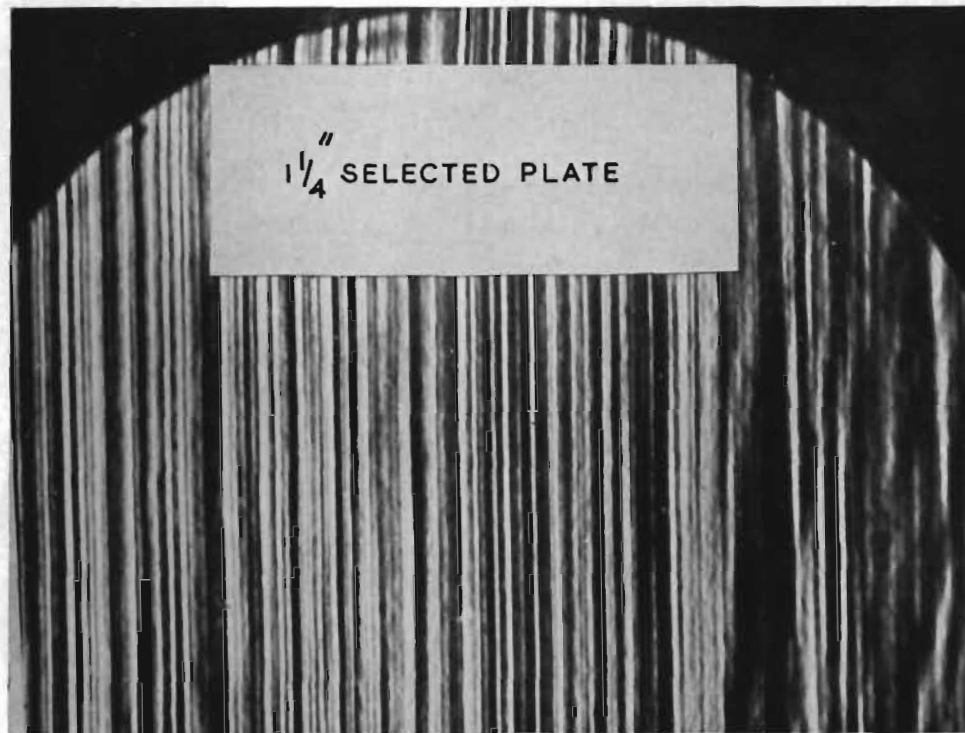


FIG. 65. Schlieren photograph of $1\frac{1}{4}$ -in. sheet of plate glass.
Knife edge parallel to striations.

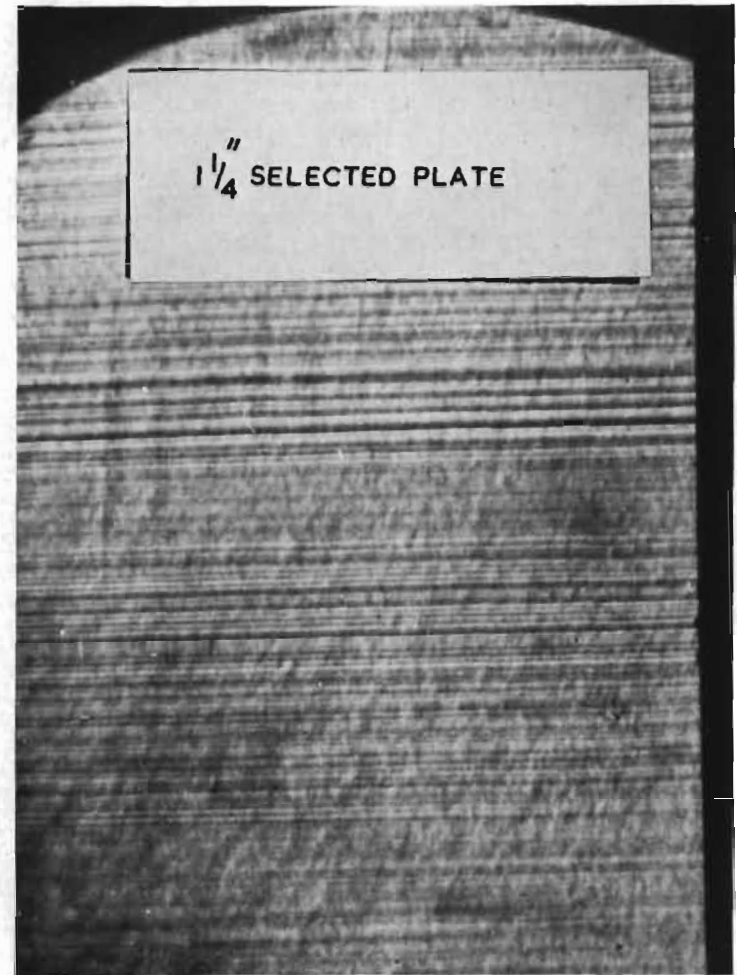


FIG. 66. Schlieren photograph of $1\frac{1}{4}$ -in. sheet of plate glass.
Knife edge normal to striations.



FIG. 67. Direct-shadow photograph of 1 1/4-in. sheet of plate glass.



FIG. 68. Direct-shadow photograph of 1-in. sheet of selected plate glass, showing surface faults.

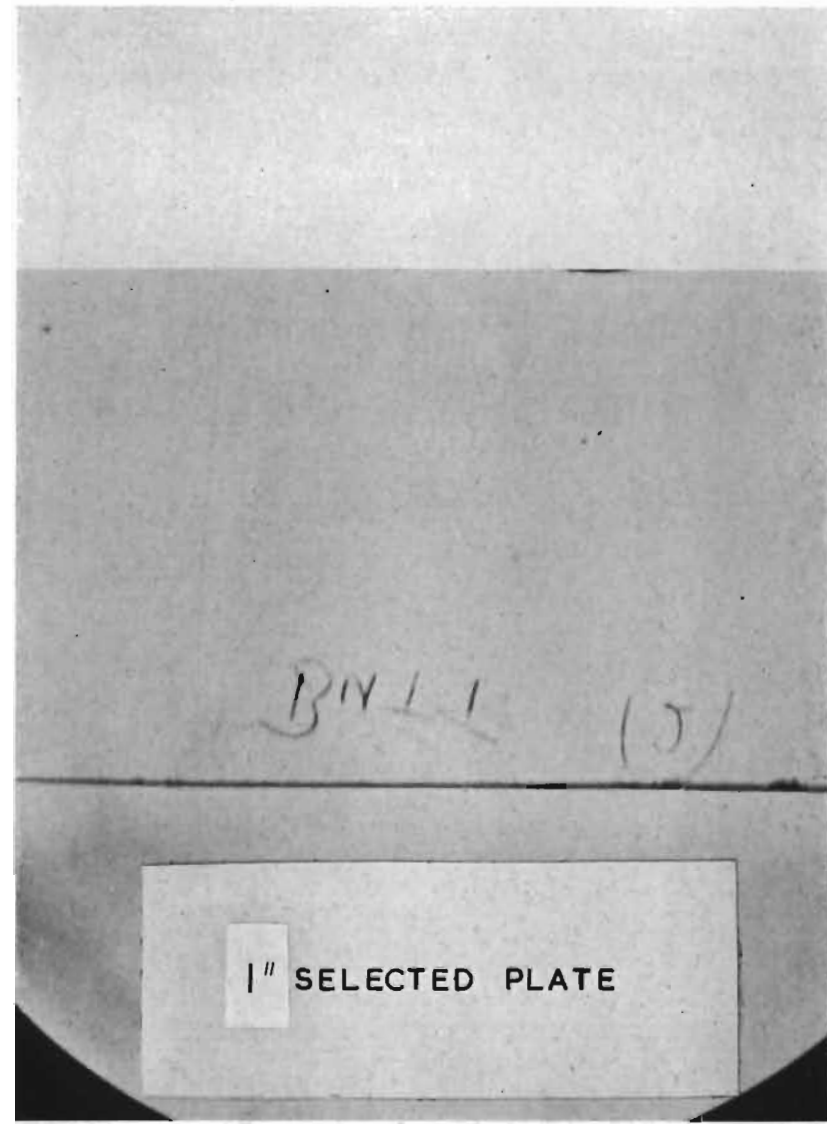


FIG. 69. Schlieren photographs of 1 in. sheet of selected plate glass showing wedge-shaped nature.

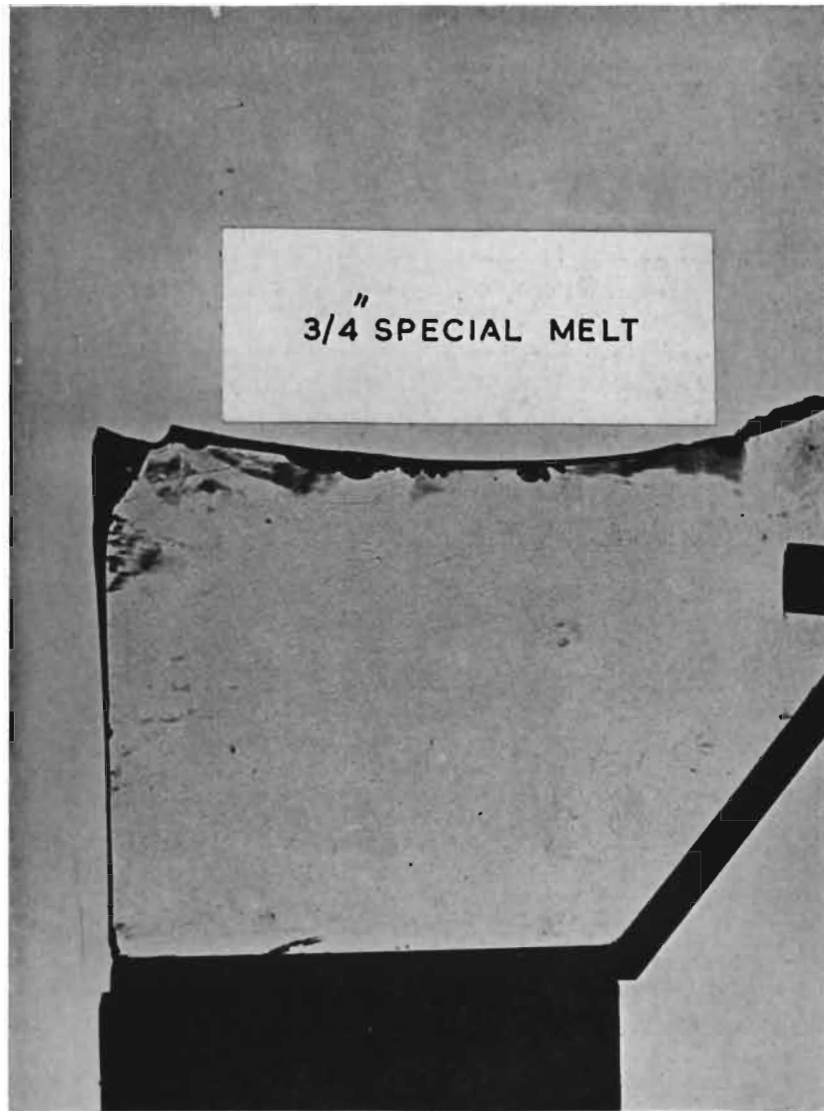


FIG. 70. Direct-shadow photograph of $\frac{3}{4}$ -in. sheet of special melt plate glass.

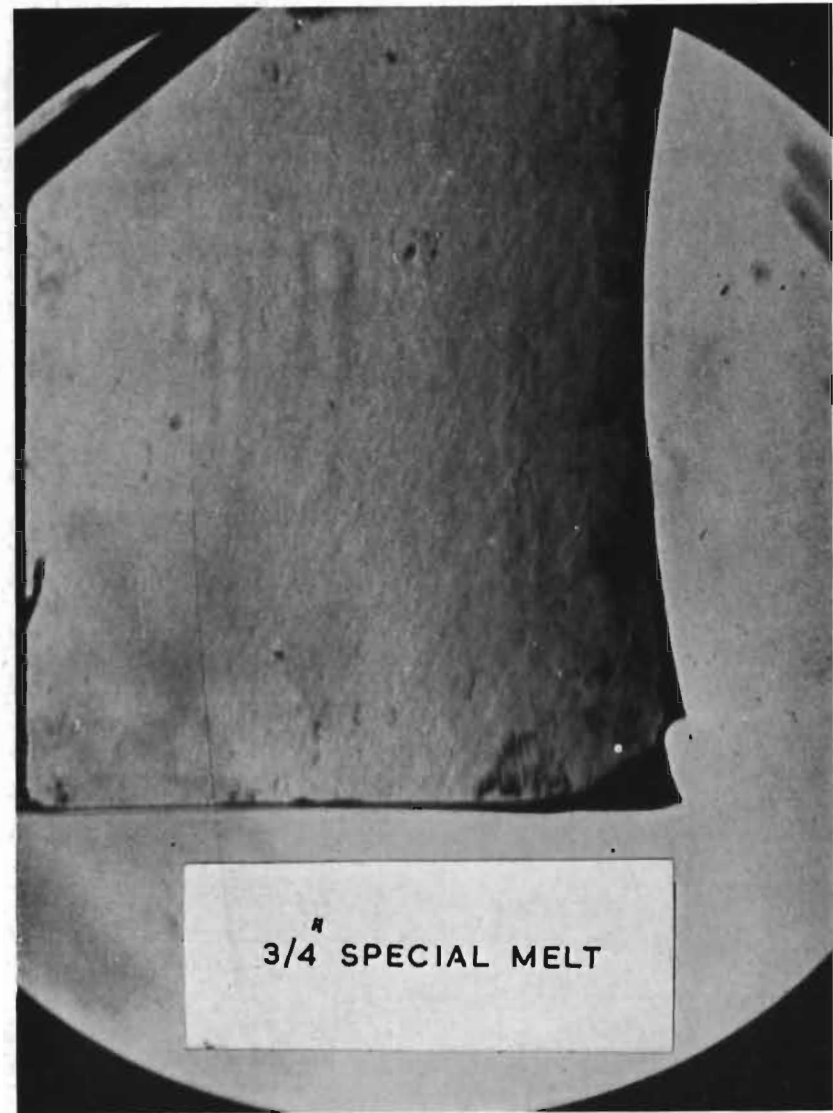


FIG. 71. Schlieren photograph of $\frac{3}{4}$ -in. sheet of special melt plate glass.

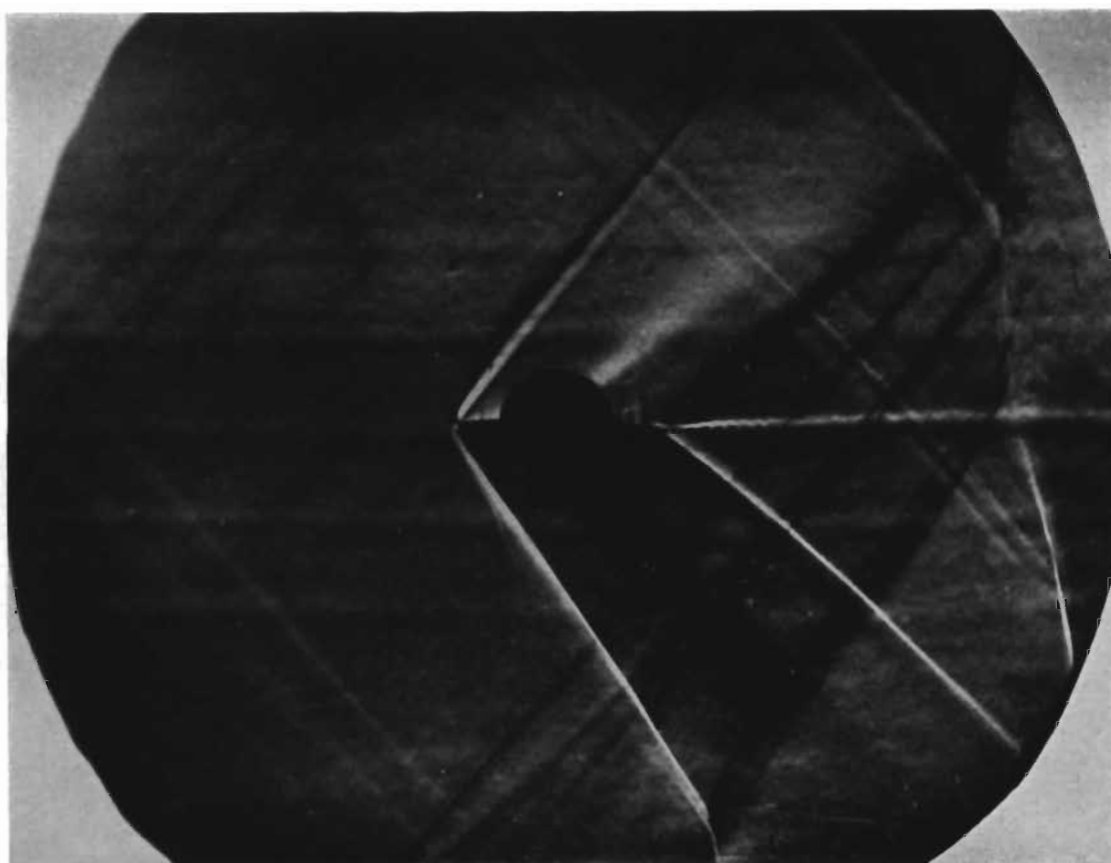


FIG. 72. Attempt to visualize stream-tubes by wakes of unheated wires.

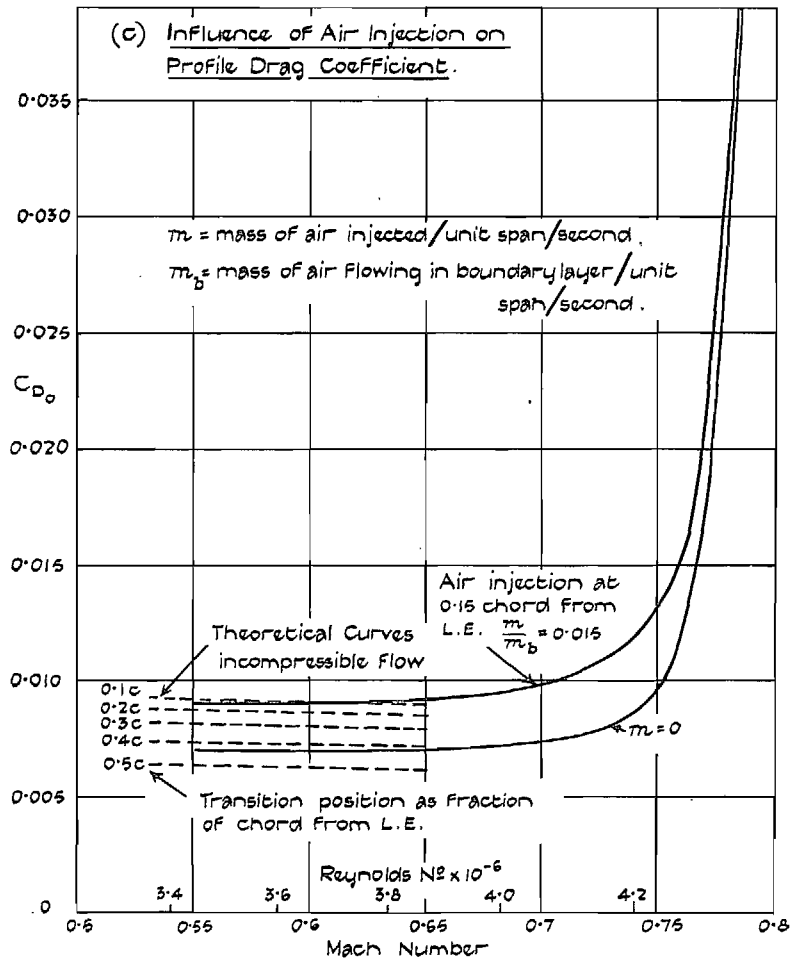
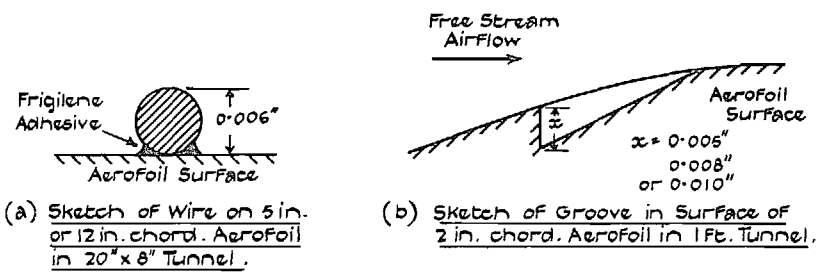
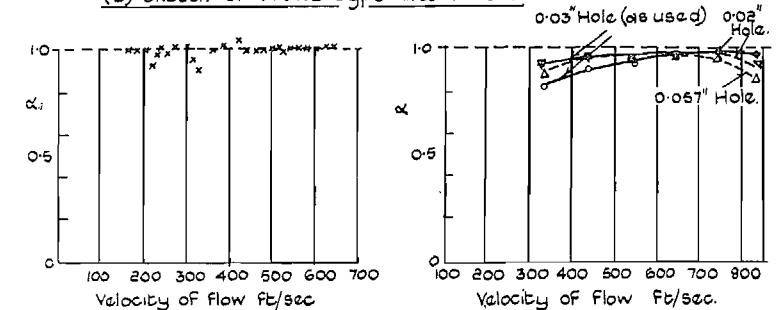
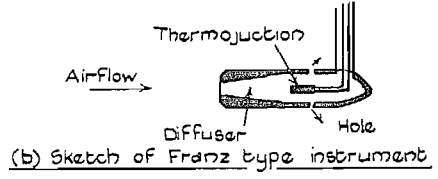
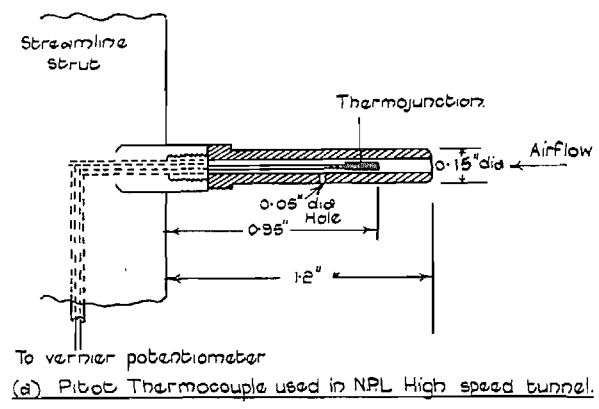


FIG. 73. Transition-fixing by wire, groove and air injection at high speed.



Note $\alpha = \frac{T_1 - T}{T_H - T}$ where T_H = Theoretical Stagnation temperature, T_1 = Measured Stagnation temperature, T = Static temperature.

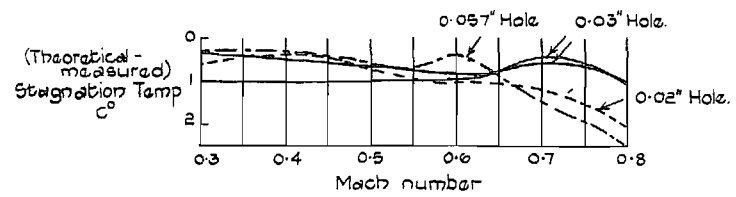


FIG. 74.

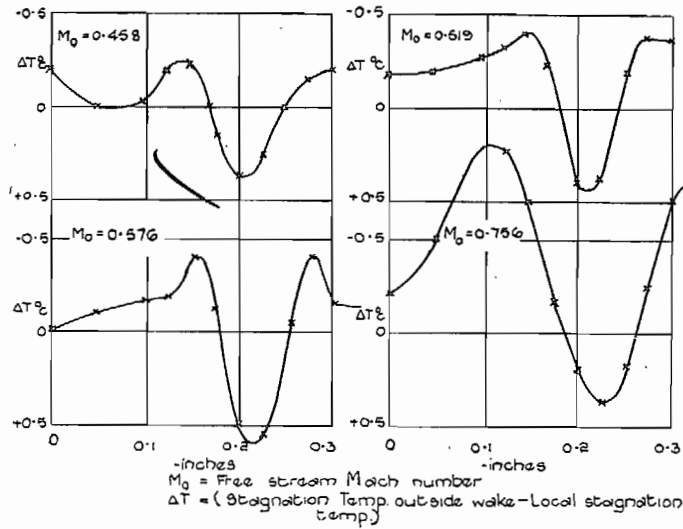


FIG. 75. Typical pitot-thermocouple traverses across wake of 2-in. chord NACA 0020 aerofoil at zero incidence (1.75-in. downstream of trailing edge).

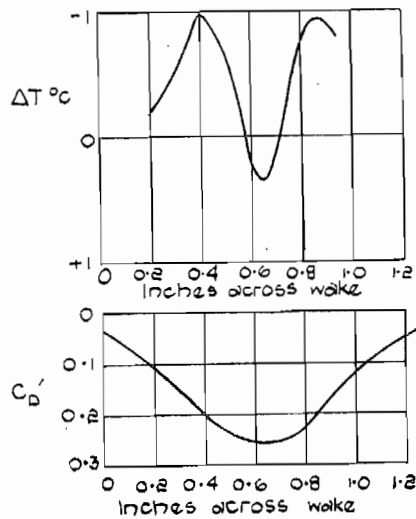
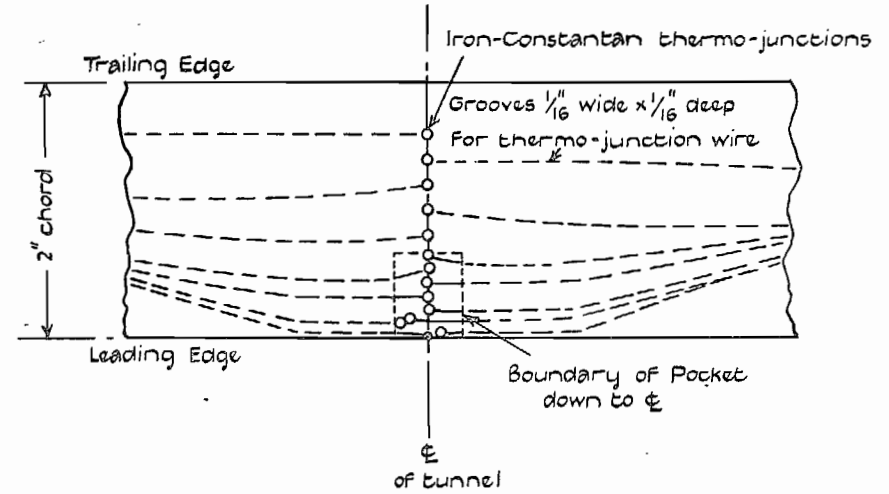


FIG. 76. Comparison of stagnation temperature and pitot-traverse in wake of 2-in. chord NACA 0020 aerofoil. After appearance of shock-wave. $M_0 = 0.756$.



Thermojunctions at 0, 0.0125, 0.025, 0.05, 0.1, 0.15, 0.2, 0.25, 0.3, 0.4, 0.5, 0.6, 0.7 and 0.8 chord from Leading Edge.

FIG. 77. Sketch of 2-in. chord NACA 0020 aerofoil for measurement of surface temperature.

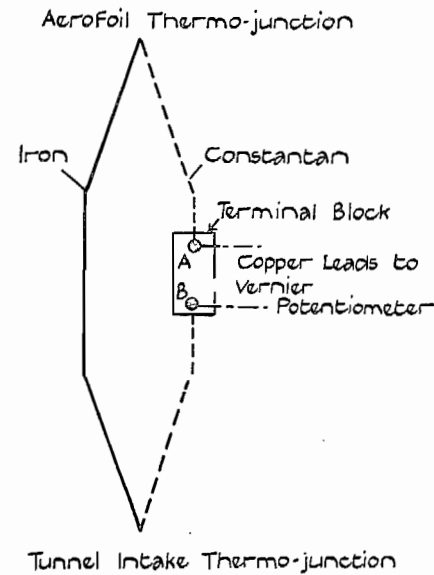


FIG. 78. Sketch of original electrical circuit. Temperature differences at junctions A and B may lead to errors.

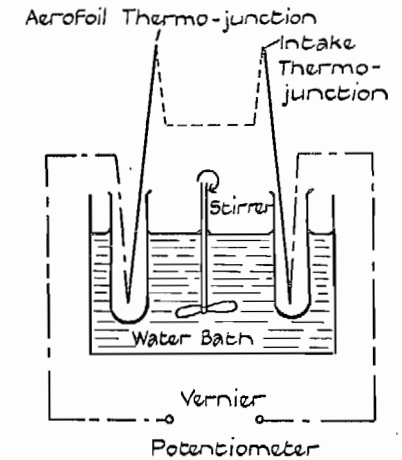


FIG. 79. Suggested modification with water bath.

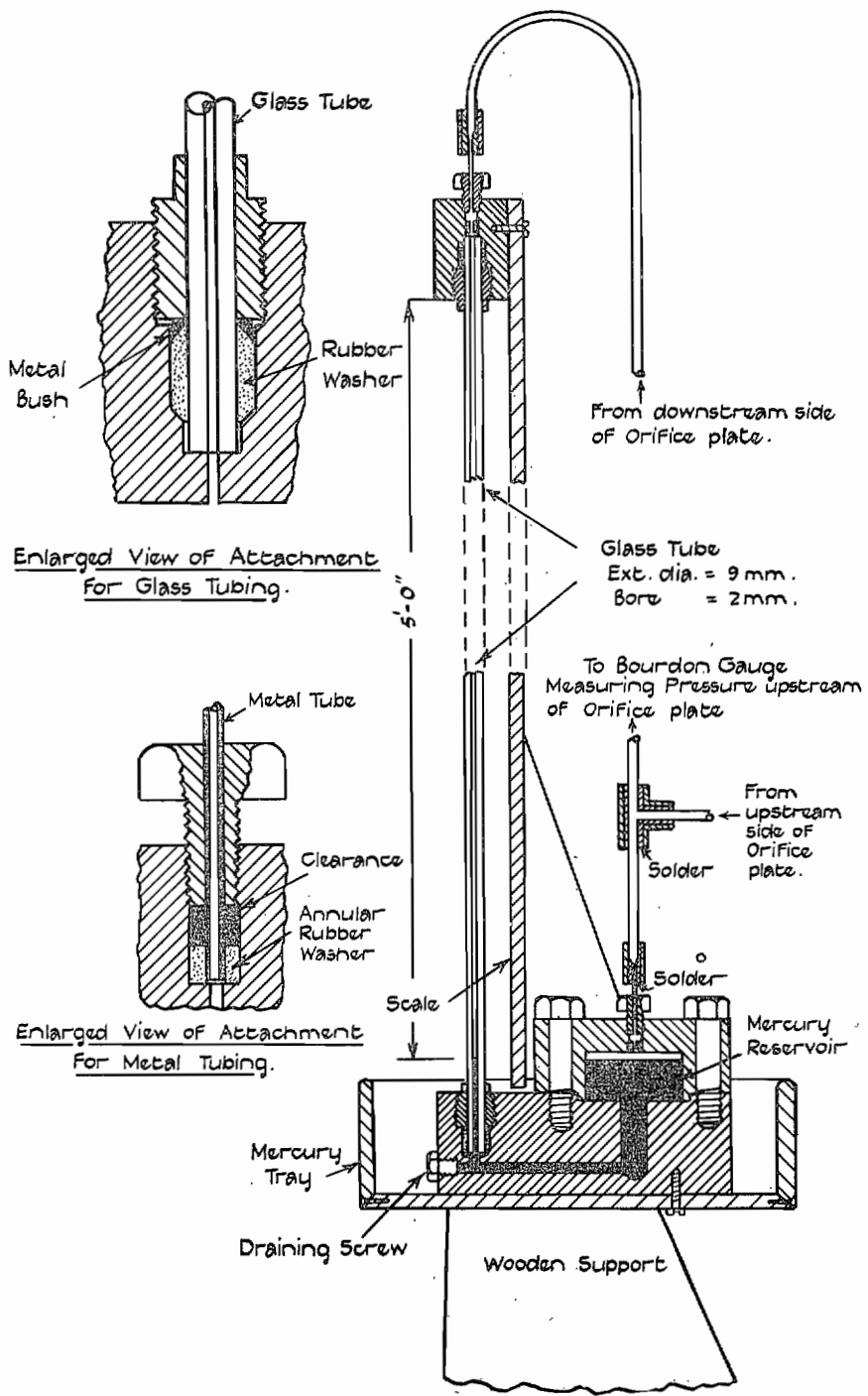


FIG. 80. General arrangement and details of manometer.

To withstand 400 lb/sq in. internal pressure and indicate differential pressures from 0 to 60 in. of mercury.

PART III

3.1. *Introduction.*—A considerable number of experiments of a systematic nature have been made at subsonic speeds in the 12-in. diameter tunnel on aerofoils supported on the electrical balance. These aerofoils usually had a 2-in. chord, and the Reynolds number range was of the order of 0.45×10^6 to 0.8×10^6 . Most of the experiments were subject to the influence of the condensation of moisture, and the only correction applied for tunnel interference was an empirical correction for blockage. Thus, to some extent, the results of these experiments must be regarded as qualitative, although in several cases satisfactory quantitative agreement has been obtained with observations made under more precise conditions and at higher Reynolds number in more modern tunnels.

The 20×8 -in. tunnel has been used almost solely for tests at subsonic speeds on aerofoils completely spanning the tunnel. The standard model chord of these tests has been 5 in., giving a Reynolds number range of from 1×10^6 to 1.9×10^6 , and in the majority of cases the experiments have included measurements of the normal surface pressure distribution and wake traverses. Owing to the time which experiments of this type require, a comparatively small number of aerofoils have been tested, and these have not formed a systematic series. Systematic series of tests are now, however, in progress.

Aerofoils fitted with moveable control surfaces have been tested in both the 12-in. diameter and 20×8 -in. tunnels at subsonic speeds, the latter including surface pressure measurements. These experiments are to be continued with a modified control shape.

Tests at supersonic speeds have been carried out in the 12-in. diameter and 5×2 -in. tunnels on a number of aerofoils including a series of round-nosed profiles. In the 12-in. diameter tunnel the measurements were made with the three component balance; in the 5×2 -in. tunnel surface-pressure measurements and flow visualization were attempted successfully. A number of experiments at supersonic speeds with aerofoils fitted with controls have been made in the 12-in. diameter tunnel.

Many miscellaneous experiments have also been made both in these three tunnels, and also in smaller tunnels specially constructed for the purpose.

It must be mentioned that the Reynolds numbers of the aerofoil tests described here are considerably below those of flight, although in certain cases, for example compressor blades, the discrepancy is not large. There is little information on the effects of Reynolds number on the flow round bodies of high Mach numbers but it is known that these effects may sometimes be considerable, particularly at transonic speeds where the flow depends essentially on the interaction of shock-waves with the boundary layer. It is possible that some of the model tests in the N.P.L. high-speed tunnels are subject to the influence of laminar separation. This possibility should be borne in mind when comparing the results of observations made in the N.P.L. high-speed tunnels at low Mach numbers with those made in low-speed tunnels at higher Reynolds numbers. Larger Reynolds numbers will be obtained at high Mach number in the new 18×14 -in. N.P.L. tunnel⁴⁹ which is designed to operate up to a stagnation pressure of three atmospheres (R up to about 7×10^6).

3.2. *Experiments at Subsonic and Transonic Speeds.*—3.2.1. *The Flow Round an Aerofoil at High Subsonic Mach Number.*—It is well known that regions exist in the neighbourhood of an aerofoil in which the velocity exceeds that of the undisturbed airstream. At very low free-stream Mach numbers (less than about 0.3 for most aerofoils) the velocity at all points in the flow field is sufficiently low to permit the compressibility of the air to be ignored. As the free-stream Mach number is increased, however, this is no longer possible. At first the influence of compressibility produces small changes in the low-speed pressure distribution (C_p) similar to those predicted by the Glauert, von Kármán-Tsein, or Temple relationships (see Refs. 156, 157, 158). With further

increase of free-stream Mach number, however, the peak velocity in the region of increased velocity close to the aerofoil surface exceeds the local speed of sound*. The free-stream Mach number at which this first occurs is usually termed the critical Mach number. More recently, however, other critical criteria have been suggested, and this together with the possibility of confusion with the free-stream Mach numbers at which large changes in the force and moment coefficients occur, has led to the use of the term first or pressure critical for the critical Mach number defined above.

Since at all Mach numbers the streamtubes of the flow round an aerofoil retain a convergent-divergent shape and a given change of the cross-sectional area of a streamtube produces a pressure change which is of opposite sign for supersonic and for subsonic flow, it is to be expected that the form of the pressure distribution over the surface will change when the critical Mach number is exceeded. This change of pressure distribution is often accompanied by changes of the force and moment coefficients. Moreover, at some free-stream Mach number above the first critical value shock-waves usually appear at the rear of the supersonic regions close to the aerofoil and these in turn modify the flow and the forces acting on the aerofoil. The changes of the force and moment coefficients with Mach number are in some cases very violent. It must be emphasised that the rapid changes of lift, drag and pitching-moment coefficient do not usually begin at a common free-stream Mach number, and that the critical Mach numbers for such coefficient changes do not usually coincide with the first or pressure critical defined above. Nor, in general, do shock-waves usually appear immediately the first critical is exceeded. The term 'shock-stall' has been used somewhat loosely to describe the more violent compressibility effects described above.

It is proposed to describe here in detail the observed phenomena which take place as the free-stream Mach number is increased to a high subsonic value for one particular aerofoil, and then to consider briefly some of the evidence concerning the influence of the shape of the aerofoil section on these phenomena. Observations on a 5-in. chord model of 1442/1547 section in the 20 × 8-in. tunnel will, therefore, be described first. This aerofoil was designed by the methods of Dr. Goldstein to have a 'roof-top' pressure distribution with low drag and high first critical Mach number. The designed low-speed lift coefficient is 0.2 (at $\alpha = 0.5$ deg), and at this incidence the von Kármán equation applied to the low-speed pressure distribution indicates a first critical Mach number of 0.694. A description of the design features of the aerofoil is given in R. & M. 2346¹⁶². The shape of the aerofoil section is shown in Fig. 1 which includes the chordwise positions of the surface pressure holes, and the theoretical and measured pressure distributions are shown in Fig. 2(a) and 2(b) for a Mach number below the first critical.

3.2.1.1. *Changes of flow pattern with free-stream Mach number.*—It is convenient to consider the variation of the pressure coefficient p/H_0 along the chord with free-stream Mach number in conjunction with photographs† taken by the direct-shadow method with an exposure of the order of 1 microsecond. This pressure coefficient is convenient since a scale of local Mach number (which is exact ahead of the shock-wave) may be appended. Two incidences only will be considered, one, the design incidence, in which the low-speed distribution has the designed 'roof-top' shape and the other a higher incidence in which the low-speed pressure distribution has a peak towards the leading edge (see Fig. 2). Observations at other incidences are discussed in R. & M. 2346¹⁶².

Fig. 3 is a control photograph at zero Mach number and indicates the position of faults in the glass tunnel walls which appear in the remainder of the photographs. Figs. 4 to 11 show a series

* Apart from the case of a symmetrical aerofoil at zero incidence, the speed of sound will be reached at different free-stream Mach numbers at the two aerofoil surfaces. Unless a statement to the contrary is made, however, the values of M_{crit} given here will refer to the free-stream Mach number at which sonic velocity is first reached anywhere on the aerofoil.

† The photographs of the flow around aerofoil G.1442/1547 are due to H. H. Pearcey.

of photographs and distributions of p/H_0 , taken over a range of free-stream Mach numbers at $\alpha = 0.5$ deg and Figs. 12 to 18 at $\alpha = 6.5$ deg. The observations were made before the Mach number gauge was installed and the Mach numbers are, therefore, not even.

At low Mach numbers the boundary layer and wake of the aerofoil are clearly visible together with an apparent distortion of the aerofoil profile at the leading edge which is due to the high rate of change of density gradient close to the forward stagnation point. There is also some evidence that the photographs indicate the position of the transition point on the aerofoil. As the speed is further increased shock-waves appear which move aft, strengthen and extend out into the flow field. Particularly at high Mach number a large separation or thickening of the boundary layer occurs at the foot of the shock-wave and the wake widens considerably. At the higher Mach numbers the shock-wave becomes bifurcated or forked at the root.

3.2.1.2. Flow-pattern changes at low incidence.—At the incidence 0.5 deg the low-speed pressure distribution is flat and slightly favourable back to about 0.6 chord from the leading edge. At $M = 0.631$ (Fig. 4) the wake is clearly visible, and there is no evidence of shock-waves since the velocity in the flow field nowhere exceeds the local speed of sound.

At $M = 0.681$ (Fig. 5) the velocity is still everywhere subsonic, but a number of wavelets are present close to the upper surface of the aerofoil. These cannot be at rest relative to the aerofoil.

At $M = 0.706$ (Fig. 6), which is above the first critical Mach number ($M = 0.694$), a small supersonic region is present on the upper surface and stronger waves are visible. The wake does not appear to have widened.

At $M = 0.733$ (Fig. 7) the supersonic region has grown and the strength of the wavelets has increased. There is still no evidence of wavelets on the lower surface.

At $M = 0.784$ (Fig. 8) the supersonic region has grown further and the shock-wave moved slightly aft and increased in amplitude. Separation has probably taken place (*see* Fig. 19) and the wake has widened. Wavelets are present on the lower surface where there is now a small supersonic region. The pressure gradient ahead of the shock-wave on the upper surface has become more favourable.

At $M = 0.835$ (Fig. 9) the supersonic regions on both surfaces have grown, the shock-waves have moved aft and strengthened. The wave roots have become bifurcated and the wake has widened considerably.

At $M = 0.855$ (Fig. 10) the bifurcation of the wave on the lower surface has become more pronounced, and the wake has widened further.

At $M = 0.876$ (Fig. 11) the wave on the lower surface has moved back almost to the trailing edge. The wave on the upper surface is very strongly bifurcated but the further increase of the wake width is not large. The pressure distribution which was at low speed favourable back to about 0.6 chord on both surfaces is now favourable back to 0.65 on the upper surface and 0.8 chord on the lower.

3.2.1.3. Flow-pattern changes at high incidence.—At the high incidence ($\alpha = 6.5$ deg) there is a suction peak near the leading edge of the aerofoil at low Mach number (Fig. 12, $M = 0.454$) the boundary layer over most of the upper surface is turbulent, and that on the lower is laminar.

At a Mach number 0.569 ($M_{\text{crit}} = 0.49$ for upper surface) there is still a velocity peak on the upper surface towards the leading edge but this has now exceeded the local speed of sound and shock-waves are visible at about $0.1c$. The wake has widened a little (Fig. 13).

At $M = 0.626$ (Fig. 14) the supersonic region on the upper surface has extended, the pressure distribution becomes slightly less peaked and the shock-waves have moved aft. The wake has further widened.

At $M = 0.675$ (Fig. 15) a definite shock-wave (in contrast to the rather diffuse waves seen at lower speeds) has formed and is apparently preceded by a second wave which may be due to a bifurcation or forking of the main shock-wave in the boundary layer of the glass walls. The wake has widened and there is some evidence that the transition position has now moved aft to the shock-wave position. The supersonic region has extended and the pressure distribution flattened.

At $M = 0.728$ (Fig. 16) the pressure distribution is favourable back to about 0.47 of the chord. The supersonic region has extended and the shock-wave moved back to about half-chord. The wake has widened.

At $M = 0.779$ (Fig. 17) the foot of the shock-wave is forked or bifurcated. Thickening of the boundary layer begins at the front limb at which the supersonic velocity also begins to fall (the fall is very much more gradual than in the case of a shock-wave without bifurcation). The width of the wake has increased considerably.

At $M = 0.829$ (Fig. 18) the bifurcation of the shock-wave and thickening of the boundary layer on the upper surface has become more pronounced and the fall of pressure at the rear of the supersonic region more gradual. A small region of supersonic velocity has appeared on the lower surface and is terminated by a shock-wave. The rapid widening of the wake has continued. The pressure distribution on both surfaces is now favourable back to at least 0.55c. Thus the increase of the favourable tendency of the pressure gradient ahead of the shock-wave is very much greater on the upper surface than it was at low incidence. Similarly, the range of shock-wave movement along the chord is greater.

3.2.1.4. *Variation of normal force and moment coefficients with free-stream Mach number.*—It is first convenient to consider the variation of the pressure coefficient C_p with free-stream Mach number. This coefficient has the advantage that $(C_p - x/c)$ curves may be integrated to give normal force and moment directly, and that such curves may therefore be used to trace the changes of overall force coefficient to their origin in the change of surface pressure distribution. To facilitate this the difference ΔC_p between the pressure coefficients on the upper and lower surfaces has also been plotted and is labelled 'Distribution of Lift'.

Fig. 19 shows the variation of the distribution of C_p along the upper and lower surfaces of the aerofoil with free-stream Mach number at the design incidence ($\alpha = 0.5$ deg). At this incidence the first critical Mach number for the upper surface is 0.694, and for the lower surface 0.77. The observations may be summarised as follows:

- (a) $M < 0.7$. The pressure coefficients on both surfaces are slightly more negative than the low-speed values, the change being roughly in accordance with the prediction of the von Kármán equation, and there is a slight rise of lift coefficient above the low-speed value. Simultaneously the moment coefficient shows a gradual fall.
- (b) $0.70 < M < 0.75$. There is a slight decrease of the suction coefficient (*i.e.*, C_p becomes more positive) over the forward part of the upper surface. The extension of the supersonic region with rearward movement and intensification of the shock waves produces an increased suction around $x/c = 0.6$. The normal von Kármán increase of suction continues on the lower surface. The effects on the upper and lower surfaces compensate each other and there is still little change of lift coefficient. The change in the distribution of lift on the upper surface causes the pitching-moment coefficient to decrease slightly.
- (c) $0.75 < M < 0.80$. The decrease of suction over the forward part of the upper surface becomes more pronounced. The rate at which the shock-wave moves back decreases but the peak suction ahead of the wave (and the wave amplitude) increases. The suction behind the wave over the whole of the rear part of the aerofoil also increases. This is probably due to the change of the effective shape of the aerofoil behind the thickening of the boundary layer. The suction coefficient on the lower surface continues to increase over the whole surface, shock-wave effects being not yet evident. The changes of pressure coefficient on the upper surface tend to compensate each other and there is a fall of lift coefficient. The fall of moment coefficient due to the change of lift distribution on the upper surface is intensified.

- (d) $0.80 < M < 0.88$. The decrease of suction over the forward part of the upper surface continues together with the increase over the rear part behind the shock-wave. The peak suction ahead of the wave does not increase and the shock-wave remains fixed.* The suction on the lower surface now develops in a similar manner to that on the upper surface at lower free-stream Mach numbers. The lift coefficient continues to fall, and the pressure coefficient changes on the lower surface due to shock-wave development are now predominant over the opposite tendencies of the upper surface producing a rapid rise of pitching moment.
- (e) $0.88 < M < 0.90$. In R. & M. 2346¹⁰² it is noted that the shock-wave on the upper surface now begins to move back (possibly being able to do so because of a modification of the effective surface curvature by the more pronounced thickening of the boundary layer behind the wave). The suction over the rear part of the aerofoil also begins to increase more rapidly. The development of the shock-wave and suction on the rear of the lower surface become less rapid. The fall of lift coefficient is arrested on account of the changes in suction at the rear of both surfaces, and simultaneously the rapid rise of moment coefficient is checked.

Fig. 20 shows a similar family of curves at high incidence (6.5 deg) where the low-speed pressure distribution has a peak near the leading edge. These may be examined in conjunction with the photographs Figs. 12 to 18, but a detailed discussion will not be given here.

3.2.1.5. *Variation of profile-drag coefficient with free-stream Mach number.*—At the design incidence ($\alpha = 0.5$ deg) the drag coefficient Figs. 21 and 22 remains approximately constant over the range of free-stream Mach number 0.4 to 0.7. At a Mach number a little above 0.7, however, the drag coefficient begins to rise rapidly. This change arises from:

- (a) Degradation of kinetic energy in shock-waves present close to the aerofoil.
- (b) Thickening or separation of the boundary layer in the neighbourhood of the sudden adverse pressure gradient where the shock-wave approaches the aerofoil surface.
- (c) Changes in the position of the transition point in the boundary layer ahead of the shock-wave due to the change of the pressure distribution in this region when shock-waves are present. This will produce changes of the skin friction ahead of the shock-wave, and also probably changes in the behaviour of the boundary layer at and downstream of the shock-waves as well as in the form of the wave itself.

Fig. 21 shows that the general form of the profile-drag curves up to an incidence of 4.5 deg is similar to that of the 0.5-deg curve, the drag rise beginning at a different Mach number at each incidence. At $\alpha = 6.5$ deg however, after an initial drag rise a check to drag rise occurs before a final and more rapid rise. The explanation of this check to the drag rise is to be found in R. & M. 2079⁷⁸ and is due to the rearward movement of the transition point with that of the shock-wave which produces an extended favourable pressure gradient ahead. At this high incidence the shock-wave and transition movement is considerable and the drag reduction due to transition movement large. Indeed in other tunnels the profile-drag coefficient has been observed to fall in some cases before the rapid rise takes place (Fig. 23).

Considering now the phenomena which occur at lower incidences, it seems that a considerable part of the drag rise must be attributed (at the Reynolds number and tunnel turbulence of the experiment) to thickening or separation of the boundary layer downstream of the shock-wave. A curve for the 'ideal' shock-wave drag calculated by the method outlined by Lock is appended to Fig. 21. There is evidence that, apart from neglecting the rise of drag due to shock-wave—boundary layer interaction, this method does not predict accurately the drag rise due to the rise of entropy through the shock-wave. Nevertheless, the rate of drag rise predicted by Lock's method is comparable with that observed ($\partial C_D / \partial M = 0.45$) at all incidences.

* The shock, however, becomes bifurcated (Figs. 9, 10, 11) and the position of the forward branch at the surface, and, therefore, that of the peak suction, is nearly constant. The rear branch continues to move back.

The photographs of the flow pattern do not show a separation of the boundary layer at the design incidence until a free-stream Mach number of about 0.8 has been reached, and it appears that much of the drag rise below this Mach number is due to boundary-layer thickening at the shock-wave. Above this Mach number bifurcation of the shock-wave takes place and the pressure coefficient over the rear part of the aerofoil departs from its constant value. Thus it appears that such bifurcation was accompanied in this experiment by separation of the boundary layer and further drag rise.

3.2.1.6. *General discussion of overall force and moment-coefficient changes.*—The variation of profile-drag coefficient with free-stream Mach number for aerofoil 1442/1547 has already been discussed in some detail and is summarised by Fig. 21. The variation of profile-drag coefficient at constant lift coefficient is shown in Fig. 22, and, apart from the initial drag fall at high lift discussed above and due to rearward transition movement, no unusual features appear.

The variation of lift coefficient with free-stream Mach number over a range of incidence is shown in Fig. 24. Except at low incidence where the initial rise is small these curves show the usual initial rise of lift coefficient followed by a sharp fall. The rise of lift coefficient, however, is never equal to that predicted by the Glauert equation apart from a very sharp rise of C_L at $\alpha = 6.5$ deg beginning at a Mach number of about 0.63. This rapid rise is attributed to a shock-wave effect and is characteristic of aerofoils with a peaked pressure distribution at low speeds.

The lift coefficient at constant Mach number is plotted against incidence in Fig. 25, and it may be seen that the lift-curve slope increases to a maximum at a Mach number of about 0.7 after which a rapid fall occurs. This is also shown in Fig. 26 where the lift curve slope $dC_L/d\alpha$ is plotted as a function of free-stream Mach number at both constant incidence and lift coefficient. The no-lift angle of incidence approximates to the theoretical value of -1.3 deg at low speeds but increases rapidly above a Mach number of about 0.75 (Fig. 27).

The quarter-chord pitching-moment coefficient at constant incidence is plotted as a function of Mach number in Fig. 28. Apart from the curve for $\alpha = 6.5$ deg these curves all show an initial gentle fall of pitching moment followed by a rapid fall and a more rapid rise at higher Mach number. Similar curves plotted at constant lift coefficient in Fig. 29 show the same general characteristics.

The distance of the centre of pressure ahead of the quarter-chord point of the aerofoil is plotted as a function of Mach number in Fig. 30. At positive lift coefficients there is a rearward centre of pressure movement with increase of Mach number. This movement increases as the lift coefficient is reduced.

The aerodynamics centre position ahead of the quarter-chord point is shown in Fig. 31, and it may be seen that although fluctuations of the position may occur with rise of free-stream Mach number the general tendency is for a rearward movement at positive lift.

The moment curve slope $dC_m/d\alpha$ is plotted as a function of free-stream Mach number in Fig. 32.

3.2.1.7. *Note on the diffuse nature of some of the shock-waves of Figs. 4 to 18.*—In general photographs taken by the direct-shadow method in the 20×8 -in. tunnel do not indicate single shock-waves on the surfaces of aerofoils particularly at the lower Mach numbers. The exposure of all the photographs is of the order of one microsecond. The diffuse nature may be due to:

- (a) Transient disturbances. Such disturbances have been photographed at Mach numbers below the first critical (*e.g.*, Fig. 5) when they cannot be at rest relative to the aerofoil. At such Mach numbers the disturbances may be of the nature of sound waves originating to the rear of the model and passing upstream. At Mach numbers a little above the first critical the disturbances may be of increased amplitude and can, therefore, move upstream in the supersonic region. Also, they may still be propagated upstream outside the supersonic region.

- (b) Spanwise variations. Variations of the shock-wave position across the span may appear on the photographic record as a diffuse wave particularly with the direct-shadow method of photography.
- (c) Interaction with the boundary layer of the tunnel wall. The double nature of the shock-wave in some of the photographs may be due to bifurcation in the boundary layers of the two glass tunnel walls. This appears to be a function of shock strength since in some of the photographs the forward part of the double wave disappears (with movement away from the aerofoil) before the rear part (*e.g.*, Fig. 18).
- (d) Oscillation of the wave. This could account for most of the observed phenomena.

3.2.2. *The Influence of the Aerofoil Shape.*—3.2.2.1. *Lift.*—The general tendency of the lift-coefficient, Mach-number curve is first an initial rise up to a Mach number of 0.7 to 0.8 for aerofoils of moderate thickness followed by a rapid fall associated with the formation of shock-waves on the aerofoil surfaces. The lift coefficient then rises again re-establishing itself at supersonic velocities and falling again as the supersonic Mach number is increased.

Influence of Aerofoil Thickness.—Thin aerofoils show an initial rise of lift coefficient with increase of free-stream Mach number from a low value. This rise appears in most cases to agree with that predicted by the Glauert formula:—

$$C_L = C_{L_0}(1 - M^2)^{-1/2} \quad \dots \quad (1)$$

where C_{L_0} is the lift coefficient in an incompressible fluid and C_L that at free-stream Mach number M . This expression applies strictly only when regions of supersonic velocity are absent and when the local velocity is everywhere nearly equal to the free-stream velocity. Thus, the Glauert equation would only be expected to apply to thin aerofoils at low incidence and Mach numbers below the first critical. Indeed it is found that thick aerofoils (greater than about 18 per cent) do not show a large initial rise of lift coefficient, and in general, this rise decreases as the aerofoil thickness is increased. This is illustrated by Figs. 33, 34, and 35,* which apply to symmetrical and cambered aerofoils respectively. The fall of lift coefficient which occurs at higher free-stream Mach numbers and is associated with the formation of shock-waves occurs at an earlier Mach number and is more severe for thick than for thin aerofoils.

The lift must re-establish itself at supersonic speeds, and some of the lift curves show this tendency at Mach numbers above that at which the loss of lift occurs. The precise shape of the lift curve in the region of Mach number close to unity, is however, not known.

Influence of camber.—The zero-lift incidence for a cambered aerofoil increases rapidly after some high subsonic Mach number has been reached. This is illustrated by Fig. 36 which shows that the no-lift angle of some aerofoils becomes positive at high Mach number. Since, however, the no-lift angle at supersonic speeds is roughly zero it seems that in these cases a fall of no-lift angle must occur at higher Mach number.

The increase of no-lift angle produces nose down changes of trim and this represents a disadvantage of the cambered aerofoil for operation above the shock stall since the no-lift angle of a symmetrical section is zero at all Mach numbers. In general the lift coefficient fall begins at a lower Mach number and is rather more severe for a cambered than for a symmetrical aerofoil being particularly severe for thick cambered aerofoils (greater than about 18 per cent). This is illustrated by Figs. 35, 37.

* For aerofoil nomenclature, see Appendix I.

Influence of trailing-edge angle.—No definite conclusions on the effect of trailing-edge angle on lift can be drawn from the results of tests in the N.P.L. tunnels. Since, however, the lift at high Mach number is largely dependent on differential movements of the shock-waves on the two aerofoil surfaces it might be expected that changes of surface curvature towards the rear of the aerofoil would be important. This is confirmed by some German experiments which show that by making the rear part of the aerofoil concave, and thus reducing the trailing-edge angle, the lift and moment characteristics at high Mach number may be improved. Thus it was found that for trailing edge angles below about 17 deg the C_m , C_L and C_L, α curves could be made approximately linear up to high Mach numbers.

Critical Mach number for lift fall.—In common with the drag and moment critical Mach numbers, the critical Mach number for lift fall does not usually coincide with the first or pressure critical Mach number. Nor does the lift critical Mach number agree exactly, in general, with the drag critical. It appears that in many cases the lift coefficient continues to rise at Mach numbers above the first critical. The agreement between the lift critical and the first critical Mach number is found to be best when the first critical is high. Thus for aerofoils with large suction peaks in the pressure distribution the lift critical occurs at a Mach number considerably in excess of the first critical, and for aerofoils with flat pressure distributions soon after the first critical.

3.2.2.2. *Pitching moment.*—The Glauert equation predicts that the quarter-chord pitching-moment coefficient will be proportional to the factor $(1 - M^2)^{-1/2}$ and will, therefore, increase in magnitude as the Mach number is raised (usually becoming more negative). The limitations of the equation are identical to those discussed in the section on lift. It is found in practice that the effects of compressibility on C_m are rather more marked than the Glauert relation would predict, and Hilton has suggested an empirical formula which is based on the Glauert relation but includes a term containing the thickness ratio of the aerofoil. The Glauert and Hilton equations are identical for an aerofoil of zero thickness. Hilton's formula gives good agreement with observation except at high C_L within roughly the limits of Mach number in which the Glauert formula is valid.

For C_{m_0} the general tendency is to become more negative as the Mach number is raised until the Mach number is reached at which the lift coefficient begins to fall. Above this Mach number C_{m_0} begins to rise rapidly (becoming less negative) towards zero. This is illustrated by Fig. 38.

Influence of aerofoil thickness.—The Mach number for rapid increase of C_{m_0} decreases with increase of aerofoil thickness. This is illustrated by the curves for EQH 1250/1050 and EQH 1550/1058 in Fig. 38 (the difference of position of the maximum centre-line ordinate should not invalidate this comparison). The quarter-chord pitching-moment slope $\partial C_m / \partial \alpha$ increases rather more rapidly with rise of Mach number from a low value for thick than for thin aerofoils. This is illustrated by Figs. 39 to 42.

Influence of camber.—The value of C_{m_0} as well as the no-lift angle are zero at all Mach numbers for a symmetrical aerofoil and this constitutes an advantage of this type of section. Fig. 43 shows the variation of the aerodynamic centre position for a number of aerofoils tested at the N.P.L. At approximately the same Mach number as that at which the lift coefficient begins to fall rapidly the position of the aerodynamic centre begins, in most cases, to move suddenly forward from the quarter-chord position. In some cases a subsequent rearward movement is apparent at a higher Mach number. This is to be expected since at supersonic speeds the aerodynamic centre is approximately at half chord.

Influence of trailing-edge angle.—German experiments indicate that the aerodynamic centre movement is most serious for aerofoils with large trailing-edge angle.

Critical Mach number for pitching moment.—In general a similar delay of pitching-moment critical Mach number beyond the first critical to that discussed under lift is observed. The pitching-moment critical appears to agree more closely with the lift critical than with the drag critical or the first critical Mach number.

3.2.2.3. *Profile drag.—Influence of aerofoil thickness.*—Tests in the N.P.L. and other high-speed tunnels indicate that the critical Mach number for drag rise decreases as the maximum thickness of the aerofoil is increased. This is illustrated by Fig. 44 which gives the results of tests in the 12-in. diameter high-speed tunnel on a family of 2-in. chord aerofoils 12, 15, 17 and 20 per cent thick, and by Fig. 45, which shows some German results.

There appears to be little conclusive evidence on the influence of aerofoil thickness on the rate of drag rise above the critical Mach number, but the effect of thickness variation does not appear to be very great. Thus an analysis of a large number of N.P.L. results has indicated that the drag-curve slope $\partial C_D/\partial M$ above the critical Mach number is about 0.45 for most aerofoils.

At supersonic speeds the drag coefficient is approximately proportional to the square of the thickness for aerofoils with the bow-wave attached to the nose.

Influence of the position of maximum thickness.—Tests at the N.P.L. and elsewhere have indicated that rearward movement of the position of maximum thickness increases the critical Mach number for drag rise. Humidity effects in both N.P.L. tunnels and wall interference in the 1-ft tunnel have, however, prevented definite conclusions being drawn as to the influence of maximum thickness position on the rate of drag rise above the critical Mach number. Experiments made in Germany indicate that rearward movement of the position of maximum thickness increases the rate of drag rise above the critical, and at such Mach numbers, therefore, a forward position may be desirable. Figs. 46 to 49 show results obtained in the 2.7-m D.V.L. tunnel on three 12 per cent symmetrical aerofoils with maximum thicknesses at 30, 40 and 50 per cent of the chord from the leading edge. It appears that a 40 per cent maximum thickness position is the optimum at small incidences for a Mach number a little above the critical, but that at higher incidence a more rearward position is preferable.

Influence of leading-edge radius.—Little evidence is available from N.P.L. experiments on the influence of leading-edge radius on the critical Mach numbers. Some German results, however, indicate that this is small in most cases.

Influence of camber.—The incidence for minimum profile drag of a cambered aerofoil decreases as the Mach number rises. This is illustrated by Fig. 21 which applies to the Goldstein 1442/1547 aerofoil. In general it appears that the critical Mach number for drag rise decreases with increase of camber for low (< 0.6) lift coefficients, and that at lift coefficients of this order the drag of a symmetrical aerofoil is then less than that of a cambered aerofoil.

Critical Mach number for drag rise.—For aerofoils with flat pressure distributions the drag begins to rise at a Mach number a little above the first or pressure critical. This is illustrated by Fig. 21, $\alpha = 0.5$ deg, for the Goldstein aerofoil and by the zero lift drag curves of Fig. 46. When the pressure distribution has large suction peaks, however, the first critical Mach number appears to bear no relationship to the critical Mach number for drag rise. This is illustrated by the high incidence curves of Fig. 46 or by Fig. 49. It has already been mentioned that a high critical Mach number for drag rise gives no indication of the performance of an aerofoil at supercritical Mach numbers, and it appears that the pressure critical is an even less satisfactory basis for estimating the performance at very high Mach numbers. This is illustrated by Figs. 47, 48, 49.

3.2.3. *Aerofoil Tests at Subsonic Speeds in the 1-ft Diameter Tunnel.*—A large number of 2-in. chord aerofoils have been tested on the balance of the 1-ft diameter tunnel at subsonic Mach numbers. Some of the more important conclusions are summarised in the foregoing paragraphs, and a complete description of the experiments is given in R. & M. 2058. A list of the aerofoils tested may also be found in the Appendix to the present paper.

The experiments were all subject to the confusing influences of humidity condensation. They were, moreover, necessarily made at low Reynolds number, and the corrections for wall interference are probably not very reliable, particularly at high Mach number. For these reasons the experimental results, particularly those of drag should be considered as qualitative rather

than quantitative in many cases. Thus, for example, a comparison between Figs. 44 and 45 which show the results of profile-drag measurements in the 12-in. N.P.L. tunnel and the 2.7-m D.V.L. tunnel indicates a considerable discrepancy.

3.2.4. *Aerofoil Tests at Subsonic Speeds in the 20 × 8-in. Tunnel.*—Observations on the 1442/1547 section have already been discussed, and those on EC 1250 and Mustang (14½ 40/1241) wing sections will be discussed later. A list of other aerofoils which have been tested in this tunnel is given in Appendix 1.

3.2.5. *Schlieren Photography in the 20 × 8-in. Tunnel.*—In addition to a large number of direct-shadow photographs of the two-dimensional flow round aerofoil models in the 20 × 8-in. tunnel, a certain number have also been taken by a schlieren method. Some typical examples are reproduced in Figs. 50 to 53 which show the flow round an N.A.C.A. propeller aerofoil (10 per cent thick at 50 per cent chord) at a Mach number of 0.84 and an incidence of -2 deg. The four photographs were taken in quick succession by four different schlieren set-ups, two with the knife-edge cut-off parallel to the chord, and two perpendicular to the chord as shown in the figures. The exposure in each case was of the order of one microsecond.

The regions of expansion and compression are clearly visible together with the positions of the shock-waves and boundary-layer separations on the aerofoil surfaces. Small amplitude waves originating near the trailing edge of the aerofoil and propagated upstream may be seen. These build up into a wave of large amplitude constituting the aerofoil shock-wave which is then at rest at the rear of the region of supersonic velocity immediately upstream. There is some evidence from the photographs that small amplitude waves may be propagated upstream round the outsides of the supersonic regions.

Wavelets in the supersonic region on the lower surface are visible in all the photographs. This may be evidence that the boundary layer in the supersonic region on this surface is turbulent. This is supported by the fact that the shock-wave on this surface is not bifurcated whilst that on the upper surface is (Ackeret having shown that for weak shocks bifurcation usually occurs only in a laminar boundary layer). At the bifurcated wave on the upper surface boundary-layer separation occurs immediately (Fig. 50) whilst at the 'near normal' shock-wave on the lower surface there is apparently no immediate boundary-layer separation (Fig. 51). The wide region of turbulence (outside the wake) visible in Figs. 50 and 51 is attributed to an effect close to the glass tunnel walls and has yet to be further investigated.

These photographs should be examined in conjunction with the pressure distributions shown in Fig. 54 which were taken simultaneously.

3.2.6. *Comparison of N.P.L. and R.A.E. High-Speed Tunnel Observations.*—The surface pressures and the profile drag of aerofoils of the Mustang section were measured in the N.P.L. 20 × 8-in. tunnel and in the R.A.E. 10 × 7-ft tunnel in 1944. The ideal design section (N.A. 73) was not reproduced in the models but the section used in the flight tests was copied. The section tested at the N.P.L. and the R.A.E. differed since the N.P.L. model included an irregularity at 0.75c (where the flap hinge was sealed in the flight tests) which was not reproduced on the R.A.E. model.

The pressure distributions measured in the two tunnels are compared in Fig. 56, and the lift, pitching moment and drag coefficients in Figs. 57, 58, 59 respectively. Whilst the results are in qualitative agreement, considerable discrepancies exist between numerical values and these are, no doubt, due in part to the differences between the shapes of the aerofoils. Other possible explanations of the differences are discussed in R. & M. 2251¹⁶⁹.

3.2.7. *Comparison of High-Speed Wind Tunnel and Flight Observations.*—The results of surface pressure-plotting experiments on the wing of a *Mustang I* aircraft in flight are given in Ref. 170, and profile-drag measurements for the same aircraft in Ref. 171. The aircraft was dived to

achieve the high Mach numbers required for the comparison with wind-tunnel observations, the highest Mach number achieved being about 0.79. Considerable care was taken to ensure that the corrections for lag in the manometer system were reliable, but even so, the pressure-plotting observations must, to some extent, be considered suspect on this score. Moreover, the difficulties associated with supporting a pitot-comb of adequate length restricted the length of comb used, and it seems that in some cases the whole of the wake was not covered. The distortion of the wing section under aerodynamic load is also a possible source of error.

At low speeds it was found that the flight and wind-tunnel results were in good agreement for pressure distribution, those of flight being roughly the means of the measurements in the R.A.E. and N.P.L. wind tunnels. Above a Mach number of about 0.7, however, considerable discrepancies occurred (*see* Fig. 60). Thus, for example, the peak suction is considerably more pronounced in flight than in the wind tunnels on both upper and lower surfaces.

The flight and wind-tunnel drag curves are compared in Fig. 61. Unfortunately the Mach number to which the flight tests could be carried was not sufficiently high to give a good comparison in the region of the critical Mach number: It appears, however, that the critical drag rise begins at a Mach number about 0.02 higher in flight than in the wind tunnel.

3.2.8. The Influence of Reynolds Number.—At low speeds the influence of the Reynolds number on the flow round a body is almost entirely confined to the boundary layer. Thus, the transition from laminar to turbulent flow in the boundary layer, the intensity of skin friction, and the position and nature of separation are, for a given shape and surface roughness; largely dependent on the Reynolds number.

At high Mach numbers when shock-waves are present in the flow between the leading and trailing edges of the body, there is considerable evidence that the nature of the interaction of the shock-wave and the boundary layer depends on the nature of the boundary layer upstream of the region of interaction. Thus, not only the nature of the shock-wave itself but also the flow downstream of the wave are dependent on the Reynolds number. It, therefore, appears that the Reynolds number may have an important influence on the distribution of normal surface pressure near and downstream of the interaction, on the normal force and moment coefficients, and also on the drag coefficient. The experimental evidence which is at present available is sufficient to support these general statements, but is not yet sufficiently conclusive to enable a precise description of the influence of Reynolds number to be made.

Fig. 62 shows the variation of the profile-drag coefficient of aerofoils of EC 1250 section with Reynolds number. The experiments were carried out in the 20 × 8-in. tunnel (apart from one set of observations on the 2-in. chord model) with aerofoils of 2, 5 and 12-in. chord. The tunnel stagnation pressure was constant throughout the experiments so that the Reynolds and Mach numbers were varied simultaneously. Mach number scales are appended to the Reynolds number scale in Fig. 62, and Reynolds number scales to the Mach number scale of Fig. 63. It appears from Fig. 63 that the profile-drag coefficient above the critical Mach number for drag rise is very little dependent on Reynolds number (over the range 0.7×10^6 to 4.3×10^6). At lower Mach numbers, however, the Reynolds number appears to be important. This is in agreement with observations in low-speed tunnels in which it is well known that the position of the transition point and the existence of laminar separation are both functions of Reynolds number. The skin friction drag will also, of course, vary with Reynolds number at constant transition position and this appears to be the explanation for the drag changes below the shock-stall in Fig. 62. It is known from flow visualization by the schlieren method and by inspection of surface pressure distributions that laminar separation occurs on 5-in. chord models in the 20 × 8-in. tunnel at low Reynolds (and, therefore, Mach) numbers.

The profile-drag measurements of Figs. 62, 63, must be suspect, particularly at high Mach number, because of the possibility of condensation of atmospheric humidity. Some drag observations made in the R.A.E. high-speed tunnel over a range of Reynolds and Mach numbers are

shown in Fig. 64. These results indicate a considerable scale effect on the absolute values of the profile-drag coefficient at all Mach numbers. This appears to be particularly so for Reynolds numbers below about one and a half million.

3.2.9. *Transition Indication.*—The results of experiments on the transition from laminar to turbulent flow on the surfaces of a 5-in. chord aerofoil model of EC 1250 section are shown in Figs. 65, 66, 67. Fig. 65(a) shows a typical deposit of atmospheric dust on the surface of an aerofoil in the 20×8 -in. tunnel. The position of transition on the surface and also the spread of turbulence behind a leaking pressure hole near the leading edge of the aerofoil is shown.

Figs. 65(b), 66, show a series of photographs taken with the EC 1250 aerofoil over a range of Mach numbers using the china-clay method⁷⁸. The corresponding pressure distributions were observed during a separate experiment, and are also shown together with the shock-wave position observed during the transition experiments. Ignoring for the moment the regions of the aerofoil span close to the tunnel walls it may be seen that the transition position moves aft as the Mach number increases, coinciding at high Mach numbers with the position of the shock-wave on the aerofoil surface. The increasingly favourable pressure gradient upstream of the shock-wave which appears as the Mach number is increased is compatible with the observed movement of the transition position. At the incidence of the experiment, the pressure gradient on the lower surface is favourable over between 0.7 and 0.8 of the chord for the whole range of Mach number, and little movement of the transition position on the lower surface is apparent with increase of Mach number (Fig. 67).

It appears from these experiments that the boundary layer immediately ahead of the shock-wave is laminar and it is known that the nature of the interaction of shock-wave and boundary layer depends on the state of the boundary layer. At the Reynolds number of flight the tendency for an early transition to turbulent flow will be considerable, and it is possible that the boundary layer upstream of the shock-wave will be turbulent so that the wind-tunnel observations discussed above may indicate a scale effect.

The rearward movement of the transition position observed in the wind-tunnel observations may be accompanied by a reduction of the skin friction over the forward part of the aerofoil. At Mach numbers below that at which the entropy rise through the shock-wave and the boundary layer thickening or separation begins to control the profile-drag coefficient it might be expected that this will show an initial fall with rising Mach number. This would be expected to be greatest when the movement of the transition position is largest, that is for aerofoils whose low-speed pressure distribution has a peak near the leading edge and is illustrated by the curves of Fig. 21 and also by Fig. 23 which shows some results from the D.V.L. 2.7-m tunnel.

The experimental observations also show the spread of turbulence at the ends of the aerofoil due to transverse contamination by the boundary layer of the tunnel wall and by any small leaks which may have been present. This does not appear to influence the centre portion of the span on which measurements are made.

The results of experiments using a sublimation indicator (Borneol) are shown in Fig. 68. The surface with this indicator is not as good as that obtained for the china-clay method, several large irregularities being present. The spread of turbulence behind these obstacles is clearly visible in the photographs as the familiar cusped shapes. Charters has shown⁹⁰ that on a flat-plate transverse contamination behind such an obstacle is in the form of a wedge. The cusped shape which is characteristic of transverse contamination on an aerofoil is attributed to the existence of a velocity gradient along the chord.

Several of the photographs shown in Figs. 4 to 18 and taken by the direct-shadow method indicate transition fairly clearly*. This method appears to show considerable promise but has several limitations, the chief of which appear to be inability of indicating spanwise variations of the transition position.

3.2.10. *The Interaction of Shock-Waves and Boundary Layers.*—For inviscid two-dimensional fluid flow along a plane surface a normal shock-wave will extend right down to the surface without change of intensity or form. In such a flow an oblique wave, incident on the surface at an angle

* See A.R.C. Current Paper. No. 10.

greater than a certain critical angle, will experience regular reflection at an angle in excess of the incident angle. The flow downstream of the reflected wave will remain parallel to the surface. If the angle of incidence is greater than the critical angle, a third (Mach) wave will appear between the surface and the point of intersection of the incident and reflected waves which will then lie at some distance from the surface. In general the static pressure will be the same behind the Mach wave and the reflected wave, but the speed, temperature, entropy and Mach number will differ, and a vortex sheet will appear at the point of intersection of the three waves and pass downstream. At the inception of this régime the Mach wave is normal to the surface, but, as the point of intersection of the three waves recedes from the surface, the Mach wave becomes increasingly curved.

In a real fluid, the velocity must fall to zero at the surface and the shock-wave cannot extend to the surface, since the velocity in the boundary layer must be subsonic near to the surface. Moreover, a shock-wave constitutes a severe adverse pressure gradient and a marked change of the nature of the boundary layer may be expected in the region of the surface near the shock-wave. The interaction of shock-waves and boundary layers is clearly of fundamental importance in the study of compressible flow round bodies and in channels. In particular the 'mixed' or 'transonic' flow round an aerofoil at high subsonic Mach numbers when local supersonic regions are present is critically dependent on this interaction. Fundamental experimental studies of the nature of shock-wave-boundary-layer interaction have been made in America, Germany, Switzerland and in this country, but further work is required before all the phenomena are fully understood.

At the N.P.L. Fage and Sargent¹¹ investigated the interaction of shock-waves of varying strength with the turbulent boundary layer on a flat plate and found that the nature of the interaction was a function of the shock strength. More recent work by Ackeret and by Liepmann has indicated that the interaction also depends on the nature of the boundary layer immediately upstream of the interaction. Thus Reynolds number and the introduction of artificial turbulence into the boundary layer were shown to have a considerable influence.

The apparatus used by Fage and Sargent is shown in Fig. 69. It consisted essentially of a 'one-sided' (Crocco-type) supersonic tunnel in which shock-waves were formed either at the breakdown from supersonic to subsonic flow, or as oblique waves from a wedge attached to one wall of the tunnel. The interaction of the shock-wave with the boundary layer of the plane wall opposite the single nozzle liner was studied. The plane wall could be traversed axially with a micrometer screw and supported the exploring tubes (static, pitot and surface tubes) used in the experiment. Direct-shadow and schlieren photographs of the flow were also taken. In order to increase the Reynolds number at the point where the interaction was studied, the tunnel was extended for a considerable distance upstream of the throat of the supersonic nozzle. The Mach number varied along the length of the plane wall, and it is difficult to give a measure of the Reynolds number at the point of interaction but it was probably about six millions. The Mach number ahead of the shock-wave was varied by the use of three separate nozzle liners and by varying the position of the breakdown shock in the expanding region of the nozzle.

Fig. 70, 71 show a number of direct-shadow and schlieren photographs of the interaction of the 'near normal' breakdown shock-wave with the boundary layer. The shock strength χ (defined as the ratio of the static pressure downstream to that upstream of the single part of the wave) varies from 1.19 (plate j) to 2.33 (plate k) through the sequence j, i, b, h, g, f, e, (a and c), d, k. All the photographs show that the foot of the shock-wave does not extend right down to the surface. At low shock strengths the foot of the shock is not forked or bifurcated, but at higher values (> 1.84) bifurcation is visible. It can be seen that the boundary layer thickens in the region of the interaction and that the thickening increases with increasing shock strength. The boundary-layer thickening is particularly severe in the case of bifurcated waves, beginning at the upstream toe of the wave foot. The apex of the bifurcated waves recedes from the surface as the shock strength increases.

Fig. 71, plates q, p and n, (o, m), show the interaction of an oblique incident wave with the boundary layer. In all cases a third (Mach) wave is visible, the point of intersection of the three waves receding from the surface as the shock strength increases. At the higher shock strengths the Mach wave bifurcates on interaction with the boundary layer in a similar manner to the near-normal waves previously discussed.

Fig. 72 shows the variation of normal pressure along the plane surface in the region of the interaction. This is plotted as the ratio of the normal pressure (p) to the atmospheric pressure (p_A). Curves of the variation of the intensity of surface friction (τ_0) along the plate are also shown. The values of τ_0 are plotted as a ratio to the intensity of surface friction (τ_0)_a just upstream of the interaction and are deduced from surface-tube observations. It may be seen that the static-pressure gradient at the surface is in no case comparable in suddenness with that which occurs through the main shock-wave at some distance from this surface. This is consistent with similar observations on the surfaces of aerofoils in the presence of shock-waves. The static pressure begins to rise at the upstream toe of the shock-wave for both bifurcated and unbifurcated waves, and the pressure gradient tends to increase with increasing shock strength. The initial rapid rise of static pressure is followed by a more gradual gradient further downstream. The intensity of surface friction falls off rapidly behind the upstream shock-wave toe and reaches zero at the higher shock strengths. At lower shock strengths the intensity of surface friction recovers after a fall to a minimum value a little downstream of the shock-wave toe.

The work (Ref. 11) includes the results of static and pitot axial traverses at various distances from the plane wall, and of lateral traverses downstream of the interaction. The theory of bifurcated shock-waves in inviscid flow is also discussed.

It is important to differentiate between phenomena associated with shock-wave-boundary-layer interaction and those associated with a finite supersonic region. In the work of Fage and Sargent, the flow was supersonic across the whole tunnel upstream of the breakdown shock-wave, but in some of Ackeret's experiments and in Leipmann's experiments the supersonic region was finite and formed by the local acceleration on a curved surface. In some of the latter experiments (examples may also be seen in some of the photographs Fig. 4 to 18) forward inclined waves were observed. These cannot arise directly from shock-wave-boundary-layer phenomena and must be attributed to reflections from the sonic boundary of the supersonic region of disturbances originating upstream, or to disturbances entering the supersonic region from the surrounding subsonic flow.

3.2.11. *Boundary-Layer Suction.*—Since a large part of the drag rise associated with the shock stall of an aerofoil appears to be due to the thickening or separation of the boundary layer at the shock-wave it might be anticipated that a reduction of drag could be achieved by the application of boundary-layer suction in this region. If the air thus removed is compressed and discharged at the free-stream density ρ_0 and velocity u_0 it can be shown that the effective total drag (allowing for the work done by the compressor) will be less than the drag of the aerofoil without suction if

$$D - D_s - \left(\frac{\varepsilon}{u_0}\right) > \left(\frac{\varepsilon_f}{u_0}\right), \quad \dots \dots \dots (2)$$

where D is the aerofoil drag without suction, D_s the drag with suction, ε the work required per unit time to raise the velocity and pressure of the suction air to the conditions of the jet exit and ε_f the work done in unit time in overcoming the losses in the ducting system. By dividing by the dynamic head based on the free-stream conditions equation (2) may be written

$$C_D - C_{D_s} - C_\varepsilon > C_{\varepsilon_f}. \quad \dots \dots \dots (3)$$

Fage and Sargent¹⁷⁵ have investigated the problem in the 5 × 2-in. tunnel using an aerofoil of 2-in. chord and N 2030 section. The adjustable walls of the tunnel were used during the experiment to minimise wall interference. The aerofoil was fitted with a forward-facing slot 0·035-in.

wide on one surface of the aerofoil; the lips of the slot were inclined at 45 deg to the chord line. The drag was measured by total-head and static-pressure traverses of the wake one chord behind the trailing edge.

In Fig. 73, the variation of C_{D_s} with the suction quantity is shown at two Mach numbers above the critical for drag rise. The suction quantity is plotted in the dimensionless form $m_s/\rho_0 u_0 c$, where m_s is the mass of air removed per unit span in unit time and c is the aerofoil chord. The drag coefficient falls at first with increase of the suction quantity but approaches a steady value beyond which further increase of suction is ineffective. The variation of drag coefficient with and without suction is plotted in Fig. 74 as a function of Mach number. The Reynolds number of these experiments was of the order of 0.7×10^6 and it is, therefore, difficult to assess the power economy which may be produced by suction at the more favourable higher Reynolds numbers of flight. Nevertheless, the fact that $(C_D - C_{D_s})$ in the experiment was of the same order as C_e suggests that power economy would be possible at higher Reynolds number.

In R. & M. 2127^{177, 178} Fage and Sargent discuss the optimum entry shape of a two-dimensional suction slot for assigned values of the slot angle and rate of flow. The cases of both laminar and turbulent boundary layers at low speeds are considered, and the shape of the slot entry for turbulent boundary-layer suction at high speeds is discussed.

It should be noted that because of the loss of total head in the boundary layer, the mass flow of air required to choke the slot is less than that predicted by the assumption of an isentropic flow from the free-stream total-head conditions. Thus, Pearcey and Rogers have found in some experiments on a Griffith aerofoil that the ratio of the former to the latter quantity was 0.90 at $M = 0.4$ and 0.78 at $M = 0.6$. The Griffith aerofoil was of 9-in. chord and symmetrical section 22 per cent thick. It was tested at zero incidence in the 20×8 -in. tunnel and had suction slots at 0.75 chord. The drag was determined by the pitot-traverse method and estimates were made of the power absorbed by the compressor (ignoring duct losses) from measurements of the mass flow of suction air and the static pressure in the slot. Examples of the experimental results are given in Fig. 75 at a Mach number of 0.60 ($M_{crit} = 0.65$). The lip radii of the two slots differed in the experiment, but the figure has been drawn for an aerofoil with two similar slots corresponding to the smaller lip radius. The estimated compressor power increases almost linearly with suction, and the combined drag ($C_{D_s} + C_e$) rises to a maximum and then falls to a minimum which is less than the drag without suction. Below the shock-stall the suction quantity for minimum drag increases with increase of Mach number. Thus, referring to the surface considered in Fig. 75 the suction quantity increased from 0.6 times the theoretical mass flow in the laminar boundary layer at $M = 0.4$ to 0.96 times this quantity at $M = 0.6$. The theoretical and experimental velocity distributions in the neighbourhood of the slot are compared in Fig. 76 and the agreement (with suction) appears to be satisfactory.

As in the earlier work of Fage and Sargent discussed above, the Reynolds number of the experiments with the Griffiths aerofoil was considerably below the full-scale value. However, an extrapolation to a Reynolds number of the order of 20×10^6 suggests that suction may be beneficial, but that the economy will be somewhat smaller at Mach numbers approaching the critical value than at low speeds. This extrapolation assumes that the boundary layer may be maintained laminar over the major part of the aerofoil ahead of the slot and, in common with conventional low-drag aerofoils, this may prove difficult in practice.

The proposed 18×14 -in. tunnel, for which the stagnation pressure may be increased to three atmospheres, will be considerably more satisfactory for suction experiments than the atmospheric 20×8 -in. tunnel, and it is hoped to continue the work discussed above in the 18×4 -in. tunnel when it becomes available.

3.2.12. *Controls on Subsonic Aerofoils.*—In 1941 an investigation of the efficiency of a conventional control surface was undertaken in the 1 ft tunnel using the three-component electric balance. The aerofoil tested was of EC 1240 section fitted with a control surface whose hinge line was at

59.5 per cent of the aerofoil chord from the leading edge. The aerofoil control combination was intended to represent a tailplane and elevator. The aerofoil was of 2-in. chord, and both aerofoil and control completely spanned the tunnel. In the original tests the gap between the aerofoil and control was not sealed and it was found that no serious loss of control (as measured by $a_2 = dC_L/d\eta$) occurred until a Mach number of 0.75–0.78 was reached. In later tests the gap was sealed, and this was found to lead to an increase of a_2 of 40 per cent at $M = 0.4$, and 60 per cent at $M = 0.7$. Loss of control was found to occur at about the same Mach number as in the gap-open condition. With the gap open a_2 was practically independent of Mach number at a value 3.0 from $M = 0.45$ to 0.73, but with the gap sealed the value of a_2 was closely represented by the equation $3.6/(1 - M^2)^{1/2}$, following the Glauert formula, over the Mach number range 0.4 to 0.7. Above $M = 0.78$ the value of a_2 fell rapidly reaching about one-half its low-speed value at about $M = 0.81$ in both the gap open and sealed conditions. A diagram of the aerofoil and control tested is given in Fig. 77, and a comparison between the values of a_2 for the gap-open and sealed conditions is given in Fig. 78. A detailed description of these experiments, which include moment and drag observations, is given in Ref. 180 and R. & M. 2227^{181, 182, 183}.

A clearer insight into the mechanism of loss of control at high Mach number may be obtained from an examination of the results of pressure-plotting experiments. Such experiments have been made in the 20 × 8-in. tunnel with an aerofoil of EC 1250 section fitted with a 25 per cent control surface. The aerofoil had a 5-in. chord, and both aerofoil and control completely spanned the working section of the tunnel between the two glass walls. These experiments, described in Ref. 184 and R. & M. 2065¹⁸⁵, were made for an incidence range (α) ± 6 deg, and a control angle (η) ± 8 deg up to a Mach number of about 0.85. The adjustable tunnel walls were used in the normal way to minimise interference, and the pressure-plotting observations were integrated to give lift, pitching moment, form drag and hinge moment. A small number of drag measurements by the wake-traverse method were made at low speeds, and at each incidence and control angle the critical Mach number for drag rise was determined. A sketch of the aerofoil and control section is given in Fig. 79. The control used was of a convex section, but it is proposed* to repeat the experiment with a concave ('hollow ground') control.

The experiment involved some 60,000 pressure observations, giving about 1000 complete pressure distributions. It was not, therefore, possible in the original published account of the experiment to include all the pressure distributions, and it is necessary here to give only a few examples.

The experiments indicated clearly the mechanism of the loss of control at high Mach number. Fig. 80 shows typical pressure distributions at $\alpha = 2$ deg and for $\eta = 0$ and 4 deg, at two Mach numbers one of which (0.68) is below the shock stall, and the other (0.84) above the shock stall. The diagram for $M = 0.68$ shows that a movement of the control surface produces a change of the pressure distribution over the whole aerofoil leading to large changes of overall force. Above the shock stall ($M = 0.84$), however, a movement of the control has no effect on the pressure distribution over the forward part of the aerofoil. In this case, the change of overall force will be small and, the control ineffective. This phenomena may be explained physically by noting that, when the velocity is everywhere subsonic, the information that the control has been moved is communicated to all parts of the aerofoil (*i.e.*, the effective camber of the whole aerofoil is changed). If a region of supersonic velocity exists close to the aerofoil surface, however, this information is trapped at the rear of the supersonic region, and the control has little influence on the pressure distribution upstream of this point. This argument is summarised in R. & M. 2065¹⁸⁵ by the remark that the shock-wave on the aerofoil surface has a masking effect on the control. The loss of control efficiency is illustrated by Fig. 81 in which the quantities a_1 and a_2 are plotted as functions of Mach number. Fig. 82 shows the variation of the quantities $\partial C_M/\partial \alpha$ and $\partial C_M/\partial \eta$ with Mach number.

* These further experiments have now been made (August, 1949).

The observed loss of control does not imply a reduction of the heaviness of the control, since even with an inefficient control, the pressure changes on the control itself produced by a control movement may be considerable. Indeed, Fig. 83 indicates that the quantity $b_2(\partial C_H/\partial \eta)$ begins to increase rapidly at about the same Mach number as that at which loss of control is observed. The experiment, therefore, indicates that whilst at high Mach number elevator (or aileron) control is lost, the control may also become heavy. It was also concluded from the experiment that the use of an all-moving tailplane (of EC 1250 section) would postpone loss of control to above $M = 0.85$.

The results may not be generally applicable since it is known that a control of convex shape may give undesirable features even at low speeds. In consequence, it is proposed to test the same aerofoil with a modified control, first concave and afterwards flat sided.

3.2.13. Tests with Brake Flaps.—A limited number of measurements were made at the request of the R.A.E. on aerofoils fitted with brake flaps in connection with the design of the Gloster F9/40 (Meteor) aeroplane. Because of the limited nature of the experiments it is not possible to draw many general conclusions from them.

The earliest tests were made in 1942 and are described in R. & M. 2211¹⁸⁶. Force measurements were made in the 12-in. diameter tunnel with a 2-in. chord model of EC 1240/0640 section, and the flow pattern photographed in the 20×8 -in. tunnel with a 5-in. chord model of (uncambered) EC 1250 section. No pressure distributions were measured in these early tests. The flap span used in the experiments was 0.3 of the aerofoil chord, and six flaps were used at equal spacings along the 12-in. aerofoil span (Fig. 84). The geometry of the plain aerofoil and of the flap combinations tested is also shown in Fig. 84. One series of experiments with a dive-recovery flap (D) was made, and the results are included in Figs. 85, 86, 87. Fig. 85 shows the change of lift, pitching moment and drag coefficients produced by the addition of the flaps to the aerofoil at three incidences and a range of Mach number. Fig. 86 shows the influence of the flaps on the quantity $\partial(\Delta C_L)/\partial \alpha$, and Fig. 87 on the position of the aerodynamic centre expressed as $\partial C_m/\partial C_L$.

A photograph of the wake and shock-wave pattern behind flap combination G (Fig. 84) on aerofoil EC 1250 at a Mach number of 0.78 is shown in Fig. 88. As in the case of most bluff bodies (compare circular cylinder, section 3.2.17 and Fig. 99) shock-waves form well aft of the body on the wake. The widening and unsteadiness of the wake and the presence of shock-waves may have an influence on a tailplane situated downstream of the mainplane. This was the subject of a continuation of the experiments described above (and in R. & M. 2211¹⁸⁶) and is reported in Ref. 188 and R. & M. 2211¹⁸⁷.

In the earlier series of experiments¹⁸⁷ a 5-in. chord aerofoil model of EC 1250 section was used with 20 pressure holes in the surface. Both upper and lower-surface flaps were at 0.65c from the leading edge. Five flap combinations were investigated, and are shown in Fig. 89. Surface-pressure measurements were made over a range of Mach number to assist in stressing the flap and aerofoil skin. The results of these observations are reported in R. & M. 2211¹⁸⁷, and, besides furnishing stressing data, give, together with the wake traverses described below, a clearer insight into the mechanism of operation of the flaps than do the overall force coefficients reported in R. & M. 2211¹⁸⁶.

Explorations of the wake at 1, 1.2 and 2.25 chord behind the trailing edge of the aerofoil, were made for all five flap combinations over a range of Mach number¹⁸⁷. It was found that apart from flap combination A (Fig. 89) the width of the wake did not increase very greatly with increase of Mach number up to a Mach number of 0.8. Above this value the wake broadened rapidly. It was observed that small changes of the flap angle had little influence on either the pressure distribution round the aerofoil or the wake width.

In Ref. 188, the results of tests made with a simplified complete model of the Gloster F.9/40 in the 20×8 -in. tunnel are reported. The purpose of the experiment was to investigate changes of trim at high speeds due to interference of the mainplane and brake flaps, on the tailplane.

A sketch of the model tested is given in Fig. 90. The mainplane was of 5-in. chord and EC 1250 section mounted between the tunnel walls and fitted with model nacelles and a model fuselage. The tailplane was of 2-in. chord and EC 1240 section, and completely spanned the tunnel. The tailplane was mounted 0.52 chord above the mainplane in order to minimise the influence of the mainplane wake, but the preliminary wake traverses described above had indicated that, at high Mach numbers this distance might not be adequate. The flexible walls of the tunnel were used in each experiment to give conditions approximating to the free-air case.

Photographs were taken by a direct-shadow method of the flow in the region of the tailplane for a range of Mach numbers without flaps, and with three flap settings. Static-pressure distributions were measured close to the tailplane surface. Typical results, shown in Fig. 91, indicate an increase of suction on the upper surface and a decrease on the lower surface with increasing flap angle. These measurements were integrated to give the lift coefficient of the tailplane (Fig. 92) but these values are of limited accuracy.

The general conclusions of this series of investigations were:

- (a) The Mach number at which shock-waves first appear on the tailplane is little affected by the presence of brake flaps on the mainplane.
- (b) As the flap angle increases there is a tendency for the shock-waves on the tailplane to become less intense for a given free-stream Mach number.
- (c) The flaps appear to produce an appreciable change of force on the tailplane at Mach numbers in excess of 0.8 accompanied by an oscillation from $M = 0.78$.
- (d) The chordwise oscillation of the shock-wave on the tailplane seems to be related to movements of the wake of the brake flaps as indicated by trails of condensed moisture. This suggests that buffeting will be experienced on the tailplane at Mach numbers above 0.78 accompanied by oscillating loads on the control surfaces as the shock-wave and breakaway crosses the hinge line and moves along the elevator chord. At Mach numbers above 0.8 a loss of control effectiveness is to be expected as the flow has broken away over most of the elevator surface. At the same time, the shock-wave appears to become more stable, and the oscillation should, therefore, diminish.

3.2.14. *Fin-Tailplane Interference.*—It is to be expected that a loss of tailplane efficiency will occur at high speeds due to interference between the rudder fin and the tailplane surface. This may be explained physically on the basis that local high-velocity regions will occur, giving rise to local shock-waves before the main shock stall of the whole tailplane occurs.

A limited number of tests were made in the 1-ft diameter tunnel with a rudder fin attached to the centre of an aerofoil supported in the electric balance and completely spanning the tunnel at the working section. The aerofoil was of EC 1240 section and of the normal 2-in. chord and the rudder was of EC 1040 section. A sketch of the model tested is given in Fig. 93. It appears that the most striking effect of the addition of the fin is the loss of lift at high speeds. This is illustrated in Fig. 93. A full account of the experiment is given in R. & M. 2138¹⁸⁷ which includes drag and moment observations.

3.2.15. *Sharp-Nosed Aerofoils at Subsonic Speeds.*—It is well known that the most efficient aerofoil sections at supersonic speeds have sharp leading and trailing edges. If such aerofoil sections are to be used for supersonic flight, their performance during the accelerating and decelerating regions of subsonic flight before and after the supersonic velocity is achieved is of interest. In particular, the maximum low-speed lift coefficient is of great importance in assessing the take-off and landing characteristics of the proposed aircraft.

Experiments have been made in the 1-ft diameter tunnel to investigate the performance of a 7½ per cent biconvex aerofoil and an 8.7 per cent faired double-wedge aerofoil (Fig. 96) at subsonic speeds. The tests were subject to the usual restriction of Reynolds number, but it may

be that the effect of Reynolds number on the stalling characteristics (and maximum lift coefficient) of a sharp-nosed aerofoil will not be large. That this is so at low Mach number has been demonstrated by some measurements^{190,191} in the Compressed Air Tunnel. The low-speed stall for both aerofoils was found to be gentle, and to occur at a lift coefficient of about 0.7 which is of the same order as that achieved by conventional symmetrical aerofoils, at the same Reynolds number.

The double-wedge aerofoil had a low-speed drag coefficient at zero incidence of 0.008; the corresponding value for the biconvex aerofoil was 0.009. For both aerofoils, however, it was found that the drag rose rapidly with increase of incidence. The variation of lift coefficient with incidence and Mach number for the faired double-wedge and biconvex aerofoils is shown in Figs. 94(a) and 94(b). Corresponding drag curves for the faired double wedge are given in Fig. 95 and for the biconvex aerofoil in Fig. 107. The maximum low-speed lift-drag ratio for both aerofoils occurs at a lift coefficient between 0.2 and 0.3 and is about 13 for the double wedge and 18 for the biconvex aerofoil. The variation of moment coefficient with incidence and Mach number for the faired double wedge is shown in Fig. 96; no unusual effects are visible.

3.2.16. *Sweep-back*.—The concept of the use of sweep-back at high speeds was not fully appreciated in this country until the results of German investigations became available at the end of the war (1945). The original suggestion has been attributed to Busemann (*see*, for example, Ref. 20). The use of sweep-back (or sweep-forward) has long been contemplated in connection with tailless aircraft, and some data on the performance of wings of this plan form at low speeds have been available for several years.

Referring to Fig. 97 which shows a wing of infinite aspect ratio in an airstream normal to the span, it would appear that, in the absence of viscosity, the flow pattern will not be altered by moving the aerofoil at any velocity in a spanwise direction. If this is done the resultant velocity of the airstream relative to the aerofoil is at an angle ψ to the span and of a greater magnitude than the chordwise component. Thus, in an inviscid fluid the component Mach number along the chord of an infinite yawed aerofoil will be $M_0 \cos \psi$, where M_0 is the free-stream Mach number and ψ the angle of yaw. This argument forms the basis for the suggested use of sweepback at high speeds since by the use of sufficient yaw the chordwise component of the Mach number may be kept below the critical values for drag rise and stability changes, at all free-stream Mach numbers. Thus, many of the more violent compressibility effects may be postponed to higher speeds by sweepback.

In practice, the theoretical increase of free-stream Mach number for drag rise is limited by the effects of viscosity, and the finite aspect ratio of the wing. In particular, a high local drag may occur at the centre junction of two swept-back wings, and outward flow of the boundary layer towards the tips may cause tip stalling. The reduction of the drag of the wing junction by the addition of a suitably designed fuselage has been the subject of some investigations.

At the N.P.L. tests have been made on two wings completely spanning a rectangular tunnel, and the variation of the profile-drag coefficient with free-stream Mach number is compared with the unyawed case in Fig. 97. Curves are added for the theoretical drag of the yawed wings deduced from the measurements of the drag of the unyawed wing. The curves do not, therefore, completely ignore the skin-friction drag component, but assume that this coefficient is not altered by the addition of yaw to the wing. It is seen that the measured drag curve for the yawed wing shows a rise at a Mach number which is higher by about 0.8 of the increase for the theoretical yawed case. Curves are also given for one aerofoil section in Fig. 97 for two different chord lengths, and the agreement between the two curves shows that the influence of tunnel interference and Reynolds number over the experimental range is small. For the other aerofoil, drag curves for two different relative humidities at the tunnel intake are given, and it appears that the influence of humidity is considerable, although the discrepancy below the shock-stall can hardly be explained on this basis.

More detailed discussions of the use of sweepback at high speeds will be found in Ref. 20, 197, 198. Some of the more interesting German experimental results are reported in Refs. 199, 200, 201, a short abstract from the latter is given in Ref. 196.

3.2.17. *Experiments with a Circular Cylinder at High Number.*—The variations of pressure distribution and drag of circular cylinders of infinite aspect ratio with Reynolds number and turbulence have been investigated at low Mach number by many workers. It is well known that with increase of Reynolds number from a low value the drag coefficient falls rapidly to a minimum value of about 0.95 at $R = 1800$, and then rises to about 1.2 at $R = 3 \times 10^4$. A marked fall then occurs from 1.2 to about 0.36 at about $R = 10^5$. The value of this critical Reynolds number is dependent on the turbulence of the airstream. Above this Reynolds number further increase produces a gradual rise of drag coefficient. A detailed discussion of these phenomena is given in Ref. 202.

The pressure distribution and drag of a circular cylinder were measured by Stanton in 1928 at Mach numbers varying from 0.25 to 0.7, and from 1.4 to 2.1 in a 3-in. diameter tunnel. The experiments were made at a constant Reynolds number of 20,000 (around which value the drag coefficient is not sensitive to R), but no corrections were applied for tunnel-wall interference. Stanton found that the drag coefficient rose slowly in a continuous curve up to his limiting subsonic Mach number of 0.7, and then fell continuously over the Mach number range 1.4 to 2.1 to a value little above the low-speed value.

Knowler and Pruden²⁰³ measured the drag of a number of cylinders (varying in diameter from 3/16 to 1 in.) on the balance of the 1-ft diameter high-speed tunnel up to Mach numbers of the order of 0.85. It was not possible to apply the usual corrections for wall interference, and a method of correction was adopted which did not permit the influences of Mach number, Reynolds number and wall interference to be separated. These experiments were continued in the 20 × 8-in. tunnel in which the flow pattern was photographed by a direct-shadow method. The form drag was deduced from pressure distributions measured in this tunnel. The experiments in the 20 × 8-in. tunnel were confined to a single model of 3/8-in. diameter, and the Reynolds number, therefore, varied as the Mach number was adjusted. The skin friction drag of a circular cylinder is probably negligible for Reynolds numbers exceeding about 10,000, and no profile-drag measurements were made in the 20 × 8-in. tunnel tests. Several assumptions on which the usual method of profile-drag measurement by wake traverse depends will probably be no longer valid for models similar to the circular cylinder. In particular, the assumption of constant stagnation temperature across the wake may be dubious.

The measurements of Knowler and Pruden (Fig. 98) show the initial gradual rise of drag coefficient with increase of Mach number observed by Stanton, and also a sudden fall of drag coefficient at a Mach number between 0.6 and 0.7 followed by a steeper rise. The Reynolds number at which this drag-coefficient fall was observed was in every case of the order of 10^5 , the logarithm of the Reynolds number for drag fall varying from 4.8 to 5.4 for cylinders of different size in the 1-ft tunnel and the 3/8-in. diameter cylinder in the 20 × 8-in. tunnel. This Reynolds number range is approximately that in which the critical Reynolds number might be expected to occur at low speeds. Whilst, therefore, the observed drag-coefficient fall is attributed in R. & M. 1933²⁰³ to the influence of Mach number alone, it appears that it may be due to the variation of Reynolds number as well.

The drag coefficient measured in the 1-ft diameter tunnel and corrected for wall interference by the method described in R. & M. 2058¹⁶⁸ is plotted as a function of Mach number in Fig. 98. Stanton's balance measurements are included for comparison. A curve of the drag coefficient deduced from measurements of the normal pressure round a 3/8-in. diameter cylinder in the 20 × 8-in. tunnel is included together with values obtained by Stanton by a similar method. The flexible walls of the 20 × 8-in. tunnel were used during the tests to minimise the wall interference. The variation of normal pressure for the 3/8-in. diameter cylinder is given in R. & M. 1933²⁰³.

Photographs of the flow pattern observed in the 20 × 8-in. tunnel at varying Mach number are shown in Fig. 99. It appears that the investigation is incomplete particularly because the effects of Reynolds and Mach numbers have not been separated. Experiments with cylinders of different diameter giving a wide range of Reynolds number in the 20 × 8-in. tunnel, where the wall interference may be minimised, would, therefore, be of considerable interest.

3.2.18. *Velocity measuring instruments.*—If p is the true static pressure, and H the total head, it may be shown that in an isentropic flow

$$\frac{H}{p} = \left(1 + \frac{\gamma - 1}{2} M^2\right)^{\gamma/(\gamma-1)} \quad \dots \quad (4)$$

Expanding, by the binomial theorem, this expression may be written

$$H - p = \frac{1}{2}\rho V^2 \left(1 + \frac{1}{4}M^2 + \dots\right), \quad \dots \quad (5)$$

which, for small values of the Mach number (M) gives the well-known relation

$$H - p = \frac{1}{2}\rho V^2. \quad \dots \quad (6)$$

Provided the Mach number is less than unity, the stagnation pressure measured at the mouth of a pitot-tube placed in a dry airstream is, to a high degree of accuracy, equal to the total head. Difficulty may be experienced in practice, however, in the measurement of static pressure (p) with instruments of the pitot-static type at high Mach numbers because of the formation of shock-waves at the rear of local regions of supersonic velocity ahead of the static holes (Fig. 100).

In 1936, a standard type of pitot-static instrument (Mark VA) with static holes 5·5 diameters behind the nose, and two other instruments one with a pointed nose and static holes 6·7 diameters downstream, and the other with a hemispherical nose and static holes 3·2 diameters downstream were tested in the N.P.L. 1-ft High Speed Tunnel. No error in the measurement of static pressure (as compared with the pressure at a hole in the tunnel wall) was observed up to a Mach number of 0·72.

In 1940, these tests were continued on two Mark VIII instruments (C and D). This type of instrument is of larger diameter than Mark V because electrical heating elements have been added. The tests were extended to a Mach number of about 0·8, and it was found that if the true velocity is given by the expression:

$$H - p' = K \frac{1}{2}\rho V^2 \left(1 + \frac{1}{4}M^2 + \dots\right), \quad \dots \quad (7)$$

where p' is the observed static pressure, the value of the factor K may be expressed in terms of the low-speed correction factor K_0 by the empirical equation

$$K/K_0 = (1 - M^2)^{0.046}, \quad \dots \quad (8)$$

to an order of accuracy of 0·1 per cent up to a Mach number of at least 0·8.

A more comprehensive series of experiments including an investigation of the influence of yaw is described by Walchner in Ref. 206. It is concluded in this paper that up to a Mach number of 0·95 and a yaw of 10 deg, the insertion of the observed pitot and static pressures in equation (5) and taking the expansion up to the term in M^2 would give the velocity correct to ± 1 per cent. The pitot-static instrument of Walchner's experiments was not unlike the Mark VIII instrument tested at the N.P.L.

A further systematic series of tests were made at the N.P.L.²²² in 1943, in which the effects of nose shape and static-hole position were investigated together with the influence of a support downstream and of a bulge similar to that of the Mark VIII (Avimo) A & B type instruments. It was found that up to a Mach number of 0·95 there was no advantage to a pointed nose over a

round nose, and that the standard Mark VIII A & B instruments were satisfactory up to a Mach number of 0.9. The Mark VIII C & D type instruments were found to be unsatisfactory at Mach numbers greater than 0.55 unless the correction described above is applied.

At supersonic speeds a shock-wave will occur ahead of the pitot tube. Provided, however, that the wave is plane and normal to the direction of motion over the region of the pitot orifice, it is still possible to deduce the true total head from an observation of the pressure at the mouth of the pitot-tube by the use of the Rayleigh correction³³. The measurement of static pressure may, however, still prove difficult.

3.2.19. *The Measurement of Surface Temperature.*—Surface-temperature measurements have been made in the 12-in. diameter tunnel on flat plates, circular cylinders, streamline-strut sections, and an aerofoil of N.2030 section. The experimental technique for the latter model is described in Ref. 219, section 2.21, and was similar for the other models. It should be noted that, at the time when these experiments were made, the tunnel intake was from the atmosphere, and all observations are therefore subject to an unknown extent to the influence of the condensation of atmospheric humidity. Such effects were particularly pronounced at the higher tunnel speeds.

Flat Plates.—Experiments with flat plates, streamline struts and circular cylinders were made by Hilton in 1937 and are reported in Ref. 207. For a laminar boundary layer on a thin flat plate placed along the stream Pohlhausen has shown that

$$T - T_1 = -\frac{1}{8} \frac{u^2}{C_p} \beta(\sigma), \quad \dots \dots \dots \quad (9)$$

where T is the free-stream temperature and T_1 the surface temperature, σ is the Prandtl number $\mu C_p/k$, where μ is the viscosity, k the thermal conductivity and C_p the specific heat at constant pressure; u is the velocity outside the boundary layer and $\beta(\sigma)$ depends on a function tabulated by Blasius.

Since it is difficult to measure T , equation (9) is transformed to an expression in terms of T_0 , the stagnation temperature on the assumption of an isentropic expansion up to the working section:—

$$\delta T \equiv T_0 - T_1 = \frac{u^2}{2C_p} \left[1 - \frac{\beta(\sigma)}{4} \right]. \quad \dots \dots \dots \quad (10)$$

Flat plates of 'Tufnol' of 2-in. chord and of thicknesses varying from 1/8 to 5/16 in. were used, the leading and trailing edges being rounded. Thermo-junctions at 1/3 and 2/3 of the chord from the leading edge were used in the experiment. Excellent agreement was obtained between the experimental and theoretical values of the slope of the curve of δT plotted as a function of u^2 for the thermo junction at 1/3-chord, but the experimental value for the 2/3-chord thermo-junction was found to be considerably less than the theoretical value. This is attributed to a transition from laminar to turbulent flow in the boundary layer between the two thermo-junction positions.

Streamline Bars.—Equation (10) was written in the form

$$\delta T = \frac{n^2 u^2}{2C_p} \left[1 - \frac{\beta(\sigma)}{4} \right], \quad \dots \dots \dots \quad (11)$$

where u is the free-stream velocity and nu the local velocity at any point. The models used were of metal, so that the effects of conduction were appreciable, nevertheless good qualitative agreement with theory was obtained at low speeds. As the speed was raised, however, it was found that the linear relationship between δT and u^2 suddenly broke down and for a small range of velocity the slope of the curve changed sign. This phenomenon was attributed to the appearance of a shock-wave on the aerofoil surface and is further discussed in R. & M. 2230²⁰³.

Circular Cylinder.—It was found that the surface temperature at the front of a ‘Tufnol’ cylinder was close to the stagnation temperature and that at the rear only about 10 per cent different from the free-stream static temperature. Thus a circular cylinder placed across the stream is an unsatisfactory shape for the thermometry of moving fluids since the temperature taken up will depend on the thermal conductivity of the cylinder.

NACA 0020.—Squire²¹¹ has shown that for a laminar boundary layer

$$\Delta T = \frac{u^2}{2JC_p} \left[1 - \frac{u_L^2}{u^2} (1 - \sigma^{1/2}) \right], \quad \dots \dots \dots (12)$$

where ΔT is the difference between the surface temperature T_s and the free-stream temperature T , u_L is the local velocity outside the boundary layer, and u the free-stream velocity. Variations of density across the boundary layer are neglected in the derivation of this expression which is, therefore, strictly applicable at low speeds only (say $M < 0.5$). For a turbulent boundary layer the value $\sigma^{1/3}$ is recommended in place of $\sigma^{1/2}$ in the light of previous experimental evidence.

Measurements with the aerofoil model described above have been compared with the expression given by Squire up to high Mach numbers in R. & M. 2230²⁰⁸, despite the strict applicability of the theory to low speeds only. As the model could not be pressure plotted, the local velocity was determined by Goldstein’s theory corrected by the application of the compressibility factor given by von Kármán. The results are expressed in terms of a temperature coefficient C_θ given by

$$C_\theta = \frac{T_s - T}{T_0 - T} = \frac{\Delta T}{T_0 - T} \quad \dots \dots \dots (13)$$

The general conclusion of the experimental work was that owing to the magnitude of the experimental errors (chiefly the effects of humidity) the observations did not confirm or deny the theory. Nevertheless, several points of interest were noted. Fig. 101 shows a typical set of curves for the variation of C_θ along the surface of the aerofoil at varying Mach number. Theoretical temperature distributions for laminar and turbulent boundary layers are added at all Mach numbers below the (first) critical. Since the quantity C_θ will be unity when the surface temperature is equal to the free-stream stagnation temperature, and zero when the surface and free-stream temperatures are equal, positive values of C_θ indicate a heating effect above the local temperature just outside the boundary layer.

It is generally agreed that this dynamic heating effect may prove a major problem in the operation of aircraft at very high speeds, and for completeness Fig. 102 is included to show the variation of stagnation temperature with flight speed, at different altitudes in the standard atmosphere. The problem of dynamic heating is also important in connection with de-icing problems.

The experiments discussed above are described in detail in R. & M. 2230²⁰⁸. It is hoped to repeat the work now that the tunnels have been fitted with return ducts and dry air may be used.

3.3. *Experiments at Supersonic Speeds.*—3.3.1. *Supersonic Tests on Sharp-Nosed Aerofoils.*—Several aerofoils have been tested in the 12-in. diameter and the 5 × 2-in. tunnels at supersonic free-stream Mach numbers.

3.3.1.1. *Tests with 3-component balance.*—2-in. chord models of biconvex (7½ per cent thick), faired double-wedge (8.7 per cent) and double-wedge (6 per cent) section have been tested in the 1-ft diameter tunnel at a Mach number of about 1.4 and some of the thinner sections also at $M = 1.2$. In general, the experimental results for lift are in good agreement with Ackeret’s theory, the experimental drag is somewhat higher than that calculated from theory (due to the skin-friction drag) and the experimental position of the centre of pressure differs slightly from that calculated from the Busemann theory.

The variation of the lift, drag, and quarter-chord pitching-moment coefficients are plotted as functions of incidence at free-stream Mach numbers of 1.25 and 1.46 for the biconvex aerofoil in Fig. 103. Curves of the lift/drag ratio are appended to the lower figure. The centre of pressure position is tabulated in this figure and agrees approximately with that calculated by the Busemann theory. Similar curves for the 8.7 per cent faired double-wedge aerofoil at $M = 1.45$ are given in Fig. 104 and at $M = 1.21$ in Fig. 105. The lift slope is consistent with that for the biconvex aerofoil, but the quarter-chord moment and centre-of-pressure position are not in agreement with theory. The centre-of-pressure position is compared with theory in Fig. 106. Observations with the 6 per cent double-wedge aerofoil are discussed in section 3.3.3 below. The variation of lift and drag coefficient with Mach number for the $7\frac{1}{2}$ per cent biconvex aerofoil over a Mach number range 0.35 to 1.45 is shown in Fig. 107. The Mach number range 0.85 to 1.25 is not attainable in the 1-ft diameter tunnel with a model present, and the curves are therefore broken over this range. Similar curves for the faired double wedge (8.7 per cent) are given in Fig. 108. The variation of the position of the centre of pressure over the same Mach number range is shown in Fig. 109 for the biconvex aerofoil. The lift-curve slope for the faired double-wedge aerofoil is given in Fig. 108.

3.3.1.2. *Pressure-plotting and flow-visualization experiments.*—Two-dimensional tests on two sharp-nosed aerofoils at a supersonic Mach number have been made in the 5×2 -in. tunnel. One aerofoil was of single-wedge section with a semi-angle 3.6 deg, and the other a double-wedge (rhombus) of the same chord (1 in.) and semi-angle. A sketch of the tunnel and one of the aerofoil models is given in Fig. 110. The observations included photography of the wave pattern by a schlieren method, and measurements of the surface and base pressures in the case of the single wedge. This model had seven pressure holes in the surface with a single pressure lead through each supporting pin so that two pressure observations could be made simultaneously, the other pressure holes being sealed. The tests were made over an incidence range -6.5 deg to $+7.5$ deg, the incidence sign being arbitrary for the symmetrical sections.

The tunnel was fitted with effuser liners designed by Bailey and Wood's approximate method¹⁴⁷. This method was known to be unsatisfactory but a more exact calculation would probably have been unjustifiable since the tunnel was not fitted with a drier, and disturbances due to moisture condensation were always present. Because of these condensation effects (which varied with the humidity of the ambient air) the least satisfactory part of the experiment was the determination of the Mach number at the 'test diamond'. Mean values of the wall pressure in this region were used to determine the Mach number, and the value thus obtained (1.40) was in good agreement with that deduced from the inclinations of the humidity waves when they were of small amplitude. The range of aerofoil incidence may be divided, theoretically, into three parts. Thus, if θ is the inclination of the surface to the stream, considered positive when the stream deflection is compressive:—

- (a) $\theta \leq 0$. For this case a Prandtl-Meyer expansion, or simple wave, will occur centered at the leading edge, and the stream will be deflected in the isentropic expansion until its direction is parallel to the surface. In the limiting case $\theta = 0$ no change of stream direction will occur, and the pressure along the surface will be equal to the free-stream pressure.
- (b) $0 < \theta < \psi$, where $\psi = 9.6$ deg for the conditions of the present experiments. For this case a compressive deviation of the stream will occur through a single plane shock-wave attached to the nose.
- (c) $\theta > 9.6$ deg. For this case the shock-wave becomes detached and curved, and the subsequent flow rotational.

Figs. 111, 112 show the observed surface pressures for the single wedge plotted as a function of stream deviation. The method by which the true aerodynamic incidence was found is described in R. & M. 2482⁴⁸ and the values of incidence plotted in Figs. 111, 112 are correct. Curves

calculated on the basis of exact inviscid theory are included in Figs. 111, 112 and it may be seen that the agreement with experiment is excellent over the greater part of surface-inclination range (b).

The pressure is sensibly constant along the chord except in range (c). The reason for this discrepancy is that the flow behind the nose shock-wave is subsonic, and because of the inclination of the aerofoil surface to the stream, the channel between the aerofoil and the tunnel wall is contracting and producing an acceleration. Thus the separation of the pressure curves at different points along the chord in Fig. 112, is an example of subsonic tunnel interference. In range (a), the agreement between theory and experiment is not as good as might have been expected, but here again the discrepancy may be attributed to tunnel interference. In this case the interference arises from the premature breakdown of the flow on the pressure side of the aerofoil; the bow-wave becomes detached and disturbances of the flow on the suction side occur.

The observed base pressure remains roughly constant over the incidence range ± 3 deg, but rises gradually outside this range where it is subject to the wall interference discussed above. The boundary layers of the glass tunnel walls may leak into the aerofoil wake at the base, and the base pressure observations are suspect for this reason. The pressures of Fig. 112 have been used to determine the lift and drag coefficients for the aerofoil. The base pressure is important in evaluating the drag, and, for this purpose, it has been assumed constant over the base; its contribution to the lift is negligible. The experimental values of lift and drag coefficient are plotted in Fig. 113 as a function of incidence.

Above $\alpha = 3$ deg the breakdown of the flow on the pressure side and the consequent modification on the suction side, due to tunnel interference, causes departures from theory. To extend the useful range of the experiment, it was assumed that the good agreement of the theoretical and experimental pressures over the range of θ unaffected by tunnel interference is a sufficient check of the theory. Accordingly the results of Fig. 113 have been extrapolated on the basis of theory along the broken lines shown in the figure. There is no reliable theory of base pressure and the measured base pressure coefficient has been accepted in the calculation of the drag coefficient. At $\alpha = 4$ deg the wave drag and base suction provide equal contributions to the total drag, but at higher incidences the wave drag component is the larger.

The agreement for lift between the exact theory and experiment is excellent, but there is a considerable discrepancy between these values and those obtained by the linearised Ackeret theory. This is of interest since good agreement with Ackeret's theory has been obtained for lift by balance measurements in the 1-ft diameter tunnels on models with fore-and-aft symmetry.

Schlieren photographs were taken with the knife-edge parallel to the chords of the aerofoils, and the angle of the bow-wave to the undisturbed stream was measured at two stations, one close to the nose and the other as far away as possible without crossing the compression waves bounding the test diamond. The results for the single wedge are shown in Fig. 114(a) where the wave angles measured at a distance from the surface are seen to be in good agreement with theory. Photographs of the flow round the single wedge are reproduced in Figs. 115 to 121 and it may be seen that the shock-wave on the suction side never disappears. This has been discussed above in connection with the departure of the surface pressures from theory in range (a). The photographs show the progressive breakdown of the flow on the pressure side with increasing incidence.

The wave angles for the double wedge are shown in Fig. 114(b). The observations here are less consistent than for the single wedge and the curvature of the bow-wave close to the leading edge is less pronounced. The photographs reproduced in Figs. 120 to 129 show that the flow breaks down at an incidence about 3 deg greater than for the single wedge because of the reduced tunnel constriction at the trailing edge. This constriction produces a tunnel interference effect on the pressure side of the aerofoil but, because the position of the bow-wave is changed, the suction side is also affected. The theoretical flow in range (b) is not reproduced, as over an incidence range of several degrees there are two weak shock-waves separated by an expansion. This is attributed to a local separation and re-attachment of the boundary layer (or a thickening of

the boundary layer followed by a thinning) close to the nose. This suggestion is supported by Fig. 129 where it is possible to follow the second shock-wave right up to the surface of the aerofoil a little aft of the nose. In order to obtain a larger-scale picture of the flow at the leading edge, the tunnel breakdown shock-wave was forced slightly ahead of the model (Fig. 130). This flow bears no relation to free-air conditions, but provides a qualitative picture of the flow at the nose behind a normal shock-wave.

3.3.2. Round-Nosed Aerofoils at Supersonic Speeds.—For given thickness and lift, the drag of a sharp-nosed aerofoil at supersonic speeds is less than that of a round-nosed aerofoil. It may, however, be argued that, since at subsonic speeds a sharp-nosed aerofoil may be inefficient, particularly on landing and take-off, an aerofoil with a round nose may be the best compromise for flight at subsonic and low supersonic Mach numbers. Moreover, structural considerations may prohibit the use of a sharp-nosed aerofoil.

In Ref. 215 Hilton describes a series of experiments on conventional round-nosed aerofoils at supersonic speeds. The experiments were made with 2-in. chord models in the 1-ft diameter tunnel using the three-component balance. The models were originally intended for subsonic tests alone, and many of them had been tested very early in the life of the tunnel. They did not, therefore, represent a systematic series of profiles and contained a mixture of aerofoil and propeller sections. Ten aerofoils were tested at $M = 1.4$ ($R = 0.81 \times 10^6$) and of these the two thinnest (4 per cent and 6 per cent) also at $M = 1.2$ ($R = 0.82 \times 10^6$). A 20 per cent aerofoil of 1.2-in. chord was also tested at $M = 1.4$ ($R = 0.49 \times 10^6$) over an extended incidence range.

Both Busemann's and Ackeret's theory break down when the bow-wave becomes detached from the leading edge, and since the bow-wave is always detached from the leading edge of a round-nosed aerofoil, neither theory applied in this case. Hilton²¹⁵ suggested a very simple method of calculating the force coefficients on such an aerofoil. The pressure coefficient at a stagnation point is readily calculated by Rayleigh's formula³³ so that the relation between pressure coefficient and stream deviation is known for the aerofoil over the range of stream deviation from zero up to the value at which the bow-wave becomes detached, and also for a stream deviation equal to a right-angle. Hilton joined the curve of pressure coefficient against stream deviation, calculated within the limits to which Busemann's theory applies, to the calculated pressure coefficient for a stream deviation of a right angle by an arbitrary curve, and showed that the calculated values of the force coefficients are not sensitive to the exact shape of this curve. He thus obtained simple theoretical expressions* for the force coefficients which in most cases were in good agreement with the experimentally measured values.

Fig. 131 shows the measured lift coefficients, and Fig. 132 the corresponding curves for drag coefficient. Fig. 133 shows experimental values for the half-chord pitching moment. The figures shown apply to a Mach number of approximately 1.4. Corresponding curves for $M = 1.2$ are given in Ref. 215.

3.3.3. Controls on Supersonic Aerofoils.—In R. & M. 2101²¹⁴, Lock has used the Busemann relation between stream deviation and pressure to derive equations for the force coefficients on typical two-dimensional supersonic aerofoil sections including the case of an aerofoil fitted with a control. In order to give an experimental comparison with these calculations, and to provide general information on the performance of control surfaces on supersonic aerofoils, experiments were made in the 1-ft diameter tunnel on aerofoil models of 2-in. chord fitted with control surfaces.

Early tests were carried out at a Mach number of 1.4 on a model of EC 1240 with a 40 per cent hinged flap. Later, tests were made with a 6 per cent double-wedge section with both flap and spoiler controls over a small range of Mach number (1.16 to 1.45). The observations on the EC 1240 aerofoil indicated that the loss or reversal of control at high subsonic speeds did not

* Since the present paper was written a number of errors have been discovered in the calculations of Ref. 215. A corrected version of the latter will be circulated as soon as possible.

persist at a supersonic speed, the coefficients a_1 , a_2 , b_2 and m having the same sign at a supersonic speed as at low speeds (notation as in R. & M. 1095). The results of these experiments are reported in Ref. 216.

The work was continued²¹² with a more conventional supersonic aerofoil in the form of a symmetrical double-wedge section of maximum thickness 6 per cent. The control consisted of a 30 per cent flap set at 4 deg to the aerofoil chord as shown in Fig. 134. For comparison, a plain aerofoil without control was also tested, and the model with a control tested in both the normal and reversed position to give information on both leading and trailing-edge flaps. The results were found to agree reasonably well with Lock's theoretical values over the range of incidence and free-stream Mach number in which the theory applies. The limit to the theory occurs when sonic speed is first reached locally at any point in the pressure field of the aerofoil, and this limit is a function of both free-stream Mach number and aerofoil incidence. The limiting values of either incidence or Mach number are usually termed the critical incidence or critical Mach number. As the critical conditions were approached the discrepancy between theory and experiment increased, and this has been attributed to the influence of tunnel interference. Fig. 135 shows the variation of lift coefficient with aerofoil incidence, control angle and Mach number for the trailing edge control and Figs. 136 and 137, show the variation of $(\partial C_L/\partial \alpha)_\eta$ and $(\partial C_m/\partial \alpha)_\eta$ with Mach number. The variation of moment coefficient with incidence, control angle and Mach number is given in Fig. 138, and curves for the drag coefficient in Figs. 139, 140.

A comparison is made in R. & M. 2197²¹² between control by leading and trailing-edge flaps and by an all-moving tailplane on the basis of the drag increase for a given increment of lift. It is concluded that most efficient control is by means of an all-moving tailplane. With the leading edge control the lift slope $\partial C_L/\partial \eta$ is roughly double that for the trailing-edge flap, but the moment changes are considerably less. The results indicate that the performance of the leading-edge control is less influenced by the boundary-layer than the control at the trailing edge. This should permit the prediction of full-scale control performance to be fairly accurate for this type of control. Moreover, wing or tailplane distortion due to control forces cannot lead to reversal with the control at the leading edge. These advantages are, however, offset by the fact that under all conditions the leading-edge control gives rise to unstable stick forces, and the drag for a given lift is higher than with a conventional control.

A further series of experiments²²¹ was made with a spoiler control on the upper surface of the 6 per cent double-wedge aerofoil. The experiments included tests with two different types of spoiler at 0.7 of the chord from the leading edge. Since the problem of control by this method depends on the behaviour of the boundary layer, the low Reynolds number of the experiment must be taken into account when assessing the value of the observations. It appeared that the control forces produced by the presence of the spoiler were small, and that these were accompanied by large drag rises.

The general conclusions which may be drawn from this series of experiments are:

- (a) Normal elevator control may be satisfactorily maintained at supersonic speeds, but the drag rise due to the operation the control is greater than with an all-moving tailplane.
- (b) The normal (trailing-edge) position of the control is more satisfactory than a leading-edge position at supersonic speeds, and both forms of control are preferable to control by spoiler.

3.4. *Miscellaneous Experiments.*—A considerable number of miscellaneous experiments have been made in both the 20 × 8-in. and 12-in. diameter tunnels during the war years at the request of various Service Departments and firms. The major part of this work has not been described in published reports but has been reported direct to the organisation which requested the investigation.

3.4.1. *Body-Wing Combinations*.—A series of tests were made in the 12-in. diameter tunnel at a Mach number of 1.4 on a number of body shapes supported at the centre of a biconvex aerofoil. Conical noses of varying angle were tested, the body itself was cylindrical and symmetrically placed on the aerofoil and was not varied during the experiment. Lift, drag, and pitching moment were measured during the experiment, the drag measurements in particular were not reliable because of the condensation of atmospheric moisture in the working section. A further series of measurements on a G.A.P. model were made on a strain-gauge sting. Lift and moment alone were measured, and this work is reported in Ref. 217.

3.4.2. *Aspect-Ratio Tests*.—A number of flat plates with faired leading and trailing edges and of varying aspect ratio and tip shape have been tested in the 12-in tunnel at a Mach number of 1.4. An aspect-ratio effect of the same order as that predicted by the calculations of R. & M. 2421²²⁰ was observed. These observations have not been published.

3.4.3. *Complete Aircraft Models*.—Measurements on a model of a *Meteor* have already been discussed¹⁸⁹. A model of the E 24/43 Miles supersonic project was tested on a strain-gauge sting in the 12-in. tunnel at a supersonic speed. Lift and moment were measured and the flow pattern was photographed by a ciné-camera. The records of these experiments are in the hands of Miles Aircraft and are unpublished.

3.4.4. *Other Tests*.—Tests have also been made on the resistance of gun barrels placed across the airstream, shells of varying shape, bomb and rocket projectile shapes, wireless aerials and engine cowlings. 'Screaming' bombs of various types have been tested in both tunnels. Fuse elements and manometric fuses have also been tested. An investigation has been made of the flow through and at the exit from gun barrels. Experiments have been carried out to investigate the influence of the boss and blade-root shape on propeller efficiency at high speed.

APPENDIX I

Table of Aerofoils Tested in High-Speed Laboratory, Aerodynamics Division, N.P.L.—
All 'Two-Dimensional'

(NOTE: For explanations see to end of Appendix, p. 175)

(1)	(2)	(3)	(4)	(5)	(6)	(7)	(8)	(9)	(10)	(11)	(12)	(13)	(14)	(15)
Usual Notation	Present Notation when different from (1)	Chord in.	1-ft Tunnel	20 × 8-in. Tunnel	Other Tunnels	Subsonic	Super-sonic	Remarks	Visualiza-tion	Balance	Pressure Plotting	Wake Traverse	Wall Pressures	References
NACA 0012	N1230	2	—	—		—	—	$C_{L \max}$ Including rounded T.E.		—		—	—	6332, 6062, 4715, 7216, 8682, 4713, 9756, R. & M. 2058, R. & M. 2209.
NACA 0015	N1530	2	—	—		—	—	$C_{L \max}$		—		—	—	4738, 6062, 7216, R. & M. 2058.
NACA 0017	N1730	2	—	—		—	—	$C_{L \max}$		—		—	—	4804, 6062, 7216, R. & M. 2058.
NACA 0020	N2030	2	—	—		—	—	$C_{L \max}$ Including yaw		—		—	—	6062, 7216, 9756, 8682, R. & M. 2058, R. & M. 1971.
173 NACA 0020	N2030	1·2	—	—		—	—	$C_{L \max}$		—		—	—	R. & M. 2058, R. & M. 1971.
NACA 2417	N1730/2040	2	—	—		—	—	$C_{L \max}$		—		—	—	5115, 6062, 7216, 6999, R. & M. 2058.
NACA 2218	N1830/2020	2	—	—		—	—	$C_{L \max}$		—		—	—	7234, 8682, R. & M. 2058.
NACA 16/12	N1050/1250	2	—	—		—	—	$C_{L \max}$		—		—	—	9756
NACA 16/15	N0650/1250	2	—	—		—	—	$C_{L \max}$		—		—	—	9756.
NACA 16/16	N1550/1250	2	—	—		—	—	$C_{L \max}$		—		—	—	—
NACA 16/21	N0750/3050	2	—	—		—	—	$C_{L \max}$		—		—	—	9756.
NACA 16/22	N1050/3050	2	—	—		—	—	$C_{L \max}$		—		—	—	9756.
NACA 16/25	N0650/3050	2	—	—		—	—	$C_{L \max}$		—		—	—	—
NACA 16/26	N1550/3050	2	—	—		—	—	$C_{L \max}$		—		—	—	—
NACA 16/32	N1050/3050	2	—	—		—	—	$C_{L \max}$		—		—	—	9756.
NACA 16/35	N0650/4950	2	—	—		—	—	$C_{L \max}$		—		—	—	—
NACA 16/36	N1550/4950	2	—	—		—	—	$C_{L \max}$		—		—	—	—
NACA 16/44	N0450/1950	2	—	—		—	—	$C_{L \max}$		—		—	—	9756.
RAF 31A	R1330/2050	2	—	—		—	—	$C_{L \max}$		—		—	—	8682, 2441, 6062, 7216, 6948, R. & M. 2058.
RAF 69	R2130/1942	2	—	—		—	—			—		—	—	6062, 7203, 2941, R. & M. 2058.
RAF 89	R2530/1942	2	—	—		—	—			—		—	—	7203, 2941, R. & M. 2058.

APPENDIX I—continued

(1)	(2)	(3)	(4)	(5)	(6)	(7)	(8)	(9)	(10)	(11)	(12)	(13)	(14)	(15)
Usual Notation	Present Notation when different from (1)	Chord in.	1-ft Tunnel	20 × 8-in. Tunnel	Other Tunnels	Subsonic	Supersonic	Remarks	Visualization	Balance	Pressure Plotting	Wake Traverse	Wall Pressures	References
RAF 6	R1533/5836	2		—		—		$C_{L \max}$					—	5272, 6532, 7026, 8682, 8041, 5862, 7615, 4726, 7216, 5862, R. & M. 2058.
EC 1240		2	—	—		—		$C_{L \max}$ Including control and brake flaps		—		—	—	
EC 1250		2	—	—		—		$C_{L \max}$		—		—	—	7216, 7278, 8682, R. & M. 2058.
EC 1240/0658		2	—	—		—		$C_{L \max}$		—		—	—	7216, 8682, R. & M. 2058.
EC 1240/0640		2	—	—		—		$C_{L \max}$		—		—	—	7216, 8682, R. & M. 2058.
EC 1250/1050		2	—	—		—				—		—	—	4708, 7216, 4713, R. & M. 2058.
EQH 1550		2	—	—		—		$C_{L \max}$		—		—	—	7216, 8682, R. & M. 2058.
EQH 1550/1058		2	—	—		—		$C_{L \max}$		—		—	—	7216, R. & M. 2058.
EQH 1250/1050		2	—	—		—		$C_{L \max}$		—		—	—	7216, R. & M. 2058.
EQH 1250/0640		2	—	—		—		$C_{L \max}$		—		—	—	7216, R. & M. 2058.
P 2040		2	—	—		—		$C_{L \max}$ Including yaw		—		—	—	4800, 6062, 7216, 8718, R. & M. 2058.
P 1240		2	—	—		—				—		—	—	4164.
G 1540/2037		2	—	—		—		$C_{L \max}$		—		—	—	7209, 7216.
H 1222	H1222/4022	2	—	—		—				—		—	—	3238, 6062.
H 1222		2	—	—		—				—		—	—	
Bristol Wing	B1430/1944	2	—	—		—				—		—	—	8960, 9203.
Double Wedge		2	—	—		—				—		—	—	
Faired														
Double Wedge	08 $\frac{1}{2}$ 50	2	—	—		—				—		—	—	R. & M. 2057.
Single Wedge	06.100	2	—	—		—				—		—	—	
Biconvex	07 $\frac{1}{2}$.50	2	—	—		—		$C_{L \max}$		—		—	—	7705.
Clark Y*	C0633/3033	2	—	—		—				—		—	—	6062.
Clark Y*	C0733/3533	2	—	—		—		$C_{L \max}$		—		—	—	
EC 1250		5	—	—		—		$C_{L \max}$ Including control and brake flaps	—	—		—	—	6378, 6662, 7067, 7176, 7278, 6378, 6662, R. & M. 2065, R. & M. 2067, R. & M. 2055, R. & M. 2079.

APPENDIX I—continued

(1)	(2)	(3)	(4)	(5)	(6)	(7)	(8)	(9)	(10)	(11)	(12)	(13)	(14)	(15)
Usual Notation	Present Notation when different from (1)	Chord in.	1-ft Tunnel	20 × 8-in. Tunnel	Other Tunnels	Subsonic	Super-sonic	Remarks	Visualiza-tion	Balance	Pressure Plotting	Wake Traverse	Wall Pressures	References
EC 1250		12		—		—		Transition Fixing	—			—		7278, R. & M. 2106.
NACA 2218	N1830/2020	5		—		—		C_z max	—			—		R. & M. 2093.
NACA 16/42	N1050/1650	5		—		—			—		—	—		
Mustang	14 $\frac{1}{2}$ 40/1241	5		—		—			—		—	—		8135.
G 1442/1547		5		—		—			—		—	—		9585.
Griffith	2245			—		—		Suction	—		—	—		10096.
NACA 0020	N2030	2			5 × 2 in.	—		Suction	—		—	—		R. & M. 1913.
H 1222		2			5 × 2 in.	—			—					
Double Wedge	0650	1			5 × 2 in.		—		—					10607.
Single Wedge	06.100	1			5 × 2 in.		—		—					10607.
EC 1250		0.35			2 $\frac{1}{4}$ -in.	—		Influence on Tunnel Performance	—		—			7812, 9490.
Double Wedge	0650	0.35			2 $\frac{1}{4}$ in.		—		—					8138, 9490.

175 Notation

(i) Aerofoil Notation .. abcd/efgh represents an aerofoil of maximum thickness ab per cent of the chord and situated at cd per cent of the chord from the leading edge. The maximum centre-line camber is ef per cent of the chord and occurs at gh per cent of the chord from the leading edge. The numerals are preceded by a number of letters which indicate the method by which the aerofoil was designed or the series to which it belongs. Thus:—

N = N.A.C.A. : R = R.A.F. : P = Piercy : G = Goldstein : B = Bristol : H = Hilton : C = Clark Y : EC = Elliptic nose, cubic tail on basic profile : EQH = Elliptic nose, quartic intermediate region, hyperbolic tail on basic profile.

(ii) Reference Notation .. R. & M. indicates that the report has been published as a Report and Memoranda of the Aeronautical Research Council. Other references are given as A.R.C. numbers unless otherwise stated.

* indicates camber-line referred to flat undersurface.

— indicates that tests have been made.

APPENDIX II

Reference List of Compressibility Reports by the Staff of the High Speed Laboratory and Others at the Aerodynamics Division, N.P.L., June, 1947

CONTENTS

1. *Development of N.P.L., H.S.T., Equipment and Technique.*
 - 1.1 General Progress.
 - 1.2 Flexible Walls.
 - 1.3 Mach Number Gauge.
 - 1.4 Strain Gauges.
 - 1.5 Pressure-Plotting Method.
 - 1.6 Drag by Wake-Transpose Method.
 - 1.7 Photographic Technique.
 - 1.8 Transition Indication.
 - 1.9 Humidity.
 - 1.10 Turbulence by Spheres.
 - 1.11 Experiments on Tunnel Design, etc.
2. *General Research (Subsonic).*
 - 2.1 Theory, Tests of Theory, etc.
 - 2.1.1 Wing forces.
 - 2.1.2 Approximation of von Kármán's formula.
 - 2.1.3 Shock-waves.
 - 2.1.4 Tunnel interference.
 - 2.1.5 Sweepback.
 - 2.1.6 Pitching-moment derivatives.
 - 2.2 Comparison with Other Tunnels and Flight.
 - 2.3 Boundary-Layer Suction.
 - 2.4 Fixing Transition.
 - 2.5 Wires on Leading Edge.
 - 2.6 Thermal Effects.
 - 2.7 Noise Effects from an Aerofoil.
 - 2.8 Circular Cylinders.
 - 2.9 Reynolds Number and Mach Number Effects.
3. *Results (Subsonic).*
 - 3.1 General.
 - 3.2 Aerofoil Sections.
 - 3.2.1 C_L and C_M of 2-in. chord by balance.
 - 3.2.2 C_L and C_M of 2-in. chord by pressure plotting.
 - 3.2.2a Maximum C_L by wall pressure.
 - 3.2.3 C_D of 2-in. chord by balance.
 - 3.2.4 C_D of 2-in. chord by wake traverse.
 - 3.2.5 C_D of 5-in. chord by wake traverse.
 - 3.2.6 Controls.
 - 3.2.7 Spoilers.
 - 3.2.8 Cut off trailing edge.
 - 3.2.9 Fin on tailplane.
 - 3.2.10 Yaw (sweepback).
 - 3.2.11 Pressure distributions.
 - 3.3 Airscrew Blade Roots.
 - 3.4 Brake Flaps.
 - 3.5 Drag of Three-Dimensional Bodies.
 - 3.6 Pressure Heads.

4. *Supersonic Work.*

- 4.1 Supersonic Tunnel Design.
- 4.2 Supersonic Theory.
- 4.3 Supersonic Tunnel Experiments.
- 4.4 Supersonic Tests in 1-ft Tunnel.
- 4.5 Other Supersonic Work.

5. *Miscellaneous.*

- 5.1 Comments on Other Work, etc.
- 5.2 Tables.

Subject	Author	A.R.C.	R. & M.	Date
<i>1. Development of N.P.L. High-Speed Tunnels, Equipment and Technique</i>				
<i>1.1. General Progress</i>				
Programme	Lock, Hilton	2282		2/36
Development of Rectangular Tunnel	Gough	2721		11/36
Programme	Hilton	3072		6/37
Problems of High-Speed Flight	Lock	<i>J.R.Ae. Soc.</i>		3/38
Further Development of Rectangular Tunnel	—	3269		11/37
Preliminary Design for Supersonic Tunnel	Lock, Collar, Goldstein	—		12/39
Interim Report	Lock, Hilton, Beavan	4343		2/40
Interim Report on Rectangular Tunnel	Beavan, Hyde	5622	2067	2/42
16 in. Supersonic Tunnel	Hilton	8080		10/44
Projected 18 × 14 in. Tunnel	Staff of H.S.T.	8545		3/45
Programme for West Aero. Tunnels	Lock, Beavan, Hilton	—		1/46
Research Programme of Aero. Division N.P.L.	—	9138		2/46
Proposed West Aero. Tunnels	Fage, Lock	9531		4/46
New Equipment in Aero. Division	Fage	10204		12/46
Aerofoil Programme at N.P.L.	Beavan, Williams	10551		5/47
<i>1.2. Flexible Walls</i>				
Interim Report on Rectangular Tunnel	Beavan, Hyde	5622	2067	2/42
Comp : Increase of Lift and Moment of EC 1250	Beavan, Hyde	6130	2055	9/42
Wall Interference in Rectangular Tunnel	Lock, Beavan	8073	2005	9/44
Limiting Speeds in Rectangular Tunnel	Beavan	8720		5/45
<i>1.3. Mach Number Gauge</i>				
	Giles	8797	2131	7/45
<i>1.4. Strain Gauges</i>				
	Wingham	8723	2316	6/45
<i>1.5. Pressure-Plotting Method</i>				
Measurements on EC 1250 with convex Control	Beavan, Hyde, Fowler	8395	2065	2/45
<i>1.6. Drag by Wake-Traversal Method</i>				
Profile Drag by Pitot Traverse	Lock	2826		1/37
Profile Drag by Pitot Traverse	Lock, Hilton, Goldstein	4709	1971	9/40
Tables	Beavan, Manwell	5326	2233	9/41
N.P.L. and U.S.A. Methods	Beavan	6658	2102	4/43
<i>1.7. Photographic Technique</i>				
Spark Photography in the Rectangular Tunnel	Hilton	5628		2/42
Observations on Wedges (Supersonic)	Valensi, Pruden		2482	
<i>1.8. Transition Indication</i>				
	Holder	8866	2079	7/45

* = Definitely to be published, R. & M. number not yet allotted.

† = In preparation.

Subject	Author	A.R.C.	R. & M.	Date
1.9. Humidity				
Effect of Condensation	Hilton, Wingham ..	6097		9/42
Effect of Condensation	Pearcey	7482	2249	2/44
Pitot and Static Readings with Condensation	Lock	8455	2249	2/45
Addendum to 7482	Pearcey	8456	*	2/45
Return Ducts to give Dry Air	Pearcey	†		
1.10. Turbulence Measurements with Spheres				
	Hyde	6086	1959	9/42
1.11. Experiments on Tunnel Design, etc.				
2½-in. Tunnel Interim Report	Knowler	7563	2448	3/44
Diffusers at high M and R	Lock	7640		4/44
Cascades in 2¼-in. Diffuser	Knowler	7756		7/44
Model Effect on Power Factor in 2¼-in. Tunnel	Knowler	7812		6/44
2¼-in. Tunnel	Knowler	8024	2448	9/44
2¼-in. Tunnel at $M = 1.45$	Knowler, Holder	8138		10/44
Diffusers	Knowler, Holder	8394		2/45
Addendum to 8394	Knowler, Holder	8668		5/45
Scale Effects on Tunnel Efficiency	Knowler, Holder	8669	2448	5/45
Supersonic Nozzle Design, Part I	Atkin	9194	2174	4/46
Injector Slots	Knowler, Holder	9490	2448	3/46
Running Time of Injector Tunnels	Holder	9902		8/46
2. General Research (Subsonic)				
2.1. Theory, Tests of Theory, etc.				
2.1.1. Wing Forces				
Glauert Effect on Lift	Hilton	3238		10/37
Effect of Thickness Ratio	Hilton	4646		7/40
Tapered Wing	Lock, Preston	5254		8/41
Lift and Moments at High Speeds	Richards	6159	2052	9/42
Empirical Formula for Moments	Hilton	6529	2195	3/43
Approximate C_M from C_L for low-drag aerofoil	Hilton	6636		4/43
Comparison of C_M Formula with R.A.E. Results	Hilton	7014	2195	4/43
Lift in the Transonic Region	Hilton	10421	2460	3/47
Negative Camber for Uniform Lift	Hilton	10452		6/47
2.1.2. Approximation of von Kármán's formula				
	Lock, Atkin	†		
2.1.3. Shock-Waves				
Problems of High-Speed Flight	Lock		<i>J.R.Ae. Soc.</i>	3/38
Possibility of Shock-Wave Obs. on Aircraft	Hilton	4204		9/39
Nature of the Shock-Stall	Relf	5542		12/41
Ideal Drag Due to Shock-Wave	Lock	5852	2512	6/42
Ideal Drag of a Shock from Experiment	Monaghan, Fowler	8286		11/44
Pitot Readings near a Shock-Wave	Fowler	8393	2468	2/45
Ideal Drag Due to Shock-Wave, Part II	Lock	8458	2512	2/45
Shock and Boundary-Layer Experiments	Fage, Sargent	8964	Ext.*	9/45
Summary and Comments on Tsien's Theory	Beavan	9550		4/46
(Second Critical Mach Number)	Beavan	9787		7/46
Ditto	Lock, Beavan, Pearcey	Paris		9/46
		Conference		
Plane Shock-Wave Formulae	Lock	N.P.L./Aero. 148		11/46
Photographs and Pressures on Goldstein I	Pearcey	†		
Photographs of Shock-wave and Boundary-Layer Oscillation.	Hilton and Fowler	11190	2692	12/47

Subject	Author	A.R.C.	R. & M.	Date
<i>2.1.4. Tunnel Interference</i>				
Profile Drag by Wake Traverse	Lock, Hilton, Goldstein	4709	1971	9/40
Linear-Perturbation Theory	Goldstein, Young	6865	1909	9/43
Wall Interference in the Rectangular Tunnel	Lock, Beavan	8073	2005	9/44
Limiting Speeds in the Rectangular Tunnel	Beavan	8720		5/45
Comparison of Various Formulae for Interference	Holder, Rogers	†		
<i>2.1.5. Sweep Back</i>				
Yaw and Sweep Back at high M	Lock, Fowler	8718		5/45
Sweep-Back Drag—Original German Tests	Beavan	9564		4/46
Yawed Aerofoil Tests	Beavan, Bumstead	10730	2458	7/47
<i>2.1.6. Pitching-Moment Derivatives</i>				
	Bratt, Chinneck	10710		7/47
<i>2.2. Comparison with Other Tunnels and Flight</i>				
Drag of NACA 2218 compared with Flight	Pearcey	6661	2093	4/43
Pressure Distribution and Drag of Mustang Model	Thompson, Marcowicz	8135	2251	8/44
	Beavan, Fowler			
<i>2.3. Boundary-Layer Suction</i>				
Suction Behind Shock-Waves	Page, Sargent	7153	1913	10/43
Addendum to 7153	Page, Sargent	7365	1913	1/44
Design of Suction Slots, Part I	Page, Sargent	7480	2127	2/44
Design of Suction Slots, Part II	Page, Sargent	8565	2127	1/45
Suction on Griffith Aerofoils	Pearcey, Rogers	10096	2511	11/46
<i>2.4. Fixing Transition</i>				
Drag with Wires and Grooves	Pearcey	6999	2252	8/43
Drag with Wires on EC 1250 12-in. chord	Pearcey	7278	2252	12/43
Fixing Transition by Blowing through Slots	Page, Sargent	7800	2106	6/44
<i>2.5. Wires on Leading Edge</i>				
	Pruden	6948		8/43
<i>2.6. Thermal Effects</i>				
Temperature in the Wake of an Aerofoil	Lock, Hilton	3647		7/38
Thermal Effects on Bodies	Hilton	2311		3/36
Ditto	Hilton	3458	Royal Soc., Vol. 168	3/38
Effect of Condensation on Temperature Measurements	Hilton	6097		9/42
Temperature Measurement in High-Speed Flow	Pearcey and others	7437		2/44
Effects of Condensation on Temperature Measurements	Pearcey	7482	2249	5/44
Surface Temperature Measurements on an Aerofoil	Hilton, Wingham	9322	2230	1/46
<i>2.7. Noise Effects from an Aerofoil, with Wires</i>				
	Hilton	3540	Phil. Mag., Vol. 30 (1940)	5/38
<i>2.8. Circular Cylinders</i>				
	Knowler, Pruden	7483	1933	2/44
<i>2.9. Reynolds Number and Mach number Effects</i>				
Pressures on EC 1250 Tail	Beavan	7067	2252	10/43
EC 1250 2, 5, 12-in. chord	Pearcey	7278	2252	12/43

Subject	Author	A.R.C.	R. & M.	Date				
3. Results (Subsonic)								
3.1. General								
Lecture to <i>R. Ae. Soc.</i>	Lock	<i>J.R. Ae. Soc.</i>		3/38				
Articles in ' <i>Aeroplane</i> '	Hilton	<i>Aeroplane</i>		4/44				
3.2. Aerofoil Sections								
3.2.1. Lift and Pitching Moment of 2-in. chord Aerofoils by Balance								
RAF 31a, 69	} Hilton	(6062) (6528)	2058	8/42				
NACA 0012, 0015, 0017, 0020, 2417								
EC 1240, 1240/0640, 1240/0658								
EC 1250, 1250/0640, 1250/1050								
EQH 1550, 1550/1508								
Clarke Y 6 per cent	} Hilton	7203	*	12/43				
Piercy 2040								
RAF 69, 89								
NACA 2218								
GR 1540/2037								
Propeller Aerofoils								
Double-Wedge Aerofoil (and supersonic)					Hilton, Pruden	7277	2057	12/43
3.2.2. Lift and Pitching Moment of 5-in. chord Aerofoils by Pressure Plotting								
EC 1250					Beavan, Hyde	6130	2055	9/42
Mustang Section					R.A.E., Beavan, Fowler	8135	2251	8/44
Goldstein Roof-Top I (1442/1547)	Pearcey, Beavan	9585	2346	4/46				
NACA 16 Propeller Section 10 per cent	Rogers	11114						
3.2.2a. Maximum Lift by Wall Pressures								
.. .. .	Beavan	{ 11084 11102 }	2678	1/48				
3.2.3. Drag of 2-in. chord Aerofoils by Balance								
RAF 31a	} Hilton	7216	2058	11/43				
NACA 0020								
EC 1240, 1240/0658								
EC 1250, 1250/0640, 1250/1050								
EQH 1550								
RAF 69, 89	} Hilton	7203	*	12/43				
NACA 0012								
NACA 0015								
NACA 0017								
NACA 2218								
NACA 2417								
EC 1240								
EC 1240/0640								
Piercy 2040								
GR 1540/2037								
Propeller Aerofoils	Hilton, Pruden, Hyde	5115		5/41				
3.2.4. Drag of 2-in. chord Aerofoils by Wake Traverse								
RAF 31a, 69, 89	} Lock, Hilton	2941		4/37				
NACA 0012, 0020								
NACA 2417	} Pearcey	6999	2252	8/43				
RAF 31a								
NACA 0012, 0020, 2218	} Beavan	8682		5/45				
EC 1240, 1240/0640, 1240/0658								
EC 1250								
EQH 1550								

Subject	Author	A.R.C.	R. & M.	Date
3.2.5. Drag of 5-in. chord Aerofoils by Wake Traverse.				
EC 1250	Beavan, Hyde	5622	2067	2/42
NACA 2218	Pearcey	6661	2093	4/43
NACA 2218, EC 1250	Pearcey	6999	2252	8/43
Mustang Section	R.A.E., Beavan, Fowler	8135	2251	8/44
Rise of Drag above M_{crit}	Beavan	8682		5/45
Goldstein Roof-Top I (1442/1547)	Pearcey, Beavan	9585	2346	4/46
NACA 16 Propeller Section 10 per cent	Rogers	11114		
3.2.6. Aerofoils with Controls				
2-in. chord EC 1240 with 40 per cent control	Hilton, Knowler	5272	*	8/41
Ditto	Hilton, Knowler	6532	*	3/43
Ditto (gap sealed)	Hilton, Knowler	7026	*	9/43
Ditto (gap sealed)	Hilton, Knowler	8041	2227	9/44
5-in. chord EC 1250 with 25 per cent convex control (advance note).	Beavan, Hyde, Fowler ..	7176	2065	11/43
Ditto	Beavan, Hyde, Fowler ..	8395	2065	2/45
3.2.7 Aerofoil with Spoiler				
22½ per cent Aerofoil	Wingham	7570	2319	3/44
6 per cent Double Wedge (also supersonic)	Pruden	9203		
3.2.8. Cut-off Trailing Edge				
NACA 0012	Sargent	6332	2209	11/42
3.2.9. Fin on Tailplane				
	Hilton, Moore, Sargent	5116	2138	5/41
3.2.10. Yawed Aerofoil Drag				
Peircey 2040	Lock, Fowler	8718	*	5/45
Peircey 2040, NACA 0020	Beavan, Bumstead	11102		
3.2.11. Pressure Distribution				
EC 1250	Beavan, Hyde	6146	2056	9/42
EC 1250 with 25 per cent convex Control	Beavan, Hyde, Fowler ..	8395	2065	2/45
Mustang Section	R.A.E., Beavan, Fowler	8135	2251	8/44
Goldstein Roof-Top I (1442/1547)	Pearcey, Beavan	9585	2346	4/46
NACA 16 Propeller Section 10 per cent	Rogers	11114		
Further EC 1250	Beavan, Hyde	10729	2625	7/47
3.3. Airscrew Blade Roots. Drag				
	Lock, Hilton, Hyde	4736	*	10/40
3.4. Brake Flaps				
On EC 1240 2-in. chord	Knowler, Pruden	5862	2211	3/43
On EC 1250 5-in. chord inc. pressures	Pruden	6378	2211	1/43
Ditto	Pruden	6662		4/43
3.5. Drag of Three-Dimensional Bodies				
Windscreens	Lock, Hilton, Beavan, Hyde, Moore.	3608 4640	2235	6/38 7/40
3.6. Pressure Heads				
Calibration of Standard	Lock, Hilton	2558	1752	8/36
Calibration of Mark VIII A.S.I.	H.S.T. Staff	4795		11/40
Static Heads	Lock, Knowler, Pearcey	6420	2386	1/43

Subject	Author	A.R.C.	R. & M.	Date
<i>4. Supersonic Work</i>				
<i>4.1. Supersonic Tunnel Design</i>				
Preliminary Design for N.P.L.	Lock, Collar, Goldstein			12/39
Proposed 16-in.	Hilton	8080		10/44
Projected 18 × 14 in.	H.S.T. Staff	8545		3/45
Supersonic Nozzle Design, Part I	Atkin	9194	2174	4/46
Proposed West Aero. Tunnels	Fage, Lock	9531		4/46
Running Times of Injector Tunnels	Holder	9902	2448	8/46
<i>4.2. Supersonic Theory</i>				
Supersonic Flight	Relf	6760		6/43
Two-Dimensional Aerofoil Theory	Lighthill	7384	1929	1/44
Conditions behind Trailing Edge of Aerofoil	Lighthill	7412	1930	1/44
Addendum to 7384	Lighthill	7571	1929	3/44
Examples of Busemann's Formula	Lock	8027	2101	9/44
Limitation of Busemann's 2nd order Theory	Hilton	9869	2524	8/46
<i>4.3. Supersonic Tunnel Experiments</i>				
Two-Dimensional Interference	Hilton	7307	2332	1/44
2½-in. Tunnel at $M = 1.45$	Knowler, Holder	8138		10/44
Diffusers	Knowler, Holder	8394		2/45
Addendum to 8394	Knowler, Holder	8668		5/45
Explorations of Two Tunnels	Holder, Burrows	8670	2448	5/45
Scale Effect on Efficiency	Knowler, Holder	8669		5/45
Injector Slots	Knowler, Holder	9490		3/46
Supersonic Running of Rectangular Tunnel	Hilton, Fowler	N.P.L./ Aero 138		3/46
<i>4.4. Supersonic Tests in 1-ft Circular Tunnel</i>				
Three Aerofoils	Hilton, Pruden	7308		1/44
Aerofoil with Elevator EC 1240	Pruden	7615	*	4/44
Biconvex Aerofoil 7½ per cent	Hilton	7705	2196	5/44
Double Wedge 8·7 per cent	Hilton, Pruden	7277	2057	12/43
Ditto	Hilton	7703	2057	5/44
Ditto with Flap 6 per cent	Pruden	8960	2197	9/45
Ditto with Spoilers 6 per cent	Pruden	9230		
Round-Nosed Aerofoils	Hilton	9756	*	6/46
Body-Wing	Wingham	8229	2771	12/44
Ram jet	Pruden	11361	2568	5/47
Spoiler Controls	Pruden	9203		12/45
Downwash Measurements	Hilton, Bumstead	10779		
<i>4.5. Other Supersonic Work</i>				
Some observations on 7·2 deg Wedges in 5 × 2-in. Tunnel	Valensi, Pruden	10607	2482	5/47
<i>5. Miscellaneous</i>				
<i>5.1. Comments on Other Work, etc.</i>				
N.P.L. and U.S.A. Wake-Traversal Calculation Methods	Beavan	6658	2102	4/43
Temperature Measurements in High-Speed Flow	Pearcey	7437		2/44
Comparison with Greene's Theory	Pearcey, Fowler	8542		3/45
Interrogation of Dr. Göthert (D.V.L.)	Lock, Holder	8880		8/45
Visit to Germany	Beavan	9066		10/45
Summary and Comments on Tsien report	Beavan	9550		4/46
<i>5.2. Tables for Compressible Flow</i>				
Index	Atkin	9893		8/46
Wake-Traversal Calculation	Lock, Hilton, Goldstein	4709	1971	9/40
Ditto	Beavan, Manwell	5326	2233	9/41

REFERENCES

- | No. | Author | Title, etc. |
|-----|------------------------------------|---|
| 1. | Durand | <i>Aerodynamic Theory</i> . Vol. I, Divn. A. Julius Springer. |
| 2. | Bairstow | <i>Applied Aerodynamics</i> . 2nd Edn., Chap. VI. Longmans, Green & Co. |
| 3. | Rayleigh | Note as to the Application of the Principle of Dynamic Similarity. R. & M. 15. 1909. |
| 4. | Durand | <i>Aerodynamic Theory</i> . Vol. III, Divn. I. Julius Springer. |
| 5. | Durand | <i>Aerodynamic Theory</i> . Vol. III, Divn. G. Julius Springer. |
| 6. | Goldstein (editor) | <i>Modern Developments in Fluid Dynamics</i> . Vol. I, Chap. I. Oxford University Press. |
| 7. | Reynolds | <i>Phil. Trans.</i> , 174, pp. 935-982. 1883. |
| 8. | Durand | <i>Aerodynamic Theory</i> . Vol. III, Divn. H. Julius Springer. |
| 9. | Bairstow | <i>Applied Aerodynamics</i> . 2nd Edn., Chap. X. Longmans, Green & Co. |
| 10. | Relf | Preliminary Note on the Nature of the 'Shock Stall'. A.R.C. 5542. (Unpublished.) |
| 11. | Fage and Sargent | Shock Wave and Boundary Layer Phenomena Near a Flat Surface. <i>Proc. Roy. Soc., A</i> , Vol. 190, 1947. A.R.C. 8964. |
| 12. | Ackeret, Feldmann and Rott | Investigations on Compression Shocks and Boundary Layers in Fast Moving Gases. Institute for Aerodynamics, E.T.H., Zurich, No. 10. A.R.C. 10,044. |
| 13. | Liepmann | The Interaction between Boundary Layer and Shock Waves in Transonic Flow. <i>J. Aero. Sci.</i> , Vol. 13, No. 12, pp. 623-637. December, 1946. |
| 14. | Donaldson | Effects of Interaction between Normal Shock and Boundary Layer. N.A.C.A. Confidential Bulletin. A.R.C. 7686. (Unpublished.) |
| 15. | Gunn | Relaxation Time Effects in Gas Dynamics. R. & M. 2338. April, 1946. |
| 16. | Kantrowitz | Heat Capacity Lag in Gas Dynamics. N.A.C.A. A.R.R. 4A22. |
| 17. | Goldstein | On Behaviour of Dry Air in a Supersonic Wind Tunnel. R. & M. 2337. April, 1946. |
| 18. | Ruhemann | <i>The Separation of Gases</i> . Oxford University Press. |
| 19. | Smelt | Proposed Programme of Work on the Drag of Aerofoils near the Speed of Sound by Measurements on Falling Bodies. A.R.C. 7817. (Unpublished.) |
| 20. | Smelt | A Critical Review of German Research on High Speed Airflow. <i>J.R. Ae. Soc.</i> , Vol. 50, No. 432. December, 1946. |
| 21. | — | Notes on the Interrogation of Dr. Göthert. A.R.C. 8880. (Unpublished.) |
| 22. | Bailey | Drag Measurements at Transonic Speeds on Freely Falling Bodies. N.A.C.A., A.C.R. No. 25 E03. A.R.C. 9234. (Unpublished.) |
| 23. | Lock and Beavan | Tunnel Interference at Compressibility Speeds Using the Flexible Walls of the Rectangular High Speed Tunnel. R. & M. 2005. September, 1944. |
| 24. | Hilton | Note on Two-Dimensional Supersonic Tunnel Interference. R. & M. 2332. December, 1943. |
| 25. | Holder | The N.P.L. High Speed Laboratory. Part II. Experimental Technique. (Part II of this Report.) |
| 26. | Holder | The N.P.L. High Speed Laboratory. Part III. Review of Experimental Results. (Part III of this Report.) |
| 27. | Thompson | Formulae and Tables for Calculating Compressible Flow. A.R.C. 8635. (Unpublished.) |
| 28. | Sutherland | <i>Phil. Mag.</i> , 31. 1893. |
| 29. | Cope | Law of Variation of Viscosity and Prandtl Number of Air at Low Temperature. A.R.C. 9287. (To be published.) |
| 30. | Taylor | The Flow of Air at High Speeds past Curved Surfaces. R. & M. 1381. |
| 31. | Hooker | The Flow of a Compressible Fluid in the Neighbourhood of the Throat of a Constriction in a Circular Wind Channel. R. & M. 1429. |
| 32. | Sauer | Flow Through Nozzles in Neighbourhood of Critical Velocity. A.R.C. 9449. (Unpublished.) |

No.	Author	Title, etc.
33.	Rayleigh	Aerial Plane Waves of Finite Amplitude. <i>Proc. Roy. Soc., A</i> , 1, XXXIV, 247. 1910.
34.	Lamb	<i>Hydrodynamics</i> . 6th Edn., Chap. X. Cambridge University Press.
35.	Hilton	Thermal Effects on Bodies in an Airstream. <i>Proc. Roy. Soc., A</i> , Vol. 168. 1938.
36.	Hilton and Wingham	Surface Temperatures on an Aerofoil at Subsonic Speeds. R. & M. 2230. January, 1946.
37.	—	—
38.	Lukasiewicz	Supersonic Diffusers. R. & M. 2501. June, 1946.
39.	Stanton	A High Speed Wind Channel for Tests on Aerofoils. R. & M. 1130.
40.	Hankins and Cope	The Flow of Gases at Sonic and Supersonic Speeds. <i>Inst. Mech. Eng. App. Mech.</i> , Vol. 155, p. 401. 1946.
41.	Stanton	On the Effect of Air Compression on Drag and Pressure Distribution on Cylinders of Infinite Aspect Ratio. R. & M. 1210. November, 1928.
42.	Stanton	Tests under Conditions of Infinite Aspect Ratio on 4 Aerofoils in a High Speed Wind Channel. R. & M. 1279.
43.	Grant	Making a Compressed Air Tunnel. <i>Aircraft Engineering</i> , Vol. 3, p. 93. 1931.
44.	Stack	The N.A.C.A. High Speed Wind Tunnel and Tests of Six Propeller Sections. N.A.C.A. Tech. Report 463.
45.	Jacobs and Abbott	The N.A.C.A. Variable Density Wind Tunnel. N.A.C.A. Tech. Reports 227 and 416.
46.	Gough	Development of Rectangular High Speed Tunnel. A.R.C. 2721. (Unpublished.)
47.	Fage and Sargent	Effect on Aerofoil Drag of Boundary Layer Suction Behind a Shock Wave. R. & M. 1913. October, 1943.
48.	Valensi and Pruden	Some Observations on Sharp Nosed Profiles at Supersonic Speed. R. & M. 2482. May, 1947.
49.	Staff of H.S.T.	The New 18 in. × 14 in. High Speed Tunnel. A.R.C. 8545. (Unpublished.)
50.	Thompson and Mair	The R.A.E. High Speed Tunnel and a Review of the Work Accomplished in 1942-1945. R. & M. 2222. September, 1946.
51.	Göthert and Matt	The D.V.L. High Speed Wind Tunnel. R.A.E. Library Translation, No. 63. A.R.C. 9149. (Unpublished.)
52. } 53. }	Holder and Knowler	The Efficiency of High Speed Wind Tunnels of the Injector Type. With an Appendix: The Efficiency of Intermittent Operation from Compressed Air Storage. R. & M. 2448. December, 1948.
54.	Crocco	High Speed Wind Tunnels. <i>L'Aerotecnica</i> , No. 3, March, 1935. A.R.C. 1915 and 1915a.
55. } 56. } 57. }	—	See Refs. 52 and 53.
58.	Goldstein	Experiments on Diffuser Design at G.A.L.C.I.T. A.R.C. 7400. (Unpublished.)
59.	Patterson	Modern Diffuser Design. <i>Aircraft Engineering</i> , Vol. X, No. 115, p. 265. September, 1938.
60. } 61. } 62. }	—	See Refs. 52 and 53.
63.	Ackeret	High-Speed Wind Tunnels. N.A.C.A Tech. Memo. No. 808. A.R.C. 8239. (Unpublished.)
64.	Stodala	<i>The Steam Turbine</i> . Constable & Co. 1905.
65.	Cheers	Note on Wind Tunnel Contractions. R. & M. 2137. March, 1945.
66.	Salter	Experiments on Thin Turning Vanes. R. & M. 2469. October, 1946.
67.	Goldstein (editor)	<i>Modern Developments in Fluid Dynamics</i> , Vol. 1, p. 255. Oxford University Press.

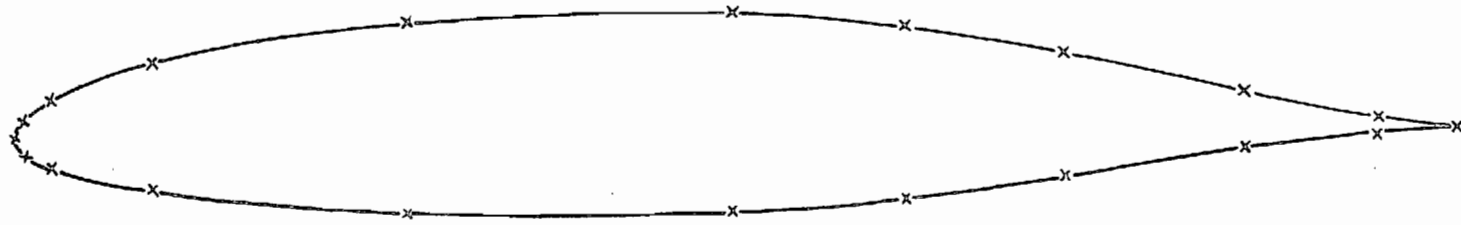
No.	Author	Title, etc.
68.	Cambridge University Aeronautics Laboratory.	The Measurement of Profile Drag by the Pitot Traverse Method. R. & M. 1688. January, 1936.
69.	Lock, Hilton and Goldstein ..	Determination of Profile Drag at High Speeds by a Pitot Traverse Method. R. & M. 1971. September, 1940.
70.	Young	Note on the Effect of Compressibility on Jones' Momentum Method of Measuring Profile Drag. R. & M. 1881. February, 1939.
71.	Young	Note on Momentum Methods of Measuring Profile Drags at High Speeds. R. & M. 1963. February, 1940.
72.	Lock	Problems of High Speed Flight as Affected by Compressibility. <i>J.R. Ae.S.</i> Vol. XLII, No. 327, pp. 93-228. March, 1938.
73.	Thompson and Mair	Research on High Speed Aerodynamics at the Royal Aircraft Establishment from 1942 to 1945. R. & M. 2222. September, 1946.
74.	Thompson and Mair	The Design of a High Speed Subsonic Wind Tunnel. A.R.C. 7409. (Unpublished.)
75.	Preston	The Interference on a Wing Spanning a Closed Tunnel arising from the Boundary Layers on the Side Walls with Special Reference to the Design of Two-Dimensional Tunnels. R. & M. 1924. March, 1944.
76.	Wingham	An Application of Strain Gauges to the Measurement of Normal Forces and Moments in High Speed Wind Tunnels. R. & M. 2316. June, 1945.
77.	Redshaw	The Electrical Measurement of Strain. <i>J.R.Ae.S.</i> , Vol. 50, No. 128. August, 1946.
78.	Holder	Transition Indication in the National Physical Laboratory 20 in. \times 8 in. High Speed Tunnel. R. & M. 2079. July, 1945.
79.	Fage and Sargent	An Air Injection Method of Fixing Transition from Laminar to Turbulent Flow in a Boundary Layer. R. & M. 2106. June, 1944.
80.	Hyde	Turbulence Measurements with Spheres in the N.P.L. High Speed Tunnels. R. & M. 1959. September, 1942.
81.	Holder	The N.P.L. High Speed Laboratory. Part I. Description of Installation. (Part I of this Report.)
82.	Hutton	The Use of Interferometers in Aerodynamics at the L.F.A., Brunswick, Germany. R. & M. 2366. July, 1946.
83.	Liepmann	Shockwave Oscillations in Wind Tunnels. <i>J. Aero. Sci.</i> , Vol. 14, No. 5, p. 295. May, 1947.
84.	Eggink	Fluctuations of Flow in High Speed Tunnels. A.R.C. 10,810. (Unpublished.)
85.	Giles	The N.P.L. Mach Number Gauge. R. & M. 2131. July, 1945.
86.	Cox	A Note on Electromagnetic Induction Micrometers. <i>J. Sci. Insts.</i> , Vol. 19, No. 8, p. 117. August, 1942.
87.	Thompson	Method of Computing C_D from Wake Traverse in High Speed Tunnel. A.R.C. 8462. (Unpublished.)
88.	—	Report of the Aeronautical Research Committee. 1931-1932.
89.	Lukasiewicz	Humidity Effects in Supersonic Flow of Air. R. & M. 2563. June, 1948.
90.	Charters, A. C., Jnr.	Transition between Laminar and Turbulent Flow by Transverse Contamination. N.A.C.A. Tech. Note No. 891. A.R.C. 6782.
91.	Klein	Micromanometers: Testing Equipment and Instruments. AVA Monographs D ₂ II 4. M.A.P. R. & T. No. 952. 1947.
92.	Pearcey	Effects of Condensation on Total Head, etc., in N.P.L. High Speed Tunnel. R. & M. 2249. February, 1944, and A.R.C. 8456. (Unpublished.)
93. } 94. }	Taylor	Pitot Pressure in Moist Air. R. & M. 2248. January, 1945.
95.	Beavan and Manwell	Tables for Use in the Determination of Profile Drag at High Speeds by the Pitot Traverse Method. R. & M. 2233. September, 1941.
96.	Young and Maas	The Behaviour of a Pitot Tube in a Transverse Total Pressure Gradient. R. & M. 1770. 1937.
97.	Smelt	Power Economy in High Speed Wind Tunnels by Choice of Working Fluid and Temperature. A.R.C. 9007. (Unpublished.)

No.	Author	Title, etc.
98.	Dodge and Davis	Vapour Pressure of Liquid Oxygen and Nitrogen. <i>J. Am. Chem. Soc.</i> , Vol. 49, pp. 610-620. 1927.
99.	Dodge and Dunbar	An Investigation of the Co-existing Liquid and Vapour Phases of Solutions of Oxygen and Nitrogen. <i>J. Am. Chem. Soc.</i> , Vol. 49, pp. 591-610. 1927.
100.	Inglis	<i>Phil. Mag.</i> (6) II, p. 640. 1906.
101.	Chambre and Chia-Chias Lin ..	On the Steady Flow of a Gas Through a Tube with Heat Exchange or Chemical Reaction. <i>J. Aero. Sci.</i> , Vol. 13, No. 10, p. 537. October, 1946.
102.	Hawthorne and Cohen	Pressure Losses and Velocity Changes due to Heat Release and Mixing in Compressible Flow. A.R.C. 7623. (Unpublished.)
103.	Binnie and Woods	The Pressure Distribution in a Convergent-Divergent Steam Nozzle. <i>Proc. I. Mech. E.</i> , Vol. 138, pp. 229-265. 1938.
104.	Wilson	<i>Phil. Trans. Roy. Soc.</i> , A, Vol. 189, p. 265. 1897.
105.	Hermann	Condensation Shock Waves in Supersonic Wind Tunnel Nozzles. R.T.P. Trans. No. 1581. A.R.C. 6185.
106.	Owen	Note on the Apparatus and Work of the W.V.A. Supersonic Institute at Kochel, S. Germany. Part I. A.R.C. 9281. (Unpublished.)
107.	McBain	<i>The Absorption of Gases and Vapour by Solids.</i> George Routledge & Sons. 1932.
108.	Hankins	Experiments on Reynolds Number Effect on Projectiles at Supersonic Speed. 6th International Congress for Applied Mechanics, Paris. September, 1946.
109.	Cope	Calculations of Reynolds Number Effect on Projectiles at Supersonic Speed. 6th International Congress for Applied Mechanics, Paris. September, 1946. See also A.R.C. 8817. (Unpublished.)
110.	Glauert	Wind Tunnel Interference on Wings, Bodies and Airscrews. R. & M. 1566. 1933.
111.	Thom	Blockage Corrections in a Closed High Speed Tunnel. R. & M. 2033. November, 1943.
112.	Young and Squire	Blockage Corrections in a Closed Rectangular Tunnel. Part I. Simple Approximate Formulae for General Application. Part II. Note on the Blockage Correction for Streamline Bodies of Revolution.
113.	Allen and Vincenti	Wall Interference in a Two-Dimensional Flow Wind Tunnel with Consideration of the Effect of Compressibility. N.A.C.A. Report No. 782. 1944.
114.	Thom and Jones	Tunnel Blockage near the Choking Condition. R. & M. 2385. August, 1946.
115.	Prandtl	<i>Aerodynamic Theory</i> (Ed. Durand). Vol. III Div. G, Sections 27-28. Julius Springer.
116.	Goldstein	Steady Two-Dimensional Flow Past a Solid Cylinder in a Non-uniform Stream, and Two-Dimensional Wind Tunnel Interference. R. & M. 1902. October, 1942.
117.	Goldstein and Young	The Linear Perturbation Theory of Compressible Flow with Applications to Wind Tunnel Interference. R. & M. 1909. July, 1943.
118.	Franke and Weinig	The Correction of the Speed of Flow and the Angle of Incidence due to Blockage by Aerofoil in a High Speed Wind Tunnel with Closed Working Section. M.O.S. Rpts. and Trans. No. 259. A.R.C. 10,268.
119.	Thom	Note on R.A.E. Report Aero. 2056 (8878)—Tunnel Blockage near the Choking Condition. A.R.C. 9095. (Unpublished.)
120.	Goldstein (editor)	<i>Modern Developments in Fluid Dynamics.</i> Vol. 1, pp. 263-264.
121.	Weyl	Analytical Methods in Optical Examination of Supersonic Flow. NAVORD Report 211-45.
122.	Schardin	Schlieren Methods and Their Application. R.A.E. Library Trans. No. 122.
123.	Byrne	Experimental Constriction Effects in High Speed Wind Tunnels. N.A.C.A. Report No. L.4107a.

No.	Author	Title, etc.
124.	Vincenti and Graham	The Effect of Wall Interference upon the Aerodynamic Characteristics of an Aerofoil Spanning a Closed-throat Circular Wind Tunnel. N.A.C.A. A.C.R. No. 5021.
125.	Derby	The Ronchi Method of Evaluating Schlieren Photographs. NAVORD Report 74-76, p. 31.
126.	Barnes and Bellinger	Schlieren and Shadowgraph Equipment for Air Flow Analysis. <i>J. Am. Opt. Soc.</i> , Vol. 35, No. 8, p. 497. August, 1945.
127.	Schardin	Theory and Application of the Mach-Zehnder Interferometer. R.A.E. Translation No. 79. Aero. Trans. No. 5. 1946.
128.	Zobel	Advances in Optical Methods of Determining Airflow. Mitteilungen der Deutsche Akademie der Luftfahrtforschung. 5008/44g. Halstead Exploiting Centre.
129.	Pack	Investigation of the Flow past Finite Wedges of 20 deg and 40 deg Apex Angle at Subsonic and Supersonic Speeds using a Mach-Zehnder Interferometer. R. & M. 2321. May, 1946.
130.	Lighthill	Two-Dimensional Supersonic Aerofoil Theory. R. & M. 1929. January, 1944.
131.	Taylor and Maccoll	<i>Proc. Roy. Soc., A</i> , Vol. 139, pp. 278-311. 1933.
132.	Owen	Note on the Apparatus and Work of the W.V.A. Supersonic Institute at Kochel, S. Germany. Part II. A.R.C. 9282. (Unpublished.)
133. } 134. }	Pearcey and Beavan	Profile Drag Measurements at Compressibility Speeds on Aerofoils with and without Spanwise Wires and Grooves. Note on Reynolds and Mach Number Effects on the Pressure Distribution on the Tail of EC 1250. R. & M. 2252. August, 1943.
135.	Pearcey	Temperature Measurement in High Speed Flow. A.R.C. 7437. (Unpublished.)
136.	Franz	Pressure and Temperature Measurement in Supercharger Investigations. N.A.C.A. Tech. Memo. 953.
137.	Oswatitsch	Kondensationserscheinungen in Überschalldüsen. <i>Z.A.M.M.</i> , Vol. 22, No. 1. 1942. R.T.P. Trans. 1905.
138.	Busemann	<i>Handbuch der Experimental-physik</i> , Wien-Harmer, Vol. 4, pp. 407-442. 1931. Translated as A.R.C. 8224.
139.	Meyer	The Method of Characteristics for Problems of Compressible Flow Involving Two Independent Variables. <i>J. Mech. and App. Maths.</i> , Vol. I, Part 2, p. 196. June, 1948. A.R.C. 9907.
140.	de Haller	The Application of a Graphic Method to some Dynamic Problems in Gases. <i>Sulzer Technical Review</i> No. 1.
141.	Atkin	Two-Dimensional Supersonic Channel Design. Part I. R. & M. 2174. November, 1945.
142.	Puckett	Supersonic Nozzle Design. <i>J. App. Mech.</i> , Vol. 68, p. A65. December, 1946.
143.	Shapiro and Edelman	Method of Characteristics for Two-Dimensional Supersonic Flow. Graphical and Numerical Procedures. <i>J. App. Mech.</i> , Vol. 14, No. 2, pp. A154-162. June, 1947.
144.	Görtler	Zum Übergang um Unterschall zu Überschallgeschwindigkeiten in Düsen. <i>Z.A.M.M.</i> , 19, pp. 325-337. 1939.
145.	Stanton	The Variation of Velocity in the Neighbourhood of the Throat of a Constriction in a Wind Channel. R. & M. 1388.
146.	Lighthill	The Hodograph Transformation in Transonic Flow. (1) Symmetrical Channels. A.R.C. 9856. (Unpublished.)
147.	Bailey and Wood	Conversion of the Stanton 3-in. High Speed Wind Tunnel to the Open Jet Type. <i>Proc. I. Mech. E.</i> , Vol. 135, p. 445. 1935.
148.	Guderley	Die Charakteristikenmethode für ebene und achsensymmetrische Überschallströmungen. <i>Jahrbuch, 1940, der Deutschen Luftfahrtforschung Flugwerk</i> , p. 1522.
149.	Cope	The Turbulent Boundary Layer in Compressible Flow. R. & M. 2840. November, 1943.

No.	Author	Title, etc.
150.	Cope	The Laminar Boundary Layer in Compressible Flow. A.R.C. 7635. (Unpublished.)
151.	Oswatitsch and Wieghardt ..	Theoretical Investigations on Steady Potential Flows and Boundary Layers at High Speeds. M.O.S. Rpts. and Trans. No. 187. A.R.C. 10,378.
152.	Ward	A Note on Compressible Flow in a Tube of Slightly Varying Cross-Section (Unpublished). Dept. of Scientific Research and Experiment, Admiralty. SRE/Airflow/24.
153.	Holder	The N.P.L. High Speed Laboratory. Part III. Review of Experimental Results. (Part III of this Report.)
154.	Richards and Burstall	The China Clay Method of Indicating Transition. R. & M. 2126. August, 1945.
155.	Royle, Bowling and Lukasiewicz..	Calibration of Two-Dimensional and Conical Supersonic Multi-nozzles. A.R.C. 11,039. (Unpublished.)
156.	Glauert	The Effect of Compressibility on the Lift of an Aerofoil. R. & M. 1135. September, 1927.
157.	von Kármán	Compressibility Effects in Aeronautics. <i>J. Aero. Sci.</i> , July, 1941, p. 19. A.R.C. 5314.
158.	Temple	Approximate Solution of the Hodograph Equations for Compressible Flow. A.R.C. 6107. (Unpublished.)
159.	Griffiths	Criterion for Wave Drag in Supersonic Flight. A.R.C. 9463. (Unpublished.)
160.	Bickley	Critical Conditions for Compressible Flow. R. & M. 2330. May, 1946.
161.	Beavan	Application of New Definition of Critical Mach Number to a Profile. A.R.C. 9787. (Unpublished.)
162.	Pearcey and Beavan	Force and Pressure Coefficients up to Mach Number 0.87 on the Goldstein Roof Top Section 1442/1547. R. & M. 2346. April, 1946.
163.	Göthert	Increase of Drag of Profiles at High Subsonic Speeds. M.O.S. Rpts. and Trans. No. 36. A.R.C. 9705. (Unpublished.)
164. } 165. }	Lock	The Ideal Drag due to Shock Wave. R. & M. 2512. February, 1945.
166.	Mair	Notes on German High Speed Tunnel Results. A.R.C. 9064. (Unpublished.)
167.	Hilton	Empirical Laws for the Effect of Compressibility on Quarter-chord Moment Coefficient and for the Choice of an Aerofoil with Small Compressibility Effect on Centre of Pressure. R. & M. 2195. March, 1943.
168.	Hilton	An Experimental Analysis of the Forces on 18 Aerofoils at High Speeds. R. & M. 2058. May, 1946.
169.	Thompson, Markowicz, Beavan and Fowler.	Pressure Distribution and Wake Traverses on Models of Mustang Wing Section in the R.A.E. and N.P.L. High Speed Tunnels. With Addendum: Pressure Distribution on a Two-dimensional Mustang Wing Model in the R.A.E. 7-ft. Wind Tunnel. R. & M. 2251. August, 1944.
170.	Charnley	Flight Measurements of Pressure Distribution around a Mustang Wing Section at High Speed. A.R.C. 8154. (Unpublished.)
171.	Charnley and Mair	Preliminary Profile Drag Measurements on a Mustang Wing in Flight at High Speeds. A.R.C. 8554. (Unpublished.)
172.	—	—
173.	Pearcey	Further Profile Drag Measurements at Compressibility Speeds for an Aerofoil with and without Spanwise Wires. R. & M. 2252. August, 1943.
174.	—	Supersonic Flow and Shockwaves. Applied Mathematics Panel, National Defence Research Committee. August, 1944.
175. } 176. }	Fage and Sargent	Effect on Aerofoil Drag of Boundary Layer Suction Behind a Shockwave. R. & M. 1913. October, 1943.
177. } 178. }	Fage and Sargent	Design of Suction Slots. R. & M. 2127. February, 1944.

No.	Author	Title, etc.
179.	Pearcey and Rogers	The Effect of Compressibility on the Performance of a Griffith Aerofoil. R. & M. 2511. November, 1946.
180.	Hilton and Knowler	Interim Report on Measurements on an Aerofoil with Elevator at High Speeds. A.R.C. 5272. (Unpublished.)
181. } 182. } 183. }	Hilton and Knowler	Lift and Pitching Moment Measurements on an EC 1240 Tailplane Elevator at High Speeds with Elevator Gap Sealed. R. & M. 2227. September, 1944.
184.	Beavan, Hyde and Fowler	Advance Note on Pressure Measurements over a Wide Mach Number Range on an Aerofoil with 25 per cent Control. Lift Moment and Hinge Moment Coefficients. A.R.C. 7176. (Unpublished.)
185.	Beavan, Hyde and Fowler	Pressure and Wake Measurements up to Mach Number 0.85 on an EC 1250 Section with 25 per cent Control. R. & M. 2065. February, 1945.
186. } 187. }	Knowler and Pruden	The Effect of Brake Flaps on an Aerofoil at High Speeds. Parts I and II. R. & M. 2211. December, 1942.
188.	Pruden	Tailplane Observations on a Model F.9 30 at High Speeds. A.R.C. 6662. (Unpublished.)
189.	Hilton, Moore and Sargent	High Speed Tunnel Measurements of Fin-tailplane Interference between EC 1040 and EC 1240 Sections. R. & M. 2138. May, 1941.
190.	Williams and Bell	Tests on a 5 per cent. Bi-convex Aerofoil in the Compressed Air Tunnel. R. & M. 2413. October, 1945.
191.	Williams, Brown and Miles	Tests on Four Circular Back Aerofoils in the Compressed Air Tunnel. R. & M. 2301. June, 1946.
192.	Hilton and Pruden	Subsonic and Supersonic High Speed Tunnel Tests of a Faired Double Wedge Aerofoil. R. & M. 2057. December, 1943.
193.	Hilton	Subsonic and Supersonic Tests on a 7½ per cent. Bi-convex Aerofoil. R. & M. 2196. May, 1944.
194.	Lock and Fowler	Yaw and Sweepback at High Mach Number. A.R.C. 8718. (Unpublished.)
195.	Beavan and Bumstead	Tests on Yawed Aerofoils in the 20 in. × 8 in. High Speed Tunnel. R. & M. 2458. July, 1947.
196.	Beavan	Drag of Sweptback Wings at High Speed—Original Model Tests in Germany. A.R.C. 9564. (Unpublished.)
197.	Mair	Relative Merits of Sweptback and Sweptforward Wings for Tailless and High Speed Aircraft. A.R.C. 9942. (Unpublished.)
198.	McKinnon Wood	Notes on Sweptback Wings for High Speeds. A.R.C. 8806. (Unpublished.)
199.	Göthert	Hochgeschwindigkeitsmessungen an einen Pfeilflügel (Pfeilwinkel = 35 deg). <i>L.G.L.</i> 156, p. 30. 1942.
200.	Koch	Drukverteilungsmessungen am schiebenden Troftügel. <i>L.G.L.</i> 156, p. 41, 1942.
201.	Ludwig	Versuchsergebnisse Pfeilflügel bei Hohen Geschwindigkeiten. <i>L.G.L.</i> 127, p. 44. 1940.
202.	Goldstein (editor)	<i>Modern Developments in Fluid Dynamics.</i> Vol. II, Chap. IX. Oxford University Press.
203.	Knowler and Pruden	On the Drag of Circular Cylinders at High Speeds. R. & M. 1933. February, 1944.
204.	Lock and Hilton	Calibration of Standard Pitot-Static Heads in the High Speed Tunnel. R. & M. 1752. 1936.
205.	H.S.T. Staff	Calibration of Mark VIII Pitot-Static Heads at High Speeds. A.R.C. 4795. (Unpublished.)
206.	Walchner	On the Effect of Compressibility on the Pressure Readings of a Prandtl Tube Situated in Flows at Subsonic Velocity. Air Ministry Trans. No. 962.
207.	Hilton	Thermal Effects on Bodies in an Airstream. <i>Proc. Roy. Soc., A</i> , Vol. 168, No. 932, pp. 43–56. October, 1938.
208.	Hilton and Wingham	Surface Temperatures on an Aerofoil at Subsonic Speeds. R. & M. 2230. January, 1946.
209.	Polhausen	<i>Z.A.M.M.</i> , I, 115–121. 1931.



x Position of pressure holes

ordinates (chords)

Leading edge radius
 $P/c = 0.01145$

x/c	0.005	0.010	0.015	0.025	0.05	0.1	0.15	0.2	0.25	0.3	0.35	0.4	0.45	0.5	0.55	0.6	0.65	0.7	0.75	0.8	0.85	0.9	0.95	1.0
y/c Upper	0.01135	0.0162	0.0200	0.0260	0.0371	0.0520	0.0625	0.0702	0.0761	0.0803	0.0830	0.0845	0.0846	0.0832	0.0804	0.0755	0.0676	0.0581	0.0476	0.0367	0.0260	0.0158	0.0069	0
y/c Lower	0.01005	0.0139	0.0167	0.0212	0.0287	0.0382	0.0445	0.0488	0.0519	0.0540	0.0552	0.0555	0.0550	0.0538	0.0515	0.0480	0.0425	0.0360	0.0291	0.0220	0.0151	0.0088	0.0036	0

FIG. 1. Goldstein roof-top aerofoil 1442/1547. 5-in chord.

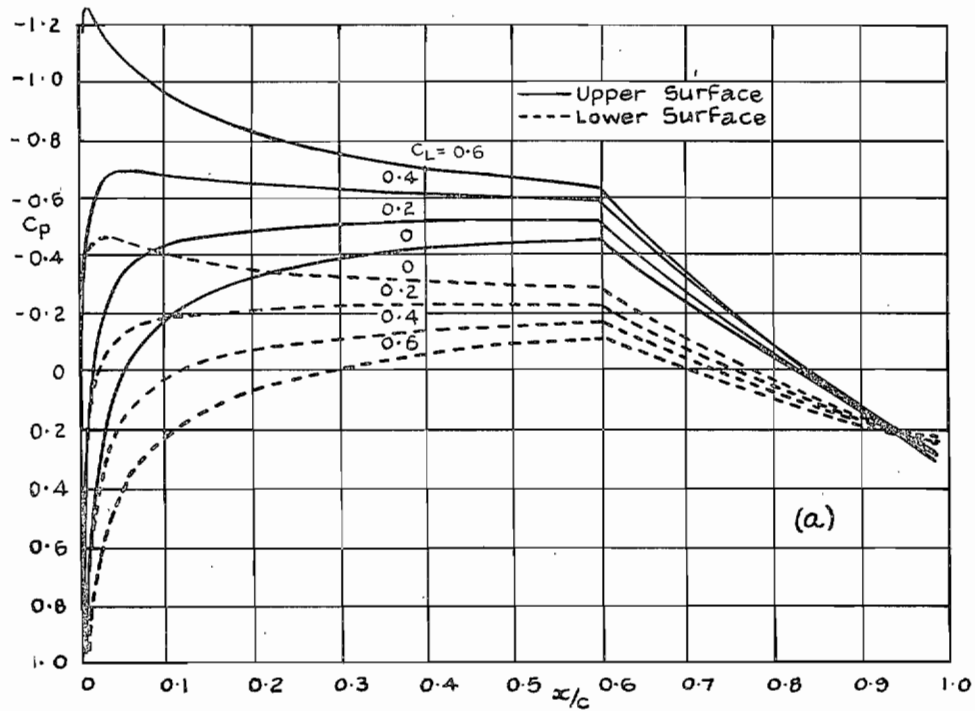


FIG. (2a). Goldstein Aerofoil 1442/1547. Calculated pressure distribution (incompressible) for $a_1 = 2\pi$.

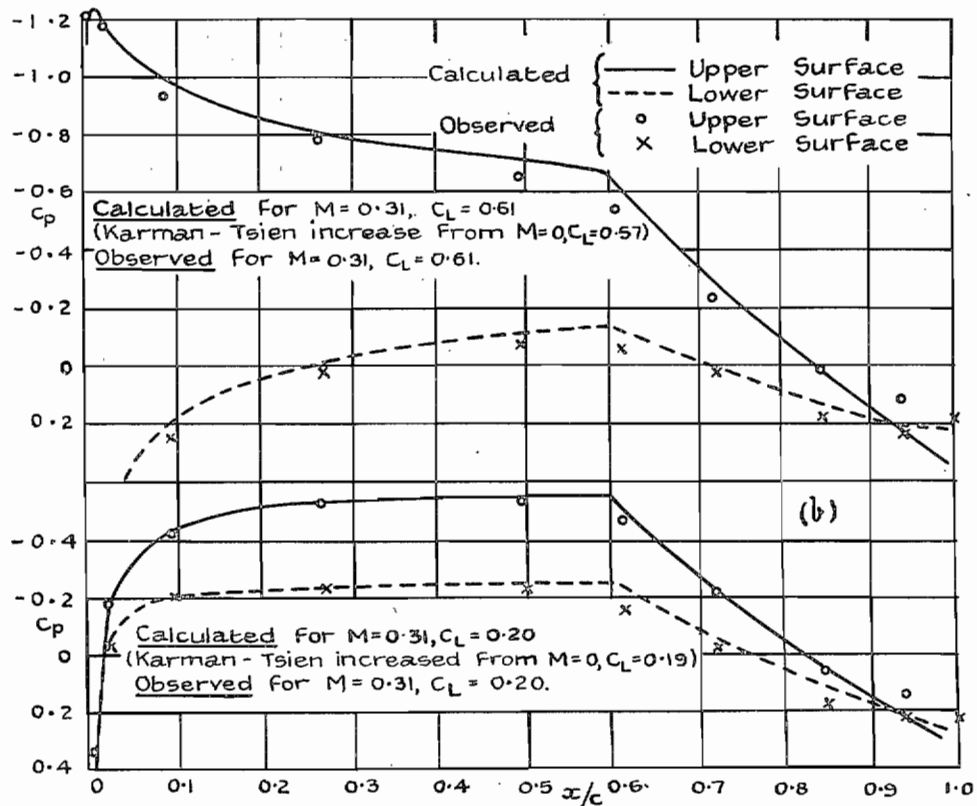
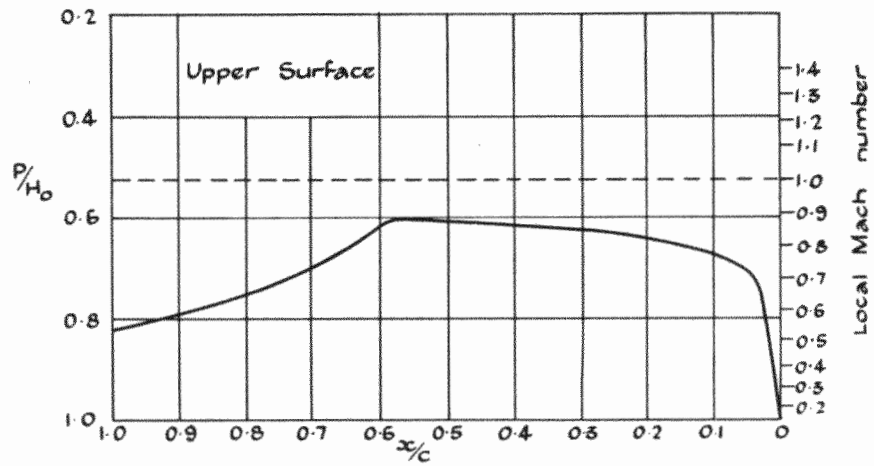


FIG. 2(b). Goldstein Aerofoil 1442/1547. Comparison of observed and theoretical (calculated incompressible plus Kármán-Tsien correction) pressures.



FIG. 3. Aerofoil G 1442/1547 at $\alpha = 0.5$ deg. Control photograph at zero Mach number.



Free Stream Mach No 0.631

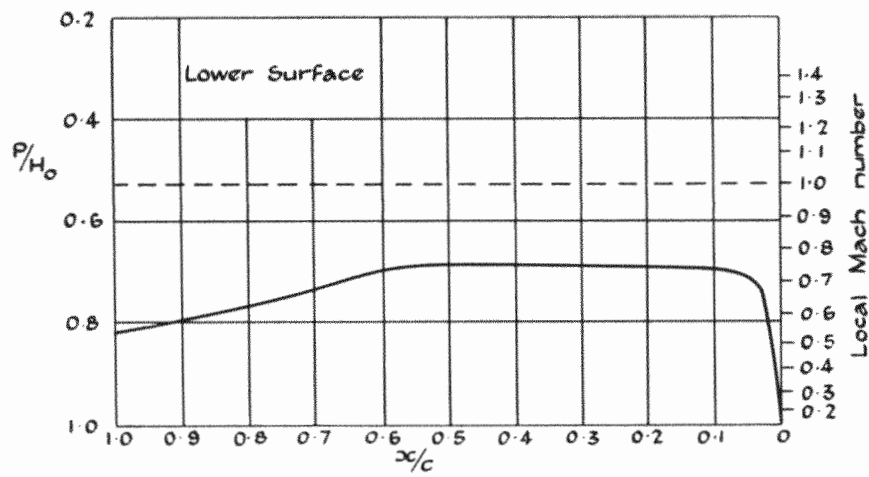
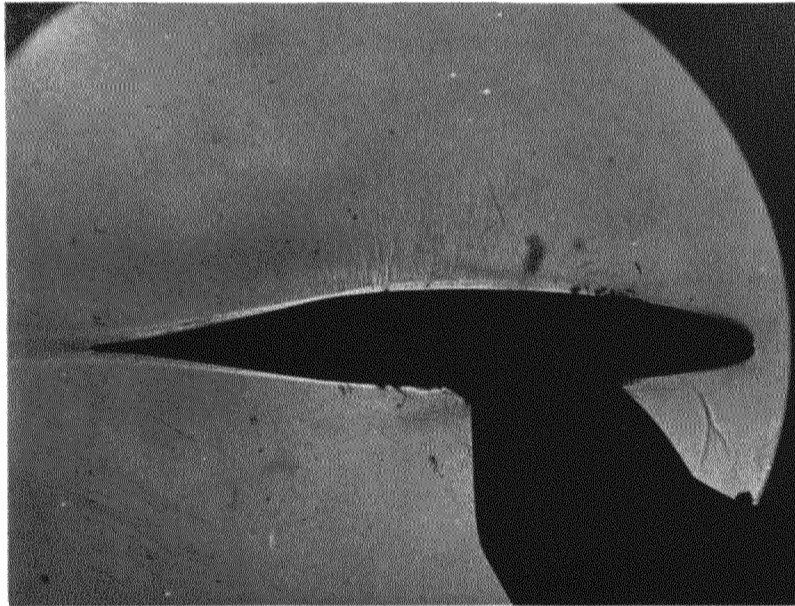
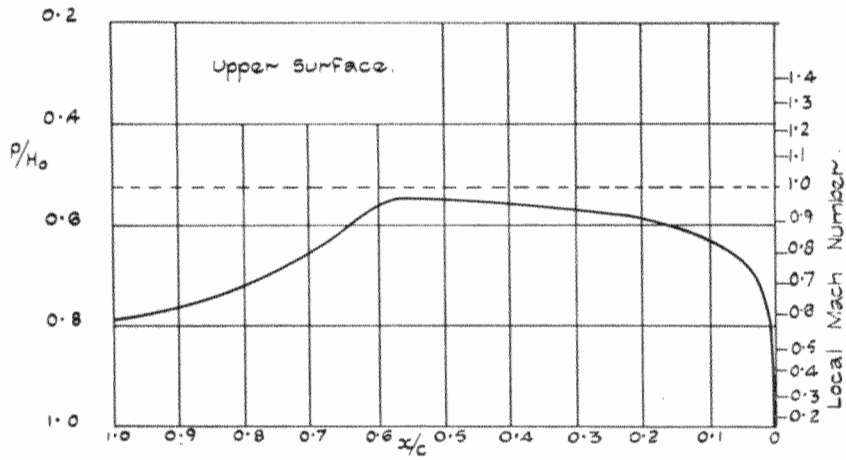


FIG. 4. Aerofoil G 1442/1547 at $\alpha = 0.5$ deg.



Free Stream Mach No 0.681

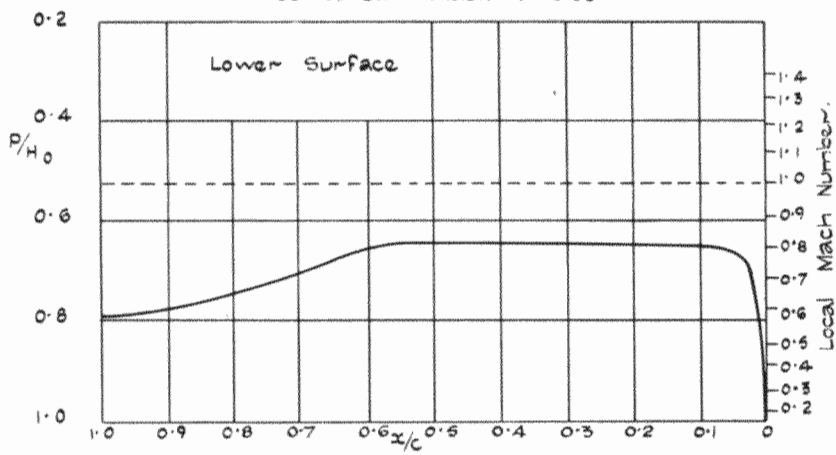
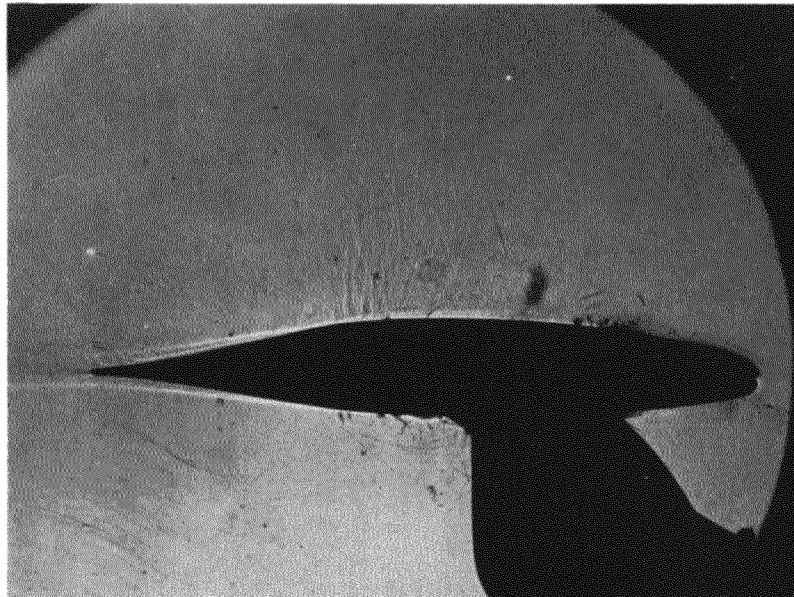
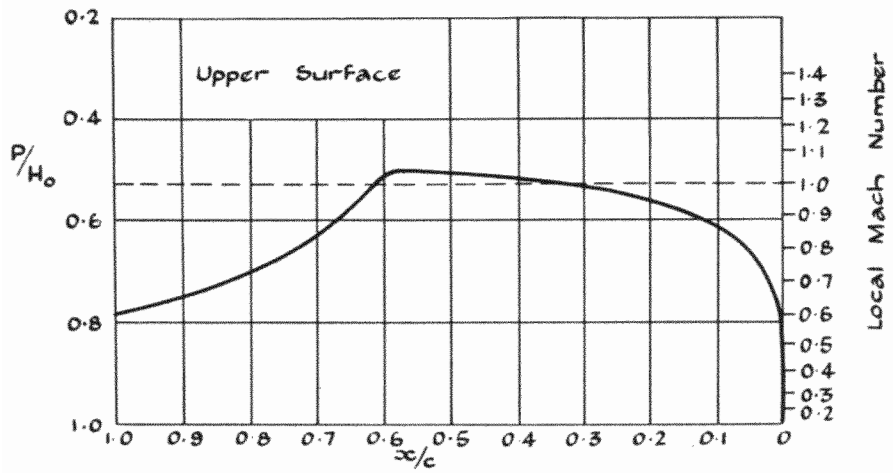


FIG. 5. Aerofoil G 1442/1547 at $\alpha = 0.5$ deg.



Free Stream Mach No 0.706

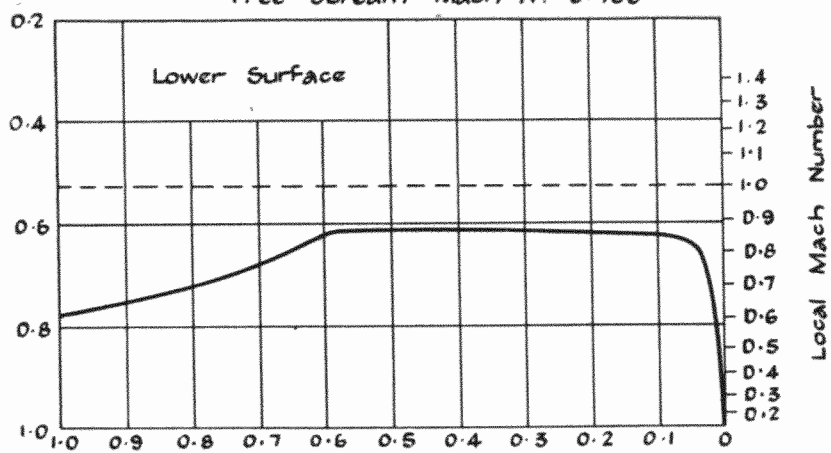
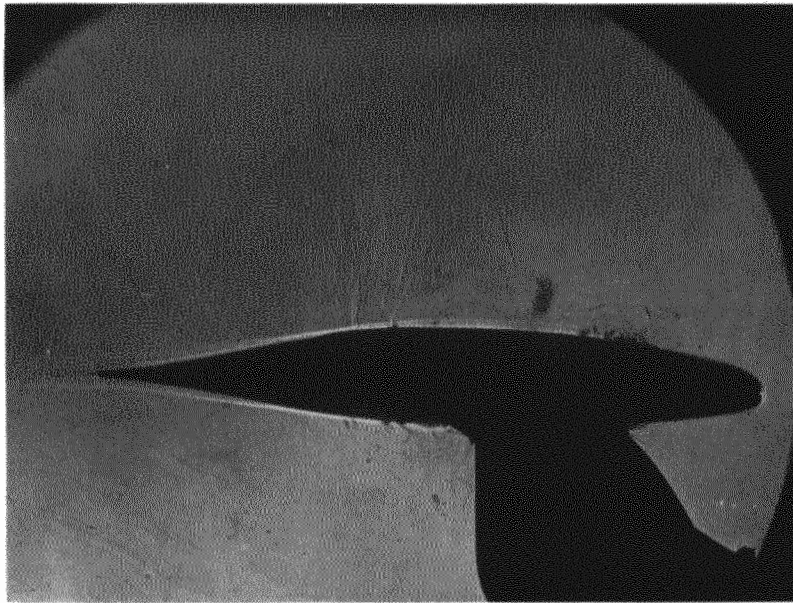
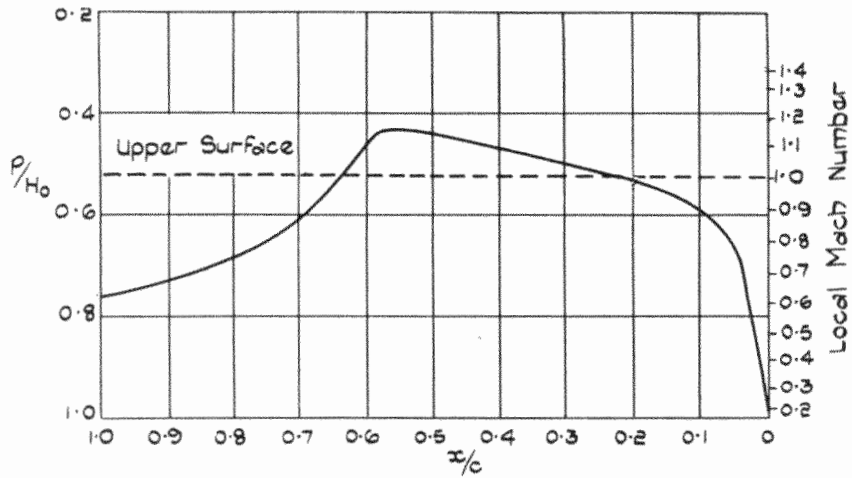


FIG. 6. Aerofoil G 1442/1547 at $\alpha = 0.5$ deg.



Free Stream Mach N^o 0.733

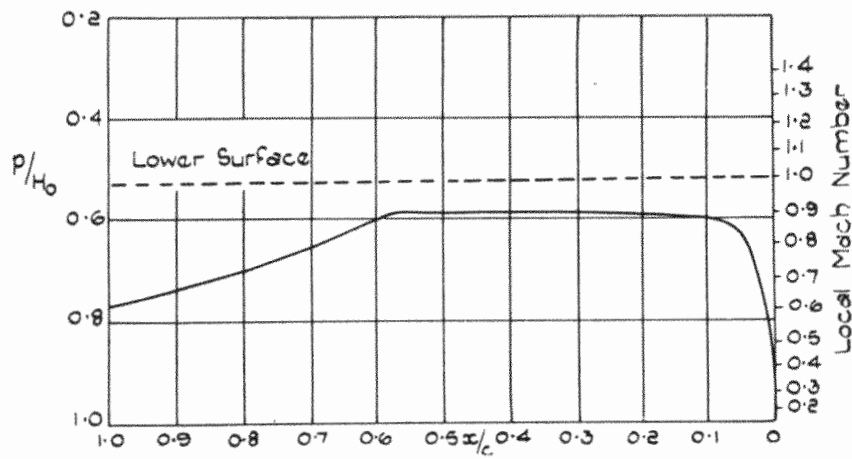


FIG. 7. Aerofoil G 1442/1547 at $\alpha = 0.5$ deg.

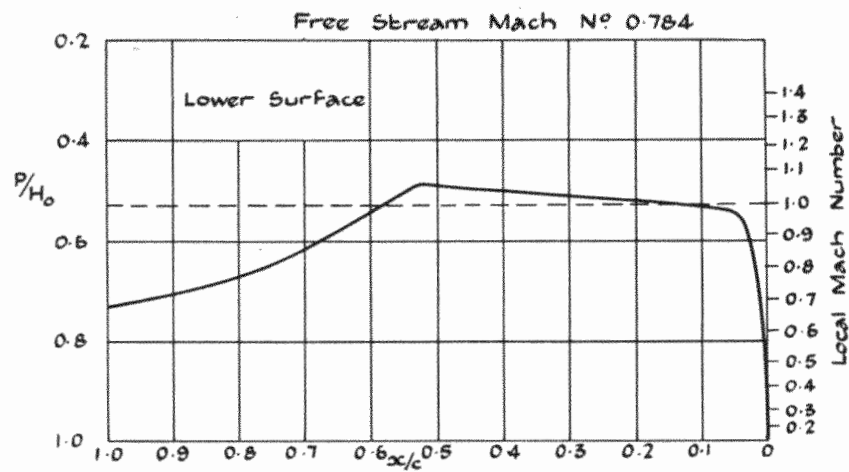
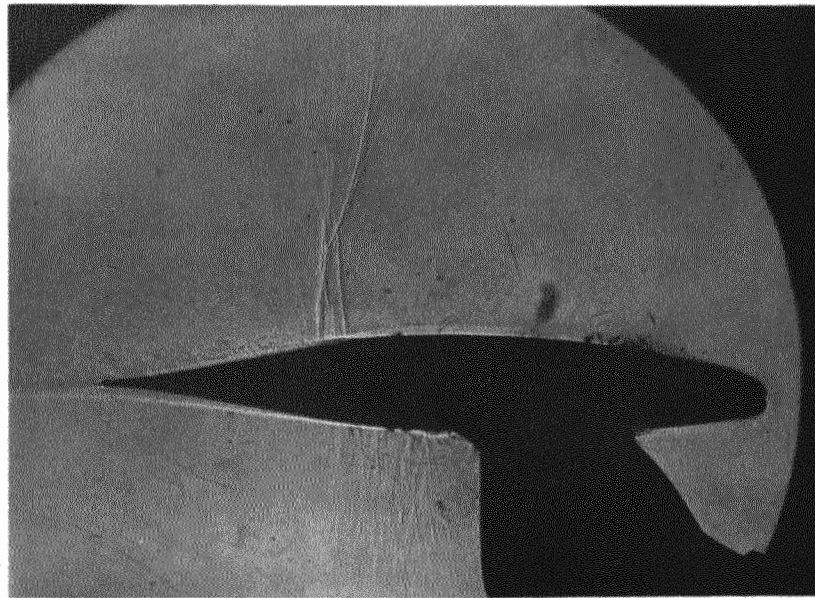
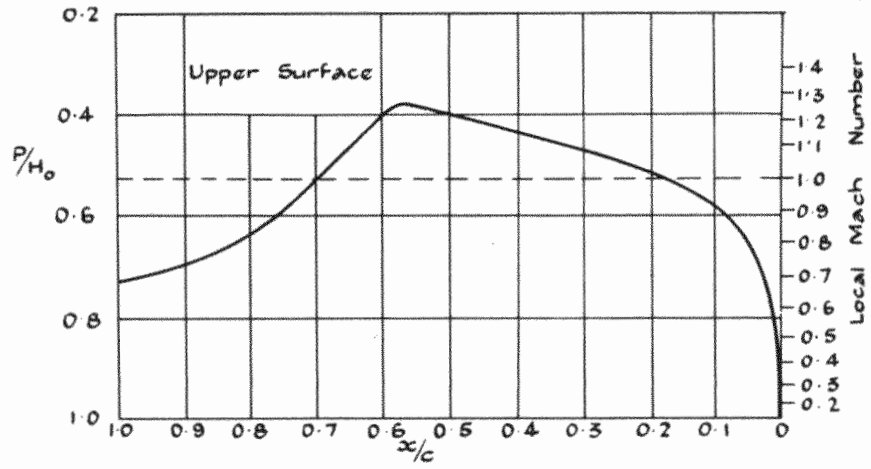


FIG. 8. Aerofoil G 1442/1547 at $\alpha = 0.5$ deg.

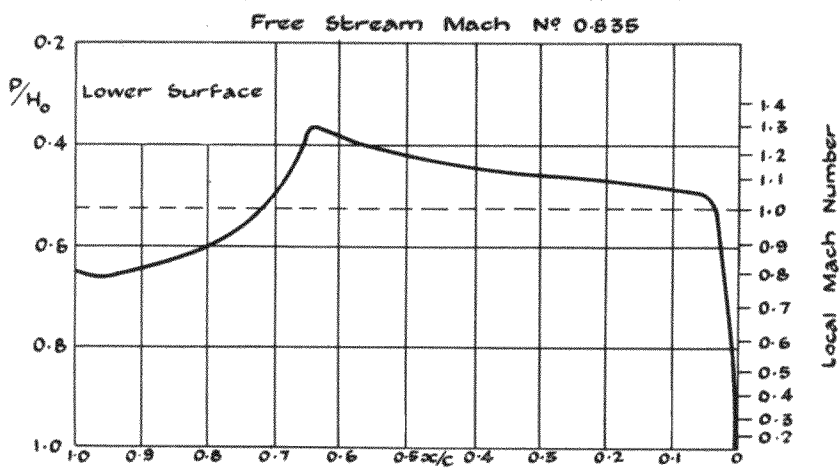
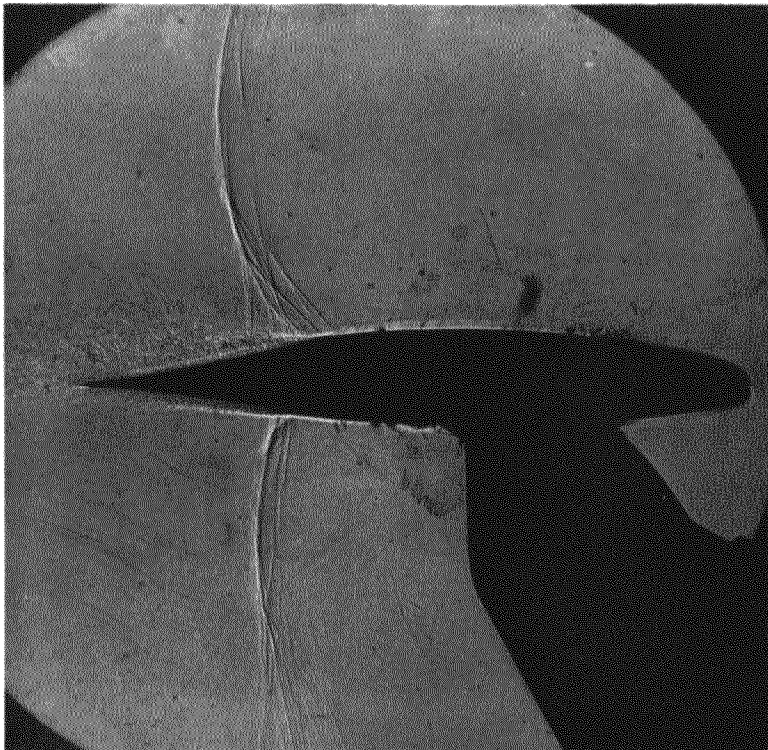
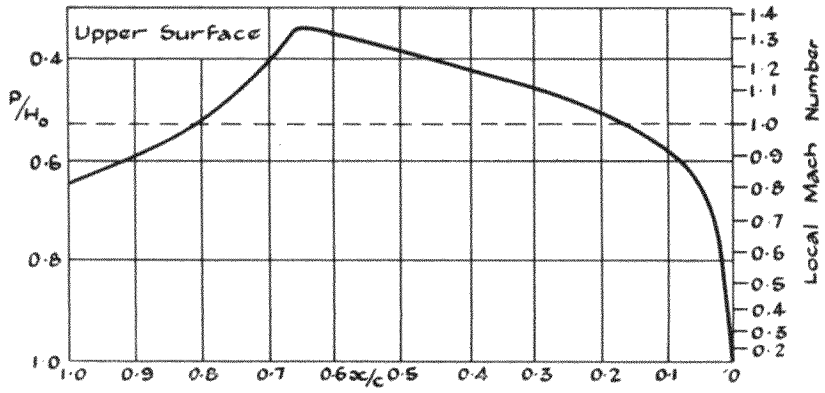
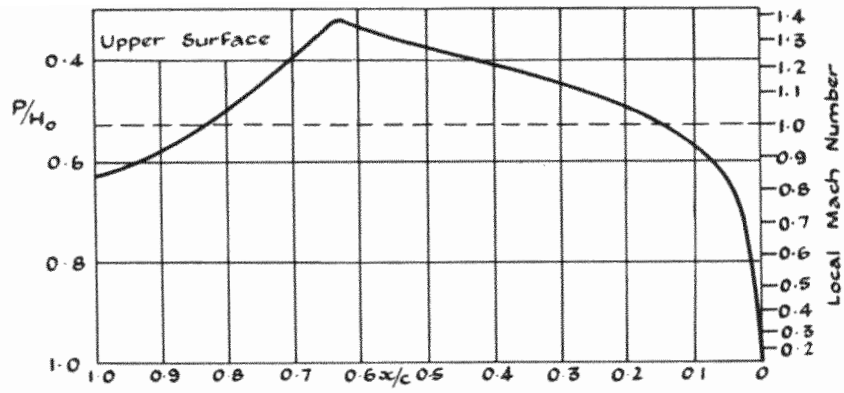


FIG. 9. Aerofoil G 1442/1547 at $\alpha = 0.5$ deg.



Free Stream Mach No 0.855

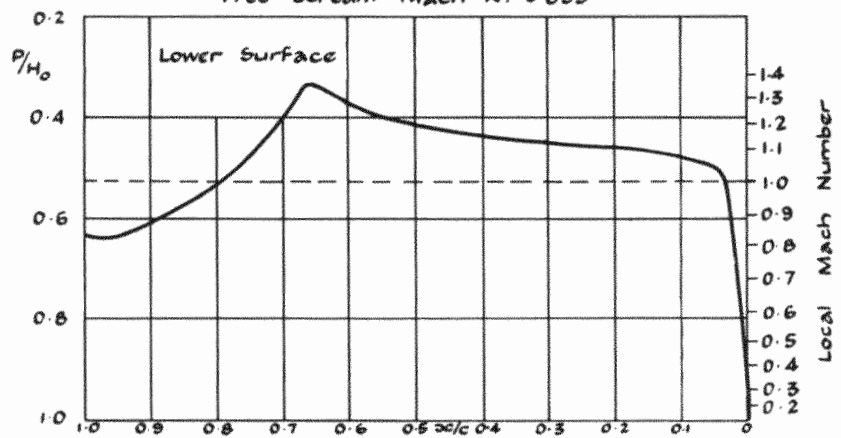
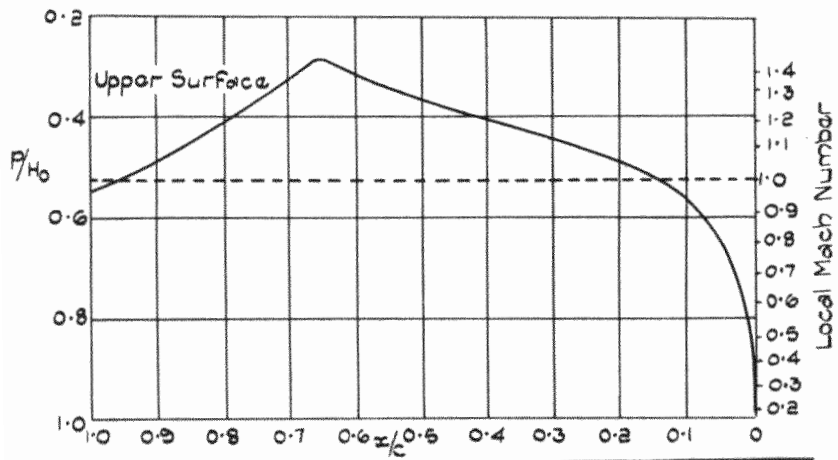


FIG. 10. Aerofoil G 1442/1547 at $\alpha = 0.5$ deg.



Free Stream Mach No 0.876

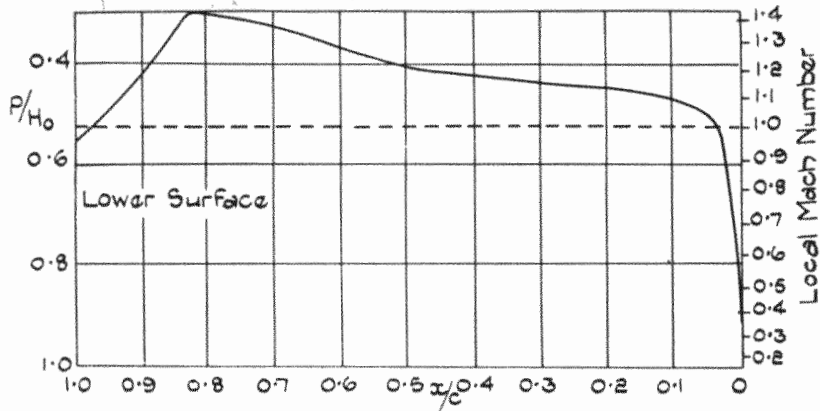
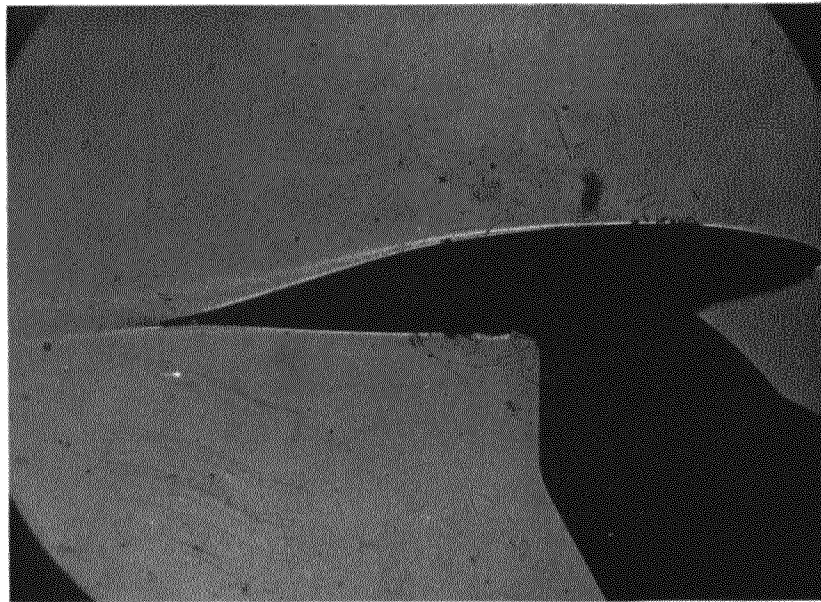
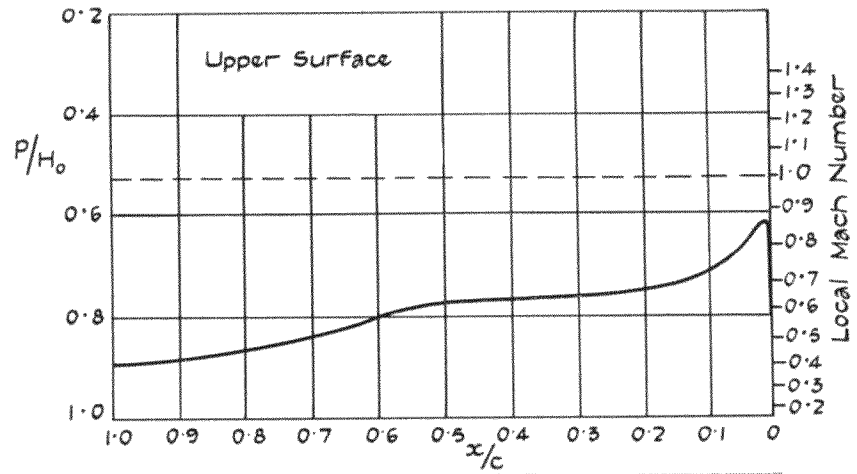


FIG. 11. Aerofoil G 1442/1547 at $\alpha = 0.5$ deg.



Free Stream Mach N° 0.454.

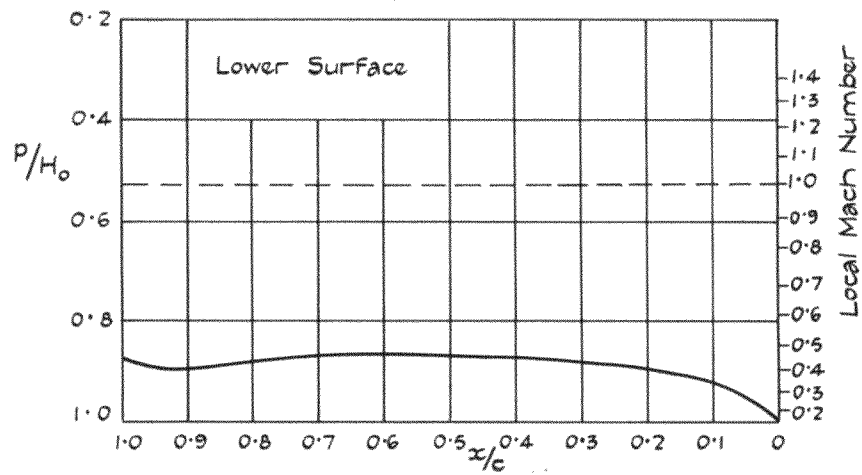
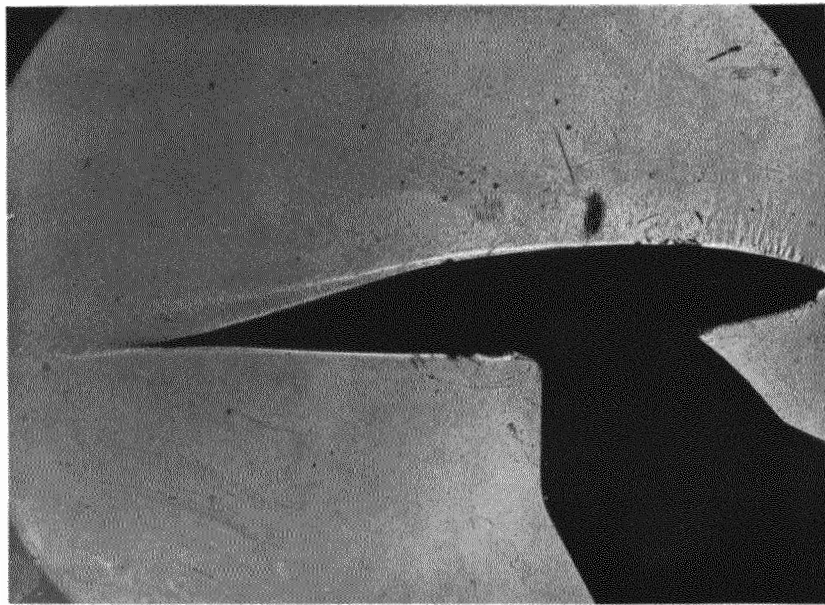
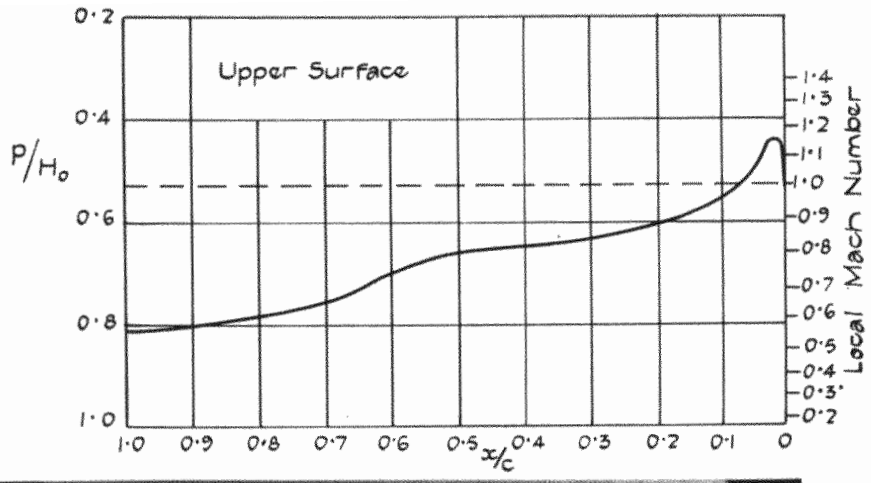


FIG. 12. Aerofoil G 1442/1547 at $\alpha = 6.5$ deg.



Free Stream Mach N° 0.569

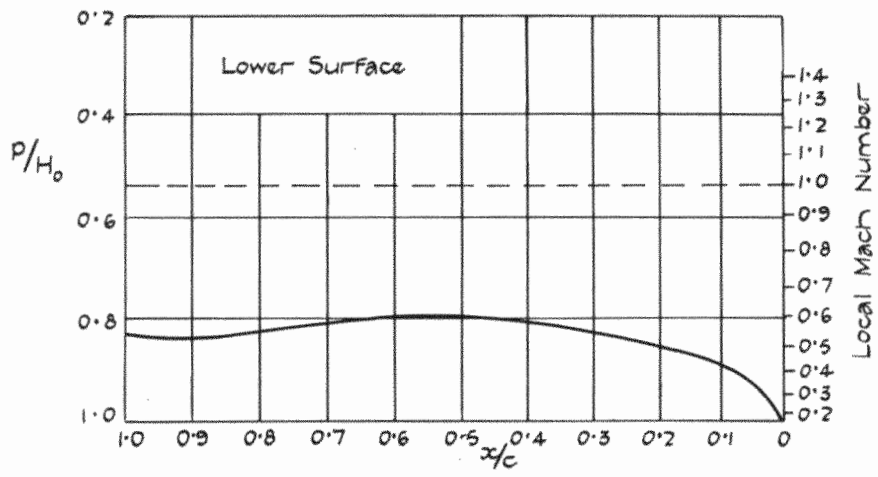
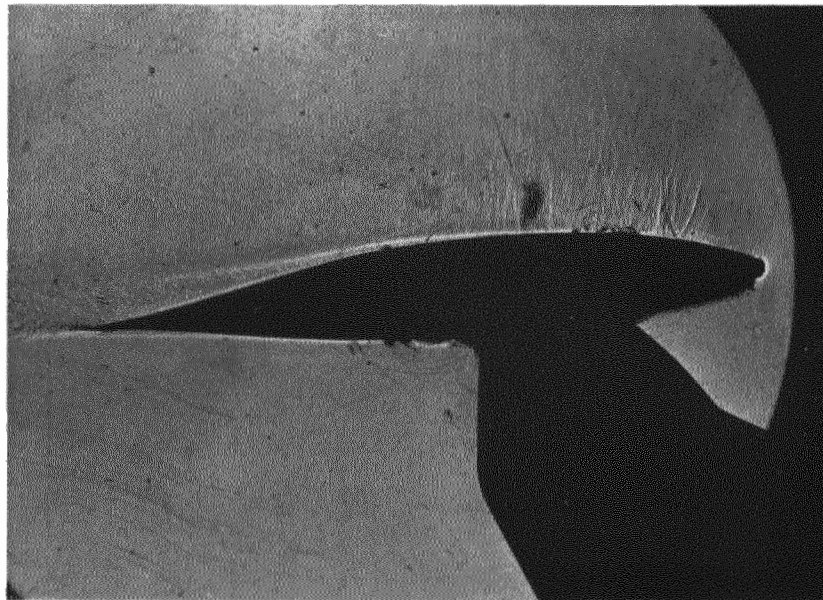
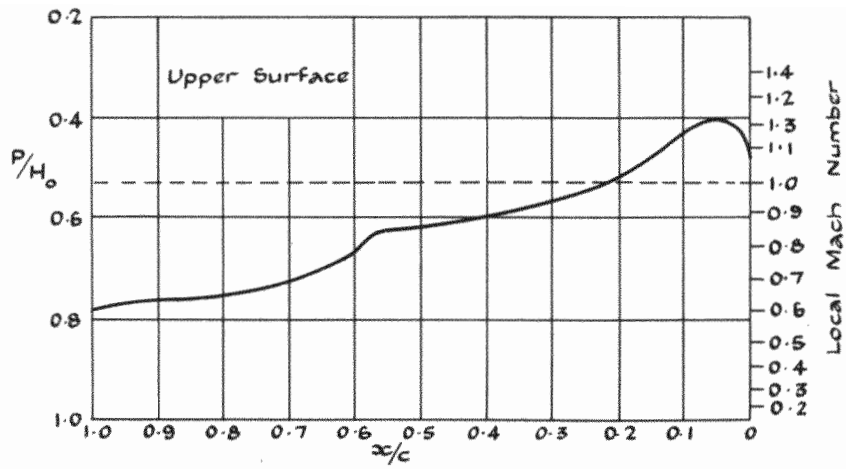


FIG. 13. Aerofoil G 1442/1547 at $\alpha = 6.5$ deg.



Free Stream Mach No 0.626

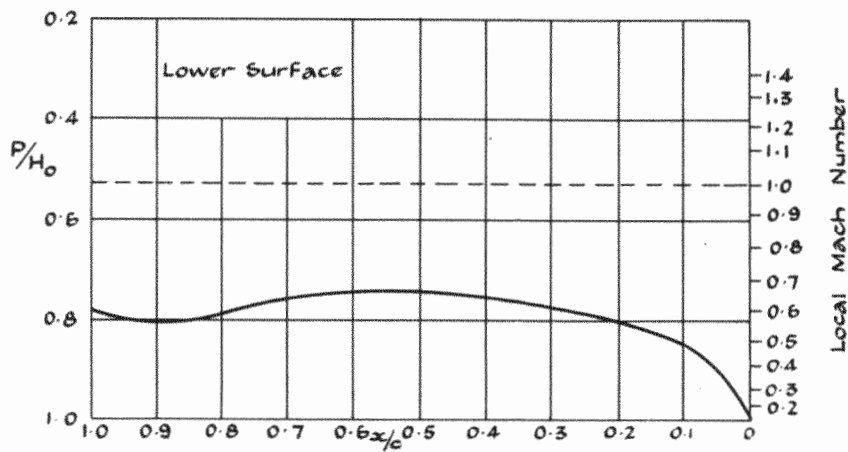
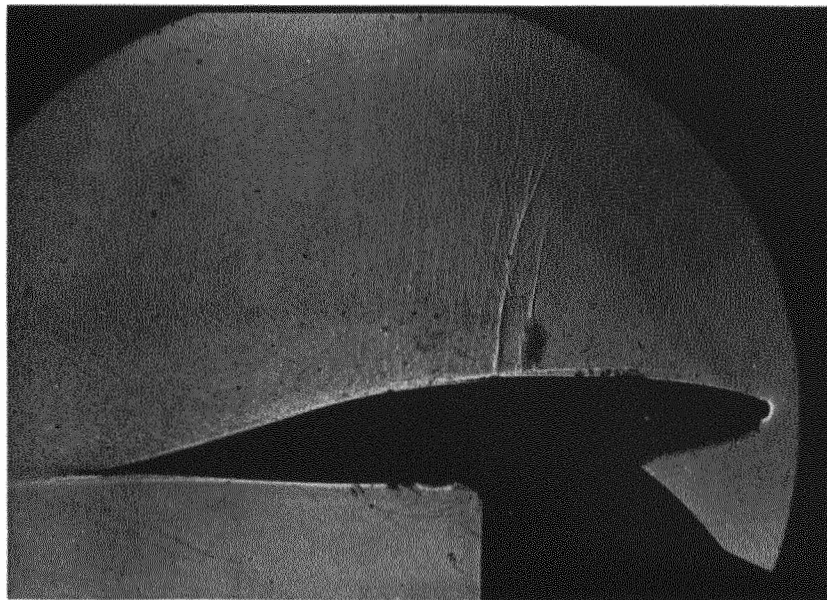
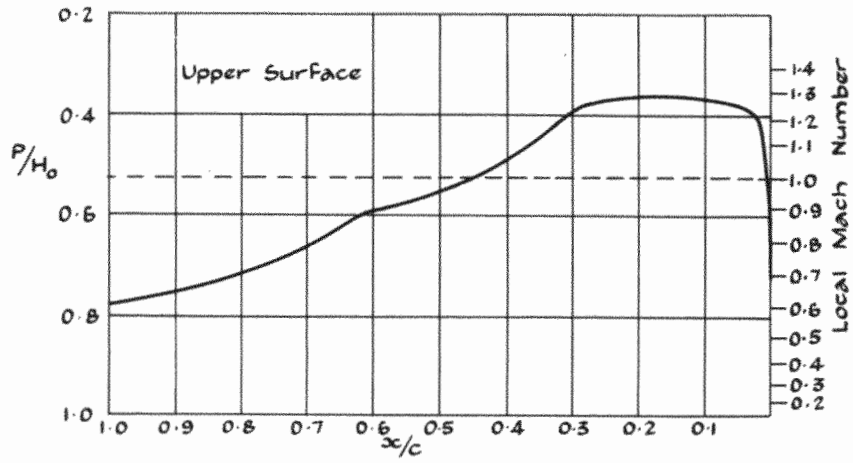


FIG. 14. Aerofoil G 1442/1547 at $\alpha = 6.5$ deg.



Free Stream Mach N° 0.675

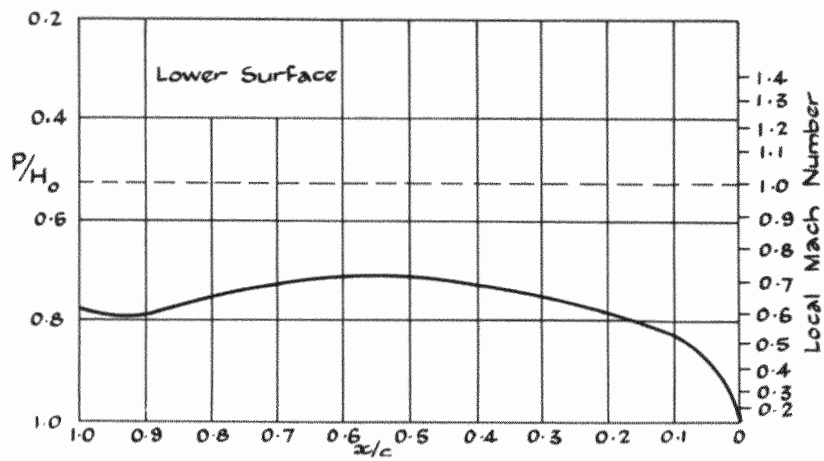
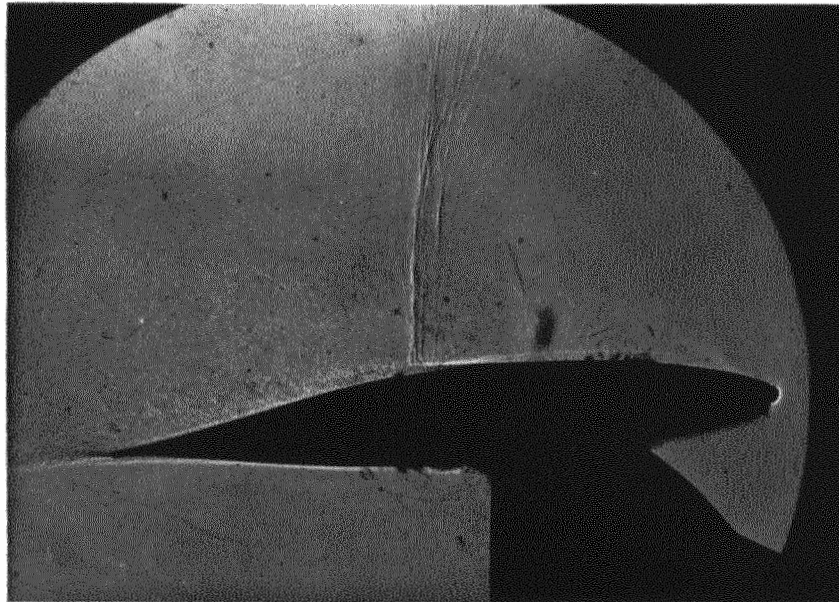
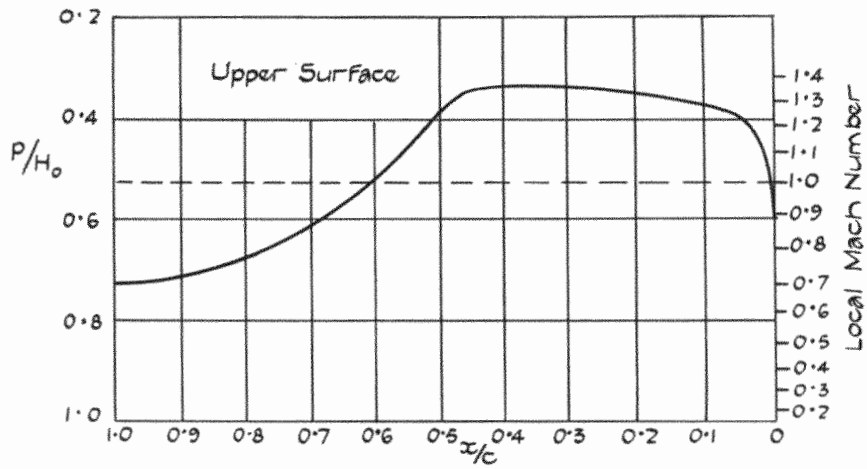


FIG. 15. Aerofoil G 1442/1547 at $\alpha = 6.5$ deg.



Free Stream Mach N° 0.728

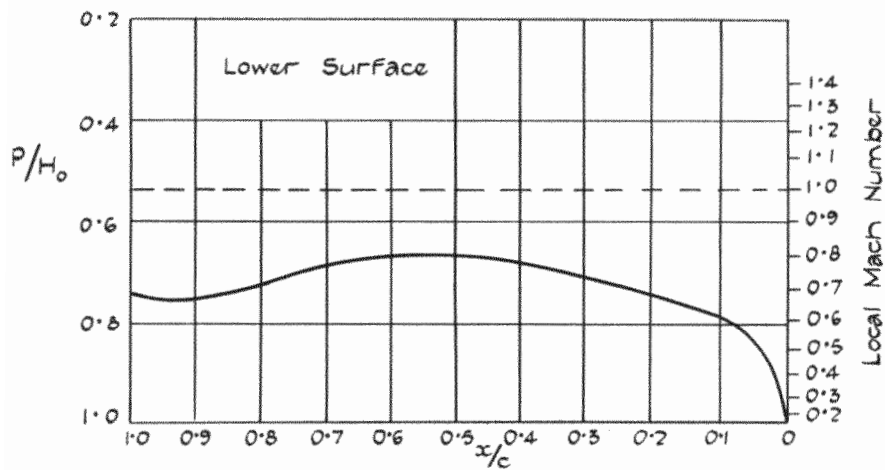


FIG. 16. Aerofoil G 1442/1547 at $\alpha = 6.5$ deg.

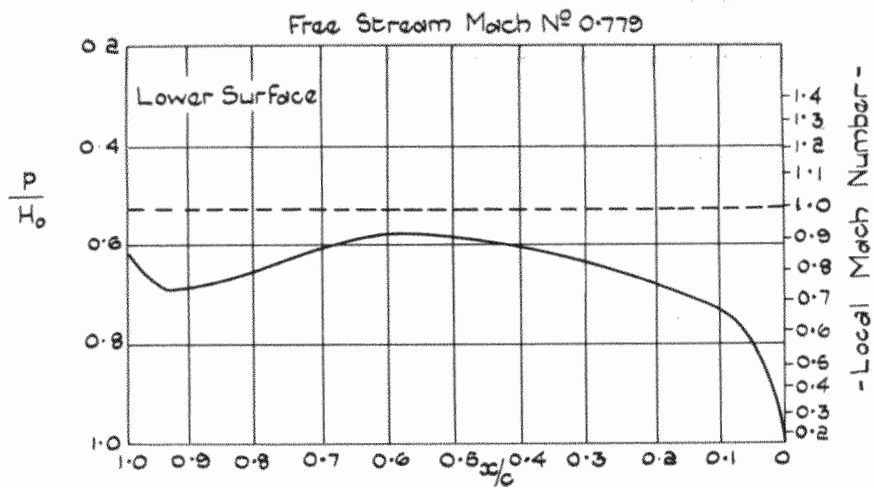
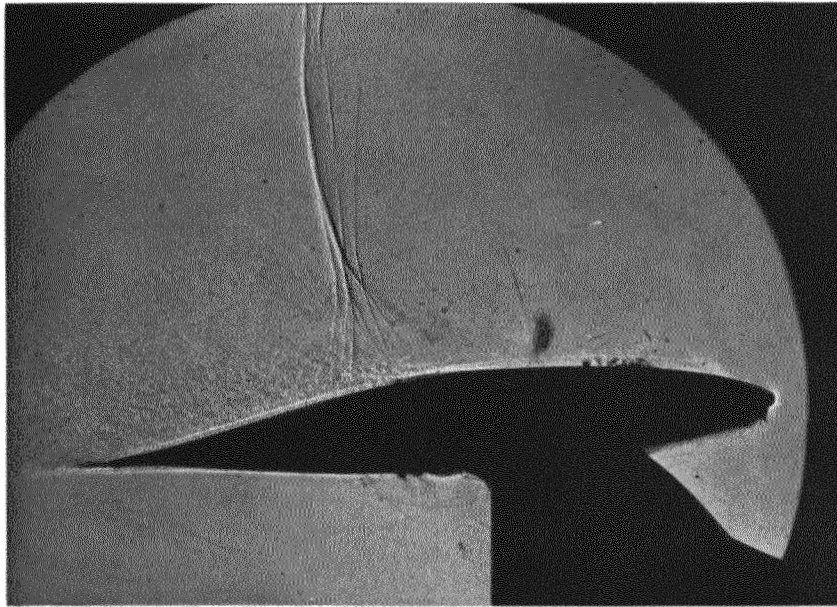
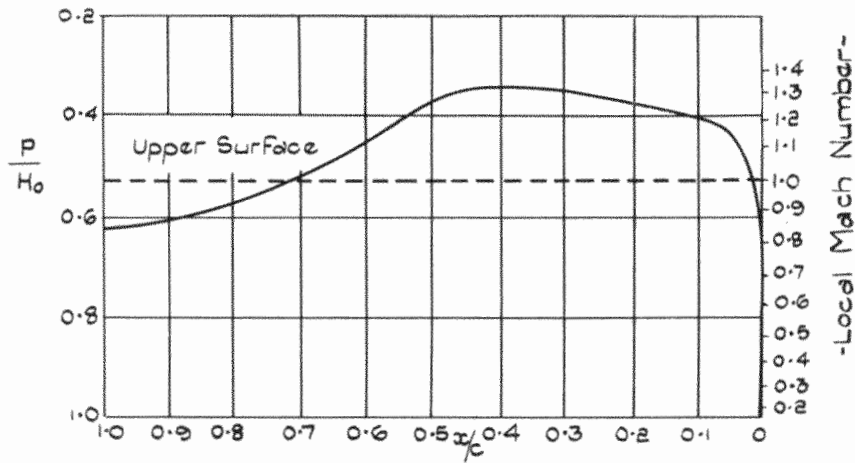
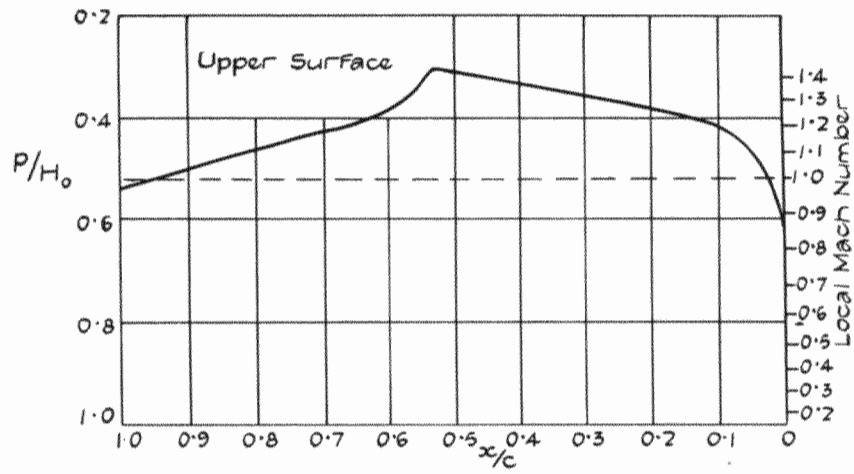


FIG. 17. Aerofoil G 1442/1547 at $\alpha = 6.5$ deg.



Free Stream Mach N° 0.829

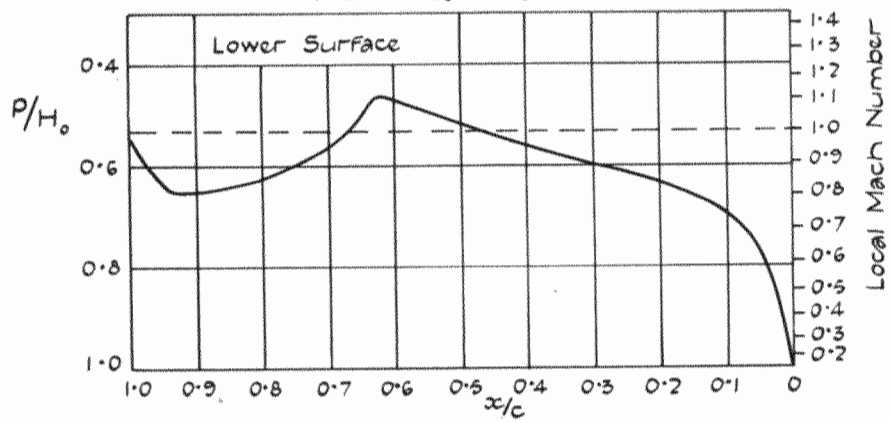


FIG. 18. Aerofoil G 1442/1547 at $\alpha = 6.5$ deg.

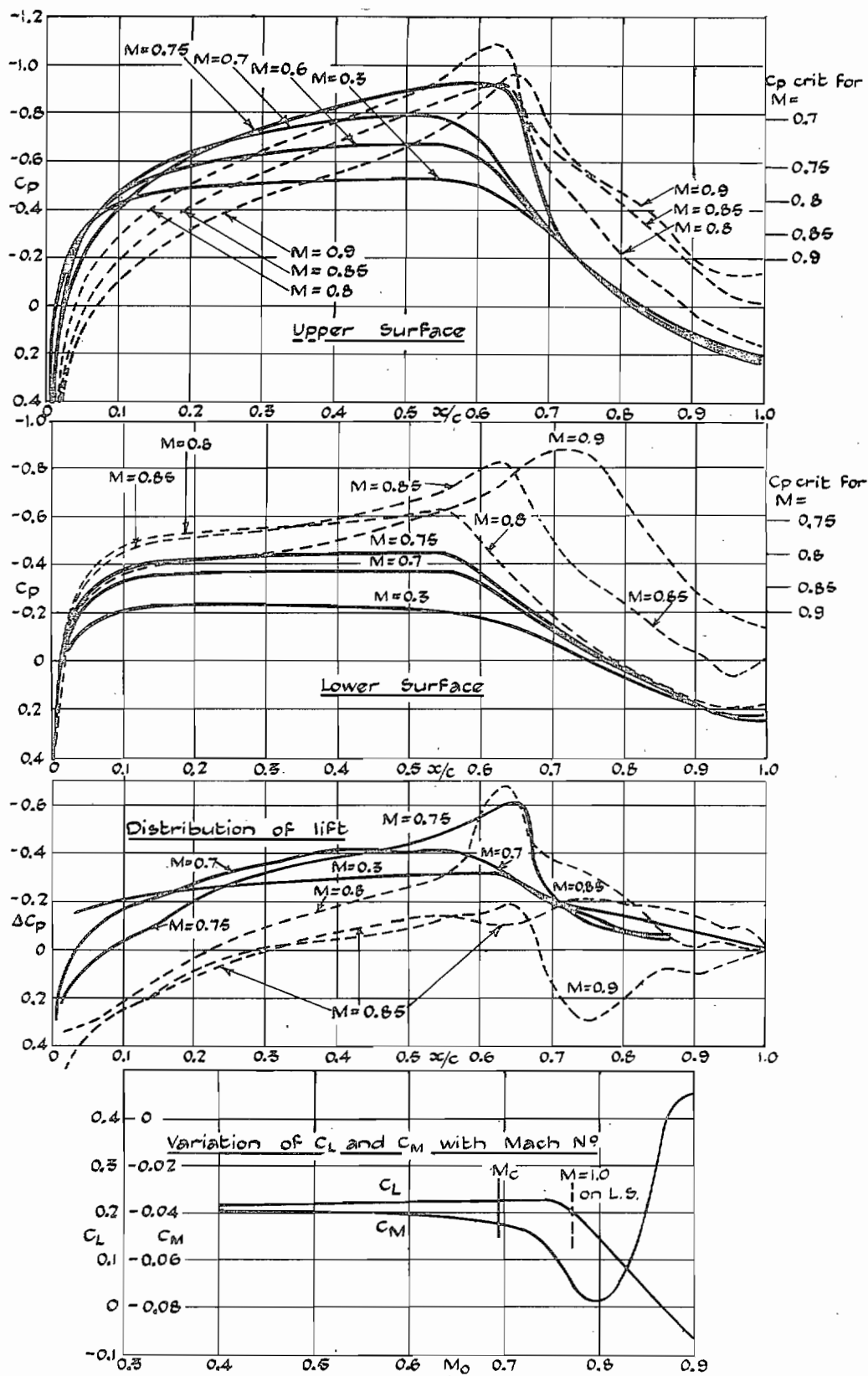


FIG. 19. Goldstein Aerofoil 1442/1547. Pressure distribution, etc., for $\alpha = 0.5^\circ$ (design incidence).

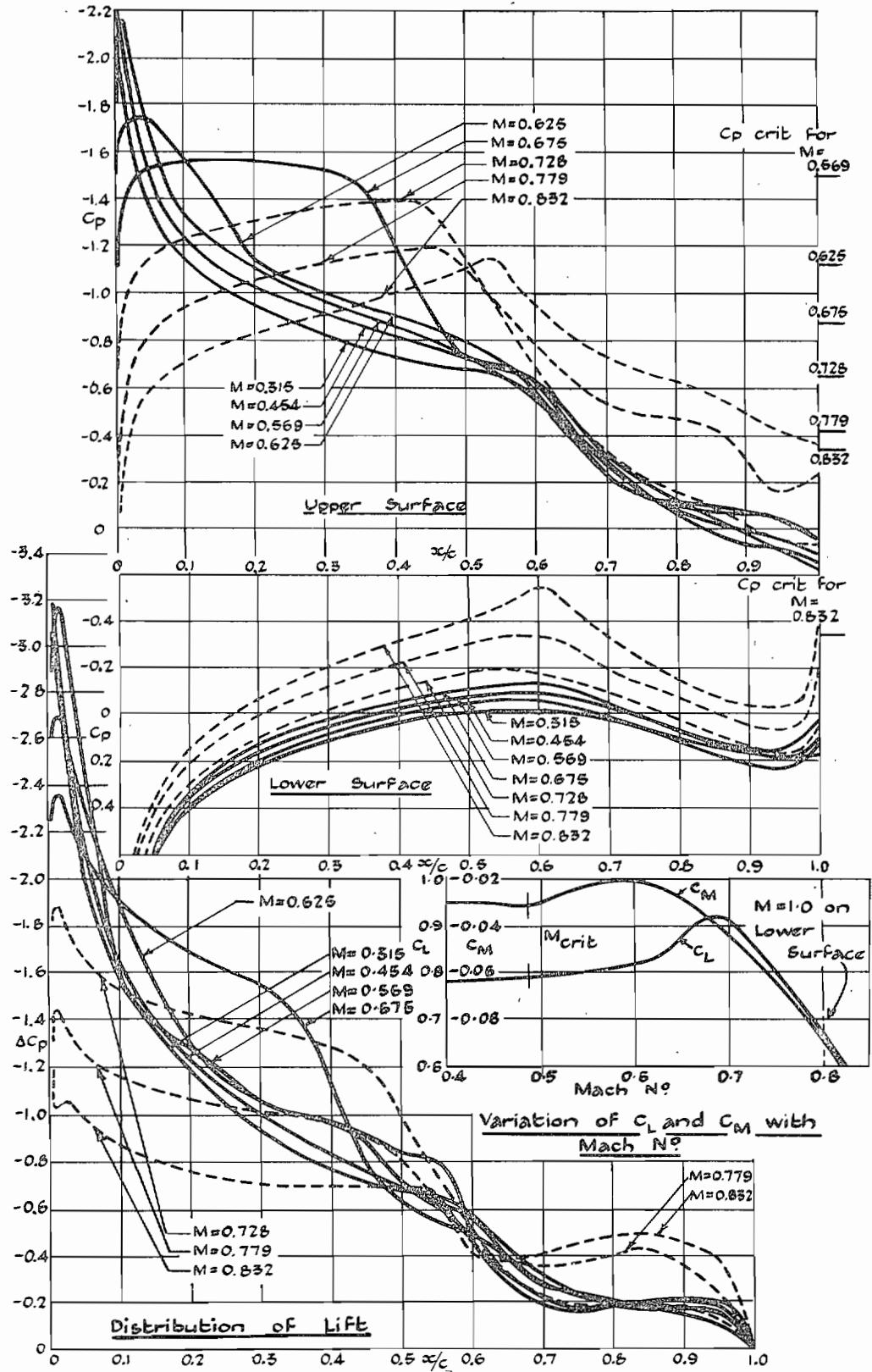


FIG. 20. Goldstein aerofoil 1442/1547. Pressure distribution, etc., for $\alpha = 6.5$ deg.

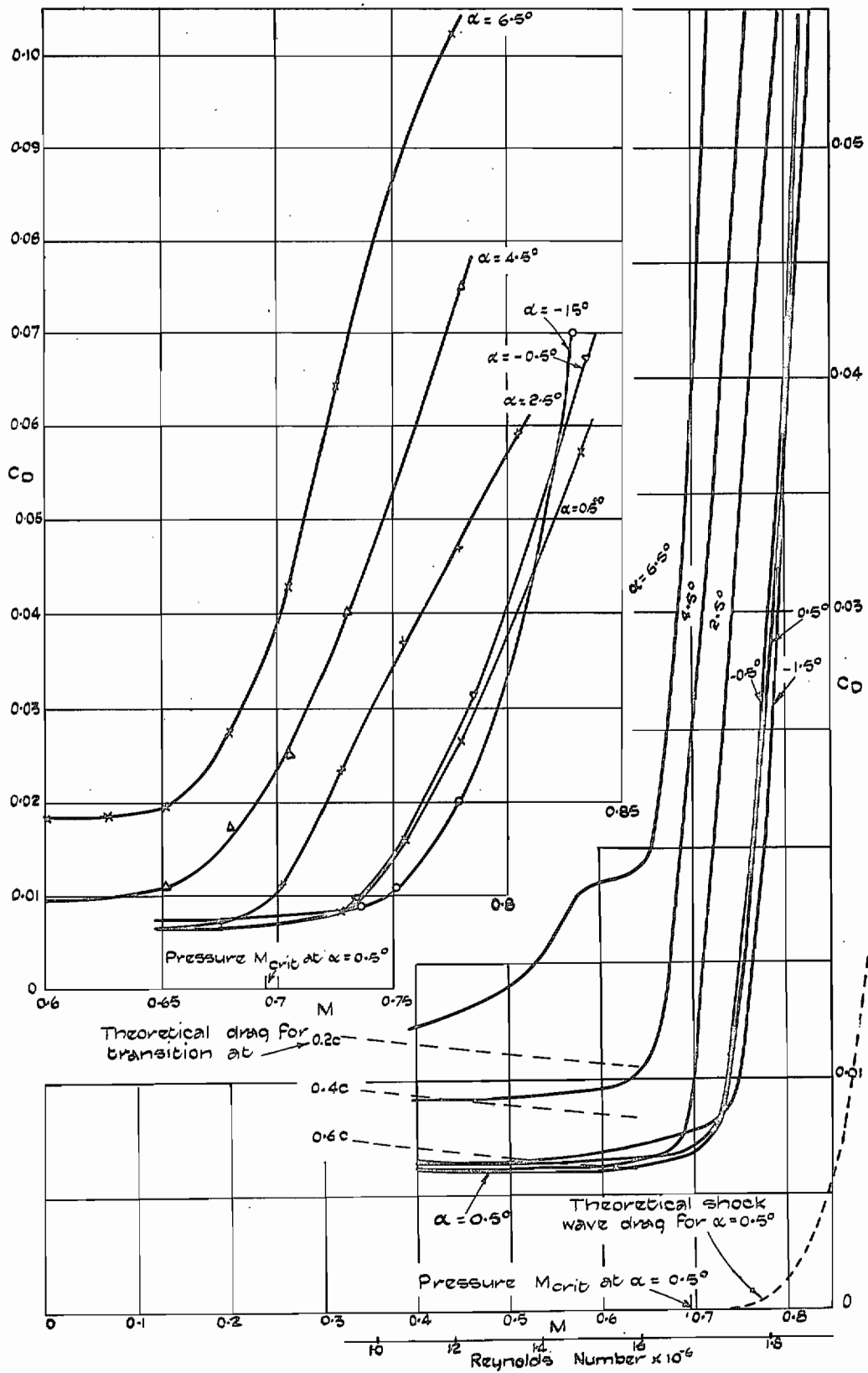


FIG. 21. Goldstein aerofoil. Variation of Profile drag with Mach number at constant incidence.

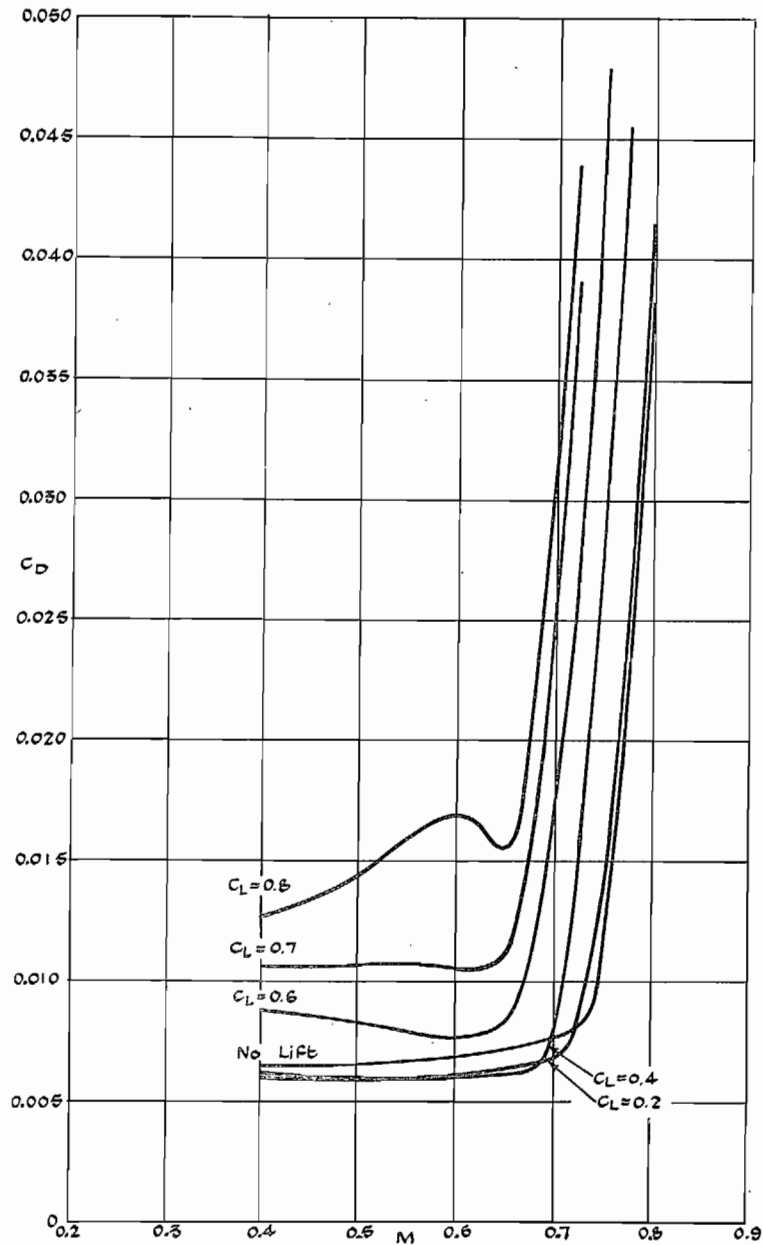


FIG. 22. Variation of Profile drag with Mach number at constant C_L . Goldstein aerofoil.

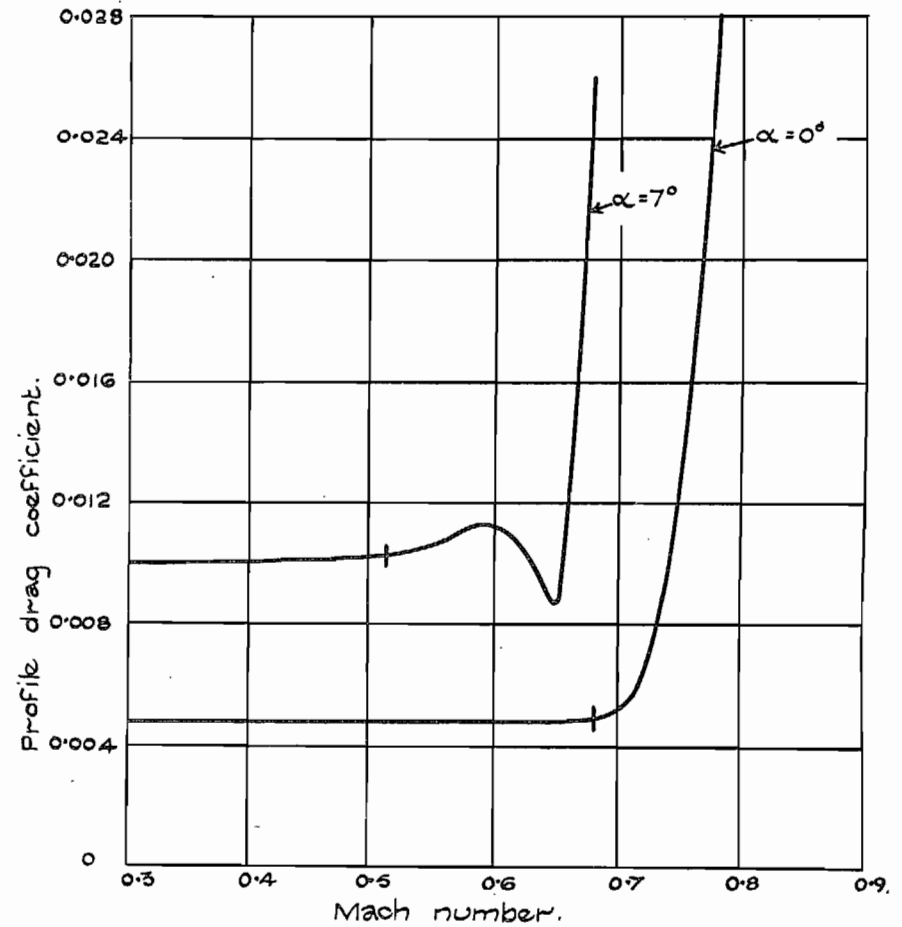


FIG. 23. Influence of transition movement on drag coefficient. (Mustang 14 1/2 40/1241 aerofoil test in 2.7m D.V.L. tunnel.)

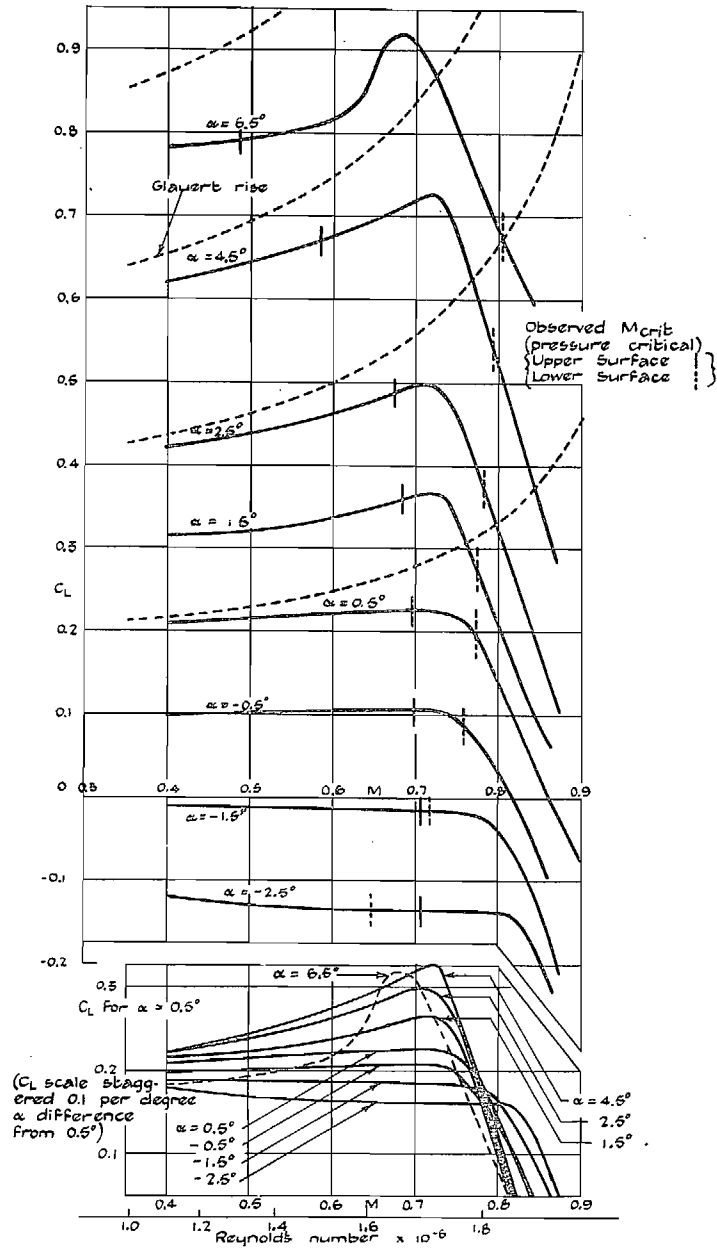


FIG. 24. Goldstein aerofoil. Variation of C_L with M at constant α .

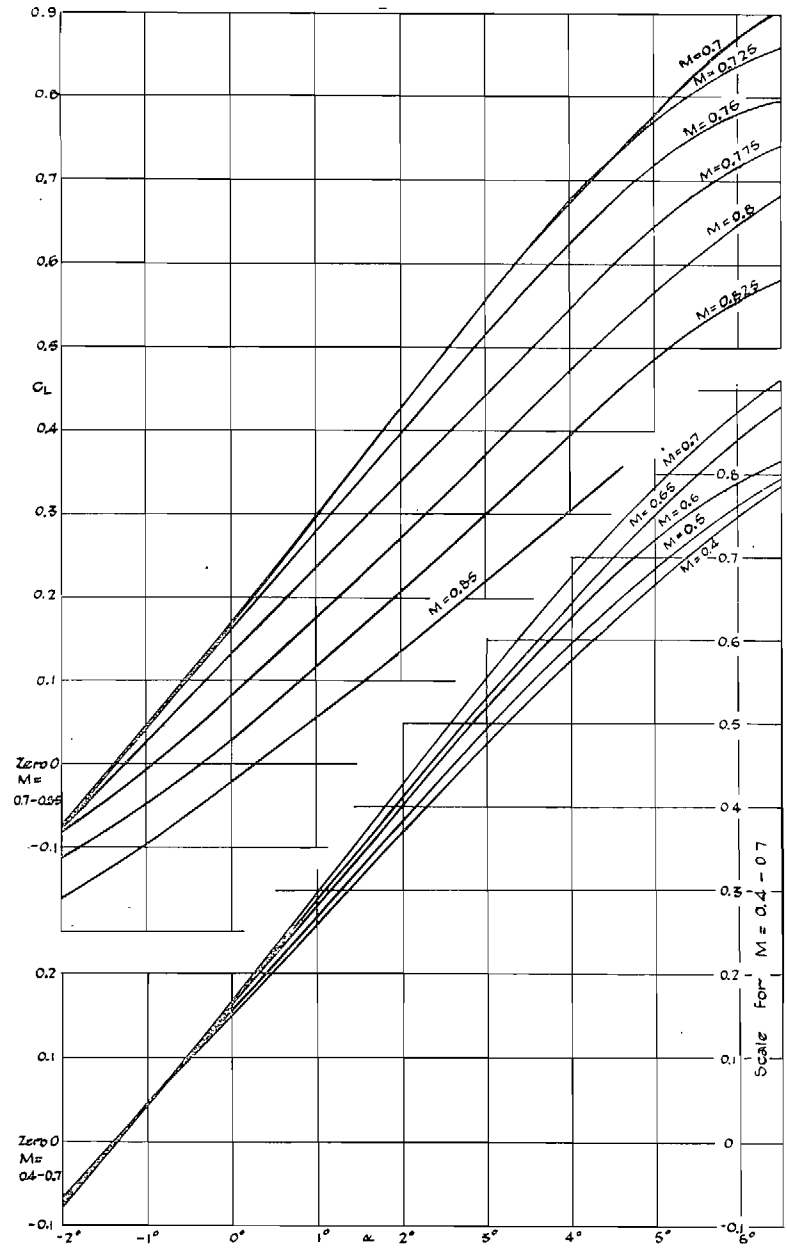


FIG. 25. Goldstein aerofoil. Variation of C_L with α at constant M .

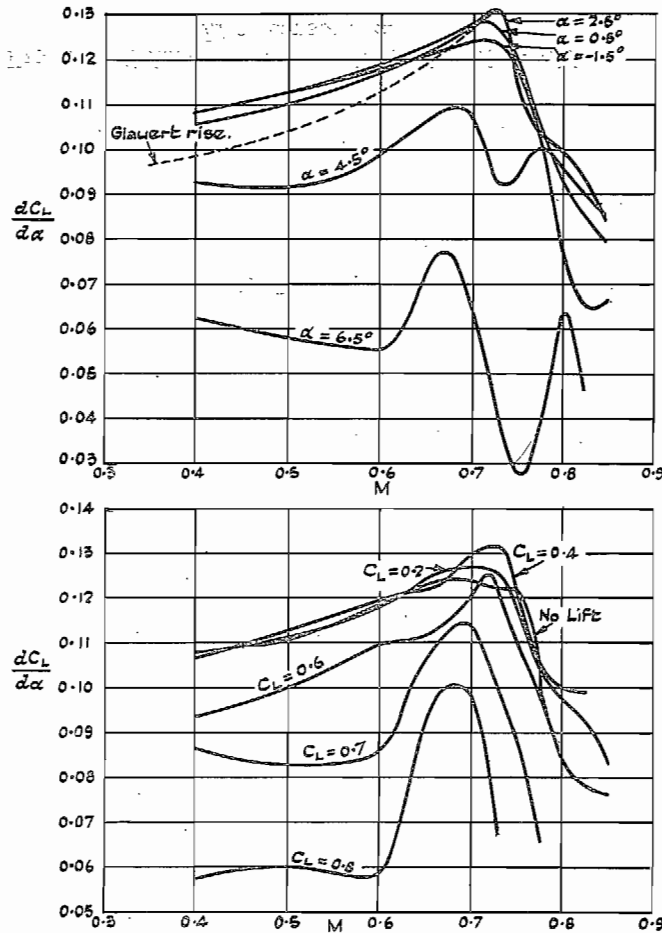


FIG. 26. Variation of $dC_L/d\alpha$ with M at constant α or C_L .

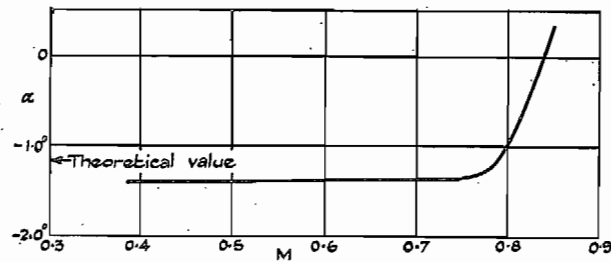


FIG. 27. Goldstein aerofoil. No-lift angle.

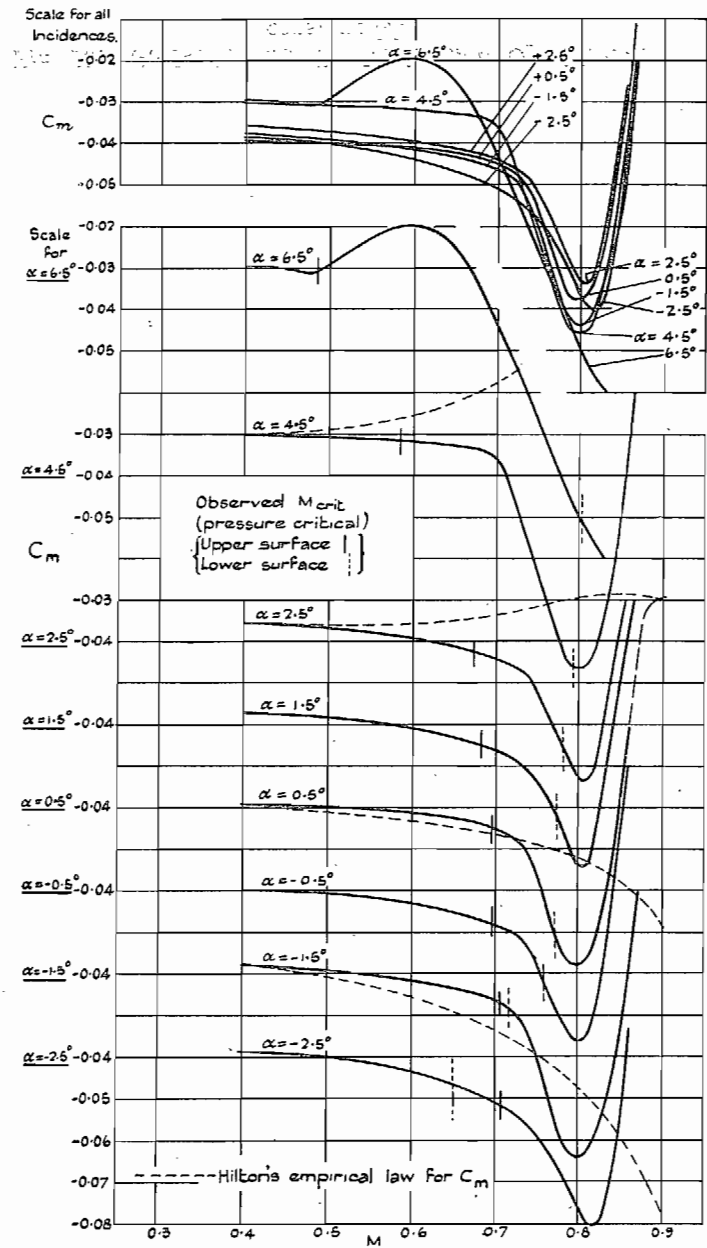


FIG. 28. Goldstein aerofoil. Variation of $\frac{1}{4}$ -chord C_m with Mach number at constant α .

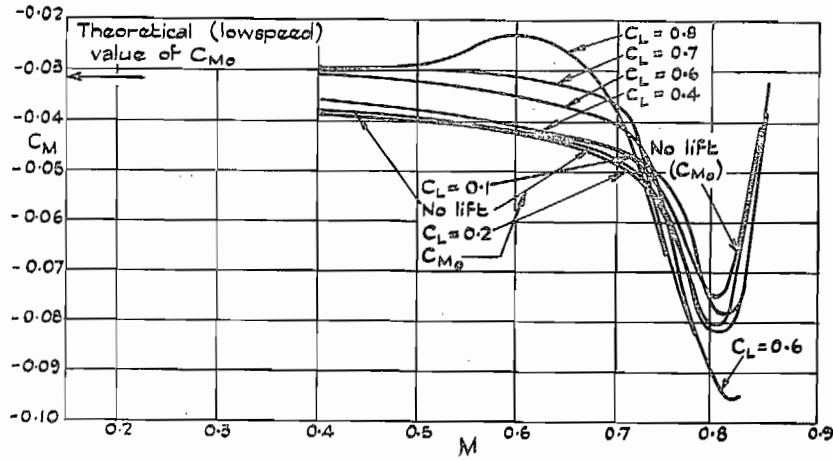


FIG. 29. Goldstein aerofoil. Variation of C_m with Mach number at constant C_L ; including C_{m0} .

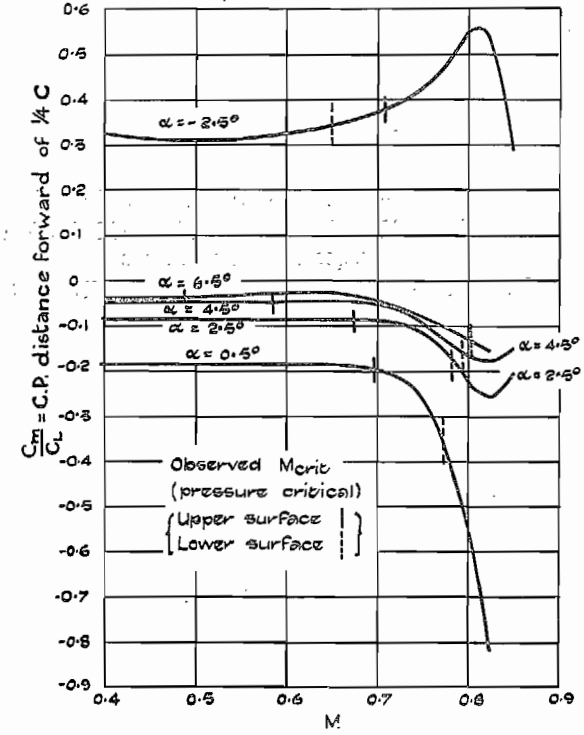


FIG. 30. Variation of C_m/C_L (C.P. position) with Mach number.

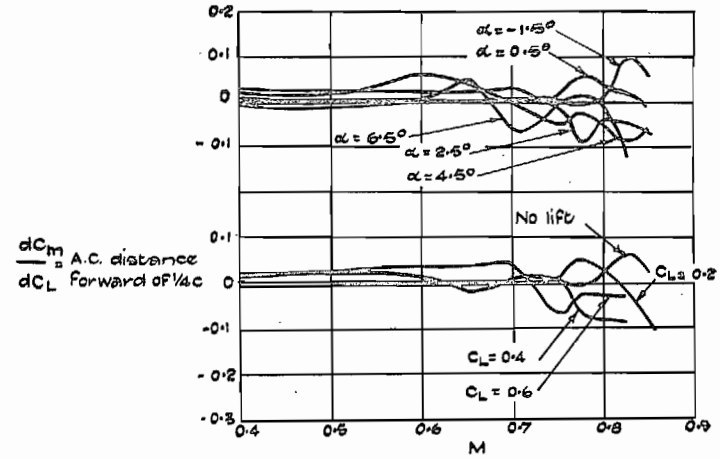


FIG. 31. Goldstein aerofoil. Variation of dC_m/dC_L and aerodynamic centre with Mach number.

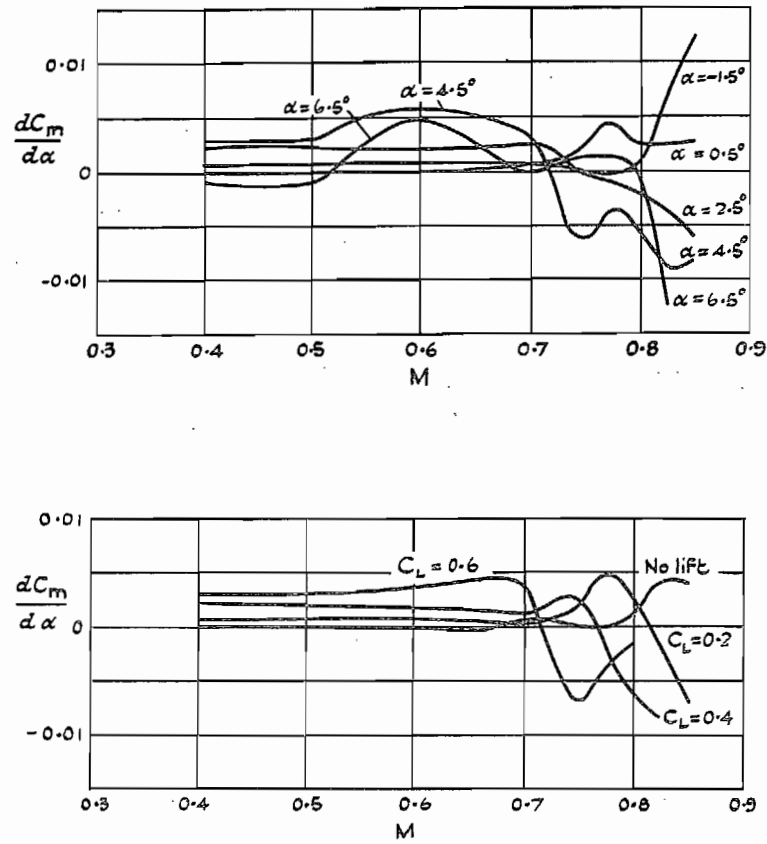


FIG. 32. Goldstein aerofoil. Variation of $dC_m/d\alpha$ with Mach number at constant α or C_L .

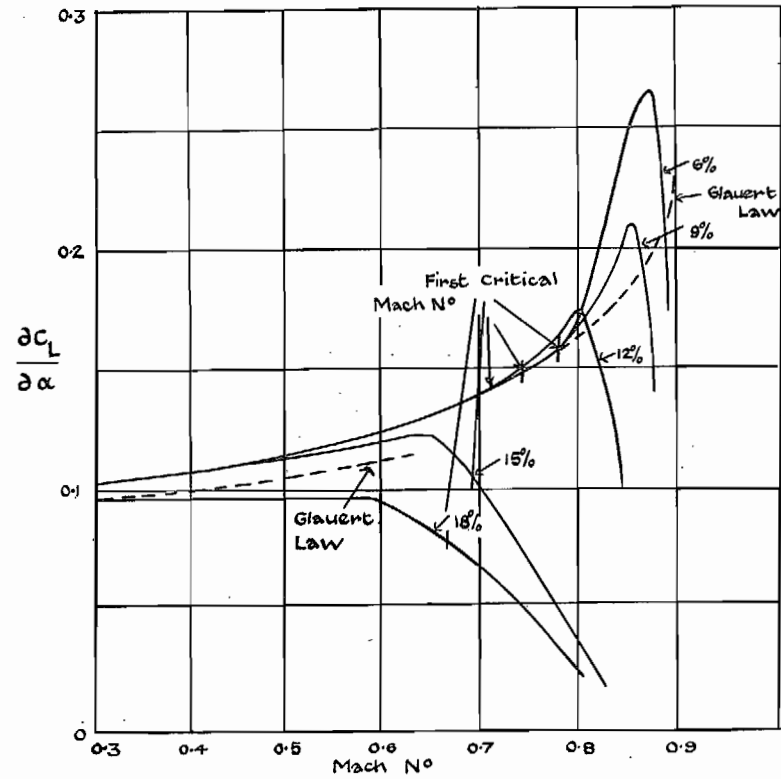


FIG. 33. Effect of thickness on lift-curve slope for symmetrical aerofoils. (N 0630, N 0930, N 1230, N 1530, N 1830.) German tests in 2.7m D.V.L. tunnel.

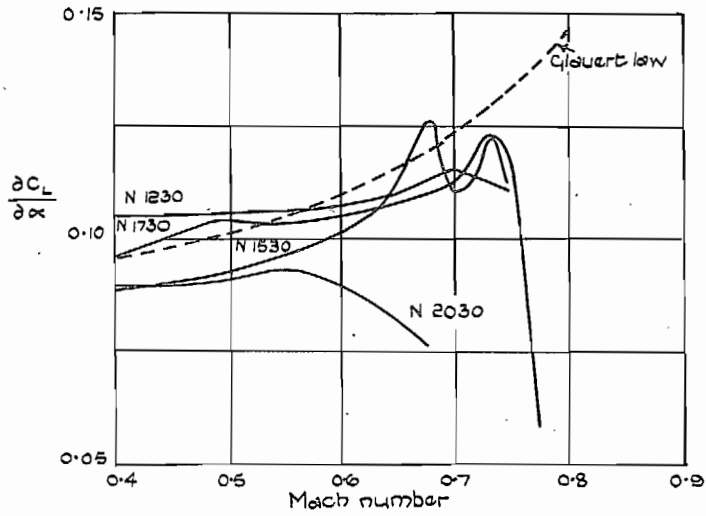


FIG. 34. Effect of thickness on lift-curve slope (N.P.L. 2-in. chord). (Symmetrical aerofoils 12, 15, 17 and 20 per cent thick at 30 per cent chord.)

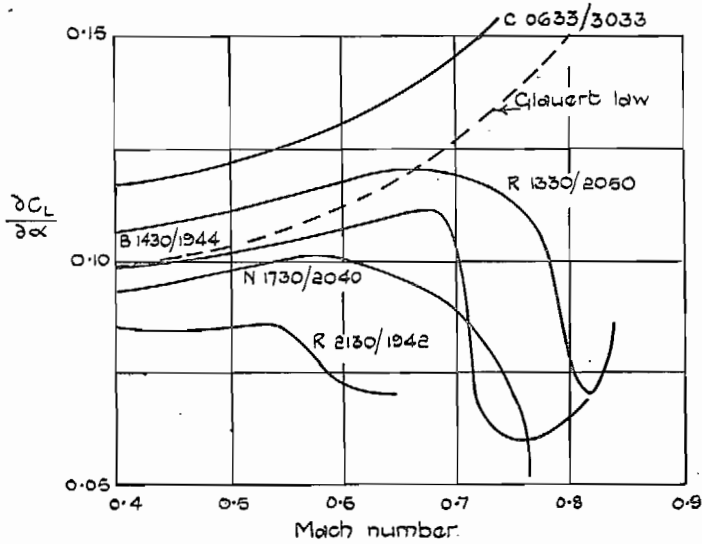


Fig. 35. Effect of thickness on lift-curve slope (N.P.L. 2-in. chord). (Cambered aerofoils 6, 13, 14, 17 and 21 per cent thick at about 30 per cent chord.)

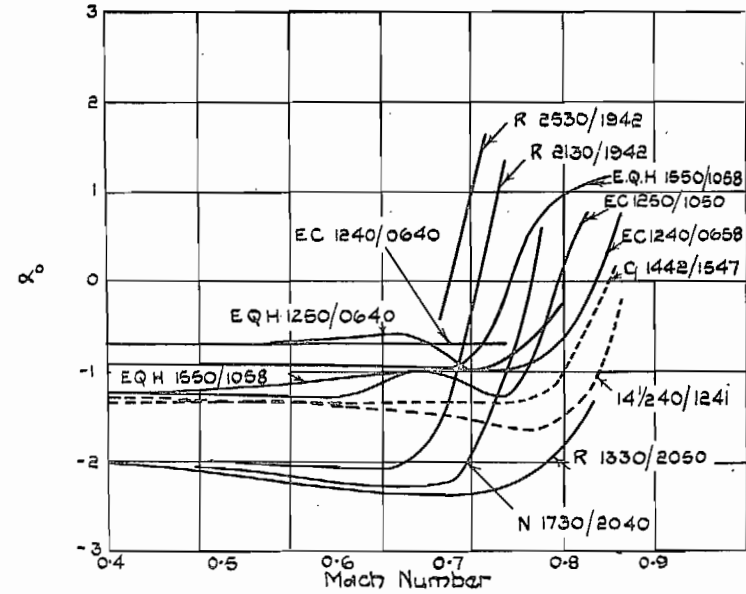


FIG. 36. Variation of no-lift angle with Mach number. Full lines 2-in. chord in 12-in. diameter Tunnel. Broken lines 5-in. chord in 20 x 8-in. tunnel.

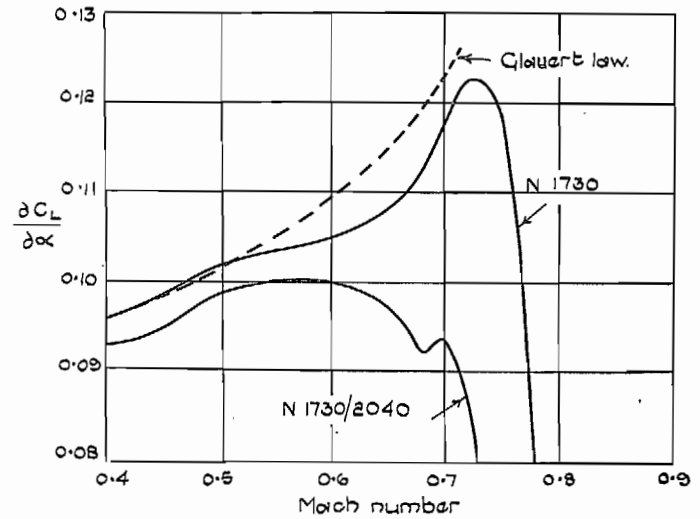


FIG. 37. Effect of camber on lift-curve slope (17 per cent thick aerofoil at 30 per cent chord).

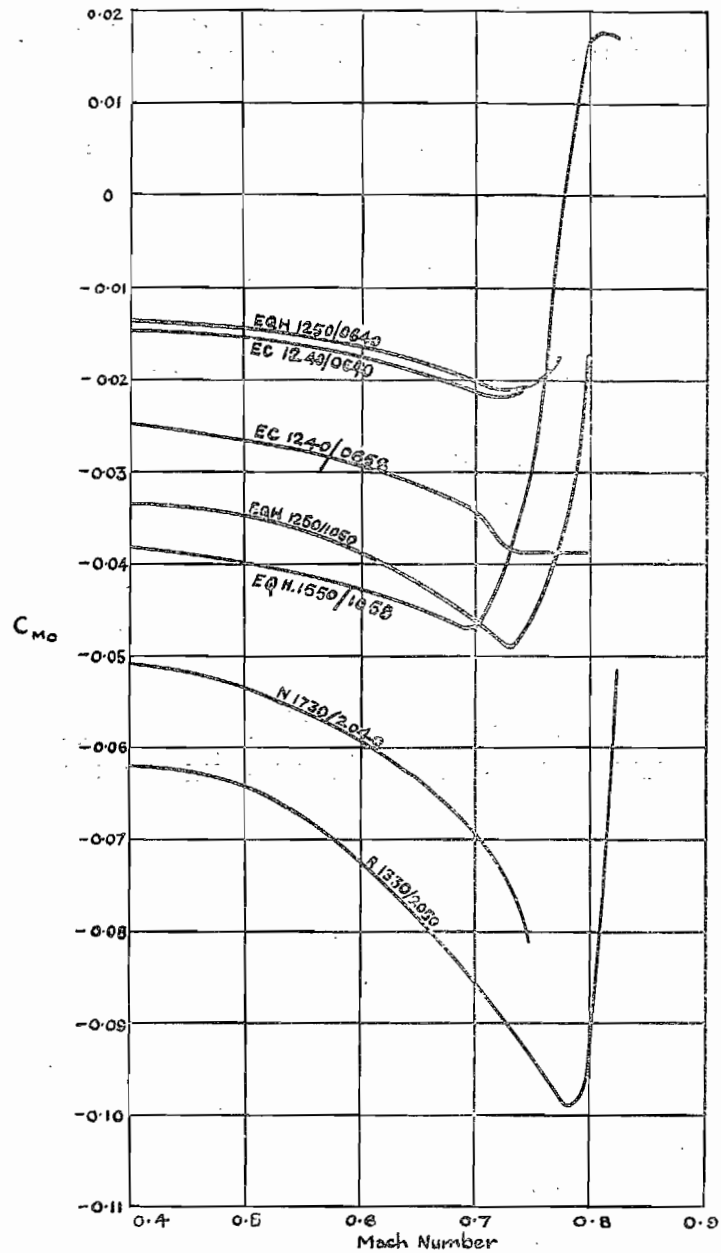


FIG. 38. Variation of pitching-moment coefficient at zero lift with Mach number for cambered aerofoils.

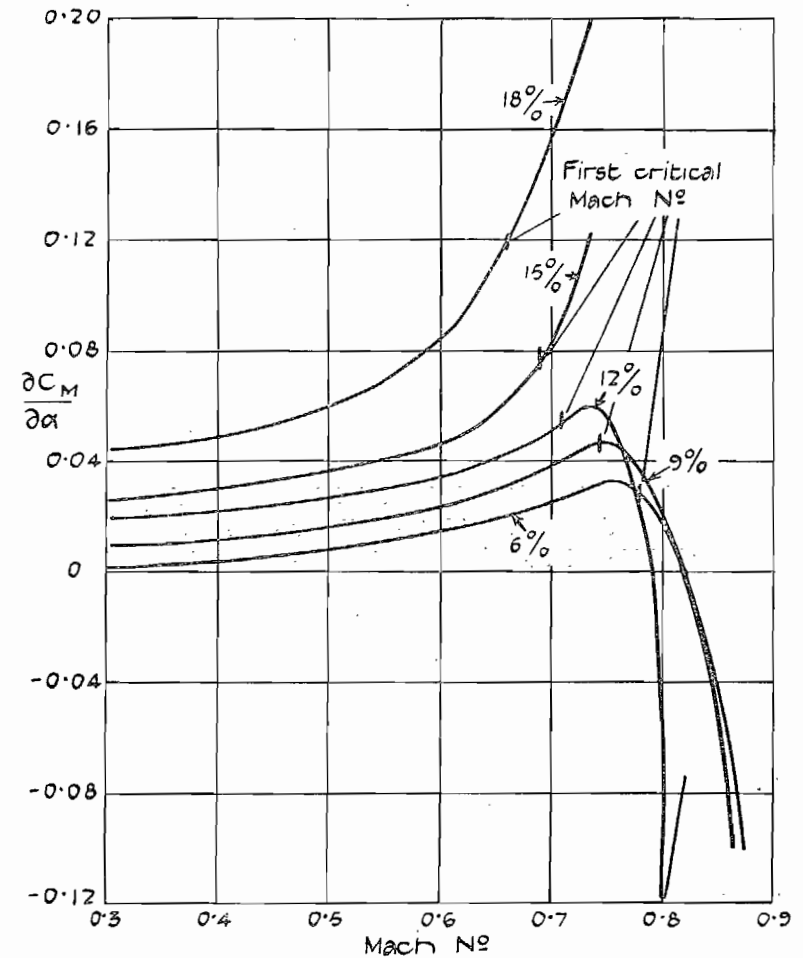


FIG. 39. Effect of thickness on moment-curve slope for symmetrical aerofoils.

(N 0630, N 0930, N 1230, N 1530, N 1830.)

German tests in 2.7m D.V.L. tunnel.

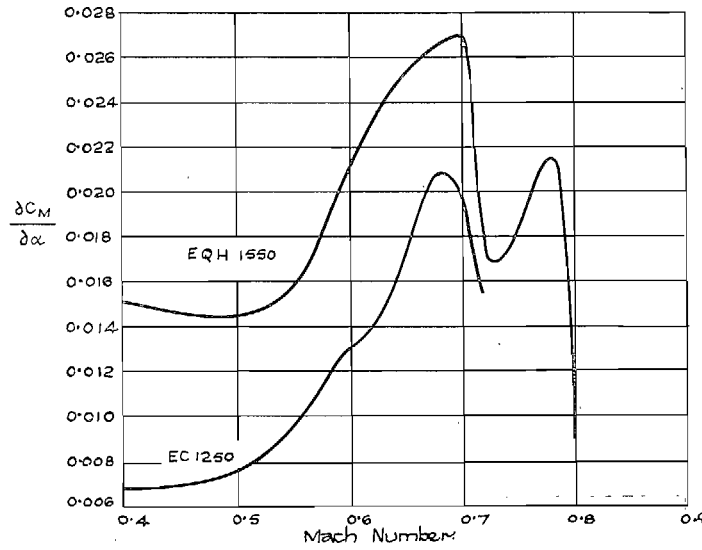
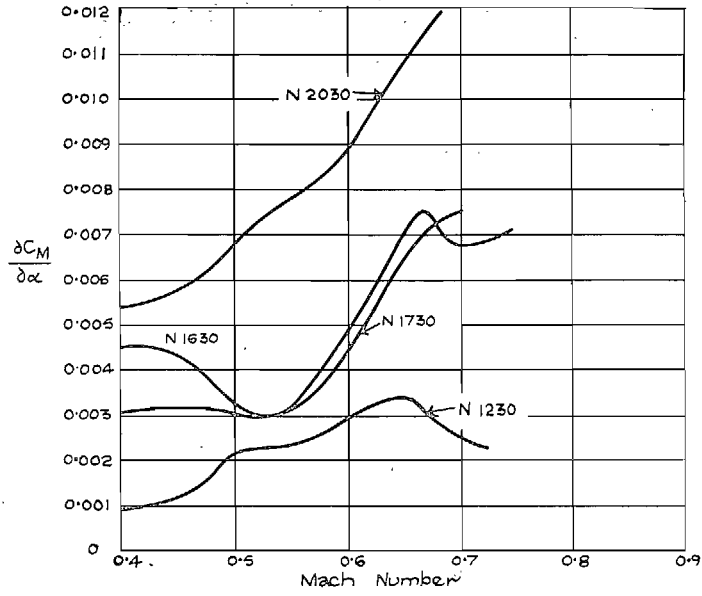


FIG. 40. Effect of thickness on moment-curve slope for symmetrical aerofoils.

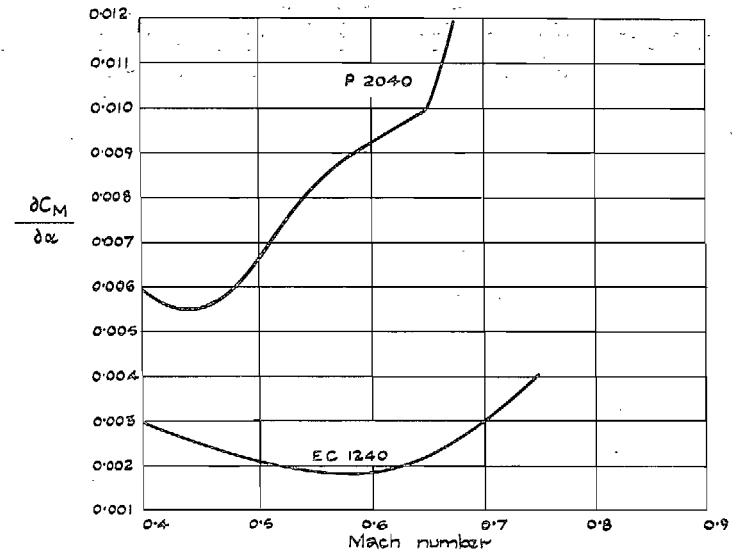


FIG. 41. Effect of thickness on moment-curve slope for symmetrical aerofoils.

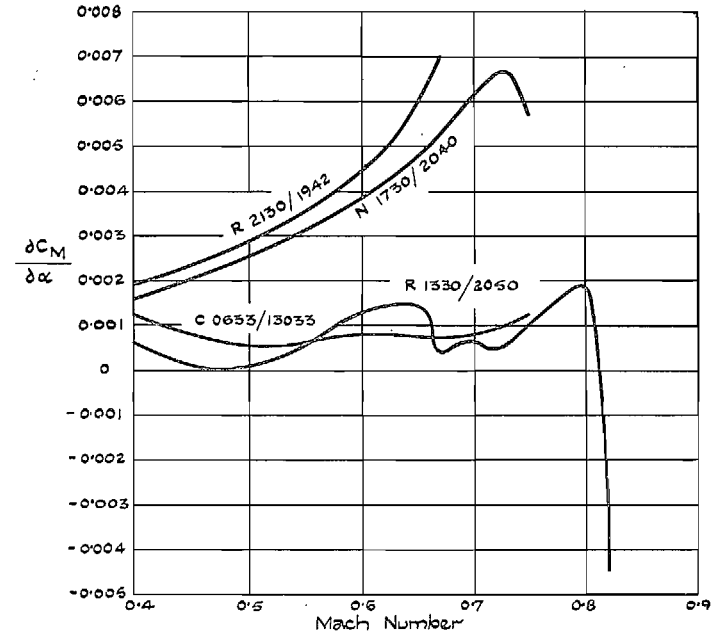


FIG. 42. Effect of thickness on moment-curve slope for cambered aerofoils.

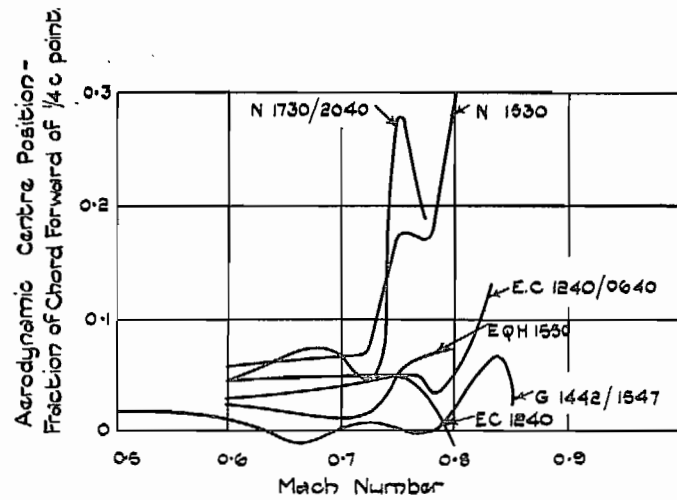


FIG. 43. Position of the aerodynamic centre.

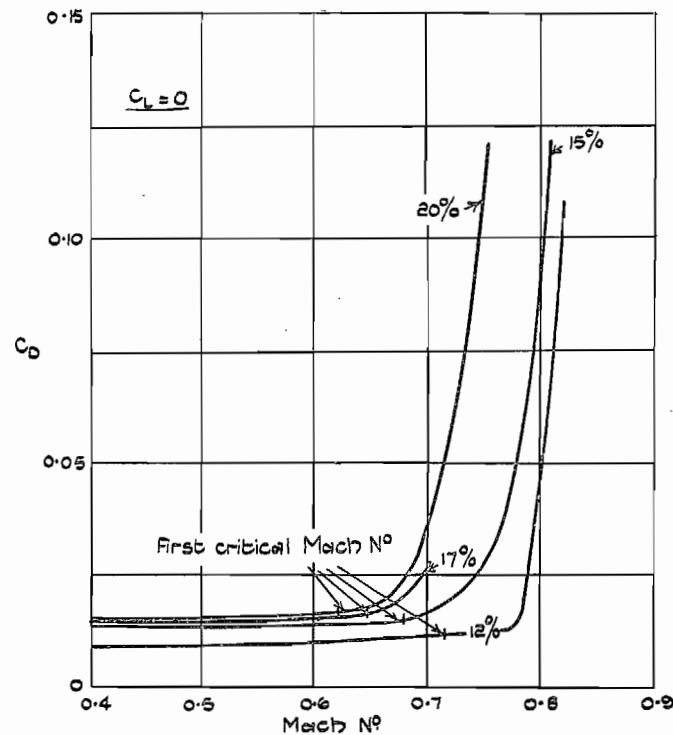


FIG. 44. Influence of thickness on drag rise
(2-in. chord in 12-in. tunnel)
(Symmetrical aerofoils N 1230, N 1530, N 1730, N 2030).

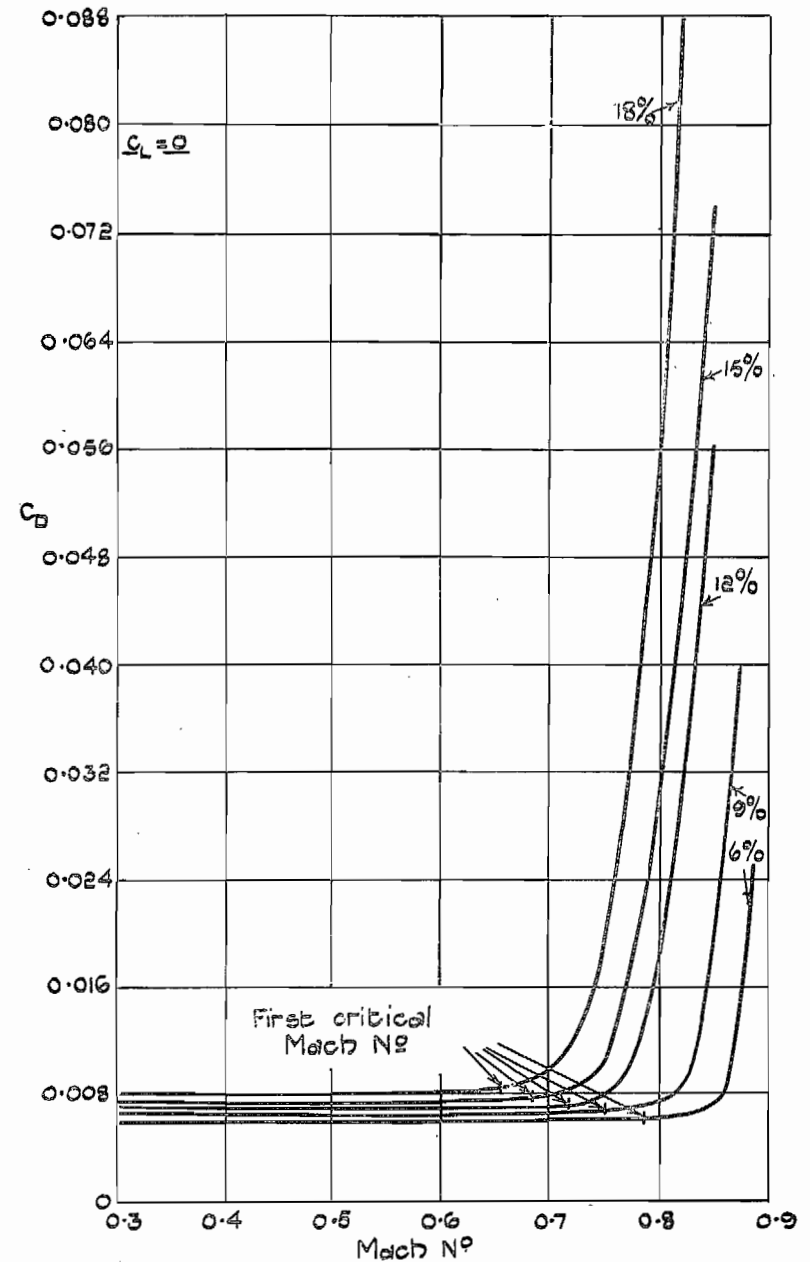


FIG. 45. Influence of thickness on drag rise.
(Symmetrical aerofoils N 0630, N 0930, N 1230, N 1530, N 1830).
German results in 2.7m D.V.L. tunnel.

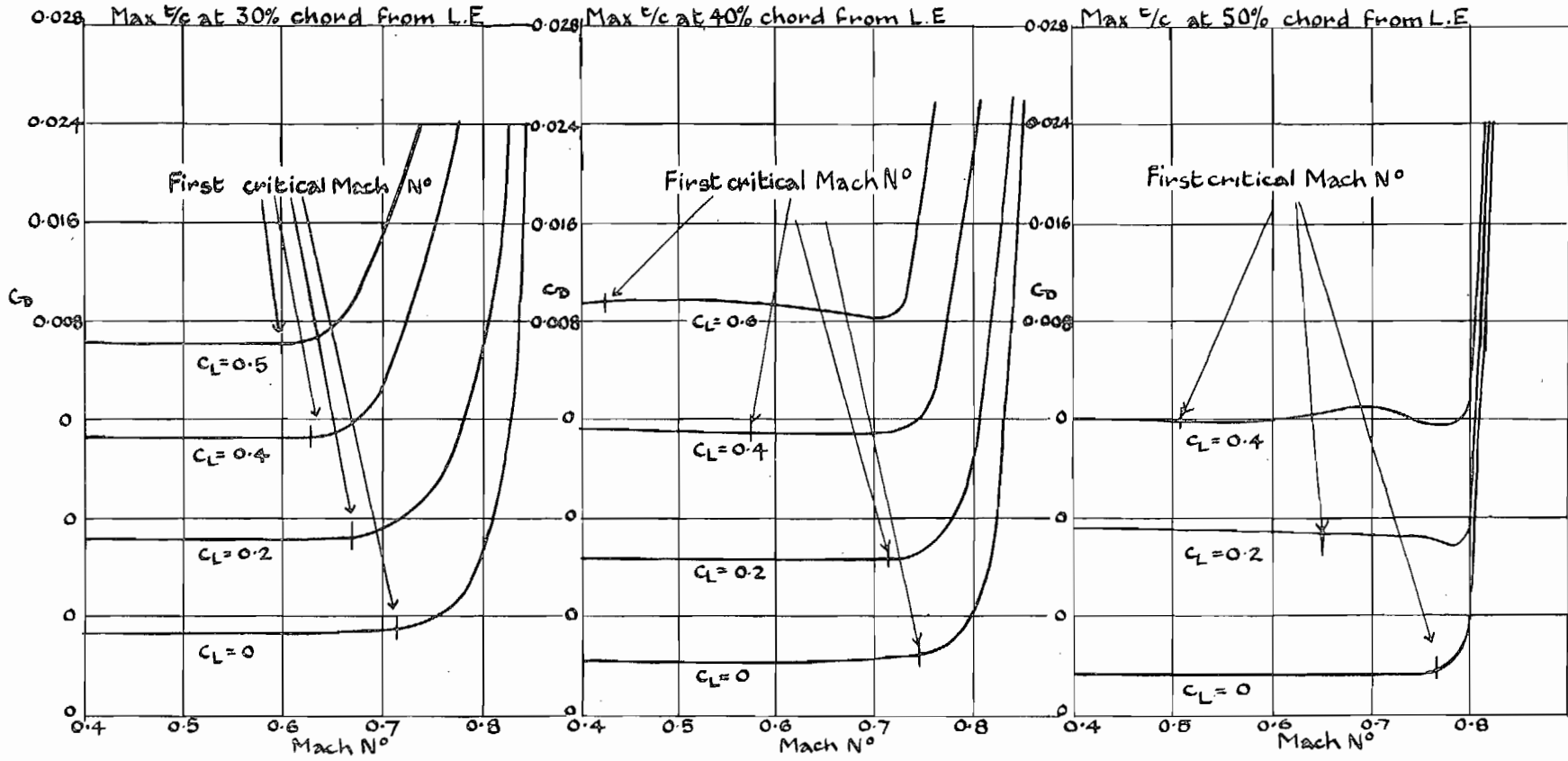


FIG. 46. Effect of position of maximum thickness on profile drag. (Symmetrical aerofoils N 1230, N 1240, N 1250.)

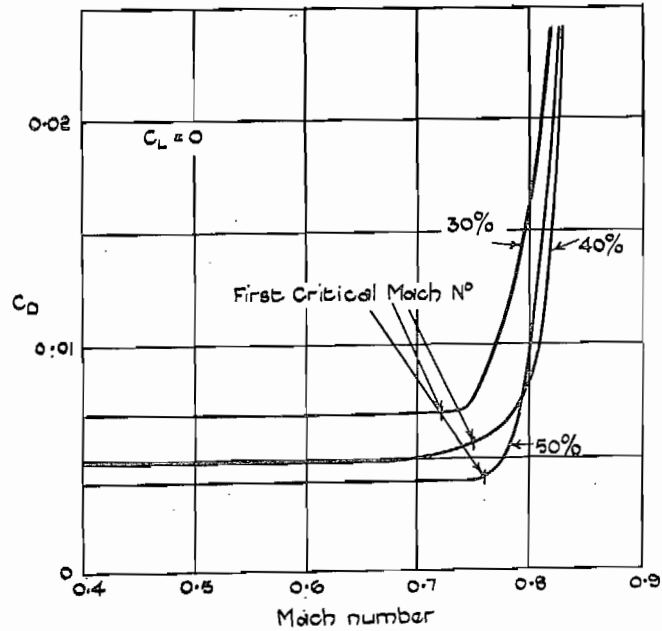


FIG. 47. Influence of maximum thickness position on drag rise.

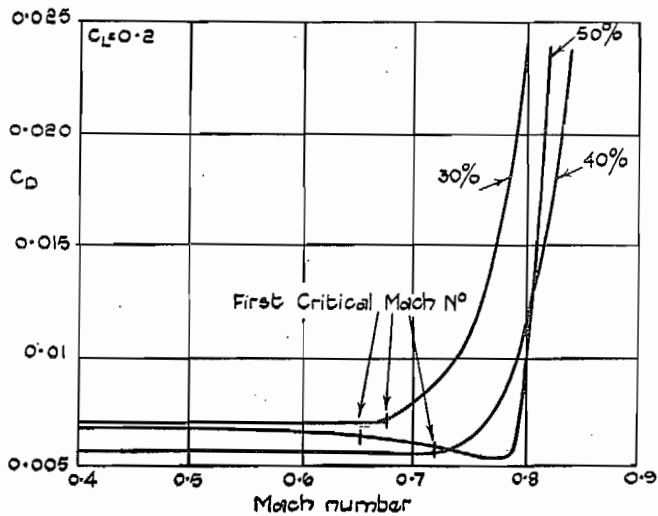


FIG. 48. Influence of maximum thickness position on drag rise.

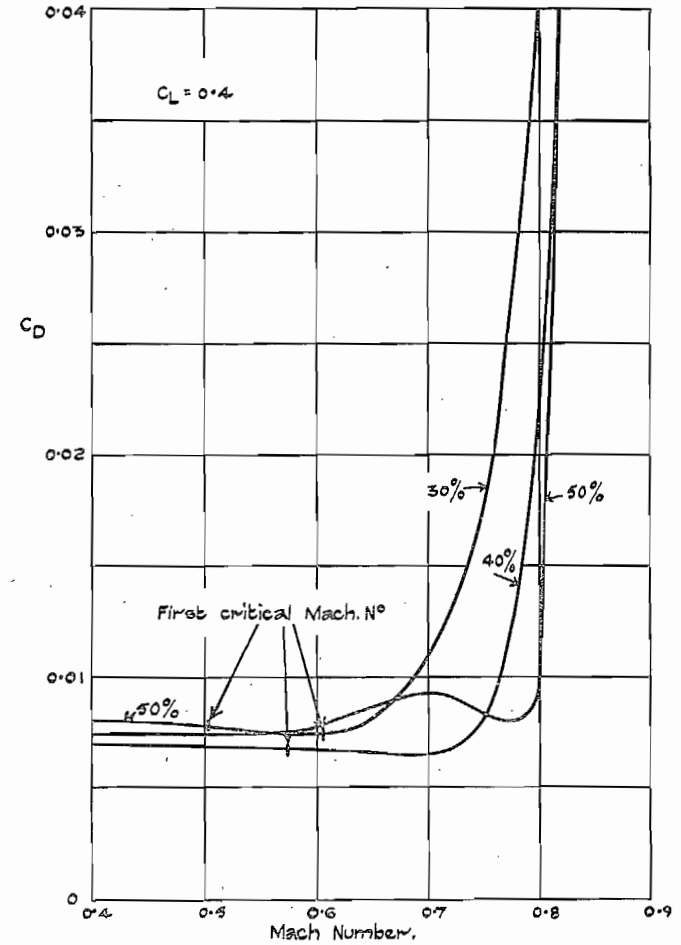
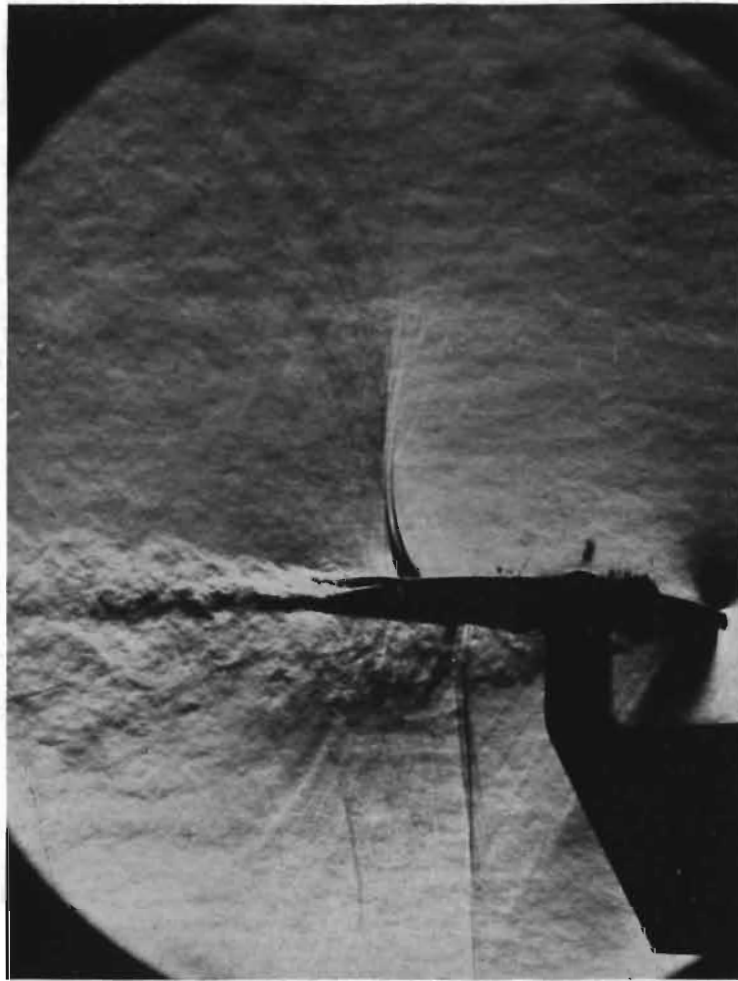


FIG. 49. Influence of maximum thickness position on drag rise.



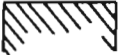
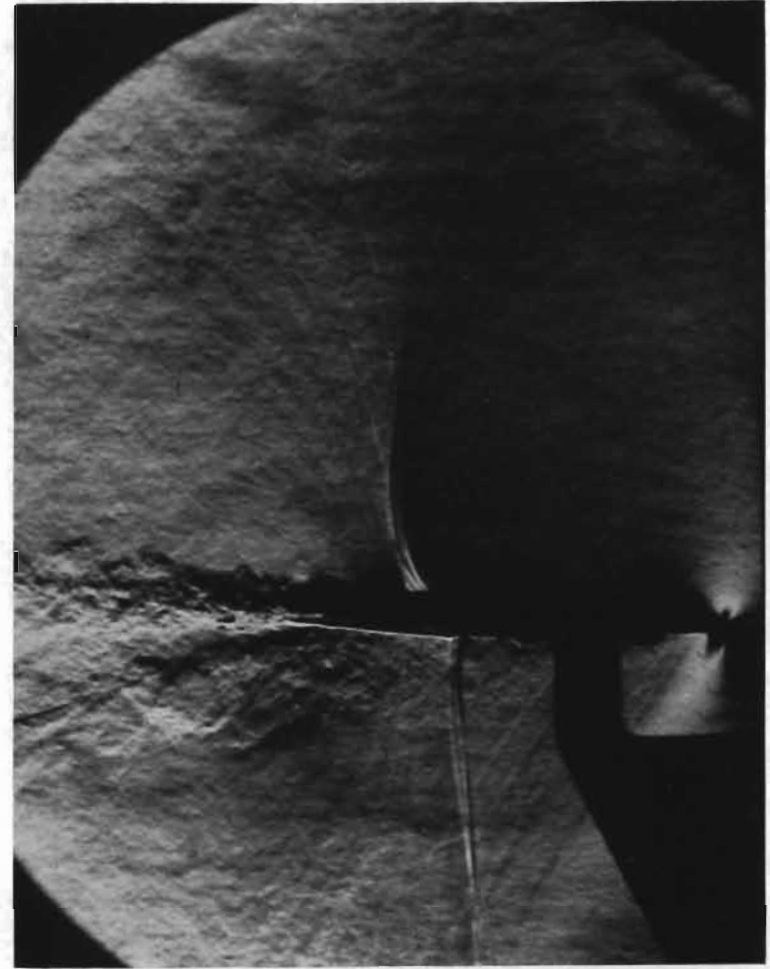
Position of Knife Edge. 

FIG. 50. Schlieren photograph of the flow around a 10 per cent NACA propeller aerofoil at $M = 0.84$, $\alpha = -2$ deg.



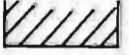
Position of Knife Edge. 

FIG. 51. Schlieren photograph of the flow around a 10 per cent NACA propeller aerofoil at $M = 0.84$, $\alpha = -2$ deg.



Position of Knife Edge.



FIG. 52. Schlieren photograph of the flow around a 10 per cent NACA propeller aerofoil at $M = 0.84$, $\alpha = -2$ deg.



Position of Knife Edge.



FIG. 53. Schlieren photograph of the flow around a 10 per cent NACA propeller aerofoil at $M = 0.84$, $\alpha = -2$ deg.

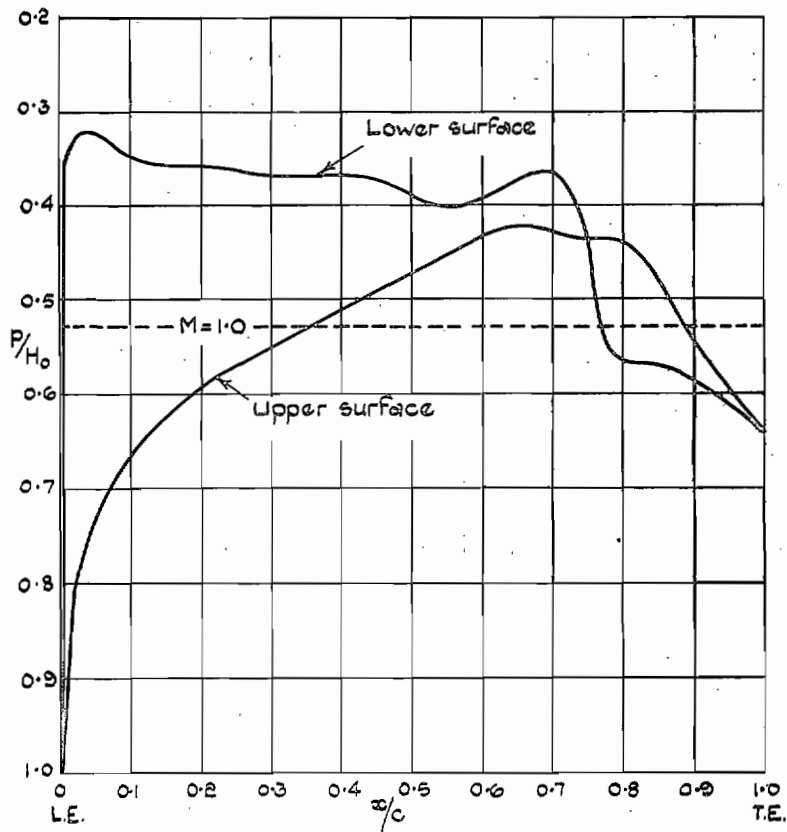


FIG. 54. Pressure distribution on 10 per cent NACA propeller aerofoil at $M = 0.84$, $\alpha = -2$ deg. (Note: This figure should be examined in conjunction with Figs. 50-53.)

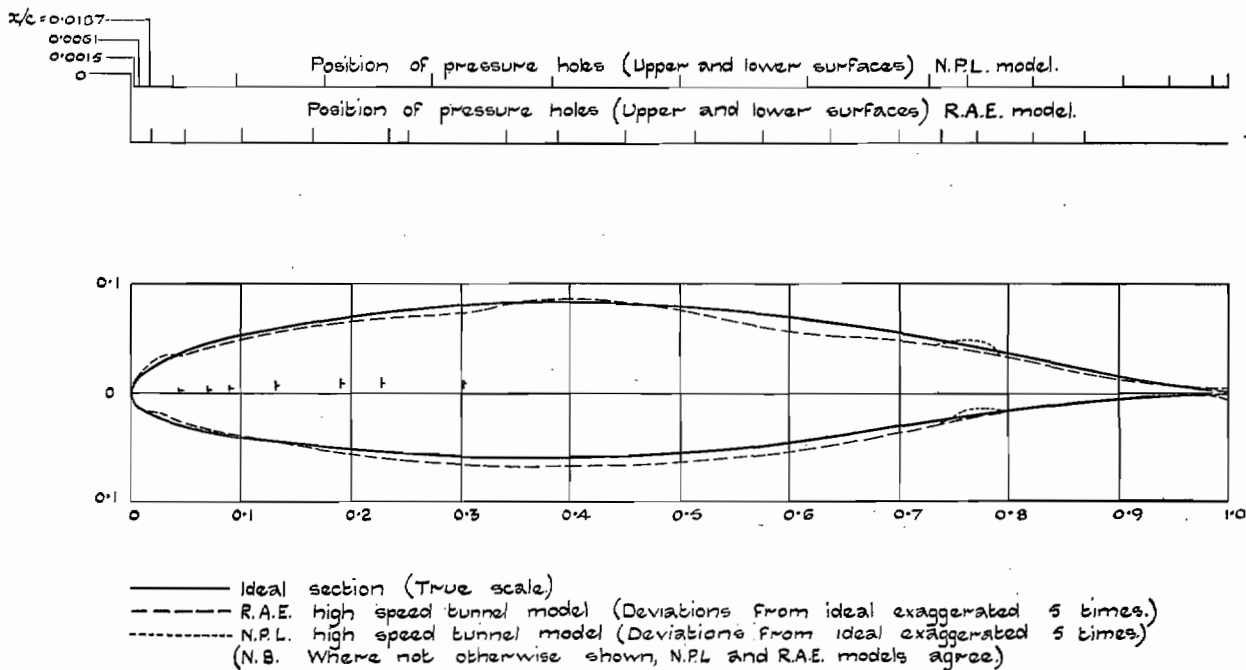


FIG. 55. Mustang wing profile, and positions of pressure holes.

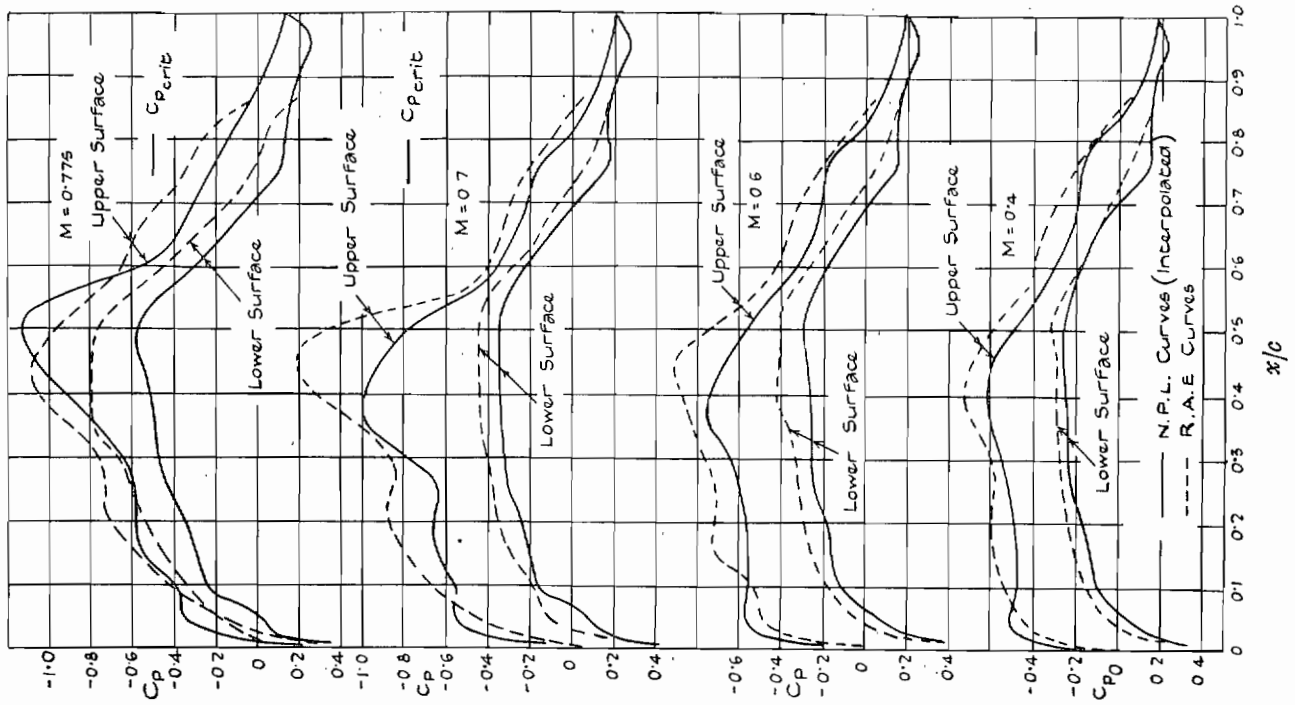


FIG. 56. Mustang wing: pressure distribution.
 $\alpha = +1$ deg. R.A.E. and N.P.L. high-speed tunnels.

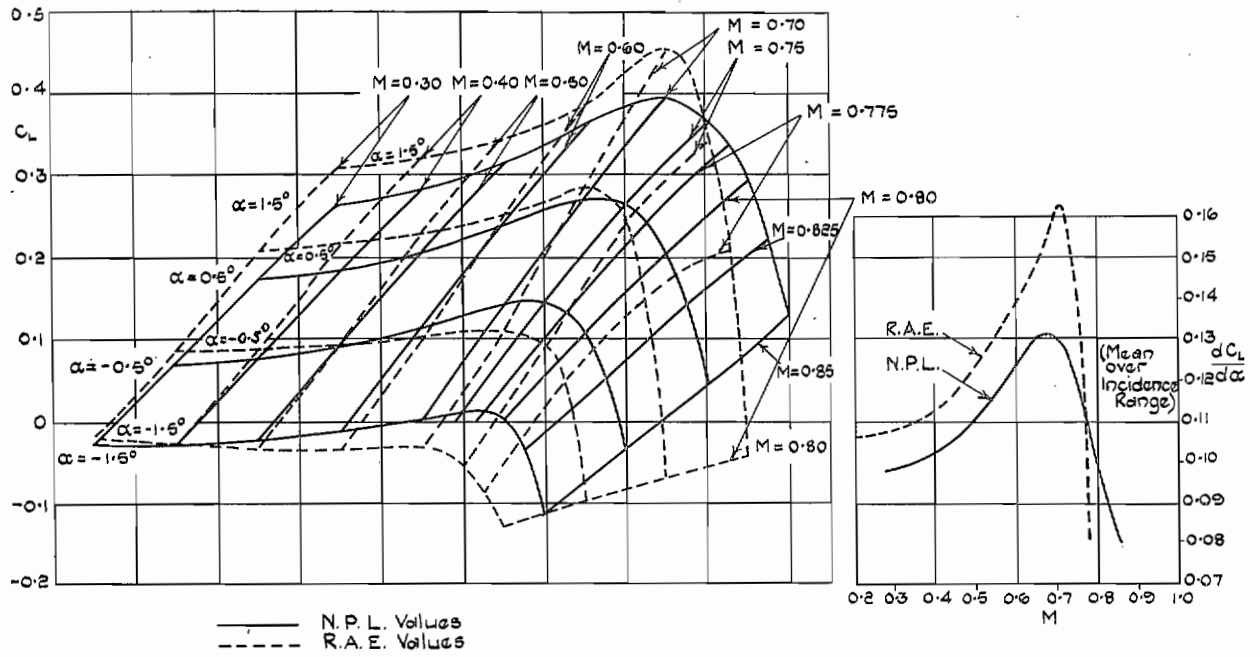


FIG. 57. Mustang wing: lift carpet. R.A.E. and N.P.L. high-speed tunnels.

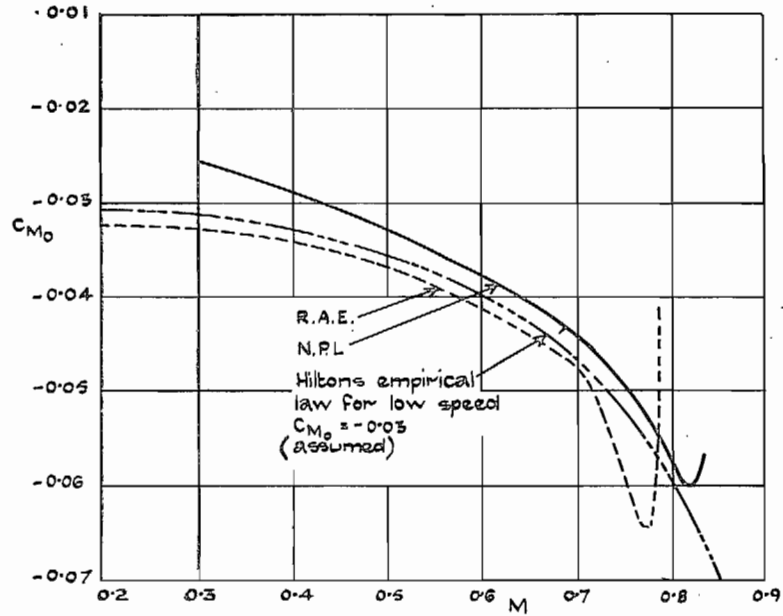


FIG. 58. Mustang wing: variation of C_{m_0} with Mach number. R.A.E. and N.P.L. high-speed tunnels.

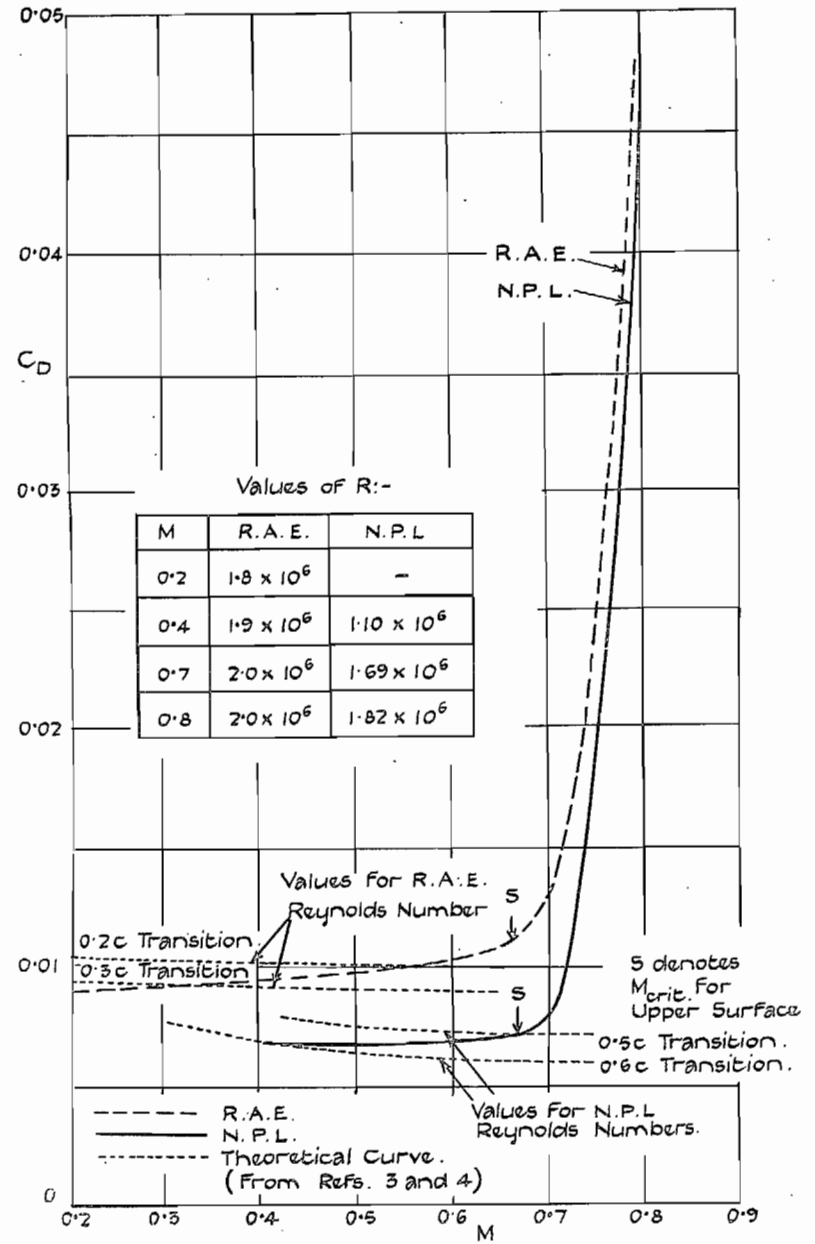


FIG. 59. Mustang wing: wake traverse drag ($\alpha = 0$). R.A.E. and N.P.L. high-speed tunnels.

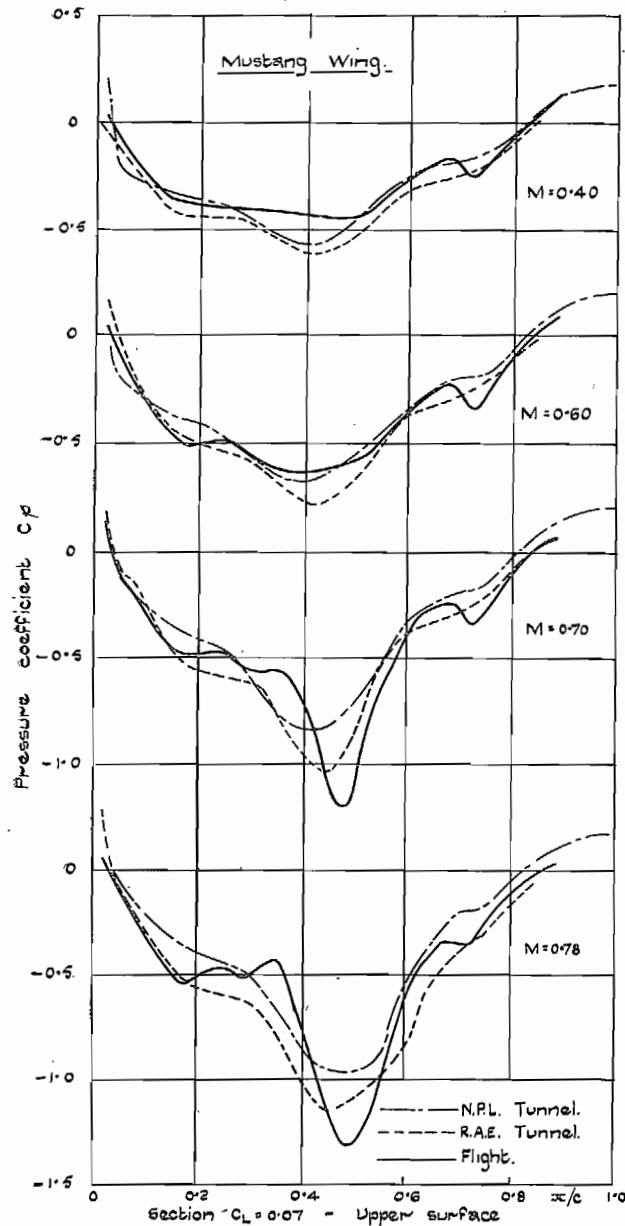


FIG. 60(a). Comparison of flight and high-speed wind-tunnel results.

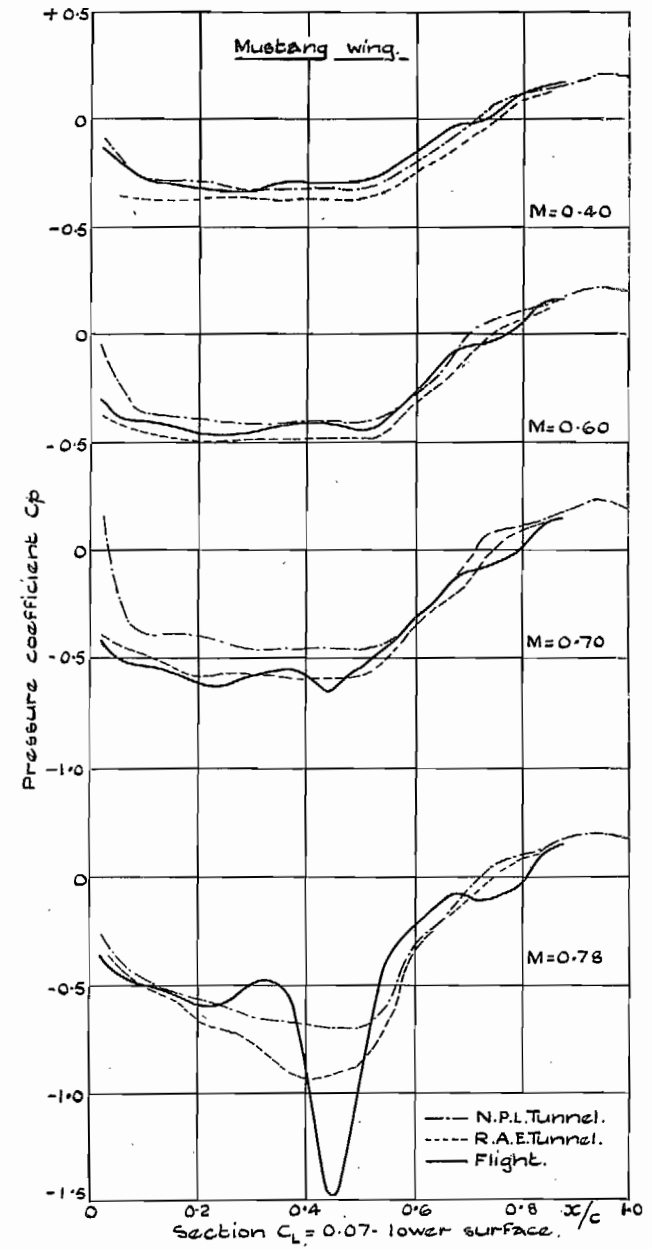


FIG. 60(b). Comparison of flight and high-speed wind-tunnel results.

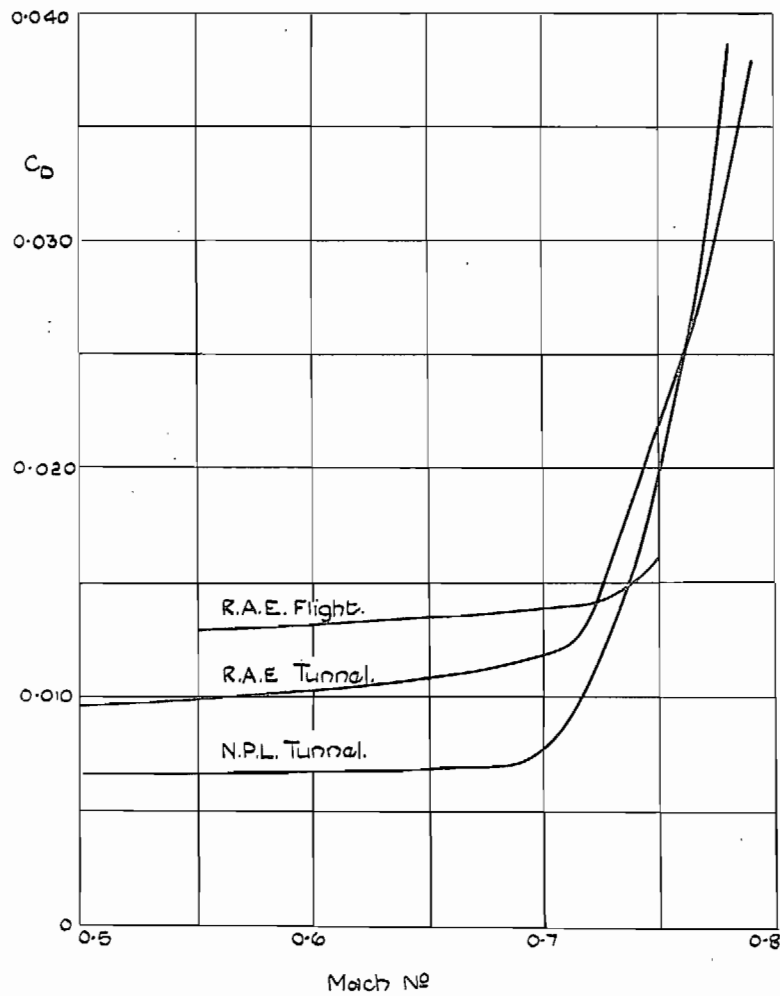


FIG. 61. Comparison of results from flight and tunnel tests. Mustang wing profile drag.

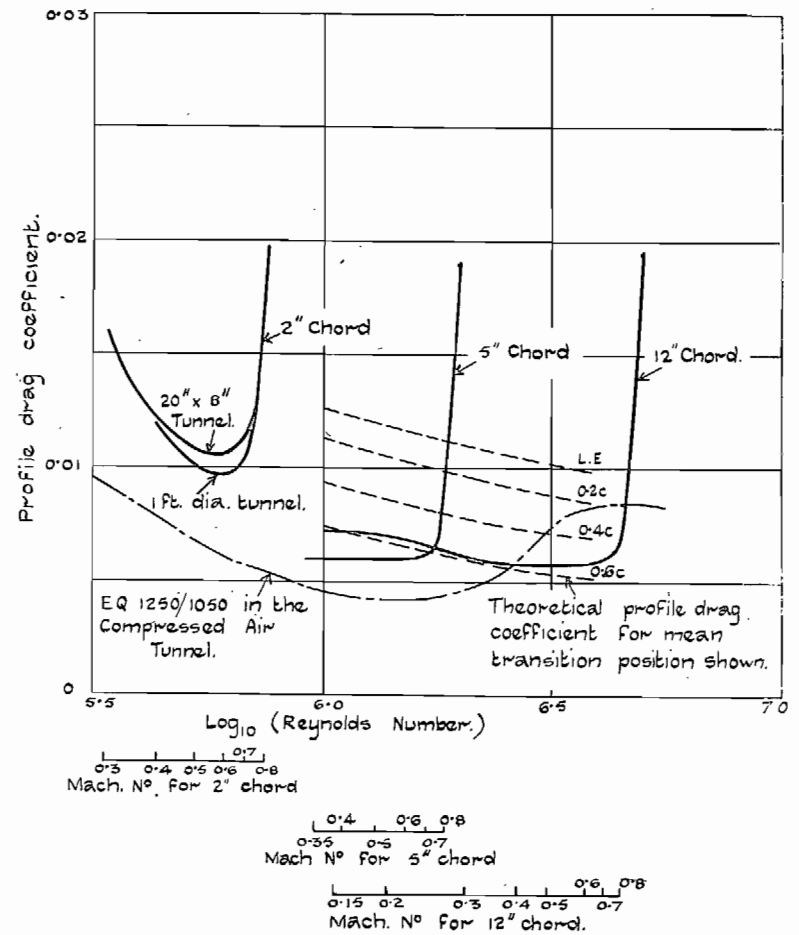


FIG. 62. Variation of profile drag with Reynolds and Mach number for EC 1250.

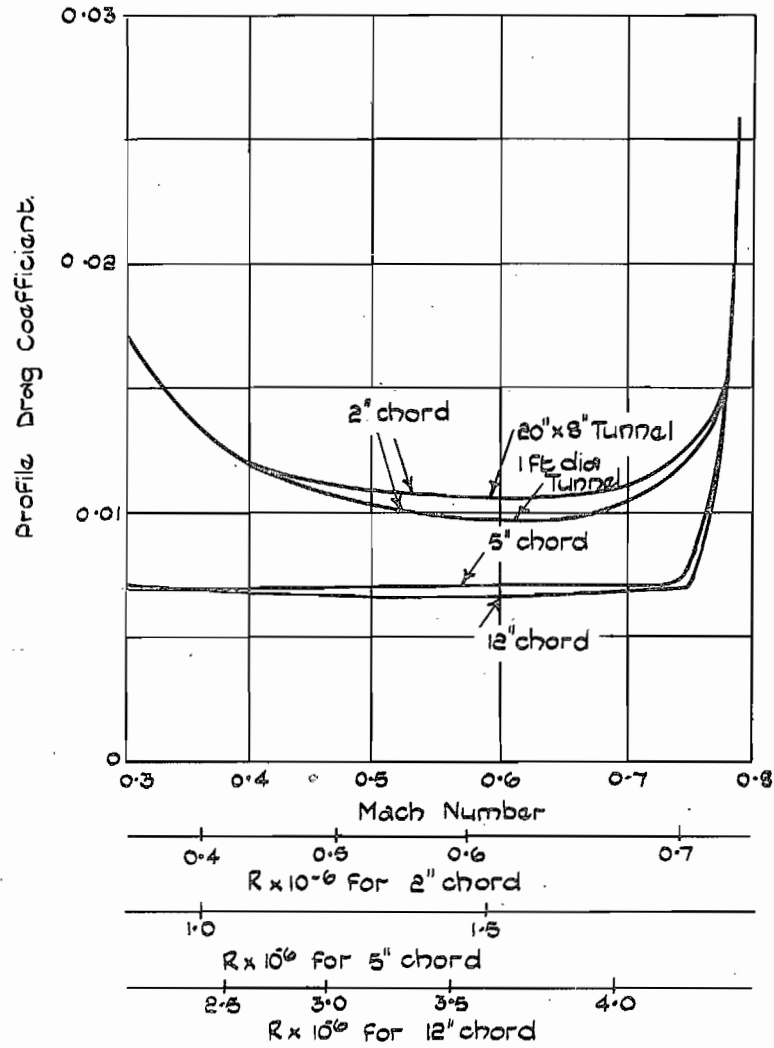


FIG. 63. Variation of profile drag with Reynolds and Mach number for EC 1250.

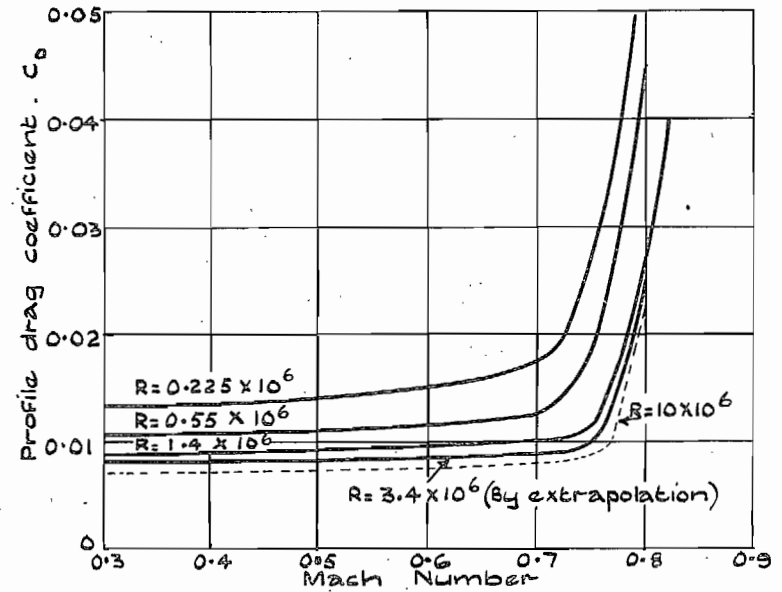


FIG. 64. Influence of Reynolds number on profile drag coefficient. (N 1530 at $\alpha = 0$ deg in R.A.E. High-Speed Tunnel.)



FIG. 65(a). Aerofoil in tunnel showing deposit of atmospheric dust aft of the transition and spread of turbulence behind obstacles on the aerofoil surface.

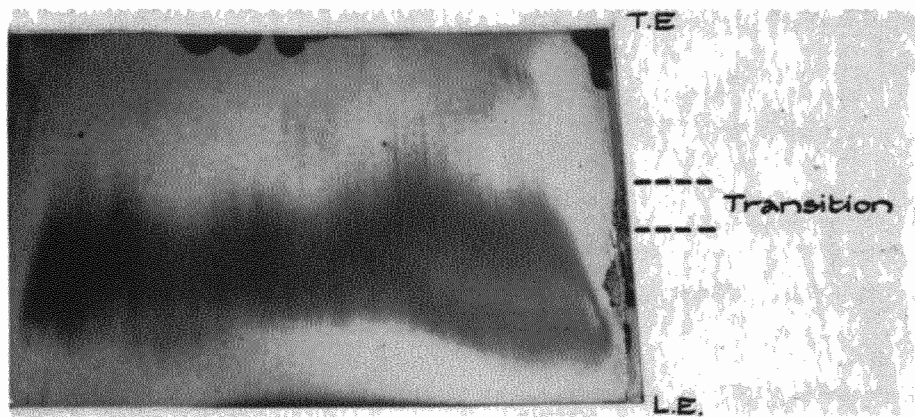


FIG. 65(b). EC 1250. Upper surface $\alpha = 2$ deg. $M = 0.3$. China-clay indicator.

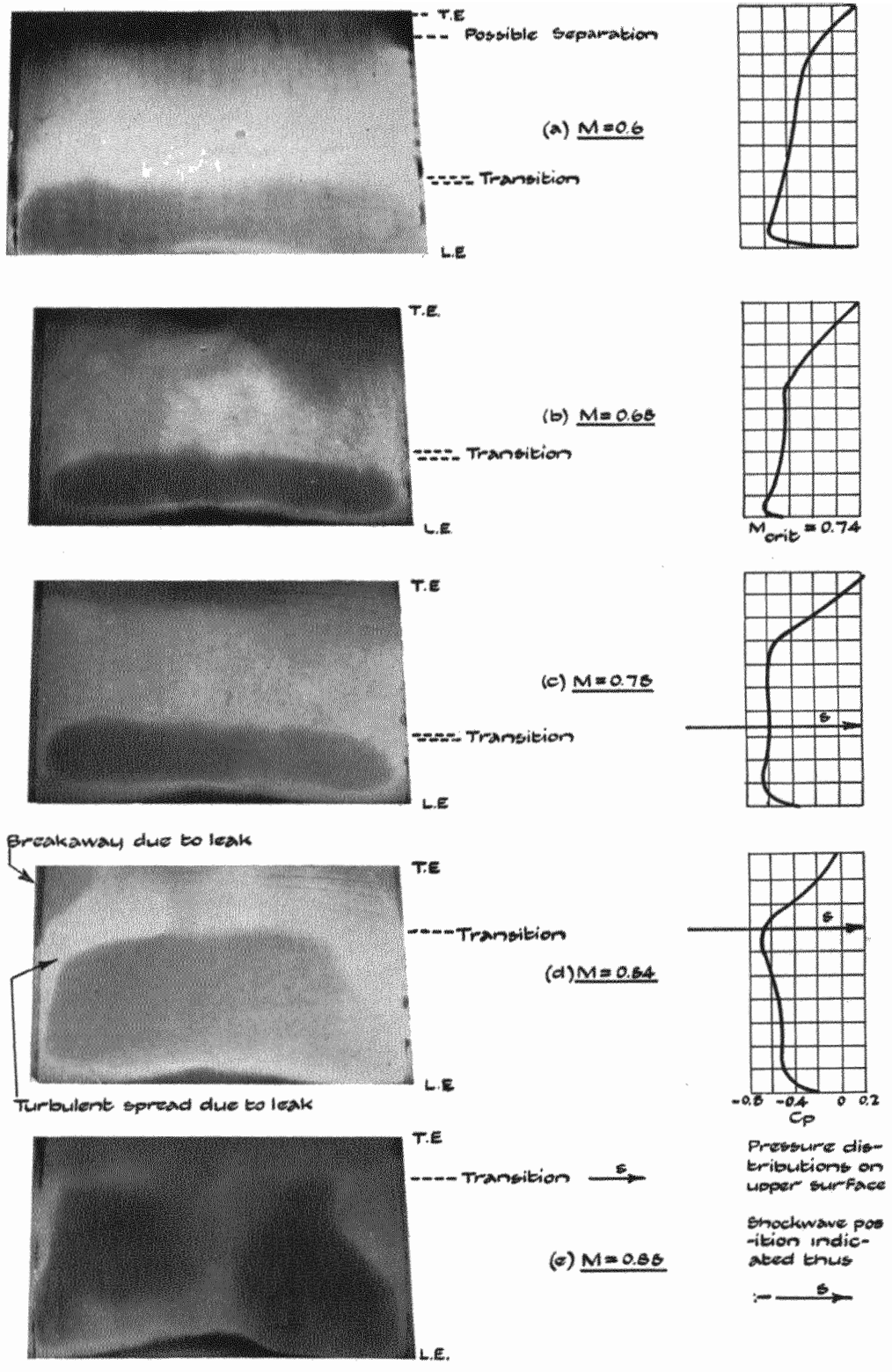


FIG. 66. EC 1250. Upper surface $\alpha = 2$ deg. China-clay indicator.

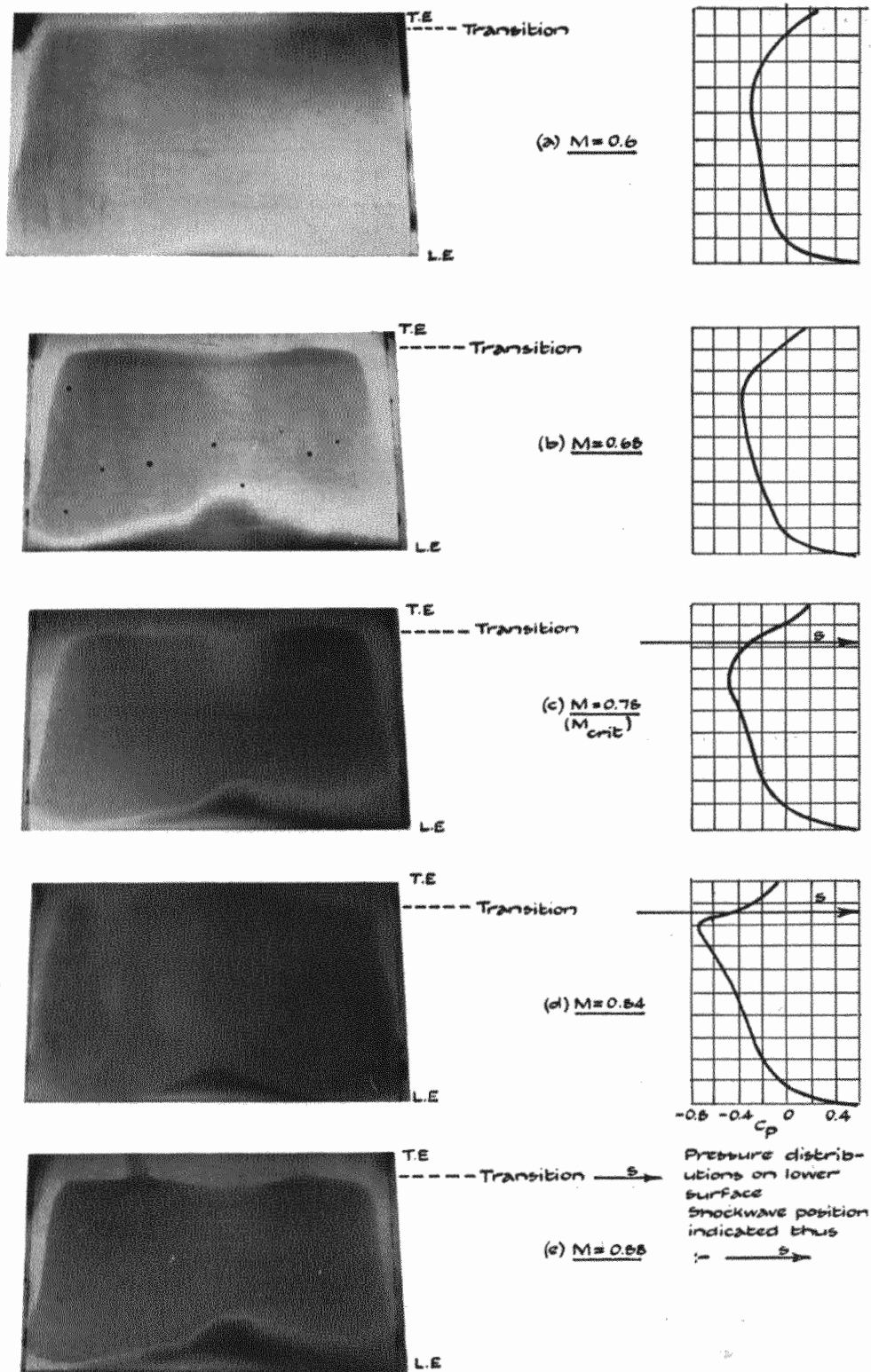


FIG. 67. EC 1250. Lower surface. $\alpha = 2$ deg. China-clay indicator.

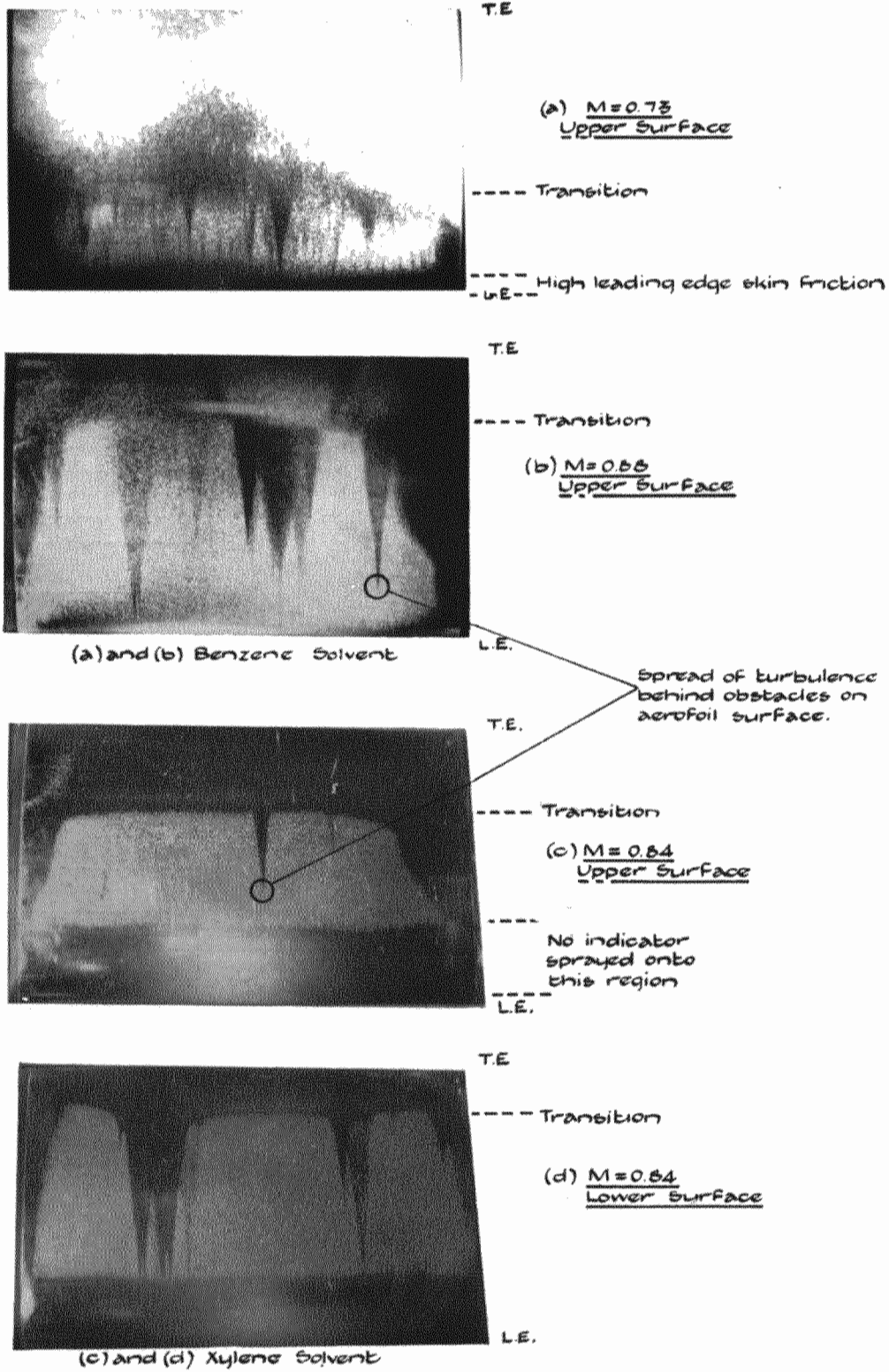
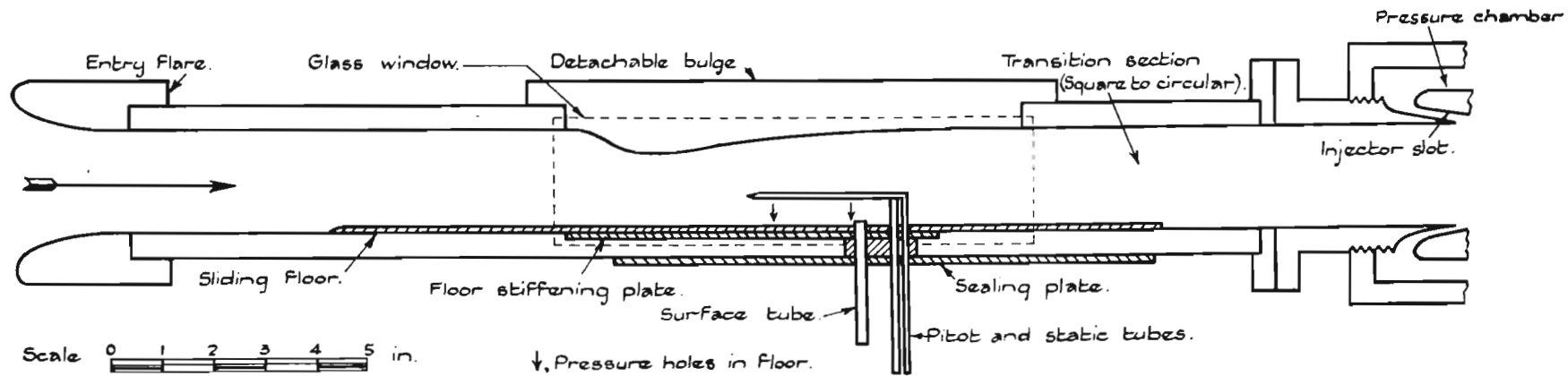


FIG. 68. EC 1250. Both surfaces. $\alpha = 2$ deg. Borneol Indicator.



235

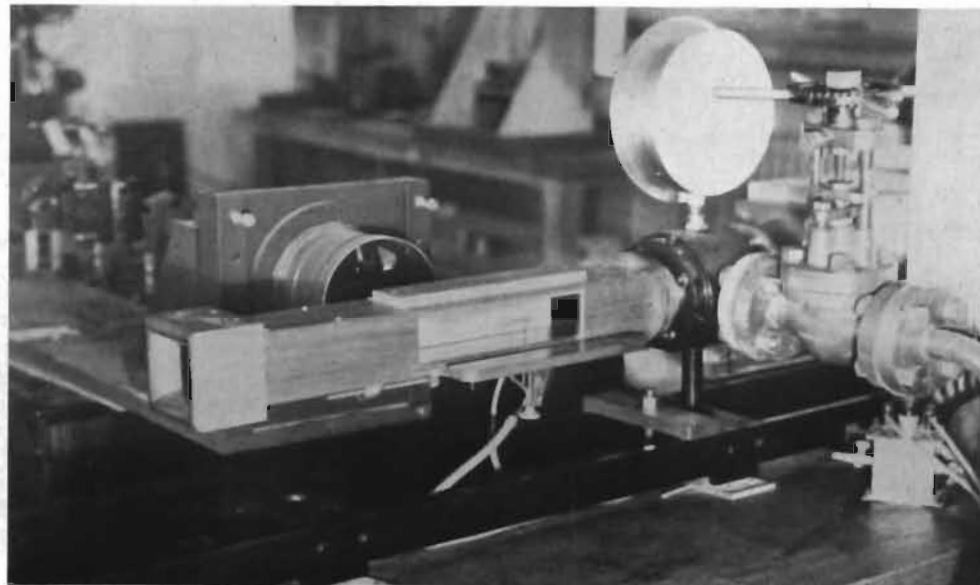
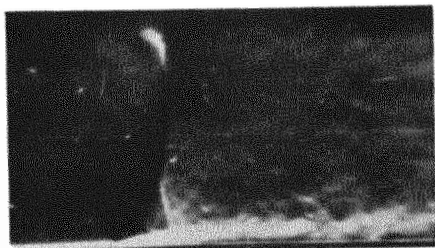
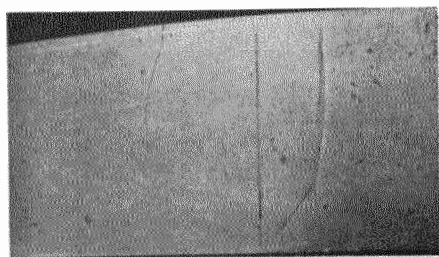


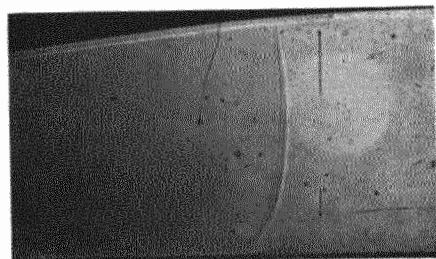
FIG. 69. Sketch and photograph of tunnel and apparatus.



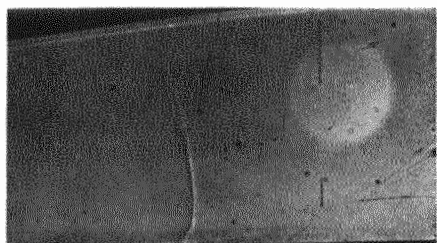
(a) $M_1 = 1.40$ $z = 2.11$



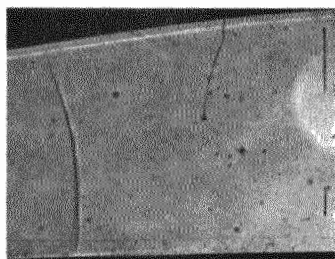
(c) $M_1 = 1.407$ $z = 2.11$



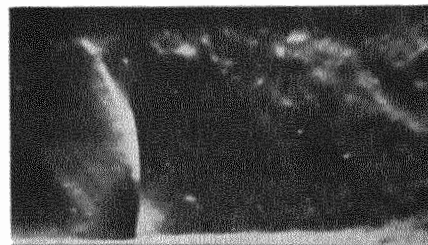
(e) $M_1 = 1.392$ $z = 2.10$



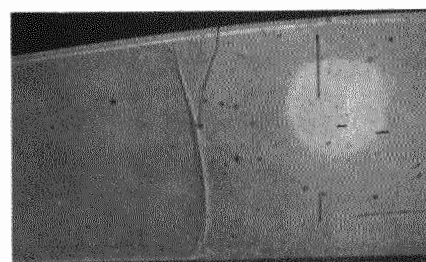
(g) $M_1 = 1.336$ $z = 1.87$



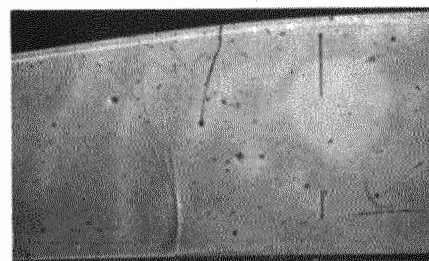
(i) $M_1 = 1.206$ $z = 1.52$



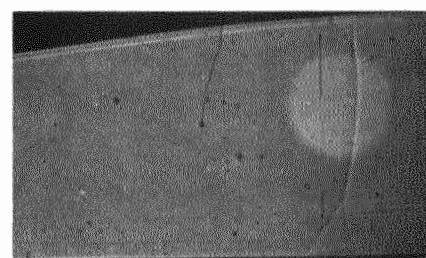
(b) $M_1 = 1.283$ $z = 1.76$



(d) $M_1 = 1.443$ $z = 2.22$



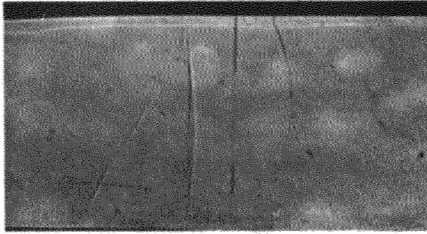
(f) $M_1 = 1.346$ $z = 1.95$



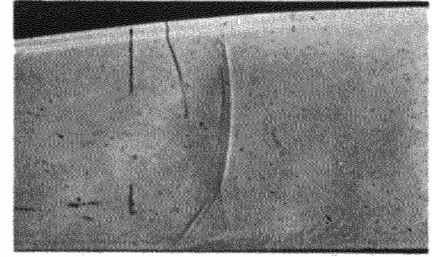
(h) $M_1 = 1.310$ $z = 1.84$

(a), (b) Töpler striation photographs.
(c) to (i) Direct-shadow photographs.

FIG. 70.



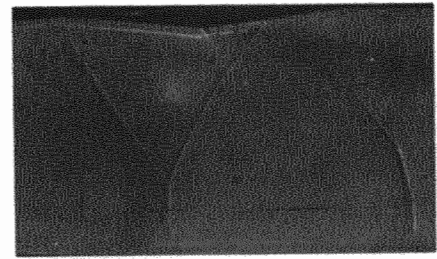
(j) $M_1 = 1.08$ $\chi = 1.19$



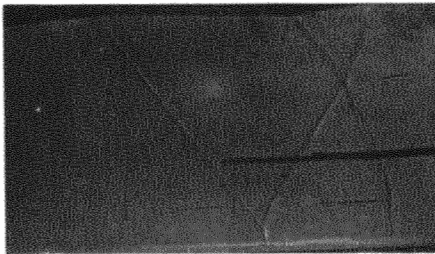
(k) $M_1 = 1.472$ $\chi = 2.33$



(l) $M_1 = 1.472$ $\chi = 2.33$



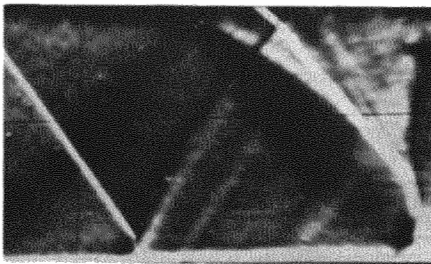
(m) $M_1 = 1.439$ $\chi = 2.25$



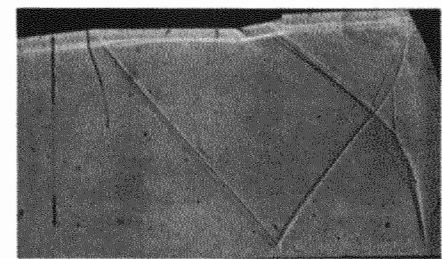
(n) $M_1 = 1.439$ $\chi = 1.76$



(o) $M_1 = 1.439$ $\chi = 2.25$



(p) $M_1 = 1.439$ $\chi = 1.76$



(q) $M_1 = 1.469$ $\chi = 1.39$

(l), (o), (p) Töpler striation photographs.
 (j), (k), (m), (n), (q) Direct-shadow photographs.

FIG. 71.

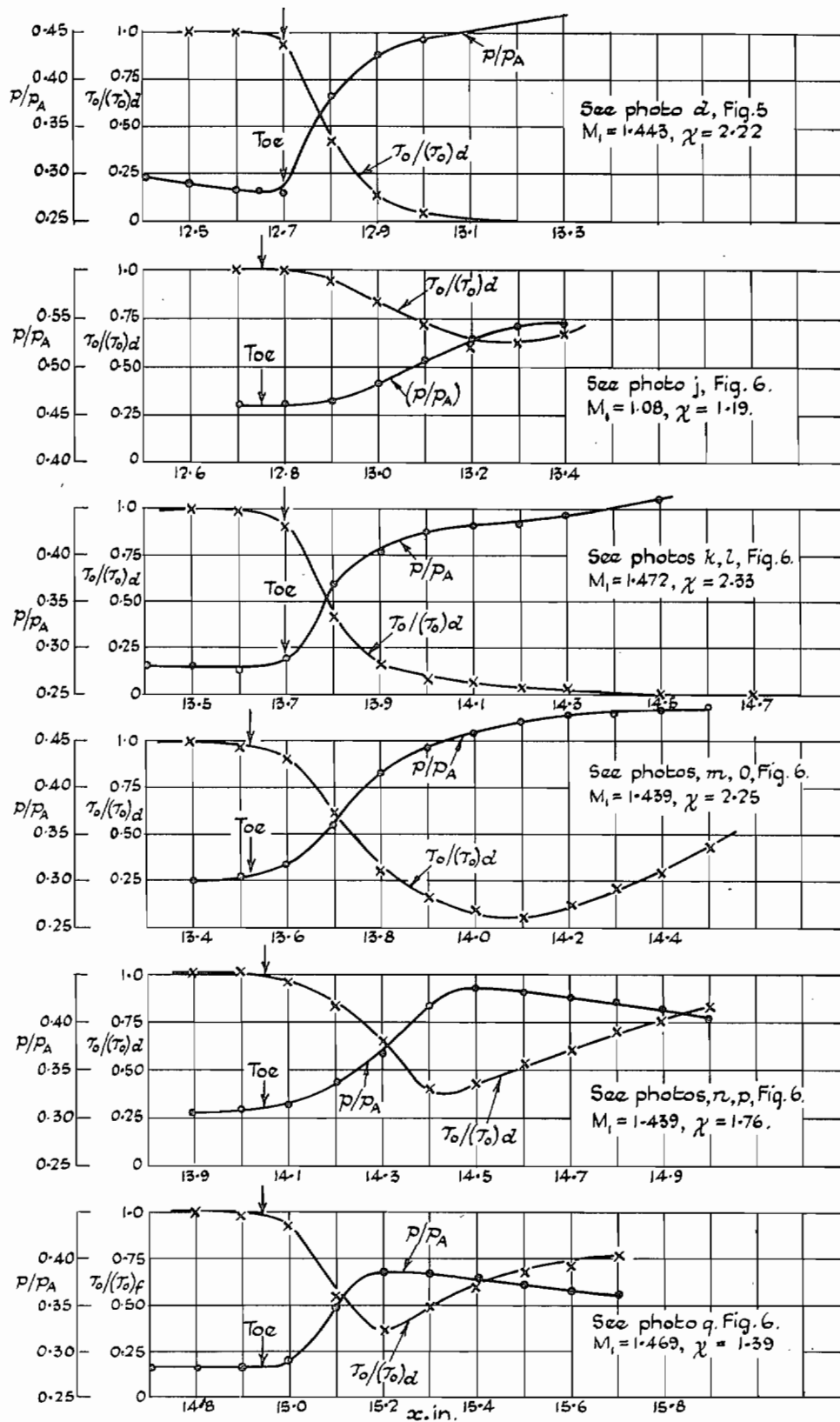


FIG. 72. Curves of normal pressure and friction on floor below shock-waves.

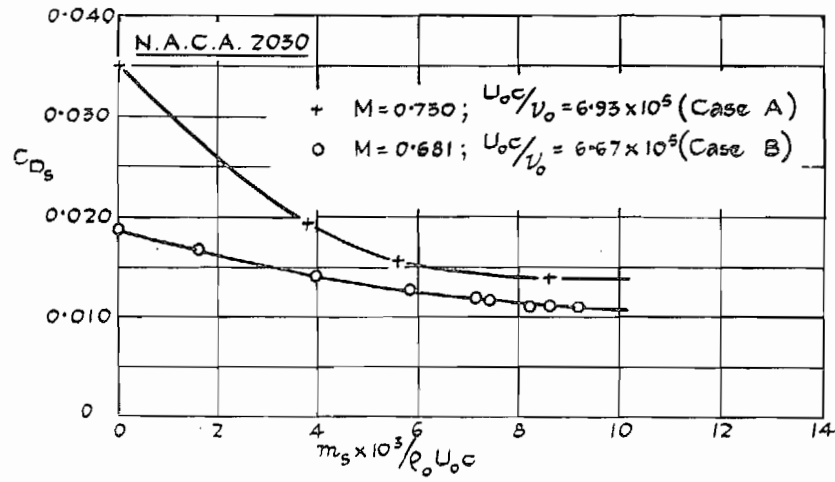


FIG. 73.

239

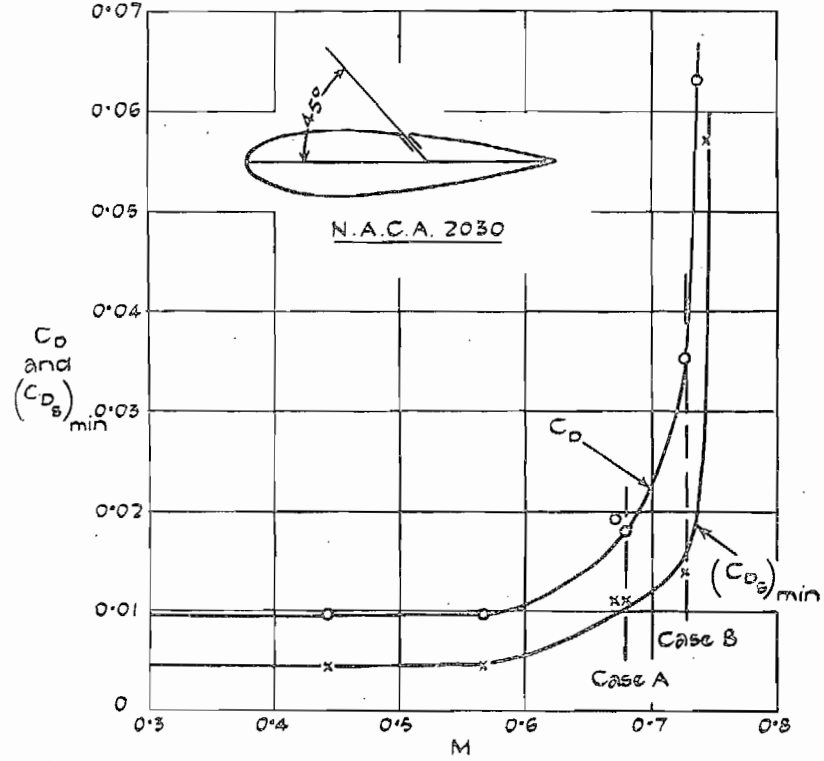


FIG. 74. Effect of suction on drag of NACA 2030. 4 deg incidence. Slot on upper surface.

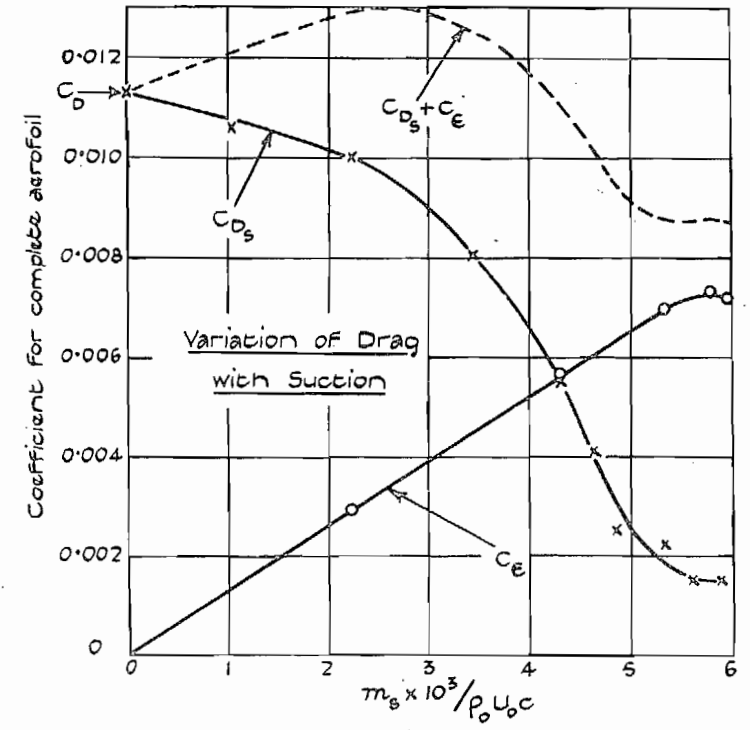


FIG. 75.

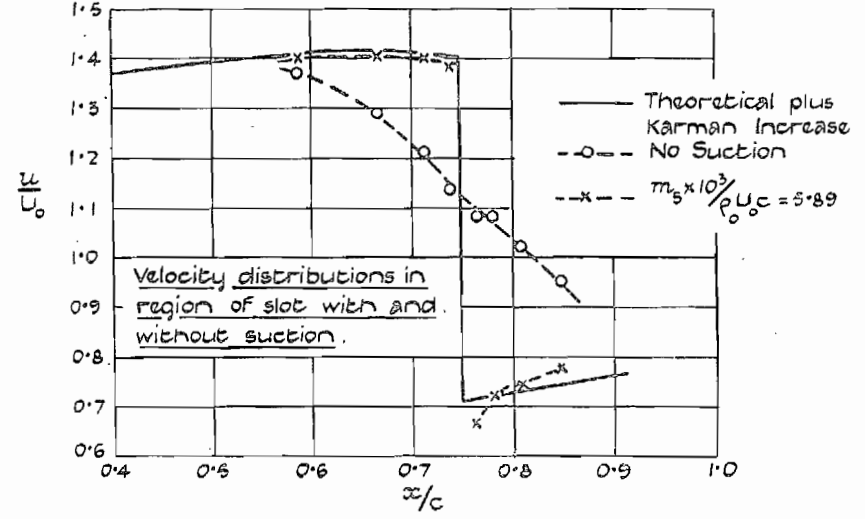


FIG. 76. 22 per cent Griffith aerofoil; incidence = 0 deg; $U_0c/V_0 = 2.76 \times 10^6$; $M = 0.6$.

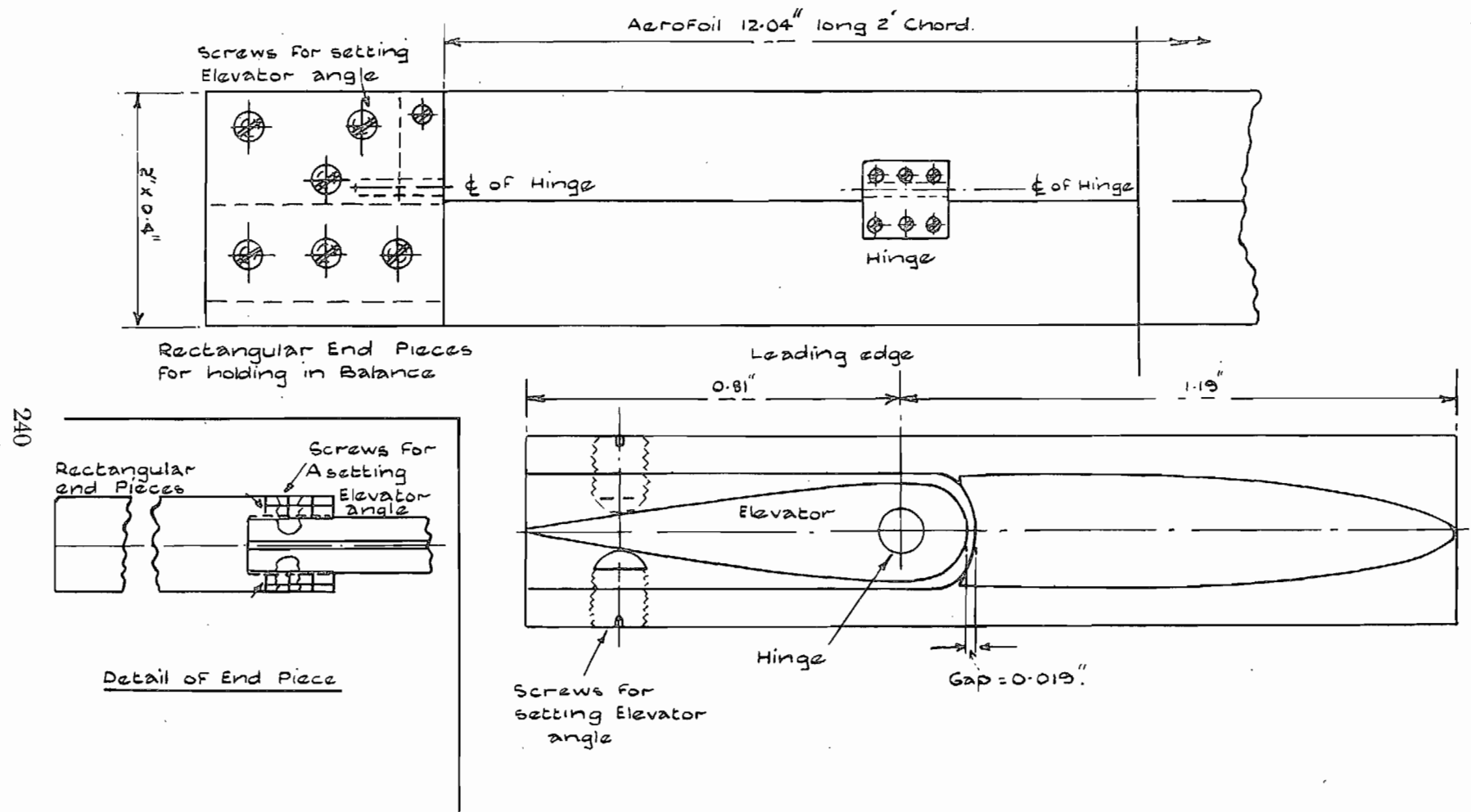


FIG. 77. EC 1240 aerofoil with hinged flap.

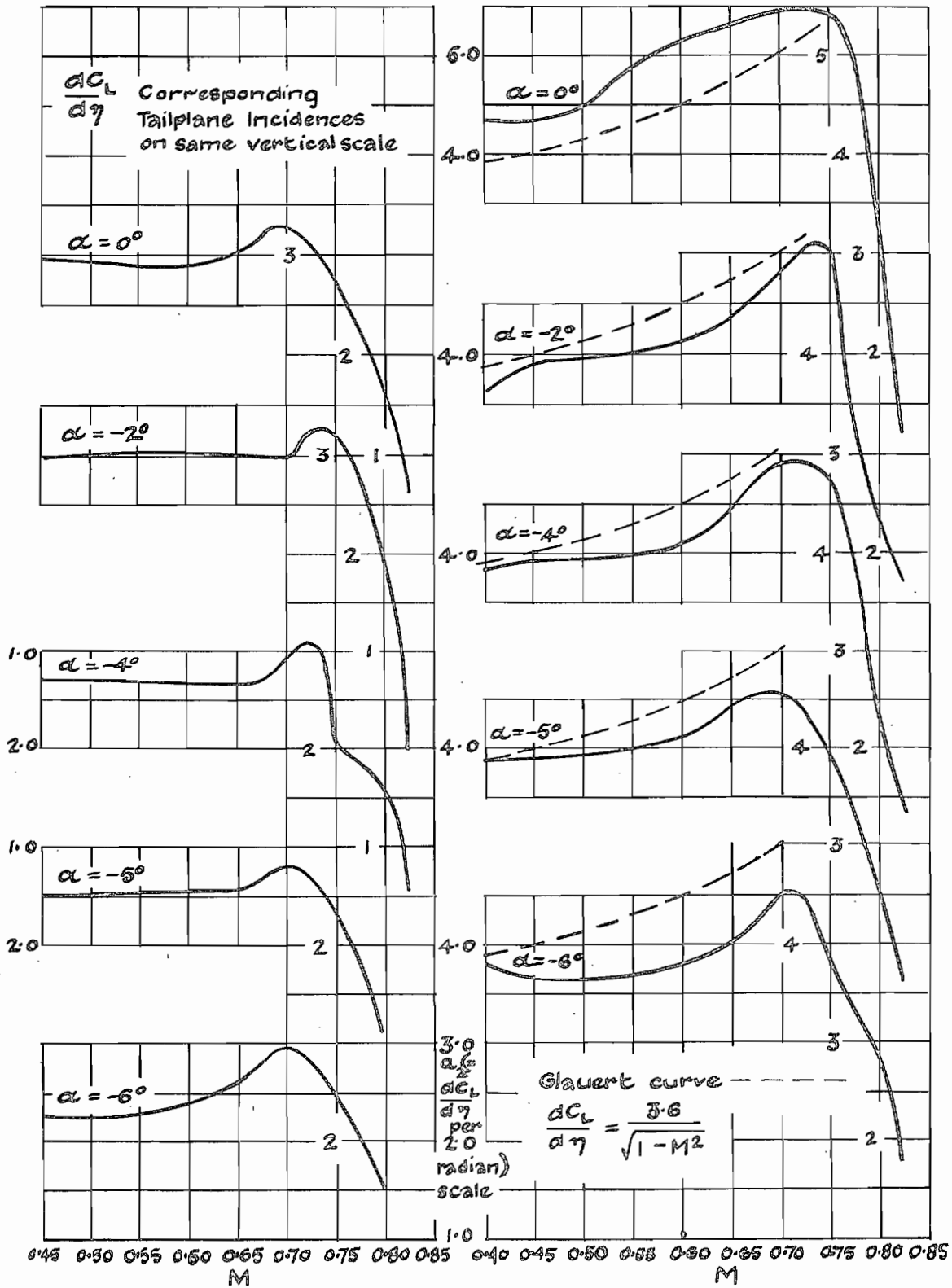
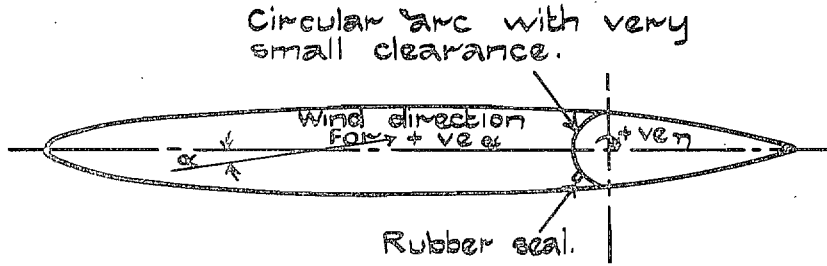


FIG. 78. EC 1240 elevator. Variation of $a_2 = dC_L/d\eta$ (η in radians) with M for various values of α .



$\frac{x}{c}$	$\frac{y}{c}$
0.005	0.008
0.010	0.012
0.015	0.015
0.025	0.020
0.1	0.036
0.15	0.043
0.2	0.048
0.25	0.052
0.3	0.055
0.35	0.057
0.4	0.059
0.45	0.060
0.5	0.060
0.55	0.060
0.6	0.058
0.65	0.056
0.7	0.053
0.75	0.048
0.8	0.042
0.85	0.034
0.9	0.025
0.95	0.014
1.0	0.001

FIG. 79. Sketch of EC 1250 with 25 per cent control. (30 pressure holes, including 10 in control surface.)

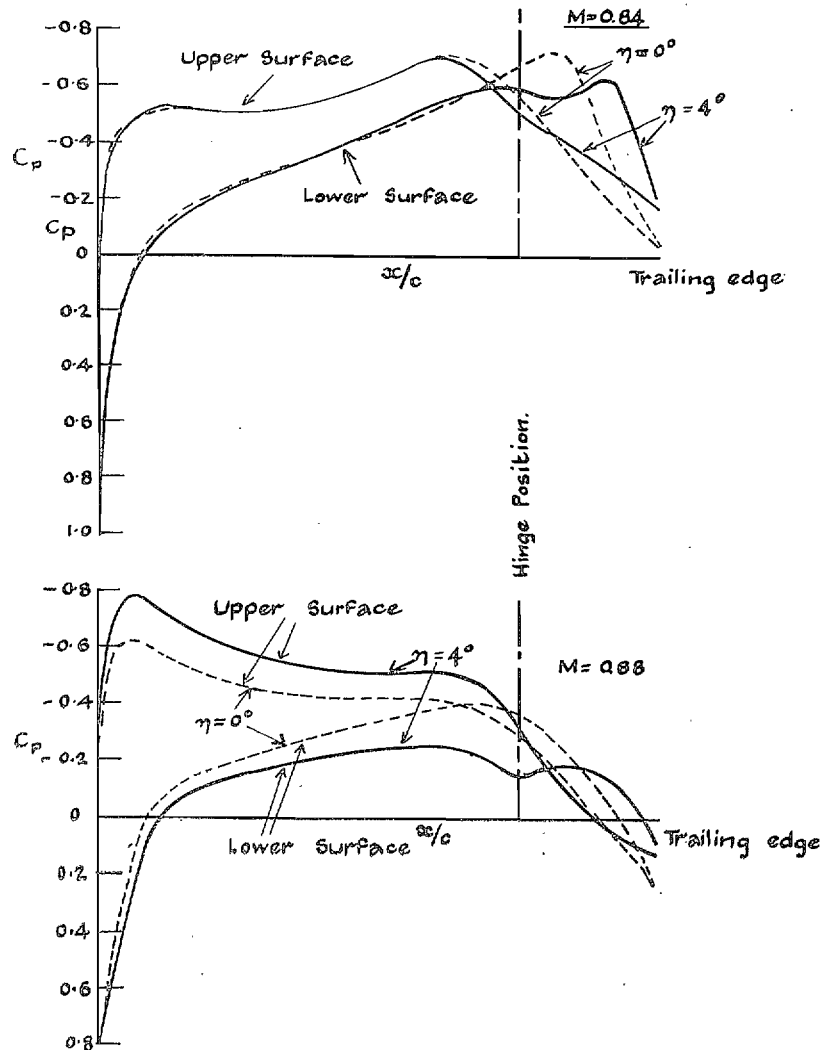


FIG. 80. Effect of shockstall upon efficiency of control surface. EC 1250 with 25 per cent control at $\alpha = 2 \text{ deg.}$ $\eta = \text{Elevator angle.}$

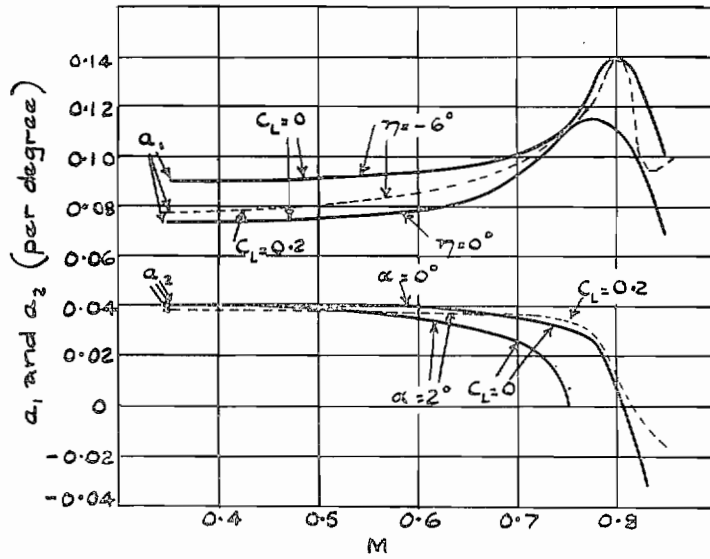


FIG. 81. Variation of $a_1 (= \partial C_L / \partial \alpha)$ and $a_2 (= \partial C_L / \partial \eta)$ with Mach number ; EC 1250 with 25 per cent control.

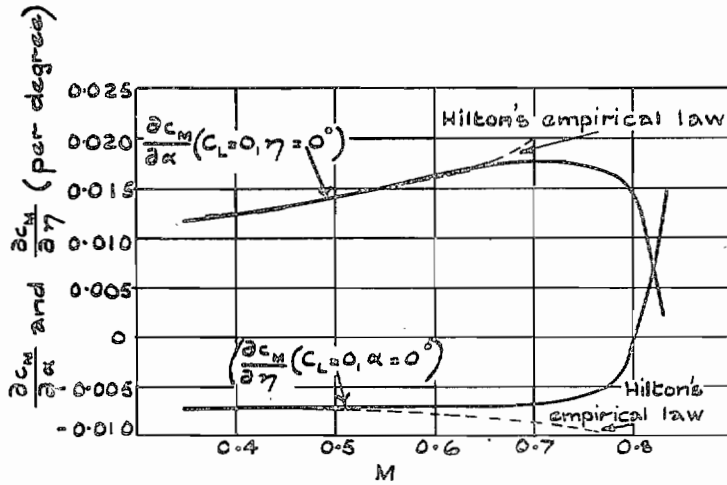


FIG. 82. Variation of $\partial C_m / \partial \alpha$ and $\partial C_m / \partial \eta$ with Mach number ; EC 1250 with 25 per cent control.

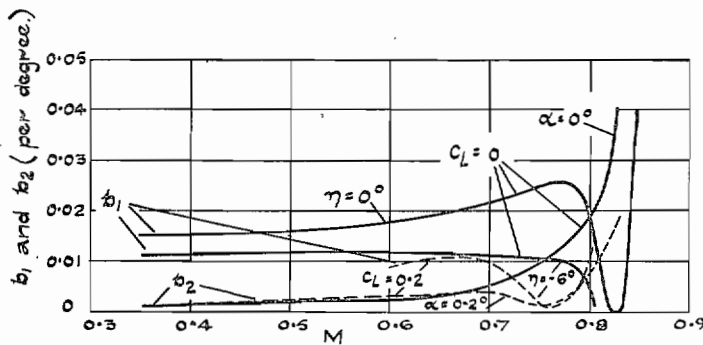
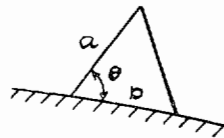
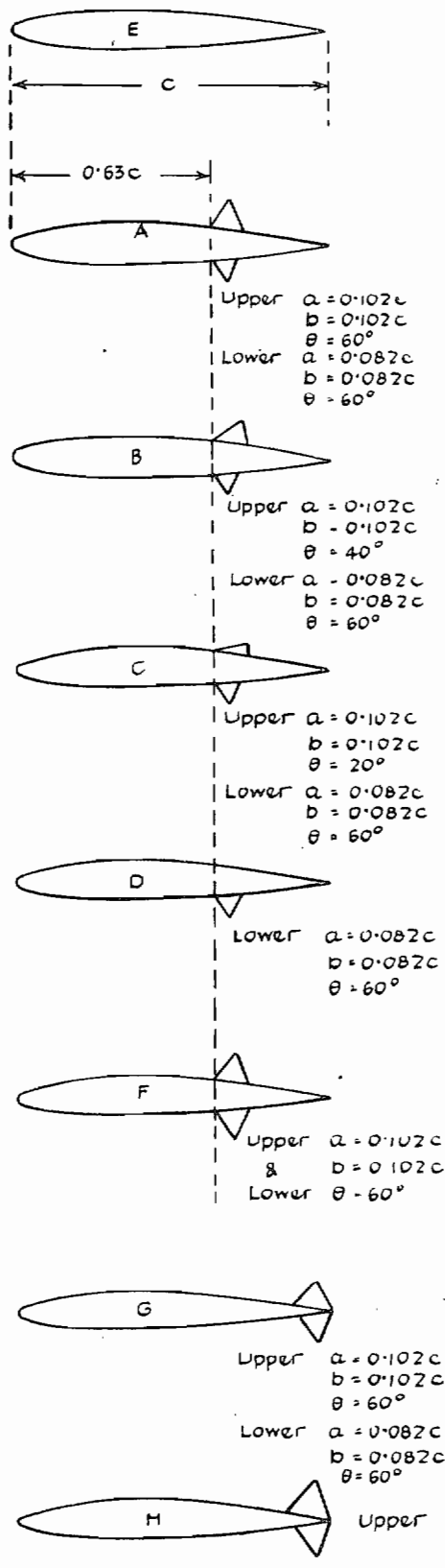
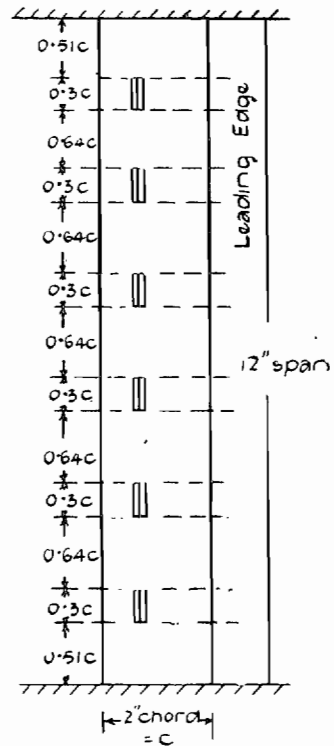


FIG. 83. Variation of $b_1 (= \partial C_H / \partial \alpha)$ and $b_2 (= \partial C_H / \partial \eta)$ with Mach number ; EC 1250 with 25 per cent control.



Sketch Indicating Notation.



Spanwise Flap Arrangement

FIG. 84. Brake flaps on 2-in. chord EC 1240/0640 aerofoil.

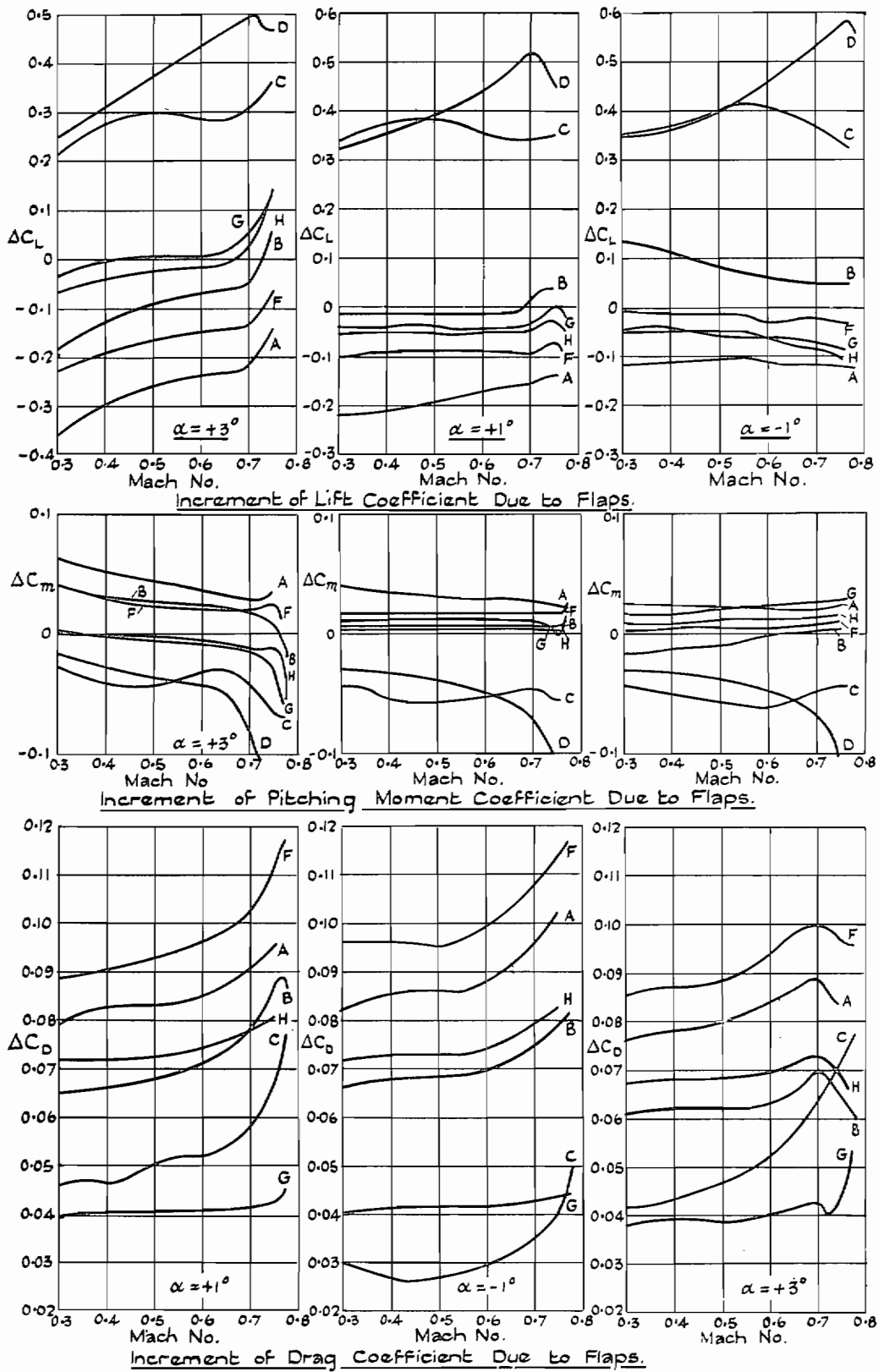


FIG. 85. Influence of brake flaps on force and moment coefficients. EC 1240/0640.

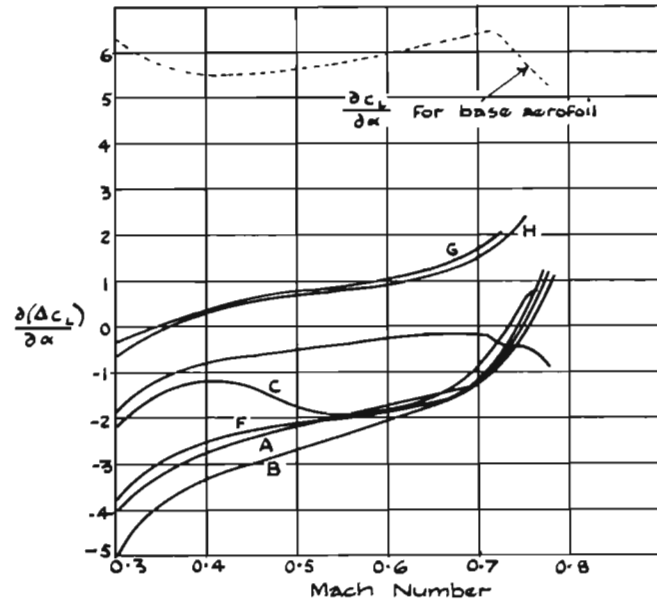


FIG. 86. Influence of brake flaps on $\partial(\Delta C_L)/\partial\alpha$ (α in radians). Aerofoil EC 1240/0640.

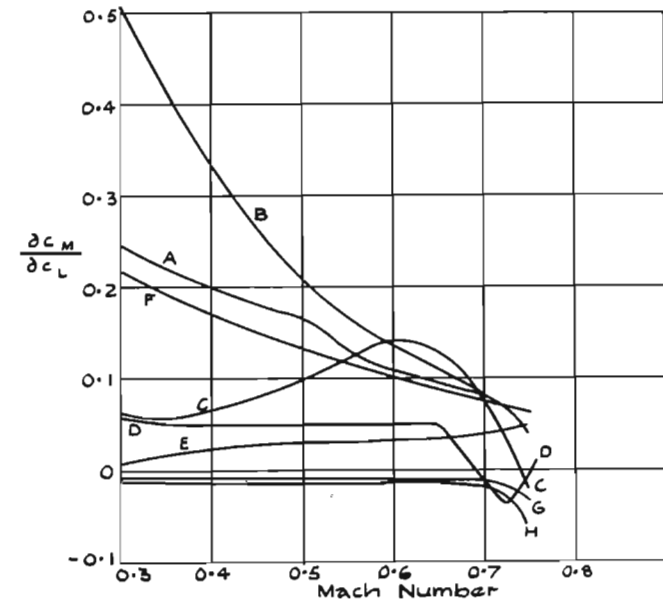


FIG. 87. Influence of brake flaps on $\partial C_M/\partial C_L$. Aerofoil EC 1240/0640.



FIG. 88. Photograph showing wake and shock-waves behind an aerofoil with brake flaps. (Combination G.) $M = 0.78$.

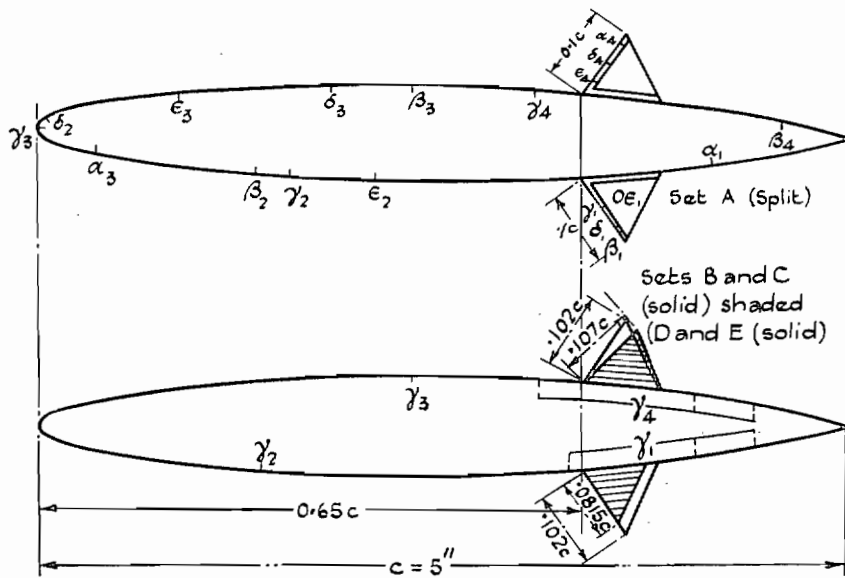
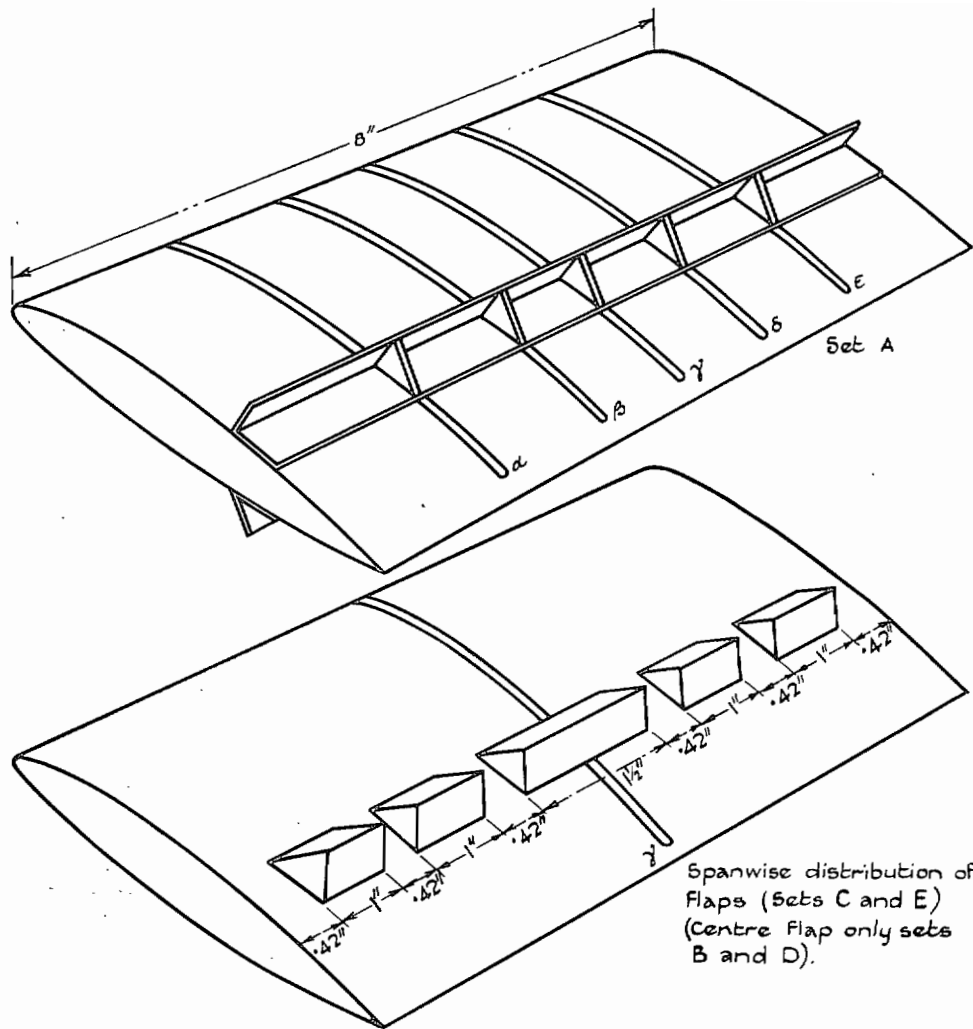
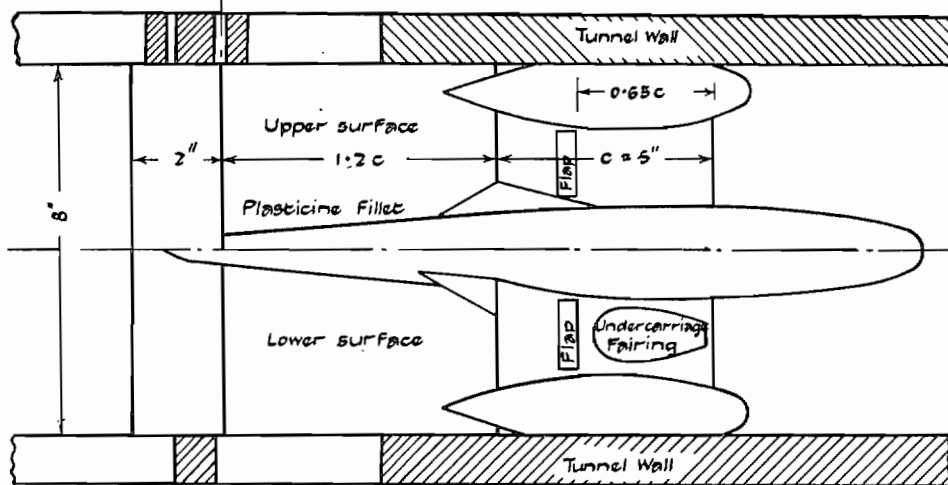
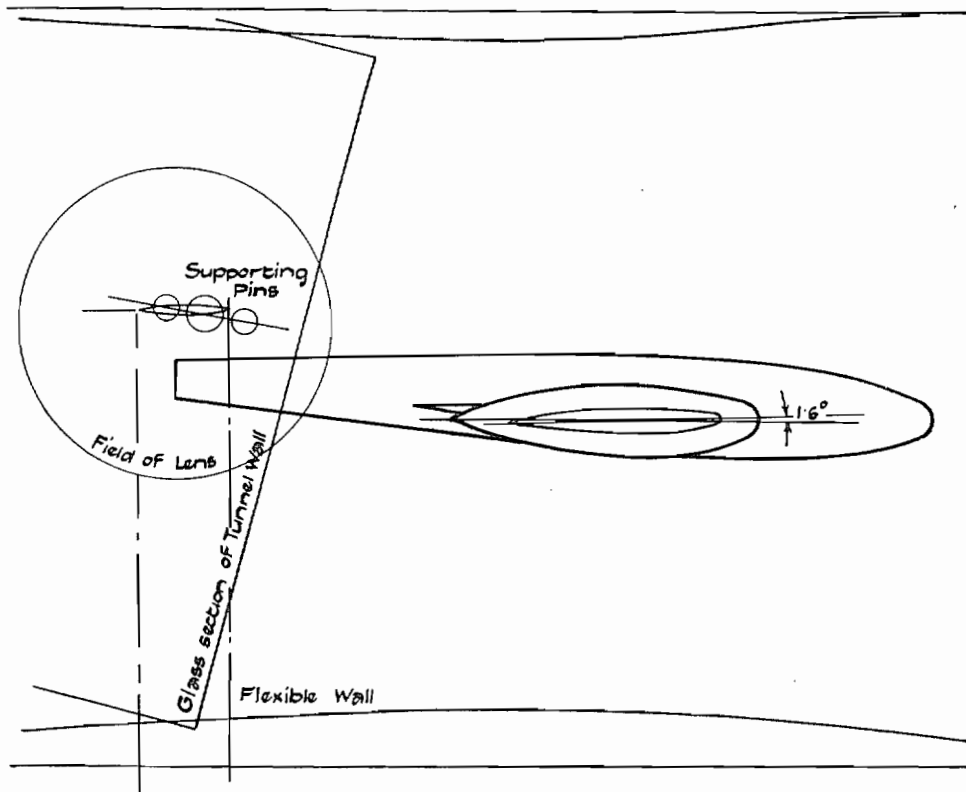


FIG. 89.



Upper surface
 $s = 0.267c$
 $d = 0.107c$

Lower surface
 $s = 0.5c$
 $d = 0.0815c$

Note in Figs. 91 & 92 the Flap combination is referred to as Flaps α/β where α is the upper and β the lower surface Flap angle.

FIG. 90.

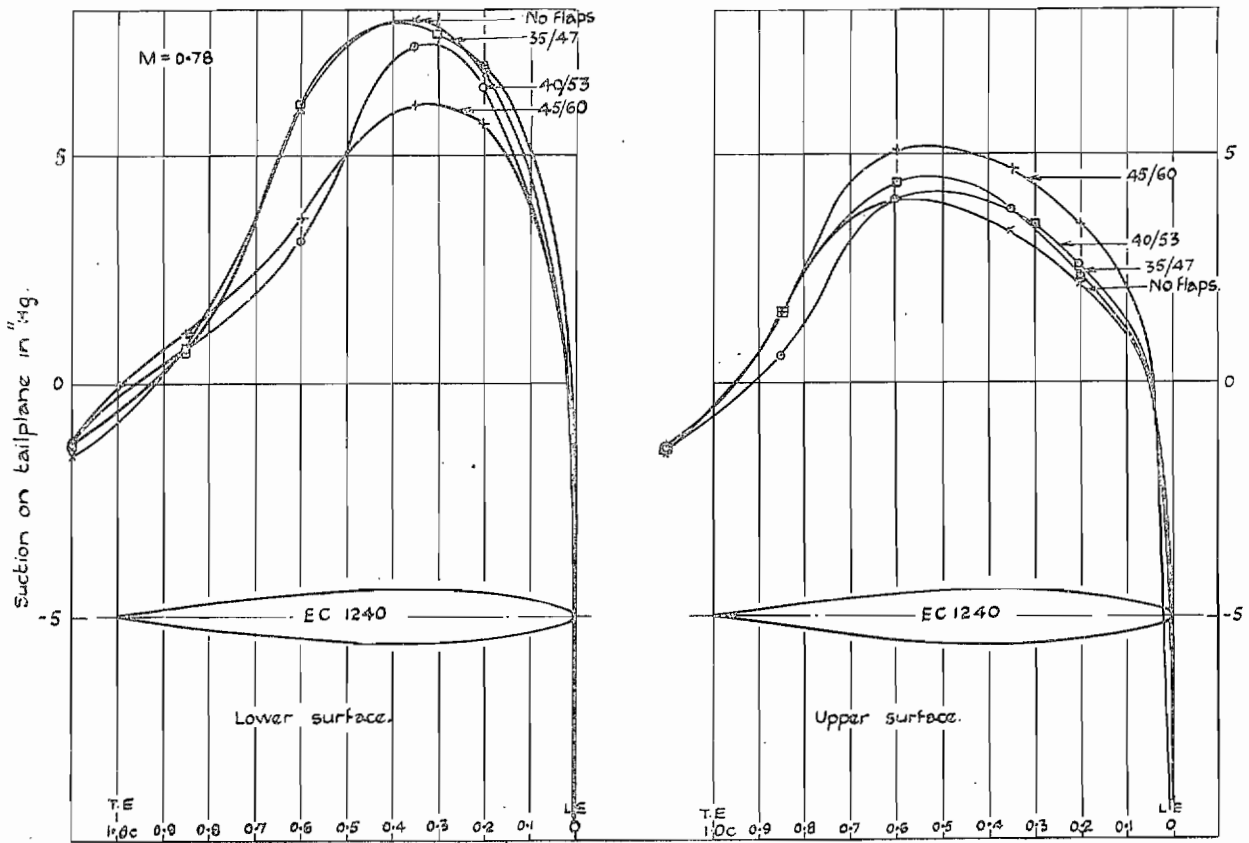


FIG. 91. Influence of brake flap on tailplane pressure distribution.

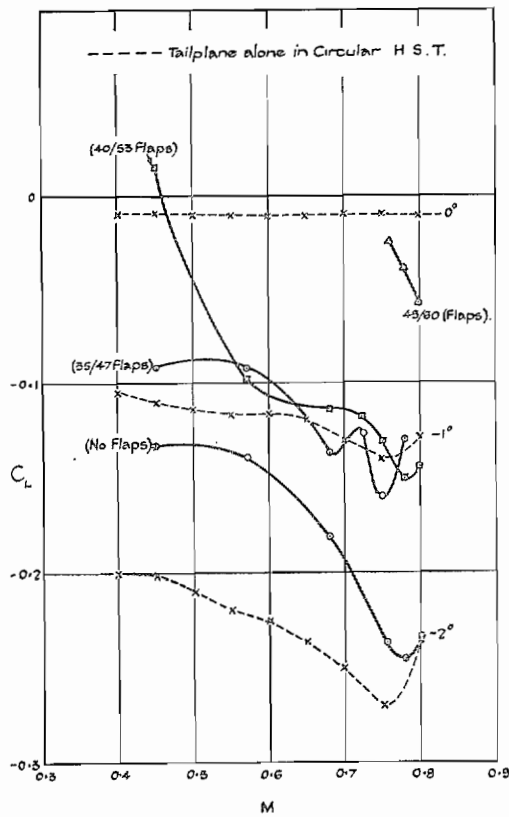
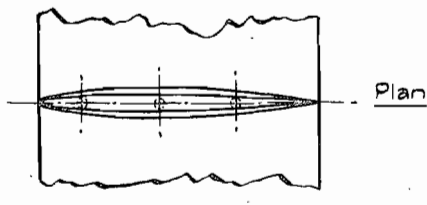
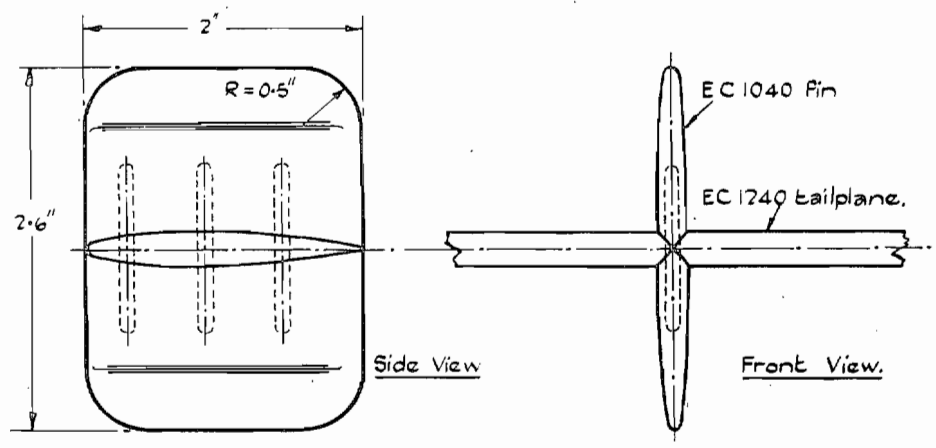


FIG. 92. Tailplane C_L against Mach number. Section EC 1240.



Sketch of EC 1240, with EC 1040 Fins.

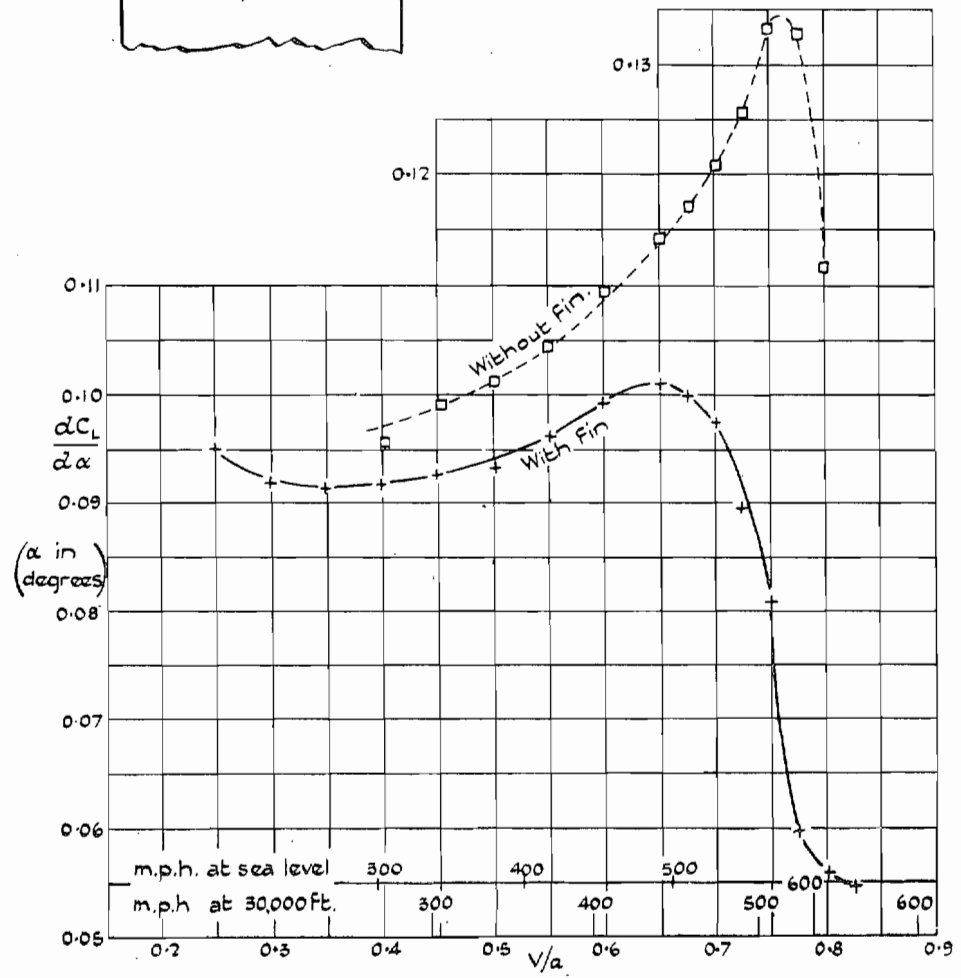


FIG. 93. Aerofoil EC 1240 with and without EC 1040 fins. Variation of lift-curve slope with Mach number.

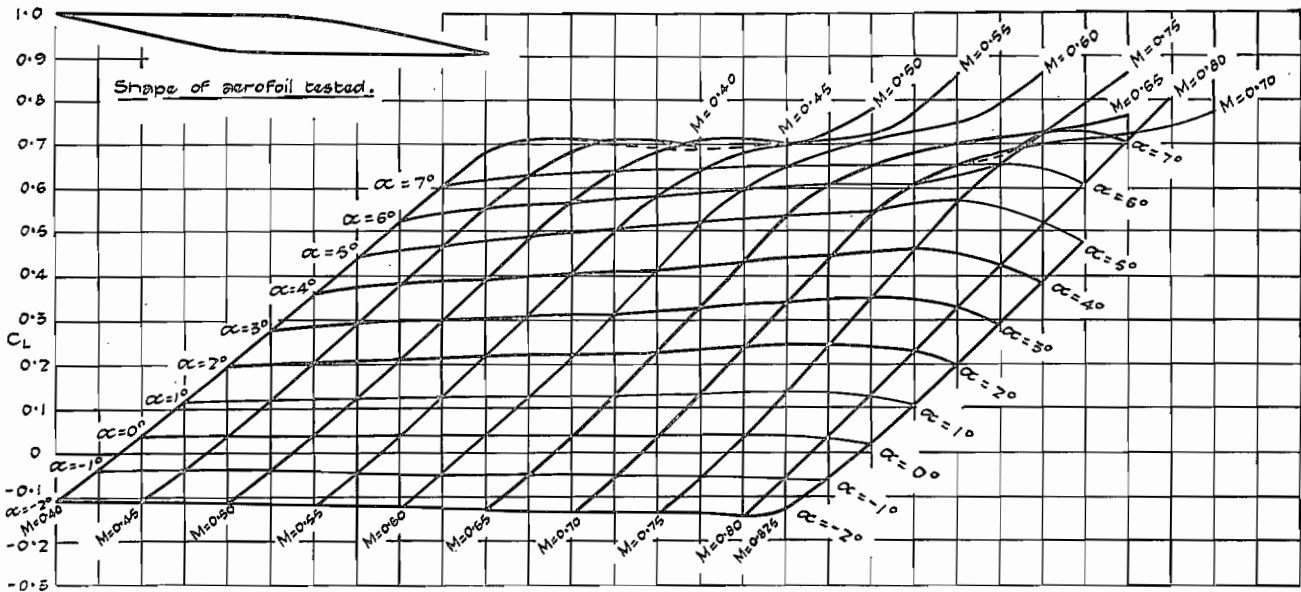


FIG. 94(a). Double-wedge aerofoil. Lift coefficient (C_L) as a function of both Mach number (M) and incidence (α).

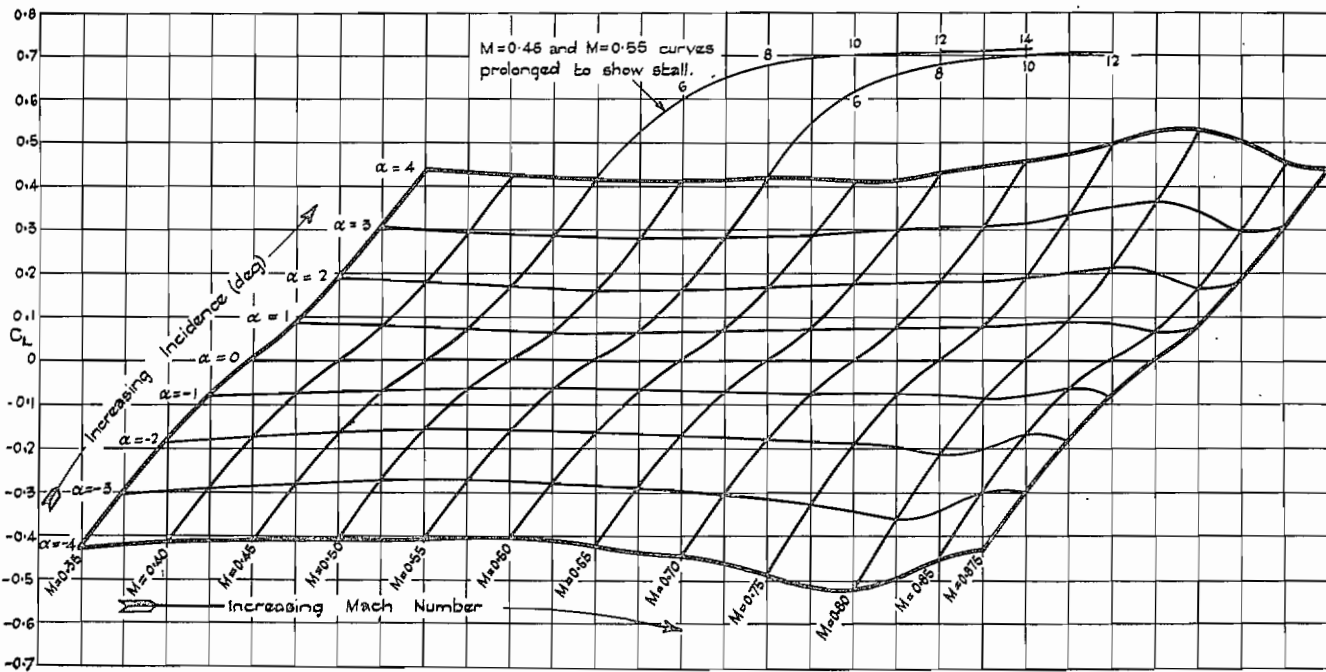


FIG. 94(b). Biconvex aerofoil. Lift coefficient (C_L) as a function of both Mach number (M) and incidence (α).

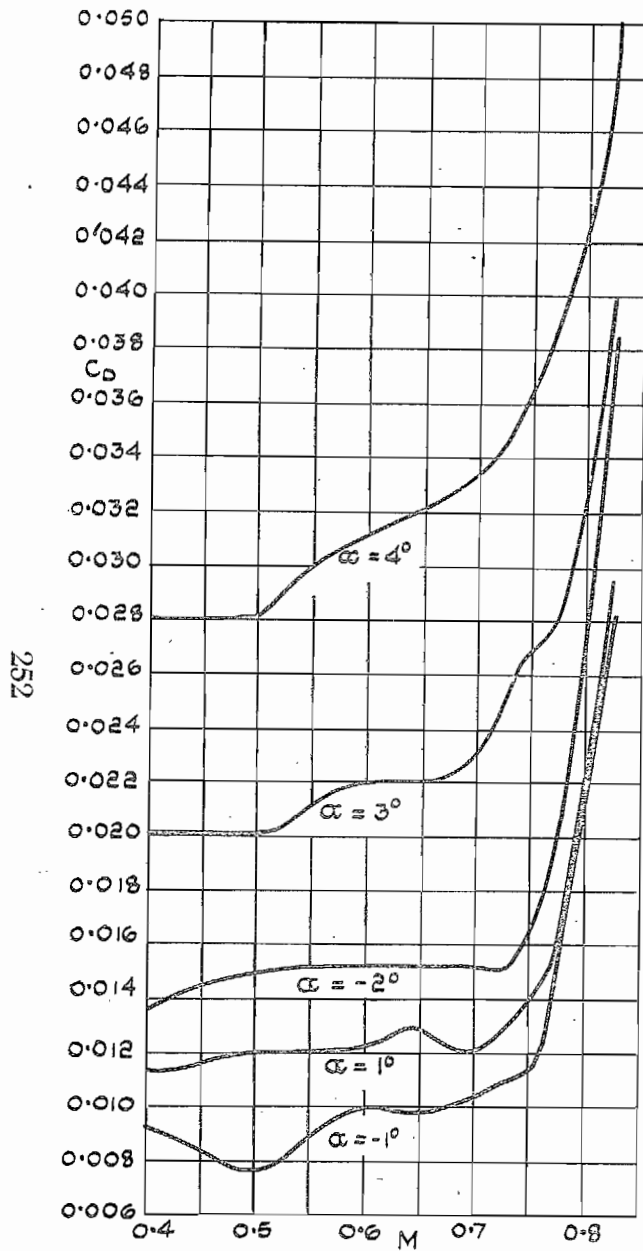
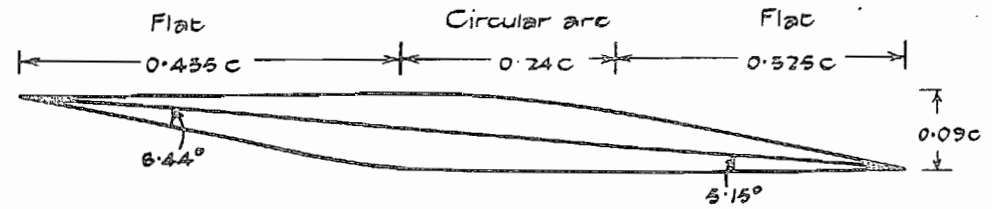


FIG. 95. Faired double-wedge aerofoil. Drag coefficient (C_D) as a function of Mach number (M) at various incidences (α).



Flats are tangential to circular arcs.
 Aerofoil shown at $+5.15^\circ$ incidence.
 Aerofoil has fore and aft symmetry
 Thickness ratio = 8.7%

Section of Aerofoil.

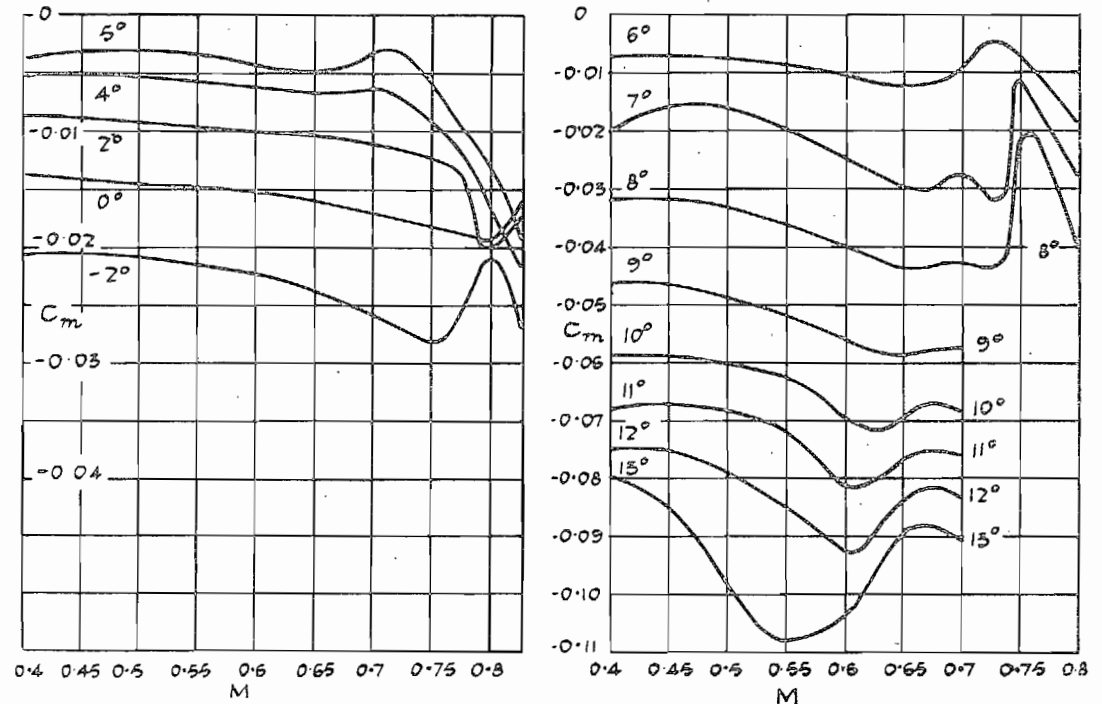
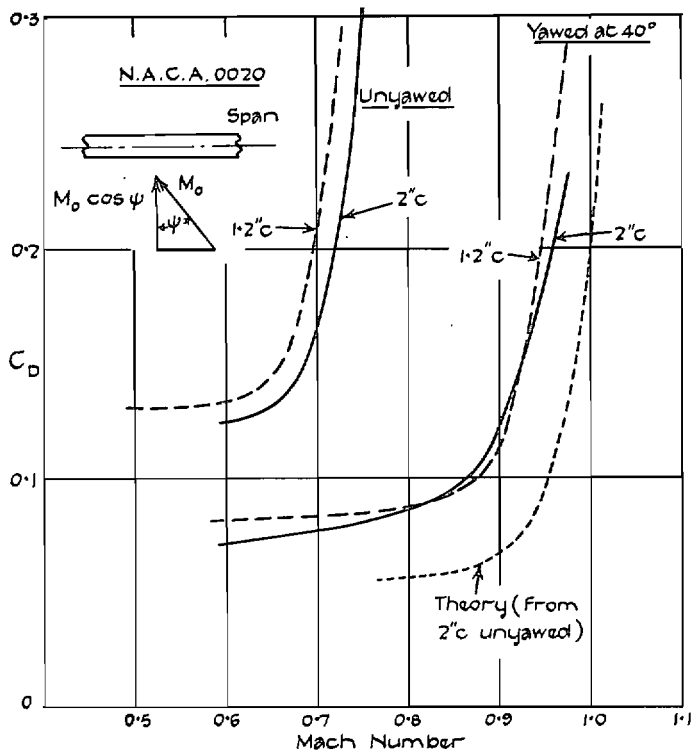
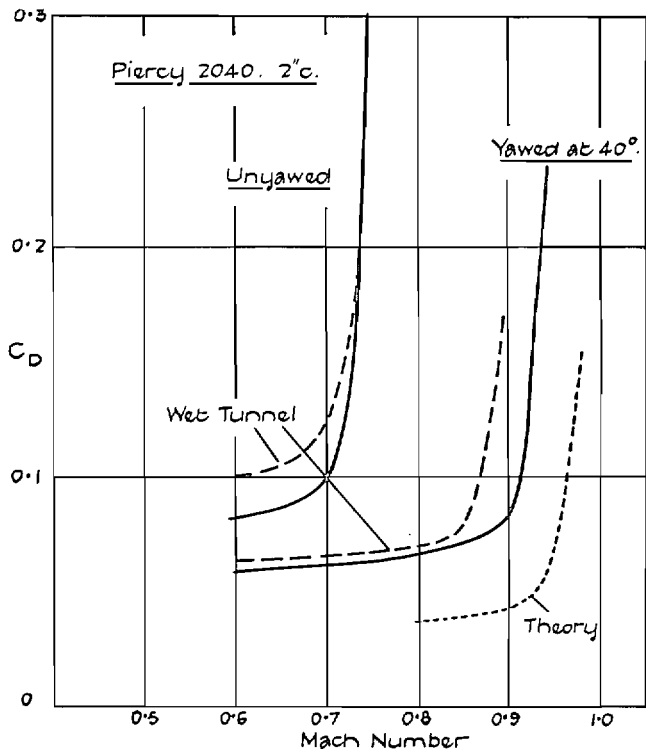


FIG. 96. Faired double-wedge aerofoil. Moment coefficient (C_m) as a function of Mach number (M) at various incidences (α).



Small Effect of Tunnel Interference.



Effect of Dry Air in the Tunnel.

FIG. 97. Delay of drag rise due to sweepback.

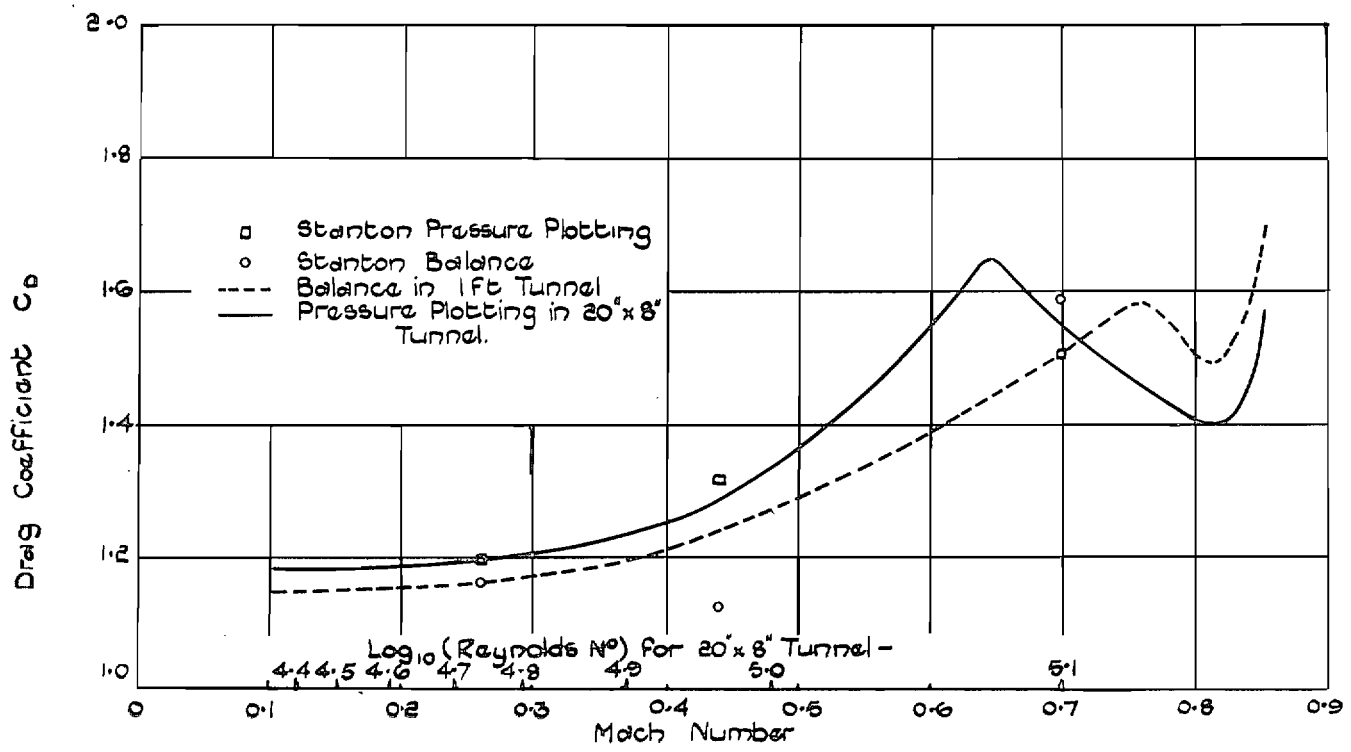


FIG. 98. Variation of drag coefficient of circular cylinder with Mach number. (Stanton's observations were made at a constant Reynolds number of 20,000.)

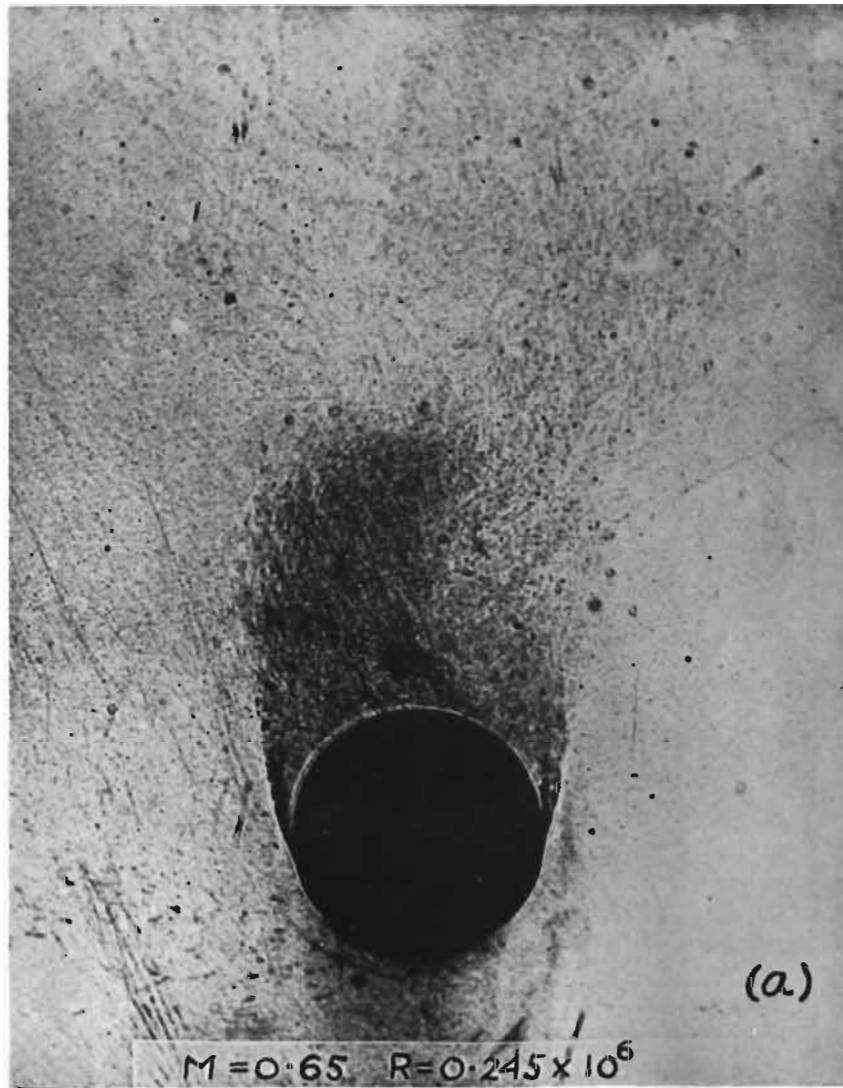


FIG. 99(a).



FIG. 99(b).

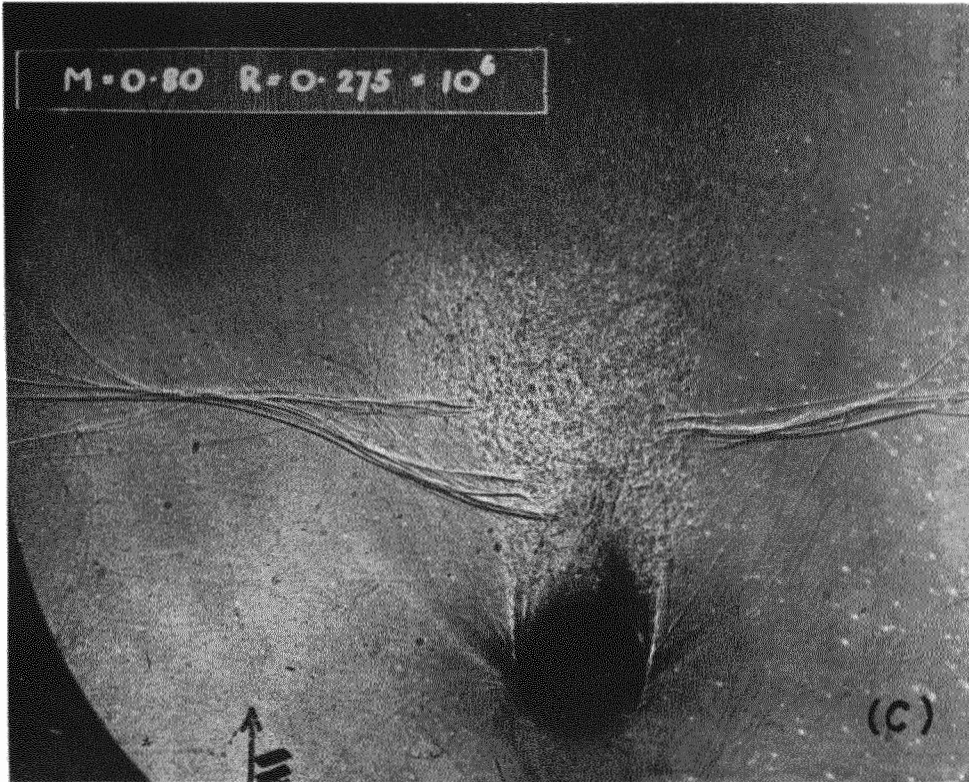


FIG. 99(c). Direct-shadow photographs of the flow around a circular cylinder.

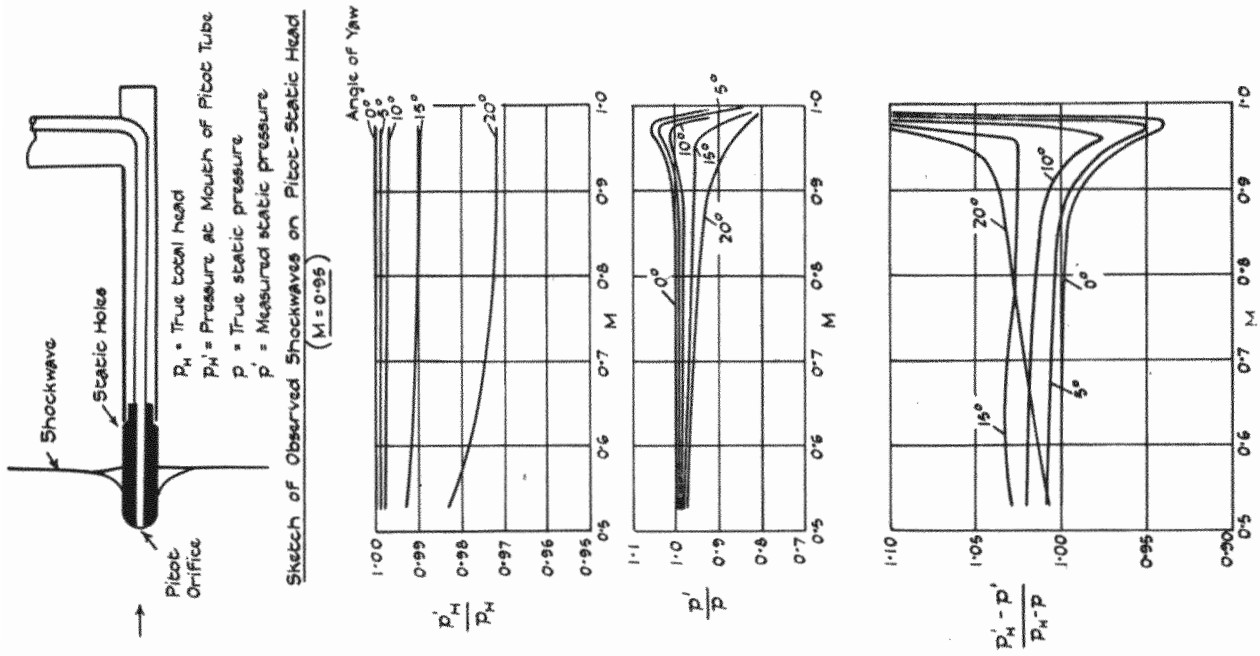


FIG. 100. Influence of compressibility and yaw on reading of pitot-static head (from Ref. 206).

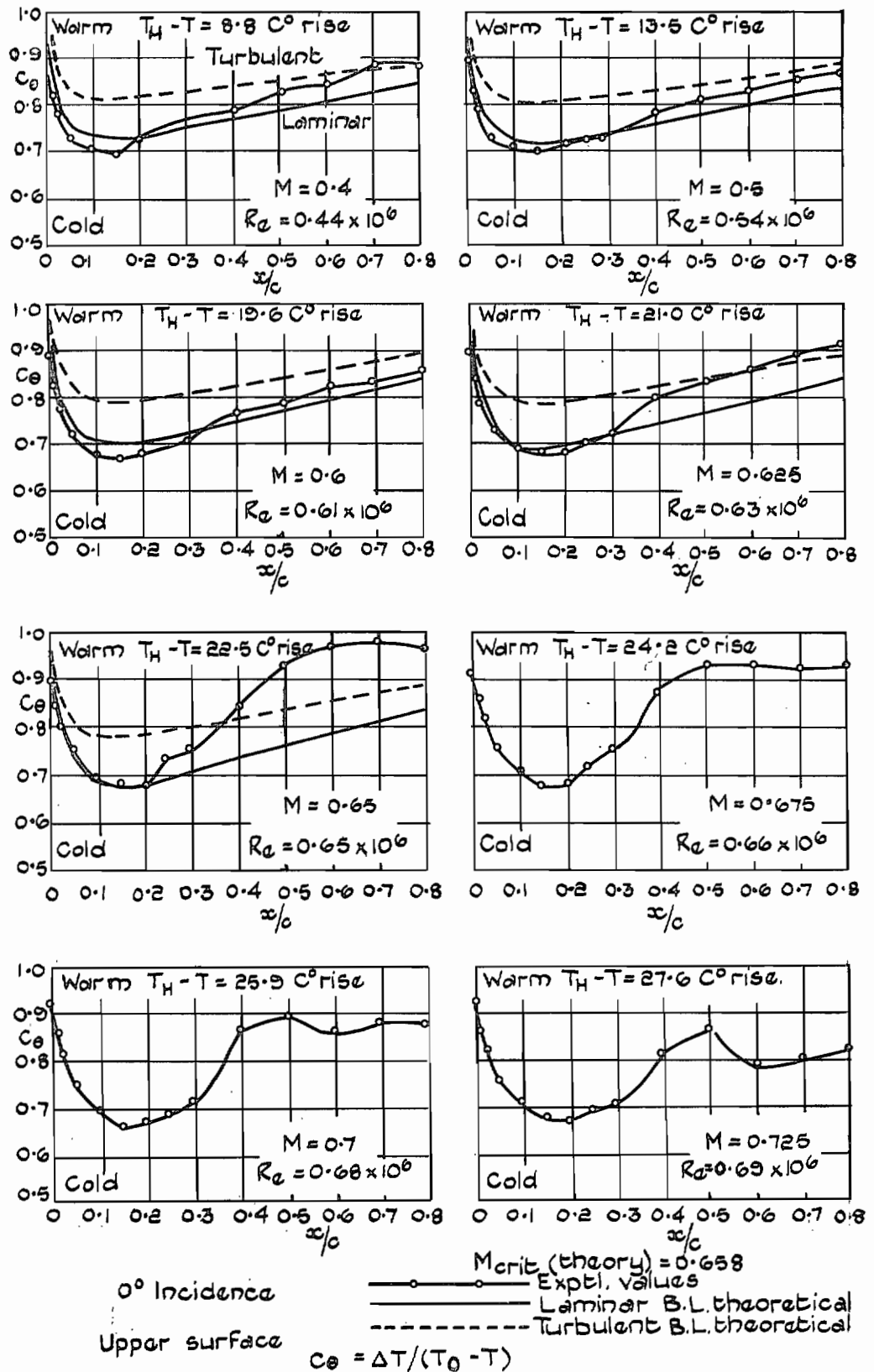


FIG. 101. Surface temperatures on N 2030 aerofoil.

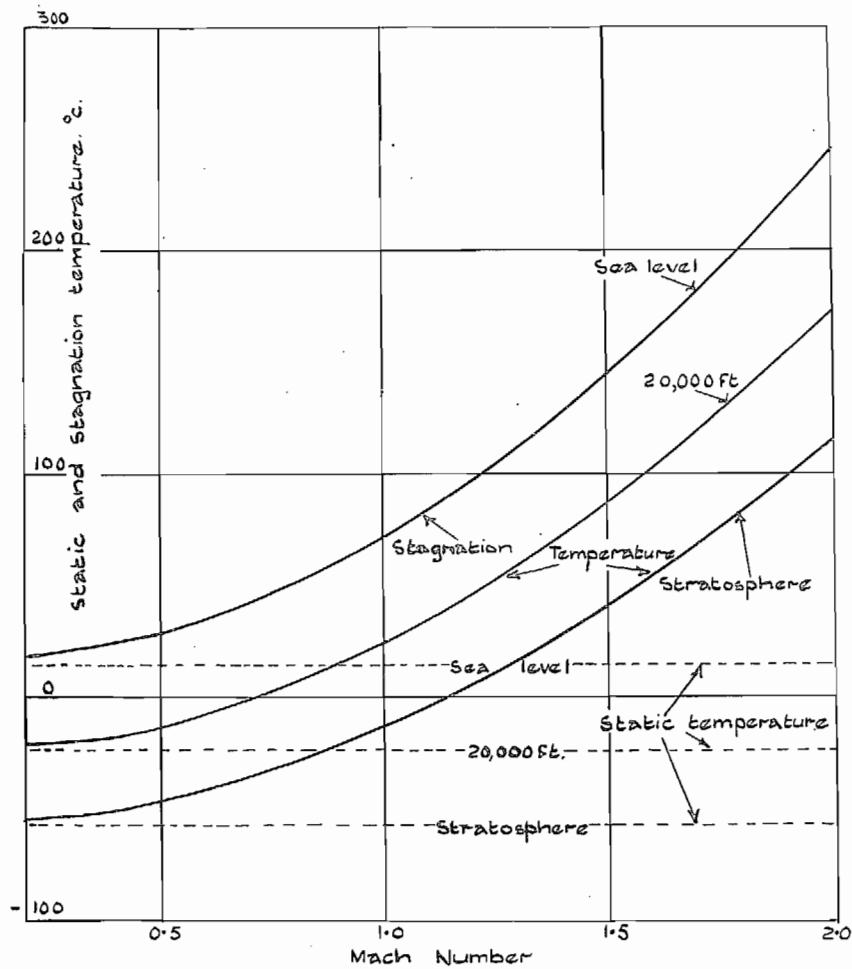


FIG. 102. Isentropic stagnation temperature at various altitudes and Mach numbers in I.C.A.N. atmosphere.

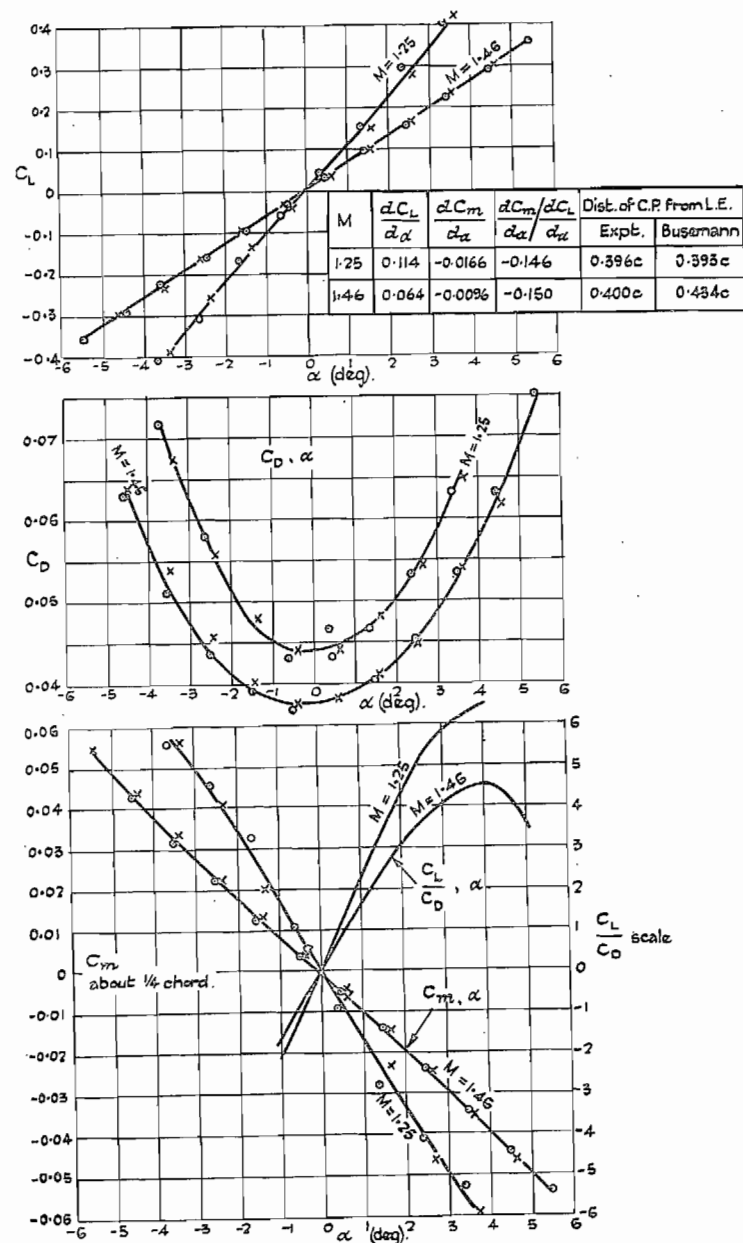


FIG. 103. Biconvex aerofoil.

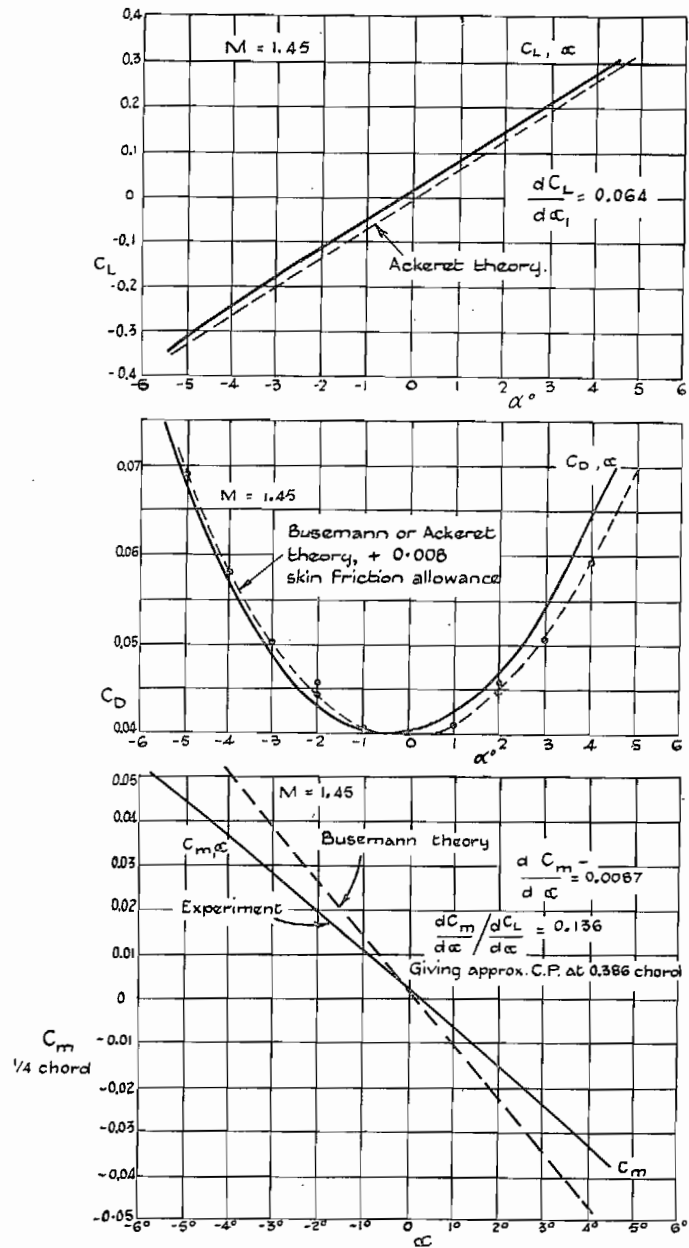


FIG. 104. Faired double-wedge aerofoil. Supersonic variation of lift, drag, quarter-chord moment and centre of pressure with incidence at $M = 1.45$.

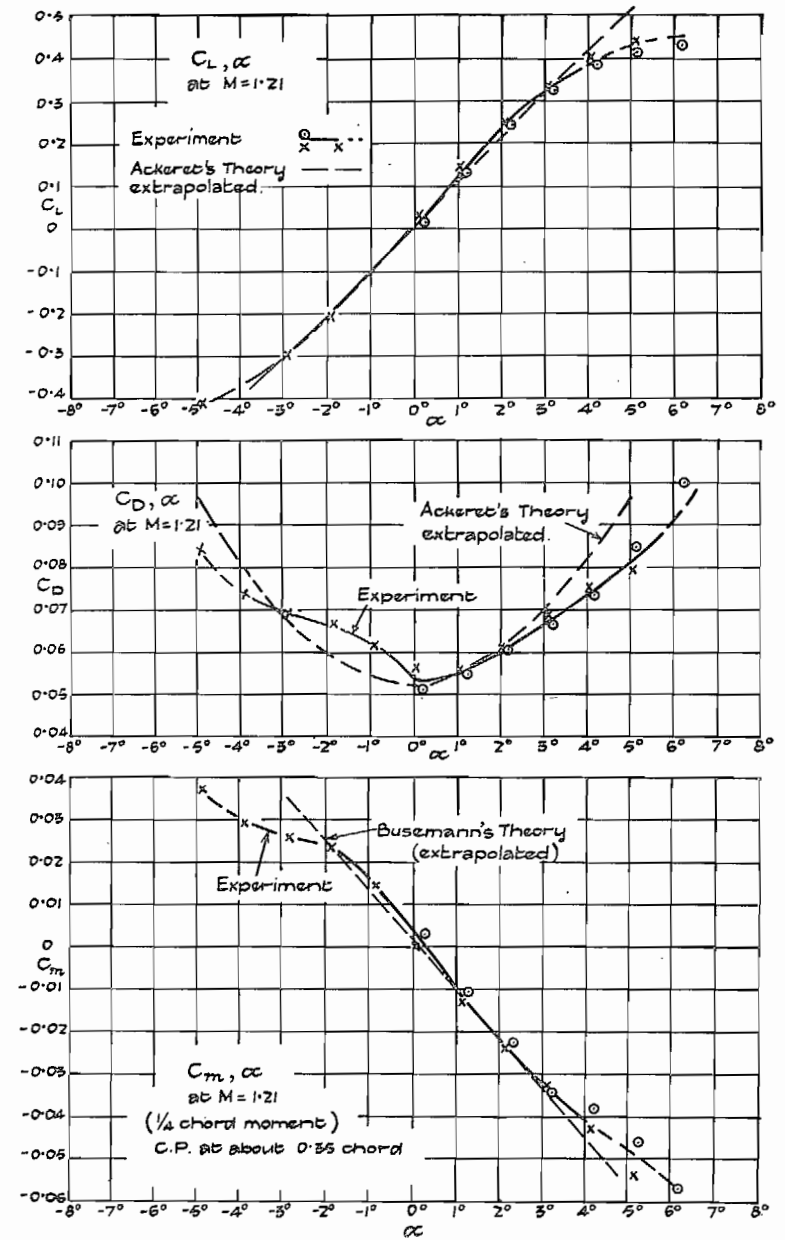


FIG. 105. Faired double-wedge aerofoil. Lift, drag and quarter-chord moment coefficients against incidence at a Mach number of 1.21, and correlation with theory.

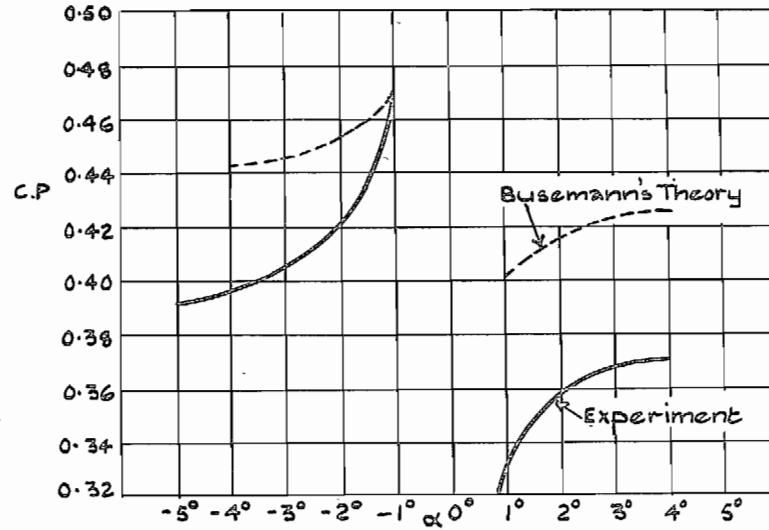


FIG. 106. Faired double-wedge aerofoil. Experimental and theoretical variation of centre of pressure with incidence at $M = 1.45$.

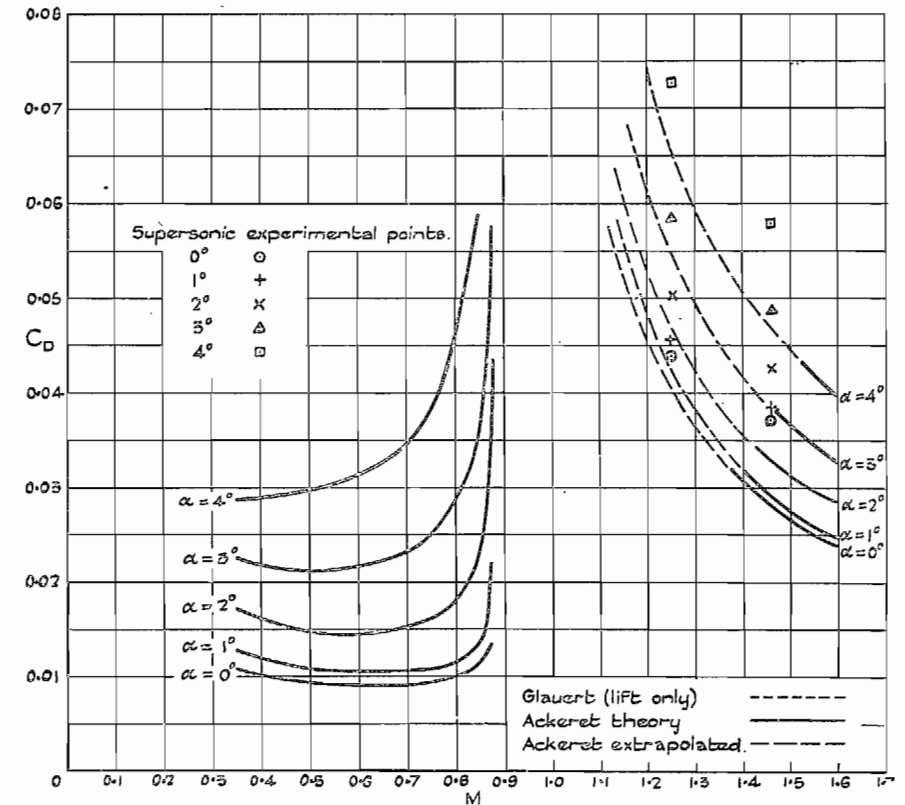
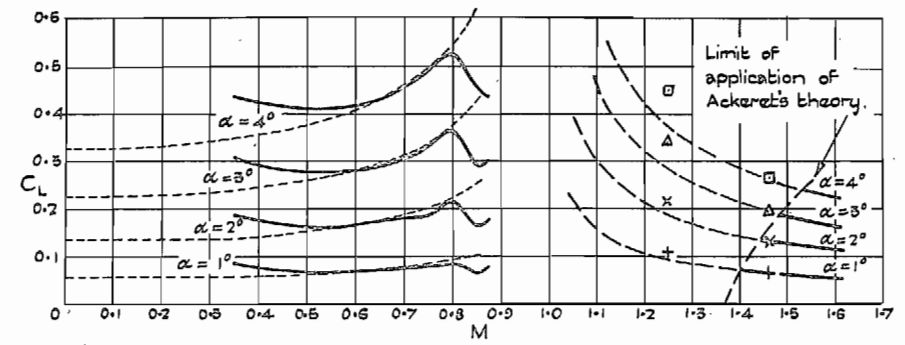


FIG. 107. Biconvex aerofoil. Subsonic and supersonic variation of C_L and C_D with Mach number. Comparison of experiment with Glauert's and Ackeret's theory.

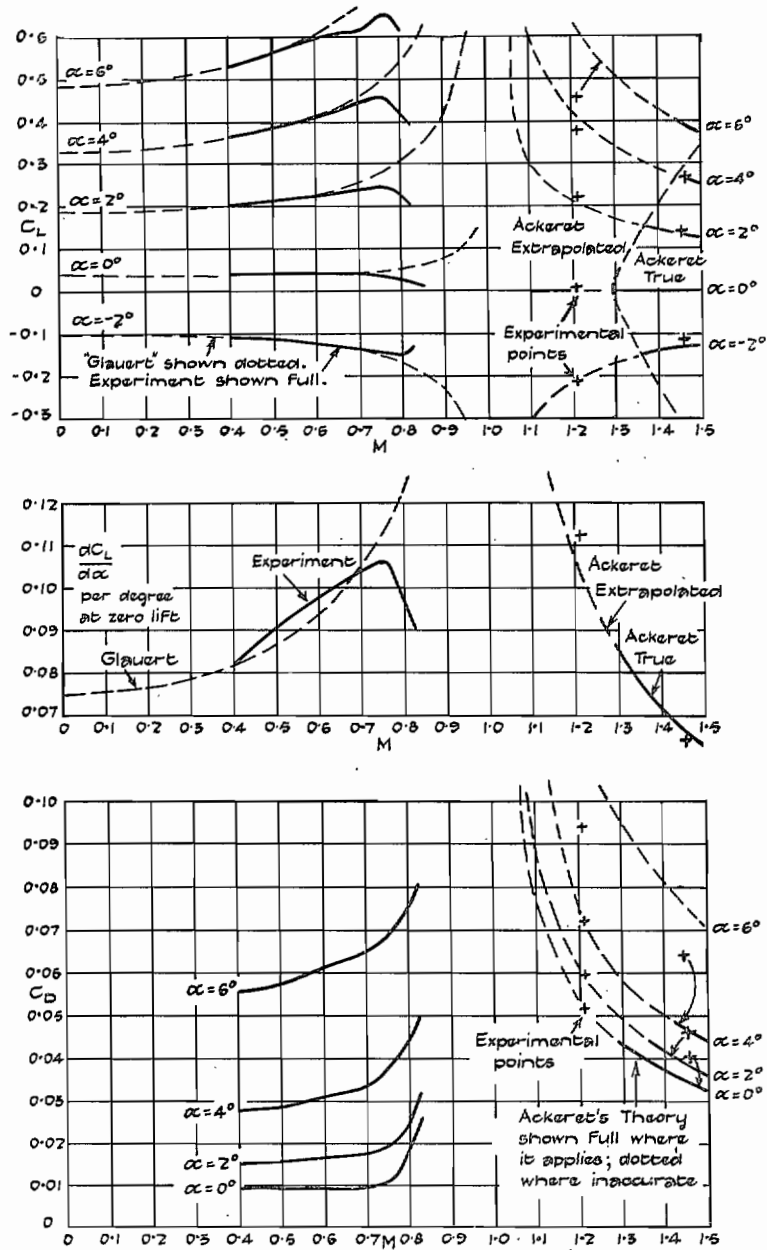


FIG. 108. Faired double-wedge aerofoil. Subsonic and supersonic variation of C_L , C_D and $dC_L/d\alpha$ with Mach number. Comparison of experiment with Glauert's and Ackeret's theories (both the latter shown dotted).

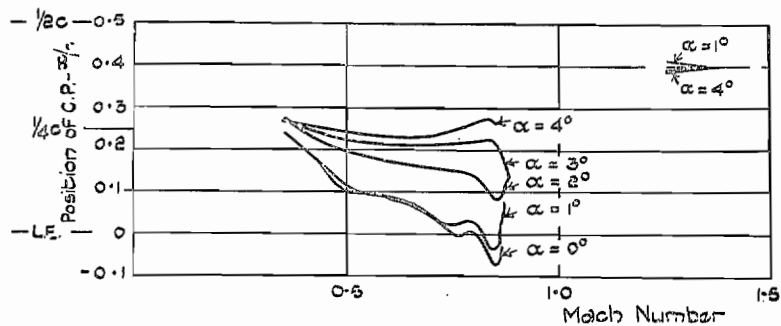


FIG. 109. Variation of centre of pressure with Mach number for $7\frac{1}{2}$ per cent biconvex aerofoil.

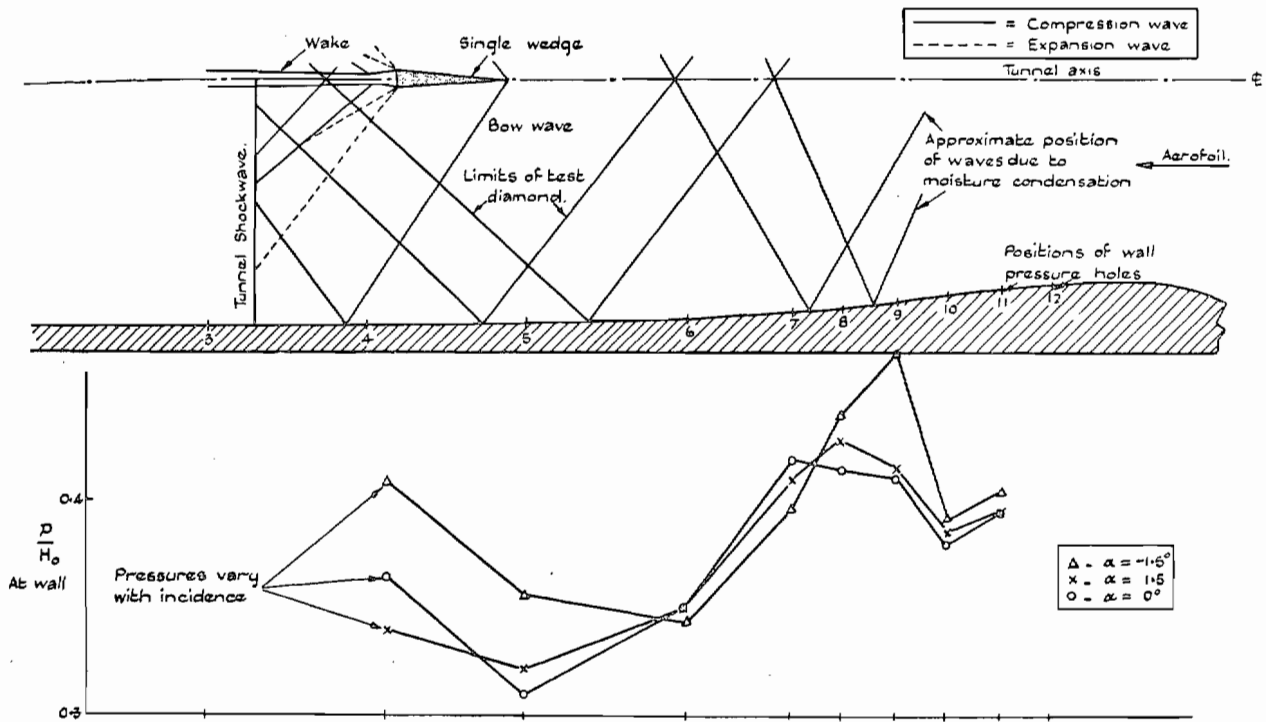


FIG. 110. Single-wedge aerofoil in 5 x 2-in. tunnel showing wave pattern and wall pressure distribution.

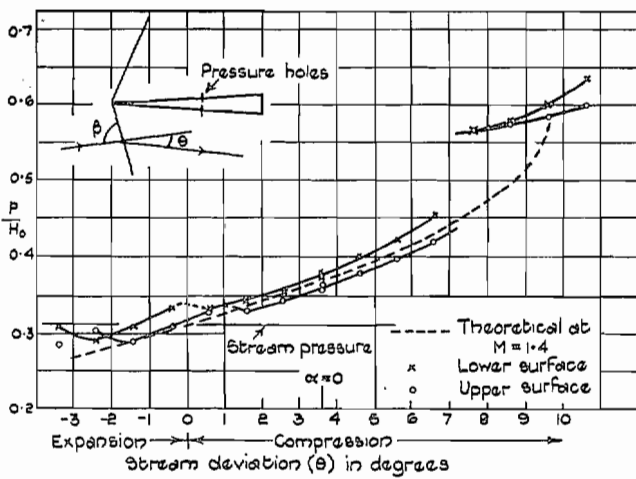


FIG. 111. Comparison of upper and lower surface pressures.

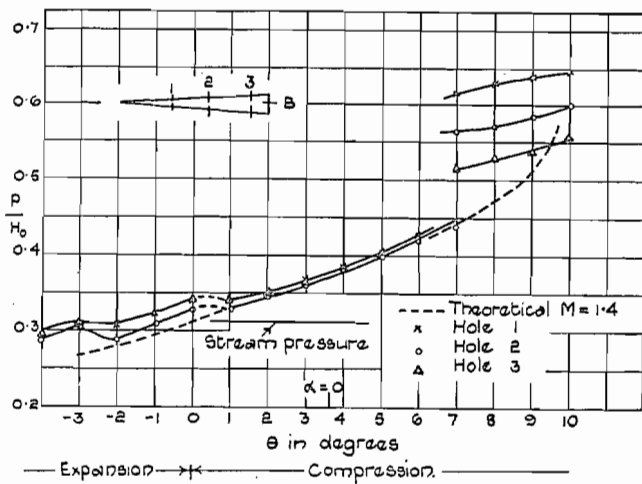


FIG. 112. Pressures on surface of single-wedge aerofoil.

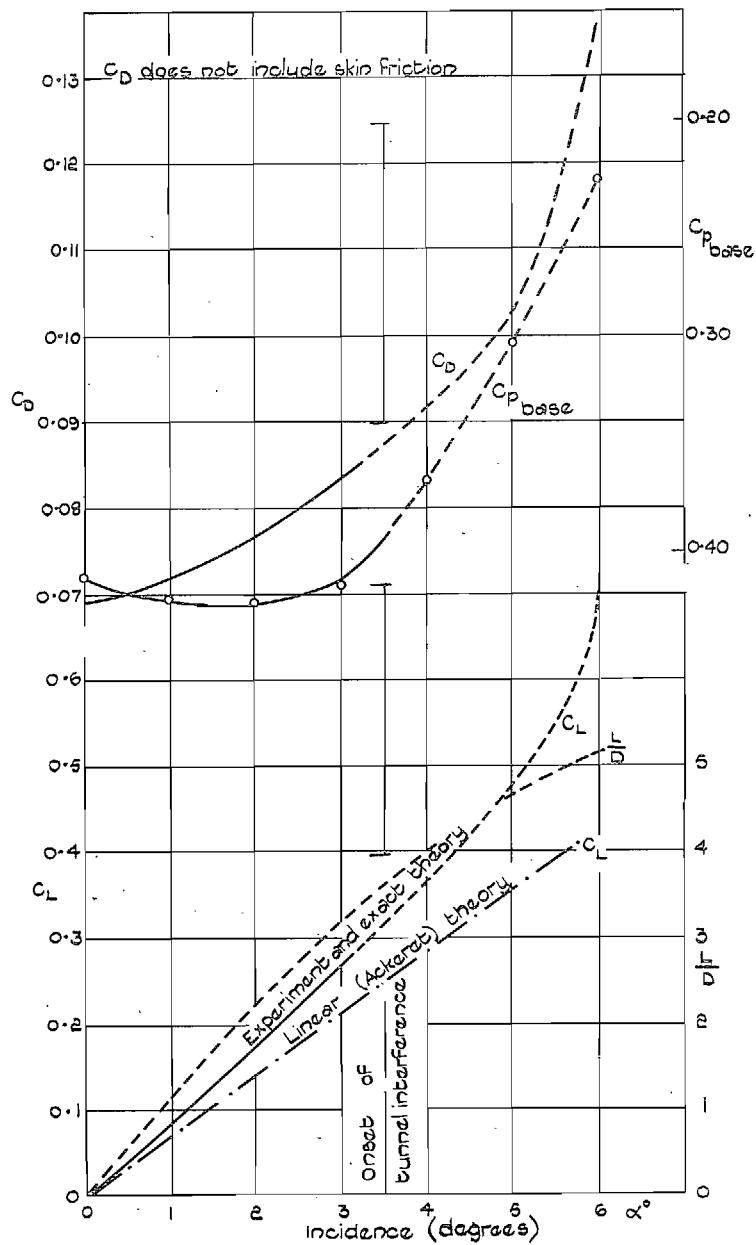


FIG. 113. Forces on wedge aerofoil.

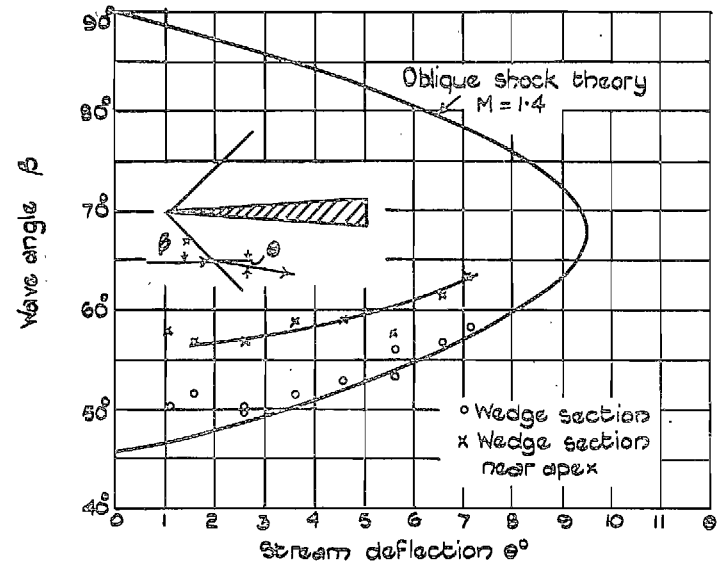


FIG. 114(a). Variation of wave angle (β) with stream deflection (θ). Wedge section.

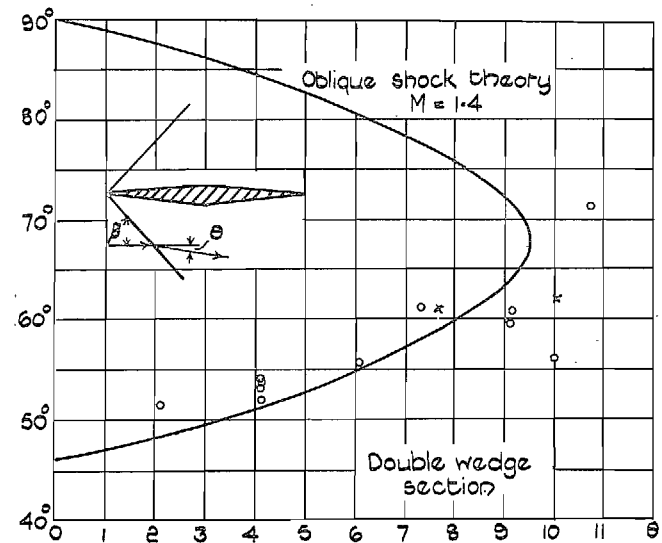


FIG. 114(b). Variation of wave angle (β) with stream deflection (θ). Double-wedge section.

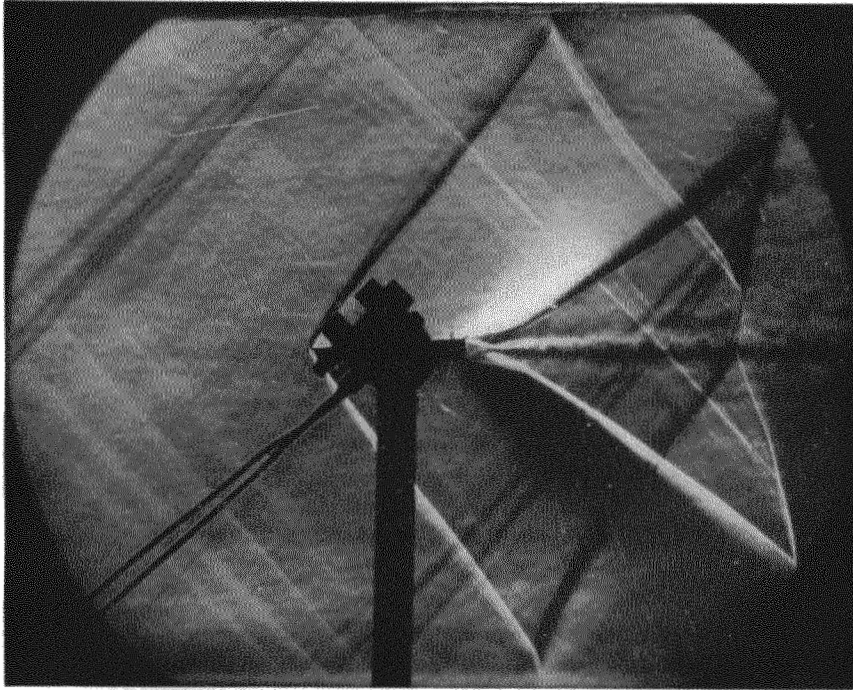


FIG. 115. Single wedge at $\alpha = 0.5$ deg. $M = 1.4$.

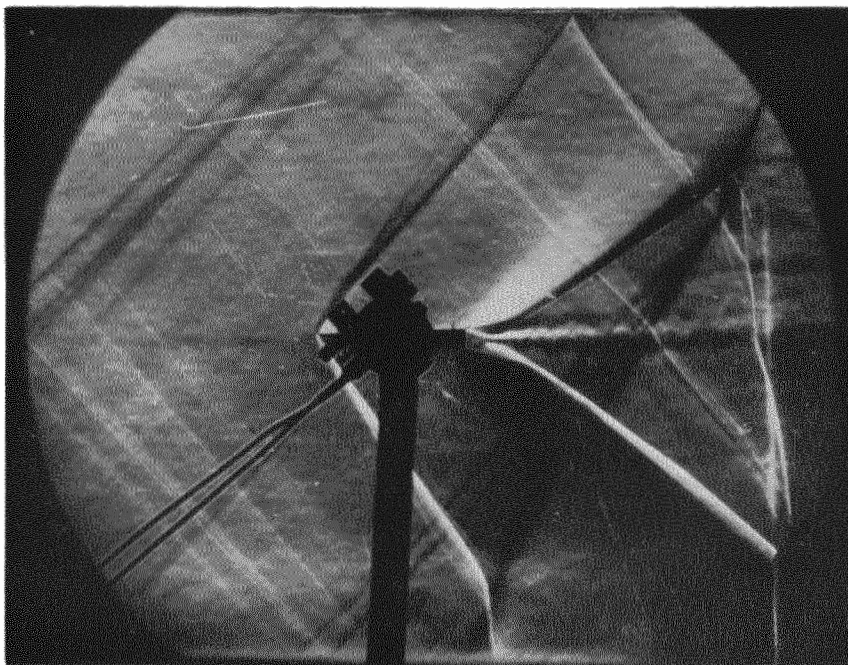


FIG. 116. Single wedge at $\alpha = 1.5$ deg. $M = 1.40$.

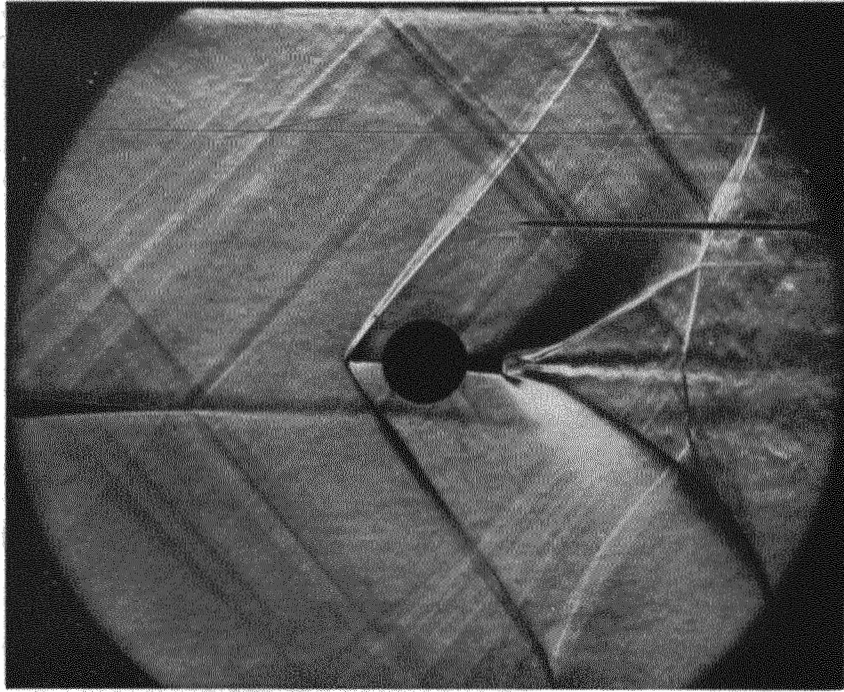


FIG. 117. Single wedge at $\alpha = 1.5$ deg. $M = 1.40$.
(Note the vortex sheet from the three shock intersection in the top right-hand corner.)

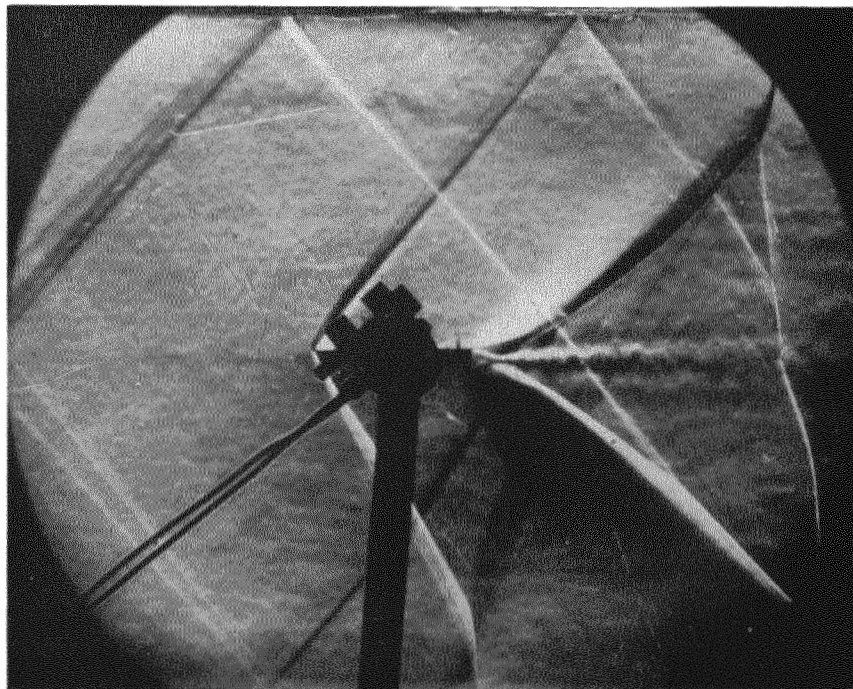


FIG. 118. Single wedge at $\alpha = 2.5$ deg. $M = 1.4$.

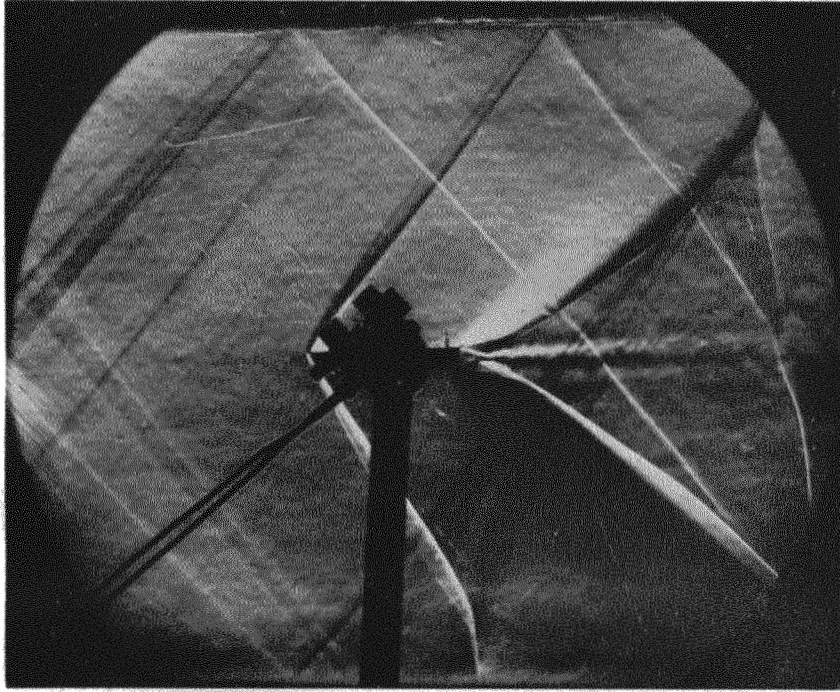


FIG. 119. Single wedge at $\alpha = 3$ deg. $M = 1.4$.

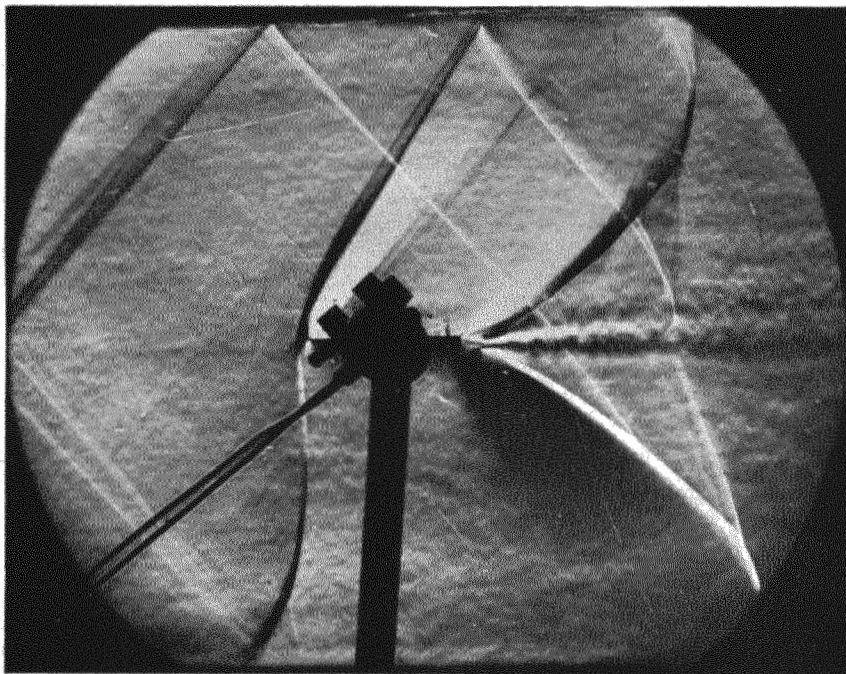


FIG. 120. Single wedge at $\alpha = 3.5$ deg. $M = 1.4$.

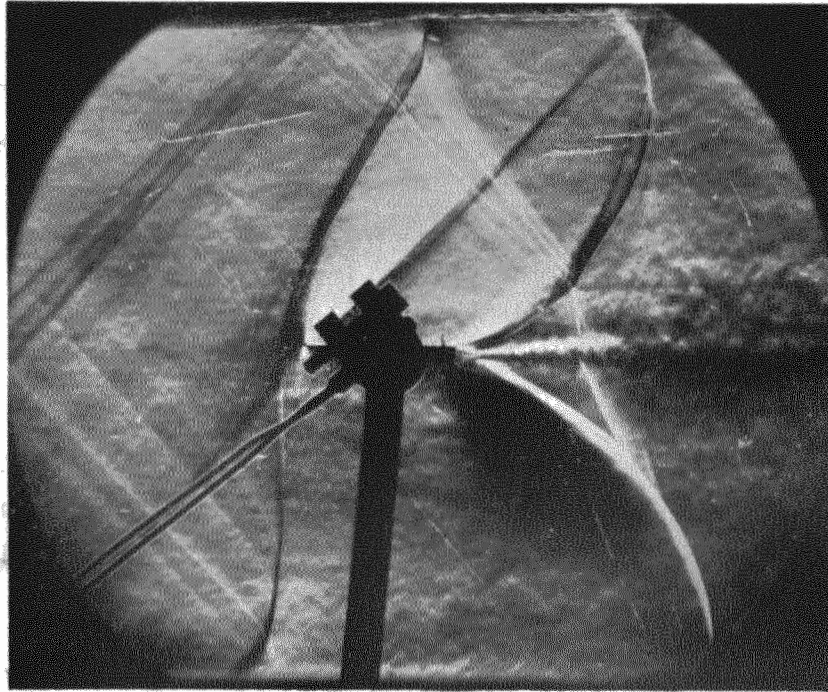


FIG. 121. Single wedge at $\alpha = 4.5$ deg. $M = 1.4$.

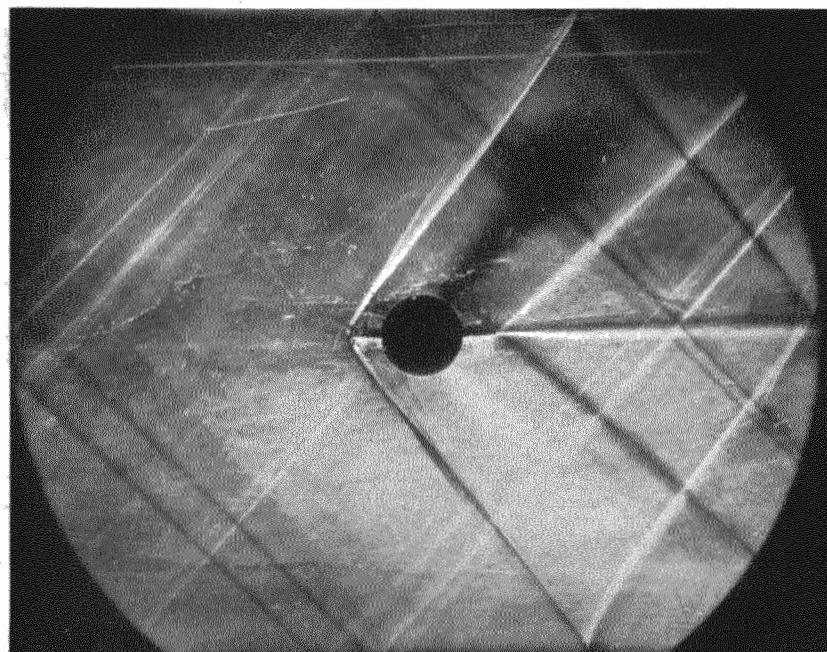


FIG. 122. Double wedge at $\alpha = 0$ deg. $M = 1.4$.

FIG. 124. Double wedge at $\alpha = 3$ deg. $M = 1.4$.

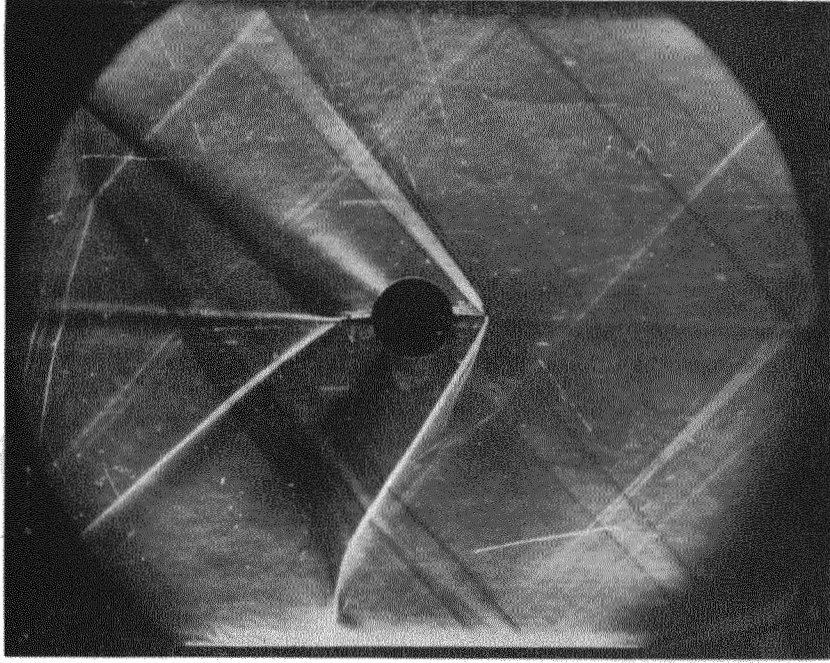
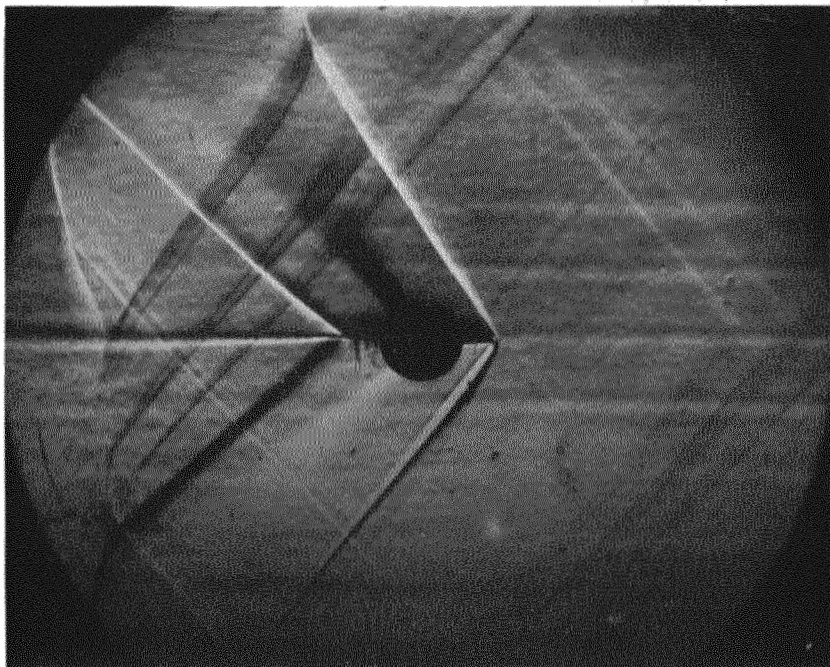


FIG. 123. Double wedge at $\alpha = 2$ deg. $M = 1.4$.



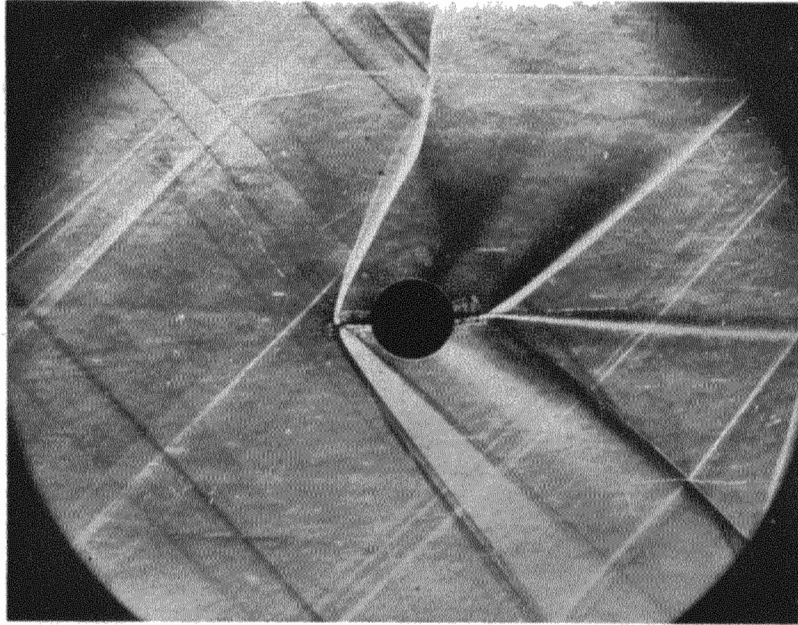


FIG. 125. Double wedge at $\alpha = 3.6$ deg. $M = 1.4$.

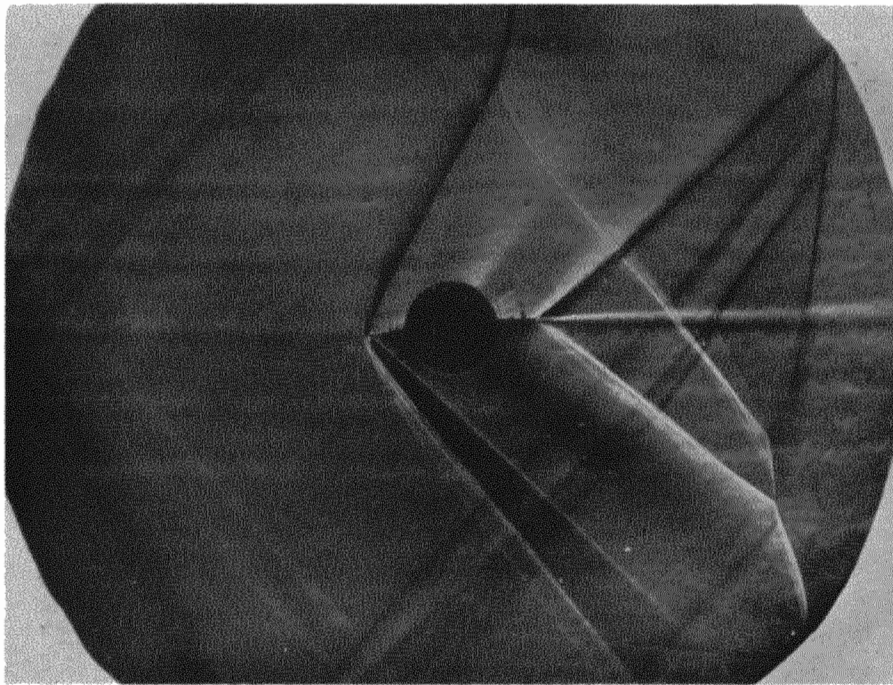


FIG. 126. Double wedge at $\alpha = 5$ deg. $M = 1.4$.

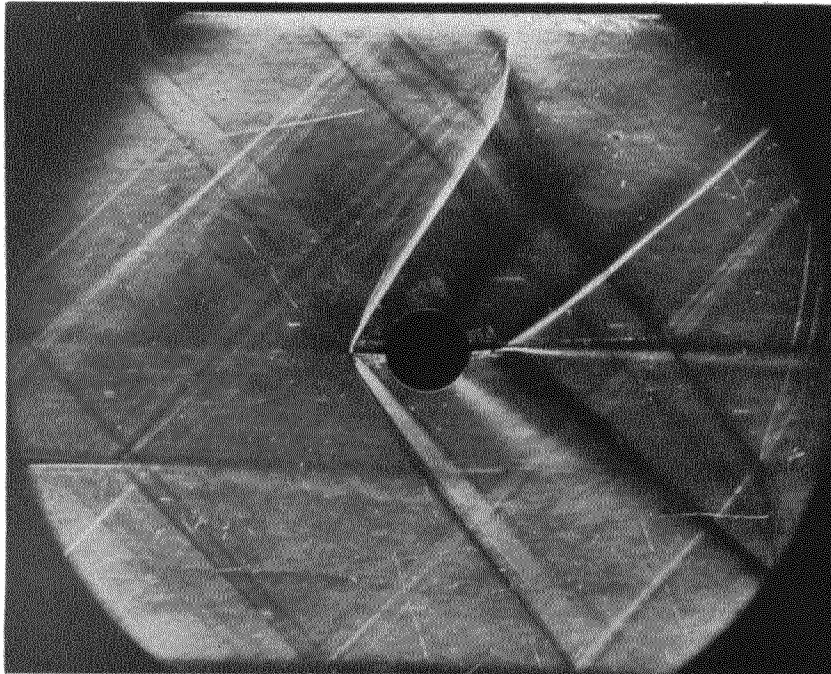


FIG. 127. Double wedge at $\alpha = 5$ deg. $M = 1.4$.

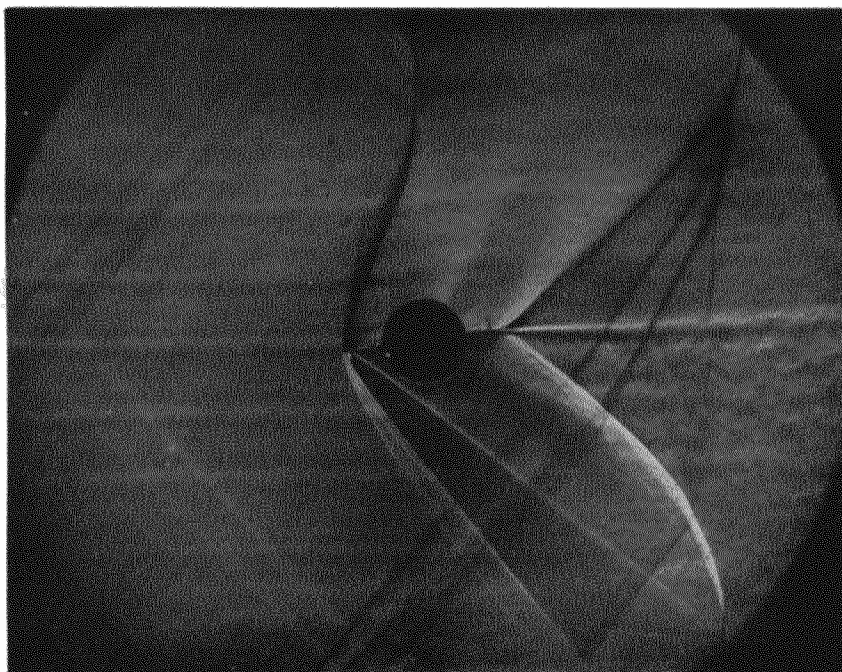


FIG. 128. Double wedge at $\alpha = 6.6$ deg. $M = 1.4$.

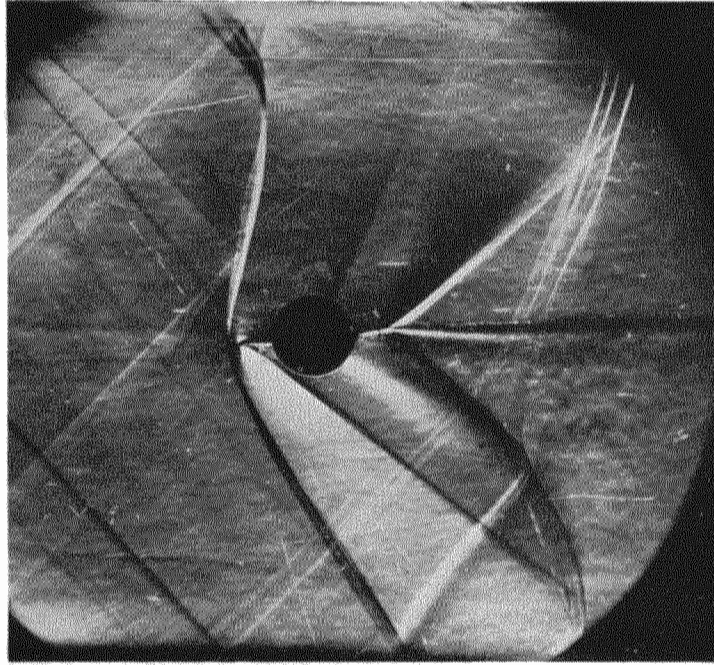


FIG. 129. Double wedge at $\alpha = 7$ deg. $M = 1.4$.

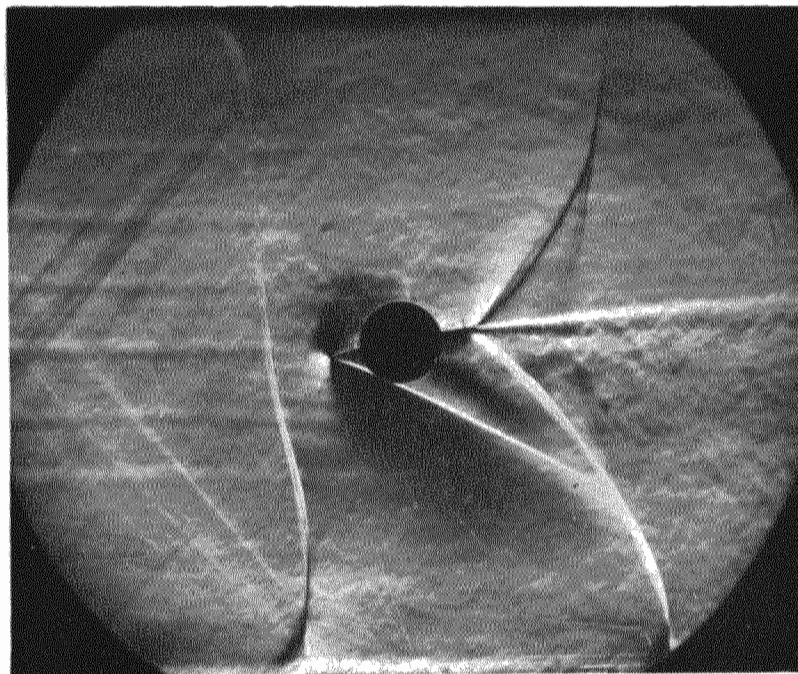


FIG. 130. Double wedge at $\alpha = 10$ deg. $M = 1.4$.

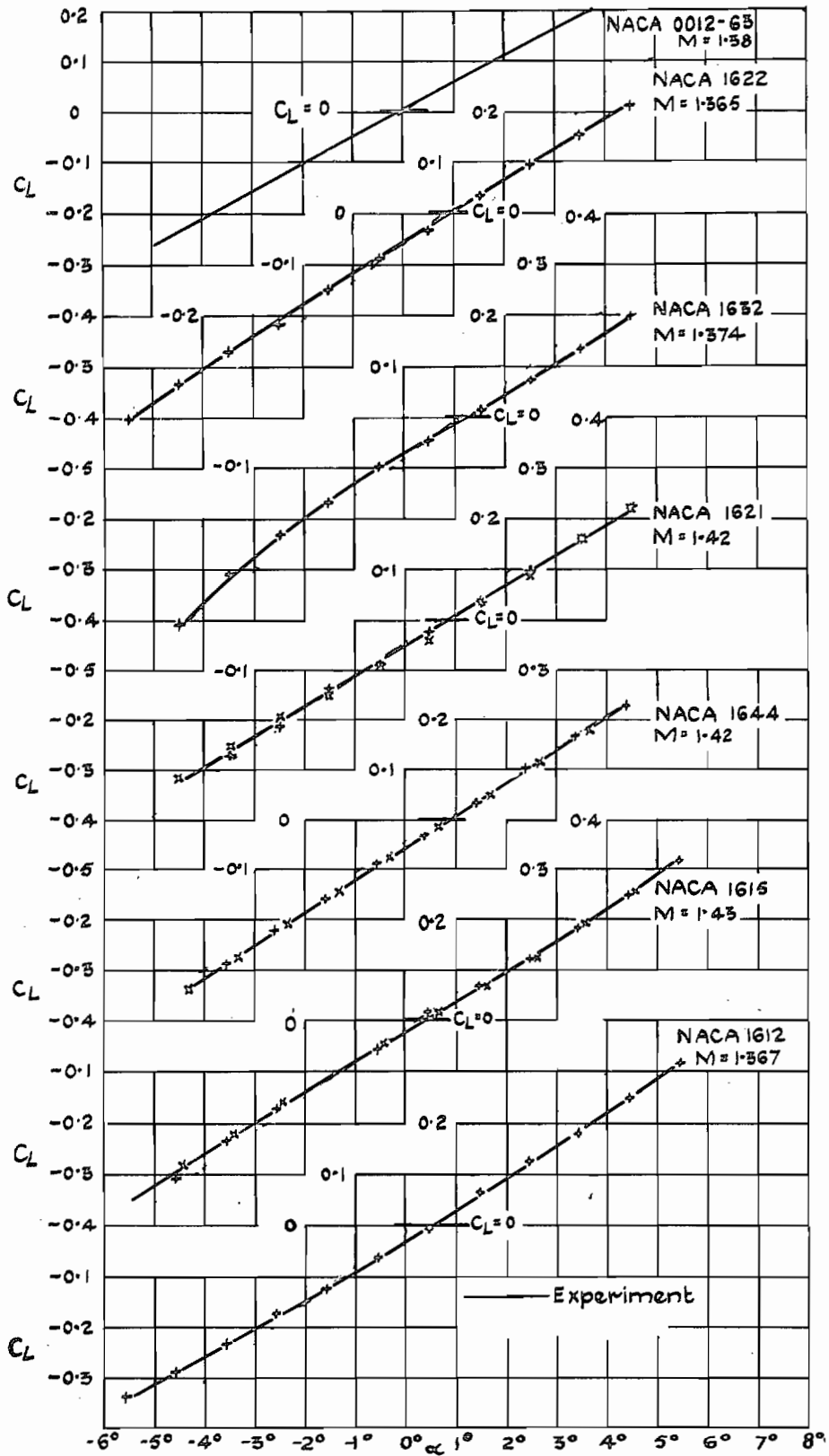


FIG. 131. Lift coefficients for round-nosed aerofoils.

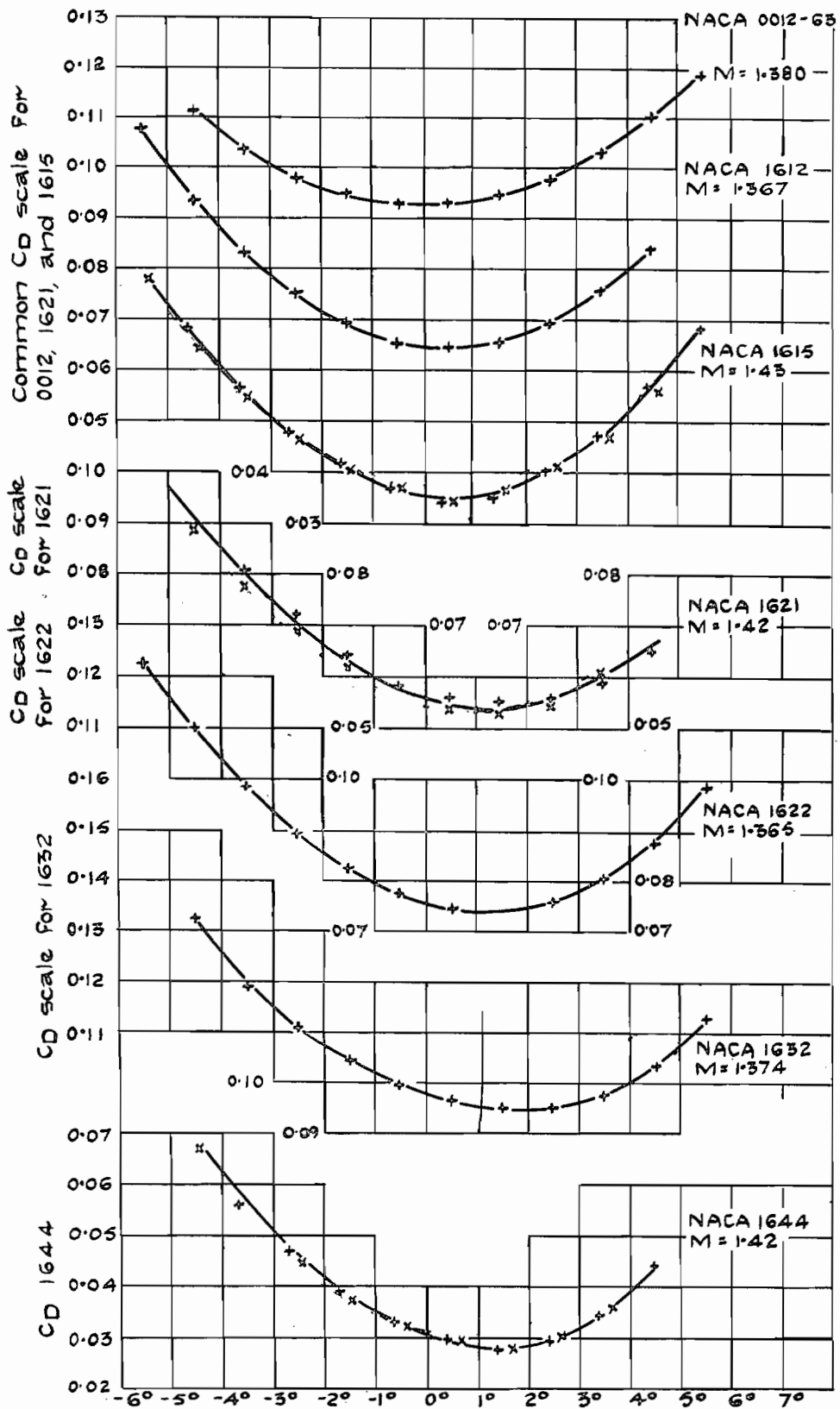


FIG. 132. Drag coefficients for round-nosed aerofoils.

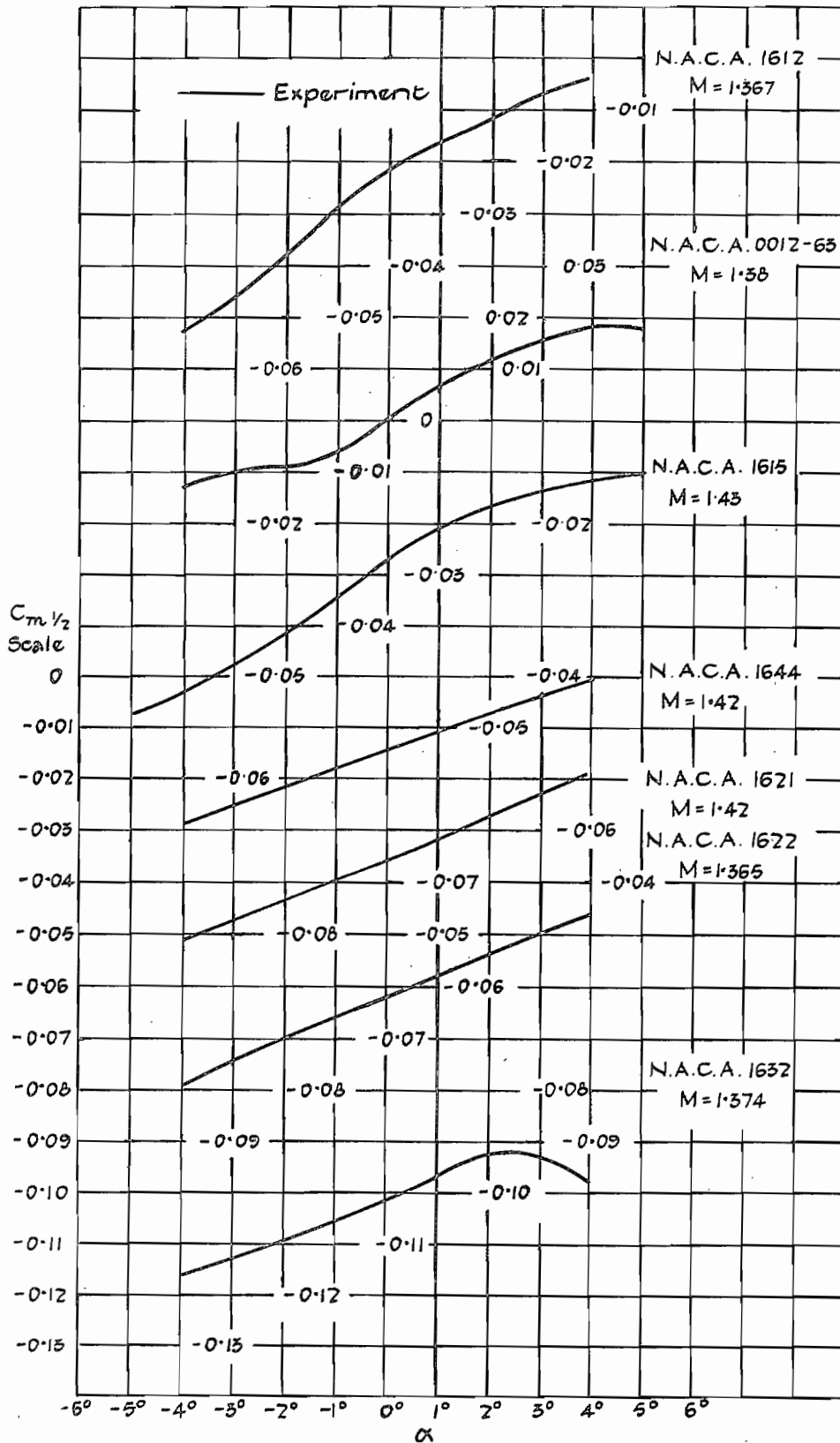


FIG. 133. Half-chord pitching-moment coefficients for round-nosed aerofoils.

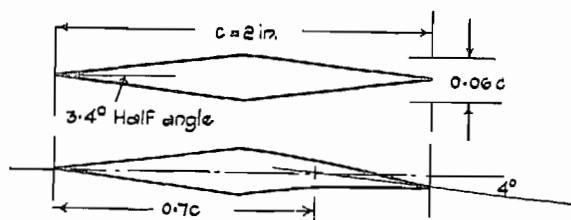


FIG. 134. Double-wedge aerofoil sections.
(Not to scale.)

274

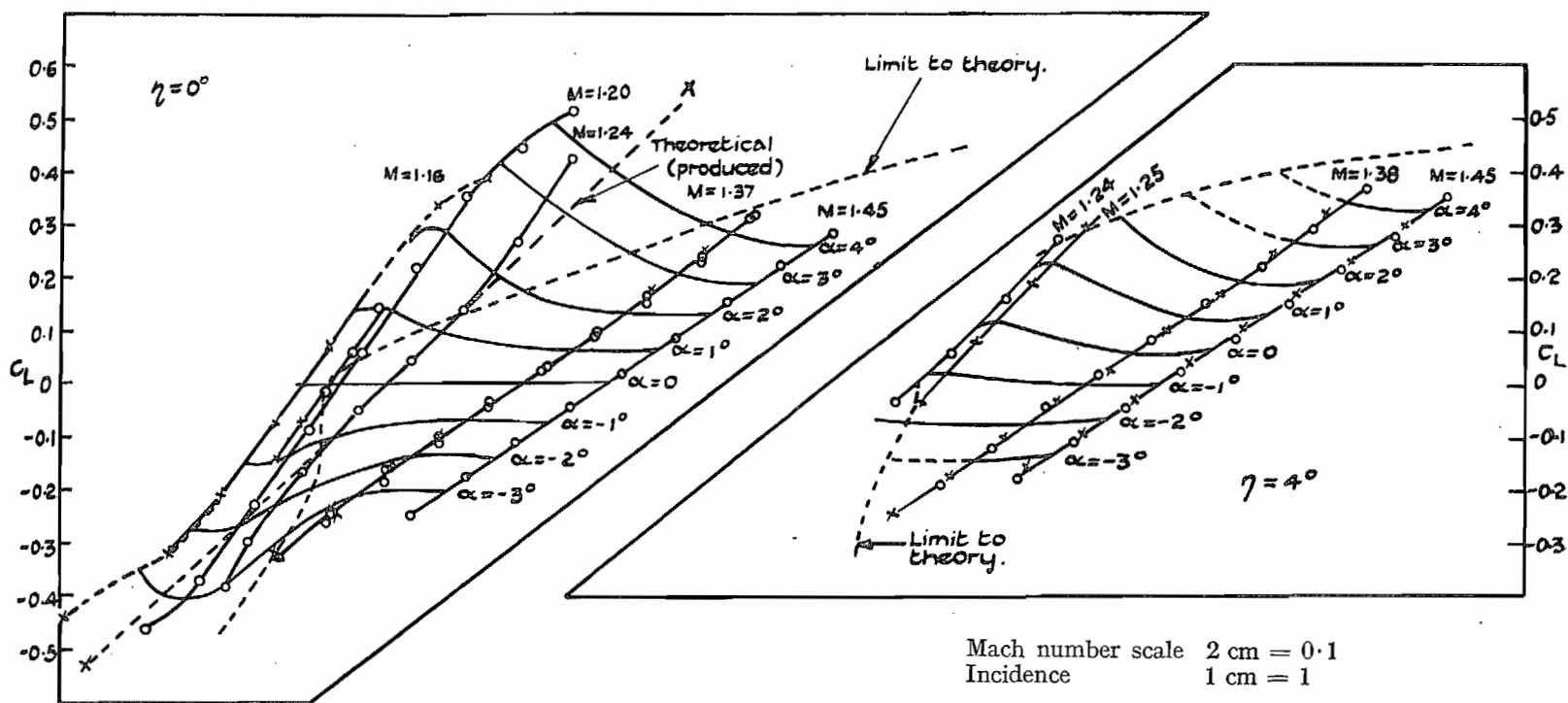


FIG. 135. Double-wedge aerofoil. The variation of C_L with α , η , and M (normal elevator).

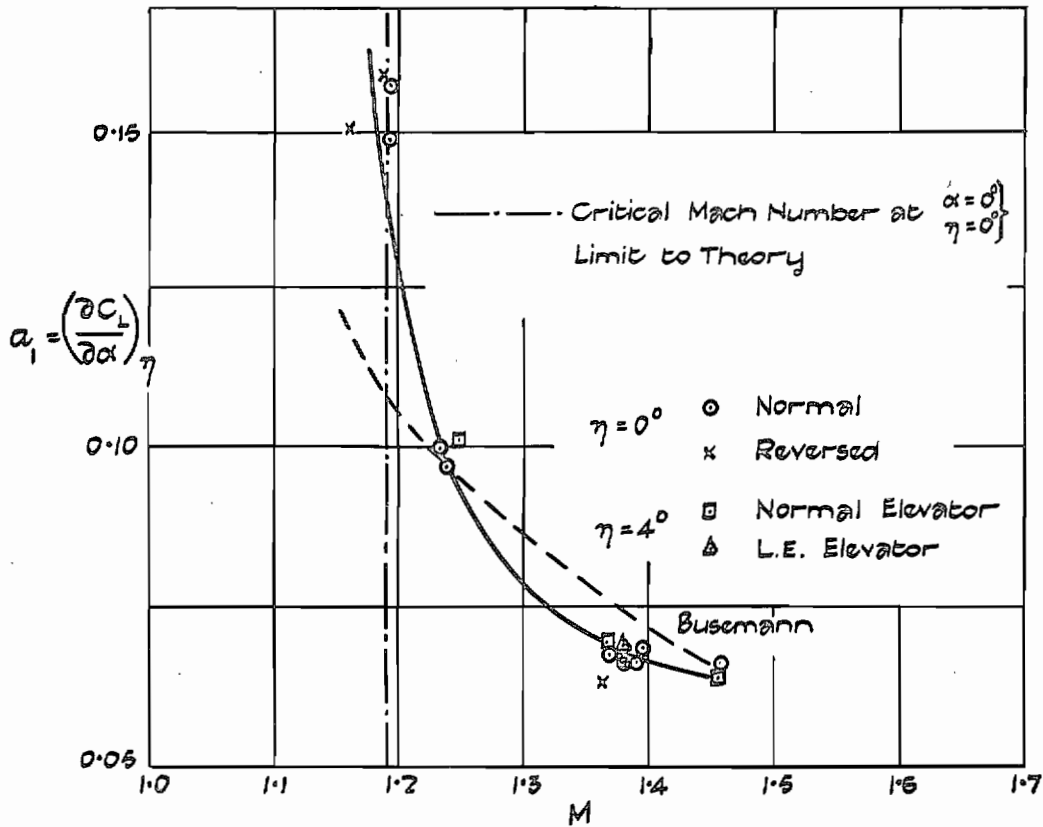


FIG. 136. Double-wedge aerofoil. Variation of a_1 with M . (α in degrees.)

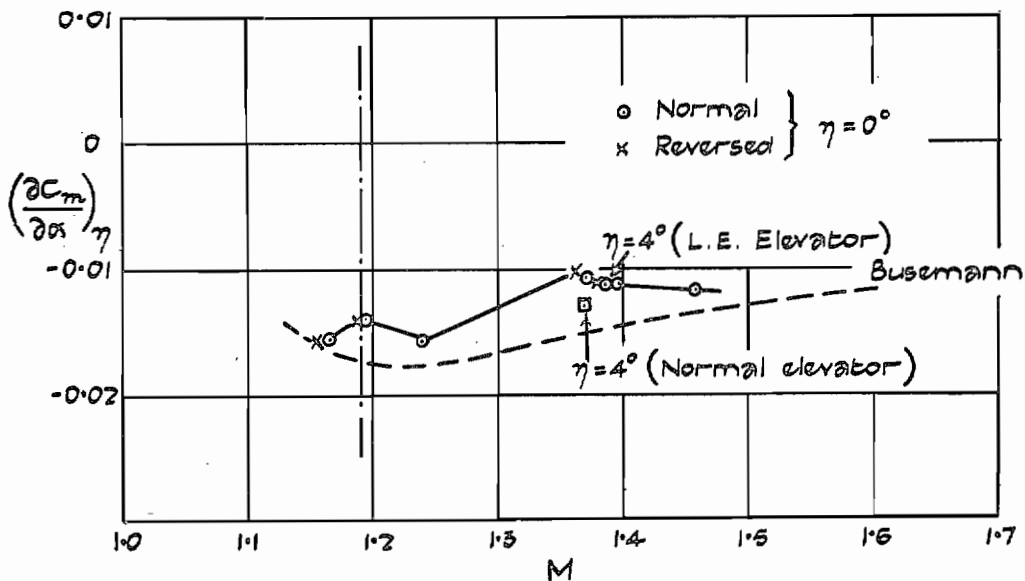


FIG. 137. Double-wedge aerofoil. Variation of $(\partial C_m / \partial \alpha)_\eta$ with M . (α in degrees.)

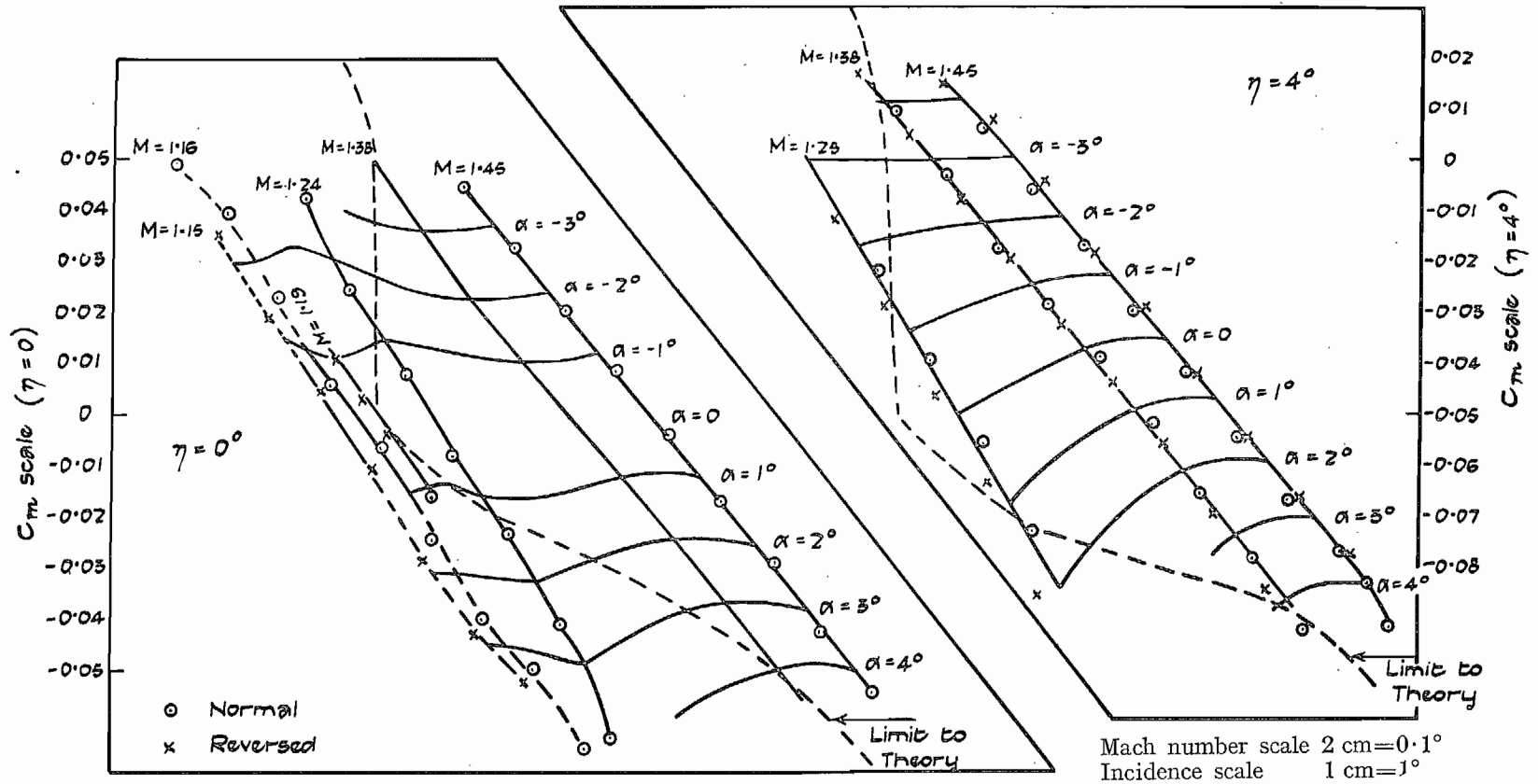


FIG. 138. Double-wedge aerofoil. The variation of C_m with α , η and M (normal elevator).

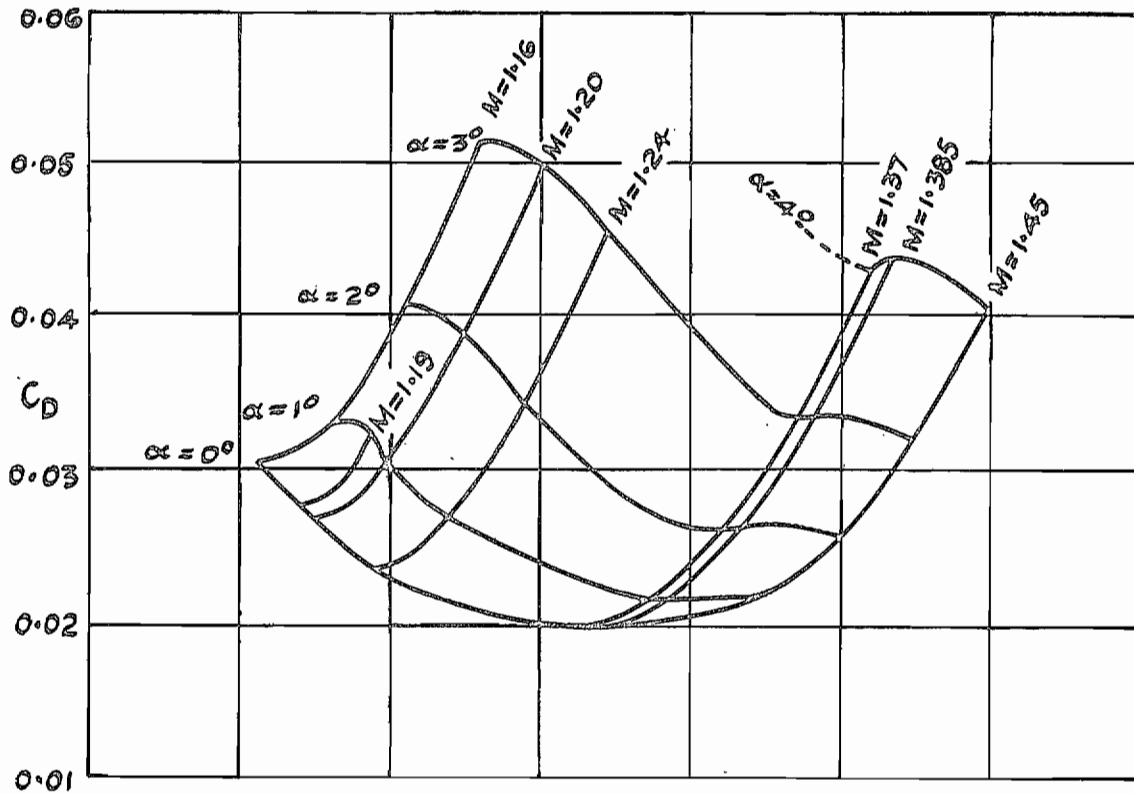


FIG. 139. Double-wedge aerofoil. Variation of C_D with α and M at $\eta = 0^\circ$.

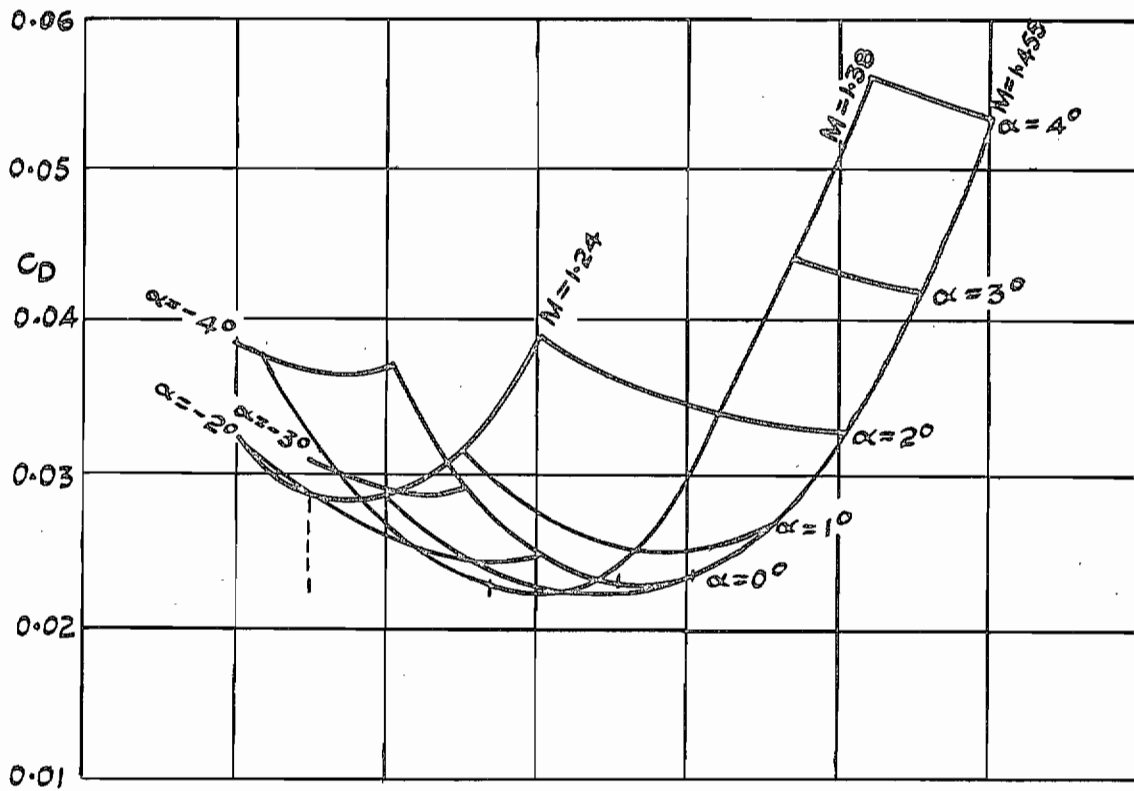


FIG. 140. Double-wedge aerofoil. Variation of C_D with α and M at $\eta = 4^\circ$.